

Advances in
**Planar Lipid Bilayers
and Liposomes**

Volume 4



Advances in
Planar Lipid Bilayers
and Liposomes

EDITORIAL BOARD

Professor Dr. Roland Benz (*Wuerzburg, Germany*)
Professor Hans G. L. Coster (*Sydney, Australia*)
Dr. Herve Duclohier (*Rennes, France*)
Dr. Yury A. Ermakov (*Moscow, Russia*)
Professor Alessandra Gliozzi (*Genova, Italy*)
Professor Dr. Ales Iglic (*Ljubljana, Slovenia*)
Dr. Bruce L. Kagan (*Los Angeles, USA*)
Professor Dr. Wolfgang Knoll (*Mainz, Germany*)
Professor Dr. Reinhard Lipowsky (*Potsdam, Germany*)
Dr. Gianfranco Menestrina (*Povo, Italy*)
Dr. Yoshinori Muto (*Gifu, Japan*)
Dr. Ian R. Peterson (*Coventry, UK*)
Professor Alexander G. Petrov (*Sofia, Bulgaria*)
Professor Jean-Marie Ruyschaert (*Bruxelles, Belgium*)
Dr. Bernhard Schuster (*Vienna, Austria*)
Dr. Masao Sugawara (*Tokyo, Japan*)
Professor Yoshio Umezawa (*Tokyo, Japan*)
Dr. Erkang Wang (*Changchun, China*)
Dr. Philip J. White (*Wellesbourne, UK*)
Professor Mathias Winterhalter (*Bremen, Germany*)
Professor Dixon J. Woodbury (*Provo, USA*)

Advances in **Planar Lipid Bilayers** **and Liposomes**

Volume 4

Editor

A. Leitmannova Liu

*Department of Physiology
Michigan State University
East Lansing, Michigan
USA*

and

*Centre for Interface Sciences
Microelectronics Department
Faculty of Engineering & Information
Slovak Technical University, Bratislava
Slovak Republic*

Founding Editor

H.T. Tien

*Department of Physiology
Michigan State University
East Lansing, Michigan
USA*



Amsterdam • Boston • Heidelberg • London • New York • Oxford
Paris • San Diego • San Francisco • Singapore • Sydney • Tokyo
An imprint of Academic Press



Academic Press is an imprint of Elsevier
84 Theobald's Road, London WC1X 8RR, UK
Radarweg 29, PO Box 211, 1000 AE Amsterdam, The Netherlands
The Boulevard, Langford Lane, Kidlington, Oxford OX5 1GB, UK
30 Corporate Drive, Suite 400, Burlington, MA 01803, USA
525 B Street, Suite 1900, San Diego, CA 92101-4495, USA

First edition 2006

Copyright © 2006 Elsevier Inc. All rights reserved

No part of this publication may be reproduced, stored in a retrieval system or transmitted in any form or by any means electronic, mechanical, photocopying, recording or otherwise without the prior written permission of the publisher

Permissions may be sought directly from Elsevier's Science & Technology Rights Department in Oxford, UK: phone (+44) (0) 1865 843830; fax (+44) (0) 1865 853333; email: permissions@elsevier.com. Alternatively you can submit your request online by visiting the Elsevier web site at <http://elsevier.com/locate/permissions>, and selecting *Obtaining permission to use Elsevier material*

Notice

No responsibility is assumed by the publisher for any injury and/or damage to persons or property as a matter of products liability, negligence or otherwise, or from any use or operation of any methods, products, instructions or ideas contained in the material herein. Because of rapid advances in the medical sciences, in particular, independent verification of diagnoses and drug dosages should be made

ISBN-13: 978-0-12-372505-9

ISBN-10: 0-12-372505-4

ISSN: 1554-4516

For information on all Academic Press publications
visit our website at books.elsevier.com

Printed and bound in USA

06 07 08 09 10 10 9 8 7 6 5 4 3 2 1

Working together to grow
libraries in developing countries

www.elsevier.com | www.bookaid.org | www.sabre.org

ELSEVIER

BOOK AID
International

Sabre Foundation

CONTENTS

Contributors	vii
Preface	ix
1. Lipid Microvesicles: On the Four Decades of Liposome Research <i>Hui-Fang Cui, Jian-Shan Ye, Angelica Leitmannova Liu and H. Ti Tien</i>	1
2. Surface Properties of Liposomes Depending on Their Composition <i>Kimiko Makino and Akira Shibata</i>	49
3. Interactions of Al and Related Metals with Membrane Phospholipids: Consequences on Membrane Physical Properties <i>Patricia I. Oteiza and Sandra V. Verstraeten</i>	79
4. Interaction of Plant Polyphenols with Liposomes <i>Tsutomu Nakayama, Katsuko Kajiya and Shigenori Kumazawa</i>	107
5. Cationic Liposomes as Transmembrane Carriers of Nucleic Acids <i>An Cao, Dominique Briane and Robert Coudert</i>	135
6. Molecular Interactions between Lipid and Its Related Substances in Bilayer Membranes <i>Tomohiro Imura, Shoko Yokoyama and Masahiko Abe</i>	191
7. Cell-Mimicking Supramolecular Assemblies Based on Polydiacetylene Lipids: Recent Development as “Smart” Materials for Colorimetric and Electrochemical Biosensing Devices <i>Chunyan Sun and Jinghong Li</i>	229
8. Budding of Liposomes – Role of Intrinsic Shape Of Membrane Constituents <i>Ales Iglic and Veronika Kralj-Iglic</i>	253
9. Electrical Properties of Aqueous Liposome Suspensions <i>F. Bordi, C. Cametti and S. Sennato</i>	281
Subject Index	321

This page intentionally left blank

CONTRIBUTORS

Masahiko Abe	191
F. Bordi	281
Dominique Briane	135
C. Cametti	281
An Cao	135
Robert Coudert	135
Hui-Fang Cui	1
Ales Iglic	253
Tomohiro Imura	191
Katsuko Kajiya	107
Veronika Kralj-Iglic	253
Shigenori Kumazawa	107
Angelica Leitmannova Liu	1
Jinghong Li	229
Kimiko Makino	49
Tsutomu Nakayama	107
Patricia I. Oteiza	79
S. Sennato	281
Akira Shibata	49
Chunyan Sun	229
H. Ti Tien	1
Sandra V. Verstraeten	79
Jian-Shan Ye	1
Shoko Yokoyama	191

This page intentionally left blank

PREFACE

Volume 4 presents recent research on liposomes based on their historic and experimental realization. Many of the contributing authors working with liposomes over many decades were in close collaboration with the late Prof. H. Ti Tien, the founding editor of this book series.

Spherical vesicles, or liposomes, were first discovered by A. Bangham around 40 years ago. It was he who first noticed the spontaneous formation of these closed bilayer structures when phospholipids were introduced to an aqueous solution. Liposomes are known in two basic types, unilamellar and multilamellar. Unilamellar liposomes are further subdivided into small unilamellar vesicles (SUV) and large unilamellar vesicles (LUV). Initially, liposomes were used primarily as a model for the cell membrane. Similar to the planar lipid bilayer membranes (BLMs) already in use, liposomes self-assembled from different kinds of phospholipids. Liposomes, however, offered advantages like stability and low-cost assembly over the conventional planar lipid BLMs. As a model system, liposomes were used to study lipid–protein interactions, membrane function, and structural properties.

As more experiments were done over the last four decades, liposomes gradually emerged as a suitable delivery system for drug molecules, proteins, nucleotides, and plasmids. A number of things make liposomes ideal delivery systems. First, they are nontoxic and biodegradable. Second, they are readily modifiable with regards to size, composition, and charge. Third, liposomes deliver their loads in a process that mirrors endocytosis. Because loads are delivered directly into the target cell, less of the “load” material (which can be very expensive) is required. Finally, liposomes can carry hydrophilic and hydrophobic loads simultaneously because loads can be stored both inside the bilayer lipid membrane (hydrophobic) and within the aqueous core (hydrophobic).

Perhaps, the most promising area of liposome research is targeted delivery. Primarily, targeting is achieved by modifying the lipid bilayer of the liposome with specific antibodies. Once in the body these liposomes will seek out cells that have corresponding receptors (or antigens). Another way of targeting the liposomes, utilizing magnetic forces, has been experimented with as well in animals. In this method, particles of iron oxide are put into liposomes along with the load. Magnets are then placed near the area of interest and serve to draw the liposomes toward that area.

In order for liposomes to circulate long enough in the body for achieving a desired effect, further modifications must be made. Conventional liposomes are quickly identified by the body’s immune system, namely macrophages, and are eliminated. Compounds like polyethylene glycol (PEG), when embedded in the liposomes’ bilayer membrane, are able to trick these defenses and increase

circulation time. PEGylated (aka “stealth”) liposomes work because the spaghetti-like PEG molecules which trail out from the liposome attract water molecules and form an aqueous cloak. Macrophages ignore these “blobs” of water, thus sparing the liposomes and their valuable cargo can continue to slip by the body’s defenses.

So we can ask a question: Where are liposomes headed? Certainly they will continue to serve as a model for biological membranes. Once suitable electrical measurement tools exist on the nano-sized level, one could expect that liposomes will be used to study electrical properties and become even more useful as a model. In addition, much more research is underway in perfecting targeted delivery and experimenting with different loads, like DNA. Gene therapy offers tremendous hope for the treatment of many diseases. Immunoliposomes are a big part of that because they can carry their loads not only in normal circulation but across the formidable blood–brain barrier. More research of liposomes and a promise land of clinical applications that is the future of this exciting scientific field. Also, the interaction of planar lipid bilayers and spherical liposomes is one of the focuses in the scientific community for the present and for the near future.

Volume 4 of this serial continues to include invited chapters on a broad range of topics, ranging from theoretical research to specific studies and experimental methods, but also refers to practical applications in many areas dealing exclusively with liposomes. The author(s) of each chapter present the results of his/her laboratory. We continue in our endeavor to focus on newcomers in this interdisciplinary field, but we welcome contributions of experienced scientists. We also try to focus on both fields: planar lipid bilayers and spherical liposomes in the further development of this scientific research worldwide. That has been one of the leading ideas of the late Prof. H. Ti Tien in establishing this book series. The contributed chapters are separate entities to themselves, but they have one common feature. They are based on spherical liposomes and their practical applications. We are grateful to all contributors for their willingness to write these chapters on liposomes in memory of the late Prof. H. Ti Tien; it is very much appreciated by the whole scientific community.

The first stage of editorial work on this volume was still based on a joint effort of the late Prof. H. T. Tien and me. I would like to express my gratitude to everybody who contributed a chapter to this volume. I value the support of the people at Elsevier, especially their understanding and help immediately after the unexpected death of Prof. H. Ti Tien. We will try our best to keep this series alive in both fields covering the planar lipid bilayers and spherical liposomes. In this way we continue to pay our respect to the scientific work and achievements of Prof. H. Ti Tien.

Angelica Leitmannova Liu
(Editor)

CHAPTER 1

Lipid Microvesicles: On the Four Decades of Liposome Research

Hui-Fang Cui,¹ Jian-Shan Ye,¹ Angelica Leitmannova Liu^{2,3,*} and H. Ti Tien²

¹*Department of Biological Sciences, National University of Singapore, 14 Science Drive 4, Singapore 117543, Singapore*

²*Membrane Biophysics Laboratory, Department of Physiology, 2201 Biomedical and Physical Sciences Building, Michigan State University, East Lansing, MI 48824, USA*

³*Center for Interface Sciences, Slovak University of Technology, Faculty of Electrical Engineering and Information Technology, Department of Microelectronics, Bratislava, Slovak Republic*

Contents

Abbreviations	2
1. Introduction	3
2. Formulation Development of Liposomes as Pharmaceutical Carriers	4
2.1. Sterically stabilized liposomes	5
2.2. Liposomes for triggered drug release	6
2.2.1. pH-sensitive liposomes	7
2.2.2. Photosensitive liposomes	10
2.2.3. Thermosensitive liposomes	12
2.2.4. Enzyme-sensitive liposomes	13
2.3. Active site-targeting liposomes	16
2.3.1. Immunoliposomes	16
2.3.2. Ligand-attached liposomes	21
3. Concluding Remarks	32
References	33

Abstract

In the past four decades, liposome research in areas ranging from biophysics and bio-reactors to medicine has been growing. This chapter focuses on the formulation development of liposomes as pharmaceutical carriers in the past 10–15 years. One of the major breakthroughs in the evolution of liposomal formulation is the development of sterically stabilized liposomes (SSL) by coating liposomes with polymer. This can sterically hinder a variety of interactions at the bilayer surface, so that the liposomes can escape the rapid uptake by macrophage cells of reticuloendothelial system, and circulate in the blood stream for a long time and passively target into sites of tumors, infection, and inflammation characterized by the presence of a leaky vasculature. With the successful development of SSL, it has been possible to investigate strategies of site-specific targeting and triggered drug release. To obtain elevated abnormal-to-normal tissue biodistribution ratio, active site-targeting liposomes were developed by attaching antibodies or ligands to

*Corresponding author. Tel: +1517 355-6475 Ext. 1347 or 1145; Fax: +1 517 432-1967 or +1 517 355-5125;
E-mail: ottova@msu.edu

the exterior surface of the polymer coating or directly to the liposome surface by chemical conjugation. In addition, several promising strategies of active triggered intracellular delivery of liposomal drugs have emerged, including external light and thermal triggering and endogenous pH and enzyme triggering. By adjusting the lipid composition and by the combination of all these strategies on a single liposome pharmaceutical carrier, a promising method for optimizing the therapeutic effect of liposomal drugs is emerging.

ABBREVIATIONS

ADM	adriamycin
AELs	anticancer ether lipids
AIPcS4	aluminumphthalocyanine tetrasulfonate
BChl	bacteriochlorophyll
BPD	benzoporphyrin derivatives
CHEMS	cholesterol hemisuccinate
Chol	cholesterol
CS	chondroitin sulfate
DC-Chol	3 β [<i>N</i> -(<i>N</i> ', <i>N</i> '-dimethylaminoethane)-carbamoyl] cholesterol
DODAP	dioleoyl dimethylammonium propane
DOPE	dioleoylphosphatidylethanolamine
DOTAP	dioleoyl-3-trimethylammonium propane
DOTMA	<i>N</i> -[1-(2,3-dioleoyloxy)propyl]- <i>N,N,N</i> -trimethylammonium chloride
DPPC	1,2-dipalmitoyl- <i>sn</i> -glycero-3-phosphocholine
DPPIsC	1,2-Di- <i>O</i> -hexadec-1'(Z)-enyl- <i>sn</i> -glyceryl-3-phosphocholine
DSPC	distearoylphosphatidylcholine
DSPE	distearoylphosphatidylethanolamine
DSPE-PEG-COOH	distearoyl- <i>N</i> -(3-carboxypropionoyl poly(ethylene glycol) succinyl)phosphatidylethanolamine
DSPG	distearoylphosphatidylglycerol
EGFR	epidermal growth factor receptor
EPC	egg phosphatidylcholine
FA-Cys-PEG-PE	folic acid-cysteine-polyethyleneglycol-phosphatidylethanolamine
FR	folate receptor
Gal-C4-Chol	cholesten-5-yloxy- <i>N</i> -(4-((1-imino-2- β -D-thiogalactosyl-ethyl)amino)alkyl)formamide
GM1	GM1 ganglioside
HSPC	hydrogenated soy phosphatidylcholine
HSV-1	herpes simplex virus 1
IL-2	interleukin-2
ILS	increased life spans
LCST	lower critical solution temperature
LDL	low-density lipids

LLO	listeriolysin O
Mal-PEG-DSPE	maleimide-derivatized poly(ethylene glycol)-distearoyl-phosphatidylethanolamine
Man-C4-Chol	cholesten-5-yloxy- <i>N</i> -(4-((1-imino-2-β-D thiomannosyl-ethyl)amino)alkyl)formamide
MLVs	multilamellar vesicles
MPEG	methoxypoly(ethylene glycol)
mPEG-DSPE	mPEG-modified-1,2-distearoyl-3- <i>sn</i> -glycerophosphoethanolamine
mPEG-SS-DSPE	<i>N</i> -[2-g-methoxypoly(ethylene glycol)- <i>K</i> -aminocarbonyl-ethyl-dithiopropionyl]-DSPE
NGPE	<i>N</i> -glutaryl-distearoylphosphatidylethanolamine
NPCs	nonparenchymal cells
OA	oleic acid
PAA	poly(acry1 amide)
PacM	poly(acrylol morpholine)
PC	phosphatidylcholine
PCs	parenchymal cells
PE	phosphatidylethanolamine
PEG	polyethylene glycol
PEG-DSPE	poly (ethylene glycol)-modified 1,2-distearoyl-3- <i>sn</i> -glycerophosphoethanolamine
PEG-PE	PEG-phosphatidylethanolamine conjugate
PG	phosphatidylglycerol
Ph(+) ALL	Philadelphia chromosome-positive acute lymphoblastic leukemia
PI	phosphatidylinositol
PLA ₂	phospholipase A ₂
poly NIPAM-co-MAA	<i>N</i> -isopropylacrylamide-methacrylic acid copolymer
PVP	poly(viny1 pyrrolidone)
RES	reticuloendothelial system
SCR	surface charge regulation
SSL	sterically stabilized liposomes
Tf	transferrin
TfR	transferrin receptors
TRX-20	3,5-dipentadecyloxybenzamidine hydrochloride
ULVs	unilamellar vesicles
VIP	vascoactive intestinal peptide
ZnPC	zinc phthalocyanine

1. INTRODUCTION

Since liposomes with solutes entrapped by closed bilayered phospholipids were produced by Alec Bangham [1] in 1965, numerous groups around the world have

been involved in liposome research, in areas ranging from biophysics and bio-reactors to medicine. Several books have extensively reviewed liposome development in the years between 1965 and 2000 [2–6]. The extensive research interest in liposomes has resulted in significant breakthroughs for the application of liposomes in medicine, particularly for the liposomal drug delivery. One of the reasons for liposomes to be considered as attractive vehicles for drug delivery is their ability to encapsulate and deliver large quantities of an unmodified drug in a single container. During the last 15 years, several liposomal drugs have been approved. The successful use of liposome as drug carriers and vaccines and in gene delivery depends entirely on both their formulation and the method of preparation [7]. The research interest in liposomology is still very high, and the formulation of liposomes, and the methods for the preparation, and the application of liposomes are so diverse that it is impossible to cover all the pertinent issues in this chapter. Thus, we will attempt to focus on the important achievements in the field of liposomal pharmaceutical carriers in the past 10–15 years as well as on the challenges that remain to be addressed and need a lot of effort to overcome.

2. FORMULATION DEVELOPMENT OF LIPOSOMES AS PHARMACEUTICAL CARRIERS

Predominately, liposomes are aggregated from amphiphiles, possessing both hydrophilic and hydrophobic groups. Liposomes may be composed of one to several hundreds of concentric bilayers, which consist of unilamellar vesicles (ULVs) and multilamellar vesicles (MLVs). The size of liposomes ranges from 20 nm to several micrometers, while the thickness of a single lamella is around 4 nm. Each lamella has a bilayered structure with the polar heads of the amphiphiles, e.g. phospholipids, on the surface of either side of the lamella, with the nonpolar tails shielded from water in the interior of the lamella. The formulation of liposomes can be adjusted to manipulate liposomal physicochemical properties, such as stability, permeability, phase behavior, and biological properties, including longevity, biodistribution, pharmacokinetics, and pharmacodynamics. The therapeutic index of liposomal drugs is greatly influenced by formulation characteristics such as particle size, lipid phase behavior, drug encapsulation method, and the presence of targeting elements.

Before 1985, despite much research progress in the field of liposomal drug carriers, researchers realized that one hurdle was to find methods to prevent the body from breaking down liposomes while they were still in the bloodstream and before they reached a site of action. Conventional liposomes are limited in effectiveness because of their rapid uptake by macrophage cells of the reticuloendothelial system (RES), predominantly in the liver and spleen [8–12]. Various attempts have been made to create a longer circulation of liposomes *in vivo* for sustained drug release. The early attempts included incorporation of specific glycolipids such as GM1 ganglioside (GM1) [13,14] and phosphatidylinositol (PI)

[15] as a stabilizing component, into liposomes. The promoted increase of circulation time by GM1 and PI was interpreted in terms of a “shielded charge”, since all these glycolipid molecules have a head group with negative charge, which is sterically hindered by a large carbohydrate residue with respect to charge–charge interaction [6]. This concept was later generalized and long-circulation liposomes were termed as sterically stabilized liposomes (SSL), indicating liposomes that sterically inhibit a variety of interactions at the bilayer surface, including hydrophobic penetration by bulky proteins [16]. Notable success with regard to SSL was not achieved until 1990, when two groups (Huang’s group [17] and Cevc’s group [18]) separately reported the long circulation of polyethylene glycol (PEG)-coated liposomes, which eventually superseded the use of the GM1- and PI-coated liposomes. The name ‘stealth (sterically stabilized) liposomes’ (‘stealth[®] liposome’ is a registered trademark of Liposome Technology, Inc.) has been given to this new class of liposomes [19]. The long-circulating SSL can passively target sites of tumors, infection, and inflammation characterized by presence of a ‘leaky’ vasculature that represents useful applications for drug delivery [20]. With the remarkable achievement of SSL, liposomes for triggered drug release as well as site-specific targeting to further improve therapeutic index have been developed rapidly in the fourth decade of liposome evolution.

2.1. Sterically stabilized liposomes

Since the development of the PEG-SSL in 1990, long-circulating liposomes have been investigated in detail and have been used in clinical practice [21,22]. It was reported that PEG-phosphatidylethanolamine (PE)-incorporated liposomes composed of phosphatidylcholine (PC)/cholesterol (Chol) (1:1) [17] or only PC [23] remained in the blood circulation 8–10 times longer than liposomes without incorporation of PEG-PE. The half-lives ($T_{1/2}$) of the PEG-liposomes after an i.v. administration, are between 5 and 13.8 h, while those of normal liposomes are approximately 0.6 h [17,23]. Compared to GM1, which is derived from bovine brain, and hydrogenated PI derived from soybeans, PEG-lipid is a much more acceptable and accessible preparation for clinical applications [6]. In addition, PEG-PE’s activity to prolong the circulation time of liposomes is greater than that of GM1 [17]. It has been shown that both the PEG chain length and the PEG chain density [23] on the liposome surface are important to the half-life of the SSL in circulation [6], while the composition of the bulk lipid bilayer allows more flexibility without influence on $T_{1/2}$ [23,24]. The optimal effect for a long $T_{1/2}$ is produced by a PEG chain approximately 2000 Da, at a density of about 5–8% of total lipids [24]. However, the $T_{1/2}$ is not influenced by the bulk lipid fluidity and the presence of net charges on the lipid membranes [23]. With regard to the influence of polymer property on the $T_{1/2}$ of liposomes, both computer simulation and experimental results have suggested that an important feature of protective polymers is their

flexibility and hydrophilicity, which allow a relatively small number of liposome-grafted polymer molecules to create a dense protective conformational cloud over the liposome surface, preventing opsonizing protein molecules from coming in contact with the liposome [25,26]. In contrast, a rigid polymer fails to form this dense protective cloud, even when it is hydrophilic [25]. Early experimental results have demonstrated that hydrophilic and flexible synthetic polymers other than linear PEG, such as branched PEG, poly(acryl amide) (PAA), poly(vinyl pyrrolidone) (PVP), poly(acrylol morpholine) (PAcM) [27], polyoxazolines [28], and polyglycerols [29], when made amphiphilic by modification at one terminus with long-chain fatty acyl or phospholipid residue, can be incorporated into the liposome surface and make the liposome a long-circulating one [26]. In addition to the polymer structure and property, the protection effects of the amphiphilic polymer–lipid conjugates also depend on the length of the hydrophobic ‘anchor’ [26]. According to the theoretical model proposed by Torchilin and Trubetsky [26], the scale of these effects might be interpreted in terms of the balance between the energy of the hydrophobic anchor’s interaction with the membrane core and the energy of polymer chain motion in the aqueous solution.

In the past decade, while PEG has remained as the gold standard for the steric protection of liposomes [30], attempts to identify other polymers that could be used to prepare long-circulating liposomes continue. For example, long-circulating liposomes were prepared using poly[*N*-(2-hydroxypropyl) methacrylamide] [31], poly *N*-vinylpyrrolidones [32], L-amino acid-based biodegradable polymer [33], and polyvinyl alcohol-conjugated lipids [34]. The common features of these polymers are flexibility, hydrophilicity, and low immunogenicity, similar to PEG. Ongoing work in the field of SSL involves interest in increasing complexity by addition of (1) selective targeting of ligands by chemical conjugation to the exterior surface of the polymer coating, (2) capabilities for triggered intracellular release of encapsulated agents into the cytoplasm, and (3) both simultaneously (see Fig. 1).

2.2. Liposomes for triggered drug release

Once liposomes target active sites by either passive or active targeting, a portion of the liposomes is taken up by cells through receptor-mediated endocytosis [35], caveolar uptake [36], and other internalization processes. For receptor-mediated endocytosis, the major type of cell internalization mechanism of liposome and liposomal drugs, the endosomes, transport their cargo to lysosomes, which may result in degradation of the carried drugs if the drugs do not escape the harsh endosomal/lysosomal environment [37]. This has stimulated investigations into the development of new approaches for triggered intracellular release of encapsulated agents into the cytoplasm. Several triggering strategies have been proposed to accomplish site-specific triggered drug release, including external light and thermo-triggering and endogenous acid and enzyme triggering.

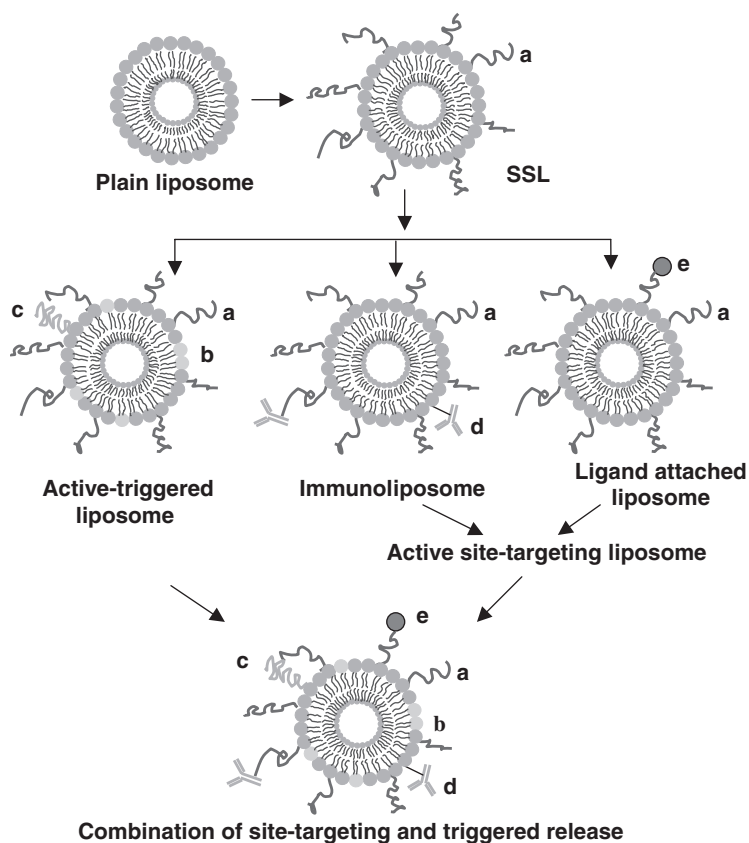


Fig. 1. Diagrammatic illustration of the formulation development of liposomes as pharmaceutical carriers from plain liposome to SSL by coating with flexible and hydrophilic polymer (a); to form active-triggered liposome by incorporating stimuli-sensitive lipids (b) or polymer (c); to form active site-targeting liposomes including immunoliposome by attaching Ab or Ab fraction (d) and ligand (e) directly to liposome surface or to the terminus of polymer; and the combination of strategies of site targeting and triggered release.

2.2.1. pH-sensitive liposomes

pH-sensitive liposomes, which can release drug upon acid triggering, have been one of the most extensively studied active triggering carriers for drug delivery. One major type of cell internalization mechanism of liposomes and liposomal drugs is endocytosis: the liposomes enter the endosomal/lysosomal pathway [35]. Within the harsh environment of the lysosome, a variety of metabolic enzymes will degrade both the carrier and the drug [37]. In order to avoid the intracellular degradation of the drug, the liposome once internalized should be able to escape the endosomes, on its way to the lysosomes [38–40]. The acidic microenvironment inside the endosome has led to extensive research on pH-sensitive liposomes that can release the drug into cytosol upon acid triggering

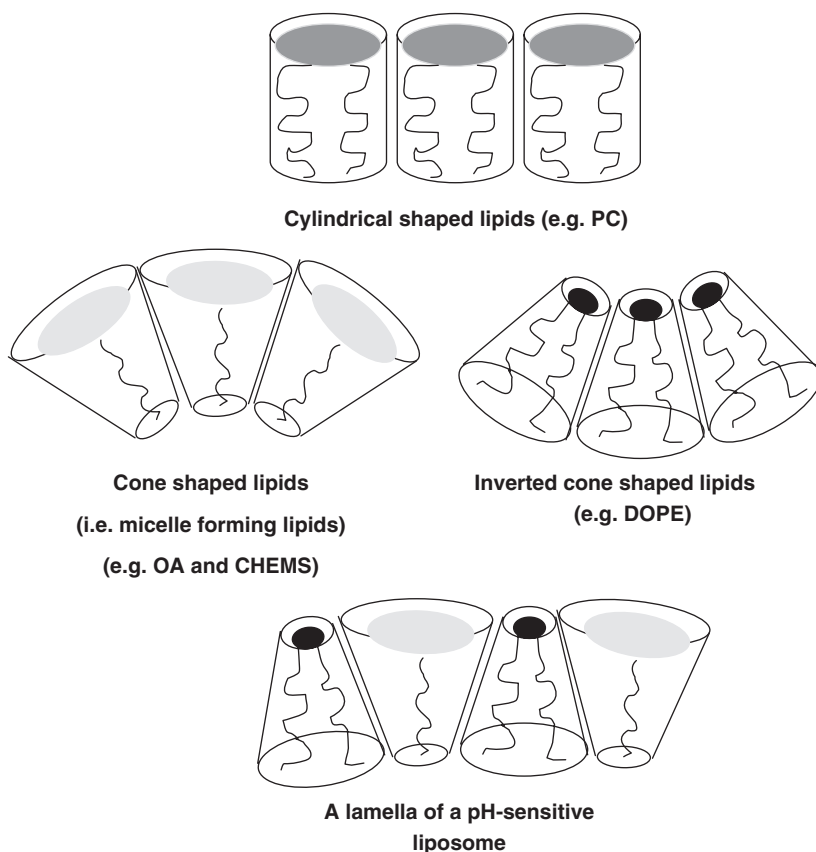


Fig. 2. Diagrammatic illustration of the assembly of a pH-sensitive liposomal lamella. Owing to the structural characteristics, DOPE alone cannot form liposome, while incorporation of lipids with large head groups, i.e. the cone-shaped lipids into DOPE can stabilize the DOPE vesicle and spontaneously lead to bilayer structure.

through fusion between bilayer membranes of the endosome and liposome [41–43]. The research on pH-sensitive liposomes focuses on the development of new lipid compositions and liposome modification with pH-sensitive polymers. Dioleoylphosphatidylethanolamine (DOPE) is a lipid with a small head group, and is therefore an inverted cone-shaped lipid (see Fig. 2), which preferably adopts inverted hexagonal phase HII at room temperature [44]. Owing to the structural characteristics, DOPE alone cannot form a liposome, but incorporation of lipids with large head groups, i.e. the cone-shaped lipids (i.e. micelle-forming lipids), into DOPE can stabilize the DOPE vesicle and spontaneously lead to bilayer structures (see Fig. 2) [40,45]. Most pH-sensitive liposomes have been the DOPE-based liposomes. To facilitate membrane fusion at low pH, during the past decade, researchers mixed DOPE with a variety of lipids, lipid derivatives, and pH-sensitive polymers to form pH-sensitive liposomes. It has been proposed that

mixing DOPE with a lipid or compound with an adequate pK_a can produce liposomes showing membrane fusion at low pH [46]. The protonation of a lipid at low pH can lead to a decreased propensity for water binding, thus resulting in lipid dehydration [40]. Since lipid hydration creates a steric barrier inhibiting, at short distances, the close proximity between the membranes of the endosome and liposome at short distances, the lipid dehydration can induce the disorganization of the membrane and drug release into the cytosol [40].

Cone-shaped, mildly acidic amphiphiles, including diacylsuccinylglycerols, more often, oleic acid (OA) and cholesterol hemisuccinate (CHEMS), have been associated with DOPE to form pH-sensitive liposomes [46,47]. The mildly acidic amphiphiles become protonated and thus partially dehydrated in an acidic environment. The dehydration of the amphiphiles leads to a change in their geometrical shape from the cone shape to a cylindrical shape, and hence it destabilizes the liposomes [39]. Collins *et al.* [47] demonstrated that liposomes composed of DOPE and diacylsuccinylglycerols are pH-sensitive and are effective drug carriers *in vitro*. DOPE/OA and DOPE/CHEMS liposomes have been extensively explored as pH-sensitive drug carriers, especially as carriers for oligonucleotides [38,48]. Between these two liposome compositions, DOPE/CHEMS liposomes have been demonstrated as attractive pH-sensitive liposomes [39,49,50]. DOPE/OA liposomes are more sensitive to acid than DOPE/CHEMS liposomes. While DOPE/OA liposomes release their content below pH 6.5, DOPE/CHEMS liposomes become leaky below pH 5.5 [48]. In addition, DOPE/OA liposomes are less stable in circulation because OA is much more easily exchanged by serum proteins than CHEMS. Addition of cholesterol into the DOPE/OA liposome formulation has been shown to greatly improve the stability of *in vivo* administration [40]. Long-circulating pH-sensitive liposomes have been achieved by adding PEG-lipid conjugates with cleavable PEG moiety into DOPE-based liposomes [51–55].

Acid-labile PEG-lipid conjugates that by themselves form micelles have been mixed with DOPE to stable liposomes at neutral pH. Thompson and his associates [45,51,52] incorporated PEG-conjugated vinyl ether lipids into DOPE liposomes. At $pH < 5$, the vinyl ether bond is hydrolyzed, resulting in the removal of the PEG moiety, so that the liposomes become fusogenic and transform to inverted hexagonal phase HII. Another well-known acid-labile bond, diortho ester, has been used to attach PEG to lipid, by Guo *et al.* [53,54]. The diortho ester bond has been originally proposed by Heller *et al.* [55] to synthesize degradable polymers which can be degraded completely within 1h at pH 5, and are reasonably stable at neutral pH.

pH-sensitive liposomes were also formulated from lipid and pH-sensitive polymers. Meyer *et al.* [56] have incorporated derivatives of *N*-isopropylacrylamide-methacrylic acid copolymer (poly NIPAM-co-MAA) into liposomes, which shows marked temperature- and pH-dependent water solubility properties. This lipid/poly NIPAM-co-MAA liposome destabilizes in acid environment resulting in the

release of its content, and maintains pH sensitivity in serum. The NIPAM copolymer provides a pH-dependent steric barrier, increasing the liposome circulation time *in vivo* [57]. Serum-stable, long-circulating PEGylated pH-sensitive liposomes were also prepared by co-incorporation of PEG-lipid conjugate and terminally alkylated poly NIPAM-co-MAA into liposomes [30,58]. In addition, the pH sensitivity has also been combined with active ligand targeting for cytosolic drug delivery for both folate and transferrin (Tf)-targeted liposomes [59–61]. To further increase the efficiency of cytosolic delivery of liposomal drugs, Lee *et al.* [62] co-encapsulated listeriolysin O (LLO), the hemolytic protein of *Listeria monocytogenes* that normally mediates bacterial passage from phagosomes into cytosol, together with other molecules (fluorescence or ovalbumin) to be delivered into pH-sensitive PE:CHEMS formulations of liposomes. Purified LLO is hemolytic and shows increased activity at low pH [63,64]. Both cytoplasmic fluorescence (brightness and number of positive cells) and antigen presentation of ovalbumin of cells are much stronger when incubated with pH-sensitive, LLO-encapsulated liposomes than when incubated with pH-sensitive, non-LLO-encapsulated liposomes or with pH-insensitive, LLO-encapsulated liposomes. The authors also demonstrated that the viability of cells after liposome uptake was similar to cells treated with buffer only.

Even though various formulations of pH-sensitive liposomes have achieved acid-triggering drug release *in vivo*, convincing clinical results have not been obtained. Control of drug-releasing kinetics is one of the main technologies that needs to be realized.

2.2.2. Photosensitive liposomes

Phototriggered release has been one of the promising strategies to improve the therapeutic index of drugs encapsulated within liposomes. Most of the phototriggered drug release from liposomes has been based on the photoinduced rearrangements of the liposome bilayer, such as isomerization, fragmentation, or polymerization [45,65,66]. Most of these approaches use visible or ultraviolet (UV) excitation. Bisby *et al.* [67,68] made use of the well-known *trans*–*cis* isomerization of azobenzenes forming a photosensitive liposome base on the lipid derivative of azobenzene-glycero-phosphocholine. Upon UV light activation, the isomerization of azobenzene-glycero-phosphocholine causes the fast release of content from liposomes in the gel phase. UV light-induced polymerization of lipid in a photosensitive PEG-liposome formulation was reported by Bondurant *et al.* [69–71]. The photosensitive PEG-liposome contains 1,2-*bis*[10-(20,40-hexadienoxy)-decanoyl]-*sn*-glycero-3-phosphocholine, which forms a cross-linked lipid network upon UV light exposure. The polymerization process of lipids causes the formation of defects in the liposome bilayer membrane and thereafter leads to the release of content. However, UV light is potentially harmful to healthy tissues, so it is not suitable for biological applications. Liposomes sensitive to visible,

far-red, and even near-infrared light have been proposed. A PEG-liposome sensitive to visible light has been reported by Mueller *et al.* [65] made by incorporation of a cyanine dye into the liposome. Zinc phthalocyanine (ZnPC), tin octabutoxyphthalocyanine, and bacteriochlorophyll (BChl) have been investigated as sensitizers to produce singlet oxygen ($^1\text{O}_2$) by light irradiation in the presence of oxygen [72–74]. The absorption peak of ZnPC is at 610 nm [75], while the absorption maximum of BChl is at 820 nm [39]. The sensitized photooxidation of plasmalogen by the $^1\text{O}_2$ has been proposed by Thompson and associates as a strategy for phototriggered content release [72,76–79]. This strategy depends on the phase transition of lamellar bilayer membrane to micellar membrane upon photooxidative cleavage of plasmenylcholines to single-chain surfactants. In addition, $^1\text{O}_2$ itself has been shown to be cytotoxic, causing peroxidative damage and cell death of tumors [80]. It is also noteworthy to mention that plasmenylcholines are abundant, naturally occurring vinyl lipids, and are also acid cleavable, and can be hydrolyzed at the vinyl bonds in acidic endosomal compartments. The double sensitive property may be utilized to control the pharmacokinetic property of liposomal drugs. Thompson and associates extended the concept of photosensitive liposomes to a photooxidative ‘cascade’-triggering pathway [77,81]. For this cascade pathway, two formulations of liposomes are co-delivered, with one kind of liposome being formulated by encapsulating Ca^{2+} in photosensitive liposomes formed from BChl and diplasmenylcholine, and the other kind of liposome being the 1,2-dipalmitoyl-*sn*-glycero-3-phosphocholine (DPPC) liposome encapsulating drugs. Photoexcitation destabilizes the photosensitive liposomes through photooxidative cleavage of diplasmenylcholine, which causes the release of Ca^{2+} . Endogenous phospholipase A_2 (PLA_2), which is a calcium-dependent enzyme, is then activated and hydrolyzes DPPC, causing drug release. Since 1,2-di-*O*-hexadec-1'(Z)-enyl-*sn*-glyceryl-3-phosphocholine (DPPIsC) liposomes are not hydrolyzed by PLA in the presence of Ca^{2+} , modification of this cascade-triggering technique may be useful for promoting endosomal release and cytoplasmic delivery of bioactive macromolecules (e.g. plasmids) from DPPIsC liposomes that co-encapsulate Ca, PLA, and the bioactive agent inside [45]. To produce localized phototoxic effect in tumor cells, BChl-IgG conjugates have been incorporated into liposomes [74]. The targeted liposomes containing Bchl-IgG conjugate was 30 times more photocytotoxic than the nontargeted liposomes containing Bchl-serine derivative, indicating that site-specific generation of oxidizing species can have a much greater biological effect than the same toxin applied systemically. Liposomal benzoporphyrin derivatives (BPD) are photosensitizers that have been demonstrated to produce peroxidative damage and cell death of intraocular tumors on stimulation [80–83]. Schmidt-Erfurth *et al.* [83] have used BPD *in vivo* to achieve complete and irreversible selective photothrombosis of corneal neovascularization with minimal toxicity to surrounding tissues. The selective photothrombosis is caused by increased metabolism of lipoproteins in proliferating cells. The combination of active targeting strategies

with phototriggered drug release may increase the site-specific drug release and therefore the bioavailability and therapeutic effect of liposomal drugs. However, photosensitive liposomal drugs are not suitable for use in the treatment of metastatic cancer, as they require that the location of the tumor be known.

2.2.3. Thermosensitive liposomes

The idea of mild local hyperthermia-triggered liposomal drug release was proposed initially by Yatvin *et al.* [84]. Their basic strategy was to design liposomes with a main phase transition temperature above physiological temperature and in a range attainable by mild local hyperthermia. Near the liquid-crystalline transition temperatures (T_c) of liposomal membrane, the bilayer membrane becomes disordered at the boundaries between solid and fluid domains of the lipid, causing release of water-soluble contents. The liposomes designed by Yatvin and associates [84,85] mainly consisted of DPPC, which has a T_c of 41 °C. By adding various proportions of distearoylphosphatidylcholine (DSPC), which has a T_c of 54 °C, the main phase transition temperature of the liposomes can be adjusted between 41 and 54 °C. In addition, hyperthermia itself has been shown to be cytotoxic [86], and can be used as a supplementary strategy for cancer therapy.

During the past decade, studies in this area have been focusing on (i) the development of new materials and formulations, (ii) efficacy studies using known thermosensitive liposomes. DPPC liposomes incorporated with fusogenic lipids, with the liposomal formulation of DPPC/elaidic acid (1:2) or DPPC/elaidic acid/elaidic alcohol (1:1:1), were deposited in A-431 tumor xenografts two to four times greater than DPPC liposomes alone, when exposed to local hyperthermia (42 °C) [87]. Various formulations of thermosensitive SSL have been proposed. Gaber *et al.* [88,89] designed PEG-coated thermosensitive SSL with a formulation of DPPC/hydrogenated soy phosphatidylcholine (HSPC)/Chol/PEG₁₉₀₀-distearoylphosphatidylethanolamine (DSPE) conjugate (100:50:30:6). These long-circulating liposomes released more than 60% of their contents when heated at 42 °C for 30 min *in vitro*. Ning *et al.* [90] formulated an SSL with PC/Chol/PEG₂₀₀₀-DSPE. Hyperthermic treatment of RIF-1 tumors in the presence of doxorubicin-loaded PC/Chol/PEG₂₀₀₀-DSPE liposomes delayed tumor growth better than either free drug with heat or liposomal drug that was not thermally activated. Careful evaluation of formulation effects on thermally induced doxorubicin release from SSL has also been undertaken [88]. These studies showed that serum proteins, particularly those derived from bovine serum, adsorb onto liposome surfaces and induce content leakage as a function of increasing cholesterol concentration and membrane fluidity, such that the addition of cholesterol to gel-phase liposomes leads to enhanced serum-induced leakage. A new liposome formulation that was optimized for doxorubicin release at 39–40 °C, was introduced by Needham and coworkers [91–93]. They kinetically trapped lyso-phospholipids into liposomal membrane in the gel phase. When the

liposomes were heated above the gel-to-fluid phase transition temperature, the lyso-phospholipids were shown to leave the bilayer, which drastically enhanced the permeability of the liposomal membrane. However, doxorubicin is not an ideal model drug to study the formulation of thermosensitive liposomes, as doxorubicin is more of a hydrophobic drug, and it is loaded with chemical gradient (pH or ammonium sulfate gradient). It is conceivable that the release of doxorubicin from liposomes may be enhanced when compared to passively loaded markers or drugs due to the destruction of the chemical gradients [94] applied when loading the liposomes [39]. When compared to the passive loading found for very stable formulations, e.g. Doxil[®] [39,95], the destruction of this gradient is considerably enhanced in several of the active liposome triggering concepts in the drug delivery field, including thermally activated liposomes.

Thermosensitive polymers, for example, poly NiPAM-co-MAA, which become water insoluble above a lower critical solution temperature (LCST), while being soluble below this temperature [96], were also incorporated into liposomes to achieve thermal triggered drug release [56,97–104]. The thermal triggering of drug release is due to the significant difference in polymer hydration below and above the LCST. Kono and co-workers [105] used a derivative of poly NiPAM, a thermally sensitive copolymer of (*N*-isopropylacrylamide)₉₈(octadecylacrylate)₂, to stabilize DOPE liposomes, which, as mentioned above, are not stable by themselves. These liposomes showed thermosensitive properties, being stable toward content (calcein) leakage below 30 °C; heating of these suspensions at 40 °C, however, leads to rapid calcein leakage within a few seconds [45,105].

Delivery of the antitumor agent melphalan encapsulated within thermosensitive liposomes with the formulation of egg phosphatidylcholine (EPC)/Chol [106] or DPPC/DSPC [107,108], with hyperthermic treatment, leads to tumor regression and extended survival times in C57B1/6 mice bearing B16F10 melanomas, relative to the same concentration of free drug either with or without applied hyperthermia.

The therapeutic effect of thermosensitive liposomal drugs has been promising; however, they may be limited to readily accessible tumors that cannot be removed surgically, because the use of hyperthermia requires that the location of the tumor be known and the tumor site be accessible to local hyperthermia [39,109].

2.2.4. Enzyme-sensitive liposomes

Liposomes destabilized by cell-associated enzymes that are upregulated in tumor and/or inflammatory tissues can lead to site-specific drug release. The enzymes used for triggering liposomal drug release have been either proteases or lipases. Two strategies have been suggested for activating liposomes by enzymes [39]. One is based on the cleavage of the lipid or lipid conjugate, resulting in the generation of fusogenic lipids that will destabilize the liposome. The other involves lipid or lipid conjugates acting as masking components that protect other

fusogenic lipids within the liposome membrane until enzymatic reaction cleaves the lipid/lipid conjugate.

Alonso and coworkers [110] have focused on using sphingomyelinase and phospholipase C as the triggering enzymes. They studied the effect of enzyme sphingomyelinase and phospholipase C on large ULVs consisting of sphingomyelin/PE/Chol (2:1:1) and PC/PE/Chol (2:1:1), respectively. With the treatment of sphingomyelinase, production of ceramides in the bilayer of sphingomyelin/PE/Chol liposomes is accompanied by leakage of the vesicle's aqueous contents and by vesicle aggregation in the absence of lipid mixing or vesicle fusion. This is in contrast to the situation of PC/PE/Chol liposomes treated with phospholipase C, for which the *in situ* generation of diacylglycerol leads to vesicle aggregation followed by vesicle fusion in the absence of leakage. Including diacylglycerol in PC/PE/Chol vesicle membranes prior to addition of phospholipase C reduced the lag time and extent of fusion (mixing of aqueous contents), while including ceramide instead of diacylglycerol in the PC/PE/Chol vesicle membranes with subsequent addition of phospholipase C reduces the lag time, though in a less marked manner, than those of diacylglycerols, but has no effect on the extent of fusion. Alonso and co-workers [111] also demonstrated that gangliosides inhibit phospholipase C-promoted fusion of the PC/PE/Chol (2:1:1) vesicles even when present at very low molar ratios, which is attributed to the combined effects of lamellar phase stabilization and phospholipase C inhibition. The inhibitory effect of gangliosides increases with the size of the oligosaccharide chain in the polar head group. Similar inhibitory effect of phospholipase C-promoted vesicle aggregation and fusion was observed by incorporating a very small amount of PEG-PE conjugate into the liposomal composition of PC/PE/Chol (2:1:1) [112]. This inhibitory effect arises from three combined and independent effects of PEG: (i) PEG moiety hinders the enzyme from reaching the membrane surface; (ii) repulsive barrier properties of surface-grafted PEG hinder liposome mixing and aggregation; (iii) PEG-PE incorporation stabilizes the lipid bilayer structure. In addition, Alonso and coworkers [113] have used sphingomyelinase and/or phospholipase C as enzymatic triggers of sphingomyelin/PC/PE/Chol (1:1:1:1) liposome to create fusogenic liposomes. When both enzymes are added together, their joint hydrolytic activities give rise to leakage-free vesicle aggregation, lipid mixing, and aqueous contents mixing, *i.e.* vesicle fusion. The lipidic end products of the two enzymes cooperate in destabilizing and fusing the membranes in a way that is never achieved through the action of any of the enzymes individually. They demonstrated that the contribution of the two enzymes is unequal: production of ceramide by sphingomyelinase facilitates the lamellar-to-nonlamellar transition in the formation of the fusion pore; while phospholipase C provides mainly a localized, asymmetric, high concentration of diacylglycerol that constitutes the trigger for the fusion process. Thus the enzymes appear to be coupled through their reaction products.

Meers and associates [114,115] used elastase as the triggering enzyme to cleave a peptide substrate covalently conjugated to fusogenic DOPE lipid. This

peptide–lipid, *N*-methoxy-succinyl-Ala-Ala-Pro-Val-DOPE, was used to form liposomes with dioleoyl dimethylammonium propane (DODAP), a pH-dependent cationic lipid in a 1:1 molar ratio. Elastase-treated liposomes displayed pH-dependent enhancement of binding, lipid mixing, and delivery of liposomal contents into cytoplasm, relative to untreated liposomes, when incubated with HL60 human leukemic cells or ECV304 endothelial cells.

Davis and Szoka [116] have utilized alkaline phosphatase, whose membrane-bound forms are overexpressed in tumor tissue [117], to destabilize liposomes consisting of cholesterol phosphate derivatives and DOPE. They showed that the liposomes could be induced to collapse upon phosphatase-catalyzed removal of the phosphate group. As described under Section 2.2.2, Thompson and his co-workers [45,77] proposed enzyme-triggered destabilization of DPPC liposomes, for which DPPC can be hydrolyzed by activated PLA₂, a Ca²⁺-dependent enzyme. Jorgensen and co-workers [39,118–122] have been focusing on utilizing secretory phospholipase A₂ (sPLA₂), which is overexpressed in inflammatory and tumor tissues [123–126], as a site-specific trigger of long-circulating liposomes [39]. Negatively charged liposomes composed of masked anticancer ether lipids (AELs), i.e. pro-AEL-PC or pro-AEL-phosphatidylglycerol (PG) caused pronounced growth inhibition of KATO III cancer cells. This result is consistent with the anionic pro-AEL-lipid (PG or PC) substrate preference of human sPLA₂ type IIA [127], which is an interfacially active enzyme that catalyzes the hydrolysis of the ester linkage in the *sn*-2 position of glycerophospholipids, producing free fatty acids and cytotoxic AELs (lysolipid AEL-PC or AEL-PG) [128,129]. Both lysolipid and free fatty acid function as permeability enhancers of membranes, which not only destabilize the liposomes, but also act as locally generated permeability enhancers [118,121,130] that increase the diffusion of the cytotoxic AELs across the cellular membrane of the target cancer cells. Pro-AEL liposomes without encapsulated drugs can be administered in large amounts, as they are considerably less toxic to the organism. In addition, the liposomes with the composition of or similar to DSPC/distearoylphosphatidylglycerol (DSPG)/DSPE-PEG₂₀₀₀ can entrap and transport conventional chemotherapeutics such as doxorubicin and cisplatin, to tumor tissues, with a mechanism similar to the pro-AEL liposomes, except that the hydrolysis products (lysolipids) of DSPC and DSPG are not cytotoxic and the drugs released from the liposomes diffuse across the cellular membrane of the target cancer cells, causing cytotoxic effect. Doxorubicin encapsulated in the sPLA₂-degradable liposomes showed significant cytotoxic activity in a colon cancer cell line, and was significantly more cytotoxic than free doxorubicin and the clinically used liposomal doxorubicin formulation, Doxil[®]. Similarly, sPLA₂ triggers the release of cisplatin from sPLA₂-degradable liposomes, resulting in a pronounced cytotoxic effect, in contrast to cisplatin encapsulated in Stealth[®] liposomes (SPI-077) [131]. Furthermore, an investigation of the cisplatin-loaded sPLA₂-degradable liposomes in preclinical studies showed an improved drug efficacy in a mouse breast cancer model (MT-3) [39].

Considering all these significant achievements of enzyme-triggered liposomal drug release as a whole, it may be speculated that by adjusting the lipid composition and the biomaterial properties of the liposomal substrate, it may be possible to finetune and optimize the liposomal tumor-specific drug release, especially by using additional active site-targeting strategies.

2.3. Active site-targeting liposomes

The combination of site targeting with active triggering can potentially lead to significantly enhanced and specific drug release at the target site, more often, tumor cells. The theoretical advantages of site targeting would include improved efficacy by virtue of higher concentrations of drug localized at the target tissue, and the potential for decreased toxicity if efficacy could be maintained using lower and fewer doses [81]. Passive liposome targeting using hydrophilic polymer conjugates that provide steric stabilization [18,132,133], has been effective for many liposomal antitumor drugs. The passive accumulation of long-circulating liposomes in tumors, often referred to as the enhanced permeability and retention effect, is due to leaky vasculature [134] and a lack of an effective drainage system [135–137] in tumor tissues. However, vascular permeability in tumors is heterogeneous with respect to tumor type and tumor microenvironment [39]; solid tumors are very heterogeneous in their vascularization and therefore not all are suitable for passive targeting treatment with liposome drugs [138]. Active targeting processes, in principle, can further improve site-specific drug delivery. Several papers have described potential methods for active liposome targeting, among these are liposomes coupled to specific antibodies [139–144] as well as liposomes coated with ligands targeting proteins expressed on cancer cell membranes or endothelial cells lining the newly generated blood vessels in the tumor [39]. Examples of such proteins are the folate receptor (FR), induced on the surface of actively growing tumor cells possibly due to increased requirements for DNA synthesis [51,145–147], the Tf receptors (TfR) [148–155] overexpressed on the surface of many tumor cells, the integrins [156–158] expressed on the endothelial cells in the neovasculature of growing tumors, vasoactive intestinal peptide (VIP) receptors [159], hyaluronan receptors [160], asialoglycoprotein receptors [161–164], chondroitin sulfate proteoglycan [165], etc. There is now ample evidence to indicate that a wide variety of active targeting mechanisms can provide an even greater degree of specificity [45].

2.3.1. Immunoliposomes

Antibody-coated liposomes, also called immunoliposomes, have been studied intensively to improve therapeutic index by accumulating liposome drugs specifically in desired tissues. With various chemical-conjugating strategies available,

the antibody can be attached directly to the head group of liposome phospholipids or to the PEG terminus of PEG-lipid conjugates. While the attachment of antibodies directly to the liposome surface has proven to be effective [166], antibodies attached to the PEG terminus are more successful, due to the better accessibility of the antibodies toward their targets [39,139,143,167,168]. The majority of research in this area relates to cancer targeting; while research using antibodies against viruses, such as herpes simplex virus 1 (HSV-1) [144] and parasites such as leishmania [169] is also being conducted. For cancer therapy, immunoliposomes can be targeted to surface molecules expressed either in the vascular system or in the extravascular system on tumor cell membranes [39]. The most readily accessible target sites for immunoliposomes are the vascular endothelial surface of growing tumors and circulating cells related to the immune system [168]. As immunoliposomes show enhanced liposome clearance [170,171], the coating of liposomes with antibodies directed against tumor-associated targets consists of a fine balance between coating with a sufficient number of antibodies to achieve target binding and tumor retention on one side, and enhanced RES clearance with an increased number of antibodies per liposome on the other [39,167,168,172,173]. A coating ratio of 10–30 antibody molecules per liposome was shown to be optimal with the most efficient delivery of drugs to tumors and limited increase in RES uptake [39,143,167,168,174].

Maruyama and co-workers [168] attached a monoclonal IgG antibody, 34A, which is highly specific to pulmonary endothelial cells, to the distal ends of liposome-PEG chain through the carboxyl groups of distearoyl-*N*-(3-carboxypropionyl poly(ethylene glycol) succinyl)phosphatidylethanolamine (DSPE-PEG-COOH), in the pre-formed liposomes with a composition of EPC/Chol (2:1) containing 6 mol% of DSPE-PEG-COOH. The immunoliposomes, directed towards a surface glycoprotein receptor (gp112), showed that more than 50% of the total dose could be found in the lungs after 30 min, which was about 1.3-fold higher than immunoliposomes without PEG coating, and 2.6-fold higher than immunoliposomes with PEG coating but with IgG 34A attached directly to the liposome lipid of *N*-glutaryl-DSPE (NGPE).

Targeting circulating B-lymphoma (Namalwa) cells *in vivo* with immunoliposomes attached to anti-CD19 antibodies, directed against the CD19 receptor of human B-cell lymphoma cells has been studied extensively [175–178]. Using the B-lymphoma as a model system, Saprà *et al.* [178] have demonstrated that internalizing epitopes (e.g. CD19) make better targets than noninternalizing epitopes (e.g. CD20) for liposomal anticancer drugs. Therapeutic experiments performed in severe combined-immunodeficient (SCID) mice inoculated *i.v.* with Namalwa cells demonstrated that administration of doxorubicin-loaded anti-CD19 liposomes resulted in significantly greater survival times than anti-CD20 liposomes. The difference in the effect between immunoliposome-targeting internalizing and noninternalizing epitopes is due to difference in the mechanism of drug delivery into the cell. When targeted liposomes bind to noninternalizing epitopes,

liposome contents are released over time at or near the cell surface, and the released drug will enter the cell by passive diffusion or normal transport mechanisms [178]. In the dynamic *in vivo* environment, the rate of diffusion and redistribution of the released drug away from the cell will exceed the rate at which the drug enters the cell, particularly for drugs such as doxorubicin, which have a large volume of distribution. The binding of targeted liposomes to internalizing epitopes triggers receptor-mediated uptake of the immunoliposomal drug package into the cell interior, where the drug contents are released subsequent to liposomal degradation by lysosomal and endosomal enzymes [178]. Harata *et al.* [176] showed that the cytotoxic effect of imatinib-encapsulated anti-CD19-liposomes on Philadelphia chromosome-positive acute lymphoblastic leukemia (Ph(+)) ALL cell lines and primary leukemia cells from patients with Ph(+)) ALL was much greater than that of free imatinib or liposomal imatinib without antibodies, with no influence on the colony formation of CD34(+) hematopoietic cells. Some problems for whole antibody molecule attached immunoliposomes have been reported, including the immunogenicity of therapeutic agents based on murine MAbs, mediated in part by the Fc region of the molecule [179–181]; enhanced removal of immunoliposomes by the cells of the mononuclear phagocyte system *via* Fc receptors on macrophages [170,172,174]; taken up of immunoliposomes containing exposed Fc regions of the antibody by tumor-associated macrophages, which limits their direct interactions with the target tumor cells [182–184]; and alteration of the biological activity of the antibody molecule during the process of thiolation of amino residues on whole IgG antibody molecules [139,185]. Concerning these problems, Sapra and co-workers [177] attached anti-CD19 antibody fragments that contain the relevant antigen-binding site, e.g. Fab' or scFv fragments *via* the thiol groups of the hinge region, to the distal end of PEG chain of maleimide-derivatized poly(ethylene glycol)-DSPE (Mal-PEG-DSPE), in the preformed liposomes composed of HSPC/Chol/mPEG-modified-1,2-distearoyl-3-*sn*-glycerophosphoethanolamine (mPEG-DSPE)/Mal-PEG-DSPE (2:1:0.08:0.02). They proved that Fab'-liposomes had longer circulation times and better therapeutic outcomes than anti-CD19-liposomes for drug doxorubicin. Internalization by endocytosis is the normal strategy associated with active targeting, as in the case of CD-19 targeting. In order that liposome drugs escape the endosomes/lysosomes before being degraded, Ishida *et al.* [175] encapsulated doxorubicin within pH-sensitive immunoliposomes coated with anti-CD19 antibodies. They demonstrated that pH-sensitive liposomes, targeted to the CD19 epitope on B-lymphoma cells, showed enhanced doxorubicin delivery into the nuclei of the target cells and increased cytotoxicity compared to non-pH-sensitive liposomes. Therapeutic studies in SCID mice inoculated with CD19+ Namalwa cells showed that all groups treated with targeted formulations had significantly higher increased life span (%ILS) than the groups treated with non-targeted formulations. In addition, the group treated with doxorubicin encapsulated in pH-sensitive immunoliposome containing *N*-[2-*g*-methoxypoly(ethylene

glycol)-K-aminocarbonylethyl-dithiopropionyl]-DSPE (mPEG-SS-DSPE), a cleavable lipid derivative of PEG, with liposome composition of DOPE/CHEMS/mPEG-SS-DSPE/Mal-PEG-DSPE[anti-CD19], had a significantly increased %ILS compared to the other targeted treatment groups (pH-sensitive PEGylated immunoliposome DOPE/CHEMS/mPEG-DSPE/Mal-PEG-DSPE[anti-CD19], containing a non-cleavable lipid derivative of PEG, and non-pH-sensitive PEGylated immunoliposome HSPC/Chol/mPEG-DSPE/Mal-PEG-DSPE[anti-CD19]). However, doxorubicin encapsulated in the pH-sensitive liposomes had a rapid leakage due to the high pH conditions used in forming stable DOPE-containing liposomes, and mPEG-S-S-DSPE-containing liposomes were rapidly cleared in blood circulation probably due to rapid cleavage of the disulfide linkage by blood components, e.g. cysteine, *in vivo*. Encapsulation of other antineoplastic drugs that are more amenable to stable loading into these pH-sensitive immunoliposome formulations may be experimentally studied to solve the drug leakage problem.

Extensive studies have also been focused on developing anti-HER2 immunoliposomes directed to target HER2-overexpressing tumors. Kirpotin, Park, and their co-workers [141,142,182,186,187] have focused on developing anti-HER2 immunoliposomes for improved cancer therapy. They [141,142,186,187] conjugated the Fab' or scFv C6.5 [142] fragments of anti-HER2 antibody to maleimide-terminated PEG-DSPE in the liposome formulation of 1-palmitoyl-2-oleoylphosphatidylcholine/Chol/poly (ethylene glycol)-modified 1,2-distearoyl-3-*sn*-glycerophosphoethanolamine (PEG-DSPE)/Mal-PEG-DSPE, and proved that HER2-overexpressing breast cancer cells incubated with the sterically stabilized immunoliposomes (anti-HER2 SSL) showed binding of liposomes followed by endocytosis *via* the coated-pit pathway, evidenced by intracellular acidification and colocalization with Tf. Parameters affecting *in vitro* binding and internalization of the anti-HER2 SSL include liposome composition, Fab' linkage site, and Fab' density [182,186]. Administration *i.v.* of doxorubicin-encapsulated anti-HER2 SSL in nude mice bearing HER2-overexpressing tumor xenografts resulted in efficient accumulation within tumor cells, while non-targeted liposomes resulted in extracellular tumor accumulation only [141,182,187]. In multiple HER2-overexpressing human breast tumor xenograft models, treatment with doxorubicin-loaded anti-HER2 immunoliposomes produces significantly increased antitumor cytotoxicity, including growth inhibition, regression, and cure [142], as compared to free doxorubicin or doxorubicin-loaded non-targeted liposomes, and significantly less systemic toxicity than free doxorubicin [141, 142,182]. Repeated administrations of anti-HER2 SSL in normal adult rats revealed no increase in clearance [141,142], confirming that anti-HER2 SSL retains the long circulation and non-immunogenicity of SSL [141]. Doxorubicin-loaded anti-HER2 SSL immunoliposome containing either recombinant human mAb HER2-Fab' or scFv C6.5 yielded comparable therapeutic efficacy [142]. In addition, Kirpotin, Park, and their co-workers [182] showed that nucleic acid-loaded cationic anti-HER2 SSL containing dioleoyl-3-trimethylammonium propane (DOTAP) can mediate efficient and specific transfection of target cells with reporter genes as well

as intracellular delivery of labeled oligonucleotides. In contrast, Goren *et al.* [188] demonstrated that although the binding of stealth liposomes attached with anti-HER2 antibody to N-87 cells (erbB-2-positive human gastric carcinoma) increased 16-fold, compared with the binding of non-targeted liposomes, doxorubicin loaded in the anti-HER2-conjugated liposomes did not cause increased *in vitro* cytotoxicity against N-87 cells. They suggested from these results that the binding of anti-HER2 immunoliposomes to N-87 cells lacks liposome internalization. Furthermore, the *in vivo* biodistribution studies in nude mice bearing subcutaneous implants of N-87 tumors showed that there was no enhancement of tumor liposome levels with administration of doxorubicin-loaded anti-HER2 immunoliposomes over plain liposomes, and both liposome preparations considerably enhanced doxorubicin concentration in the tumor compared with free drug administration, and antitumor activities of targeted and non-targeted liposomes were similar. Therefore they suggested that efficacy is dependent on drug delivery to the tumor and that the rate-limiting factor of liposome accumulation in tumors is the liposome extravasation process, irrespective of liposome affinity or targeting to tumor cells. This controversy may be caused by some of the critical issues [39] faced in the field of active targeting: (i) internalization by endocytosis is the normal strategy associated with active targeting. The drug then has to escape the endosomes/lysosomes before being degraded, a process that may depend on the method of drug encapsulation; (ii) when liposomes accumulate in the interstitial compartment due to extravasation and bind to the first line of target cells, liposomes with strongly binding ligands may obstruct the pathway for accumulation of more liposomes.

Many other antibodies conjugated to immunoliposomes directed against cancer-associated antigens have been investigated. For example, the antibody CC52, which is directed against rat colon adenocarcinoma CC531 lines, was attached to PEGylated liposomes and resulted in the specific accumulation of liposomes in a rat model of metastatic CC531 [30,189]. A single-chain Fv fragment (scFv A5) directed against human endoglin (CD105) overexpressed on proliferating endothelial cells, with an additional cysteine residue at the C-terminus of the scFv fragment, was coupled to sulfhydryl-reactive lipids incorporated into the lipid bilayer of liposomes [190]. The anti-CD105 immunoliposomes showed rapid and strong binding to human endoglin-expressing endothelial cells (HUVEC, HDMEC), and internalization of the liposomes as evidenced by a perinuclear accumulation. *In vitro*, doxorubicin-loaded anti-CD105 immunoliposomes showed greater cytotoxicity towards endothelial cells, compared to untargeted liposomes and free doxorubicin. Nucleosome-specific antibodies capable of recognizing various tumor cells through tumor cell surface-bound nucleosomes improved Doxil (Alza) targeting to tumor cells and increased its cytotoxicity [30,191]. Immunoliposomes containing the novel antitumoral drug fenretinide, and targeting the ganglioside GD2, induced apoptosis in neuroblastoma and melanoma cell lines, and demonstrated strong antineuroblastoma activity both *in vitro* and *in vivo* in mice [30,192]. Doxorubicin-loaded immunoliposomes tagged with the F(ab')₂

of an mAb GAH, recognizing positively to human gastric, colorectal, and mammary cancer cells, exhibited significantly superior antitumor effects against GAH-positive WiDr-Tc and SW837 xenografts, compared with non-targeting liposome doxorubicin [193]. These results led to a phase I clinical trial of the GAH-immunoliposomes (MCC-465) for patients with metastatic colorectal cancer [193,194], which defined the maximum tolerated dose, dose-limiting toxicity, recommended phase II dose, and pharmacokinetics of MCC-465, and proved that MCC-465 was well tolerated. Epidermal growth factor receptor (EGFR)-targeted immunoliposomes have been specifically delivered to a variety of tumor cells that overexpress EGFR [30,195]. Immunoliposomes targeted to the internalizing EGFR on the surface of ovarian carcinoma cells (OVCAR-3), co-encapsulating a pH-dependent fusogenic peptide (diINF-7) and diphtheria toxin A (DTA) chain, which inhibits protein synthesis when delivered into the cytosol of target cells, showed cytotoxicity toward OVCAR-3 cells; while the immunoliposomes not encapsulating diINF-7 peptide did not [196]. This result suggests the necessity and the enhanced performance of the combination of active targeting and triggered release for effectively delivering liposome drugs into cytosol.

2.3.2. Ligand-attached liposomes

2.3.2.1. Folate-attached liposomes

Folic acid is a vitamin that is essential for the biosynthesis of nucleotides, and is consumed in elevated quantities by proliferating cells. It is transported across the plasma membrane using either of two membrane-associated proteins, the reduced folate carrier or the folate receptor (FR). The former is found in virtually all cells and constitutes the primary pathway responsible for uptake of physiological folates [145]. The latter is found primarily on polarized epithelial cells and activated macrophages [197]. FR is upregulated in many human cancers, including malignancies of the ovary, brain, kidney, breast, myeloid cells, and lung, and FR density appears to increase as the stage/grade of the cancer worsens [145]. In addition, it has been reported that tumors that survive standard chemotherapy commonly have higher levels of FR [198]. Therefore, FR constitutes a useful target for tumor-specific drug delivery. FR may be further qualified as a tumor-specific target, since it generally becomes accessible to intravenous drugs only after malignant transformation [145]. That is, access to the folate receptor in those normal tissues that express it can be severely limited due to its location on the apical (externally facing) membrane of polarized epithelia. However, upon epithelial cell transformation, cell polarity is lost and FR becomes accessible to targeted drugs in circulation.

The precise mechanism of FR transport of folic acid into cells (the route of entry) remains unresolved; however, it is clear that physiologic folates [199], folate conjugates [200,201], and folate-attached liposomes [202] move across the plasma membrane into the cytoplasm *via* receptor-mediated endocytosis. After

folate conjugates were internalized by FR-positive KB cells, the endosomal pH was measured by Low and associates [203]. Of the 99 randomly selected folate conjugate-containing endosomes examined, most had internal pH values between 4.7 and 5.8, with some as low as 4.3. The most frequent pH encountered in these compartments was 5.0. Folate-attached liposomes have been investigated as FR-targeted drug carriers specifically delivering to cancer cells *in vitro* and *in vivo*. *In vitro* investigations have shown that folate targeting enhances the cytotoxicity of liposomal drugs against FR-expressing tumor cells; while the therapeutic data of *in vivo* studies hitherto, are still fragmentary and appear to be formulation- and tumor model-dependent.

Since prolonged circulation is a prerequisite for tumor accumulation of liposomes [94,204] and PEGylated liposomes are the best basis for a formulation that confers a long half-life in circulation [205], most folate-attached liposome formulations investigated are PEGylated liposomes. Low and associates [202] first established the possibility of delivering FR-targeted PEGylated liposomes into living cells. Upon incorporating folic acid-PEG₃₃₅₀-PE lipid conjugate into calcein-encapsulating liposomes of ~66 nm diameter, the folate-tethered liposomes were seen to enter cultured FR-bearing KB cells by FR-mediated endocytosis. PEG spacers of short and intermediate lengths were unable to mediate association of folate-conjugated liposomes with receptor-bearing cells; therefore, the authors assumed that the spacer length of PEG₃₃₅₀ (Mr ~3350, ~250 Å long) was necessary to permit the folate to penetrate cell surface obstructions in its search of an unoccupied FR. Similar results were observed by Gabizon *et al.* [205,206], i.e., mPEG₂₀₀₀-DSPE significantly interfered with the binding and uptake of liposomes targeted with 0.5% folate-PEG₂₀₀₀-DSPE [206], and increase of PEG length in the folate conjugate to Mr 3350 results in a major improvement of the targeting effect, but cannot entirely overcome the interference with binding to FR [205]. Two options to further improve the targeting effect were proposed: (i) extend further the PEG length of the folate conjugate; (ii) design a cleavable PEG-lipid. Both of these two strategies need to be tested and optimized. Studies by Low and colleagues [202,207] and Gabizon *et al.* [206,208] demonstrated that a molar fraction of 0.2–0.5% folate-PEG-DSPE is sufficient for effective interaction with the cell membrane FR. The remaining liposomal PEG would be in the form of the standard mPEG–DSPE conjugate. However, a recent study by Leamon and co-workers [209] indicated that optimal binding is obtained with low levels of 0.03% folate-PEG-lipid, about 10-fold less than those commonly used in previous studies. The authors hypothesize that at high surface density, a folate–folate interaction prevents folate binding to the receptor [209]. Researchers demonstrated that doxorubicin encapsulated in FR-targeting liposomes exhibited superior and selective cytotoxicity against FR(+) tumor cells *in vitro* [207], and greater tumor growth inhibition and higher increase in life span *in vivo* [210,211], compared with nontargeted liposomal doxorubicin (L-DOX). Low and associates [207] demonstrated that doxorubicin encapsulated in

DSPC/Chol/folate-PEG₃₅₀₀-DSPE (56:40:0.1) liposomes or DSPC/Chol/PEG₂₀₀₀-DSPE/folate-PEG₃₅₀₀-DSPE (56:40:4:0.1) liposomes, was 86 and 2.7 times cytotoxic than nontargeted liposomal doxorubicin and free doxorubicin respectively, and was specifically delivered to KB cells without harming co-cultured normal cells. Incorporation of 4 mol% PEG₂₀₀₀-DSPE does not reduce the uptake or cytotoxicity of folate-PEG-liposomal doxorubicin. Recently, Pan *et al.* [211] combined the application of FR-targeted liposomal doxorubicin with the induction of FR, using all-*trans* retinoic acid treatment to mouse ascites leukemia models generated using KG-1 cells, and increased the cure rate from 10% to 60%, compared with FR-targeted liposomal doxorubicin alone.

In addition to doxorubicin, some other FR-targeted liposomal anticancer drugs [212,213] as well as genes [209] and antisense oligonucleotides [214,215] have been investigated *in vitro* and/or *in vivo*. It was demonstrated that both the cellular uptake and the cytotoxicity of FR-targeted liposomal daunorubicin were much stronger in various tumor cells such as KB oral carcinoma cells, Chinese hamster ovary, and KG-1 human acute myelogenous leukemia cells [212]. *In vivo*, Pan *et al.* [213] evaluated FR-targeted liposomal daunorubicin in an FR+ L1210JF murine ascites tumor model for therapeutic efficacy, and demonstrated that mice treated with folate-coated liposomal daunorubicin showed significantly greater tumor inhibition and 40.7% greater increase in life span compared with those that received identical doses of non-FR-targeted liposomal daunorubicin. Meanwhile, free daunorubicin given at the same dose failed to prolong the survival of the treated mice. Furthermore, Low and associates [214] showed that folate-PEG-liposome-encapsulated antisense oligonucleotides targeted against the human EGF were efficiently and non-destructively delivered into KB cancer cells, resulting in nearly quantitative growth inhibition and gross morphological abnormalities. However, Leamon and co-workers [215] indicated that the *in vitro* delivery of antisense oligonucleotides encapsulated in folate-coated liposomes was very efficient, whereas *in vivo* delivery results were less promising. In contrast, the study by the same group [209] on FR-targeted gene delivery of cationic lipid-based transfection complex, comprising of protamine-condensed plasmid DNA, a mixture of cationic and neutral lipids, and a folic acid-cysteine-PEG-PE (FA-Cys-PEG-PE) conjugate, demonstrated that both *in vitro* and *in vivo*, folate-labeled formulations produced an 8- to 10-fold increase in tumor-associated luciferase expression, as compared with the corresponding non-targeted cationic lipid/DNA formulations. They showed that *in vitro*, as little as 0.01 to 0.3% of FA-Cys-PEG-PE was needed to produce optimal targeted expression of plasmid DNA, while *in vivo* use of a disseminated intraperitoneal L1210A tumor model resulted in maximum transfection activity occurring with intraperitoneally administered formulations that contained 0.01 mol% of the FA-Cys-PEG-PE targeting lipid.

To promote the escape of liposomal contents from endosomes, Low and co-workers [216] encapsulated the anticancer drug cytosine arabinoside, together

with a fusogenic peptide whose conformation changes upon acidification and thereby initiates membrane fusion [217], into folate-PEG liposomes, and observed that the cytotoxicity of the drug increased ~100-fold by simple folate targeting, and another 10-fold by encapsulation of the fusogenic peptide. More significantly, encapsulation of cytosine arabinoside into FR-targeting pH-sensitive DPPIC/DSPE-PEG₃₃₅₀-folate (99.5:0.5) liposomes, composed of synthetic, naturally occurring, pH-sensitive fusogenic lipid diplasmenylcholine DPPIC, enhanced cytotoxicity to KB cells by 6000-fold, compared with free drug [51]. Therefore, folate-coated liposomes are compatible with the use of active triggers, e.g. acid-triggered liposomes.

2.3.2.2. Transferrin-attached liposomes

Tf comprise a family of large (molecular mass ca. 80 kDa) nonheme iron-binding glycoproteins [218]. The principal biological function of Tf is thought to be related to iron-binding properties [218]. With a concentration of 2.5 mg/ml, 30% of the transferrins in blood plasma are occupied with iron [219]. The binding of apo-Tf and iron-Tf to TfR is pH dependent: apo-Tf binds to TfR only at acidic pH and iron-Tf binds at neutral or higher pH [220]. Human TfR1 appears to be expressed in all nucleated cells in the body [218], but differs in levels of expression [221,222]. It is expressed on rapidly dividing cells, with 10,000 to 100,000 molecules per cell commonly found on tumor cells or cell lines in culture [223]. In contrast, in nonproliferating cells, expression of TfR1 is low or frequently undetectable [218]. Site-specific targeting of Tf-conjugated liposomal photosensitizers, anticancer drugs, and therapeutic genes into primarily proliferating malignant cells that overexpress TfR has been shown to be a promising strategy to enhance the cytotoxicity and the therapeutic effect of the photosensitizers [151,224] and drugs [152,225], and the expression efficiency of the genes [155,226–229].

In higher organisms, one principal pathway of cellular uptake of iron-Tf is by the receptor-mediated endocytosis *via* clathrin-coated pits, which bud from the plasma membrane as membrane-bound vesicles or endosomes [230–232]. After the iron-Tf-TfR1 complex enters into the endosomal compartment, upon maturation and loss of the clathrin coat, the endosome becomes competent to pump protons in a process energized by ATPase, and the endosomal lumen is rapidly acidified to a pH of about 5.5 [233–235]. At this pH, the binding of iron to Tf is weakened, leading to iron release from the protein [218], and the resultant apo-Tf-TfR1 complex is then recruited through exocytic vesicles back to the cell surface. At extracellular physiological pH, apo-Tf dissociates from its receptor owing to its low affinity at pH 7.4, and is released into the circulation and reutilized [231,236,237]. The uptake of Tf-liposome conjugates has been elucidated to be a similar receptor-mediated endocytosis process [60,149,238], but the internalization process of Tf-liposome conjugates is slower than that of unmodified Tf [60]. In addition, in contrast to the recyclable nature of Tf, liposome-attached Tf

together with encapsulated contents, e.g. rhodamines were retained in vesicular compartments [60]. To promote the escape of liposomal encapsulated contents from endosomes/lysosomes, a pH-sensitive fusogenic peptide was introduced into liposomal membranes using a cholesteryl moiety for anchoring [60]. With the incorporation of the pH-sensitive fusogenic peptide into the liposomal membranes, the encapsulated contents, e.g. rhodamines were efficiently released and diffused into the cytosol. However, intracellular trafficking of Tf-lipoflex conjugates by confocal microscopy also demonstrated that DNA and Tf entered the endosome (or lysosome) from the plasma membrane [238] and finally colocalize at the perinuclear space [155] and in the nucleus [155,238], indicating that plasmid DNA enters into the nucleus not only as a free form but also as an associated form complexed with Tf-liposomes [238].

Tf-mediated targeting of liposomal photosensitizer aluminum phthalocyanine tetrasulfonate (AIPcS4) [224,239] has been demonstrated to show higher intracellular accumulation and photocytotoxicity to HeLa cells [239] and human AY-27 transitional-cell carcinoma cells [224] *in vitro*, and more selective tumoral tissue accumulation of AIPcS4 in rats bearing AY-27 cell-derived bladder tumors *in vivo* [224], than free AIPcS4 and non-targeting liposomal AIPcS4. The high photocytotoxicity of Tf-liposomal AIPcS4 *in vitro* was shown to be the result of a high intracellular concentration in tumor cells, which could be lowered dramatically by incubating the conjugate with a competing Tf concentration [239]. The chemotherapeutic drug doxorubicin, encapsulated in Tf-coupled PEG liposomes (Tf-PEG-liposomes), in which Tf was covalently linked to the distal terminal end of PEG chains on the external surface of PEG-liposomes, can be delivered *in vitro* to C6 glioma, which overexpress TfR with the extent of overexpression correlated to the severity of the tumor, with much higher efficiency compared with non-targeting liposome populations [153]. *In vivo* administration of cisplatin-encapsulated Tf-PEG-liposomes in nude mice with peritoneal dissemination of human gastric cancer cells showed high liposome and cisplatin levels in ascites [152]. Compared with the non-targeting liposomal cisplatin-administered group, the Tf-PEG liposomal cisplatin demonstrated significantly lower uptake of liposomes in the liver and spleen, significantly higher liposome uptake and cisplatin levels in disseminated tumor cells of ascites, and the greater omentum, and significantly higher survival rates [152].

For targeting gene delivery, association of Tf with cationic liposome-DNA complexes (lipoplexes), in particular, the negatively charged pH-sensitive fusogenic complexes [240,241], significantly facilitated efficient transfection in many cell lines, including HeLa [240–242], K-562 cells [241], squamous cell carcinoma of the head and neck (SCCHN) cells [229], human osteosarcoma (HOSM-1) cells [229], and lung carcinoma cells Calu3 and H292 [243], even in the presence of serum. This vector was also effective in transfection of epithelial and lymphoid cell lines, as well as the corneal endothelium [226] and human macrophages, especially with the use of optimized lipid/DNA (\pm) charge ratios [244]. Considerable

research has been made toward delivery of the tumor suppressor gene p53 *via* cationic liposome-based vectors [218]. The p53 gene has been shown to be involved in the control of DNA damage-induced apoptosis, and malfunction of this p53-mediated apoptotic pathway could be one mechanism by which tumors become resistant to chemotherapy or radiation [218]. *In vitro*, the exogenous wild-type (wt) p53 was expressed at high levels in Tf-liposome-DNA-transfected radiation-resistant SCCHN cells, and resulted in the restoration of radiation-induced apoptotic pathway [228,229]. The radiation-induced apoptosis was directly proportional to the level of exogenous wt p53 in the tumor cells. *In vivo*, intratumoral injection of the Tf-liposome-p53 complex into the SCCHN cell-induced nude mouse xenografts resulted in a higher number of transfected tumor cells, when compared with transfection by non-targeting liposomes [228]. In addition, intravenous administration of the Tf-liposome-p53 complex markedly sensitized established SCCHN nude mouse xenograft tumors to radiotherapy [229]. The combination of systemic Tf-liposome-p53 gene therapy and radiation resulted in complete tumor regression and inhibition of their recurrence even 6 months after the end of the entire treatment [229]. The Tf-attached PEG-liposomes intravenously administered to the rats after 90 min of transient middle cerebral occlusion can target post-ischemic cerebral endothelium *in vivo* [154]. The expression of TfR in the cerebral endothelium increased with a peak at 1 day after the re-perfusion, and returned to the control level by 6 days, and at 2 days, about 70% of TfR-positive vascular endothelium was double-labeled with Tf-PEG [154].

The Tf-dependent uptake of Tf-PEG-liposomes to various organs is liposomal size dependent and the size dependency is tissue dependent [148]. In liver and brain, Tf-dependent uptake was found to be dependent on the size of the liposomes used. For small liposomes with a diameter of 60–80 nm, uptake of Tf-PEG-liposome by liver and brain was more efficient than that of non-targeting PEG-liposomes. On the other hand, the size dependency of Tf-dependent uptake was not observed in the heart. Therefore, controlling the size of Tf-PEG-liposomes may be useful for the success of tissue targeting.

The studies so far collectively suggest that the systematic delivery of therapeutic drugs, photosensitizers, anticancer drugs, and genes by the Tf-attached liposomal delivery system has the potential to improve the therapeutic index and transfection efficiency of drugs and genes.

2.3.2.3. Glycosylated liposomes

Receptors for carbohydrates such as the asialoglycoprotein receptor exclusively on hepatocytes, and the mannose receptor on macrophages and liver endothelial cells, produce opportunities for cell-specific liposomal targeting [164]. Asialoglycoprotein receptor is promising for liver targeting since it expresses at large numbers on hepatocytes [245] and exhibits high affinity and a rapid internalization rate [246]. To target the asialoglycoprotein receptors on liver parenchymal cells

(PCs), extensive research has been focused on galactosylated [163,245,247–251], including lactosylated liposomes [252]. In contrast, mannosylated liposomes have been studied to target the mannose receptors on liver nonparenchymal cells (NPCs) [253–256], and splenic macrophages [257]. Mannose receptor-positive liver NPCs, such as sinusoidal endothelial cells and Kupffer cells are involved in various diseases and disorders of the liver, such as Gaucher disease [258], hepatic ischemia/re-perfusion injuries [259], and viral infection [260]; while splenic macrophages are the sites where the parasite *Leishmania donovani* resides and multiplies [257]. Therefore effective targeting of drugs, genes, and antigens to liver NPCs by mannosylated liposomes would be one important strategy to achieve high therapeutic index. The physiological properties of the galactosylated and mannosylated liposomes can influence the accessibility of the liposomes to the cell surface and therefore the amount delivered to the hepatocytes and NPCs, respectively [164]. Liver sinusoids have discontinuous capillaries and show large inter-endothelial junctions, i.e. fenestrations of up to 150 nm [261], and they are linked to the highly phagocytic Kupffer cells [164]. The structure of the liver requires that the galactosylated liposomes must be condensed to 150 nm in diameter, while the size of mannosylated liposomes for targeting Kupffer cells can exceed this value [164].

Galactosylation and mannosylation of liposomes can be achieved through incorporation of synthetic glycolipids on the surface of liposomes. For this purpose, different types of glycolipids have been synthesized. Hashida and associates [164,248,262,263] have synthesized cholesten-5-yloxy-*N*-(4-((1-imino-2- β -D-thiogalactosylethyl)amino)alkyl)formamide (Gal-C4-Chol), and cholesten-5-yloxy-*N*-(4-((1-imino-2- β -D thiomannosylethyl)amino)alkyl)formamide (Man-C4-Chol) [254,255], two novel cholesterol derivatives possessing galactose and mannose residues as a targetable ligand for liver PCs and NPCs, respectively. In addition, these glycosylated cholesterol derivatives possess cationic charge necessary for DNA binding, and therefore have been used to form cationic liposome/plasmid DNA complexes for gene targeting [164,248,254,262,263], and also to form galactosylated neutral liposomes with DSPC for hepatocyte-selective targeting of lipophilic drugs [245,250] and immunomodulators [255]. The biodistribution and pharmacokinetic studies [253] of the intravenous-injected liposomes showed that the liposomes composed of DSPC, cholesterol, and Gal-C4-Chol (or Man-C4-Chol) with the molar ratio of 60:35:5 were rapidly eliminated from the circulating blood and preferentially recovered in the liver. The uptake ratios by liver PCs and NPCs (PCs/NPCs ratios) for the dose of 0.5% galactosylated and mannosylated liposomes were found to be 15.1 and 0.6, respectively. Further experimental results suggested the uptake of galactosylated and mannosylated liposomes by the liver was *via* asialoglycoprotein receptors in PCs and mannose receptors in NPCs, respectively. More interestingly, Hashida and associates [253] found that at high dose (5%), galactosylated liposomes were taken up by NPCs rather than by PCs, and suggested that galactosylated liposomes administered at

a high dose would also be taken up by NPCs *via* fucose receptors that are considered to act as galactose particle receptors [264]. It was suggested by Hashida and co-workers [253] that at high doses, saturation of the asialoglycoprotein receptors in PCs occurs and the contribution of the galactose particle receptors in NPCs with a lower affinity becomes predominant. Incorporating 1% of PEG₃₅₀-DSPE into the galactosylated liposomes can control the delivery rate of galactosylated liposomes to liver PCs (i.e. reduce the blood elimination rate) without loss of their targeting capability [247]. For cationic liposomes containing Gal-C4-Chol, *N*-[1-(2,3-dioleoyloxy)propyl]-*N,N,N*-trimethylammonium chloride (DOTMA), and Chol, the administration of the cationic liposome/plasmid DNA complexes to perfused liver revealed that the tissue binding and cellular internalization rates were higher for the galactosylated cationic liposome complexes compared with the control i.e., non-galactosylated liposome complexes [262]. The PCs/NPCs uptake ratio was as high as unity, which was much higher than that of the control liposome complexes [262]. With the targeting property of the Gal-C4-Chol- and Man-C4-Chol-containing liposomes, liver-specific gene transfection and targeting drug delivery have been achieved. Intraportal injection of the DOTMA/Chol/Gal-C4-Chol (1:0.5:0.5) galactosylated liposome-plasmid DNA complex into mice caused one order of magnitude higher gene expression in the liver than naked DNA and DOTMA/Chol (1:1) liposome-DNA complexes [248]. In a similar way, high gene expression was observed in the liver after intravenously injecting mice with Man-C4-Chol/DOPE (6:4) mannosylated liposome/plasmid DNA complex, whereas 3 β [*N,N'*-dimethylaminoethane]-carbonyl cholesterol (DC-Chol)/DOPE (6:4) control liposome/plasmid DNA complex only showed marked expression in the lung [254]. The mannosylated liposome/DNA complexes in the liver were observed preferentially in NPCs due to recognition by mannose receptors in NPCs [254]. The hepatocyte-selective gene expression of the Gal-C4-Chol-containing liposome/plasmid DNA complex is dependent on the composition of the liposomes, charge ratio of the cationic liposomes to DNA, and other factors based on physicochemical considerations. Gene expression for galactosylated cationic liposomes containing 3 β [*N,N'*-dimethylaminoethane]-carbonyl cholesterol, Gal-C4-Chol, and DOPE was 10 times lower than that of the DOTMA/Chol/Gal-C4-Chol (1:0.5:0.5) galactosylated liposomes [248]. As far as the charge ratio of DOTMA/Chol/Gal-CA-Chol (1:0.5:0.5) liposomes to plasmid DNA was concerned, complexes with charge ratios of 2.3–3.1 produced maximal gene expression in the liver after intraportal injection of the complexes [248]. Similar results were observed for intravenous administration of Man-C4-Chol/DOPE (6:4) cationic liposomes/plasmid DNA complex in mice. Transfection efficiency after intravenous administration of the complex at charge ratios (+:–) of 2.3 and 3.1 in liver and spleen, respectively, expressing a mannose receptor on the cell surface was higher than that in the lung; while the transfection efficiency at a charge ratio (+:–) of 4.7 was found to be highest in the lung, suggesting a non-specific interaction [265]. Incorporation of polyethylenimine (PEI), a molecule showing a

pH-buffering capacity in endosomes and DNA-condensing activity, into the Man-C4-Chol/DOPE (6:4) cationic liposomes/plasmid DNA complex, increased the uptake and transfection activity in mouse peritoneal macrophages 2-fold and 6-fold, respectively, compared to those obtained without incorporating PEI [266]. The presence of an essential amount of sodium chloride (NaCl) during the formation of cationic liposome/plasmid DNA complexes (lipoplexes) stabilizes the lipoplexes according to the surface charge regulation (SCR) theory [263]. After intraportal administration, the hepatic transfection activity of galactosylated SCR lipoplexes (5 and 10 mM NaCl solution in lipoplex) was approximately 10- to 20-fold higher than that of galactosylated conventional lipoplexes in mice. For galactosylated neutral liposomes containing Gal-C4-Chol of composition of DSPC/Chol/Gal-C4-Chol (60:35:5), model lipophilic drug prostaglandin E1 (PGE1) [245,250] and probucol [245,250] have been incorporated in the liposomes, and found to selectively target hepatocytes. However, probucol incorporated in the liposomes exhibited lower liver uptake than liposomes, suggesting that substantial release of probucol from liposomes had taken place before the liposomes were taken up in the liver [250]. In contrast, probucol incorporated in the galactosylated neutral liposomes with the composition of EPC/Chol/Gal-C4-Chol (60:35:5) was more stably incorporated under *in vivo* conditions [250].

In addition to Gal-C4-Chol and Man-C4-Chol, some other types of glycosylated lipids have been synthesized and used for construction of liposomes. Wang and his co-workers [249] synthesized four types of amphiphilic glycolipid molecules bearing galactose residues, namely octodecyl galactoside, octodecyl lactoside, cholesteryl galactoside, and cholesteryl lactoside, and mixed the glycolipids with pH-sensitive lipids DC-Chol/DOPE in a molar ratio of 1:6:4, to prepare hepatocyte-targeting pH-sensitive liposomes. Among the glycosylated lipids used, the DNA/liposome complexes containing octodecyl galactoside had the highest *in vitro* HepG2 cells (liver cells)-targeting property and gene transfection efficiency [249]. Zhang and associates [251] synthesized cholesterylated thio-galactosides with different lengths of oligoethylene glycol spacer and formulated galactosylated liposome–polycation–DNA complexes. The complexes containing galactosylated lipids with spacers of 3 and 4 ethylene glycol units significantly improved the levels of gene expression in cultured hepatoma cells, HepG2 and SMMC-7721; while those with spacers of 1 and 2 ethylene glycol units did not, compared with the complexes containing non-galactosylated lipids [251]. This result is consistent with the one observed by Sasaki *et al.* [267], who demonstrated that among the oligoethylene glycol-coupled galactolipids tested, the galactolipids with a tri- or tetraethylene glycol moiety as spacer caused the greatest accumulation of liposomes in the liver. In addition, they showed that the galactolipids with a tri- or tetraethylene glycol moiety as spacer exposed galactosyl moiety on the surface of liposomes, while those with a mono- or diethylene glycol spacer did not [267]. Sasaki and co-workers [268] also synthesized branched galactosyllipid and demonstrated that the difference in accumulation of liposomes

between non-branched galactosyllipid and branched galactosyllipid was not large. They proved that liver accumulation of liposomes depends more on the density of galactosyl residues. The spacer effect of PEG-coupled galactolipids on the surface exposure of galactosyl moiety and the biodistribution of liposomes were also investigated by Shimada *et al.* [269]. The galactose moiety is separated from a diacylglyceride lipid anchor by PEG chains of 10, 20, or 40 oxyethylene residues (PEG_{10/20/40}), and the galactosylated-PEG-lipids (Gal-PEG-Lip) are incorporated in the bilayer of liposomes. They demonstrated that only the liposomes containing the Gal-PEG₁₀-Lip aggregated with the *Ricinus communis* agglutinin 120 [269]. Furthermore, they illustrated that 90% of the intravenously injected Gal-PEG₁₀-Lip containing liposomes in rats was taken up by liver, and only less than 1% was taken up by spleen, compared to 19% by liver and 6% by spleen for liposomes without Gal-PEG₁₀-Lip [269]. However, they demonstrated that the increased liver uptake of Gal-PEG₁₀-Lip-containing liposomes was almost entirely attributable to increased uptake by the Kupffer cells and they suggested that this very specific and efficient recognition by the Kupffer cells could be attributed to interaction with the galactose particle receptor on these cells [269]. This somewhat unexpected result is possibly due to the dose effect of liposomes. Hashida and associates [253] have already demonstrated that at high dose (5%), galactosylated liposomes were taken up by NPCs rather than by PCs, and suggested that galactosylated liposomes administered at a high dose will also be taken up by NPCs *via* fucose receptors, which act as galactose particle receptors. In contrast, Nag and Ghosh [270] demonstrated that liposomes containing galactose-tagged PEG₂₀₀₀-DSPE conjugates (Gal-PEG₂₀₀₀-DSPE) much favored the uptake by PCs, with the ratio of intra-hepatic distribution of PCs to NPCs being 93:7, compared to 47:53 and 40:60 for PEG₂₀₀₀-DSPE containing liposomes and conventional liposomes (containing lipids neither PEGylated nor galactosylated), respectively. On the other hand, mannosylation of both the conventional liposomes and the PEGylated liposomes (i.e. SSL) shifted the distribution toward Kupffer cells [270]. Furthermore, significant liver antimetastatic effects of galactosylated liposomal antitumor drug adriamycin (ADM) [163] and immunochemotherapeutic cytokine interleukin-2 (IL-2) [271] have been demonstrated.

Optimization of the glycosylated lipid structure, lipid composition of the liposomes, charge ratio for cationic liposomes, and other factors based on physicochemical considerations, should lead to more specific and effective drug and gene delivery.

2.3.2.4. Other ligand-attached liposomes

Several other ligands, designed to target specific receptors that are overexpressed on target cells (especially cancer cells), and certain specific membrane molecules on pathological cells [30], have been attached to liposomes for actively

targeting delivery of drugs, genes, and diagnostic agents. For example, $\alpha_v\beta_3$ -integrins are overexpressed on actively proliferating endothelium and represent a possible target to disrupt the angiogenic process of tumor growth [156]. The phage display library selection of peptides targeting to tumor blood vessels demonstrated that the Arg–Gly–Asp (RGD) tripeptide showed the most efficient binding to the $\alpha_v\beta_3$ -integrin receptor [156]. Cyclic RGD peptide has been coupled to the PEG-terminus of PEG-liposome encapsulating antitumor drug doxorubicin to target the receptor $\alpha_v\beta_3$ -integrins expressed on the endothelial cells of a doxorubicin-resistant C26 colon cancer xenograft model [157]. Doxorubicin encapsulated in the RGD-attached PEG-liposome inhibited tumor growth in the colon carcinoma model, whereas control liposomal (plain PEG-liposome) doxorubicin failed to decelerate tumor growth [157]. In another example, RGD-attached PEG-liposomal doxorubicin showed higher intracellular uptake of doxorubicin by B16 cells *in vitro* and higher antitumor activity in terms of tumor growth inhibition and mice survival time prolongation *in vivo* compared to plain PEG-liposomal doxorubicin [272]. Similarly, integrin GPIIb–IIIa forms upon platelet activation, which is an acute response to balloon-induced vascular injury, and is strongly implicated in the pathogenesis of luminal restenosis through release of chemical mediators such as platelet-derived growth factor (PDGF) [273,274]. RGD peptide-coated liposomes with the composition of DSPE/DSPE-PEG₃₄₀₀-RGD (95:5) have been demonstrated to bind platelets at levels substantially greater than the control DSPE/DSPE-PEG₂₀₀₀ (95:5) liposomes, representing a means to target liposome-encapsulated anticoagulant or antiplatelet therapeutics [158]. Another receptor, VIP receptor (VIP-R), which is about five times overexpressed in human breast cancer compared to normal breast tissue [275,276], has become an attractive molecular target for breast cancer targeting. VIP, a 28-amino acid mammalian neuropeptide, has been covalently attached to the surface of SSL that encapsulated a radionuclide to target VIP-R on the surface of human breast cancer cells for breast cancer imaging, and resulted in significantly more accumulation of radionuclide in breast cancers than plain SSL [159]. For antineovascular therapy, peptides specifically homing to tumor angiogenic vessels have been isolated from a phage-displayed random peptide library [277,278]. ADM [276] and 5P-O-dipalmitoylphosphatidyl 2P-C-cyano-2P-deoxy-1-L-D-arabinopentofuranosylcytosine (DPP-CNDAC) [279], a hydrophobized derivative of the novel antitumor nucleoside CNDAC, were encapsulated in liposomes modified with APRPG, one of the angiogenic homing peptides, and strongly suppressed tumor growth compared with the same number of doses of unmodified liposomal drugs [277,279], with the increase of life span of the treated mice [279]. EGFR-targeted immunoliposomes have been specifically delivered to a variety of tumor cells that overexpress EGFR [30,195]. The hyaluronan-specific receptors CD44 and hyaluronan-mediated motility receptor (RHAMM) are found at low levels on epithelial, hematopoietic, and neuronal cells, and are overexpressed (one or both) in roughly all cancer types [160,280,281]. *In vivo*, mitomycin

C-encapsulated and hyaluronan-coated liposomes with the composition of PC/PE/Chol (3:1:1) were demonstrated to be accumulated 33- and 5-fold higher in tumor-bearing lungs, compared with free drug and non-hyaluronan-coated liposomal drugs, respectively [160]. Key indicators of therapeutic responses, tumor progression, and metastatic burden and survival were superior in animals receiving hyaluronan-coated liposomal mitomycin C, than those receiving non-hyaluronan-coated liposomal drug and free drug [160]. In addition, coating the liposomes with hyaluronan turned the liposomes into long-circulating species through its many hydroxyl residues, over a time frame similar to (or better than) that reported for PEG-coated liposomes [160]. It has been found that an increased level of chondroitin sulfate (CS) expression on the cell surface is often associated with malignant transformation and the progression of tumor cells [165,282–286]. Kimura and co-workers have developed long-circulating PEG-liposomes that contain a new cationic lipid 3,5-dipentadecyloxybenzamidinium hydrochloride (TRX-20), and this TRX-20 PEG-liposomes with the composition of HSPC/Chol/TRX-20/PEG-DSPE (50:42:8:0.75) bound preferentially to certain CSs, such as CS B, CS D, and CS E, whereas PEG-liposomes lacking TRX-20 showed no significant binding to any of the glycosaminoglycans tested [165]. Consequently, the TRX-20 PEG-liposomes, but not plain PEG liposomes, in *in vitro* studies, avidly bound to and were readily internalized by highly metastatic tumor cells such as LM8G5 and ACHN cells, which express large amounts of CS on the cell surface [165,287]. It was found that systemically injected TRX-20 PEG-liposomes preferentially accumulated in the liver and in solid s.c. LM8G5 tumors [165]. When administered to mice with glomerulonephritis, the TRX-20 PEG-liposomes selectively accumulated in glomerular mesangial lesions where vascular permeability was increased and CSs were abundantly expressed, and TRX-20 PEG-liposome-encapsulated prednisolone showed an increased therapeutic efficacy, compared with the free drug [288]. Furthermore, cisplatin-loaded TRX-20 PEG-liposomes effectively killed the CS-expressing tumor cells *in vitro*, whereas cisplatin-PEG-liposomes lacking TRX-20 were totally ineffective. *In vivo* in mice bearing an s.c. LM8G5 tumor, the TRX-20 PEG-liposomal cisplatin was significantly more effective in reducing the local tumor growth, suppressing metastatic spreading of LM8G5 tumor cells to the liver, and increasing the survival time, compared to plain PEG-liposomal cisplatin or free cisplatin [165].

3. CONCLUDING REMARKS

Research on the liposomal formulation towards site-specific active targeting and controlled cytoplasmic delivery of drugs, genes, antisense oligonucleotides, diagnostic imaging materials, etc. is a growing area. The targeting strategies of coating the liposomes with antibodies or other ligands can significantly improve the accumulation and internalization of liposomes, and may, in some

cases, result in an increased bioavailability of the encapsulated drugs/genes. The combination of active triggering strategies with site-specific targeting strategies is therefore of crucial importance for improving therapeutic index. In the future, more efforts are required to optimize the liposome formulations for optimal rate of drug release, and to develop stable liposomes for storage and a variety of quality control assays for liposomal formulations. With all these efforts accompanying the development of new strategies in material synthesis, and the advances in understanding the molecular basis of diseases, we believe that more clinical success on liposomal drugs can be achieved, and more liposomal pharmaceuticals can be launched in the market in the foreseeable future.

REFERENCES

- [1] A.D. Bangham, M.M. Standish, J.C. Watkins, Diffusion of univalent ions across the lamellae of swollen phospholipids, *J. Mol. Biol.* 13 (1965) 238–252.
- [2] H.T. Tien, *Bilayer Lipid Membranes (BLM): Theory and Practice*, Marcel Dekker, New York, 1974.
- [3] M.J. Ostro, *Liposomes*, Marcel Dekker, New York, 1983.
- [4] M. Rosoff (Ed.), *Vesicles*, Marcel Dekker, New York, 1996.
- [5] H.T. Tien, A. Ottova-Leitmannova, *Membrane biophysics: as viewed from experimental bilayer lipid membranes*, *Planar Lipid Bilayers and Spherical Liposomes*, Elsevier, Amsterdam, 2000.
- [6] D. Papahadjopoulos, Steric stabilization, an overview, in: A.S. Janoff, (Ed.), *Liposomes Rational Design*, Marcel Dekker, New York, 1999, pp. 1–12.
- [7] S. Chatterjee, D.K. Banerjee, Preparation, isolation, and characterization of liposomes containing natural and synthetic lipids, in: S.C. Basu, M. Basu (Eds.), *Liposome Methods and Protocols*, Humana Press Inc., Totowa, NJ, 2002, pp. 3–16.
- [8] S.C. Silverstein, R.M. Steinman, Z.A. Cohn, Endocytosis, *Ann. Rev. Biochem.* 46 (1977) 669–722.
- [9] Y.J. Kao, R.L. Juliano, Interactions of liposomes with the reticuloendothelial system. Effects of reticuloendothelial blockade on the clearance of large unilamellar vesicles, *Biochim. Biophys. Acta* 677 (1981) 453–461.
- [10] J.H. Senior, Fate and behavior of liposome *in vivo* – A review of controlling factors, *CRC, Crit. Rev. Ther. Drug. Car. Syst.* 3 (1987) 123–193.
- [11] G. Gregoriadis (Ed.), *Liposomes as Drug Carriers: Recent Trends and Progress*, Wiley, Chichester, 1988.
- [12] K.J. Hwang, Liposome pharmacokinetics, in: M.J. Ostro, (Ed.), *Liposomes: From Biophysics to Therapeutics*, Marcel Dekker, New York, 1987, pp. 109–156.
- [13] T.M. Allen, A. Chonn, Large unilamellar liposomes with low uptake into the reticuloendothelial system, *FEBS Lett.* 223 (1987) 42–46.
- [14] T.M. Allen, C. Hansen, J. Rutledge, Liposomes with prolonged circulation time: factors affecting uptake by reticuloendothelial and other tissues, *Biochim. Biophys. Acta* 981 (1989) 27–35.
- [15] N.M. Wassef, F. Roerdink, E.C. Richardson, C.R. Alving, Suppression of phagocytic function and phospholipid metabolism in macrophages by phosphatidylinositol liposomes, *Proc. Natl. Acad. Sci. USA* 81 (1984) 2655–2659.
- [16] D.D. Lasic, F.J. Martin, A. Gabizon, S.K. Huang, D. Papahadjopoulos, Sterically stabilized liposomes: a hypothesis on the molecular origin of the extended circulation time, *Biochim. Biophys. Acta* 1070 (1991) 187–192.

- [17] A.L. Klibanov, K. Maruyama, V.P. Torchilin, L. Huang, Amphipatic polyethyleneglycols effectively prolong the circulation time of liposomes, *FEBS Lett.* 268 (1990) 235–238.
- [18] G. Blume, G. Cevc, Liposomes for the sustained drug release *in vivo*, *Biochim. Biophys. Acta* 1029 (1990) 91–97.
- [19] T.M. Allen, Stealth™ liposomes: avoiding reticuloendothelial uptake, in: G. Lopez-Berenstein, I.J. Fidler (Eds.), *Liposomes in the Therapy of Infectious Diseases and Cancer*, Alan R. Liss, New York, 1989, pp. 405–415.
- [20] M.C. Woodle, Controlling liposome blood clearance by surface-grafted polymers, *Adv. Drug Deliver. Rev.* 32 (1998) 139–152.
- [21] A.A. Gabizon, Pegylated liposomal doxorubicin: metamorphosis of an old drug into a new form of chemotherapy, *Cancer Invest.* 19 (2001) 424–436.
- [22] D.Lasic, F.Martin (Eds.), *Stealth® Liposomes*, CRC Press, Boca Raton, FL, 1995.
- [23] G. Blume, G. Cevc, Molecular mechanism of the lipid vesicle longevity *in vivo*, *Biochim. Biophys. Acta* 1146 (1993) 157–168.
- [24] M.C. Woodle, K.K. Matthay, M.S. Newman, J.E. Hidayat, L.R. Collins, C. Redemann, F.J. Martin, D. Papahadjopoulos, Versatility in lipid compositions showing prolonged circulation with sterically stabilized liposomes, *Biochim. Biophys. Acta* 1105 (1992) 193–200.
- [25] V.P. Torchilin, V.G. Omelyanenko, M.I. Papisov, A.A. Bogdanov Jr., V.S. Trubetsky, J.N. Herron, C.A. Gentry, Poly(ethylene glycol) on the liposome surface: on the mechanism of polymer-coated liposome longevity, *Biochim. Biophys. Acta* 1195 (1994) 11–20.
- [26] V.P. Torchilin, V.S. Trubetsky, Which polymers can make nanoparticulate drug carriers long circulating? *Adv. Drug Deliver. Rev.* 16 (1995) 141–155.
- [27] V.P. Torchilin, M.I. Shtilman, V.S. Trubetsky, K. Whiteman, A.M. Milstein, Amphiphilic vinyl polymers effectively prolong liposome circulation time *in vivo*, *Biochim. Biophys. Acta* 1195 (1994) 181–184.
- [28] M.C. Woodle, C.M. Engbers, S. Zalipsky, New amphipathic polymer-lipid conjugates forming long-circulating reticuloendothelial system-evading liposomes, *Bioconjugate Chem.* 5 (1994) 493–496.
- [29] K. Maruyama, S. Okuizumi, O. Ishida, H. Yamauchi, H. Kikuchi, M. Iwatsuru, Phosphatidyl polyglycerols prolong liposome circulation *in vivo*, *Int. J. Pharm.* 111 (1994) 103–107.
- [30] V.P. Torchilin, Recent advances with liposomes as pharmaceutical carriers, *Nat. Rev. Drug Discov.* 4 (2005) 145–160.
- [31] K.R. Whiteman, V. Subr, K. Ulbrich, V.P. Torchilin, Poly(HPMA)-coated liposomes demonstrate prolonged circulation in mice, *J. Lipid Res.* 11 (2001) 153–164.
- [32] V.P. Torchilin, T.S. Levchenko, K.R. Whiteman, A.A. Yaroslavov, A.M. Tsatsakis, A.K. Rizos, E.V. Michailova, M.I. Shtilman, Amphiphilic poly *N*-vinylpyrrolidones: synthesis, properties and liposome surface modification, *Biomaterials* 22 (2001) 3035–3044.
- [33] J.M. Metselaar, P. Bruin, L.W.T. de Boer, T. de Vringer, C. Snel, C. Oussoren, M.H.M. Wauben, D.J.A. Crommelin, G. Storm, W.E. Hennink, A novel family of L-amino acid-based biodegradable polymer-lipid conjugates for the development of long-circulating liposomes with effective drug-targeting capacity, *Bioconjugate Chem.* 14 (2003) 1156–1164.
- [34] H. Takeuchi, H. Kojima, H. Yamamoto, Y. Kawashima, Evaluation of circulation profiles of liposomes coated with hydrophilic polymers having different molecular weights in rats, *J. Control. Release* 75 (2001) 83–91.
- [35] S. Ohkuma, B. Poole, Fluorescence probe measurement of the intralysosomal pH in living cells and the perturbation of pH by various agents, *Proc. Natl. Acad. Sci. USA* 75 (1978) 3327–3331.
- [36] J.E. Schnitzer, P. Oh, E. Pinney, J. Allard, Filipin-sensitive caveolae-mediated transport in endothelium: reduced transcytosis, scavenger endocytosis, and capillary permeability of select macromolecules, *J. Cell Biol.* 127 (1994) 1217–1232.

- [37] A. Huang, S.J. Kennel, L. Huang, Interactions of immunoliposomes with target cells, *J. Biol. Chem.* 258 (1983) 14034–14040.
- [38] D.C. Drummond, M. Zignani, J.C. Leroux, Current status of pH-sensitive liposomes in drug delivery, *Prog. Lipid Res.* 39 (2000) 409–460.
- [39] T.L. Andresen, S.S. Jensen, K. Jorgensen, Advanced strategies in liposomal cancer therapy: problems and prospects of active and tumor specific drug release, *Prog. Lipid Res.* 44 (2005) 68–97.
- [40] E. Fattal, P. Couvreur, C. Dubernet, Smart delivery of antisense oligonucleotides by anionic pH-sensitive liposomes, *Adv. Drug Deliver. Rev.* 56 (2004) 931–946.
- [41] S. Simoes, J.N. Moreira, C. Fonseca, N. Duzgunes, M.C. de Lima, On the formulation of pH-sensitive liposomes with long circulation times, *Adv. Drug Deliver. Rev.* 56 (2004) 947–965.
- [42] G. Cevc, H. Richardsen, Lipid vesicles and membrane fusion, *Adv. Drug Deliver. Rev.* 38 (1999) 207–232.
- [43] I.M. Hafez, P.R. Cullis, Roles of lipid polymorphism in intracellular delivery, *Adv. Drug Deliver. Rev.* 47 (2001) 139–148.
- [44] E.Y. Shalaev, P.L. Steponkus, Phase diagram of 1,2-dioleoylphosphatidylethanolamine (DOPE): water system at subzero temperatures and at low water contents, *Biochim. Biophys. Acta* 1419 (1999) 229–247.
- [45] O.V. Gerasimov, J.A. Boomer, M.M. Qualls, D.H. Thompson, Cytosolic drug delivery using pH- and light-sensitive liposomes, *Adv. Drug Deliver. Rev.* 38 (1999) 317–338.
- [46] D.C. Litzinger, L. Huang, Phosphatidylethanolamine liposomes: drug delivery, gene transfer and immunodiagnostic applications, *Biochim. Biophys. Acta* 1113 (1992) 201–227.
- [47] D. Collins, D.C. Litzinger, L. Huang, Structural and functional comparisons of pH-sensitive liposomes composed of phosphatidylethanolamine and three different diacylsuccinylglycerols, *Biochim. Biophys. Acta* 1025 (1990) 234–242.
- [48] P. Venugopalan, S. Jain, S. Sankar, P. Singh, A. Rawat, S.P. Vyas, pH-sensitive liposomes: mechanism of triggered release to drug and gene delivery prospects, *Pharmazie* 57 (2002) 659–671.
- [49] C.J. Chu, J. Dijkstra, M.Z. Lai, K. Hong, F.C. Szoka, Efficiency of cytoplasmic delivery by pH-sensitive liposomes to cells in culture, *Pharm. Res.* 7 (1990) 824–834.
- [50] V.A. Slepishkin, S. Simoes, P. Dazin, M.S. Newman, L.S. Guo, M.C.P. de Lima, Sterically stabilized pH-sensitive liposomes. Intracellular delivery of aqueous contents and prolonged circulation *in vivo*, *J. Biol. Chem.* 272 (1997) 2382–2388.
- [51] Y. Rui, S. Wang, P.S. Low, D.H. Thompson, Dipalmitoylcholine-folate liposomes: an efficient vehicle for intracellular drug delivery, *J. Am. Chem. Soc.* 120 (1998) 11213–11218.
- [52] J. Shin, P. Shum, D.H. Thompson, Acid-triggered release *via* dePEGylation of DOPE liposomes containing acid-labile vinyl ether PEG-lipids, *J. Control. Release* 91 (2003) 187–200.
- [53] X. Guo, F.C. Szoka Jr., Steric stabilization of fusogenic liposomes by a low-pH sensitive PEG-diortho ester-lipid conjugate, *Bioconjugate Chem.* 12 (2001) 291–300.
- [54] X. Guo, J.A. MacKay, F.C. Szoka Jr., Mechanism of pH-triggered collapse of phosphatidylethanolamine liposomes stabilized by an ortho ester polyethyleneglycol lipid, *Biophys. J.* 84 (2003) 1784–1795.
- [55] J. Heller, K.J. Himmelstein, Poly(ortho ester) biodegradable polymer systems, *Methods Enzymol.* 112 (1985) 422–436.
- [56] O. Meyer, D. Papahadjopoulos, J.C. Leroux, Copolymers of *N*-isopropylacrylamide can trigger pH sensitivity to stable liposomes, *FEBS Lett.* 421 (1998) 61–64.
- [57] E. Roux, R. Stomp, S. Giasson, M. Pezolet, P. Moreau, J.C. Leroux, Steric stabilization of liposomes by pH-responsive *N*-isopropylacrylamide copolymer, *J. Pharm. Sci.* 91 (2002) 1795–1802.

- [58] E. Roux, C. Passirani, S. Scheffold, J.P. Benoit, J.C. Leroux, Serum-stable and long-circulating, PEGylated pH-sensitive liposomes, *J. Control. Release* 94 (2004) 447–451.
- [59] M.J. Turk, J.A. Reddy, J.A. Chmielewski, P.S. Low, Characterization of a novel pH-sensitive peptide that enhances drug release from folate-targeted liposomes at endosomal pHs, *Biochim. Biophys. Acta* 1559 (2002) 56–68.
- [60] T. Kakudo, S. Chaki, S. Futaki, I. Nakase, K. Akaji, T. Kawakami, K. Maruyama, H. Kamiya, H. Harashima, Transferrin-modified liposomes equipped with a pH-sensitive fusogenic peptide: an artificial viral-like delivery system, *Biochemistry* 43 (2004) 5618–5628.
- [61] G. Shi, W. Guo, S.M. Stephenson, R.J. Lee, Efficient intracellular drug and gene delivery using folate receptor targeted pH-sensitive liposomes composed of cationic/anionic lipid combinations, *J. Control. Release* 80 (2002) 309–319.
- [62] K.D. Lee, Y.K. Oh, D.A. Portnoy, J.A. Swanson, Delivery of macromolecules into cytosol using liposomes containing hemolysin from *Listeria monocytogenes*, *J. Biol. Chem.* 271 (1996) 7249–7252.
- [63] C. Geoffroy, J.L. Gaillard, J.E. Alouf, P. Berche, Purification, characterization, and toxicity of the sulfhydryl-activated hemolysin listeriolysin O from *Listeria monocytogenes*, *Infect. Immun.* 55 (1987) 1641–1646.
- [64] D.A. Portnoy, R.K. Tweten, M. Kehoe, J. Bielecki, Capacity of listeriolysin O, streptolysin O, and perfringolysin O to mediate growth of *Bacillus subtilis* within mammalian cells, *Infect. Immun.* 60 (1992) 2710–2717.
- [65] A. Mueller, B. Bondurant, D.F. O'Brien, Visible-light-stimulated destabilization of PEG-liposomes, *Macromolecules* 33 (2000) 4799–4804.
- [66] V.C. Anderson, D.H. Thompson, Triggered release of hydrophilic agents from plasmalogen liposomes using visible light or acid, *Biochim. Biophys. Acta* 1109 (1992) 33–42.
- [67] R.H. Bisby, C. Mead, C.G. Morgan, Wavelength-programmed solute release from photosensitive liposomes, *Biochem. Biophys. Res. Commun.* 276 (2000) 169–173.
- [68] R.H. Bisby, C. Mead, C.G. Morgan, Active uptake of drugs into photosensitive liposomes and rapid release on UV photolysis, *Photochem. Photobiol.* 72 (2000) 57–61.
- [69] B. Bondurant, A. Mueller, D.F. O'Brien, Photoinitiated destabilization of sterically stabilized liposomes, *Biochim. Biophys. Acta* 1511 (2001) 113–122.
- [70] B. Bondurant, D.F. O'Brien, Photoinduced destabilization of sterically stabilized liposomes, *J. Am. Chem. Soc.* 120 (1998) 13541–13542.
- [71] T. Spratt, B. Bondurant, D.F. O'Brien, Rapid release of liposomal contents upon photoinitiated destabilization with UV exposure, *Biochim. Biophys. Acta* 1611 (2003) 35–43.
- [72] D.H. Thompson, O.V. Gerasimov, J.J. Wheeler, Y.J. Rui, V.C. Anderson, Triggerable plasmalogen liposomes: improvement of system efficiency, *Biochim. Biophys. Acta* 1279 (1996) 25–34.
- [73] Y. Fu, P.D. Sima, J.R. Kanofsky, Singlet-oxygen generation from liposomes: a comparison of 6b-cholesterol hydroperoxide formation with predictions from a one-dimensional model of singlet-oxygen diffusion and quenching, *Photochem. Photobiol.* 63 (1996) 468–476.
- [74] S. Gross, A. Brandis, L. Chen, V. Rosenbach-Belkin, S. Roehrs, A. Scherz, Y. Salomon, Protein-A-mediated targeting of bacteriochlorophyll-IgG to *Staphylococcus aureus*: a model for enhanced site-specific photocytotoxicity, *Photochem. Photobiol.* 66 (1997) 872–878.
- [75] X. Zhou, A.M. Ren, J.K. Feng, X.J. Liu, Theoretical studies on the one- and two-photon absorption of tetrabenzoporphyrins and phthalocyanines, *Can. J. Chem.* 82 (2004) 19–26.
- [76] P. Shum, J.M. Kim, D.H. Thompson, Phototriggering of liposomal drug delivery systems, *Adv. Drug Deliver. Rev.* 53 (2001) 273–284.

- [77] N.J. Wymer, O.V. Gerasimov, D.H. Thompson, Cascade liposomal triggering: light-induced Ca^{2+} release from diplasmenylcholine liposomes triggers PLA_2 -catalyzed hydrolysis and contents leakage from DPPC liposomes, *Bioconjugate Chem.* 9 (1998) 305–308.
- [78] J.H. Collier, B.H. Hu, J.W. Ruberti, J. Zhang, P. Shum, D.H. Thompson, P.B. Messersmith, Thermally and photochemically triggered self-assembly of peptide hydrogels, *J. Am. Chem. Soc.* 123 (2001) 9463–9464.
- [79] Z.Y. Zhang, P. Shum, M. Yates, P.B. Messersmith, D.H. Thompson, Formation of fibrinogen-based hydrogels using phototriggerable diplasmalogen liposomes, *Bioconjugate Chem.* 13 (2002) 640–646.
- [80] U. Schmidt-Erfurth, T.J. Flotte, E.S. Gragoudas, K. Schomacker, R. Bringeuber, T. Hasan, Benzoporphyrin-lipoprotein-mediated photodestruction of intraocular tumors, *Exp. Eye Res.* 62 (1996) 1–10.
- [81] S. Ebrahim, G.A. Peyman, P.J. Lee, Applications of liposomes in ophthalmology, *Surv. Ophthalmol.* 50 (2005) 167–182.
- [82] U. Schmidt-Erfurth, T. Hasan, T. Flotte, E. Gragoudas, R. Birngruber, Photodynamic therapy of experimental, intraocular tumors with benzoporphyrin-lipoprotein, *Ophthalmology* 91 (1994) 348–356.
- [83] U. Schmidt-Erfurth, T. Hasan, K. Schomacker, T.J. Flotte, R. Birngruber, *In vivo* uptake of liposomal benzoporphyrin derivative and photothrombosis in experimental corneal neovascularization, *Lasers Surg. Med.* 17 (1995) 178–188.
- [84] M.B. Yatvin, J.N. Weinstein, W.H. Dennis, R. Blumenthal, Design of liposomes for enhanced local release of drugs by hyperthermia, *Science* 202 (1978) 1290–1293.
- [85] J.N. Weinstein, R.L. Magin, M.B. Yatvin, D.S. Zaharko, Liposomes and local hyperthermia: selective delivery of methotrexate to heated tumors, *Science* 204 (1979) 188–191.
- [86] M.W. Dewhirst, L. Prosnitz, D. Thrall, D. Prescott, S. Clegg, C. Charles, J. MacFall, G. Rosner, T. Samulski, E. Gillette, S. LaRue, Hyperthermic treatment of malignant diseases: current status and a view toward the future, *Semin. Oncol.* 24 (1997) 616–625.
- [87] S. Zellmer, G. Cevc, Tumor targeting *in vivo* by means of thermolabile fusogenic liposomes, *J. Drug Target.* 4 (1996) 19–29.
- [88] M.H. Gaber, K. Hong, S.K. Huang, D. Papahadjopoulos, Thermosensitive sterically stabilized liposomes: formulation and *in vitro* studies on the mechanism of doxorubicin release by bovine serum and human plasma, *Pharm. Res.* 12 (1995) 1407–1416.
- [89] M.H. Gaber, N.Z. Wu, K.L. Hong, S.K. Huang, M.W. Dewhirst, D. Papahadjopoulos, Thermosensitive liposomes: extravasation and release of contents in tumor microvascular networks, *Int. J. Radiat. Oncol. Biol. Phys.* 36 (1996) 1177–1187.
- [90] S. Ning, K. Macleod, R.M. Abra, A.H. Huang, G.M. Hahn, Hyperthermia induces doxorubicin release from long-circulating liposomes and enhances their anti-tumor efficacy, *Int. J. Rad. Oncol.* 29 (1994) 827–834.
- [91] D. Needham, G. Anyarambhatla, G. Kong, M.W. Dewhirst, A new temperature-sensitive liposome for use with mild hyperthermia: characterization and testing in a human tumor xenograft model, *Cancer Res.* 60 (2000) 1197–1201.
- [92] G. Kong, G. Anyarambhatla, W.P. Petros, R.D. Braun, O.M. Colvin, D. Needham, M.W. Dewhirst, Efficacy of liposomes and hyperthermia in a human tumor xenograft model: importance of triggered drug release, *Cancer Res.* 60 (2000) 6597–6950.
- [93] D. Needham, M.W. Dewhirst, The development and testing of a new temperature-sensitive drug delivery system for the treatment of solid tumors, *Adv. Drug Deliver. Rev.* 53 (2001) 285–305.
- [94] A.A. Gabizon, Stealth liposomes and tumor targeting: one step further in the quest for the magic bullet, *Clin. Cancer Res.* 7 (2001) 223–225.

- [95] A. Gabizon, H. Shmeeda, Y. Barenholz, Pharmacokinetics of PEGylated liposomal doxorubicin: review of animal and human studies, *Clin. Pharmacokinet.* 42 (2003) 419–436.
- [96] K. Kono, Thermosensitive polymer-modified liposomes, *Adv. Drug Deliver. Rev.* 53 (2001) 307–319.
- [97] H.G. Schild, Poly(*N*-isopropylacrylamide): experiment, theory and application, *Prog. Polym. Sci.* 17 (1992) 163–249.
- [98] H. Feil, Y.H. Bae, F.J. Jan, S.W. Kim, Effect of comonomer hydrophilicity and ionization on the lower critical solution temperature of *N*-isopropylacrylamide copolymers, *Macromolecules* 26 (1993) 2496–2500.
- [99] M. Shibayama, S. Mizutani, S. Nomura, Thermal properties of copolymer gels containing *N*-isopropylacrylamide, *Macromolecules* 29 (1996) 2019–2024.
- [100] K. Kono, K. Yoshino, T. Takagishi, Effect of poly(ethylene glycol) grafts on temperature-sensitivity of thermosensitive polymer-modified liposomes, *J. Control. Release* 80 (2002) 321–332.
- [101] H. Ringsdorf, J. Venzmer, F.M. Winnik, Interaction of hydrophobically modified poly *N*-isopropylacrylamides with model membranes – or playing a molecular accordion, *Angew Chem. Int. Ed.* 30 (1991) 315–318.
- [102] H. Ringsdorf, J. Simon, F.M. Winnik, Interactions of hydrophobically modified poly(*N*-isopropylacrylamides) with liposomes – fluorescence studies, *ACS Symp. Ser.* 532 (1993) 216–240.
- [103] K. Kono, R. Nakai, K. Morimoto, T. Takagishi, Thermosensitive polymer-modified liposomes that release contents around physiological temperature, *Biochim. Biophys. Acta* 1416 (1999) 239–250.
- [104] K. Kono, A. Henmi, T. Takagishi, Temperature-controlled interaction of thermosensitive polymer-modified cationic liposomes with negatively charged phospholipids membranes, *Biochim. Biophys. Acta* 1421 (1999) 183–197.
- [105] H. Hayashi, K. Kono, T. Takagishi, Temperature-controlled release property of phospholipid vesicles bearing a thermosensitive polymer, *Biochim. Biophys. Acta* 1280 (1996) 127–134.
- [106] T.P. Chelvi, S.K. Jain, R. Ralhan, Hyperthermia-mediated targeted delivery of thermosensitive liposome-encapsulated melphalan in murine tumors, *Oncol. Res.* 7 (1995) 393–398.
- [107] P.T. Chelvi, S.K. Jain, R. Ralhan, Heat-mediated selective delivery of liposome-associated melphalan in murine melanoma, *Melanoma Res.* 5 (1995) 321–326.
- [108] C.P. Tamiz, R. Ralhan, Enhanced antitumor effect of radiation in combination with heat-sensitive liposome-encapsulated drug and hyperthermia on murine tumors, *J. Clin. Biochem. Nutr.* 19 (1995) 137–146.
- [109] G. Kong, M.W. Dewhirst, Hyperthermia and liposomes, *Int. J. Hyperthermia* 15 (1999) 345–370.
- [110] M.B. Ruiz-Arguello, G. Basanez, F.M. Goni, A. Alonso, Different effects of enzyme-generated ceramides and diacylglycerols in phospholipid membrane fusion and leakage, *J. Biol. Chem.* 271 (1996) 26616–26621.
- [111] G. Basanez, G.D. Fidelio, F.M. Goni, B. Maggio, A. Alonso, Dual inhibitory effect of gangliosides on phospholipase C-promoted fusion of lipidic vesicles, *Biochemistry* 35 (1996) 7506–7513.
- [112] G. Basanez, F.M. Goni, A. Alonso, Poly(ethylene glycol)-lipid conjugates inhibit phospholipase C-induced lipid hydrolysis, liposome aggregation and fusion through independent mechanisms, *FEBS Lett.* 411 (1997) 281–286.
- [113] M.B. Ruiz-Arguello, F.M. Goni, A. Alonso, Vesicle membrane fusion induced by the concerted activities of sphingomyelinase and phospholipase C, *J. Biol. Chem.* 273 (1998) 22977–22982.
- [114] C.C. Pak, R.K. Erukulla, P.L. Ahl, A.S. Janoff, P. Meers, Elastase-activated liposomal delivery to nucleated cells, *Biochim. Biophys. Acta* 1419 (1999) 111–126.

- [115] P. Meers, Enzyme-activated targeting of liposomes, *Adv. Drug Deliver. Rev.* 53 (2001) 265–272.
- [116] S.C. Davis, F.C. Szoka Jr., Cholesterol phosphate derivatives: synthesis and incorporation into a phosphatase and calcium-sensitive triggered release liposome, *Bioconjugate Chem.* 9 (1998) 783–792.
- [117] J.L. Millan, W.H. Fishman, Biology of human alkaline phosphatases with special reference to cancer, *Crit. Rev. Clin. Lab. Sci.* 32 (1995) 1–39.
- [118] J. Davidsen, K. Jorgensen, T.L. Andresen, O.G. Mouritsen, Secreted phospholipase A₂ as a new enzymatic trigger mechanism for localized liposomal drug release and absorption in diseased tissue, *Biochim. Biophys. Acta* 1609 (2003) 95–101.
- [119] K. Jorgensen, C. Vermehren, O.G. Mouritsen, Enhancement of phospholipase A₂-catalyzed degradation of polymer grafted PEG-liposomes: effects of lipopolymer-concentration and chain-length, *Pharm. Res.* 16 (1999) 1491–1493.
- [120] T.L. Andresen, O.G. Mouritsen, M. Begtrup, K. Jorgensen, Phospholipase A₂ activity: dependence on liposome surface charge and polymer coverage, *Biophys. J.* 82 (2002) 148A–148A.
- [121] T.L. Andresen, J. Davidsen, M. Begtrup, O.G. Mouritsen, K. Jorgensen, Enzymatic release of antitumor ether lipids by specific phospholipase A₂ activation of liposome-forming prodrugs, *J. Med. Chem.* 47 (2004) 1694–1703.
- [122] K. Jorgensen, T. Kiebler, I. Hylander, C. Vermehren, Interaction of a lipid-membrane destabilizing enzyme with PEG-liposomes, *Int. J. Pharm.* 183 (1999) 21–24.
- [123] S. Yamashita, M. Ogawa, K. Sakamoto, T. Abe, H. Arakawa, J. Yamashita, Elevation of serum group II phospholipase A₂ levels in patients with advanced cancer, *Clin. Chim. Acta* 228 (1994) 91–99.
- [124] T. Abe, K. Sakamoto, H. Kamohara, Y. Hirano, N. Kuwahara, M. Ogawa, Group II phospholipase A₂ is increased in peritoneal and pleural effusions in patients with various types of cancer, *Int. J. Cancer* 74 (1997) 245–250.
- [125] J.Z. Jiang, B.L. Neubauer, J.R. Graff, M. Chedid, J.E. Thomas, N.W. Roehm, S.B. Zhang, G.J. Eckert, M.O. Koch, J.N. Eble, L. Cheng, Expression of Group IIA secretory phospholipase A₂ is elevated in prostatic intraepithelial neoplasia and adenocarcinoma, *Am. J. Pathol.* 160 (2002) 667–671.
- [126] J.P. Laye, J.H. Gill, Phospholipase A₂ expression in tumours: a target for therapeutic intervention? *Drug Discov. Today* 8 (2003) 710–716.
- [127] A.G. Buckland, D.C. Wilton, Anionic phospholipids, interfacial binding and the regulation of cell functions, *Biochim. Biophys. Acta* 1483 (2000) 199–216.
- [128] O.G. Berg, M.H. Gelb, M.D. Tsai, M.K. Jain, Interfacial enzymology: the secreted phospholipase A₂-paradigm, *Chem. Rev.* 101 (2001) 2613–2654.
- [129] D.A. Six, E.A. Dennis, The expanding superfamily of phospholipase A₂ enzymes: classification and characterization, *Biochim. Biophys. Acta* 1488 (2000) 1–19.
- [130] J. Davidsen, O.G. Mouritsen, K. Jorgensen, Synergistic permeability enhancing effect of lysophospholipids and fatty acids on lipid membranes, *Biochim. Biophys. Acta* 1564 (2002) 256–262.
- [131] S. Bandak, D. Goren, A. Horowitz, D. Tzemach, A. Gabizon, Pharmacological studies of cisplatin encapsulated in long-circulating liposomes in mouse tumor models, *Anticancer Drugs* 10 (1999) 911–920.
- [132] B. Uziely, S. Jeers, R. Isacson, K. Kutsch, D. Wei-Tsao, Z. Yehoshua, E. Libson, F.M. Muggia, A. Gabizon, Liposomal doxorubicin: antitumor activity and unique toxicities during two complementary phase I studies, *J. Clin. Oncol.* 13 (1995) 1777–1785.
- [133] M.R. Ranson, J. Carmichael, K. O'Byrne, S. Stewart, D. Smith, A. Howell, Treatment of advanced breast cancer with sterically stabilized liposomal doxorubicin: results of a multicenter phase II trial, *J. Clin. Oncol.* 15 (1997) 3185–3191.
- [134] R.K. Jain, Delivery of molecular and cellular medicine to solid tumors, *J. Control. Release* 53 (1998) 49–67.

- [135] H. Maeda, Y. Matsumura, Tumorotropic and lymphotropic principles of macromolecular drugs, *Crit. Rev. Ther. Drug Carrier Syst.* 6 (1989) 193–210.
- [136] L.W. Seymour, Passive tumor targeting of soluble macromolecules and drug conjugates, *Crit. Rev. Ther. Drug Carrier Syst.* 9 (1992) 135–187.
- [137] F. Yuan, M. Leunig, S.K. Huang, D.A. Berk, D. Papahadjopoulos, R.K. Jain, Microvascular permeability and interstitial penetration of sterically stabilized (stealth) liposomes in a human tumor xenograft, *Cancer Res.* 54 (1994) 3352–3356.
- [138] S.H. Jang, M.G. Wientjes, D. Lu, J.L.S. Au, Drug delivery and transport to solid tumors, *Pharm. Res.* 20 (2003) 1337–1350.
- [139] T.M. Allen, E. Brandeis, C.B. Hansen, G.Y. Kao, S. Zalipsky, A new strategy for attachment of antibodies to sterically stabilized liposomes resulting in efficient targeting to cancer cells, *Biochem. Biophys. Acta* 1237 (1995) 99–108.
- [140] O. Zelphati, F.C. Szoka Jr., Liposomes as a carrier for intracellular delivery of antisense oligonucleotides: a real or magic bullet? *J. Control. Release* 41 (1996) 99–119.
- [141] J.W. Park, D.B. Kirpotin, K. Hong, R. Shalaby, Y. Shao, U.B. Nielsen, J.D. Marks, D. Papahadjopoulos, C.C. Benz, Tumor targeting using anti-her2 immunoliposomes, *J. Control. Release* 74 (2001) 95–113.
- [142] J.W. Park, K. Hong, D.B. Kirpotin, G. Colbern, R. Shalaby, J. Baselga, Y. Shao, U.B. Nielsen, J.D. Marks, D. Moore, D. Papahadjopoulos, C.C. Benz, Anti-HER2 immunoliposomes: enhanced efficacy attributable to targeted delivery, *Clin. Cancer Res.* 8 (2002) 1172–1181.
- [143] P. Sapra, T.M. Allen, Ligand-targeted liposomal anticancer drugs, *Prog. Lipid Res.* 42 (2003) 439–462.
- [144] S.G. Norley, D. Sendele, L. Huang, B.T. Rouse, Inhibition of herpes simplex virus replication in the mouse cornea by drug containing immunoliposomes, *Invest. Ophthalmol. Vis. Sci.* 28 (1987) 591–595.
- [145] Y. Lu, P.S. Low, Folate-mediated delivery of macromolecular anticancer therapeutic agents, *Adv. Drug Deliver. Rev.* 54 (2002) 675–693.
- [146] O. Aronov, A.T. Horowitz, A. Gabizon, D. Gibson, Folate-targeted PEG as a potential carrier for carboplatin analogs. Synthesis and *in vitro* studies, *Bioconjugate Chem* 14 (2003) 563–574.
- [147] Y.J. Lu, P.S. Low, Immunotherapy of folate receptor-expressing tumors: review of recent advances and future prospects, *J. Control. Release* 91 (2003) 17–29.
- [148] H. Hatakeyama, H. Akita, K. Maruyama, T. Suhara, H. Harashima, Factors governing the *in vivo* tissue uptake of transferrin-coupled polyethylene glycol liposomes *in vivo*, *Int. J. Pharm.* 281 (2004) 25–33.
- [149] O. Ishida, K. Maruyama, H. Tanahashi, M. Iwatsuru, K. Sasaki, M. Eriguchi, H. Yanagie, Liposomes bearing polyethyleneglycol-coupled transferrin with intracellular targeting property to the solid tumors *in vivo*, *Pharm. Res.* 18 (2001) 1042–1048.
- [150] A.S. Derycke, P.A. De Witte, Transferrin-mediated targeting of hypericin embedded in sterically stabilized PEGliposomes, *Int. J. Oncol.* 20 (2002) 181–187.
- [151] A. Gijssens, A. Derycke, L. Missiaen, D. de Vos, J. Huwyler, A. Eberle, P. de Witte, Targeting of the photocytotoxic compound AIPcS4 to HeLa cells by transferring conjugated PEGliposomes, *Int. J. Cancer* 101 (2002) 78–85.
- [152] H. Iinuma, K. Maruyama, K. Okinaga, K. Sasaki, T. Sekine, O. Ishida, N. Ogiwara, K. Johkura, Y. Yonemura, Intracellular targeting therapy of cisplatin-encapsulated transferrin-polyethylene glycol liposome on peritoneal dissemination of gastric cancer, *Int. J. Cancer* 99 (2002) 130–137.
- [153] D.A. Eavarone, X. Yu, R.V. Bellamkonda, Targeted drug delivery to C6 glioma by transferrin-coupled liposomes, *J. Biomed. Mater. Res.* 51 (2000) 10–14.
- [154] N. Omori, K. Maruyama, G. Jin, F. Li, S.J. Wang, Y. Hamakawa, K. Sato, I. Nagano, M. Shoji, K. Abe, Targeting of post-ischemic cerebral endothelium in rat by liposomes bearing polyethylene glycol-coupled transferrin, *Neurol. Res.* 25 (2003) 275–279.

- [155] N. Joshee, D.R. Bastola, P.W. Cheng, Transferrin-facilitated lipofection gene delivery strategy: characterization of the transfection complexes and intracellular trafficking, *Hum. Gene Ther.* 13 (2002) 1991–2004.
- [156] W. Arap, R. Pasqualini, E. Ruoslahti, Cancer treatment by targeted drug delivery to tumor vasculature in a mouse model, *Science* 279 (1998) 377–380.
- [157] R.M. Schiffelers, G.A. Koning, T.L.M. ten Hagen, M.H.A.M. Fens, A.J. Schraa, A.P.C.A. Janssen, R.J. Kok, G. Molema, G. Storm, Anti-tumor efficacy of tumor vasculature-targeted liposomal doxorubicin, *J. Control. Release* 91 (2003) 115–122.
- [158] B.J. Lestini, S.M. Sagnella, Z. Xu, M.S. Shive, N.J. Richter, J. Jayaseharan, A.J. Case, K. Kottke-Marchant, J.M. Anderson, R.E. Marchant, Surface modification of liposomes for selective cell targeting in cardiovascular drug delivery, *J. Control. Release* 78 (2002) 235–247.
- [159] S. Dagar, A. Krishnadas, I. Rubinstein, M.J. Blend, H. Onyuksel, VIP-grafted sterically stabilized liposomes for targeted imaging of breast cancer: *in vivo* studies, *J. Control. Release* 91 (2003) 123–133.
- [160] D. Peer, R. Margalit, Loading mitomycin C inside long-circulating hyaluronan targeted nano-liposomes increases its antitumor activity in three mice tumor models, *Int. J. Cancer* 108 (2004) 780–789.
- [161] J.S. Remy, A. Kichler, V. Mordvinov, F. Schuber, J.P. Behr, Targeted gene transfer into hepatoma cells with lipopolyamine-condensed DNA particles presenting galactose ligands: a stage toward artificial viruses, *Proc. Natl. Acad. Sci. USA* 92 (1995) 1744–1748.
- [162] M.A. Zanta, O. Boussif, A. Adib, J.P. Behr, *In vitro* gene delivery to hepatocytes with galactosylated polyethylenimine, *Bioconjugate Chem.* 8 (1997) 839–844.
- [163] I. Matsuda, H. Konno, T. Tanaka, S. Nakamura, Antimetastatic effect of hepatotropic liposomal adriamycin on human metastatic liver tumors, *Surg. Today* 31 (2001) 414–420.
- [164] M. Hashida, M. Nishikawa, F. Yamashita, Y. Takakura, Cell-specific delivery of genes with glycosylated carriers, *Adv. Drug Deliver. Rev.* 52 (2001) 187–196.
- [165] C.M. Lee, T. Tanaka, T. Murai, M. Kondo, J. Kimura, W. Su, T. Kitagawa, T. Ito, H. Matsuda, M. Miyasaka, Novel chondroitin sulfate-binding cationic liposomes loaded with cisplatin efficiently suppress the local growth and liver metastasis of tumor cells *in vivo*, *Cancer Res.* 62 (2002) 4282–4288.
- [166] G.A. Koning, H.W.M. Morselt, A. Gorter, T.M. Allen, S. Zalipsky, G.L. Scherphof, J.A.A.M. Kamps, Interaction of differently designed immunoliposomes with colon cancer cells and Kupffer cells. An *in vitro* comparison, *Pharm. Res.* 20 (2003) 1249–1257.
- [167] K. Maruyama, T. Takizawa, T. Yuda, S.J. Kennel, L. Huang, M. Iwatsuru, Targetability of novel immunoliposomes modified with amphipathic poly(ethylene glycol)s conjugated at their distal terminals to monoclonal antibodies, *Biochim. Biophys. Acta* 1234 (1995) 74–80.
- [168] K. Maruyama, O. Ishida, T. Takizawa, K. Moribe, Possibility of active targeting to tumor tissues with liposomes, *Adv. Drug Deliver. Rev.* 40 (1999) 89–102.
- [169] S. Mukherjee, L. Das, L. Kole, S. Karmakar, N. Datta, P.K. Das, Targeting of parasite-specific immunoliposome-encapsulated doxorubicin in the treatment of experimental visceral leishmaniasis, *J. Infect. Dis.* 189 (2004) 1024–1034.
- [170] J.A. Harding, C.M. Engbers, M.S. Newman, N.I. Goldstein, S. Zalipsky, Immunogenicity and pharmacokinetic attributes of poly(ethyleneglycol)-grafted immunoliposomes, *Biochim. Biophys. Acta* 1327 (1997) 181–192.
- [171] G.A. Koning, J.A. Kamps, G.L. Scherphof, Interference of macrophages with immunotargeting of liposomes, *J. Liposome Res.* 12 (2002) 107–119.
- [172] D. Aragnol, L. Leserman, Immune clearance of liposomes inhibited by an anti-Fc receptor antibody *in vivo*, *Proc. Natl. Acad. Sci. USA* 83 (1986) 2699–2703.
- [173] J.T. Derksen, H.W. Morselt, G.L. Scherphof, Uptake and processing of immunoglobulin-coated liposomes by subpopulations of rat liver macrophages, *Biochim. Biophys. Acta* 971 (1988) 127–136.

- [174] K. Mruyama, E. Holmber, S.J. Kennel, A. Klibanov, V. Torchilin, L. Huang, Characterization of *in vivo* immunoliposome targeting to pulmonary endothelium, *J. Pharm. Sci.* 79 (1990) 978–984.
- [175] T. Ishida, M.J. Kirchmeier, E.H. Moase, S. Zalipsky, T.M. Allen, Targeted delivery and triggered release of liposomal doxorubicin enhances cytotoxicity against human B lymphoma cells, *Biochim. Biophys. Acta* 1515 (2001) 144–158.
- [176] M. Harata, Y. Soda, K. Tani, J. Ooi, T. Takizawa, M. Chen, Y. Bai, K. Izawa, S. Kobayashi, A. Tomonari, F. Nagamura, S. Takahashi, K. Uchimar, T. Iseki, T. Tsuji, T.A. Takahashi, K. Sugita, S. Nakazawa, A. Tojo, K. Maruyama, S. Asano, CD19-targeting liposomes containing imatinib efficiently kill Philadelphia chromosome-positive acute lymphoblastic leukemia cells, *Blood* 104 (2004) 1442–1449.
- [177] P. Sapra, E.H. Moase, J. Ma, T.M. Allen, Improved therapeutic responses in a xenograft model of human B lymphoma (Namalwa) for liposomal vincristine Versus liposomal doxorubicin targeted *via* anti-CD19 IgG2a or Fab' fragments, *Clin. Cancer Res.* 10 (2004) 1100–1111.
- [178] P. Sapra, T.M. Allen, Internalizing antibodies are necessary for improved therapeutic efficacy of antibody-targeted liposomal drugs, *Cancer Res.* 62 (2002) 7190–7194.
- [179] R.W. Schroff, K.A. Foon, S.M. Beatty, R.K. Oldham, A.C. Morgan Jr., Human anti-mouse immunoglobulin responses in patients receiving monoclonal antibody therapy, *Cancer Res.* 45 (1985) 879–885.
- [180] N.C. Phillips, J. Dahman, Immunogenicity of immunoliposomes: reactivity against species-specific IgG and liposomal phospholipids, *Immunol. Lett.* 45 (1995) 149–152.
- [181] P. Carter, Improving the efficacy of antibody-based cancer therapies, *Nat. Rev. Cancer* 1 (2001) 118–129.
- [182] J.W. Park, K. Hong, D.B. Kirpotin, O. Meyer, D. Papahadjopoulos, C.C. Benz, Anti-HER2 immunoliposomes for targeted therapy of human tumors, *Cancer Lett.* 118 (1997) 153–160.
- [183] S.K. Huang, K.D. Lee, K. Hong, D.S. Friend, D. Papahadjopoulos, Microscopic localization of sterically stabilized liposomes in colon carcinoma-bearing mice, *Cancer Res.* 52 (1992) 5135–5143.
- [184] G.L. Scherphof, J.A.A.M. Kamps, G.A. Koning, *In vivo* targeting of surface-modified liposomes to metastatically growing colon carcinoma cells and sinusoidal endothelial cells in the rat liver, *J. Liposome Res.* 7 (1997) 419–432.
- [185] C.B. Hansen, G.Y. Kao, E.H. Moase, S. Zalipsky, T.M. Allen, Attachment of antibodies to sterically stabilized liposomes: evaluation, comparison and optimization of coupling procedures, *Biochim. Biophys. Acta* 1239 (1995) 133–144.
- [186] D. Kirpotin, J.W. Park, K. Hong, S. Zalipsky, W.L. Li, P. Carter, C.C. Benz, D. Papahadjopoulos, Sterically stabilized anti-HER2 immunoliposomes: design and targeting to human breast cancer cells *in vitro*, *Biochemistry* 36 (1997) 66–75.
- [187] D.B. Kirpotin, J.W. Park, K. Hong, Y. Shao, R. Shalaby, G. Colbern, C.C. Benz, D. Papahadjopoulos, Targeting of liposomes to solid tumors: the case of sterically stabilized anti-HER2 immunoliposomes, *J. Liposome Res.* 7 (1997) 391–417.
- [188] D. Goren, A.T. Horowitz, S. Zalipsky, M.C. Woodle, Y. Yarden, A. Gabizon, Targeting of stealth liposomes to erbB-2 (Her/2) receptor: *in vitro* and *in vivo* studies, *Br. J. Cancer* 74 (1996) 1749–1756.
- [189] J.A. Kamps, G.A. Koning, M.J. Velinova, H.W.M. Morselt, M. Wilkens, A. Gorter, J. Donga, G.L. Scherphof, Uptake of long-circulating immunoliposomes, directed against colon adenocarcinoma cells, by liver metastases of colon cancer, *J. Drug Targ.* 8 (2000) 235–245.
- [190] T. Völkel, P. Hölig, T. Merdan, R. Müller, R.E. Kontermann, Targeting of immunoliposomes to endothelial cells using a single-chain Fv fragment directed against human endoglin (CD105), *Biochim. Biophys. Acta* 1663 (2004) 158–166.
- [191] A.N. Lukyanov, T.A. Elbayoumi, A.R. Chakilam, V.P. Torchilin, Tumor-targeted liposomes: doxorubicinloaded long-circulating liposomes modified with anti-cancer antibody, *J. Control. Release* 100 (2004) 135–144.

- [192] L. Raffaghello, G. Pagnan, F. Pastorino, E. Cosimo, C. Brignole, D. Marimpietri, E. Bogenmann, M. Ponzoni, P.G. Montaldo, Immunoliposomal fenretinide: a novel antitumoral drug for human neuroblastoma, *Cancer Lett.* 197 (2003) 151–155.
- [193] T. Hamaguchi, Y. Matsumura, Y. Nakanishi, K. Muro, Y. Yamada, Y. Shimada, K. Shirao, H. Niki, S. Hosokawa, T. Tagawa, T. Kakizoe, Antitumor effect of MCC-465, PEGylated liposomal doxorubicin tagged with newly developed monoclonal antibody GAH, in colorectal cancer xenografts, *Cancer Sci.* 95 (2004) 608–613.
- [194] Y. Matsumura, M. Gotoh, K. Muro, Y. Yamada, K. Shirao, Y. Shimada, M. Okuwa, S. Matsumoto, Y. Miyata, H. Ohkura, K. Chin, S. Baba, T. Yamao, A. Kannami, Y. Takamatsu, K. Ito, K. Takahashi, Phase I and pharmacokinetic study of MCC-465, a doxorubicin (DXR) encapsulated in PEG immunoliposome, in patients with metastatic stomach cancer, *Ann. Oncol.* 15 (2004) 517–525.
- [195] C. Mamot, D.C. Drummond, U. Greiser, K. Hong, D.B. Kirpotin, J.D. Marks, J.W. Park, Epidermal growth factor receptor (EGFR)-targeted immunoliposomes mediate specific and efficient drug delivery to EGFR- and EGFRVIII-overexpressing tumor cells, *Cancer Res.* 63 (2003) 3154–3161.
- [196] E. Mastrobattista, G.A. Koning, L. van Bloois, A.C.S. Filipe, W. Jiskoot, G. Storm, Functional characterization of an endosome-disruptive peptide and its application in cytosolic delivery of immunoliposome-entrapped proteins, *J. Biol. Chem.* 277 (2002) 27135–27143.
- [197] N. Nakashima-Matsushita, T. Homma, S. Yu, T. Matsuda, N. Sunahara, T. Nakamura, M. Tsukano, M. Ratnam, T. Matsuyama, Selective expression of folate receptor beta and its possible role in methotrexate transport in synovial macrophages from patients with rheumatoid arthritis, *Arthritis Rheum.* 42 (1999) 1609–1616.
- [198] G. Toffoli, A. Russo, A. Gallo, C. Cernigoi, S. Miotti, R. Sorio, S. Tumolo, M. Boiocchi, Expression of folate-binding protein as a prognostic factor for response to platinum-containing chemotherapy and survival in human ovarian cancer, *Int. J. Cancer* 79 (1998) 121–126.
- [199] B.A. Kamen, A. Capdevila, Receptor-mediated folate accumulation is regulated by the cellular folate content, *Proc. Natl. Acad. Sci. USA* 83 (1986) 5983–5987.
- [200] C.P. Leamon, P.S. Low, Delivery of macromolecules into living cells: a method that exploits folate receptor endocytosis, *Proc. Natl. Acad. Sci. USA* 88 (1991) 5572–5576.
- [201] J.J. Turek, C.P. Leamon, P.S. Low, Endocytosis of folate–protein conjugates: ultrastructural localization in KB cells, *J. Cell Sci.* 106 (1993) 423–430.
- [202] R.J. Lee, P.S. Low, Delivery of liposomes into cultured KB cells *via* folate receptor-mediated endocytosis, *J. Biol. Chem.* 269 (1994) 3198–3204.
- [203] R.J. Lee, S. Wang, P.S. Low, Measurement of endosomal pH following folate receptor-mediated endocytosis, *Biochim. Biophys. Acta* 1312 (1996) 237–242.
- [204] A. Gabizon, D. Papahadjopoulos, Liposome formulations with prolonged circulation time in blood and enhanced uptake by tumors, *Proc. Natl. Acad. Sci. USA* 85 (1988) 6949–6953.
- [205] A. Gabizon, H. Shmeeda, A.T. Horowitz, S. Zalipsky, Tumor cell targeting of liposome-entrapped drugs with phospholipid-anchored folic acid-PEG conjugates, *Adv. Drug Deliver. Rev.* 56 (2004) 1177–1192.
- [206] A. Gabizon, A.T. Horowitz, D. Goren, D. Tzemach, F. Mandelbaum-Shavit, M.M. Qazen, S. Zalipsky, Targeting folate receptor with folate linked to extremities of poly(ethyleneglycol)-grafted liposomes: *in vitro* studies, *Bioconjugate Chem.* 10 (1999) 289–298.
- [207] R.J. Lee, P.S. Low, Folate-mediated tumor cell targeting of liposome-entrapped doxorubicin *in vitro*, *Biochim. Biophys. Acta* 1233 (1995) 134–144.
- [208] D. Goren, A.T. Horowitz, D. Tzemach, M. Tarshish, S. Zalipsky, A. Gabizon, Nuclear delivery of doxorubicin *via* folate-targeted liposomes with bypass of multidrug-resistance efflux pump, *Clin. Cancer Res.* 6 (2000) 1949–1957.

- [209] J.A. Reddy, C. Abburi, H. Hofland, S.J. Howard, I. Vlahov, P. Wils, C.P. Leamon, Folate-targeted, cationic liposome-mediated gene transfer into disseminated peritoneal tumors, *Gene Ther.* 9 (2002) 1542–1550.
- [210] X.Q. Pan, H. Wang, R.J. Lee, Antitumor activity of folate receptor-targeted liposomal doxorubicin in a KB oral carcinoma murine xenograft model, *Pharm. Res.* 20 (2003) 417–422.
- [211] X.Q. Pan, X. Zheng, G.F. Shi, H.Q. Wang, M. Ratnam, R.J. Lee, Strategy for the treatment of acute myelogenous leukemia based on folate receptor-targeted liposomal doxorubicin combined with receptor induction using all-trans retinoic acid, *Blood* 100 (2002) 594–602.
- [212] S. Ni, S.M. Stephenson, R.J. Lee, Folate receptor-targeted delivery of liposomal daunorubicin into tumor cells, *Anticancer Res.* 22 (2002) 2131–2135.
- [213] X.Q. Pan, R.J. Lee, *In vivo* antitumor activity of folate receptor-targeted liposomal daunorubicin in a murine leukemia model, *Anticancer Res.* 25 (2005) 343–346.
- [214] S. Wang, R.J. Lee, G. Cauchon, D.G. Gorenstein, P.S. Low, Delivery of antisense oligonucleotides against the human epidermal growth factor receptor into cultured KB cells with liposomes conjugated to folate *via* polyethyleneglycol, *Proc. Natl. Acad. Sci. USA* 92 (1995) 3318–3322.
- [215] C.P. Leamon, S.R. Cooper, G.E. Hardee, Folate-liposome-mediated antisense oligodeoxynucleotide targeting to cancer cells: evaluation *in vitro* and *in vivo*, *Bioconjugate Chem.* 14 (2003) 738–747.
- [216] K. Vogel, S. Wang, R.J. Lee, J. Chmielewski, P.S. Low, Peptide-mediated release of folate-targeted liposome contents from endosomal compartments, *J. Am. Chem. Soc.* 118 (1996) 1581–1586.
- [217] N.K. Subbarao, R.A. Parente, F.C. Szoka Jr., L. Nadasdi, K. Pongracz, pH-dependent bilayer destabilization by an amphipathic peptide, *Biochemistry* 26 (1987) 2964–2972.
- [218] Z.M. Qian, H.Y. Li, H.Z. Sun, K.P. Ho, Targeted drug delivery *via* the transferrin receptor-mediated endocytosis pathway, *Pharmacol. Rev.* 54 (2002) 561–587.
- [219] A. Leibman, P. Aisen, Distribution of iron between the binding sites of transferrin in serum – Methods and results in normal human subjects, *Blood* 53 (1979) 1058–1065.
- [220] H. Kawabata, R.S. Germain, P.T. Vuong, T. Nakamaki, J.W. Said, H.P. Koeffler, Transferrin receptor 2- α supports cell growth both in iron-chelated cultured cells and *in vivo*, *J. Biol. Chem.* 275 (2000) 16618–16625.
- [221] M. Davies, J.E. Parry, R.G. Sutcliffe, Examination of different preparations of human placental plasma membrane for the binding of insulin, transferrin and immunoglobulins, *J. Reprod. Fertil.* 63 (1981) 315–324.
- [222] C.A. Enns, H.A. Suomalainen, J.E. Gebhardt, J. Schroder, H.H. Sussman, Human transferrin receptor: expression of the receptor is assigned to chromosome 3, *Proc. Natl. Acad. Sci. USA* 79 (1982) 3241–3245.
- [223] T. Inoue, P.G. Cavanaugh, P.A. Steck, N. Brunner, G.L. Nicolson, Differences in transferrin response and numbers of transferrin receptors in rat and human mammary carcinoma lines of different metastatic potentials, *J. Cell Physiol.* 156 (1993) 212–217.
- [224] A.S.L. Derycke, A. Kamuhabwa, A. Gijssens, T. Roskams, D. De Vos, A. Kasran, J. Huwyler, L. Missiaen, P.A.M. de Witte, Transferrin-conjugated liposome targeting of photosensitizer AIPcS4 to rat bladder carcinoma cells, *J. Natl. Cancer I* 96 (2004) 1620–1630.
- [225] D.A. Eavarone, X. Yu, R.V. Bellamkonda, Targeted drug delivery to C6 glioma by transferrin-coupled liposomes, *J. Biomed. Mater. Res.* 51 (2000) 10–14.
- [226] P.H. Tan, W.J. King, D. Chen, H.M. Awad, M. Mackett, R.I. Lechler, D.F.P. Larkin, A.J.T. George, Transferrin receptor-mediated gene transfer to the corneal endothelium, *Transplantation* 71 (2001) 552–560.

- [227] L.N. Xu, K.F. Pirollo, E.H. Chang, Transferrin-liposome-mediated p53 sensitization of squamous cell carcinoma of the head and neck to radiation *in vitro*, *Hum. Gene Ther.* 8 (1997) 467–475.
- [228] L.A. Xu, K.F. Pirollo, W.H. Tang, A. Rait, E.H. Chang, Transferrin-liposome-mediated systemic p53 gene therapy in combination with radiation results in regression of human head and neck cancer xenografts, *Hum. Gene Ther.* 10 (1999) 2941–2952.
- [229] M. Nakase, M. Inui, K. Okumura, T. Kamei, S. Nakamura, T. Tagawa, p53 gene therapy of human osteosarcoma using a transferrin-modified cationic liposome, *Mol. Cancer Ther.* 4 (2005) 625–631.
- [230] Z.M. Qian, P.L. Tang, Mechanism of iron uptake by mammalian cells, *Biochim. Biophys. Acta* 1269 (1995) 205–214.
- [231] Z.M. Qian, P.L. Tang, Q. Wang, Iron crosses the endosomal membrane by a carrier-mediated process, *Prog. Biophys. Mol. Biol.* 67 (1997) 1–15.
- [232] P. Aisen, Transferrin, the transferrin receptor and the uptake of iron by cells, *Metal. Ions Biol. Syst.* 35 (1998) 535–631.
- [233] A. Dautry-Varsat, A. Ciechanover, H.F. Lodish, pH and the recycling of transferrin during receptor-mediated endocytosis, *Proc. Natl. Acad. Sci. USA* 80 (1983) 2258–2262.
- [234] R.D. Klausner, J.V. Ashwell, J. Van Renswoude, J.B. Harford, K.R. Bridges, Binding of apotransferrin to K562 cells: explanation of the transferrin cycle, *Proc. Natl. Acad. Sci. USA* 80 (1983) 2263–2266.
- [235] S. Paterson, N.J. Armstrong, B.J. Iacopetta, H.J. McArdle, E.H. Morgan, Intravesicular pH and iron uptake by immature erythroid cells, *J. Cell Physiol.* 120 (1984) 225–232.
- [236] E.H. Morgan, Cellular iron processing, *J. Gastroenterol. Hepatol.* 11 (1996) 1027–1030.
- [237] E.H. Morgan, Mechanisms of iron transport into rat erythroid cells, *J. Cell Physiol.* 186 (2001) 193–200.
- [238] S.M. Lee, J.S. Kim, Intracellular trafficking of transferrin-conjugated liposome/DNA complexes by confocal microscopy, *Arch. Pharmacol. Res.* 28 (2005) 93–99.
- [239] A. Gilsens, A. Derycke, L. Misslaen, D. De Vos, J. Huwylar, A. Eberle, P. De Witte, Targeting of the photocytotoxic compound AIPcS4 to HeLa cells by transferring conjugated PEGliposomes, *Int. J. Cancer* 101 (2002) 78–85.
- [240] C.T. De Iarduya, N. Düzgünes, Efficient gene transfer by transferrin lipoplexes in the presence of serum, *Biochim. Biophys. Acta* 1463 (2000) 333–342.
- [241] K. Kono, Y. Torikoshi, M. Mitsutomi, T. Itoh, N. Emi, H. Yanagie, T. Takagishi, Novel gene delivery systems: complexes of fusigenic polymer-modified liposomes and lipoplexes, *Gene Ther.* 8 (2001) 5–12.
- [242] S. Simões, V. Slepishkin, R. Gaspar, M.C. De Pedroso, N. Düzgünes, Gene delivery by negatively charged ternary complexes of DNA, cationic liposomes and transferrin or fusigenic peptides, *Gene Ther.* 5 (1998) 955–964.
- [243] K. Yanagihara, H. Cheng, P.W. Cheng, Effects of epidermal growth factor, transferrin and insulin on lipofection efficiency in human lung carcinoma cells, *Cancer Gene Ther.* 7 (2000) 59–65.
- [244] M.C.P. De Lima, S. Simoes, P. Pires, R. Gaspar, V. Slepishkin, N. Düzgünes, Gene delivery mediated by cationic liposomes: from biophysical aspects to enhancement of transfection, *Mol. Membr. Biol.* 16 (1999) 103–109.
- [245] S. Kawakami, C. Munakata, S. Fumoto, F. Yamashita, M. Hashida, Novel galactosylated liposomes for hepatocyte-selective targeting of lipophilic drugs, *J. Pharm. Sci.* 90 (2001) 105–113.
- [246] E. Wagner, Application of membrane-active peptides for nonviral gene delivery, *Adv. Drug Deliver. Rev.* 38 (1999) 279–289.
- [247] C. Managit, S. Kawakami, M. Nishikawa, F. Yamashita, M. Hashida, Targeted and sustained drug delivery using PEGylated galactosylated liposomes, *Int. J. Pharm.* 266 (2003) 77–84.

- [248] S. Kawakami, S. Fumoto, M. Nishikawa, F. Yamashita, M. Hashida, *In vivo* gene delivery to the liver using novel galactosylated cationic liposomes, *Pharm. Res.* 17 (2000) 306–313.
- [249] S.Y. Wen, X.H. Wang, L. Lin, W. Guan, S.Q. Wang, Preparation and property analysis of a hepatocyte targeting pH-sensitive liposome, *World J. Gastroenterol.* 10 (2004) 244–249.
- [250] Y. Hattori, S. Kawakami, F. Yamashita, M. Hashida, Controlled biodistribution of galactosylated liposomes and incorporated probucol in hepatocyte-selective drug targeting, *J. Control. Release* 69 (2000) 369–377.
- [251] X. Sun, L. Hai, Y. Wu, H.Y. Hu, Z.R. Zhang, Targeted gene delivery to hepatoma cells using galactosylated liposome-polycation-DNA complexes (LPD), *J. Drug Target.* 13 (2005) 121–128.
- [252] S. Matsukawa, M. Yamamoto, K. Ichinose, N. Ohata, N. Ishii, T. Kohji, K. Akiyoshi, J. Sunamoto, T. Kanematsu, Selective uptake by cancer cells of liposomes coated with polysaccharides bearing 1-aminolactose, *Anticancer Res.* 20 (2000) 2339–2344.
- [253] S. Kawakami, J. Wong, A. Sato, Y. Hattori, F. Yamashita, M. Hashida, Biodistribution characteristics of mannosylated, fucosylated, and galactosylated liposomes in mice, *Biochim. Biophys. Acta* 1524 (2000) 258–265.
- [254] S. Kawakami, A. Sato, M. Nishikawa, F. Yamashita, M. Hashida, Mannose receptor-mediated gene transfer into macrophages using novel mannosylated cationic liposomes, *Gene Ther.* 7 (2000) 292–299.
- [255] P. Opanasopit, M. Sakai, M. Nishikawa, S. Kawakami, F. Yamashita, M. Hashida, Inhibition of liver metastasis by targeting of immunomodulators using mannosylated liposome carriers, *J. Control. Release* 80 (2002) 283–294.
- [256] N. Garcon, G. Gregoriadis, M. Taylor, J. Summerfield, Mannose-mediated targeted immunoadjuvant action of liposomes, *Immunology* 64 (1988) 743–745.
- [257] L. Kole, L. Das, P.K. Das, Synergistic effect of interferon- γ and mannosylated liposome-incorporated doxorubicin in the therapy of experimental visceral leishmaniasis, *J. Infect. Dis.* 180 (1999) 811–820.
- [258] T. Ohashi, S. Boggs, P. Robbins, A. Bahnson, K. Patrene, F.S. Wei, J.F. Wei, J. Li, L. Lucht, Y. Fei, Efficient transfer and sustained high expression of the human glucocerebrosidase gene in mice and their functional macrophages following transplantation of bone marrow transduced by a retroviral vector, *Proc. Natl. Acad. Sci. USA* 89 (1992) 11332–11336.
- [259] Y.G. Lee, S.H. Lee, S.M. Lee, Role of Kupffer cells in cold/warm ischemia – reperfusion injury of rat liver, *Arch. Pharmacol. Res.* 23 (2000) 620–625.
- [260] F.T. Hufert, J. Schmitz, M. Schreiber, H. Schmitz, P. Racz, D.D. von Laer, Human Kupffer cells infected with HIV-1 *in vivo*, *J. Acquired Immun. Deficiency Syndrome* 6 (1993) 772–777.
- [261] Y. Takakura, R.I. Mahato, M. Hashida, Extravasation of macromolecules, *Adv. Drug Deliver. Rev.* 34 (1998) 93–108.
- [262] S. Fumoto, F. Nakadori, S. Kawakami, M. Nishikawa, F. Yamashita, M. Hashida, Analysis of hepatic disposition of galactosylated cationic liposome/plasmid DNA complexes in perfused rat liver, *Pharm. Res.* 20 (2003) 1452–1459.
- [263] S. Fumoto, S. Kawakami, Y. Ito, K. Shigeta, F. Yamashita, M. Hashida, Enhanced hepatocyte-selective *in vivo* gene expression by stabilized galactosylated liposome/plasmid DNA complex using sodium chloride for complex formation, *Mol. Ther.* 10 (2004) 719–729.
- [264] J. Kuiper, H.F. Bakkeren, E.A.L. Bissen, T.J.C. Van Berkel, Characterization of the interaction of galactose-exposing particles with rat Kupffer cells, *Biochem. J.* 299 (1994) 285–290.
- [265] S. Kawakami, Y. Hattori, Y. Lu, Y. Higuchi, F. Yamashita, M. Hashida, Effect of cationic charge on receptor-mediated transfection using mannosylated cationic liposome/plasmid DNA complexes following the intravenous administration in mice, *Pharmazie* 59 (2004) 405–408.

- [266] A. Sato, S. Kawakami, M. Yamada, F. Yamashita, M. Hashida, Enhanced gene transfection in macrophages using mannosylated cationic liposome-polyethylenimine-plasmid DNA complexes, *J. Drug Target* 9 (2001) 201–207.
- [267] A. Sasaki, N. Murahashi, H. Yamada, A. Morikawa, Syntheses of novel galactosyl ligands for liposomes and the influence of the spacer on accumulation in the rat liver, *Biol. Pharm. Bull.* 18 (1995) 740–746.
- [268] N. Murahashi, H. Ishihara, A. Sasaki, M. Sakagami, H. Hamana, Hepatic accumulation of glutamic acid branched neogalactosyllipid modified liposomes, *Biol. Pharm. Bull.* 20 (1997) 259–266.
- [269] K. Shimada, J.A. Kamps, J. Regts, K. Ikeda, T. Shiozawa, S. Hirota, G.L. Scherphof, Biodistribution of liposomes containing synthetic galactose-terminated diacylglycerol-poly(ethyleneglycol)s, *Biochim. Biophys. Acta* 1326 (1997) 329–341.
- [270] A. Nag, P.C. Ghosh, Assessment of targeting potential of galactosylated and mannosylated sterically stabilized liposomes to different cell types of mouse liver, *J. Drug Target* 6 (1999) 427–438.
- [271] K. Okuno, K. Nakamura, A. Tanaka, K. Yachi, M. Yasutomi, Hepatic immunopotential by galactose-entrapped liposomal IL-2 compound in the treatment of liver metastases, *Surg. Today, Jpn. J. Surg.* 28 (1998) 64–69.
- [272] X.B. Xiong, Y. Huang, W.L. Lu, H. Zhang, X. Zhang, Q. Zhang, Enhanced intracellular uptake of sterically stabilized liposomal doxorubicin *in vitro* resulting in improved antitumor activity *in vivo*, *Pharm. Res.* 22 (2005) 933–939.
- [273] C. Wu, Y. Chen, G. Hsiao, C. Lin, C. Liu, J. Sheu, Mechanisms involved in the inhibition of neointimal hyperplasia by abciximab in a rat model of balloon angioplasty, *Thromb. Res.* 101 (2001) 127–138.
- [274] H. Le Breton, E.F. Plow, E.J. Topol, Role of platelets in restenosis after percutaneous coronary revascularization, *J. Am. Coll. Cardiol.* 28 (1996) 1643–1651.
- [275] J.C. Reubi, *In vitro* identification of vasoactive intestinal peptide receptors in human tumors: implications for tumor lipoimaging, *J. Nucl. Med.* 36 (10) (1995) 1846–1853.
- [276] J.C. Reubi, *In vitro* identification of VIP receptors in human tumors: potential clinical implications, *Ann. NY Acad. Sci.* 805 (1996) 753–759.
- [277] N. Oku, T. Asai, K. Watanabe, K. Kuromi, M. Nagatsuka, K. Kurohane, H. Kikkawa, K. Ogino, M. Tanaka, D. Ishikawa, H. Tsukada, M. Momose, J. Nakayama, T. Taki, Anti-neovascular therapy using novel peptides homing to angiogenic vessels, *Oncogene* 21 (2002) 2662–2669.
- [278] T. Asai, M. Nagatsuka, K. Kuromi, S. Yamakawa, K. Kurohane, K. Ogino, M. Tanaka, T. Taki, N. Oku, Suppression of tumor growth by novel peptides homing to tumor-derived new blood vessels, *FEBS Lett.* 510 (2002) 206–210.
- [279] T. Asaia, K. Shimizua, M. Kondo, K. Kuromia, K. Watanabea, K. Oginob, T. Takib, S. Shutoc, A. Matsudac, N. Okua, Anti-neovascular therapy by liposomal DPP-CNDAC targeted to angiogenic vessels, *FEBS Lett.* 520 (2002) 167–170.
- [280] H. Li, L. Guo, J.W. Li, N. Liu, R. Qi, J. Liu, Expression of hyaluronan receptors CD44 and RHAMM in stomach cancers: relevance with tumor progression, *Int. J. Oncol.* 17 (2000) 927–932.
- [281] V. Abetamann, H.F. Kern, H.P. Elsasser, Differential expression of the hyaluronan receptors CD44 and RHAMM in human pancreatic cancer cells, *Clin. Cancer Res.* 2 (1996) 1607–1618.
- [282] V.P. Chiarugi, C.P. Dietrich, Sulfated mucopolysaccharides from normal and virus transformed rodent fibroblasts, *J. Cell. Physiol.* 99 (1979) 201–206.
- [283] M. Alini, G.A. Losa, Partial characterization of proteoglycans isolated from neoplastic and nonneoplastic human breast tissues, *Cancer Res.* 51 (1991) 1443–1447.
- [284] E.B. Olsen, K. Trier, K. Eldov, T. Ammitzboell, Glycosaminoglycans in human breast cancer, *Acta Obstet. Gynecol. Scand.* 67 (1988) 539–542.
- [285] R.A. Reisfeld, D.A. Cheresh, Human tumor antigens, *Adv. Immunol.* 40 (1987) 323–377.

- [286] T.F. Bumol, R.A. Reisfeld, Unique glycoprotein–proteoglycan complex defined by monoclonal antibody on human melanoma cells, *Proc. Natl. Acad. Sci. USA* 79 (1982) 1245–1249.
- [287] T. Harigai, M. Kondo, M. Isozaki, H. Kasukawa, H. Hagiwara, H. Uchiyama, J. Kimura, Preferential binding of polyethylene glycol-coated liposomes containing a novel cationic lipid, TRX-20, to human subendothelial cells *via* chondroitin sulfate, *Pharm. Res.* 18 (2001) 1284–1290.
- [288] J. Liao, K. Hayashi, S. Horikoshi, H. Ushijima, J. Kimura, Y. Tomino, Effect of steroid-liposome on immunohistopathology of IgA nephropathy in ddY mice, *Nephron* 89 (2001) 194–200.

CHAPTER 2

Surface Properties of Liposomes Depending on their Composition

Kimiko Makino^{1,2,*} and Akira Shibata³

¹*Faculty of Pharmaceutical Sciences, Tokyo University of Science, Yamazaki Noda-shi Chiba, 278-8510, Japan*

²*Center for Drug Delivery Research, Tokyo University of Science, Yamazaki Noda-shi Chiba, 278-8510, Japan*

³*Faculty of Pharmaceutical Sciences, The University of Tokushima, Sho-machi Tokushima-shi Tokushima, 770-8505, Japan*

Contents

1. Lipid Diversity and Distribution in Biological Membranes	50
2. Classification and Characterizations of Liposomes	51
2.1. Classification of liposomes	51
2.2. Surface activity of phospholipids	53
2.3. Hydration and conformation of headgroups	54
2.4. Phase transition	57
2.5. Osmotic effects	60
2.6. Electric surface properties of liposomes	63
3. Surface Modification of Liposomal Membranes	67
3.1. <i>In vivo</i> stability	67
3.2. Membrane fusion	70
3.3. Liposome–cell interactions	72
References	74

Abstract

Since the discovery of liposomes in the middle of the 20th century, much attention has been focused on their physicochemical properties and on the liposome design from their potential value as drug carriers in drug delivery systems. Also, from a biological interest, liposomes have been studied as biomimetic cells, since biological membrane is composed of lipids, proteins, and carbohydrates. In this chapter, lipid compositions, shapes of lipids, diversity, and distribution in biological membranes will be discussed in terms of their functions. Physicochemical properties of liposomes, such as hydration of lipid headgroup, size, osmotic effects, and surface charges, which affect the stability and loading efficacy of drugs in liposomes, will be discussed. The modification of liposome surfaces with glycolipids and hydrophilic polymers stabilizes the liposomes and increases the loading efficiency of drugs. By the modification of liposome surfaces with polyethylene glycol (PEG), the circulation time of liposomes after being administered to blood is prolonged, since PEGylated liposomes have an ability to escape from the uptake by reticuloendothelial system. Liposomes, the surfaces of which are modified by hydrophilic polymers, have been studied as injectable

*Corresponding author. Corresponding author. Faculty of Pharmaceutical Sciences, Tokyo University of Science. Yamazaki Noda-shi Chiba, 278-8510, Japan Tel: +81-471-21-3662; Fax: +81-471-21-3662;
E-mail: makino@rs.noda.tus.ac.jp

drug carriers for passive targeting of anticancer drugs to cancer tissue. In addition, positively charged liposomes have recently been studied as DNA transfection agents.

1. LIPID DIVERSITY AND DISTRIBUTION IN BIOLOGICAL MEMBRANES

The biological membrane is a complex aggregate of lipids, proteins, and carbohydrates, formed as a result of non-covalent interactions. The functions of a membrane are determined by its chemical composition, physical state, and mode of organization, all of which are interdependent [1]. Biological membranes contain an astonishing variety of lipids of more than 100 molecular species [2]. Phosphatidylcholine (PC), which is one of the major lipid species of mammalian membranes, forms a stable bilayer. Phosphatidylethanolamine (PE), a second major lipid, has the ability to promote the bilayer-to-hexagonal phase transition that may facilitate membrane fusion. Sphingomyelin (SM) has a molecular shape and hydration properties similar to PC. Cholesterol (Chol) is present in most mammalian membranes, but in very different amounts in different organelles [3]. Chol alone is incapable of forming membrane structures, but in the presence of equimolar proportions with PC stabilizes bilayer structures. Although Chol has several different functions in eukaryotic cells, two of its primary and essential roles are to decrease permeability and increase the stability of membrane bilayers [4,5]. Chol and SM are chemically as well as functionally different, and they colocalize in the same membrane compartment [4]. Lateral assemblies of SM and Chol may function as platforms in membranes for different cellular processes [5]. The glycolipids (GLs), which can also include carbohydrate-containing glycerol-based lipids, form micelles or bilayers and play major roles as cell-surface-associated antigens and recognition factors in eukaryotes [6].

Phospholipid molecules contain different polar head groups and two very hydrophobic hydrocarbon chains. Polar head groups can be zwitterionic, such as PC, PE, and SM or negatively charged, such as phosphatidylinositol (PI), phosphatidylserine (PS), phosphatidylglycerol (PG), phosphatidic acid (PA), and cardiolipin (CL) depending on the pH. Membranes contain a fixed fraction of charged phospholipids. Their charges vary in quantity and distribution within their headgroup regions. The charge distribution determines the extent and type of interaction with foreign molecules at the membrane surface [7]. The two hydrocarbon chains of phospholipid molecules are of different lengths and consist of different degrees of unsaturation. Glycerol-based phospholipids have a saturated fatty acid esterified at the 1-position of the glycerol backbone and an unsaturated fatty acid at the 2-position. In addition, the fatty acid composition shows very large variations mainly with respect to the content of the fatty acids such as C_{16:0}, C_{18:0}, C_{24:0}, and C_{24:1} for bovine brain SMs [8]. These variations affect the physical properties of liposomes, such as thermotropic behavior and osmotic activity.

The lipid bilayer as the main structural feature of the plasma membrane is highly non-homogeneous due to lipid asymmetry. The individual lipid species are distributed over the inner and outer monolayers of membrane bilayers in a highly asymmetrical fashion [9]. The outer monolayer of the bilayer is primarily composed of PC, SM, and glycolipids and the inner monolayer contains PS and PE, with lesser amounts of PC and SM. A general feature of plasma membrane asymmetry is that most of the phospholipids with a net negative charge at physiological pH are located in the cytosolic half of the bilayer. Steric and electrostatic interactions between phospholipid head groups are primarily responsible for the asymmetry [10]. Phospholipids with higher degrees of unsaturation tend to reside preferentially in the outer monolayer.

2. CLASSIFICATION AND CHARACTERIZATIONS OF LIPOSOMES

Owing to their amphiphilic nature, phospholipid molecules have the property of forming spontaneously well-organized bilayer structures in water. The primary driving force behind this phospholipid bilayer formation is the entropy of water due to the change in water structure around the hydrophobic portions of phospholipid molecules. Hydrophobic effect, with $\sim 4 \text{ kJ mol}^{-1}$ per CH_2 group, plays the main role in the stabilization of the lipid bilayer, but the hydrogen bonding and dipole–dipole interactions, with energies of $4\text{--}40 \text{ kJ mol}^{-1}$, are also dominant in the region of the polar headgroups of phospholipid molecules [11].

The types of phospholipids are important for the determination of the exact state of liposomes. Israelachvili *et al.* [12] defined a packing parameter (P) of phospholipid molecules on their organization by the following equation:

$$P = V/SL_c \quad (1)$$

where V is the hydrophobic volume, S the average surface area occupied by the polar region of the amphiphilic molecule at the air/water interface, and L_c the extended length of the hydrophobic region. Cylinder-like phospholipid molecules with packing parameters between 0.8 and 1.1, preferably around 1, will form liposomal bilayer structure, whereas molecules with much lower- or higher-packing parameters will self-assemble as micelles or hexagonal type II (H_{II}) phase, respectively. Changing the composition, temperature, pH, and ionic strength in the medium may lead to change in the packing parameter.

2.1. Classification of liposomes

There are now a large variety of techniques for preparing liposomal systems. Some of the major procedures are summarized in Table 1. Liposomes are mainly classified into four types on the basis of the number of lamellae and size, and they

Table 1. Methods of preparation and characteristics of the liposomes

Method of preparation	Type of liposome	Size (nm)	Reference
Vortexing thin lipid film with aqueous solution	MLV	400–5000	[13,14]
Sonication	SUV	25–50	[15]
French press	SUV	30–50	[16]
Ethanol injection	SUV	30–110	[17]
Detergent dialysis	LUV	100–200	[18,19]
Ether injection	LUV	150–250	[20]
Freeze and thaw	LUV	50–500	[21]
Reversed-phase evaporation	LUV	200–900	[22]
GUV	GUV	5000–50,000	[23,24]

are multilamellar vesicles (MLVs) of large size, small unilamellar vesicles (SUVs) (liposomes) of small size, large unilamellar vesicles (LUVs) of large size, and giant unilamellar vesicles (GUVs) $> 5 \mu\text{m}$ in diameter. MLVs consist of concentric bilayers with water entrapped between the bilayers and have a relatively large diameter ($> 400 \text{ nm}$) [13,14]. Increasing the amount of water incorporated between the bilayers increases the repeat distances and decreases the bilayer thickness. Individual MLVs are rather heterogeneous, and spherical onion-like, oblong, and tubular structures of various sizes coexist. The MLVs have been mainly used for physical studies on bilayer organization and motional properties of individual lipids within a membrane structure. SUVs can be prepared directly from MLVs by sonication [15], passage through French press [16], or ethanol injection [17]. The size of SUVs is in the range 20–50 nm diameter, although it is dependent a little on the type of the lipid that constitutes liposomes. The radius of curvature of SUV is so small that the ratio of the number of lipid molecules in the inner and outer monolayers is approximately 1:2. Therefore, the geometric packing constraints of SUV with large curvature disorder the structural features in comparison with LUV. The LUVs are prepared by the our commonly used methods detergent dilution [18,19], ether injection [20], freezing and thawing [21], and reverse-phase evaporation [22]. The LUVs system is a more useful membrane model and the mean diameter is in the range between 50 and 200 nm. The thermodynamic behaviors of SUV and LUV bilayers differ. This follows from the constraints on packing the lipid molecules in a bilayer membrane with a large radius of curvature. GUVs are also useful as cell models involving proteins or intact cells. The successful preparation of GUVs at ionic strength close to

physiological conditions requires the incorporation of 10–20% of a charged lipid, such as PS, PG, or CL, into PC bilayers [23,24]. The LUVs and GUVs have advantages for stability, trapped volumes, and trapping efficiencies. Characteristics of the liposome variously change in composition, particle sizes, membrane fluidity, and charge of the membrane surface, together with the method of liposome preparation.

2.2. Surface activity of phospholipids

The monolayer of the phospholipid resembles half-bilayer leaflets in the biomembranes and thus serves as an excellent model for the biomembranes, including the nature, stability, and packing characteristics of the phospholipids. When phospholipids are spread onto the subphase water surface, monomolecular layer of well-aligned phospholipid molecules is formed. The hydrophilic group is in contact with water, while their hydrocarbon chains extend above water surface and associate with each other. The alignment of lipid molecules on the water surface significantly decreases the surface tension of water. Amphiphilic character of phospholipids is responsible for the surface activity. The surface area per phospholipid molecule is important in understanding or quantitating the asymmetric distribution of lipids in membranes, lipid diffusivity, interactions between acyl chains and polar head groups, surface charge density, and non-bilayer structures such as the hexagonal phase. The surface area at zero surface pressure in the surface pressure–surface area isotherm can predict the cross-sectional area of closely packed phospholipid molecules in the bilayer membranes [25,26]. Two-dimensional phase transition between solid (condensed) and fluid liquid crystalline phases in phospholipid monolayers has been analyzed in terms of their surface pressure–surface area and area–temperature isotherms [27]. Phospholipid molecules in the monolayer in the fluid state are close to each other and tilt with respect to the subphase surface, whereas the molecules in the solid state are packed as closely as possible and are perpendicular to the subphase surface. The monolayers in the solid state, which are indicated by the almost vertical surface pressure–surface area isotherms, show lower compressibility compared with that in the fluid liquid crystalline state [25,26]. The monolayer phase state is important in determining the extent to which the presence of Chol in mixed monolayer reduces the average molecular packing density of either glycerol-based phospholipids or simple sphingolipids such as galactosylceramide [28]. For the evaluation of miscibility in mixed phospholipid monolayers as functions of composition, chain lengths, and temperature the surface phase rule applies [29]. The lateral diffusion coefficient of the component in mixed monolayers can be estimated from the theory of random walks [30].

2.3. Hydration and conformation of headgroups

In the liposomal membrane, phospholipids are densely packed with their polar heads preferentially oriented parallel to the bilayer plane. The polar region of phospholipid constitutes an interface between the bulk aqueous phase and the hydrophobic core of the membrane and is strongly hydrated. Hydration of the phospholipid head group at the interface loosens the packing in that region due to the weakening of the electrostatic interaction and/or the accommodation of water molecules between adjacent phosphate groups. The extent of the hydration depends on the effective size of the polar part and also the effective molecular geometry [1]. It has been estimated that the thickness of a fluid PC bilayer membrane is $\sim 50 \text{ \AA}$, comprising the hydration layer, polar head group, and hydrocarbon chains [31]. There exists a very steep gradient for relative permittivity ϵ_r in the region of a half-bilayer leaflet of about 25 \AA thickness [32]. The lipid membrane/water interface represents an interface between a bulk aqueous phase of high relative permittivity ($\epsilon_r \approx 78$ at 25°C) and the alkane-like phase which is built up by the lipid hydrocarbon chains of very low relative permittivity ($\epsilon_r \approx 2$). The relative permittivity of water in the immediate vicinity of lipid polar head groups at the interface is estimated at around 20–30.

Zwitterionic PC and PE, as major components of the membrane surface matrix, determine surface global properties characterizing its environment, where other lipids are presented. Choline methyl groups are hydrophobic, and adjacent water molecules are hydrogen-bonded between themselves, forming a hydration shell around the PC head group. It is estimated that about 25–30 water molecules are needed to fully hydrate the choline head group, whereas the ethanolamine head group requires only 10–12 water molecules [33]. The ammonium group of PE readily forms hydrogen bonds with water molecules as well as with the oxygen atom of neighboring molecules phosphate groups.

Negative net charges such as PS, PA, PG, or PI and positive charge such as sphingosine differ in magnitude and location within the interface. Phospholipids with a net negative charge differ with respect to the large quantity of water trapped between adjacent bilayers with motional characteristics of free water from non-charged phospholipids. The ability of charged phospholipid bilayers to incorporate large quantities of water to swell up to bilayers of about 140 \AA (three times larger than the original thickness) is ascribed to electrostatic. The number of water molecules in the hydration shell depends on the phase state of lipids, the types of lipid head groups, acyl chain composition, and the presence of *cis*-double bonds. Dehydration of liposomal membranes induces phase separation [35]. The negatively charged head groups interact stoichiometrically with divalent ions such as Ca^{2+} and displace water molecules hydrogen-bonded to this group. This leads to a tighter packing in the polar group that is propagated to the hydrocarbon chains and to a decrease in bilayer permeability [11]. Dehydration such as that taking place upon the binding of Ca^{2+} to PS in bilayer has a dramatic

effect on the physical state of the phospholipid. In general, the ease with which an isothermal, solution-induced phase transition is induced increases with the relative lipid hydrophobicity. PC, PG, and CL consequently are more susceptible to such transitions than PE, PS, or PA [36]. Charged phospholipids are always more amenable to an isothermal phase transition than the zwitterionic lipids, in the surface charge density-depending manner.

Langner and Kubica [34] have stressed the physiological significance of residual charge distribution within the lipid head group and membrane environment, such as charge, lipid, and water dipoles located within the interface to the effective electrostatic surface potential and the effect of the relative permittivity gradient on local interfacial electrostatics. A schematic drawing of selected lipids of both sides of the plasma membrane, as an example of the biological membrane, is shown in Fig. 1. The inner and outer plasma membranes consist of a substantial amount of zwitterionic lipids (PC, SM, and PE) similar in residual charge distribution, but different otherwise. PC and SM are located on the outer surface, and PE is on the inner surface of the plasma membrane. Zwitterionic lipids of the outer layer have choline moieties in the interface region. Choline groups are well hydrated and do

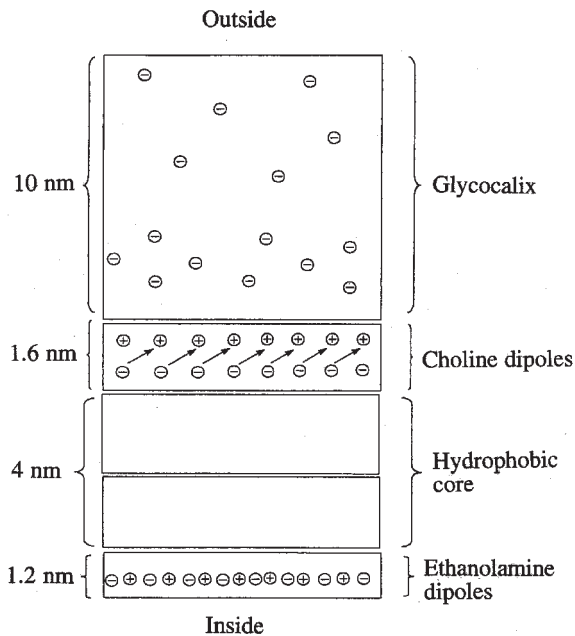


Fig. 1. An electrostatic model of the plasma membrane. Assuming that lipids are mixed, there are no charged lateral domains. The glycocalyx has a spread negative charge associated with the sialic acids of glycolipids and glycoproteins. Under the glycocalyx is the choline region where charge separation induces an electric field associated with P–N dipoles. The uncharged hydrophobic core of the lipid bilayer gives way to the intracellular membrane surface formed predominantly of PE, with ethanolamine groups parallel to the membrane surface [34].

not form hydrogen bonds. The interaction of PC with water molecules induces a cooperative conformational change in the polar group of PC such that the $\text{PO}_4(-)-\text{N}(+)$ dipole of the phosphorylcholine group changes from a conformation coplanar with the bilayer plane to the one in which this dipole is more nearly perpendicular to the bilayer plane. The conformation of the dipole of the PE in the presence of water is coplanar with the bilayer plane, enabling effective charge neutralization between adjacent phosphodiester and ammonium groups [34]. These conformational changes in the polar group are coupled to changes in the packing and molecular motion of the hydrocarbon chains of phospholipids.

For fully hydrated phospholipids, the interfacial region of a fluid phospholipid bilayer membrane comprises a dynamic mixture of various components of phospholipid molecules with very different physical and chemical properties, such as the hydration layer, phosphorylcholine moiety, glycerol backbone, ester carbonyls, and the first methylene segments [31,37]. Figure 2 shows illustration of the methylene/water boundary and the dynamic thickness of a fluid bilayer [31]. Therefore, this region of the bilayer can be generally characterized as one of tumultuous chemical heterogeneity because of the thermal motion of the bilayer.

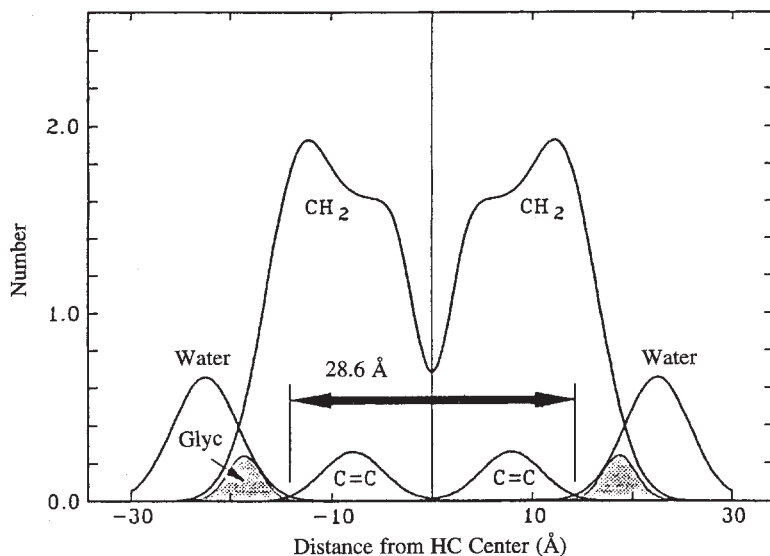


Fig. 2. Illustration of the methylene/water boundary and the dynamic thickness of a fluid bilayer. The glycerol groups precisely mark the water/methylene boundary for DOPC at 66% RH. The large arrow indicates the minimum instantaneous thickness of the bilayer taken as the transbilayer separation of the extreme edges of the water distributions defined by their intersections with the double-bond distributions. This thickness is defined as the dynamic thickness. Here it is 28.6 Å, which is several angstroms smaller than the equivalent hydrocarbon slab thickness. However, as the hydration of the bilayer increases, the dynamic thickness is expected to decrease dramatically. Note that thermal motion causes a small but significant overlap of the water and double-bond distributions [31].

Thus, a molecule binding to the interface should necessarily interact both with the head group as well as the hydrocarbon region. Phospholipids are also free to diffuse laterally in the bilayer plane and polar heads undergo fast vibrational and rotational motions by spontaneous thermal fluctuation. As a consequence, strong interactions exist between lipid polar head groups which, in addition to their dynamics, make feasible the exchange of ions, in particular of protons, between adjacent lipid molecules [32]. This dynamic image of the bilayer may give a clue to the approach for the problem of how molecules in the aqueous phase can penetrate the bilayer. Because of the thermal motion, there can be a higher probability of polar molecules, such as water penetrating, at least transiently, deeper into the hydrocarbon core [31]. The charge density and sign through changes in the phospholipid head groups determine the extent and strength of interaction with associated molecules [38].

2.4. Phase transition

Phospholipids exhibit a variety of phases, depending on the lipid species, composition, and temperature as well as ambient conditions. Phospholipid membrane phases are commonly grouped into crystalline, gel, and fluid liquid crystalline membrane phases. A generalized sequence of thermotropic phase transition for phospholipids that exhibit limiting hydration is indicated by the following (proceeding from low to high temperature) [39]:

$$L_c \rightarrow L_\beta \rightarrow P_{\beta'} \rightarrow L_\alpha \rightarrow Q_{II} \rightarrow H_{II} \quad (2)$$

where L_c is the crystalline phase, L_β the hydrated lamellar gel phase with ordered lipid chains not tilted to the bilayer normal, $P_{\beta'}$ the lamellar gel phase with ordered lipid chains tilted to the bilayer normal, L_α the fluid lamellar liquid crystalline phase, Q_{II} the cubic phase, and H_{II} the hexagonal phase. Not all of these phases and transitions necessarily appear for a single phospholipid. This depends on the molecular structure of the particular phospholipid. In general, the transition from lamellar to non-lamellar phases would be first inverted Q_{II} and then inverted H_{II} .

Both multilamellar and unilamellar liposomes undergo structural changes at the phase transition temperature [40]. These changes do not affect the gross spherical closed bilayer structure of liposomes. The gel-to-liquid crystalline phase transition temperature as well as the enthalpy, entropy, and cooperativity associated with this transition are lower for the SUVs than for the MLVs [39]. The enthalpy of the liposome phase transition, ΔH_t , can be determined from the excess specific heat involved in the transition, measured by differential scanning calorimetry (DSC) [40,41]. The entropy change at the transition, ΔS_t is determined using the following equation:

$$\Delta H_t = T_t \Delta S_t \quad (3)$$

where T_t is the transition temperature.

At the liposome phase transition, the changes in van der Waals interactions, *trans*–*gauche* isomerism, head group interactions, and lipid hydration contribute to the transition enthalpy. In the case of non-lamellar phase transitions, changes in curvature elastic energy and chain packing restrictions also play an important role. The transition entropy is dominated principally by changes in the population of chain rotational isomers, the ordering of water molecules of hydration layer, and by intermolecular contributions [39]. Data for gel-to-fluid liquid crystalline phase transitions of PC [42–47], PE [48,49], and SM [50] are shown in Table 2. For PC, there is an increase in the gel-to-fluid liquid crystalline phase transition temperature by $\sim 20^\circ\text{C}$ as each two-hydrocarbon unit is added and a corresponding increase in enthalpy ($\sim 10\text{ kJ mol}^{-1}$), and the phase transition temperature and enthalpy are significantly sensitive to the head group constituent. Inclusion of double bond for PC molecules results in a remarkable decrease in the transition temperature [47]. The relative position of choline and phosphate groups in the zwitterionic dipalmitoylphosphatidylcholine (DPPC) bilayer may differ between gel and liquid crystalline states. There exist significant differences in the phase behavior and in the physicochemical properties in general of PC and PE as major lipids in biological membranes. For example, the gel-to-liquid crystalline transition temperature is significantly lower for PC than for the analogous PE (Table 2). The L_x – H_{II} phase transition temperature in PEs decreases with increasing hydrocarbon chain length [51]. In addition to an ability to adopt a gel or liquid crystalline bilayer organization, phospholipids can adopt entirely different liquid crystalline structures on hydration and one of their structures is the *hexagonal* H_{II} arrangement, in which all biological membranes contain an appreciable

Table 2. Gel-to-liquid crystalline phase transition for phospholipids in aqueous suspensions

Lipid	T_c ($^\circ\text{C}$)	ΔH (kJ mol^{-1})	Reference
DMPC	24.0, 23.9	22.6, 25.5	[42,43]
DPPC	41.4, 41.7	36.0, 40.5	[42,44]
DSPC	54.1, 55.1	44.3, 43.1	[42,45]
DBPC	75	62.3	[46]
DOPC	–22	31.8	[47]
DLPE	30.5	14.6	[48,49]
DMPE	49.1, 49.0	23.8, 23.8	[48,49]
DPPE	63.0, 63.2	36.8, 36.8	[48,49]
NPSM	41.3	28.5	[50]
NSSM	52.8	74.9	[50]

DMPC, Dimyristoyl phosphatidylcholine; DPPC, Dipalmitoyl phosphatidylcholine; DSPC, Distearoyl phosphatidylcholine; DBPC, Dibehenoyl phosphatidylcholine; DOPC, Dioleoyl phosphatidylcholine; DLPE, Dilauloyl phosphatidylethanolamine; DMPE, Dimyristoyl phosphatidylethanolamine; DPPE, Dipalmitoyl phosphatidylethanolamine; NPSM, *N*-palmitoyl sphingomyelin; NSSM, *N*-stearoyl sphingomyelin.

fraction (up to 40 mol%) of lipid species [52]. PEs form either lamellar or hexagonal (H_{II}) phases depending on temperature, water content, and their hydrocarbon chain composition [53]. Non-lamellar phase formation can be triggered by alteration in lipid hydrocarbon chain length, degree of unsaturation, head groups, hydration, and temperature [54]. The phase behavior of the membrane is also influenced by changes taking place in the interface, such as solute binding. At the phase transition temperature, the compressibility of the membrane is high and there is a maximum in permeability.

Considering complex mixtures of phospholipids in biological membranes, it is of great importance to understand the polymorphic phase behavior of such mixtures in well-defined model systems. These studies have revealed the highly diverse behavior of mixing for phospholipid species in hydrated bilayers from nearly ideal mixing in both liquid crystalline and gel phases [55,56] to limited miscibility [57] or complete immiscibility [58], particularly, in gel phase bilayers. In general, the mixing of a bilayer-forming PC system to H_{II} -forming PE system has the effect of tending to stabilize the lamellar phase [59,60]. For mixtures of PE with charged phospholipids such as PS, PG, and PI [60], the phase behavior is more complicated. For PE/PS mixtures, lowering the pH can induce an L_{α} - H_{II} phase transition [60,61]. For equimolar mixtures of PC with CL, a cubic phase can be induced by low levels of Ca^{2+} [62]. The miscibility of binary PE mixture with different acyl chain lengths is poorer in hydrated bilayer than in non-hydrated bulk phase [63]. Adding SM to PC/PE liposomes enhances outer monolayer packing. Thus, SM stabilizes the lamellar state of PC/PE liposomes. Chol is known to be membrane protective in phospholipid bilayers. Increasing Chol in PC membranes reduces membrane fluidity above and increases it below the transition temperature. Incorporation also of Chol to PC membranes increases lamellar-phase hydrocarbon-chain order [64]. PC/PE/Chol-liposomes are more unstable than PC/PE liposomes and undergo mainly rupture instead of fusion. The addition of the lamellar phase-forming digalactosyl diacylglycerol (DGDG) to the H_{II} phase-forming monogalactosyl diacylglycerol (MGDG) stabilizes the bilayer lamellar phases [65].

Glycosphingolipids (GSLs) are important constituents of membranes of the central nervous system. GSLs exhibit a variety of carbohydrate sequences and composition in the oligosaccharide chain; the fatty acid and long-chain base heterogeneity is more uniform compared to the variations in the polar head group [66]. The oligosaccharide chain has a marked influence on their thermotropic behavior, intermolecular packing, and surface electrical potential [66]. The transition temperature and enthalpy of GSLs decrease proportionally to the complexity of the polar head group and show a linear dependence with the intermolecular spacings. Interactions occurring among GSLs and phospholipids induce changes of the molecular area and surface potential that depend on the type of GSL. Large changes of the molecular free energy, asymmetry ratio, and phase state of the GSLs-containing structure can be triggered by small changes

of the molecular parameters, lipid composition, and lateral surface pressure [66]. The studies on the thermotropic behavior of mixtures of DPPC with natural GSL (galactosylceramide, phrenosine, kersasine, glucosylceramide, lactosylceramide, sulfatide, G_{M3} , G_{M1} , G_{D1a} , and G_{T1b}) in dilute aqueous dispersions over the entire composition range show that the pretransition of DPPC is abolished and the cooperativity of the main transition decreases sharply at mole fractions of GSLs below 0.2 [67]. A limited quantity (1–6 molecules of DPPC per molecule of GLS) can be incorporated into a homogeneously mixed lipid phase. Domains of DPPC, immiscible with the rest of a mixed GSL/DPPC phase that shows no cooperative phase transition, are established as DPPC exceeds a certain proportion in the system.

2.5. Osmotic effects

The addition of water-soluble solutes into liposome suspensions may alter interaction between the phospholipid molecules at the bilayer surface. Thereby, osmotic gradients change the bilayer properties of liposomes such as elastic, permeability, and partition coefficients, perhaps by altering the area per lipid at the membrane surface [68]. The direction and magnitude of the osmotic gradient are closely associated with osmotic gradient-induced bilayer fusion. Under suitable conditions, liposomes are only permeable to water and result in osmotic shrinkage for hypertonic solutions and swelling for hypotonic solutions. The initial water permeability velocity (v_0) through liposomal membranes induced by the hypertonic stress of solute was determined from [69]:

$$v_0 = \{d(1/A)/dt\}_{t=0}/(1/A)_{t=0} \quad (4)$$

where $A_{t=0}$ is the absorbance of liposome suspension extrapolated to the time of solute injection ($t = 0$). Since v_0 is proportional to the initial velocity of volume change of the liposomes, (dV/dt) the following relationship holds [70]

$$v_0 = k(dV/dt)_{t=0} = kP_w SRT\Delta C_s \quad (5)$$

where P_w is the water permeability coefficient, S the surface area of the membrane, ΔC_s the difference between the concentrations of solute outside and inside liposomal membrane, and k a constant. Initial velocity of water permeabilities depends on the nature of the bilayer membranes, the electrolyte gradients, and the presence of additives [68,70]. The effect of the negatively charged CL on the bilayer properties of non-charged PC membranes was studied by monitoring the water permeability of the liposomes (LUVs) caused by osmotic shrinkage in hypertonic glucose solution [71]. Incorporation of small amounts of CL into PC membranes causes a significant decrease in their water permeability associated with stabilization of the membrane structure. The incorporation of CL stabilizes the intermolecular hydrogen-bonded network including water molecules of the hydration layers at the bilayer surface that are important for the stable bilayer

configuration of the PC molecules. The effect of the local anesthetic tetracaine on the water permeability of the phospholipid bilayer has been examined using liposomes composed of various molar ratios of negatively charged CL to non-charged PC by monitoring their osmotic shrinkage in hypertonic glucose solution [72]. Typical time-course of shrinkage of liposomes of CL/PC (2/98, mol/mol) caused by the addition of hypertonic glucose solution is measured as absorbance increase at 450 nm (Fig. 3). A linear relationship is observed between the reciprocal of the absorbance change and the reciprocal of the concentration of glucose at least up to 50 mM, indicating that phospholipids in the liposomes are tightly arranged and the liposomes behave as perfect osmometers. Addition of tetracaine caused slight increase in the optical absorbance at 450 nm (A'_0) owing to slight aggregation of liposomes, and A'_0 became constant after about 2 min. This absorbance is greatly enhanced by hypertonic osmotic shock induced by the addition of 20 mM glucose and the absorbance attains a certain constant level (A_∞) after < 10 min. Increase in the absorbance (A) is associated with shrinkage and/or aggregation of liposomes. The initial velocity of liposome shrinkage (v_0) reflects the barrier ability of the liposomes against water permeation, because the possible effect of liposome aggregation is unlikely in the initial stage of osmotic shock. Therefore, the v_0 value determined from equation (4) may be used as an index of the change in the membrane structure induced by tetracaine. Increase in

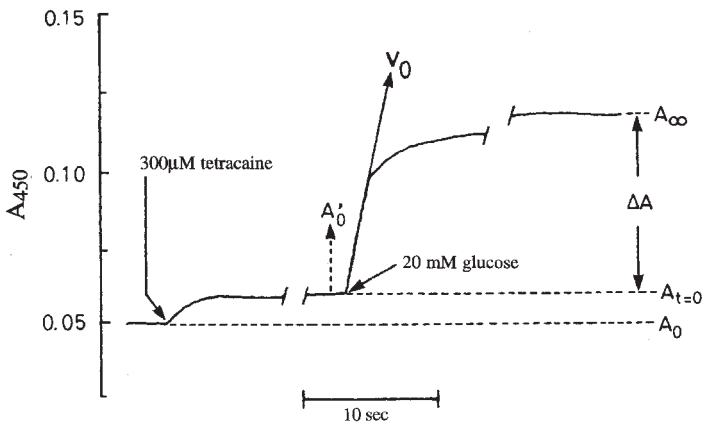


Fig. 3. Typical time course of shrinkage of liposomes of CL/PC (2/98 mol/mol) caused by addition of hypertonic glucose solution measured as absorbance increase at 450 nm. Liposomes are suspended in an isotonic solution of 10 mM Tris-HCl buffer (pH 7.3) containing 300 μ M tetracaine, and incubated for 2 min at 30°C. Then, glucose at a final concentration of 20 mM was added rapidly. Change in the absorbance was monitored, and values of A_0 (absorbance of liposome suspension), A'_0 (absorbance after addition of tetracaine), $A_{t=0}$ (absorbance extrapolated to $t = 0$ just after addition of glucose), and A_∞ (absorbance at the plateau level after glucose addition) are read. v_0 is the initial velocity of absorbance change and ΔA the difference between A_∞ and $A_{t=0}$ [72].

v_0 is dependent on P_w and S , but S would not change greatly on binding of tetracaine under the present experimental conditions in which the concentrations of tetracaine are much lower than those generally used in studies of its effect on membrane lysis. Thus, initial velocity of the absorbance change can be regarded essentially to represent the velocity of water permeation. Figure 4 shows the effects of tetracaine on the permeability of liposomal membranes to water, v_0 , induced by osmotic shock on addition of 20 mM glucose. In the experiments, liposome composed of various molar ratios of negatively charged CL to non-charged PC (CL/PC liposomes) are used. With all liposomes carrying various negative surface charges, there is a distinct concentration of tetracaine that causes a sharp peak of maximum shrinkage of liposomes due to water efflux on hypertonic osmotic shock induced by injection of glucose into the medium. It is noteworthy that below and above the concentration C_{max} of tetracaine, which needs to induce maximum shrinkage, the values of v_0 are almost the same. Thus, at a certain concentration, tetracaine loosens the tight arrangement of phospholipid molecules, allowing water to penetrate rapidly through the phospholipid bilayer according to the osmotic pressure, but at higher concentrations than C_{max} , tetracaine restores the perturbed membrane structure to the

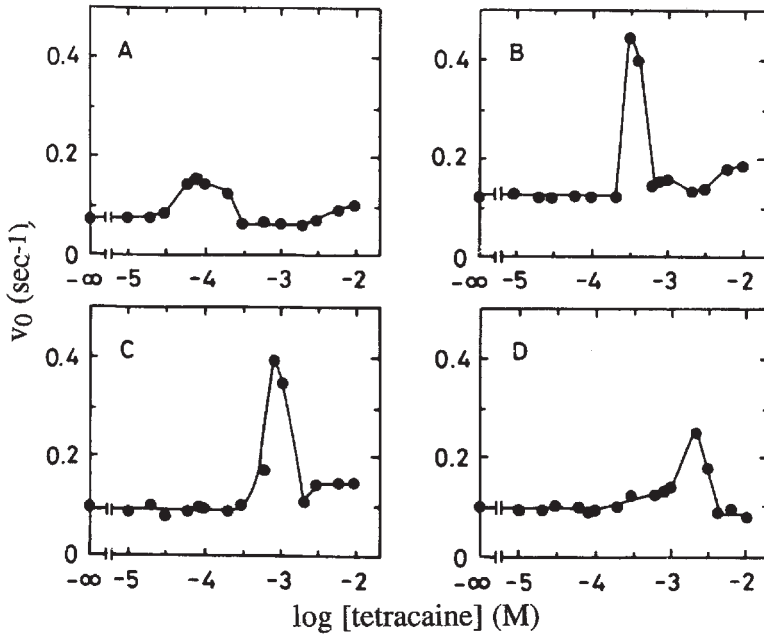


Fig. 4. Effect of tetracaine on the absorbance change of liposome suspension. The initial velocity of shrinkage v_0 is plotted against the tetracaine concentration on a log scale. Experimental conditions are as for Fig. 1. The molar ratios of CL/PC in liposomes are: (A) 0:100; (B) 2:98; (C) 5:95; and (D) 10:90. The value at $-\infty$ indicates that without tetracaine [72].

level in the absence of tetracaine. The finding that A'_0 is almost the same with all liposomes suggests that the binding of tetracaine does not affect the size of liposomes. The value of C_{\max} increases with the increase in the content of the negatively charged CL in the liposomes. The membrane integrity of the mixed PC/CL liposomes is governed mainly by the electrical charge of phospholipid polar headgroups when phospholipid bilayers are in the highly fluid state, and that positively charged amine tetracaine molecules neutralize the negative surface charge of the CL-containing membranes, lowering the barrier for water permeation through the lipid bilayers.

2.6. Electric surface properties of liposomes

The surface properties and structures of liposomes are affected by lipid phase transition, lipid composition, adsorption of small molecules such as ions, local anesthetics, and amphiphilic drugs; and adsorption of polymer molecules such as PEG and proteins, as described in Sections 2.3, 2.4, and 2.5, which could be detected by the usage of microelectrophoretic measurements [73–75]. Zeta potential measurements of liposomes provide us with direct information on the structure of lipid headgroup. From the data of zeta potential measurements, it is possible to predict how the lipid headgroups on the liposome surface move depending on temperature and ionic strength. PC, which is the most commonly used phospholipid to prepare liposomes, is a neutral lipid, having one phosphatidyl group and one choline group in the molecule. The neutral liposomes composed of DPPC, DMPC, and distearylphosphatidylcholine (DSPC) exhibit non-zero zeta potentials in an electric field even when they are dispersed in solution at pH 7.4 [38,76]. In solutions of low-ionic strength, the zeta potential is negative and decreases in magnitude with increasing ionic strength. With further increase in the ionic strength, the zeta potential reverses its sign in some cases. The non-zero mobility of the liposomes in the external electric field can be explained by a model shown in Fig. 5. In the surface area of liposomes, lipid molecules are considered to be arranged in such a way that the hydrophilic groups are located on the surface of liposomes. In this model, changes in the zeta potential caused by the increase of ionic strength are due to a structural change of the headgroup region of the liposomes. The reversal of the zeta potential can be explained with the changes in the direction of the dipole connecting the negative charge of phosphatidyl group and the positive charge of choline group in the headgroup of the lipid molecule [34,77–81], as has been mentioned in Section 2.3. Consider a membrane immersed in an electrolyte solution of bulk concentration n . The membrane has a surface layer of thickness d . In this surface layer, two charge sheets are located parallel to the surface on the membrane core/solution interface at a separation of d , with charge densities σ_1 and σ_2 , respectively, and that one lies on the outer surface with σ_1 and the other on the inner surface with σ_2 .

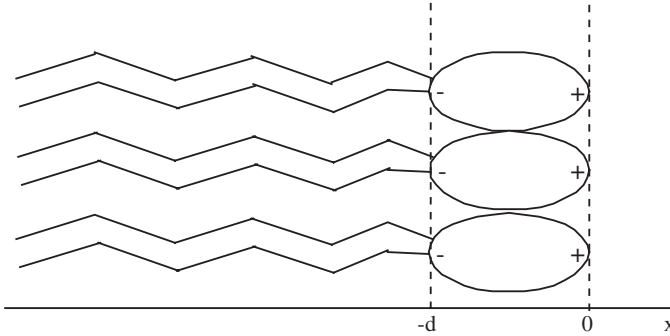


Fig. 5. Schematic representation of the headgroup region [82].

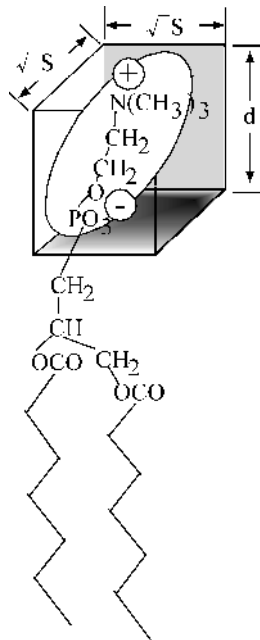


Fig. 6. Lipid headgroup region [82].

Here, $\sigma_1 = -\sigma_2$, since the numbers of negatively charged groups and positively charged groups are equal. Also, the surface area S occupied by one charged group is introduced, as shown in Fig. 6. Then, $\sigma_1 = e/S$ and $\sigma_2 = -e/S$, when the positive sheet faces the bulk solution. Electrolyte ions can penetrate into the region between the two sheets. Solution of the Poisson–Boltzmann equation with the boundary conditions for $\kappa d \ll 1$ give the following equation for d/\sqrt{S} :

$$\frac{d}{\sqrt{S}} = \text{sgn}(\zeta) \sqrt{\frac{2\epsilon_0\epsilon_r|\zeta|}{e\kappa}} \tag{6}$$

where ζ is the zeta potential and $\text{sgn}(\zeta)$ is $+1$ for $\zeta > 0$, and -1 for $\zeta < 0$, κ the Debye–Hückel parameter, e the elementary electric charge, ε_r and ε_0 are the relative permittivity of the electrolyte solution and the permittivity of vacuum, respectively. The separation d is the distance from the position of the choline group to that of the phosphatidyl group in the direction normal to the surface of liposomes. When the actual distance between the phosphatidyl group and choline group is ℓ , the value of d lies between $-\ell$ and $+\ell$ depending on the direction of the headgroup to the surface, as shown in Fig. 7. The values of d/\sqrt{S} are more negative in the solution at lower ionic strength. As the ionic strength increases, the value becomes less negative and changes its sign from negative to positive. The direction of the lipid headgroup changes from stage I to stage III on increasing the ionic strength, as shown in Fig. 8. Also, the direction of the lipid headgroup is sensitive to temperature. At the phase transition temperature of the lipid, the phosphatidyl group lies in the outermost region of the surface and the choline group is in the innermost region. At the temperature where the gel-to-liquid crystalline phase transition occurs, the electrophoretic mobility remarkably changes [82].

Adsorption of ions on liposome surfaces affects the electrophoretic mobility of liposomes. Metal cations adsorb on the surfaces of neutral liposomes composed of PC and change the electrophoretic mobility values.

Monovalent metal cations can reduce the negative surface potential by decreasing the thickness of the diffusion double layer, while multivalent cations can bind to the ionizable groups of acidic lipids forming Stern plate [83–90]. Effects of both mono- and divalent ions upon the bilayer-to-hexagonal phase transition can be explained by ion-binding and preferential hydration. Monovalent cations bind to multilamellar PC/PS vesicles with decreasing association constant in the sequence $\text{Li}^+ > \text{Na}^+ > \text{NH}_4^+ > \text{K}^+ > \text{Rb}^+ > \text{Cs}^+ > \text{tetraethylammonium}^+$ and

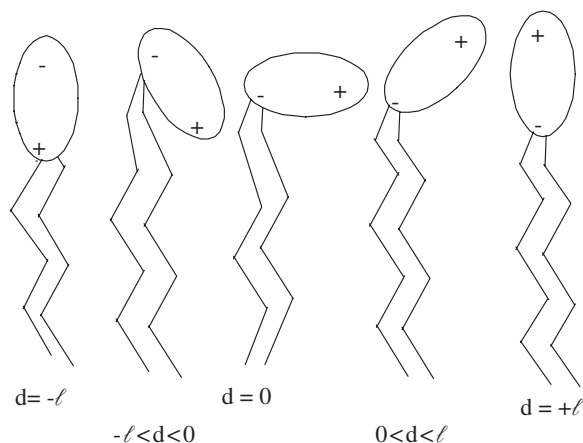


Fig. 7. Model for the conformation of lipid headgroup [82].

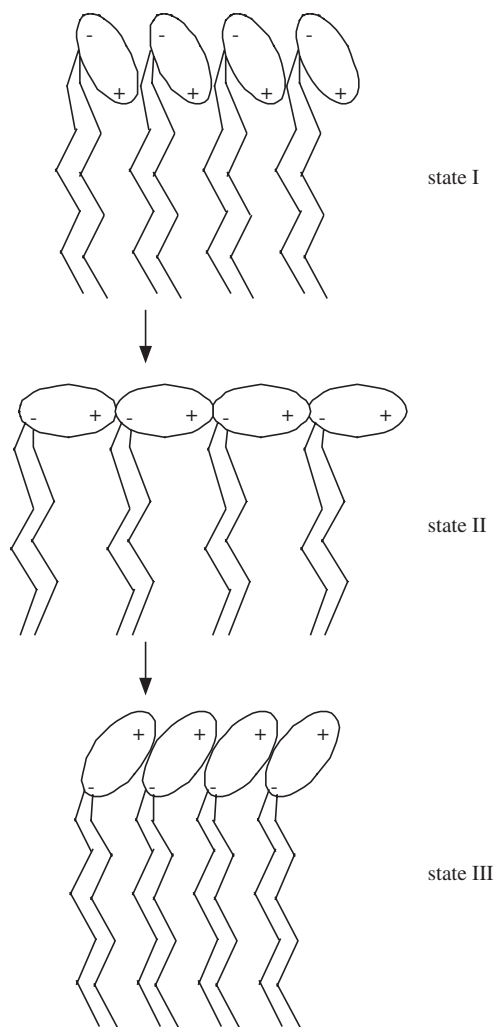


Fig. 8. Changes in the direction of the lipid headgroups depending on ionic strength [82].

tetramethylammonium⁺. Among the alkali metal ions, Li⁺ and Na⁺ belong to the “hydration-structure making” group together with H⁺, OH⁻, and Ca²⁺. On the other hand, K⁺, Rb⁺, and Cs⁺ are called “structure breakers” together with NH₄⁺, Cl⁻, and urea [91]. The binding affinity of divalent cations is reported to be in the sequence of Mn²⁺ > Ca²⁺ > Mg²⁺ [83–85]. Trivalent cations change zeta potential from negative to positive by adsorbing to PC with much higher affinity than the divalent cations [87,92].

Anions also adsorb on the liposome surfaces composed of neutral lipids and then reduce the electrophoretic mobility of these liposomes. The sequence for anion affinities to DMPC liposome surface is reported as follows: trinitrophenol

$> \text{ClO}_4^- > \text{I}^- > \text{SCN}^- > \text{Br}^- > \text{NO}_3^- > \text{Cl}^- \approx \text{SO}_4^{2-}$ [93]. The increase in the negative electrophoretic mobility is observed at the chain-melting temperature, which is related to an increase in maximum charge density rather than a change in the affinity constant with temperature.

The important role of water in the membrane structure is explained by the fact that hydration of lipids leads to significant changes in thermodynamic parameters of their main phase transition depending on headgroup structure, as described in Section 2.3. The ordering of the water molecules at the membrane surface may be the reason of the main part of dipole potential at the membrane boundaries and the hydration forces. The ability of ions to adsorb at the lipid surface seems to correlate with their effects on the dipole ordering with the significant changes in the lipid–lipid interactions and their clusterization [77,94–96].

3. SURFACE MODIFICATION OF LIPOSOMAL MEMBRANES

The surface properties of phospholipid liposomes can be modified in many ways by the incorporation of various types of lipids, proteins, and synthetic amphiphiles into the membrane bilayers [40,97]. The simple modifications without chemical reactions are to vary the composition of the liposome surface by controlling the amount of phospholipid or glycolipids incorporated into the liposomal membranes. Glycolipids are incorporated by anchoring their two acyl chains into the bilayers. Many membrane proteins are anchored to the bilayer with the aid of a fatty acid, such as myristic or palmitic acid, which are covalently linked to the protein [98]. The modifications of liposomal surfaces by a chemical reaction involve anchoring of the macromolecules such as polysaccharides and synthetic polymers to the membrane surface.

3.1. *In vivo* stability

The success in developing stabilized liposomal preparations is due to surface modification of liposome with glycolipids or surface-grafted hydrophilic polymers. The term “stability of liposome” involves chemical stability of the constituents, stability of physical properties, such as size and lamellarity or stability toward cellular uptake in biological fluids [99]. When the surface nature of the liposomes is altered by the lipid molecules with different polar head groups and/or the environmental conditions, such as ionic concentration or temperature, the bilayers can alter the stability and take on various shapes and surfaces [100]. For example, lowering the pH for liposomes consisting of PE/PS mixtures can induce an $L\alpha$ – H_{II} phase transition [60,61].

pH-sensitive liposomes are introduced as a tool to deliver encapsulated drugs to tumors, whose environment is slightly lower in pH than those of normal tissues.

Incorporation of PE as the main lipid component of pH-sensitive liposomes determines the pH sensitivity and capacity to be destabilized and/or fusion at acidic pH [101]. The incorporation of Chol or ganglioside or Chol/hemisuccinate (Chol/HS) can enhance the stability of pH-sensitive liposomes in plasma and serum to deliver the pH-sensitive liposomes to the target cell safely. pH-sensitive liposomes composed of dioleoylphosphatidylethanolamine (DOPE)/Chol-HS as a delivery system for epitope peptides to induce cytotoxic T lymphocyte responses show effective immune response to destroy cancer cells. A pH-sensitive liposome formulation bearing a tertiary alkylated *N*-isopropylacrylamide (NIPAM) copolymer was characterized with regard to its pH responsiveness and its surface property by Roux *et al.* [102]. *In vivo*, the NIPAM-coated liposomes exhibit a prolonged circulation time (1.6-fold longer than the control formulation) in rats.

In general, small Chol-rich liposomes composed of non-charged phospholipids with saturated long alkyl chains exhibit relatively prolonged circulation in plasma [99]. Chol interacts favorably with SMs, whereas its interaction with PCs is much weaker. In the Chol-incorporated SM liposomes, SM can form additional hydrogen bonds and this may confer its special nature. Chol-rich DSPC liposomes show prolonged circulation compared with DPPC. The advantage of DSPC may be because of the increase in the gel to liquid crystalline phase transition temperature. Incorporation of specific natural glycolipids results in prolonged circulation as compared with control liposome compositions [103]. In the use of the liposomes as a material for chemoembolization therapy against cancer, the incorporation of monosialoganglioside GM1 in the bilayer can avoid considerably rapid clearance of liposomes from the circulation by cells of the mononuclear phagocytic system (MPS) [104]. Inclusion of ganglioside in PC/Chol LUVs greatly induces their susceptibility to lysis and contents leakage induced by plasma components. Increasing rigidity decreases interactions of liposomes with high-density lipoproteins and increases circulation times. Surface modification of liposomes by coating with materials such as peptides, saccharides, or block copolymers or by incorporation of specific glycolipids can reduce the uptake by MPS and results in prolonged circulation [105]. The circulation time depends on surface properties such as hydrophobicity [106], charge [107], and fluidity of liposomes [108].

For liposomal delivery systems, PEG-derivatized PE (PEG-PE) provides a synthetic alternative to ganglioside G_{M1} , a naturally occurring glycosylated lipid and contributes to an increase in the circulation time. The PEG-PE significantly affects structure and phase behavior in systems with varying bilayer compositions. The particular efficiency of surface-bonded PEG chains is explained by the steric repulsive barrier around the liposomes provided by the covalently bonded PEG [109,110]. The surface conformations of PEG depend on the surface density and molecular weight of the PEG grafted to the PEGylated lipid molecules in the liposomal membranes [111,112]. The controlling factor is the distance between the PEG chains in the lipid bilayer. Most of the studies with PEG-containing

membranes have been performed with liposomes composed of non-charged lipids such as PC, SM, and Chol. Indeed, the PEG-liposomes containing negatively charged PS bind high amounts of plasma proteins and are removed from the circulation within minutes after *in vivo*. Chiu *et al.* [114] have utilized the well-characterized binding interactions of blood coagulation proteins with negatively charged PS-containing liposomes as a model for evaluating the surface properties of PEG on such liposomes. They demonstrated that incorporating 15 mol% DSPE-PEG 2000 into PS liposomes results in circulation times comparable to that obtained with non-charged liposomes containing 5 mol% DSPE-PEG2000. 15 mol% DSPE-PEG2000 may be effective in protecting PS liposomes from the high-affinity, PS-mediated binding of plasma proteins.

The permeability of liposomes incorporating a range of DPPE-PEG5000 mol% is studied as a function of temperature and liposome composition [115]. The activation energies for glucose permeability decrease from 90 to 23 kJ mol⁻¹. The decrease in the activation energy with increasing temperature is attributed to an increasing number of bilayer defects as the content of PEG-grafted lipid in the liposomes is increased. The permeability of calcein across egg PC or DMPC liposomes containing PEG-DSPE increases with increase in concentration of PEG-DSPE in the liposomes. On the other hand, the permeability decreases with a low amount of PEG-Chol (below 20% Chol-PEG) and increases with a high amount of it. The permeabilities of DPPC/negatively charged dicetylphosphate (DCP) liposomes incorporating hydrophobic peptides (poly(γ -dodecyl-glutamate), poly(benzyl-glutamate), poly(leucine), and poly(valine)) as protein model to glucose have been examined by Shibata *et al.* [116,117]. These polypeptides are obtained from the polymerization of monomeric amino acids in liposome matrix and their secondary structures consist of the mixture of the α -helix and the β -sheet. The permeability is larger for the peptide-incorporated DPPC/DCP liposomes than the control ones without peptide. The bulky side groups of the hydrophobic peptides in the bilayers may perturb the orientation and packing of lipid molecules in the bilayer membranes.

The *in vivo* characteristics of liposomes coated with a polyvinyl alcohol having a long alkyl chain at the end of the molecule (PVA-R) as an injectable drug carrier for passive targeting of drugs have been evaluated by Takeuchi *et al.* [118]. The circulation and distribution of the small unilamellar liposomes (100 nm in diameter) with various lipid compositions, such as the different Chol contents or the different charges, are examined with their intravenous administration in rats. The PVA-R-coated liposomes show significantly prolonged circulation compared to that of non-coated ones. The prolonged circulation of PVA-R-coated liposomes is attributed to their fewer uptakes in liver and spleen. They conclude that not only the hydrophilic property but the sterically stabilizing effect of the coating layer is important in prolonging the circulation of the particulate drug carriers with less MPS uptake. Furthermore, Takeuchi *et al.* [119] prepared mucoadhesive liposomes by coating multilamellar liposomes with Carbopol (CP) or chitosan (CS).

The positively charged multilamellar liposomes (stearylamine (SA)/DPPC) or the negatively charged multilamellar liposomes (DCP/DPPC) could be coated with CP or CS. Mucoadhesive properties of both the resultant polymer-coated liposomes (CP- and CS-liposomes) and the positively or negatively non-coated liposomes (non-liposome) are evaluated using the rat intestine. The order is CS-liposome \geq CP-liposome $>$ positively charged non-liposome $>$ negatively charged non-liposome. The adhesive property of CP-liposome decreases on increasing the medium pH, and this is owing to the electrostatic repulsion between CP-liposome and the mucus layer.

3.2. Membrane fusion

As the major structural components of biomembranes, phospholipids are obviously important in membrane fusion process. The bilayer structures and physical properties, such as bilayer dehydration [120], lipid composition [121,122], lipid packing [123], bilayer curvature [124], and non-bilayer phases [125] contribute to the membrane fusion process. There are at least three distinct steps involved in the molecular mechanism of fusion: membrane aggregation, bilayer destabilization, and then merging of the membrane components. Non-bilayer lipid phases may be indirectly involved in each of these steps. When the temperature exceeds the L_{α} to H_{II} phase transition temperature, T_H , the liposomes undergo a contact-mediated lysis; i.e., the mixing of aqueous contents associated with fusion is abolished. Above T_H , there is also a large amount of lipid mixing as the liposome membranes are transformed to H_{II} phase precursors and the bilayers cease to exist [126]. As is the case with many membranes, H^+ , K^+ -ATPase-rich tubulovesicles in parietal cells are dominated by phospholipids such as PC, PE, PS, PI, and PA. Duman *et al.* [127] demonstrated that tubulovesicles should be triggered to fuse with protein-free liposomes. They examined the ability of tubulovesicles to undergo fusion with PC-based liposomes containing a variety of common membrane lipids of various shapes and charges. Negatively charged lipids such as PS, PA, and PI are best able to enhance liposome-tubulovesicle fusion. The surface charge of liposomes may perturb the lipid organization and structure in the fusing membranes by acting through an electric field at close proximity. The surface charge imparted by the lipids is responsible for the enhancement of liposome fusion. Hydration of the lipid head group is an important parameter in connection with membrane fusion. As the lipid head groups are necessarily hydrophilic, and often charged, a shell of water is associated with the liposomal membrane surface, representing a barrier to membrane fusion [34]. Hydration of biological membranes is strong, because of their high content of PC in which the choline head group is very strongly hydrated [33].

Non-bilayer-forming PE favors interbilayer close approach because of its limited head group hydration and promotes fusion by destabilizing the bilayer state

[128]. PE favors Ca^{2+} -induced fusion of PC/PS LUVs [129] and PEG-mediated fusion of both LUVs and SUVs [130]. The concentration of divalent cations required for the fusion of PS-containing liposomes increases with an increase in the number of liposome [131]. Isothermal induction of crystalline structure by the addition of Ca^{2+} to PS containing liposome systems results in fusion to form the large bilayer structures [132]. In addition, lipids with inverted structure, such as lysophospholipids provide an attractive intermediate structure for fusion. The role of PS in biomembrane fusion is in facilitating the lipid rearrangements required during the fusion process.

E. Haque *et al.* [133] systematically evaluated the PEG-mediated membrane fusion of liposomes using model membranes with complex lipid composition involving dioleoyl phosphatidylcholine (DOPC), DOPE, DOPS, bovine brain SM, and Chol in order to identify lipid compositions that produce highly fusogenic membranes. A liposome system composed of four lipids, DOPC/DOPE/SM/Chol, fuses optimally at a 35/30/15/20 molar ratio in the presence of PEG. Each lipid in liposome plays a part in optimizing the membrane for fusion. PE disrupts the outer monolayer packing and enhances fusion and rupture, without significantly altering the interbilayer approach. An optimal ratio of DOPC/DOPE (35/30) produces a balance between fusion and rupture. Chol destabilizes PE and PC/PE bilayers. Chol induces the formation of H_{II} in preference to the lamellar phase and also negative curvature in DOPC and DOPE monolayers [134]. Adding SM to PC/PE liposomes dramatically reduces both fusion and rupture. In addition, liposomes composed of PC/SM/Chol are non-fusogenic even at high PEG concentrations. Chol and SM, when present at an optimal ratio of 7/6 in liposomes containing the optimal PC/PE ratio, reduce rupture without significantly reducing fusion. The optimal SM/Chol ratio (3/4) also enhances outer monolayer packing. SM alone reduces both rupture and fusion.

Positively charged phospholipid derivative ethylphosphatidylcholine, EDOPC, recently developed as DNA transfection agents, forms bilayers indistinguishable from those of natural phospholipids and undergoes fusion with negatively charged POPG bilayers [135]. Membrane fusion could also be involved in the actual formation of lipoplexes from liposomes and DNA and, indeed, addition of DNA or anionic electrolytes to cationic amphiphile dispersions leads to considerable membrane mixing. An extensive group of experiments has been done to characterize lipid mixing between oppositely charged membranes as a function of surface charge densities on one set of liposomes, the other set of liposomes being fully charged, both positively as well as negatively. Lipid mixing between EDOPC and DOPG liposomes can be significant between highly charged cationic liposomes and weakly charged anionic liposomes, especially at high ionic strength. DOPG/EDOPC (1:1) dispersions with no net charge undergo lipid mixing with cationic liposomes; surface heterogeneity and/or phase polymorphism may account for the unusual behavior of DOPG/EDOPC mixtures.

3.3. Liposome–cell interactions

Many reports have demonstrated the delivery of biologically active agents to cells with a variety of liposomal formulations [136–138]. Papisov [137] has evaluated the relationship between liposome structure and pharmacokinetics on the basis of the mechanistic analysis of each elementary process of liposome transfer and interactions with biological milieu. Interaction of liposomes with cells and blood proteins, mass transfer models, and effects of boundary diffuse layer resulting from surface modification provide quantitative approaches to relating the observed biological effects to structural factors such as size, charge, rigidity, and headgroup composition.

The interactions of various types of liposomes with hepatocytes have been examined in detail by Scherphof and Kamps [138]. Large PS-containing liposomes of 200–400 nm diameter accumulate to a substantial proportion in the hepatocytes. However, this is not observed for those liposomes in which the PS-containing liposomes is replaced by PG. The difference between PS- and PG-liposomes is explained by the following mechanism: PS-liposomes are somehow forced through the fenestration by a mechanism that does not apply to PG-liposomes. The probability of this mechanism is enhanced by demonstrating that *in vivo* uptake of large PS-containing liposomes by hepatocytes is greatly reduced when the highly unsaturated brain-PS is replaced by the fully saturated DSPS and, likewise, the egg PC by DSPC. These far more rigid liposomes apparently are not able to cross the endothelial barrier in the liver and therefore do not gain access to the hepatocytes. It is likely that the liposomes need to be deformed when passing through the fenestrations. Lack of deformability, as a result of increased rigidity, will deny access of liposomes to the hepatocytes. A structure on the endothelial surface recognizes the PS moiety of the liposomes, but does not bind it strongly enough to result in an irreversible interaction. Such a structure could be the scavenger receptor that specifically recognizes, binds, and internalizes the negatively charged PS liposomes in the absence of serum.

In order to optimize the intracellular delivery of drugs to cells, methods are required for increasing the uptake of liposomes into cells. Recently Fenske *et al.* [139] demonstrated a new method for enhancing the interaction of liposomes with cells using a novel class of cationic PEG-lipid (CPL) conjugates. This is a non-specific targeting approach that involves increasing the electrostatic attraction between liposomes and cells by the incorporation of positively charged lipid molecules into preformed vesicles. The positively charged molecules are novel structures wherein a cationic head group (containing 1–4 positive charges) is separated from the phospholipid anchor and thus from the liposome surface by a flexible, hydrophilic polymer, in this case PEG. A novel class of cationic PEG-lipid (CPL) conjugates has been characterized for its ability to insert into preformed vesicles and enhance *in vitro* cellular binding and uptake of neutral and sterically

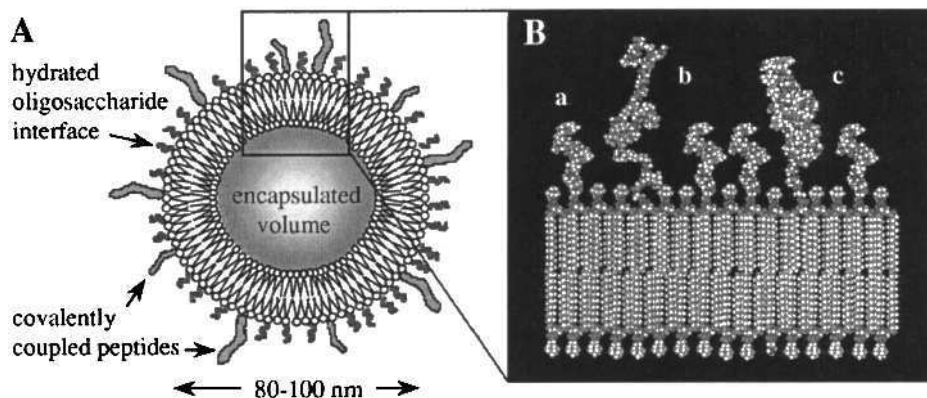


Fig. 9. Molecular schematic of a surface-modified liposomal drug delivery vehicle for intravascular targeting. (A) The liposome surface consists of a glycocalyx-like oligosaccharide layer to minimize non-specific interactions and peptide ligands to mediate selective receptor targeting. (B) Composite molecular model showing glycolipids hydrating the surface of the phospholipid bilayer (a), an RDG peptide coupled to the liposome through a poly(ethylene oxide) spacer (b), and a hypothetical coagulation factor VII peptide for targeting tissue factor (TF) on vascular endothelial cells (c) [140].

stabilized DOPE/DODAC/PEGCerC₂₀ liposomes. Five types of CPL with 1–4 positive charges in the headgroup insert into the external leaflet of the LUVs in a manner dependent on temperature, time, CPL/lipid ratio, and LUV composition. The presence of CPLs in LUVs results in dramatic increases in the binding and uptake of vesicles by BHK cells *in vitro*.

Lestini *et al.* [140] have considered three components of liposome design as drug delivery liposomes: (1) identification of candidate cell surface receptors for targeting; (2) identification of ligands that maintain binding specificity and affinity; and (3) prevention of rapid non-specific clearance of liposomes into the reticuloendothelial organs. They have presented their work on developing liposomal surface modifications that address both targeting specificity and liposome longevity. Such a liposome design is depicted in Fig. 9. An arginine–glycine–aspartic acid (RDG)-containing peptide is used as a model ligand to target liposomes to the integrin GPIIb-IIIa on activated platelets. Liposomes containing an RGD peptide bind to activated platelets, while apparently avoiding platelet aggregation owing to modest affinity of the peptide. With respect to the oligosaccharide incorporated into liposomes, liposome clearance rates are sensitive to changes in liposome diameter caused by the incorporation of surfactants into the lipid bilayer. Therefore, in the design of liposomal surface modifications meant to alter liposome circulation times, molecular geometry must be carefully controlled to provide sufficient surface coverage without disrupting liposome structure.

REFERENCES

- [1] P.K.J. Kinnunen, A. Kõiv, J.Y.A. Lehtönen, M. Rytomaa, *Chem. Phys. Lipids* 73 (1994) 181–207.
- [2] L.L.L. van Deenen, J. de Gier, in: D. Surgenor, (Ed.), *The Red Blood Cell*, Academic Press, New York, 1974, pp. 147–213.
- [3] S. Raffy, J. Teissie, *Biophys. J.* 76 (1999) 2072–2080.
- [4] T.J. McIntosh, S.A. Simon, D. Needham, C.H. Huang, *Biochemistry* 24 (1985) 8–14.
- [5] T. Harder, K. Simons, *Curr. Opin. Cell. Biol.* 9 (1997) 534–542.
- [6] B. Libin, D. Chiu, in: J.R. Sheppard, V.A. Anderson, J.W. Eaton (Eds.), *Membrane and Genetic Disease*, Alan R. Liss, New York, 1982, pp. 137–164.
- [7] Y. Feng, Z.-W. Yu, P.J. Quinn, *Chem. Phys. Lipids* 114 (2002) 149–157.
- [8] Y. Barenholz, in: M. Sinitzky, (Ed.), *Physiology of Membrane Fluidity*, Vol. 1, CRC Press, Boca Raton, FL, 1984, pp. 131–173.
- [9] P.R. Cullis, M.J. Hope, in: D.E. Vance, J.E. Vance (Eds.), *Biochemistry of Lipids and Membranes*, The Benjamin/Cummings Publishing Company, California, 1985, pp. 25–72.
- [10] J.A. Berden, N.W. Barber, G.K. Radda, *Biochim. Biophys. Acta* 375 (1975) 186–208.
- [11] H. Hauser, in: F. Franks, (Ed.), *Water: A Comprehensive Treatise*, Plenum Press, New York, 1975, pp. 209–297, Chapter 4.
- [12] J.N. Israelachvili, S. Maceljia, R.G. Horn, Q. Rev. *Biophys.* 13 (1980) 121–200.
- [13] A.D. Bangham, M.M. Standish, J.C. Watkins, *J. Mol. Biol.* 13 (1965) 238–252.
- [14] S.C. Kinsky, in: S. Fleischer, L. Parker (Eds.), *Methods in Enzymology*, Vol. 32, Academic Press, New York, 1974, pp. 501–513.
- [15] C. Huang, *Biochemistry* 8 (1969) 344–352.
- [16] Y. Barenholz, S. Amselem, D. Lichtenberg, *FEBS Lett* 99 (1979) 210–214.
- [17] J.M.H. Kremer, M.W.J.v.d. Esker, C. Pathmanoharan, P.H. Wiersema, *Biochemistry* 16 (1977) 3932–3935.
- [18] L.T. Mimms, G. Zampighi, Y. Nozaki, C. Tanford, J.A. Reynolds, *Biochemistry* 20 (1981) 833–840.
- [19] O. Zumbuehl, H.G. Weder, *Biochim. Biophys. Acta* 640 (1981) 252–262.
- [20] D.W. Deamer, *Ann. New York Acad. Sci.* 308 (1978) 250–257.
- [21] U. Pick, *Arch. Biochem. Biophys.* 212 (1981) 186–194.
- [22] F. Szoka, D. Papahadjopoulos, *Proc. Natl. Acad. Sci. USA* 75 (1978) 4194–4198.
- [23] N. Oku, J.F. Scheerer, R.C. MacDonald, *Biochim. Biophys. Acta* 692 (1982) 384–388.
- [24] A. Moscho, O. Orwar, D.T. Chiu, B.P. Modi, R.N. Zare, *Proc. Natl. Acad. Sci. USA* 93 (1996) 11443–11447.
- [25] J.T. McIntosh, S.A. Simon, *Biochemistry* 25 (1986) 4948–4956.
- [26] J.H. Fendler, *Membrane Mimetic Chemistry*, Wiley, New York, 1982, pp. 78–99, Chapter 4.
- [27] O. Albrecht, H. Gruler, E. Sackman, *J. Phys. (Orsay, France)* 39 (1978) 301–313.
- [28] S. Ali, J.M. Smaby, H.L. Brockman, R.E. Brown, *Biochemistry* 33 (1994) 2900–2906.
- [29] G.L. Gaines Jr., *Insoluble Monolayers at Liquid–Gas Interfaces*, Interscience Publishers, New York, 1966, pp. 281–299, Chapter 6.
- [30] T. Loughram, M.D. Hatlee, L.K. Patterson, J.J. Kozak, *J. Chem. Phys.* 72 (1980) 5791–5797.
- [31] M.C. Wiener, S.H. White, *Biophys. J.* 61 (1992) 434–447.
- [32] J.F. Tocanne, J. Teissie, *Biochim. Biophys. Acta* 1031 (1990) 111–142.
- [33] K.V. Damodaran, K.M. Merz, *Biophys. J.* 66 (1994) 1076–1087.
- [34] M. Langner, K. Kubica, *Chem. Phys. Lipids* 101 (1999) 3–35.
- [35] J.Y.A. Lehtonen, P.K.J. Kinnunen, *Biophys. J.* 68 (1995) 525–535.
- [36] G. Cevc, *Chem. Phys. Lipids* 57 (1991) 293–307.
- [37] R.E. Jacobs, S.H. White, *Biochemistry* 28 (1989) 3421–3437.

- [38] M.N. Jones, *Adv. Colloid Interf. Sci.* 54 (1995) 93–128.
- [39] D. Marsh, *Chem. Phys. Lipids* 57 (1991) 109–120.
- [40] J.H. Fendler, *Membrane Mimetic Chemistry*, Wiley, New York, 1982, pp. 113–183, Chapter 6.
- [41] A.G. Lee, *Biochim. Biophys. Acta* 472 (1977) 237–281.
- [42] D.A. Wilkinson, J.F. Nagle, in: C.G. Knight, (Ed.), *Liposomes*, Elsevier, North-Holland, Biomedical Press, Amsterdam, 1981, pp. 273–298.
- [43] J. Stümpel, A. Nicksch, H. Eible, *Biochemistry* 20 (1981) 662–665.
- [44] H.J. Hinz, J.M. Sturtevant, *J. Biol. Chem.* 247 (1972) 6071–6075.
- [45] J.T. Mason, C.-H. Huang, R.L. Biltonen, *Biochemistry* 20 (1981) 6086–6092.
- [46] M.C. Phillips, R.M. Williams, D. Chapman, *Chem. Phys. Lipids* 3 (1969) 234–244.
- [47] D. Chapman, J. Urbina, K.M. Keough, *J. Biol. Chem.* 249 (1974) 2512–2521.
- [48] D.A. Wilkinson, J.F. Nagle, *Biochemistry* 20 (1981) 187–192.
- [49] H.H. Mantsch, S.C. Hsi, K.W. Butler, D.G. Cameron, *Biochim. Biophys. Acta* 728 (1983) 325–330.
- [50] Y. Barenholz, J. Suurkuusk, D. Mountcastle, T.E. Thompson, R.L. Biltonen, *Biochemistry* 15 (1976) 2441–2447.
- [51] J.M. Seddon, G. Cevc, R.D. Kaye, D. Marsh, *Biochemistry* 23 (1984) 2634–2644.
- [52] P.R. Cullis, B. De Kruijff, M.J. Hope, A.J. Verkleij, R. Nayar, S.B. Farren, C.P.S. Tilcock, *Structural properties of lipids and their functional roles in biological membranes*. in: R.C. Aloia (Ed.), *Membrane Fluidity in Biology*, Vol. 1, Academic Press, New York, 1983, pp. 39–81.
- [53] R.N. Lewis, R.N. McElhaney, *Biophys. J.* 64 (1993) 1081–1096.
- [54] P.R. Cullis, M.J. Hope, C.P. Tilcock, *Chem. Phys. Lipids* 40 (1986) 127–144.
- [55] H.D. Dorfler, G. Brezesinski, P. Miethe, *Chem. Phys. Lipid* 48 (1988) 245–254.
- [56] S. Ali, H.-N. Lin, R. Bittman, C.-H. Huang, *Biochemistry* 28 (1989) 522–528.
- [57] I.V. Polozov, J.G. Molotkovsky, L.D. Bergelson, *Chem. Phys. Lipids* 69 (1994) 209–218.
- [58] J.W. Brauner, R. Mendelsohn, *Biochim. Biophys. Acta* 861 (1986) 16–24.
- [59] M.W. Tate, S.M. Gruner, *Biochemistry* 26 (1987) 231–236.
- [60] R.M. Epand, R. Bottega, *Biochim. Biophys. Acta* 944 (1988) 144–154.
- [61] C.P.S. Tilcock, P.R. Cullis, *Biochim. Biophys. Acta* 641 (1981) 189–201.
- [62] B. De Kruijff, A.J. Verkleij, J. Leunissen-Bijvelt, C.J.A. Van Echteld, J. Hille, H. Rijnbout, *Biochim. Biophys. Acta* 693 (1982) 1–12.
- [63] Y. Nibu, T. Inoue, *Chem. Phys. Lipids* 76 (1995) 159–169.
- [64] J.A. Barry, K. Gawrisch, *Biochemistry* 34 (1995) 8852–8860.
- [65] A. Khan, L. Rilfors, Å. Wielslander, G. Lindblom, *Eur. J. Biochem.* 116 (1981) 215–220.
- [66] B. Maggio, G.D. Fidelio, F.A. Cumar, R.K. Yu, *Chem. Phys. Lipids* 42 (1986) 49–63.
- [67] B. Maggio, T. Ariga, J.M. Sturtevant, R.K. Yu, *Biochemistry* 24 (1985) 1084–1092.
- [68] S.M. Gruner, *Materials properties of liposomal bilayers*. in: M.J. Ostro, (Ed.), *Liposomes: From Biophysics to Therapeutics*, Marcel Dekker, New York, 1987, pp. 1–34, Chapter 1
- [69] M.C. Blok, L.L.M. Van Deenen, J. De Gier, *Biochim. Biophys. Acta* 433 (1976) 1–12.
- [70] T. Inoue, H. Kamaya, I. Ueda, *Biochim. Biophys. Acta* 812 (1985) 393–401.
- [71] A. Shibata, K. Ikawa, T. Shimooka, H. Terada, *Biochim. Biophys. Acta* 1192 (1994) 71–78.
- [72] T. Shimooka, A. Shibata, H. Terada, *Biochim. Biophys. Acta* 1104 (1992) 261–268.
- [73] D.G. Fatouros, S.G. Antimisiaris, *J. Colloid Interf. Sci.* 251 (2002) 271–277.
- [74] J.A. Cohen, V.A. Khorosheva, *Colloids Surf. A Physicochem. Eng. Aspects* 195 (2001) 113–127.
- [75] K. Ahmed, P.W. Muiruri, G.H. Jones, M.J. Scott, M.N. Jones, *Colloids Surf. A Physicochem. Eng. Aspects* 194 (2001) 287–296.
- [76] H. Matsumura, K. Furusawa, *Phospholipid membranes*, in: H. Ohshima and K. Furusawa (Eds.), *Electrical Phenomena at Interfaces, Fundamentals, Measurements*,

- and Applications, 2nd edition, Revised and Expanded, Marcel Dekker, New York, 1998, pp. 519–533.
- [77] G. Cevc, *Biochemistry* 26 (1987) 6305–6310.
- [78] K.C. Sehgal, W.F. Pickard, C.M. Jackson, *Biochim. Biophys. Acta* 552 (1979) 11–22.
- [79] V. Vogel, D. Möbius, *Thin Solid Films* 159 (1988) 73–81.
- [80] V. Vogel, D. Möbius, *J. Colloid Interf. Sci.* 126 (1988) 408–420.
- [81] C.M. Roland, M.J. Zuckermann, A. Geogallas, *J. Chem. Phys.* 86 (1987) 5852–5858.
- [82] K. Makino, T. Yamada, M. Kimura, T. Oka, H. Ohshima, T. Kondo, *Biophys. Chem.* 41 (1991) 175–183.
- [83] D. Papahadjopoulos, *Biochim. Biophys. Acta* 163 (1968) 240–254.
- [84] T. Seimiya, S. Ohki, *Biochim. Biophys. Acta* 298 (1973) 546–561.
- [85] S. Ohki, R. Sauve, *Biochim. Biophys. Acta* 511 (1978) 377–387.
- [86] K. Hammond, M.D. Roboiras, I.G. Lyle, M.N. Jones, *Colloids Surf.* 10 (1984) 143–153.
- [87] M.D. Roboiras, M.N. Jones, *Colloids Surf.* 15 (1985) 239–247.
- [88] R.H. Ottewill, M.C. Rastogi, A. Watanabe, *Trans. Farad. Soc.* 56 (1960) 854–865.
- [89] R.H. Ottewill, A. Watanabe, *Kolloid-Z.* 170 (1960) 132–139.
- [90] K. Furusawa, H. Kakoki, H. Matsumura, *Bull. Chem. Soc. Jpn.* 57 (1984) 3413–3418.
- [91] R. Kraayenhof, G.J. Sterk, H.W. Wong Fong Sang, K. Krab, R.M. Epand, *Biochim. Biophys. Acta* 1282 (1996) 293–302.
- [92] M.A. Akeson, D.N. Nunns, R.G. Burau, *Biochim. Biophys. Acta* 986 (1989) 33–40.
- [93] S.A. Tatulian, *Biochim. Biophys. Acta* 736 (1983) 189–195.
- [94] S.A. Simon, C.A. Fink, A.K. Kenworthy, T.J. McIntosh, *Biophys. J.* 59 (1991) 538–546.
- [95] K. Gawrish, D. Ruston, J. Zimmerberg, A. Parsegian, R.P. Rand, N. Fuller, *Biophys. J.* 61 (1992) 1213–1223.
- [96] Y.A. Ermakov, S.S. Makhmudova, A.Z. Averbakh, *Colloids Surf. A Physicochem. Eng. Aspects* 140 (1998) 13–22.
- [97] M.N. Jones, *Adv. Drug Deliv. Rev.* 13 (1994) 215–249.
- [98] H.P. Haagsman, R.V. Diemel, *Comparative Biochem. Physiol. Part A* 129 (2001) 91–108.
- [99] M.C. Woodle, D.D. Lasic, *Biochim. Biophys. Acta* 1113 (1992) 175–199.
- [100] S. Ohki, K. Arnold, *Methods Enzymol.* 367 (2003) 253–268.
- [101] J.-S. Chang, M.-J. Choi, *Methods Enzymol.* 373 (2003) 127–137.
- [102] E. Roux, R. Stomp, S. Giasson, M. Pezolet, P. Moreau, J.-H. Leroux, *J. Pharm. Sci.* 91 (2002) 1795–1802.
- [103] G. Scherphof, J. Damen, J. Wilschut, in: G. Gregoriadis, (Ed.), *Liposome Technology*, Vol. 3, CRC Press, Boca Raton, FL, 1981, pp. 205–224.
- [104] T.M. Allen, A. Chonn, *FEBS Lett.* 223 (1987) 42–46.
- [105] J.H. Senior, *Crit. Rev. Ther. Drug Carrier Syst.* 2 (1987) 123–193.
- [106] T. Ishida, K. Funato, S. Kojima, R. Yoda, H. Kiwada, *Int. J. Pharm.* 156 (1997) 27–37.
- [107] A. Choun, P.R. Cullis, D.V. Devine, *J. Immunol.* 146 (1991) 4234–4241.
- [108] H.M. Patel, *Crit. Rev. Ther. Drug Carrier Syst.* 9 (1992) 39–90.
- [109] K. Hristova, A.K. Kenworthy, T.J. McIntosh, *Macromolecules* 28 (1995) 7693–7699.
- [110] F.K. Bedu-Addo, L. Huang, *Adv. Drug Delivery Rev.* 16 (1995) 235–247.
- [111] D. Needham, N. Stoicheva, D.V. Zhelev, *Biophys. J.* 73 (1997) 2615–2629.
- [112] H. Du, P. Chandaloy, S.W. Hui, *Biochim. Biophys. Acta* 1326 (1997) 236–248.
- [113] A. Klibanov, K. Maruyama, A.M. Beckerleg, V.P. Torchilin, L. Huang, *Biochim. Biophys. Acta* 1062 (1992) 142–148.
- [114] G.N.C. Chiu, M.B. Bally, L.D. Mayer, *Biochim. Biophys. Acta* 1510 (2001) 56–69.

- [115] A.R. Nicholas, M.J. Scott, N.I. Kennedy, M.N. Jones, *Biochim. Biophys. Acta* 1463 (2000) 167–178.
- [116] A. Shibata, S. Yamashita, Y. Ito, T. Yamashita, *Biochim. Biophys. Acta* 854 (1986) 147–150.
- [117] A. Shibata, K. Nakajima, S. Ueno, T. Yamashita, *Chem. Pharm. Bull.* 42 (1994) 1151–1153.
- [118] H. Takeuchi, H. Kojima, H. Yamamoto, Y. Kawashima, *J. Controlled Release* 68 (2000) 195–205.
- [119] H. Takeuchi, Y. Matsui, H. Yamamoto, Y. Kawashima, *J. Controlled Release* 86 (2003) 235–242.
- [120] H. Wu, L. Zheng, B.R. Lentz, *Biochemistry* 35 (1996) 12602–12611.
- [121] T.G. Brock, K. Nagaprakash, D.I. Margolis, J.E. Smolen, *J. Membr. Biol.* 141 (1994) 139–148.
- [122] I. Martin, J.M. Ruyschaert, *FEBS Lett.* 405 (1997) 351–355.
- [123] J. Lee, B.R. Lentz, *Biochemistry* 36 (1997) 421–431.
- [124] S. Nir, J. Wilschut, J. Bentz, *Biochim. Biophys. Acta* 688 (1982) 275–278.
- [125] H. Ellens, D.P. Siegel, D. Alford, P.L. Yeagle, L. Boni, L.J. Lis, P.J. Quinn, J. Bentz, *Biochemistry* 28 (1989) 3692–3703.
- [126] J. Bentz, H. Ellens, F.C. Szoka, *Biochemistry* 26 (1987) 2105–2116.
- [127] J.G. Duman, Elasa Lee, G.Y. Lee, G. Singh, J.G. Forte, *Biochemistry* 43 (2004) 7924–7939.
- [128] J. Marra, J. Israelachvili, *Biochemistry* 24 (1985) 4608–4618.
- [129] N. Duzgunes, J. Wilschut, R. Fraley, D. Papahadjopoulos, *Biochim. Biophys. Acta* 642 (1981) 182–195.
- [130] Q. Yang, Y. Gui, L. Li, S.W. Hui, *Biophys. J.* 73 (1997) 277–282.
- [131] S. Ohki, *J. Membr. Biol.* 77 (1984) 265–275.
- [132] D. Papahadjopoulos, G. Poste, W.J. Vail, *Studies on membrane fusion with natural and model membranes in: E.D. Korn (Ed.), Methods in Membrane Biology, Vol. 10, Plenum, New York, 1978, pp. 1–121.*
- [133] M.D. Emdadul Haque, T.J. McIntosh, B.R. Lentz, *Biochemistry* 40 (2001) 4340–4348.
- [134] Z. Chen, R.P. Rand, *Biophys. J.* 73 (1997) 267–276.
- [135] D.P. Pantazatos, S.P. Pantazatos, R.C. MacDonald, *J. Membr. Biol.* 194 (2003) 129–139.
- [136] K. Balasubramanian, A.J. Schroit, *J. Biol. Chem.* 273 (1998) 29272–29277.
- [137] M.I. Papisov, *Adv. Drug Delivery Rev.* 32 (1998) 119–138.
- [138] G.L. Scherphof, J.A.A.M. Kamps, *Prog. Lipid Res.* 40 (2001) 149–166.
- [139] D.B. Fenske, L.R. Palmer, T. Chen, K.F. Wong, P.R. Cullis, *Biochim. Biophys. Acta* 1512 (2001) 259–272.
- [140] B.J. Lestini, S.M. Sagnella, Z. Xu, M.S. Shive, N.J. Richter, J. Jayaseharan, A.J. Case, K. Kottke-Marchant, J.M. Anderson, R.E. Marchant, *J. Controlled Release* 78 (2002) 235–247.

This page intentionally left blank

CHAPTER 3

Interactions of Al and Related Metals with Membrane Phospholipids: Consequences on Membrane Physical Properties

Patricia I. Oteiza^{1,2,*} and Sandra V. Verstraeten²

¹Departments of Nutrition and Environmental Toxicology, University of California, Davis, CA 95616, USA

²Department of Biological Chemistry, IQUIFIB (UBA-CONICET), School of Pharmacy and Biochemistry, University of Buenos Aires, Junín 956, C1113AAD, Buenos Aires, Argentina

Contents

1. Aluminum and Related Cations: General Properties	81
2. Effects of Al and Related Cations on Membrane Physical Properties	82
2.1. Studies in synthetic membranes (liposomes)	82
2.1.1. <i>trans</i> -interactions	83
2.1.2. <i>cis</i> -interactions	84
2.2. Studies in biological membranes	88
3. Relationship between Al-Mediated Changes in Membrane Physical Properties and Membrane-Associated Processes	90
3.1. Lipid oxidation	90
3.1.1. Effects on Fe ²⁺ -initiated lipid oxidation	91
3.1.2. Membrane-independent effects in the pro-oxidant action of Al	96
3.2. Effects of Al on phosphoinositide hydrolysis	98
Concluding Remarks	102
Acknowledgements	103
References	103

Abstract

The capacity of aluminum (Al) and a group of trivalent cations that are chemically and physically related to Al (scandium, beryllium, yttrium, gallium, and lanthanum) to promote changes in membrane rheology will be discussed. These multivalent cations are recognized neurotoxicants, which have high affinity for cellular acidic molecules, especially those containing one or more phosphate groups. In negatively charged liposomes, these metals bind to membrane phospholipids establishing either *trans*- or *cis*-interactions that differentially affect the physical properties of the bilayer. As a consequence of *trans*-interactions, Al and related metals promote the aggregation and fusion of vesicles. *cis*-interactions lead to the formation of clusters of negatively charged phospholipids (phosphatidyl serine, polyphosphoinositides). In these discrete regions of the bilayer, the mobility of the acyl chains is reduced as well as the hydration of the phospholipid head-groups, resulting in an increase in the membrane permeability. In addition, the membrane surface potential is altered, due to the loss of surface negative charges.

*Corresponding author. Tel: 1-530-754-6074; Fax: 1-530-752-8966;
E-mail: poteiza@ucdavis.edu

The observed alterations of membrane physical properties associated with metal–lipid interactions could have profound effects on membrane-associated processes.

For example, although Al and related cations have no redox capacity in biological systems, they can stimulate Fe^{2+} -induced lipid oxidation. We have shown that, among other possible mechanisms, Al and related metals-induced alterations on membrane fluidity and hydration create an environment that enhance the oxidant activity of Fe^{2+} . This mechanism could occur not only *in vitro* but also *in vivo* since, in an animal model of prenatal exposure to Al, a lower fluidity of brain myelin associated with a higher content of end products of lipid oxidation was observed. In this model we found a higher myelin content of galactolipids, lipids that can also decrease membrane fluidity and favor the propagation of lipid oxidation. Independently of its effects on membranes, Al can also facilitate oxidation reactions through a direct interaction with oxidant species.

Furthermore, Al-membrane interactions affect the metabolism of polyphosphoinositides. In liposomes containing a mixture of brain phosphoinositides, Al also caused membrane rigidification and lateral phase separation. Although Al did not affect the activity of the enzyme phospholipase C, a marked decrease in the activity of phosphatidyl inositol-specific phospholipase C (PI-PLC) was observed. The activity of PI-PLC was fully recovered when vesicles were disrupted by the addition of Triton X-100. The effects of Al on PI-PLC activity can be attributed to the formation of discrete clusters enriched in polyphosphoinositides that limit the accessibility of the enzyme to its substrates.

In summary, in this paper we will discuss the consequences of Al and related metals interactions with membranes. These metals cause alterations in membrane physical properties, which affect lipid oxidation rates and phosphoinositide hydrolysis. However, Al-mediated changes in membrane rheology could also affect other membrane-associated processes such as signal transduction events, membrane transport, and the functionality of receptors. These mechanisms could contribute to Al neurotoxicity.

Abbreviations

16-AP	16-(9-anthroyloxy)palmitic acid
6-AS	6-(9-anthroyloxy)stearic acid
12-AS	12-(9-anthroyloxy)stearic acid
C_6 -NBD-PE	2-(6-(7-nitrobenz-2-oxa-1,3-diazol-4-yl)amino)hexanoyl-1-hexadecanoyl- <i>sn</i> -glycero-3-phosphoethanolamine
CNPase	2',3'-cyclic nucleotide-3'-phosphohydrolase
DMPC	dimyristoyl phosphatidyl choline
DPH	1,6-diphenyl-1,3,5-hexatriene
EPR	electronic paramagnetic resonance
GP	generalized polarization
Laurdan	6-dodecanoyl-2-dimethylaminonaphthalene
PC	phosphatidyl choline
PI-PLC	phosphoinositide-specific phospholipase C
PLC	phospholipase C
PPI	polyphosphoinositides
PS	phosphatidyl serine
ROS	reactive oxygen species
TBARS	2thiobarbituric acid-reactive substances

1. ALUMINUM AND RELATED CATIONS: GENERAL PROPERTIES

Aluminum (Al) is a heavy metal present in high amounts in the earth's crust, where it represents 8% of the total components. Even when the bioavailability of this metal is low due to the formation of Al-silicate complexes, certain environmental and industrial factors could raise Al availability. Among other factors, environmental contamination, acid rain, water purification treatment with Al compounds, the use of Al as food additives, and certain pharmacological and therapeutic treatments, could lead to an increased exposure of humans to this metal [1].

In humans, Al could be absorbed through the gastrointestinal tract [2], the olfactory and oral epithelium [3], and the skin [4]. Once absorbed, Al circulates in the bound form mainly to transferrin and citrate [5] and could be deposited in several tissues and organs. Specially, the brain has a high susceptibility to Al toxicity. To avoid the inflow of this toxic metal, the brain has an active efflux of this cation at the blood-brain barrier level, mediated by a monocarboxylate transporter [6,7].

It has been proposed that Al deposition in tissues can determine the alteration of numerous metabolic pathways. In this way, alterations in phosphoinositides metabolism [8], in cholinergic [9] and glutamatergic [10] neurotransmission, in microtubule-dependent transport [11], and DNA alterations [12] have been reported both *in vitro* and *in vivo*.

Even when Al is a non-redox cation in biological systems, it can promote *in vitro* lipid oxidation in the presence of a redox-metal (Fe^{2+}) in liposomes, in microsomal membranes and in erythrocytes [13–15]. *In vivo*, the accumulation of Al in the brain determines the increase in the amount of lipid peroxidation products [16,17].

Al shares certain chemical and physical properties with other metals that belong to group III of the elements. This group is divided into two subgroups, the first formed by scandium (Sc), yttrium (Y), and lanthanum (La), and the second that includes gallium (Ga) and indium (In). In the ionic state, Sc and Y have the highest similarity to Al since all these cations have an electronic configuration similar to inert gases (Table 1). On the other hand, Ga and In have filled d orbital that confers certain properties close to those of inert gases. As shown in Table 1, these four cations have a lower charge density respect to that of Al, and therefore, they have a lower polarizing capacity. All these cations are amphoteric, although Sc is slightly more alkaline than Al while Ga is more acidic. Finally, beryllium (Be) is the first metal of the group II of the elements. Even when Be has the same charge density and electronegativity than Al (Table 1), its lower atomic charge and coordination number are important differences that could be reflected in the behavior of this particular cation.

In the present work, we will summarize the investigations performed in our laboratory in the last decade oriented to understand select mechanisms that

Table 1. Atomic properties of Al³⁺ and related cations

Cation	Al ³⁺	Ga ³⁺	In ³⁺	Sc ³⁺	Y ³⁺	Be ²⁺	La ³⁺
Ionic radii(Å)	0.51	0.62	0.79	0.73	0.89	0.35	1.51
Charge density(z/r)	5.66	4.84	3.80	4.11	3.37	5.71	1.99
Coordination number	(4), 6	6	6	6	6–8	(3), 4	6
Electronic configuration	IG(Ne)	3d ¹⁰	4d ¹⁰	IG(Ar)	IG(Kr)	IG(He)	IG(Xe)
Electronegativity	1.5	1.6	1.7	1.3	1.3	1.5	1.1

IG, inert gas electronic configuration.

Reproduced with permission from Environmental Health Perspectives [1].

could participate in Al toxicity. We specially focused on the possible interactions between this metal and membrane lipids, and how these interactions could affect membrane physical properties and subsequently, membrane-related processes. We compared the effects of Al with those of other related cations, to elucidate if they could exert similar actions on membrane rheology. The differential effect of divalent and trivalent cations on membrane physical properties will be discussed.

2. EFFECTS OF Al AND RELATED CATIONS ON MEMBRANE PHYSICAL PROPERTIES

2.1. Studies in synthetic membranes (liposomes)

Liposomes were used in these studies since they are a well-defined and controlled system, in which the lipid composition can be defined by the user. In liposomes, we investigated the effects on the interactions of Al and related cations with membranes and their consequences on certain membrane physical properties. In most of the studies, liposomes composed of brain phosphatidyl choline (PC) and brain phosphatidyl serine (PS) in a 60:40% molar ratio were used. These two lipids were selected taking into consideration that:

- (a) PC is the major phospholipid in brain membranes, representing a 40% of total phospholipids [18].
- (b) PS is also present in brain membranes although at a lower concentration (13% of total phospholipids [18]). PS is the most abundant negatively charged phospholipid in biological membranes and has two characteristics that were relevant to understand the interaction of Al with membranes:
 - (i) The headgroup contains a serine moiety that, due to its negative charge, constitutes a preferential binding site for cationic compounds through electrostatic interactions [19].
 - (ii) In the nervous system PS is particularly enriched in polyunsaturated fatty acids [20], substrates of oxidants-mediated lipid oxidation.

(c) PC and PS mixtures spontaneously form planar bilayers [21] due to the tubular shape of these phospholipids. Therefore the obtained vesicles resemble biological membranes.

Working with liposomes composed of PC and PS at a 60:40% molar ratio, we performed two kinds of studies, evaluating the inter-vesicle interactions (*trans*-interactions) and the intrinsic properties of the bilayer (*cis*-interactions).

2.1.1. *trans*-interactions

First, we investigated the effects of Al and related cations on membrane aggregation and fusion. Liposomes are stable structures that do not spontaneously interact, specially the negatively charged liposomes that have an important electrostatic repulsion between the charged headgroup of phospholipids. Therefore, vesicles will aggregate when a decrease in their electrostatic repulsion occurs [22]. For example, liposome aggregation can occur in the presence of multivalent cations, such as Ca^{2+} , which neutralizes superficial charges, promoting the intercrossing of PS molecules located in neighbor vesicles, and the partial dehydration of the membrane surface [23,24].

In our experimental system, we found that Al, Sc, Ga, In, Be, Y, and La significantly promoted membrane aggregation [25]. These metals had a higher aggregating action than that reported for divalent cations, since the metal concentration required to attain a significant aggregation was approximately 60 times lower than that reported for Ca^{2+} . This difference could be ascribed to a higher electrostatic interaction of the Al and related metals with the negatively charged membranes.

Although vesicle aggregation precedes membrane fusion, aggregation *per se* does not constitute a sufficient condition to promote fusion. For example, Mg^{2+} causes a massive liposome aggregation but in contrast to Ca^{2+} , it does not promote membrane fusion [26]. To understand the differences between the behavior of these two cations, it is necessary to consider that the fusion takes place when a certain energetic barrier is overcome, barrier that is the resultant between the electrostatic repulsion among lipid polar headgroups and their hydration forces [23]. These two forces prevent the hydrophobic interactions between lipid bilayers. Metals that can only neutralize membrane charges, but that do not dehydrate the polar headgroups, such as Mg^{2+} , will only cause membrane aggregation.

Our results showed that Al and related cations not only caused membrane aggregation but also induced fusion [15,25]. Liposome fusion kinetics after the interaction with these cations showed a biphasic behavior, with a fast initial phase within the first minute of incubation, and a slower phase that reached a maximal effect after 30 min of incubation [25]. This result is in agreement with the kinetics of metal-induced liposome aggregation, which was completed within the first 5 min of incubation.

Al and related cations had a maximal effect on liposome fusion at lower concentrations than those reported for other divalent cations. While for trivalent cations the maximal fusion was observed at 20–100 μM , for Ca^{2+} the required concentration was higher than 9 mM [27,28]. Our results indicated that, in order to obtain a similar fusogenic effect, Ca^{2+} , Zn^{2+} , and Cd^{2+} had to be present in concentrations that were 15–500 times higher than those for the trivalent cations [25].

2.1.2. *cis*-interactions

In the early stage of Ca^{2+} binding to the membrane, the cation forms *cis* complexes with PS [29], resulting in the segregation of lipids in the lateral phase of the bilayer. Through this mechanism, Ca^{2+} generates lipid microdomains enriched in PS that constitute a nuclei to a number of molecular events that lead to the membrane fusion, such as lipid dehydration and formation of *trans* complexes with PS, among others [30]. In phospholipid binary mixtures, lateral phase separation could be a result of a partial miscibility of the components [31], or due to changes in thermodynamical conditions, such as temperature or ionic strength [32].

In PC/PS liposomes, we investigated whether Al and related cations could promote lipid segregation, and the results were compared with those obtained in PC/PS/galactolipid liposomes. In PC/PS liposomes, Al and related cations (10–200 μM) significantly promoted lipid lateral phase separation (Fig. 1) [33]. The extent of this Al-mediated effect depended on the amount of phosphatidyl serine in the membrane (Fig. 1). Thus, liposomes composed exclusively of phosphatidyl serine were more sensitive to Al-mediated effects on phase separation than PC/PS liposomes.

A significant and positive correlation ($r^2 = 0.99$, $P < 0.001$) was observed between the magnitude of the effects in PC/PS and in PS liposomes (See inset to Fig. 1) suggesting that this process is driven by the interactions of Al with negatively charged membranes. The presence of galactolipids in the membrane enhanced Al (10–100 μM)-mediated lateral phase separation [34]. In galactolipid-containing vesicles, a spontaneous lipid segregation was observed that depended on galactolipid concentration in the membrane. This phenomenon was previously described by Ruocco *et al.* [35], who demonstrated in DMPC liposomes that at galactolipids concentrations higher than 23 mol%, two lipid phases coexist in the bilayer. The first contains lipids in gel phase, where approximately a 23% of galactolipids are entrapped, and the second is mainly composed of galactolipids in crystal phase. Although in our system, lipids are from brain origin, and therefore contain all the fatty acids that are naturally present in the central nervous system (CNS), which favors lipids miscibility, we also observed the spontaneous segregation of galactolipids. The finding of a higher lateral phase separation effect of Al in galactolipids-containing liposomes compared to liposomes devoid of galactolipids, suggest that this metal could enhance the natural formation of lipid domains in the membrane. In the range of galactolipid concentrations used for the experiments, Al could act at two different

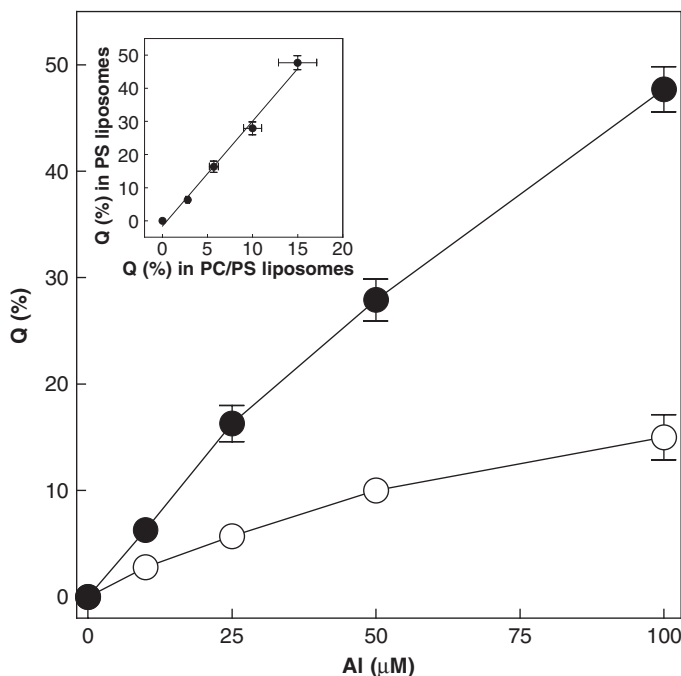


Fig. 1. Effect of Al on lipid lateral phase separation. PC/PS (○) or PS (●) liposomes containing the fluorescent probe C₆-NBD-PE were incubated in the presence of Al (0–100 μM), and the lipid lateral phase separation was evaluated as the decrease in fluorescence intensity due to quenching. Results are shown as mean ± SEM of four independent experiments. Inset: Correlation between Al-mediated lipid lateral phase separation in PC/PS (60:40 molar ratio) and in PS liposomes.

Data taken from Verstraeten [40].

levels: first, completing the formation of galactolipid-enriched domains spontaneously generated and second, acting on phospholipid-enriched domains where Al could promote the separation of PS from PC.

As a consequence of the movement of phospholipids in the bilayer during metal-induced lateral phase separation unspecific pores can be generated, through which small molecules can leak, resulting in alterations of membrane permeability. This effect is higher in sonicated vesicles, used in our study, since these liposomes have a higher mechanical rigidity associated with a higher curvature radii [36]. Working with PC/PS liposomes we found that Al and related cations (10–100 μM) promoted the release to the external media of the fluorescent probe 5(6)-carboxyfluorescein [15,25]. The capacity of Al to permeabilize membranes could be particularly relevant in the cell damage associated with Al-intoxication, since this metal accumulates in lysosomes [37]. Thus, Al could induce the liberation of the lysosomal content to the cytoplasm, inducing cellular damage and/or death.

On the other hand, during lateral phase separation, phospholipids adopt an energetically favorable disposition in the bilayer, releasing water molecules from their headgroups. This newly adopted disposition could cause the immobilization of the phospholipids involved in metal binding, effect that propagates into the membrane hydrophobic core. Thus, we next investigated whether Al could promote membrane dehydration and rigidification.

Working with PC/PS liposomes containing the fluorescent probe Laurdan, we evaluated the effects of Al and related cations on phospholipid hydration. According to Parasassi and Gratton [38], the blue and red components of the Laurdan fluorescence spectrum could be altered by a decrease in the polarity of its environment. This effect is a direct consequence of a lesser penetration of water molecules into the bilayer, affecting their interaction with the excited state dipole of Laurdan. In our experimental system, Al and related cations (10–200 μM) promoted the displacement of water molecules from the hydration shell of membrane phospholipids [39]. The finding of lower water content in the membrane would *per se*, trigger the alteration of other membrane physical properties, including the interaction with neighbor vesicles. In fact, we observed a positive correlation between metal-mediated membrane dehydration and the capacity of these cations to induce membrane fusion [40]. These results are in accordance to those previously described for Ca^{2+} , where the displacement of water molecules from the bilayer decreases the repulsion between the charged vesicles, and leads to membrane aggregation and fusion [23].

We also investigated the effect of these cations on membrane fluidity using electronic paramagnetic resonance (EPR) and fluorescent techniques. First, working with PC/PS liposomes containing the fluorescent probe 1,6-diphenyl hexatriene (DPH) we found that Al and related cations (10–100 μM) significantly decreased membrane fluidity, as evidenced by an increase in the DPH order parameter [25]. This effect was also observed in PC/PS:galactolipid liposomes, although in this system a differential effect was observed [34]. In these liposomes, galactolipids caused *per se* a decrease in membrane fluidity, due to its high content of saturated, long-chain fatty acids. However, the addition of Al (100 μM) significantly decreased membrane fluidity, but only when galactolipids concentration was lower than 20 mol% [34], while at higher galactolipids contents, Al did not affect membrane fluidity. The lack of an additional effect of Al at higher galactolipids concentration suggests that the rigidity of phospholipids domains had already reached the maximal value, or that, given DPH evaluates the average membrane fluidity with no specificity for different lipid domains, the changes caused by Al in the phospholipids-enriched domains would be masked by the higher rigidity in the galactolipids-enriched domains.

As mentioned above, DPH homogeneously distribute in the bilayer and provides information on the global fluidity of the membrane. Given that Al promotes lateral phase separation, and therefore generates PS-enriched domains in PC/PS liposomes, we investigated the possibility that the fluidity in PS-domains could

be lower than in PC-domains. For this purpose, we used two EPR probes, 7-doxyl PS and 7-doxyl PC, inserted in PC/PS liposomes. In the presence of Al, we observed a decrease in the membrane fluidity that affected both kinds of lipid domains (Fig. 2). However, the effect of Al was significantly higher in the PS-enriched domains [40] compared to PC-enriched domains, indicating that Al–PS interactions could have a higher impact on membrane lipid organization.

We next investigated whether the lower membrane fluidity due to Al was caused by the formation in the membrane of discrete lipids domains where the fatty acids were in gel phase. DMPC/DMPS liposomes were used in order to attain an homogeneous system where the only variable was the polar headgroup. Both phospholipids are completely miscible, and in this system a unique transition temperature is observed, close to 30°C [39]. From the variation in the generalized polarization (GP) of the fluorescent probe Laurdan, it is possible to estimate the relative proportion of lipids in each phase [38]. In these liposomes Al (100 μ M)

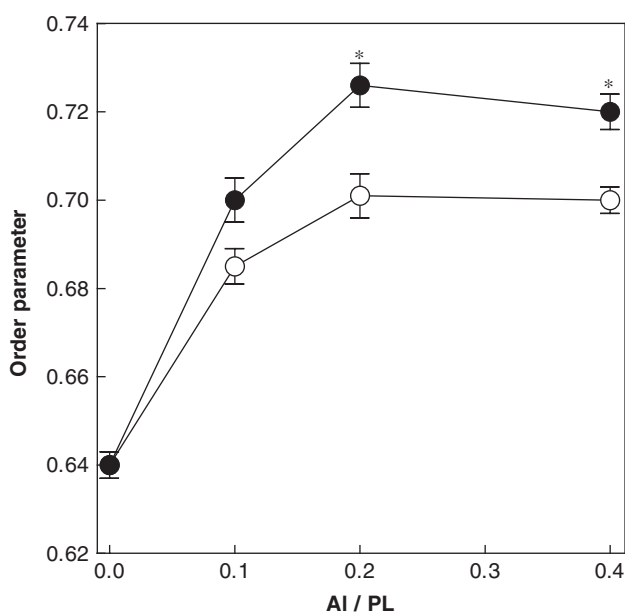


Fig. 2. Effect of Al on membrane fluidity in PS- and PC-enriched domains. PC/PS liposomes containing 1.5 mol% of the spin probes 7-doxyl PS (●) or 7-doxyl PC (○) were incubated for 5 min at 22°C in the presence of increasing amounts of Al to attain an Al to phospholipid (PL) molar ratio within the range of 0.1–0.4. After incubation, the EPR spectra were recorded and the order parameter calculated as indicated in [69].

Results are shown as mean \pm SEM of three independent experiments. * is significantly different from the values obtained using the probe 7-doxyl PC ($P < 0.01$, two-way ANOVA test).

Data taken from Verstraeten [40].

caused a 20% increase in the amount of lipids in gel phase that corresponded to a 2°C displacement in the lipid transition temperature [38].

In contrast to DMPC/DMPG liposomes, brain PC/PS liposomes presented the behavior characteristic of a homogeneous liquid-crystalline phase between 10 and 45°C. In the presence of Al (10–200 μM) and at 37°C, Laurdan GP corresponding to the excitation and emission spectra curves moved toward higher values with increasing Al concentrations. However, the shapes of the curves were unaltered [40] suggesting that in these liposomes Al did not cause a detectable variation in the lipid phase state. The lack of an Al-mediated effect on the phase state of lipids could be related to the variety in the fatty acids composition of brain phospholipids, both in length and saturation degree. Membranes formed by natural phospholipids do not show a neat transition temperature, that could be lower than 10°C [41]. In addition, using this methodology the coexistence of lipids domains could be detected only when the molecular ratio of the gel and liquid-crystalline phases is in the range from 30% to 70% [38]. Both below and above this range, a single homogeneous phase is observed, with the properties of the more concentrated phase being slightly modified by the presence of the other [38].

The effects of Al on membrane lipid packing and lateral phase separation are significantly more pronounced than those exerted by divalent cations. Even at concentrations as high as 200 μM, calcium and zinc had no effects on membrane lipid packing or lateral phase separation [42,43] while lead [42] induced lateral separation but at a lower extent than Al.

2.2. Studies in biological membranes

As described above, Al is a neurotoxicant that produces a myriad of changes in the physical properties of synthetic membranes. However, biological membranes are more complex, containing a variety of molecules. Therefore, our interest was next centered in how Al could affect the physical properties in different brain membranes.

First, we worked with a human neuroblastoma cell line (IMR-32) to study the interactions of Al with their plasma membrane. Taking into account that neuroglial cells do not incorporate Al from the medium [44] in spite of the ionic bonds that could be established between the metal and the cell plasma membrane, and that the modification of membrane physical properties can be an early event that could trigger neuronal dysfunction, we hypothesized that the consequences of Al-plasma membrane interactions may have a profound biological relevance.

In non-differentiated IMR-32 cells we observed that Al (10–100 μM) significantly affected the fluidity of cell plasma membrane [45]. However, when the experiments were performed using IMR-32 cells differentiated to a cortical neuron phenotype, Al not only promoted the loss of plasma membrane fluidity, but the magnitude of the effect was significantly higher than that of the non-differentiated cells [45]. We found that differentiated cell plasma membranes were significantly

more fluid than the membranes from the non-differentiated cells. In order to understand these differences, we characterized their lipid composition. We found that although no relevant differences were observed in phospholipid composition, differentiated cells have a higher cholesterol content and a higher relative content of polyunsaturated fatty acids [45]. Both cholesterol and unsaturated fatty acid contents are important factors that modulate membrane fluidity.

Accordingly, when lipid phase state was evaluated using the fluorescent probe Laurdan, Al caused a differential effect in both kinds of cells. In the presence of Al (10–50 μM), Laurdan GP curve corresponding to the excitation spectrum was displaced toward higher values. In non-differentiated IMR-32 cells, the magnitude of Al effect on Laurdan GP was significantly higher than that observed in differentiated cells [45]. Again, the difference between both cell types could be ascribed to the difference in the relative content of unsaturated fatty acids, since as discussed in the previous section, saturated and unsaturated fatty acids have a differential response to Al-mediated effects.

Even when Al promoted lipid lateral phase separation both in differentiated and non-differentiated IMR-32 cells, the magnitude of the effect was similar in both cell types. We can speculate that, if Al-mediated lateral phase separation results from Al-binding to more than one acidic phospholipid that leads to their clustering, the similar phospholipid composition in differentiated and non-differentiated cells explains the lack of a differential effect due to Al.

Another membrane that could potentially be susceptible to Al-mediated effects on bilayer physical properties is the brain myelin membrane. Myelin is a particular membrane highly enriched in lipids, representing the 70% of membrane dry weight. Therefore, this membrane could constitute an environment where Al-induced changes in membrane physical properties would be favored.

To test this hypothesis, a model of chronic Al-intoxication in mice during gestation and early development was used. The amount of Al administered in this model was chosen taking into account the Al ingestion in humans submitted to a chronic antacid treatment with $\text{Al}(\text{OH})_3$ -containing compounds. This model was previously reported to cause Al deposition in the brain, and a delay in the time necessary for animals to acquire new abilities, but not on their capacity to perform an already acquired skill [46].

We evaluated in this experimental model the impact of the amount of Al administered to mice on enzymes from different cell types that could be inhibited at high Al concentrations. In this regard, we measured the activity of glutamine synthase (marker of glial cells), acetylcholinesterase (marker of neuronal cells) and 2',3'-cyclic nucleotide-3'-phosphohydrolase (CNPase, marker of oligodendroglial cells). In this model, no alterations in the activity of these enzymes were observed in Al-intoxicated animals [40]. The normal activity of acetylcholinesterase could be a parameter of a low or moderate Al-intoxication, since in severe Al-intoxication an alteration in the cholinergic metabolism was reported, leading to a decreased acetylcholinesterase activity [9,47].

In mice, the formation of myelin in the CNS occurs in the postnatal period. One of the main enzymes that are measured as an indicator of myelin maturation is CNPase. The normal CNPase activity found in the Al-intoxicated animals suggested that the amount of Al administered to these mice did not interfere with the normal myelin deposition.

At day 40 postnatal, the amount of Al measured in brain myelin was higher in the Al-intoxicated mice compared to control animals [48]. Similar to that previously observed in liposomes, Al treatment determined a lower membrane fluidity, as evaluated from DPH fluorescence polarization [48]. Even when the increase in DPH order parameter in Al-intoxicated mice myelin membranes was relatively small (2.4%) with respect to control animals, this result is comparable to those reported for erythrocyte membranes incubated *in vitro* in the presence of Al [49].

When myelin from Al-intoxicated and control animals was characterized for its lipid and protein composition, several differences were found. In both experimental groups, myelin protein and cholesterol content were similar [34]. However, the concentration of phospholipids in Al-intoxicated mice was 37% higher, while galactolipids content was 104% higher than those of control mice [34]. The findings that Al toxicity can be associated with the presence of an abnormal myelin suggests that changes in myelin composition could contribute to the lower learning ability found in Al-intoxicated mice [46]. As explained in the previous section, galactolipids play a crucial role in the modulation of Al-induced changes in membrane physical properties, causing a decrease in membrane fluidity and the spontaneous segregation of lipids in the lateral phase of the bilayer [34], thus facilitating the deleterious effects of Al on membrane rheology.

3. RELATIONSHIP BETWEEN AI-MEDIATED CHANGES IN MEMBRANE PHYSICAL PROPERTIES AND MEMBRANE-ASSOCIATED PROCESSES

3.1. Lipid oxidation

Oxygen has a key role in higher organisms, which use this gas for their normal metabolic functions leading to energy production. However, it has been demonstrated that the exposure to high oxygen concentrations (>21%) is toxic to most of the living organisms. This finding led Gershman and coworkers [50] to propose that the noxious effects of oxygen are caused by the formation of free radicals, molecular species that have a high reactivity. These and other active species are called as a whole reactive oxygen species (ROS). ROS oxidize polyunsaturated lipid molecules in a process usually called lipid oxidation.

Lipid oxidation can be triggered by different agents, such as redox-active metals (iron, copper), organic or inorganic compounds that could decompose rendering free radical derivatives, UV light, ionizing energy, etc. In biological

systems, the role of iron (Fe^{2+}) is particularly relevant in the initiation of lipid peroxidation, since this metal interacts with molecular oxygen forming superoxide anion, which in turn, renders hydroxyl radical, the specie with the highest oxidant capacity known until now. On the other hand, Fe^{3+} generated from Fe^{2+} oxidation, can also trigger lipid oxidation through its reaction with lipid hydroperoxides normally present in biological membranes. Through both mechanisms, iron can initiate lipid oxidation reactions.

The CNS is particularly sensitive to ROS-mediated damage [51] since:

- (a) The brain has a high oxygen consumption rate, representing approximately 20% of the total oxygen consumed by the organism.
- (b) Brain membranes are enriched in polyunsaturated fatty acids that are preferential substrates of ROS-mediated oxidation.
- (c) In the brain, the activity of the enzymes responsible for detoxifying ROS (catalase, superoxide dismutase, and glutathione peroxidase) is lower than that found in other organs and tissues.
- (d) The iron concentration in the brain is high [52], specially in the substantia nigra, caudate-putamen, and globus pallidus. During certain processes that involve cerebral tissue lesions, such as ischemia followed by reperfusion, high amounts of iron are liberated from its stores, which can initiate the oxidative damage to cellular components.
- (e) Finally, many neurotransmitters are auto-oxidizable molecules. For example, dopamine, its precursor L-DOPA, and noradrenaline could, by reaction with molecular oxygen generate superoxide anion, hydrogen peroxide and active quinones, and all of them could initiate oxidative damage to cells.

All these factors make the nervous tissue a preferential target for the noxious action of ROS, which could be involved in a number of pathologies that affect the CNS.

For the above reasons, we centered the attention on the possible interactions between Al and two oxidant species: Fe^{2+} and melanine, a compound generated from the auto-oxidation of dopamine.

3.1.1. *Effects on Fe^{2+} -initiated lipid oxidation*

First, we investigated the effects of Al on Fe^{2+} -initiated lipid oxidation evaluated as the formation of 2thiobarbituric acids-reactive substances (TBARS). Results were compared to those obtained for Al-related cations.

Working with PC/PS (60:40 molar ratio) liposomes we observed that Fe^{2+} -induced lipid oxidation presented a biphasic behavior. We found a slow component of TBARS formation during the first 60 min of incubation at 37°C , with a rate constant of 0.012 ± 0.003 nmol TBARS/mg phospholipid/min. This initial stage was followed by a faster component, with a rate constant of TBARS production of 0.14 ± 0.02 nmol

TBARS/mg phospholipids/min that continued until 120 min of incubation. It is important to stress that at least until 120 min of incubation, TBARS production did not reach a maximal value, indicating that during the incubation period, the substrates of lipid oxidation were not exhausted.

The simultaneous addition of Al and Fe^{2+} stimulated the oxidant capacity of Fe^{2+} *per se* [15,25]. Similarly, all the Al-related cations assessed stimulated Fe^{2+} -triggered lipid oxidation [25]. In this group, La showed the highest stimulatory capacity, reaching the maximal effect at a 20 μM concentration [25]. On the other hand, Y and Al displayed their highest action at 50 μM concentration, while Ga and Be did not reach a maximum effect in all the range of concentrations tested (10–200 μM) [25]. Finally, Be, the only divalent cation of this group had the lowest stimulatory capacity.

The stimulatory effect of Al and related cations on Fe^{2+} -mediated lipid oxidation showed a strong dependency on the pH of incubation media, being higher at acidic pH [40]. Thus, we observed that at pH 5.5 the amount of TBARS measured in the presence of these cations was between 2.6- and 4 times higher than that obtained at physiological pH. Similar to Al, Sc, Ga, In, Be, Y, and La have acidic properties, and therefore, at neutral pH the polyhydroxylated species of these metals are predominant. As pH gradually decreases in the media, the raise in proton concentration displaces the equilibrium toward the formation of free cation (Me^{7+}). The fact that the stimulation of TBARS production by the metals was higher at acidic pH, which strongly suggests that the ionic specie involved in this process is the free cation rather than the polyhydroxylated species [40]. In this way, Martin [53] calculated that at pH 7, the amount of free Al is in the picomolar order and that $\text{Al}(\text{OH})_3$ predominates. However, when in the media molecules are present with Al-binding capacity, such as phospholipids, the phosphate and/or carboxylate groups present in these macromolecules quelate Al and displace the $\text{Al}(\text{OH})_3$ hydrolysis equilibrium toward the formation of the free cation. Consequently, the amount of Al bound to the membranes at pH ~ 7 is higher than the free cation concentration in the aqueous media. This effect can be magnified at acid pH.

Interestingly, membrane disruption due to liposomes treatment with the non-ionic detergent Triton X-100 did not affect the oxidant capacity of Fe^{2+} . This cation can interact with the membranes, cleaving the lipid hydroperoxides naturally present in them, which, due to their hydrophilic nature, are located in the water–lipid interface. Therefore, the accessibility of Fe^{2+} to these lipid hydroperoxides need not be limited by the presence of a detergent.

On the contrary, in liposomes treated with Triton X-100 the stimulatory effect of Al and related cations was abolished [40]. This finding indicates that the capacity of Al and related cations to stimulate lipid oxidation requires the presence of an organized bilayer structure. As discussed above, it is in this context of an organized bilayer where these cations can exert their effects on membrane physical properties, and those changes could create an environment where the propagation of lipid oxidation will be enhanced.

Supporting this, we observed that the presence of galactolipids in the membranes enhances the stimulatory effect of Al on Fe^{2+} -triggered lipid oxidation. We found that in PC/PS and PC/PS/galactolipid liposomes, the magnitude of Fe^{2+} -initiated lipid oxidation was similar in both liposome populations (17.2 ± 0.7 and 17.2 ± 1.9 nmol TBARS/mg phospholipid, respectively). The presence of Al (100 μM) significantly increased TBARS content in both types of liposomes. However, in galactolipid-containing membranes, the stimulatory action of Al on lipid oxidation was significantly higher (45 ± 1 nmol TBARS/mg phospholipids) with respect to that in PC/PS liposomes (29 ± 2 nmol TBARS/mg phospholipids) [34].

In our experimental model, positive correlations between the capacity of Al and related cations to promote membrane aggregation ($r^2 = 0.71$, $P < 0.01$, Fig. 3A), fusion ($r^2 = 0.80$, $P < 0.005$, Fig. 3B), and rigidification ($r^2 = 0.91$, $P < 0.001$, Fig. 3C and D) and the stimulation of Fe^{2+} -initiated lipid oxidation were observed. The magnitude of metal action on lipid oxidation was higher in those membranes in which the fluidity of the bilayer was low [33]. This finding is in accordance with those reported by Cervato *et al.* [54] who demonstrated that arachidonic acid inserted in dipalmitoyl-PC was oxidized by Fe^{2+} at a higher rate when liposomes were incubated at temperatures lower than the transition temperature of the lipids, and thus, at low bilayer fluidity. Supporting this, we observed a positive correlation ($r^2 = 0.89$, $P < 0.01$) between the changes in the relative proportion of lipids in gel phase due to Al and related cations interaction with the membrane and the magnitude of Fe^{2+} -initiated lipid oxidation (Fig. 3E) [39]. Moreover, McLean and Hagaman [55], observed a higher oxidation of palmitoyl-arachidonoyl-PC at temperatures below their transition temperature, effect that these authors attribute to the decrease in membrane fluidity as well as to the formation of microdomains enriched in oxidizable lipids. However, this effect was not observed in cholesterol-containing membranes, which modulates their fluidity [56].

Finally, we also observed a positive correlation ($r^2 = 0.90$, $P < 0.005$) between the capacity of Al and related cations to induce lateral phase separation and to stimulate lipid oxidation (Fig. 3C). This finding could be due to the fact that, during the formation of acid phospholipids-enriched domains in the membrane, there is a local increase in polyunsaturated fatty acids content, and their higher proximity could cause an increase in Fe^{2+} -induced lipid oxidation rates [55].

From our experimental results we proposed a mechanism to explain the stimulatory effect of Al and related cations on Fe^{2+} -initiated membrane lipid oxidation that is summarized in Fig. 4.

Al and related cations interact with the polar headgroup of membrane phospholipids forming *cis*- and *trans*-complexes. As a consequence of *trans*-interactions, these metals promote, initially, the aggregation of the vesicles, followed by their fusion.

cis-interactions, preferentially with negatively charged phospholipids, cause their rearrangement in the lateral phase of the bilayer, resulting in the formation of microdomains enriched in PS. Along this process, phospholipids adopt in the

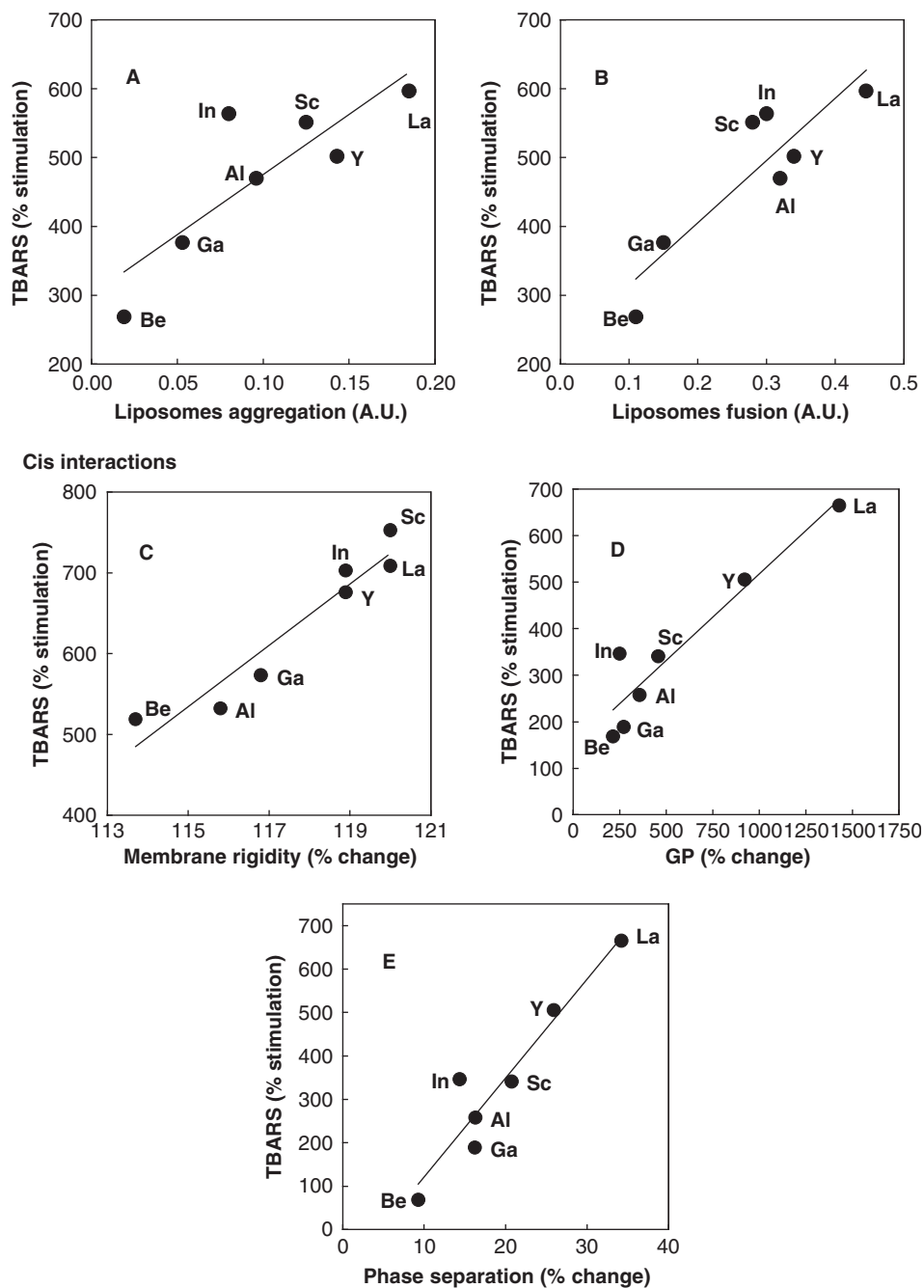


Fig. 3. Correlation between the capacity of Al and related metals to stimulate Fe^{2+} -initiated lipid oxidation and to induce liposome (A) aggregation, (B) fusion, (C) rigidification, (D) change in lipid phase state, and (E) lateral phase separation.

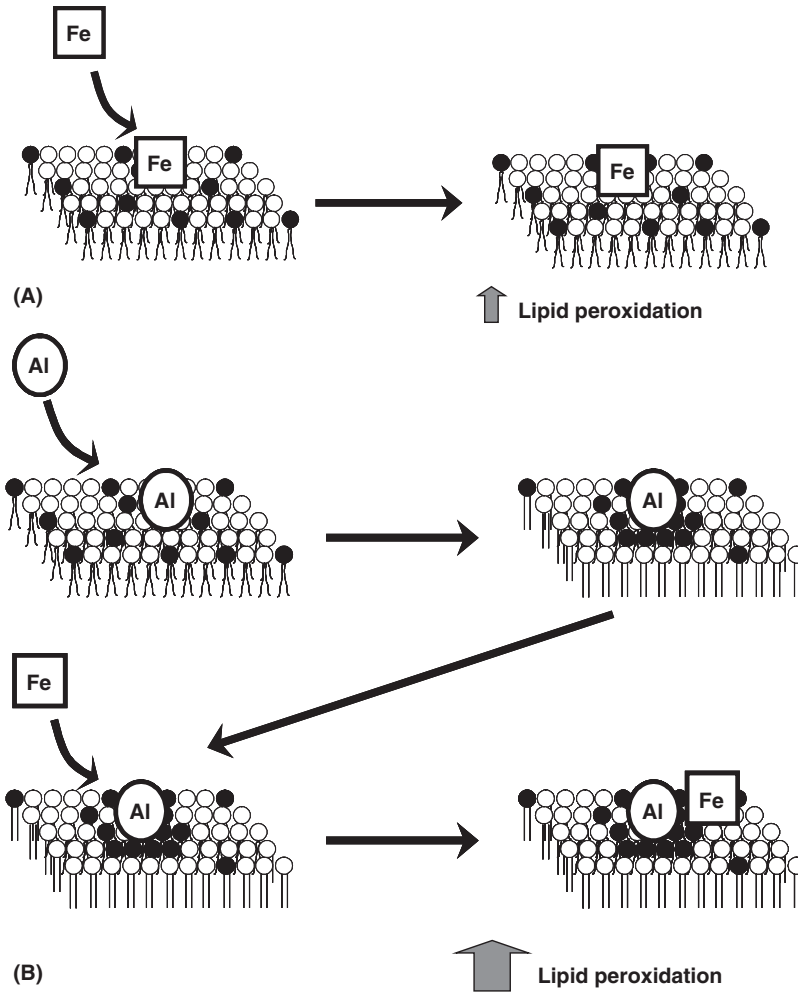


Fig. 4. Mechanism proposed for the stimulatory capacity of Al and related metals on Fe^{2+} -initiated lipid oxidation. \circ = PC; \bullet = negatively charged phospholipid.

bilayer a more energetically favorable disposition, with liberation of water molecules that hydrate the polar headgroup of phospholipids. This newly adopted disposition immobilizes the polar headgroups involved in metal–membrane binding, and this immobilization affects not only the water–lipid interface but propagates into the hydrophobic region of the membrane.

Since a high percentage of fatty acids in brain PS are polyunsaturated, the effects of Al and related metals causing a local increase in PS with decreased lipid mobility could be the determinant of an increase in lipid peroxidation rates, by favoring the propagation of lipid oxidation. In biological membranes, the extent of Al effects on membrane rheology could be limited by the presence of proteins and cholesterol. This latter molecule has two main properties that could limit the

propagation of lipid oxidation. First, cholesterol differentially modulates lipid ordering in membrane domains, increasing fluidity in those domains where lipids are in gel phase, and decreasing fluidity in those with fluid lipids. On the other hand, cholesterol also could act as a chain breaker of lipid oxidation.

Supporting this proposed mechanism, we found that both, in isolated brain myelin and in myelin from Al-treated mice [48] a higher susceptibility to be oxidized in the presence of Al. This higher susceptibility of myelin membrane could not be explained in terms of a higher content of acidic phospholipids that could act as Al-binding sites, or to a higher concentration of oxidizable lipids, or to a deficiency in the amount of antioxidants [48]. On the contrary, the particular susceptibility of myelin to be oxidized in the presence of Al could be attributed to its characteristic composition in lipids and proteins. As discussed previously, in this membrane the lipid to protein ratio is 70:30, while in other biological membranes this ratio is generally the opposite. Therefore, the myelin membrane constitutes an environment that could favor the effects of Al on membrane physical properties. In this environment, Al could induce the loss of membrane fluidity and the formation of acidic lipid clusters, and both effects would enhance the propagation of lipid oxidation, similar to that observed in liposomes. This hypothesis is supported by the finding that *in vitro*, Al and related cations stimulate lipid oxidation both in myelin and in liposomes with a similar pattern of effect (Sc, Y, and La > Al, Ga, In > Be). On the contrary, in synaptic membranes where the relative lipid content is lower (30%), not only the magnitude of the stimulation was lower, but no differences were observed among the effects of the different metals.

Lead, although having a lower effect than Al, also interacts with negatively charged liposomes and induces lateral phase separation. The capacity of lead to stimulate Fe²⁺-initiated lipid oxidation is, as observed for Al, associated with its capacity to bind to the membrane and to promote changes in membrane physical properties that facilitate the propagation of lipid oxidation. This is also supported by the dependence of the stimulatory effect of lead on lipid oxidation, on membrane negative charge density and on the integrity of the bilayer [42]. In agreement with the mechanism proposed for Al, related metals, and lead, zinc, that also bind to negatively charged membranes but does not affect neither membrane lipid packing nor lateral phase separation, acts inhibiting Fe²⁺-initiated lipid oxidation [43]. Zinc acts as an antioxidant by occupying potential iron-binding sites in the membrane, thus preventing the initiation/propagation of iron-triggered lipid oxidation [43].

3.1.2. Membrane-independent effects in the pro-oxidant action of Al

Al can also promote oxidative damage through a direct interaction between the metal and oxidant species. Early work from Fridovich and coworkers proposed that Al can enhance the oxidating capacity of superoxide by neutralizing its negative charge [57]. Recently, based on this and other experimental data [57,58], it has been hypothesized that Al forms a superoxide semireduced radical ion [59].

Al and iron accumulates at high concentrations in particular regions of the brain in Parkinson's disease [60,61]. Neuromelanin is a complex pigment mainly located in neurons from the substantia nigra and locus coeruleus. The finding that the highly melanized dopaminergic neurons are those that degenerate in Parkinson's disease suggests that melanin could be involved in the process of neuronal degeneration and death. Melanins are redox-active polymers. The autoxidation of semiquinone and hydroquinone residues present in melanin generate superoxide anion and hydrogen peroxide, which in the presence of transition metals can lead to the formation of highly reactive species. Significantly, high Al and iron concentrations were found in melanized neurons of the substantia nigra from patients with Parkinson's disease [61].

On the basis of the capacity of Al to stimulate Fe^{2+} -initiated lipid oxidation and on the presence of high concentrations of both metals in neuromelanin, we tested the capacity of Al and related cations to modulate oxidative reactions in the presence of melanin [58]. In the experiments described in Section 3.1.1, the magnitude of the stimulatory effect on Fe^{2+} -initiated lipid oxidation was $\text{Y, Sc, La} > \text{In, Ga, Al} > \text{Be}$. In the presence of melanin, Y, Sc, and La had no effect on TBARS production and the order of magnitude of the effects of the other cations was $\text{Ga} > \text{Al} > \text{Be}$. The differences in the observed effects of Al on liposome lipid oxidation in the presence of the different initiators indicate that, in the case of melanin, the effects of Al are not related to its capacity to induce changes in membrane physical properties. On the basis of the capacity of melanin to autoxidize and generate ROS, we investigated if Al could act stimulating melanin-initiated lipid oxidation by interacting with melanin-generated oxidant species. To test this hypothesis, different antioxidant substances and enzymes as well as metal chelators were used to investigate the potential oxidant species involved. Superoxide dismutase, which metabolizes superoxide anion, but not catalase, which metabolizes hydrogen peroxide, inhibited TBARS formation, both in the presence of melanin or melanin and Al (Fig. 5). Two scavengers of hydroxyl radicals, mannitol and dimethyl sulfoxide, did not affect lipid oxidation. Two metal chelators, desferal and EDTA completely prevented melanin-initiated TBARS production in the absence or presence of Al (Fig. 5). This experiment supports the involvement of transition metals (iron) in the generation of ROS by melanin and on the involvement of an interaction Al-superoxide anion, with the generation of a specie of higher oxidative capacity than superoxide anion *per se*, in the stimulation by Al of melanin-initiated lipid oxidation.

This conclusion is supported by the finding that Ga, Al, and Be also stimulates NADH oxidation promoted by Rose Bengal [58]. When illuminated, Rose Bengal generates several different oxidant species including superoxide anion, hydrogen peroxide, hydroxyl radical, and singlet oxygen. Similarly to the results obtained for melanin, from the different antioxidants tested, only superoxide dismutase inhibited the oxidation of NADH mediated by Al and rose Bengal, pointing again the participation of an Al-superoxide anion specie with high oxidant capacity in the

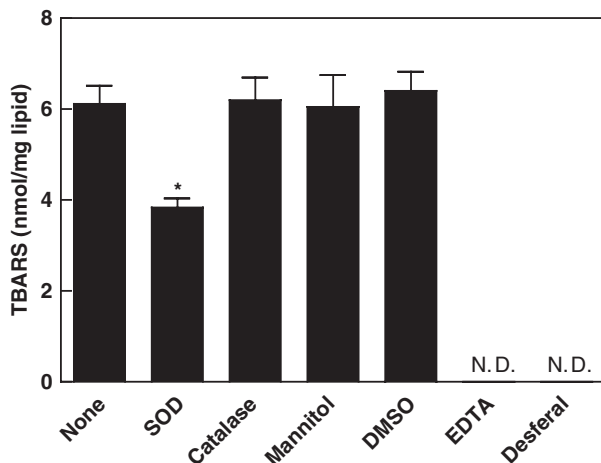


Fig. 5. Effect of antioxidants on the stimulatory effect of Al on melanin induced TBARS production. PC/PS (60:40 molar ratio) liposomes were incubated at 37°C in the presence of 40 µg/ml melanin and 50 µM Al. After 90 min of incubation, lipid oxidation was evaluated as TBARS formation. Results are shown as the mean ± SEM of four independent experiments. ND = nondetectable. Data taken from Meglio and Oteiza [58].

pro-oxidant action of Al [57–59]. A similar mechanism was found to occur for the lead-mediated oxidation of NADH [42].

On the basis of the above results, we have proposed that the interaction among melanin, iron, and Al can lead to oxidative stress in highly melanized dopaminergic neuron, which could trigger neuronal dysfunction and/or death in Parkinson's disease.

3.2. Effects of Al on phosphoinositide hydrolysis

Several biological ligands, such as neurotransmitters, neuromodulators, and certain hormones, exert their physiological actions through an intracellular second-messenger system, in which the receptor–ligand complex stimulates the turnover of polyphosphoinositides (PPI). This metabolic pathway is inhibited by Al, both *in vitro* and *in vivo* [62–64]. The inhibitory effect of Al on phosphoinositide-mediated cell signaling cascade could be attributed to a metal interaction with, at least, one of the major components of this system: the membrane receptor, the G protein associated to the receptor, the enzyme phosphoinositide-specific phospholipase C (PI-PLC), or with its substrates. The two first possibilities were discarded by Shafer and Mundy [8], and we investigated the two second mechanisms.

We hypothesized that Al could alter the physical properties of PPI-containing membranes, causing a decrease in the accessibility of PI-PLC to its substrates. To investigate this hypothesis, we first evaluated whether the presence of PPI enhanced Al-mediated changes in membrane rheology.

Al-binding to PPI-containing liposomes was significantly higher compared to PC liposomes [65]. In the latter, the recovery of non-bound Al was nearly a 100%, suggesting that weaker ionic bonds are established between Al and the zwitterionic phospholipid PC. Interestingly, in PPI-containing liposomes, Al remained bound to the lipids even when the vesicles were disrupted by the addition of a non-ionic detergent, which indicates the high-ionic bonds between Al and PPI phosphate groups.

Another way to evaluate the interaction of a cation with a membrane is to measure the changes in membrane surface potential after the addition of the cation. In agreement with the fact that PPI have a net negative charge, the surface potential of PPI-containing liposomes was lower than that observed in PC liposomes [65]. As expected, Al (10–100 μM) binding to the membrane caused an increase in the surface potential of PC/PPI liposomes, an effect that not only depended on Al concentration but also on PPI relative proportion in the bilayer [65]. For example, 2.5 μM Al caused an increase in PC liposomes surface potential of 0.05 mV, while in PC/PPI (60:40 molar ratio) liposomes the increase was of 1.55 mV.

In our experimental model, and similar to that observed in liposomes and in cultured cells, Al interaction with PPI phosphate groups caused the segregation of these lipids, forming clusters enriched in PPI. According to the higher Al-binding to PPI-containing membranes, a higher extent of lipid lateral phase separation was observed in these membranes compared to PC liposomes [65], effect that not only depended on Al concentration but also on the amount of PPI present in the membranes. This could be explained in terms of the amount of potential binding sites for Al, and the physical distance between PPI. In liposomes containing only a 10 molar% of PPI, a larger spatial separation between the PPI phosphate groups could lead to the binding of Al to the membrane with a stoichiometry of one Al per phospholipid. In contrast, in PPI-enriched membranes (p. e. in 40 molar% liposomes), Al could bind to phosphate groups present in vicinal PPI moieties at an Al/phospholipid ratio of 1:2 or 1:3. This would enhance Al-induced clustering of PPI in the lateral phase of the bilayer. Supporting this, Al did not induce aggregation in this system, as evaluated from steady-state light scattering, implying that in PPI-containing membranes *cis*-interactions would be kinetically and thermodynamically more favorable than *trans*-interactions.

Similar to the above-described results, in this experimental model Al caused a decrease of membrane fluidity [65]. Again, the magnitude of the Al-mediated membrane rigidification depended not only on Al concentration but also on PPI relative amount in the bilayer. In this case, membrane fluidity was investigated

using three fluorescent probes: 6-AS, 12-AS, and 16-AP. These probes sense changes in membrane fluidity in their surroundings at different depths of the bilayer. While 6-AS evaluates the fluidity in a region close to the water–lipid interface, 12-AS and 16-AP locate in deeper regions of the membrane and sense the fluidity in the hydrophobic core of the bilayer. Al caused a decrease in membrane fluidity close to the polar headgroups of phospholipids, but this rigidifying effect propagated into the hydrophobic region [65], being the magnitude of the change higher in the deepest regions of the bilayer than in the liposome surface.

We finally investigated how Al-induced changes on PPI-containing membranes rheology could affect the activity of the enzyme PI-PLC. For the experiments, we worked with PI-PLC isolated from bovine brain. The obtained protein had a lower molecular weight than the three PI-PLC present in the brain, and was formerly known as the α isoform of PI-PLC which corresponded to an active hydrolytic fragment of the δ isoform [66]. This enzyme did not affect PC, PI, or PIP concentrations, but specifically hydrolyzed PIP₂ [65]. The activity of the enzyme toward its substrate in intact liposomes was similar to that obtained after liposomes disruption with a non-ionic detergent, indicating that the enzyme had complete accessibility to its substrate in liposome membranes.

Al caused a significant and concentration-dependent decrease in PIP₂ hydrolysis by PI-PLC [65]. The apparent inhibitory concentration was 2.5 μ M Al, slightly higher than that reported for the δ isoform of PI-PLC (0.2 μ M) [67]. Interestingly, the inhibitory effect of Al was abolished when liposomes were disrupted into micelles. When Triton X-100 was added to PPI-containing liposomes, this detergent determined the spatial separation of PIP₂ molecules that were previously clustered by Al. However, the strength of Al interaction with PPI phosphate groups is high enough to remain bound even in the presence of a detergent. Therefore, a possible interaction of Al with the catalytic site of PI-PLC that could result in the enzyme inactivation was discarded. Also, the possibility that the detergent could *per se* release Al from its binding sites, especially to those containing extra phosphate groups, was ruled out.

Interestingly, when PPI-containing liposomes were incubated in the presence of the enzyme PLC, Al had no effect on PLC activity [68]. This finding is in close agreement with the fact that, although Al binds to PC, the strength of this binding is lower, and therefore Al could be easily displaced from its binding to this phospholipid.

Together, our experimental data (summarized in Fig. 6) suggest that Al-binding to membrane PPI results in changes in membrane physical properties, such as membrane surface potential, lipid clustering, and fluidity. Consequently, PI-PLC has a decreased accessibility to its substrate, resulting in a decreased hydrolysis of PIP₂. Through this mechanism, rather than through a direct interaction of the metal with the enzyme, Al could interfere with other PPI-associated processes that occur in cells.

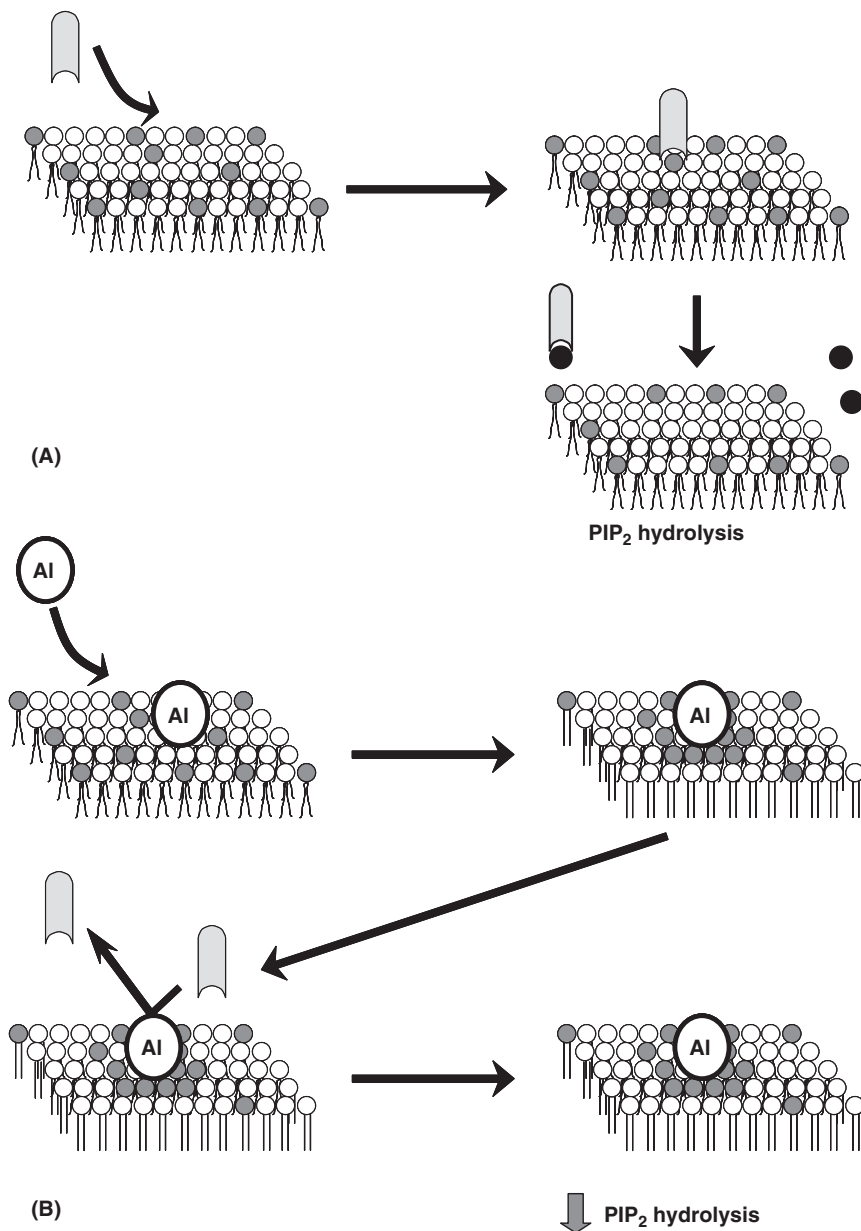


Fig. 6. Mechanism proposed for the inhibitory action of Al and related metals on phosphoinositide hydrolysis. \square = PI-PLC; \bullet = inositol 1,4,5-trisphosphate.

CONCLUDING REMARKS

Al is a neurotoxic metal which has been implied not only in the pathological effects associated with high Al exposure but as a factor contributing to the initiation and/or progression of different neurological disorders. The mechanisms involved in the deleterious effects of Al are not completely understood but the high affinity of the metal for membrane lipids points biological membranes as a major target of its damaging effect.

Evidence from other laboratories and ours has shown that Al can interact with model membranes and promote liposome aggregation, fusion, lateral phase separation, membrane rigidification, and dehydration of the polar head groups. Any of these effects could *per se* affect membrane-associated processes. But different aspects should be considered in the action of Al on biological membranes: (a) the high affinity of the metal for negatively charged phospholipids could determine high local concentrations of the metal in certain membrane domains and/or lead to the accumulation of the metal in certain types of membranes or organelles; (b) the presence of certain lipids, such as galactolipids, can modulate the local effects of Al on membranes; and (c) Al could have generalized effects on biological membranes but, most probably, it will affect select processes occurring in particular domains of the membranes.

The mentioned effects of Al on membrane rheology are not limited to model membranes. They also occur in isolated biological membranes and in cellular (neuroblastoma cells) and animal models of Al toxicity. This effect depends on the composition of the biological membranes, which was evidenced by the differential effects found in myelin and synaptosomal membranes and between differentiated and non-differentiated neuroblastoma cells.

We have found that through its interaction with membranes Al affects two membrane related processes: (a) the rate of membrane lipid oxidation, which can alter the function and/or the physical properties of the bilayer, and also release to the media products of lipid oxidation which can oxidize or modify distant molecules such as DNA, and (b) the hydrolysis of PIP₂ which leads to the formation of inositol-1,4,5-trisphosphate and diacylglycerol, which mediates an increase in the intracellular Ca²⁺ concentration and activate protein kinase C, respectively, and constitute the initiation of a number of relevant signaling events.

In summary, Al interaction with biological membranes and the associated alterations in membrane physical properties could be a key event in Al neurotoxic effects. The consequences of Al interactions with membranes could be multiple, considering the numerous events that occur at the membrane level, such as membrane selective permeability, the transport of different molecules, the function of membrane associated proteins (enzymes, receptors), the modulation of select signaling cascades, etc. Further research will help to elucidate this hypothesis as well as to understand the potential contribution of Al to neurological disorders.

ACKNOWLEDGEMENTS

This work has been supported by grants from the University of Buenos Aires, Fundación Antorchas, and CONICET, Argentina.

REFERENCES

- [1] P.O. Ganrot, Metabolism and possible health effects of aluminum, *Environ. Health. Perspect.* 65 (1986) 363–441.
- [2] T.H. Ittel, Determinants of gastrointestinal absorption and distribution of aluminium in health and uraemia, *Nephrol. Dial Transplant* 8 (Suppl. 1) (1993) 17–24.
- [3] E. Roberts, Alzheimer's disease may begin in the nose and may be caused by aluminosilicates, *Neurobiol. Aging* 7 (1986) 561–567.
- [4] C. Exley, Does antiperspirant use increase the risk of aluminium-related disease, including Alzheimer's disease? *Mol. Med. Today* 4 (1998) 107–109.
- [5] R.A. Yokel, M. Wilson, W.R. Harris, A.P. Halestrap, Aluminum citrate uptake by immortalized brain endothelial cells: implications for its blood-brain barrier transport, *Brain Res.* 930 (2002) 101–110.
- [6] R. Yokel, S. Rhineheimer, R. Brauer, P. Sharma, D. Elmore, P. McNamara, Brain aluminum clearance is slow, *Tox. Sci.* 54 (2000) 35.
- [7] R. Yokel, S. Rhineheimer, P. Sharma, D. Elmore, P. McNamara, Entry, half-life, and desferrioxamine-accelerated clearance of brain aluminum after a single ^{26}Al exposure, *Toxicol. Sci.* 64 (2001) 77–82.
- [8] T.J. Shafer, W.R. Mundy, H.A. Tilson, Aluminum decreases muscarinic, adrenergic, and metabotropic receptor-stimulated phosphoinositide hydrolysis in hippocampal and cortical slices from rat brain, *Brain Res.* 629 (1993) 133–140.
- [9] D. Julka, R. Sandhir, K.D. Gill, Altered cholinergic metabolism in rat CNS following aluminum exposure: implications on learning performance, *J. Neurochem.* 65 (1995) 2157–2164.
- [10] M. Llansola, M.D. Minana, C. Montoliu, R. Saez, R. Corbalan, L. Manzo, V. Felipo, Prenatal exposure to aluminum reduces expression of neuronal nitric oxide synthase and of soluble guanylate cyclase and impairs glutamatergic neurotransmission in rat cerebellum, *J. Neurochem.* 73 (1999) 712–718.
- [11] P.I. Oteiza, M.S. Golub, M.E. Gershwin, J.M. Donald, C.L. Keen, The influence of high dietary aluminum on brain microtubule polymerization in mice, *Toxicol. Lett.* 47 (1989) 279–285.
- [12] R. Ahmad, M. Naoui, J.F. Neault, S. Diamantoglou, H.A. Tajmir-Riahi, An FTIR spectroscopic study of calf-thymus DNA complexation with Al(III) and Ga(III) cations, *J. Biomol. Struct. Dyn.* 13 (1996) 795–802.
- [13] J.M. Gutteridge, G.J. Quinlan, I. Clark, B. Halliwell, Aluminium salts accelerate peroxidation of membrane lipids stimulated by iron salts, *Biochim. Biophys. Acta* 835 (1985) 441–447.
- [14] G.J. Quinlan, B. Halliwell, C.P. Moorhouse, J.M. Gutteridge, Action of lead(II) and aluminium (III) ions on iron-stimulated lipid peroxidation in liposomes, erythrocytes and rat liver microsomal fractions, *Biochim. Biophys. Acta* 962 (1988) 196–200.
- [15] P.I. Oteiza, A mechanism for the stimulatory effect of aluminum on iron-induced lipid peroxidation, *Arch. Biochem. Biophys.* 308 (1994) 374–379.
- [16] C.G. Fraga, P.I. Oteiza, M.S. Golub, M.E. Gershwin, C.L. Keen, Effects of aluminum on brain lipid peroxidation, *Toxicol. Lett.* 51 (1990) 213–219.
- [17] P.I. Oteiza, C.L. Keen, B. Han, M.S. Golub, Aluminum accumulation and neurotoxicity in Swiss-Webster mice after long-term dietary exposure to aluminum and citrate, *Metabolism* 42 (1993) 1296–1300.
- [18] W. Norton, in: P. Morell (Ed.), *Myelin*. Plenum Press, New York, 1977.

- [19] I. Haller, M.J. Freiser, Structural changes in bilayer membranes by multivalent ions, *Biochim. Biophys. Acta* 455 (1976) 739–748.
- [20] C.H. Lee, A.K. Hajra, Molecular species of diacylglycerols and phosphoglycerides and the postmortem changes in the molecular species of diacylglycerols in rat brains, *J. Neurochem.* 56 (1991) 370–379.
- [21] D. Atkinson, H. Hauser, G.G. Shipley, J.M. Stubbs, Structure and morphology of phosphatidylserine dispersions, *Biochim. Biophys. Acta* 339 (1974) 10–29.
- [22] D. Papahadjopoulos, W.J. Vail, C. Newton, S. Nir, K. Jacobson, G. Poste, R. Lazo, Studies on membrane fusion. III. The role of calcium-induced phase changes, *Biochim. Biophys. Acta* 465 (1977) 579–598.
- [23] J. Wilschut, N. Duzgunes, D. Hoekstra, D. Papahadjopoulos, Modulation of membrane fusion by membrane fluidity: temperature dependence of divalent cation induced fusion of phosphatidylserine vesicles, *Biochemistry* 24 (1985) 8–14.
- [24] R. New, in: D. Rickwood, B. Hames, (Eds.), *Liposomes, a practical approach*, IRC Press, Oxford, England, 1990.
- [25] S.V. Verstraeten, P.I. Oteiza, Sc^{3+} , Ga^{3+} , In^{3+} , Y^{3+} , and Be^{2+} promote changes in membrane physical properties and facilitate Fe^{2+} -initiated lipid peroxidation, *Arch. Biochem. Biophys.* 322 (1995) 284–290.
- [26] A. Chattopadhyay, E. London, Parallax method for direct measurement of membrane penetration depth utilizing fluorescence quenching by spin-labeled phospholipids, *Biochemistry* 26 (1987) 39–45.
- [27] J. Wilschut, N. Duzgunes, D. Papahadjopoulos, Calcium/magnesium specificity in membrane fusion: kinetics of aggregation and fusion of phosphatidylserine vesicles and the role of bilayer curvature, *Biochemistry* 20 (1981) 3126–3133.
- [28] K.D. Barfield, D.R. Bevan, Fusion of phospholipid vesicles induced by Zn^{2+} , Cd^{2+} , and Hg^{2+} , *Biochem. Biophys. Res. Commun.* 128 (1985) 389–395.
- [29] S.W. Hui, N.B. He, Molecular organization in cholesterol-lecithin bilayers by X-ray and electron diffraction measurements, *Biochemistry* 22 (1983) 1159–1164.
- [30] D. Papahadjopoulos, G. Poste, B.E. Schaeffer, W.J. Vail, Membrane fusion and molecular segregation in phospholipid vesicles, *Biochim. Biophys. Acta* 352 (1974) 10–28.
- [31] K. Jorgensen, M.M. Sperotto, O.G. Mouritsen, J.H. Ipsen, M.J. Zuckermann, Phase equilibria and local structure in binary lipid bilayers, *Biochim. Biophys. Acta* 1152 (1993) 135–145.
- [32] K. Jorgensen, O.G. Mouritsen, Phase separation dynamics and lateral organization of two-component lipid membranes, *Biophys. J.* 69 (1995) 942–954.
- [33] S.V. Verstraeten, L.V. Nogueira, S. Schreier, P.I. Oteiza, Effect of trivalent metal ions on phase separation and membrane lipid packing: role in lipid peroxidation, *Arch. Biochem. Biophys.* 338 (1997) 121–127.
- [34] S.V. Verstraeten, C.L. Keen, M.S. Golub, P.I. Oteiza, Membrane composition can influence the rate of Al^{3+} -mediated lipid oxidation: effect of galactolipids, *Biochem. J.* 333 (1998) 833–838.
- [35] M.J. Ruocco, G.G. Shipley, E. Oldfield, Galactocerebroside-phospholipid interactions in bilayer membranes, *Biophys. J.* 43 (1983) 91–101.
- [36] E.A. Disalvo, Leakage from egg phosphatidylcholine vesicles induced by Ca^{2+} and alcohols, *Biochim. Biophys. Acta* 905 (1987) 9–16.
- [37] D.R. Crapper, S. Quittkat, S.S. Krishnan, A.J. Dalton, U. De Boni, Intranuclear aluminum content in Alzheimer's disease, dialysis encephalopathy, and experimental aluminum encephalopathy, *Acta Neuropathol. (Berl.)* 50 (1980) 19–24.
- [38] T. Parasassi, E. Gratton, Membrane lipid domains and dynamics as detected by Laurdan fluorescence, *J. Fluorescence* 5 (1995) 59–69.
- [39] S.V. Verstraeten, P.I. Oteiza, Effects of Al^{3+} and related metals on membrane phase state and hydration: correlation with lipid oxidation, *Arch. Biochem. Biophys.* 375 (2000) 340–346.

- [40] S.V. Verstraeten. Mechanisms of the oxidative damage to membranes mediated by aluminum and the related cations. Effects *in vitro* and *in vivo*. [Doctoral Thesis]. Buenos Aires, Argentina: University of Buenos Aires, 2000 165 p.
- [41] R.R. Brenner, Effect of unsaturated acids on membrane structure and enzyme kinetics, *Prog. Lipid Res.* 23 (1984) 69–96.
- [42] V.N. Adonaylo, P.I. Oteiza, Pb^{2+} promotes lipid oxidation and alterations in membrane physical properties, *Toxicology* 132 (1999) 19–32.
- [43] M.P. Zago, P.I. Oteiza, The antioxidant properties of zinc: interactions with iron and antioxidants, *Free Radic. Biol. Med.* 31 (2001) 266–274.
- [44] A. Campbell, D. Hamai, S.C. Bondy, Differential toxicity of aluminum salts in human cell lines of neural origin: implications for neurodegeneration, *Neurotoxicology* 22 (2001) 63–71.
- [45] S.V. Verstraeten, A.G. Erlejman, M.P. Zago, P.I. Oteiza, Aluminum affects membrane physical properties in human neuroblastoma (IMR-32) cells both before and after differentiation, *Arch. Biochem. Biophys.* 399 (2002) 167–173.
- [46] M.S. Golub, B. Han, C.L. Keen, M.E. Gershwin, R.P. Tarara, Behavioral performance of Swiss Webster mice exposed to excess dietary aluminum during development or during development and as adults, *Toxicol. Appl. Pharmacol.* 133 (1995) 64–72.
- [47] H. Bielarczyk, M. Tomaszewicz, A. Szutowicz, Effect of aluminum on acetyl-CoA and acetylcholine metabolism in nerve terminals, *J. Neurochem.* 70 (1998) 1175–1181.
- [48] S.V. Verstraeten, M.S. Golub, C.L. Keen, P.I. Oteiza, Myelin is a preferential target of aluminum-mediated oxidative damage, *Arch. Biochem. Biophys.* 344 (1997) 289–294.
- [49] C. Weis, A. Haug, Aluminum-altered membrane dynamics in human red blood cell white ghosts, *Thromb. Res.* 54 (1989) 141–149.
- [50] R. Gerschman, D.L. Gilbert, S.W. Nye, P. Dwyer, W.O. Fenn, Oxygen poisoning and x-irradiation: a mechanism in common, *Science* 119 (1954) 623–626.
- [51] C.P. LeBel, S.C. Bondy, Oxygen radicals: common mediators of neurotoxicity, *Neurotoxicol. Teratol.* 13 (1991) 341–346.
- [52] M.B. Youdim, Iron in the brain: implications for Parkinson's and Alzheimer's diseases, *Mt. Sinai J. Med.* 55 (1988) 97–101.
- [53] R.B. Martin, The chemistry of aluminum as related to biology and medicine, *Clin. Chem.* 32 (1986) 1797–1806.
- [54] G. Cervato, P. Viani, M. Masserini, C. Di Iorio, B. Cestaro, Studies on peroxidation of arachidonic acid in different liposomes below and above phase transition temperature, *Chem. Phys. Lipids* 49 (1988) 135–139.
- [55] L.R. McLean, K.A. Hagaman, Effect of lipid physical state on the rate of peroxidation of liposomes, *Free Radic. Biol. Med.* 12 (1992) 113–119.
- [56] H. Mowri, S. Nojima, K. Inoue, Effect of lipid composition of liposomes on their sensitivity to peroxidation, *J. Biochem. (Tokyo)* 95 (1984) 551–558.
- [57] S. Kong, S. Liochev, I. Fridovich, Aluminum(III) facilitates the oxidation of NADH by the superoxide anion, *Free Radic. Biol. Med.* 13 (1992) 79–81.
- [58] L. Meglio, P.I. Oteiza, Aluminum enhances melanin-induced lipid peroxidation, *Neurochem. Res.* 24 (1999) 1001–1008.
- [59] C. Exley, The pro-oxidant activity of aluminum, *Free Radic. Biol. Med.* 36 (2004) 380–387.
- [60] E.C. Hirsch, J.P. Brandel, P. Galle, F. Javoy-Agid, Y. Agid, Iron and aluminum increase in the substantia nigra of patients with Parkinson's disease: an X-ray microanalysis, *J. Neurochem.* 56 (1991) 446–451.
- [61] P.F. Good, C.W. Olanow, D.P. Perl, Neuromelanin-containing neurons of the substantia nigra accumulate iron and aluminum in Parkinson's disease: a LAMMA study, *Brain Res.* 593 (1992) 343–346.
- [62] L.J. McDonald, M.D. Mamrack, Aluminum affects phosphoinositide hydrolysis by phosphoinositidase C, *Biochem. Biophys. Res. Commun.* 155 (1988) 203–208.

- [63] L.J. McDonald, M.D. Mamrack, Phosphoinositide hydrolysis by phospholipase C modulated by multivalent cations La^{3+} , Al^{3+} , neomycin, polyamines, and melittin, *J. Lipid Mediat. Cell Signal* 11 (1995) 81–91.
- [64] A.C. Nostrandt, T.J. Shafer, W.R. Mundy, S. Padilla, Inhibition of rat brain phosphatidylinositol-specific phospholipase C by aluminum: regional differences, interactions with aluminum salts, and mechanisms, *Toxicol. Appl. Pharmacol.* 136 (1996) 118–125.
- [65] S.V. Verstraeten, P.I. Oteiza, Al^{3+} -mediated changes in membrane physical properties participate in the inhibition of polyphosphoinositide hydrolysis, *Arch. Biochem. Biophys.* 408 (2002) 263–271.
- [66] G.D. Taylor, J.A. Fee, D.F. Silbert, S.L. Hofmann, PI-specific phospholipase C alpha from sheep seminal vesicles is a proteolytic fragment of PI-PLC delta, *Biochem. Biophys. Res. Commun.* 188 (1992) 1176–1183.
- [67] L.J. McDonald, M.D. Mamrack, Phosphoinositide hydrolysis by phospholipase C modulated by multivalent cations $\text{La}(3^+)$, $\text{Al}(3^+)$, neomycin, polyamines, and melittin, *J. Lipid Mediat. Cell Signal* 11 (1995) 81–91.
- [68] S.V. Verstraeten, M.S. Villaverde, P.I. Oteiza, Al^{3+} -mediated changes on membrane fluidity affects the activity of PI-PLC but not of PLC, *Chem. Phys. Lipids* 122 (2003) 159–163.
- [69] E. de Paula, S. Schreier, Use of a novel method for determination of partition coefficients to compare the effect of local anesthetics on membrane structure, *Biochim. Biophys. Acta* 1240 (1995) 25–33.

CHAPTER 4

Interaction of Plant Polyphenols with Liposomes

Tsutomu Nakayama,* Katsuko Kajiya, and Shigenori Kumazawa

Laboratory of Functional Food Science and COE program in the 21st Century, School of Food and Nutritional Sciences, University of Shizuoka, 52-1 Yada, Shizuoka 422-8526, Japan

Contents

1. Introduction	108
2. General Methods	109
2.1. Measurement of the amount of a polyphenol incorporated into liposomes	109
2.2. Measurement of where a polyphenol is located in lipid bilayers	111
2.3. Measurement of membrane damage caused by a polyphenol	111
2.4. Partition coefficient	111
2.5. Colony formation assay for cytotoxic activity of a polyphenol	112
2.6. Colony formation assay for antioxidant activity of a polyphenol	112
3. Affinity of Polyphenols for Lipid Bilayers	112
3.1. Gallic acid esters	112
3.2. Caffeic acid esters	113
3.3. Curcuminoids	114
3.4. Flavonols	114
3.5. Isoflavones	114
4. Interactions of Catechins with Liposomes	116
4.1. Factors affecting the affinity of catechins for lipid bilayers	116
4.1.1. Structure–activity relationships	116
4.1.2. External factors	119
4.2. Location of catechin in the lipid bilayers	122
4.3. Membrane damage caused by catechins	123
4.4. Antibacterial activity of (+)-catechin derivatives and their interaction with liposomes	124
5. Direct Evidence of Incorporation of EGCg into Lipid Bilayers by Solid-State Nuclear Magnetic Resonance	126
6. Conclusion	130
Acknowledgments	130
References	130

Abstract

The biological activities of plant polyphenols have been examined by various methods *in vitro* and *in vivo* for prediction of their ability to prevent human diseases. Their activities found in *in vitro* experiments with cultured mammalian cells should reflect the amount incorporated into the cells during incubation. Since no transporter specific to plant polyphenols has been found in mammalian cells, it is supposed that most polyphenols are

*Corresponding author. Tel.: +81-54-264-5522; Fax: +81-54-264-5551;
E-mail: nakayatu@smail.u-shizuoka-ken.ac.jp

incorporated into the cells by passive transport and the amount incorporated is related to the affinity of the polyphenol for the cell membranes. In general, measurements of the amount of a polyphenol incorporated into the cell membranes or the cells are difficult and inaccurate, because the amount is very low and some polyphenols are unstable and metabolized immediately after incorporation. We developed a method to measure the amount of polyphenols incorporated into the lipid bilayers of liposomes with a dense internal aqueous phase. The higher relative density of the liposomes than that of water enabled to separate the medium and the liposomes by ultracentrifugation for a short time after incubation. Consequently, the amount of a polyphenol incorporated into the separated liposomes was selectively measured. With this method, the affinities of various kinds of plant polyphenols, including phenyl propanoids, gallic acid esters, curcumin, flavonoids and isoflavones have been investigated. In particular, interaction of tea catechins with lipid bilayers has been investigated in detail. Epicatechin (EC), epigallocatechin (EGC), epicatechin gallate (ECg) and epigallocatechin gallate (EGCg) are the major components of polyphenols in green tea infusions. EGCg is the most abundant among these compounds. The reported biological activities of EC and EGC were often lower than those of their corresponding gallic acid esters, i.e., ECg and EGCg. We clarified that EC and EGC had lower affinities for the lipid bilayers of liposomes than ECg and EGCg. This indicates that the interaction of tea catechins with the lipid bilayer partly governs their activities. In addition to the presence of the gallic acid ester, the number of the hydroxyl groups on the B-ring and the steric character of the C-ring affected the affinity of the catechins for the lipid bilayers. Furthermore, the external factors such as salt concentration in an aqueous medium of the liposome suspension, the electric charges of the lipid bilayers and the presence of EC governed the affinity of EGCg for the lipid bilayers. The interaction of EGCg with a model membrane was also examined by solid state ^{31}P and ^2H NMR. These NMR observations provide direct experimental evidence that EGCg molecule interacts with the lipid bilayers. Using liposomes with a dense internal aqueous phase, we also clarified that ECg and EGCg were located on the surface of the lipid bilayers and perturbed the membrane structure.

1. INTRODUCTION

The biological activities of polyphenols contained in plant foods such as vegetables, fruits and teas have been examined by various methods *in vitro* and *in vivo* for prediction of their ability to prevent human diseases. The activity evaluated in experiments *in vitro* with cultured mammalian or bacterial cells should reflect the amount incorporated into the cells. Some tea polyphenols tightly bound 67 kDa laminin receptor [1] and inhibited sodium-dependent glucose transporter by a competitive mechanism [2]. But, so far neither transporter nor receptor specific to any plant polyphenols has been found in mammalian cells. It is supposed that most polyphenols are incorporated into the cells by passive transport and the amount incorporated is related to the affinity of the polyphenol for the cell membranes. For example, some polyphenols suppress the cytotoxicity of hydrogen peroxide toward mammalian and bacterial cells [3–7]. The structure–activity relationships obtained from those experiments suggested that the amount of the compounds incorporated governs the dose-dependency. Measurements of the amounts of a compound incorporated into cells during a certain incubation period

are difficult and inaccurate, because the amount is very low and some polyphenols are metabolized in the cells and/or excluded to the surrounding medium immediately after incorporation. Thus, accurate methods to measure the amount of polyphenols incorporated into model membranes are needed to compare the affinities of a series of polyphenols. In the pharmaceutical sciences, liposome-partitioning systems have been used to investigate the relationship between the biological activity of compounds and their interaction with lipid bilayers. On the other hand, there have been a few reports on the affinity of polyphenols for model membranes. Formerly, no quantitative method to analyze a polyphenol incorporated into model membranes was established. One problem in measurement is the difficulty of separation of the liposomes from the aqueous medium after incubation of the polyphenols. We developed a method to measure the amounts of polyphenols incorporated into the lipid bilayers of liposomes with a dense internal aqueous phase. The higher relative density of the liposomes than that of the surrounding medium enabled to separate the medium and the liposomes by ultracentrifugation for a short time after incubation. Consequently, the amount of a polyphenol incorporated into the liposomes was selectively measured. With this method, the affinities of various kinds of plant polyphenols, including phenyl propanoids, gallic acid esters, curcumin, flavonoids and isoflavones were measured. In particular, interaction of tea catechins with lipid bilayers has been investigated in detail to apply the methods to the liposomes with a dense internal aqueous phase.

2. GENERAL METHODS

The methods to investigate the interaction of polyphenols with liposomes with a dense internal aqueous phase and some general methods in this chapter were described here.

2.1. Measurement of the amount of a polyphenol incorporated into liposomes

Phosphatidylcholine from egg yolk (egg PC) (100 mg) was dissolved in a small amount of chloroform (Fig. 1). The solution was put in a round-bottomed flask and evaporated using a rotary evaporator. The thin film of egg PC on the inner surface of the flask was dried with a vacuum pump. Then, 300 mM aqueous glucose solution (10 ml) was poured into the flask and the mixture was sonicated in an ultrasonic cleaner. The resulting solution of multilamellar vesicles (MLV) was transferred into a 50 ml plastic centrifuge tube and bubbled with N₂ gas. The sealed tube was placed in water in the cavity of a sonicator with a cup-horn and sonicated for 10 min. The liposomal solution was diluted 10 times with phosphate-buffered saline (PBS) (pH 7.4), and untrapped glucose was removed by

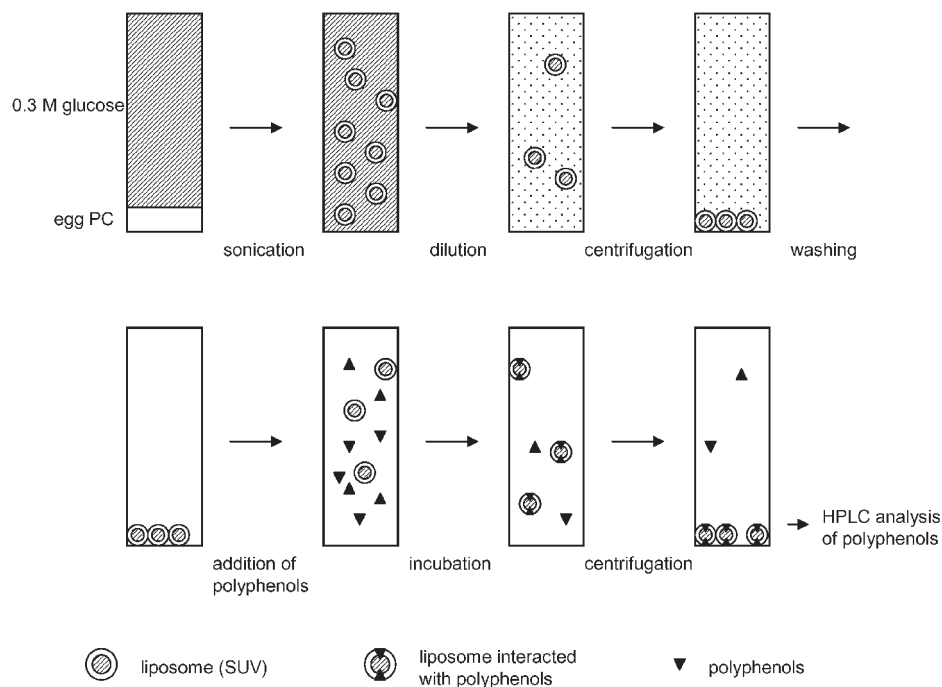


Fig. 1. The protocol of the measurement of a polyphenol incorporated in the lipid bilayers.

centrifugation at 130,000 g for 5 min at 20°C. The liposomes in the sediment were suspended in PBS, pH 7.4 with the final concentration of egg PC in the liposomal solution to 1 mg/ml exactly. Since the density of the internal aqueous phase of the liposomes, small unilamellar vesicles (SUV), was higher than that of the external solution, all liposomes were sedimented readily by centrifugation. In a typical experiment due to measure the amount of a polyphenol incorporated into the lipid bilayers, a polyphenol solution in ethanol (0.1 ml) was added to 0.9 ml of the liposome solution in PBS and the mixture was vortexed. After incubation for 20 min at 20°C, the mixture was centrifuged at 130,000 g for 5 min. After being suspended with PBS and centrifuged again, the liposomes containing the polyphenol were dissolved with 1 ml of ethanol. The amount of the polyphenol in the ethanol solution was measured by high-performance liquid chromatography (HPLC) with a UV detector. The calculated amount of the polyphenol coprecipitated with the liposomes is defined as the amount incorporated into liposomes, which might also reflect the amount of the polyphenol bound to the surface of the lipid bilayers. Except for catechins, the amount of a polyphenol incorporated into the liposomes are proportional to its amounts added to the liposomal solution in the range tested. Thus, the results are expressed as the percentage of the incorporated amount to the added amount.

2.2. Measurement of where a polyphenol is located in lipid bilayers

Location of a polyphenol in the lipid bilayers of liposomes was estimated by measurement of fluorescence of 2-(9-anthroyloxy)stearic acid (2-AS) or 12-(9-anthroyloxy)stearic acid (12-AS) in the lipid bilayers. In the presence of 400 nmol of 2-AS or 12-AS, 100 mg of egg PC was dissolved in a small amount of chloroform. The solution was put in a flask and the solvent evaporated off. The thin film of egg PC on the inner surface of the flask was dried with a vacuum pump. Then, 300 mM aqueous glucose solution (10 ml) was poured into the flask and the mixture was vortexed. The MLV was prepared in the solution by freezing and thawing repeatedly. The liposome solution was diluted 10 times with PBS, and untrapped glucose was removed by centrifugation. The liposomes in the sediment were suspended in PBS. The final concentration of egg PC in the liposome solution was adjusted to 1 mg/ml. The final concentration of 2-AS or 12-AS was 4 μ M. After incubation with a polyphenol for 10 min, the MLV was purified by centrifugation and suspended with PBS. The fluorescence of 2-AS (excitation: 362 nm, emission: 446 nm) or 12-AS (excitation: 381 nm, emission: 446 nm) in the lipid bilayer was measured. The fluorescence intensity was calculated as percent of the fluorescence intensity of 2-AS or 12-AS in the absence of the polyphenol.

2.3. Measurement of membrane damage caused by a polyphenol

Membrane damage of liposomes caused by a polyphenol was analyzed by the amount of calcein that leaked from calcein-trapped liposomes. Egg PC was sonicated in the presence of 300 mM glucose and 100 μ M calcein to prepare SUV with a dense internal aqueous phase containing calcein. The procedures of liposome purification were the same as described in Section 2.1. The required amount of a polyphenol was added to the liposome solution, and the solution was incubated at 20°C for 1 h. The external medium of the liposomes was collected by centrifugation at 130,000 *g* for 5 min. Fluorescence of calcein leaking from the internal aqueous phase to the external medium was measured with excitation at 488 nm and emission at 520 nm. The degree of calcein leakage was calculated as percent of the fluorescence intensity of completely released calcein from the liposomes after treatment with 1 wt% Triton X-100 (polyethylene glycol mono-4-octylphenyl ether).

2.4. Partition coefficient

In the case of a hydrophilic polyphenol such as catechins, its solution in the same buffer used for the liposome experiments such as PBS was vigorously mixed with the same volume of 1-octanol. In the case of the lipophilic polyphenol, its solution in 1-octanol was vigorously mixed with the same volume of the buffer. After centrifugation at 200 *g* for 10 min, the amount of the polyphenol in each layer was

measured by HPLC. The partition coefficient of each catechin was then calculated. The results were expressed as common logarithms.

2.5. Colony formation assay for cytotoxic activity of a polyphenol

In order to clarify the correlation between the cytotoxicity and lipophilicity, the cytotoxicity of a polyphenol was examined by a colony formation assay as an index of a simple biological activity *in vitro*. Chinese hamster lung fibroblast V79 cells were seeded in Petri dishes (~100 cells/dish) and incubated in 5 ml of a minimum essential medium (MEM) supplemented with 10% heat-inactivated fetal bovine serum (FBS) in a humidified atmosphere of 5% CO₂ in air at 37°C for 2 h. After changing the medium to FBS-free MEM, a dimethylsulfoxide solution of a polyphenol (50 µl) was added to the medium, but no polyphenol was added to the control medium. The cells were incubated in these media for 4 h and subsequently in MEM supplemented with FBS for 5 days. Then, the number of the colonies stained with a Giemsa solution was counted. The survival rate (% of control) was calculated by dividing the number of colonies in the medium containing the polyphenol by that in the control medium. Each result is expressed as the mean and standard deviation of four separate cultures.

2.6. Colony formation assay for antioxidant activity of a polyphenol

Chinese hamster V79 cells were seeded in dishes (~100 cells/dish) and incubated in a MEM supplemented with FBS. After the medium had been changed to MEM without FBS, the cells were incubated with indicated concentrations of a polyphenol. After being washed with HEPES-buffered saline HBS (pH 7.3), the cells were incubated with 150 µM H₂O₂ in HBS. After 5 days of culturing, the number of the colonies was counted. The cell survival (% of control) was calculated by dividing the number of colonies of the cells treated with H₂O₂ and/or the respective polyphenol by the number of colonies of untreated control cells.

3. AFFINITY OF POLYPHENOLS FOR LIPID BILAYERS

3.1. Gallic acid esters

The amount of lauryl gallate incorporated into the liposomes was the highest among three gallic acid esters, followed by propyl and methyl gallates (Fig. 2) [8]. Gallic acid was not detected in the liposomes. This result indicates that the affinity of a gallic acid ester for the lipid bilayers depends simply on the chain length of its ester moiety. It has been already reported that 200 nM lauryl gallate, 20 µM propyl gallate and 80 µM methyl gallate were necessary for complete protection against

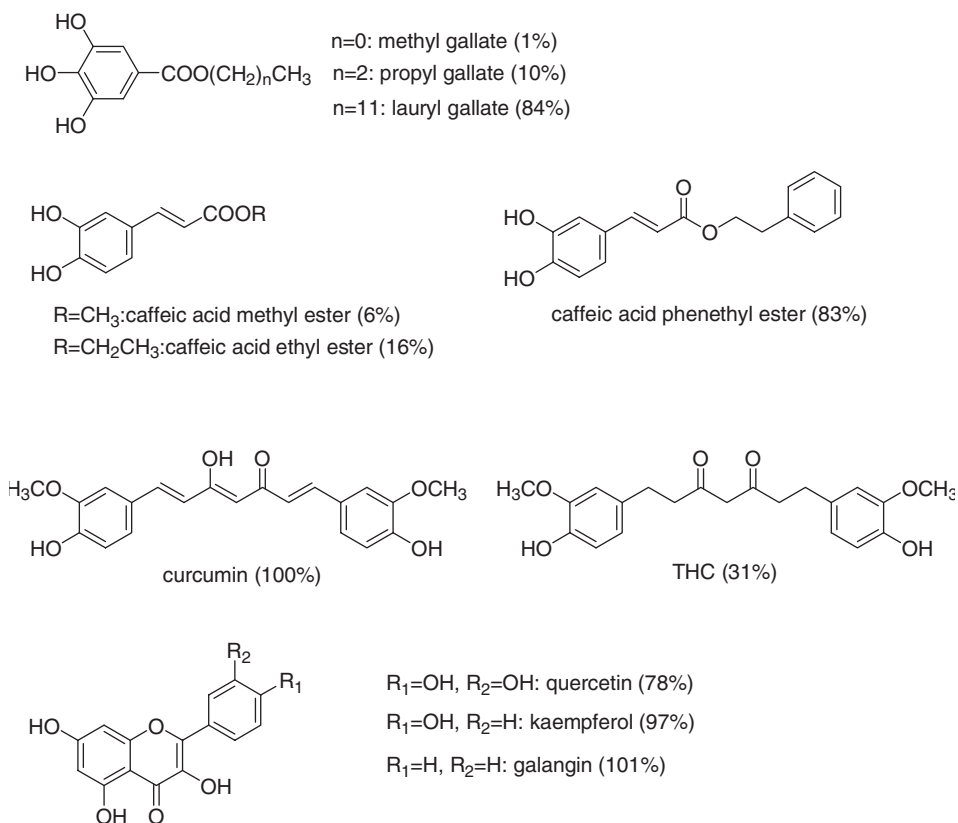


Fig. 2. Chemical structures of gallic acid esters, caffeic acid esters, curcuminoids and flavonols with their ratios incorporated into the liposomes. Source: Data were taken from Refs. [8,11] with permission from the Publisher.

H₂O₂-induced cytotoxicity [3], and that lauryl gallate was the most effective among the gallic acid esters for lowering the SOS induction raised by H₂O₂ [5]. These results support our hypothesis that gallic acid esters with higher affinities exhibit biological activities in lower concentrations.

3.2. Caffeic acid esters

The incorporated amount of caffeic acid phenethyl ester was the highest among the caffeic acid esters, followed by caffeic acid ethyl and methyl esters (Fig. 2) [8]. Caffeic acid was not incorporated into liposomes. The ethyl and methyl esters suppressed H₂O₂-induced cytotoxicity and DNA single-strand breaks, but caffeic acid did not [6]. Dose dependencies of the phenethyl ester, the ethyl ester and the methyl ester on the protection against H₂O₂-induced cytotoxicity [9] indicate that the phenethyl ester was the most effective, followed by the ethyl ester. Thus, the

biological activities examined in these studies reflect the affinity of the esters for the lipid bilayers. The phenethyl ester is a natural caffeic acid ester found in some kinds of propolis [10]. Inhibitory effects of the phenethyl ester on azoxymethane-induced biochemical changes and aberrant crypt foci formation in rat colon, growth of human leukemia HL-60 cells and activation of nuclear transcription factor NF- κ B have been reported (reviewed in ref. [9]). After the phenethyl ester and other caffeic acid esters are supposed to be hydrolyzed by esterase, the resulting caffeic acid should be the very compound exerting those inhibitory effects in the cells, i.e., their affinities for the cell membranes should determine their apparent biological activities.

3.3. Curcuminoids

Curcumin is the major yellow component of turmeric. Colorless tetrahydrocurcumin (THC) is a metabolite of curcumin. The affinity of THC was lower than that of curcumin (Fig. 2) [8], which exhibited cytotoxicity in the cultured cells at concentrations lower than did THC [7]. The flexible and bulky structure of THC might make its incorporation into the lipid bilayers difficult when compared to curcumin. On the other hand, the high affinity for the lipid bilayers of curcumin should be partly ascribed to its rigid and planar structure because of the conjugated system, which also causes its yellow color. It is natural that the three-dimensional interaction of these compounds with the phospholipid bilayers of the liposomes simulate well with that of the cell membranes of cultured cells.

3.4. Flavonols

The affinity for lipid bilayers of the three flavonols, galangin, kaempferol and quercetin, which respectively have no, one and two hydroxyl groups on the B-ring was compared (Fig. 2) [11]. The percentage incorporated into the liposomes was the lowest in quercetin, followed by kaempferol and galangin. These results show that the number of phenolic hydroxyl groups on the B-ring was inversely correlated with the lipophilicity of the flavonols. The cytotoxicity of these compounds by using Chinese hamster lung fibroblast V79 cells was examined to clarify the correlation between the lipophilicity and cytotoxicity. Among the three compounds, galangin was the most toxic, followed by kaempferol and quercetin [11]. This suggests that the lipophilicity governed the amount of flavonol incorporated into the cells and, consequently, the cytotoxicity.

3.5. Isoflavones

Isoflavones occurring ubiquitously in plants such as soybeans exhibit estrogen-like activity. Consumption of isoflavones has been suggested to protect against

hormone-related cancers and cardiovascular diseases [12,13]. The biological activities of numerous isoflavones have been evaluated by various methods *in vitro* with cultured mammalian cells, bacterial cells and low-density lipoproteins (LDL). Some activities have been attributed to the affinity for estrogen receptors [14]. Since the amount incorporated into cells or lipoproteins during incubation is supposed to be another factor, the affinity of isoflavones and their glucosides for lipid bilayers was investigated [15].

Figure 3 indicates that the proportion of an aglycone incorporated into the lipid bilayers was higher than that of its corresponding glucoside. Biochanin A and formononetin with a methoxyl group at 4'-position of the B-ring showed higher affinity for the lipid bilayers than the other aglycones such as genistein and daidzein. Among three glucosides, sissotrin with a methoxyl group at 4'-position of the B-ring showed the highest affinity. The difference of the structures of each pair of compounds, i.e., daidzein vs. genistein, formononetin vs. biochanin A, daidzin vs. genistin, is the absence vs. the presence of a hydroxyl group at 5-position of the A-ring. The percentage of the incorporated amount to the added amount of genistein was higher than the corresponding value of daidzein. Similar results were obtained in the cases of their derivatives with a methoxyl group at 4'-position of the B-ring, i.e., biochanin A and formononetin. The higher activity of genistein than daidzein has been ascribed to its higher affinity for the estrogen receptors [14]. The antioxidant activities against LDL oxidation and inhibitory effects on cell growth in the presence of genistein were stronger than those in the presence of daidzein [16–21]. These results suggest that the affinity for lipid bilayers also affects the activity *in vitro*, especially where the estrogen receptors have no role. Hydroxyl groups are usually expected to increase hydrophilicity as

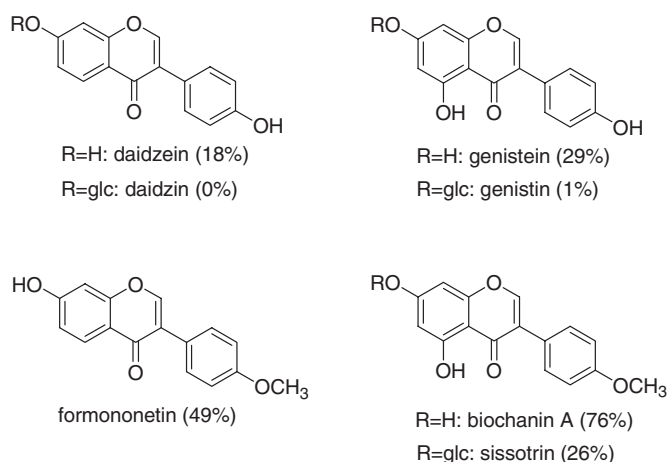


Fig. 3. Chemical structures of isoflavones with their ratios incorporated into the liposomes. The “glc” represents glucosyl moiety. Source: Data were taken from Ref. [15] with permission from the Publisher.

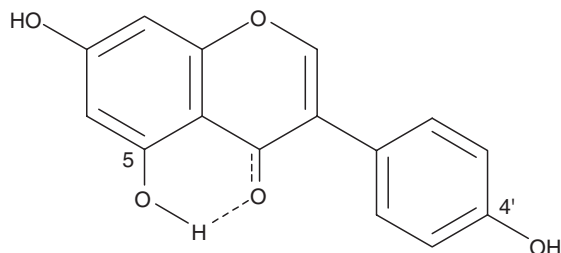


Fig. 4. The proposed six-membered ring in the chemical structure of genistein.

in the case of flavonols described in Section 3.4. Thus, the results seem to be peculiar to the hydroxyl group at 5-position of the A-ring of isoflavones. We postulate that this hydroxyl group forms a six-membered aromatic ring as shown in Fig. 4, resulting in the enhancement of the lipophilicity of the compound. Formation of a similar six-membered ring in the structure of quercetin has been already proposed [22]. The cytotoxic activities of the four aglycones were compared as follows [15]: biochanin A > formononetin > genistein > daidzein. This result indicates that the presence of a hydroxyl group at 5-position of the A-ring and a methoxyl group at 4'-position of the B-ring independently enhanced the cytotoxicity. This is in accordance with the increasing effects of both groups on the proportion of the isoflavones incorporated into the lipid bilayers. Lower binding affinities of formononetin and biochanin A for estrogen receptors α and β than those of genistein and daidzein [14] indicate that these receptors have no role in the cytotoxicity mentioned above. Thus, the cytotoxic activities of the isoflavones estimated by the colony formation assay with V79 cells should be attributed to their affinity for the lipid bilayers. In conclusion, the biological activities of isoflavones evaluated *in vitro* could be governed by their affinity for the lipid components in the cases where the estrogen receptors have no role.

4. INTERACTIONS OF CATECHINS WITH LIPOSOMES

4.1. Factors affecting the affinity of catechins for lipid bilayers

4.1.1. Structure–activity relationships

Catechins are present in fruits and tea infusions. A wide range of biological effects of tea catechins such as antimutagenicity, anticarcinogenicity, antitumorogenicity, antioxidant, antihypercholesterolemia and antibacterial activities have been reported. Usually, the order of the activity of various catechins differs in each case. Some examples of the order of activity of the *cis*-type (epi type) catechins reported previously are as follows. Growth inhibition of human lung cancer cell line: epicatechin gallate (ECg) > epigallocatechin gallate (EGCg) > epigallocatechin (EGC) > epicatechin (EC) [23]; inactivation effects on

human type-A influenza virus, $ECg > EGCg \gg EGC$ [24]; inhibitory effects on the oxidative modification of LDL, $EGCg > ECg > EGC > EC$ or $EGCg > ECg \gg EC > EGC$ [25,26]; antibacterial activity against *Clostridium botulinum*, $EGCg > ECg > EGC > EC$ [27]. These results indicate that the gallic acid esters of catechins such as EGCg and ECg always show higher activities than the catechins without the galloyl moiety such as EGC and EC. Furthermore, it has been reported that EGCg and ECg showed strong interactions with lipid bilayers [28,29]. We postulated that the differences in these activities were partly based on the amounts of compounds incorporated into the lipid bilayers. Tea catechins are classified into *cis*- and *trans*-type from the configuration of the two hydrogens at the 2- and 3-positions on the C-ring (Fig. 5). Green tea infusion contains a large amount of *cis*-type catechins and a small amount of *trans*-type catechins. Saeki *et al.* [30] reported that EGCg showed higher apoptosis-inducing activity than GCg in cultured cells. Tsuchiya [28,31] clarified by measuring fluorescence polarization of liposomal membranes that *cis*-type catechins were more effective for reducing membrane fluidity than *trans*-type catechins. These results suggest that a *cis*-type catechin has higher affinity for the cell membranes than its corresponding *trans*-type catechin. We compared the affinity of *cis*-type catechins, i.e., EC, EGC, ECg and EGCg, and *trans*-type catechins, i.e., catechin (C), gallocatechin (GC), catechin gallate (Cg) and gallocatechin gallate (GCg), for the lipid bilayers [32,33].

Figure 6 shows the typical dose effects of tea catechins on the amount incorporated. Unlike other polyphenols, dose effects of catechins are not linear but convex. In *cis*-type catechins, the amount of ECg incorporated was the highest, followed by EGCg and EC. In *trans*-type catechins, the amount of Cg incorporated was highest, followed by GCg and C. The lower affinity of EC and EGC than that of the corresponding gallic acid ester, ECg and EGCg, implies that the presence of the ester bond contributes to the higher hydrophobicity of the gallic acid esters. The affinity of ECg was higher than that of EGCg, and the affinity of EC was higher than that of EGC. This indicates that three hydroxyl groups in the B-ring of gallocatechins such as EGC and EGCg lowered their hydrophobicity and consequently their affinity for the lipid bilayers in comparison with EC and ECg that have two hydroxyl groups in the B-ring. Furthermore, the amount of ECg incorporated was higher than that of Cg, and the amount of EGCg incorporated was higher than that of GCg. Thus, the affinity of *trans*-type catechins with a galloyl moiety for the lipid bilayers could be lower than that of the respective *cis*-type catechins. The partition coefficients of tea catechins in an 1-octanol/PBS system decreased in the same order (Table 1). The *trans*-type catechins tend to have a lower partition coefficient than the *cis*-type catechins.

Figure 7 shows the stereochemical structures of ECg and Cg. The hydrophobic domain of ECg is liable to protrude into lipid bilayers and lie in contact with the inner lipophilic region, because other hydrophilic domains do not conceal the hydrophobic domain. On the other hand, the hydrophobic domain of Cg is hard to

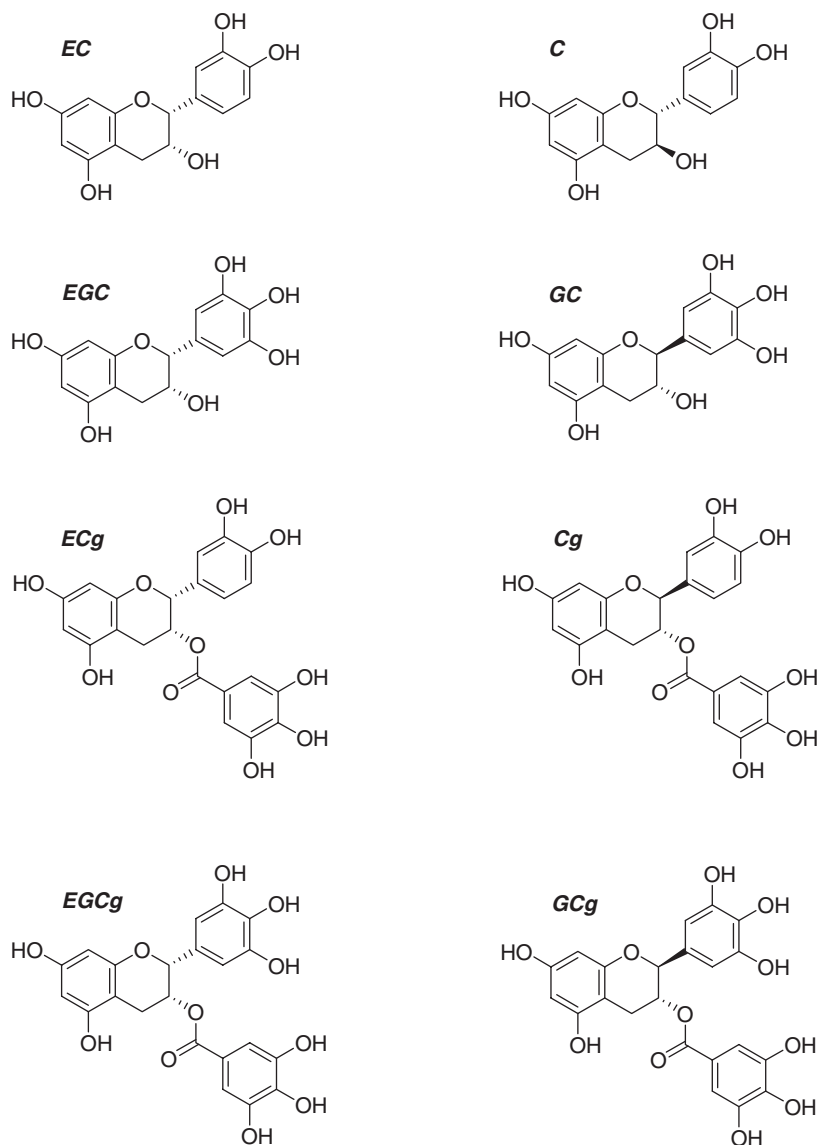


Fig. 5. Chemical structures of tea catechins.

protrude into lipid bilayers, because the hydrophobic domain is located at the center of the molecule, and the hydrophilic domains of A-ring, B-ring and the galloyl moiety interfere with the contact of the hydrophobic domain in the inner lipophilic region of the lipid bilayers.

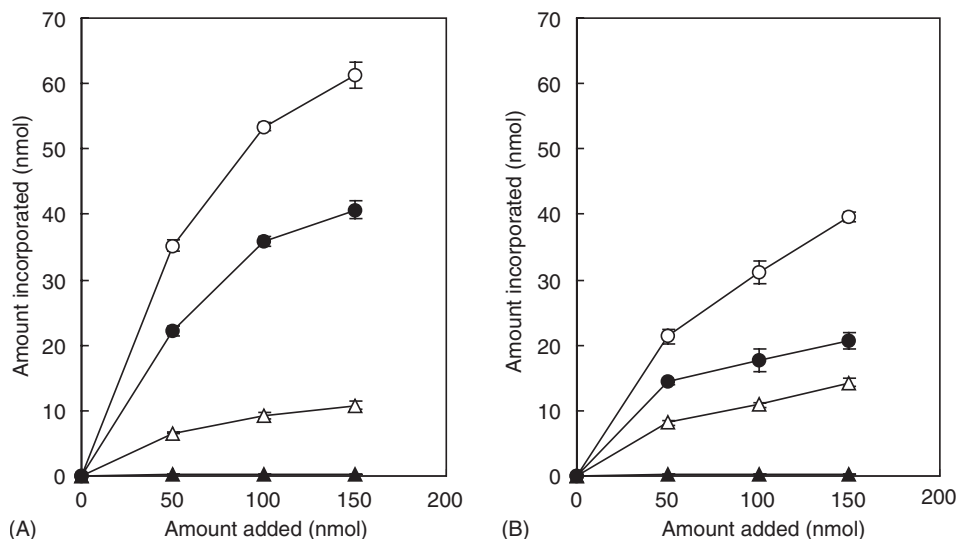


Fig. 6. Dose effects of (A) *cis*-type catechins and (B) *trans*-type catechins on the amount incorporated into the liposomes. (A) ○, ECg; ●, EGCg; △, EC; ▲, EGC. (B) ○, Cg; ●, GCg; △, C; ▲, GC. (From Ref. [33] with permission from the Publisher.)

Table 1. Partition coefficients of tea catechins evaluated with an 1-octanol/PBS system

<i>cis</i> -type catechins	$\log P$	<i>trans</i> -type catechins	$\log P$
ECg	1.79 ± 0.05	Cg	1.63 ± 0.05
EGCg	1.41 ± 0.03	GCg	1.35 ± 0.07
EC	0.30 ± 0.01	C	0.38 ± 0.00
EGC	-0.10 ± 0.00	GC	-0.40 ± 0.00

Note: The results are shown as the mean value of four independent experiments with the SD.

Source: From Ref. [33] with permission from the Publisher.

4.1.2. External factors

The effects of the salt concentration of the medium, the electric charges of the lipid bilayers, and the presence of other catechins were investigated [34]. The amounts of EC, ECg and EGCg incorporated into the lipid bilayers increased as the salt concentration was increased (Table 2). The partition coefficient of each catechin evaluated with an 1-octanol/PBS system also increased as the salt concentration was increased [34]. These results indicate that the partition coefficient and the affinity of the catechins for lipid bilayers strongly depended on the salting-out effect of the aqueous medium. Thus, the *in vitro* activities of a catechin can be expected to depend on the salt concentration of the medium.

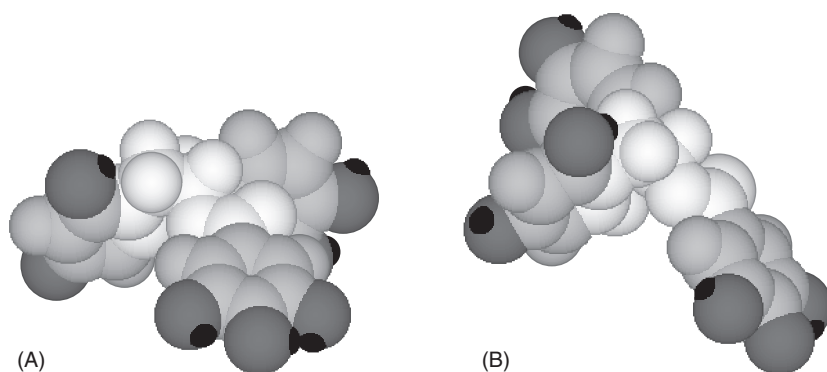


Fig. 7. Space filling model of (A) ECG (B) and Cg. Stereochemical structures were depicted by CS Chem 3D version 6.0 software (Cambridge Soft, USA). A restrained molecular dynamics method was used to calculate the energetically minimum structures of the compounds. The colorless moiety is the hydrophobic domain and the dark color moiety is the hydrophilic domain. (From Ref. [33] with permission from the Publisher.)

Table 2. Amount incorporated into the lipid bilayers of tea catechins in various concentrations of PBS^a

Tea catechin	Incorporation into lipid bilayers (%) ^b		
	1/4 PBS	1/2 PBS	PBS
EGC	0.0 ± 0.0	0.0 ± 0.0	0.0 ± 0.0
EC	9.2 ± 0.4	16.3 ± 0.6	28.8 ± 0.4
EGCg	38.0 ± 0.0	44.5 ± 0.8	46.9 ± 0.1
ECg	53.2 ± 0.4	56.6 ± 0.0	68.1 ± 4.0

^a PBS (pH 7.4) diluted 1-, 2- and 4-fold with water was used as PBS, 1/2 PBS and 1/4 PBS, respectively, and contained 0.9%, 0.45% and 0.225% NaCl, respectively.

^b Each result is shown as the mean ± value SD of four independent experiments.

Source: From Ref. [34] with permission from the Publisher.

The antibacterial activity of catechins is higher against Gram-positive bacteria than that of Gram-negative bacteria [35–38]. The outer membrane of Gram-positive bacteria consists of a thick peptidoglycan layer. Gram-negative bacteria have an external membrane consisting of a phospholipid and lipopolysaccharide outside a thin peptidoglycan layer. Ikigai *et al.* [38] reported that EGCg caused leakage of 5,6-carboxyfluorescein, a fluorescence substance, entrapped in the intraliposomal space and the amount of 5,6-carboxyfluorescein that leaked from the liposomes with negative charge was lower than that leaking from the control liposomes. They explained that the resistance of Gram-negative bacteria to EGCg was attributed to the presence of negatively charged lipopolysaccharides.

To verify their explanation directly, we investigated the effect of the electric charge of the membrane on the affinity of tea catechins for the lipid bilayers [34]. The control liposomes prepared from PC alone do not have net electric charge. On the one hand, the liposomes containing 10% phosphatidyl serine (PS) or dicetylphosphate (DCP) have negative charge, and those containing stearyl amine (SA) have positive charge. The amounts of ECg and EGCg incorporated into the lipid bilayers containing PS or DCP were distinctly lower than those incorporated into the control liposomes (Table 3). On the other, their amounts incorporated into the lipid bilayers containing SA were similar to those incorporated into the control liposomes. These results indicate that electrostatic repulsion between each catechin and the membranes with negative charge in the presence of PS or DCP lowered the affinity.

The constituents of the green tea extracts had a synergistic or additive effect on cancer preventive activity, because the green tea extract had a stronger effect than the same amount of each catechin [39,40]. On the assumption that these synergistic effects were due to enhanced incorporation of the catechins into the cells, the affinity of a catechin for the lipid bilayer in the presence of other catechins was examined. Figure 8 shows that the amount of EGCg and ECg incorporated into the lipid bilayers was increased by the addition of EC. Similar enhancing effects of EC on the partition coefficient of ECg or EGCg in an 1-octanol/PBS system were also observed [34]. Suganuma *et al.* [39,40] reported that EC dose-dependency enhanced apoptosis of the PC-9 human lung cancer cell line induced by EGCg and that the [³H] EGCg incorporation into PC-9 cells was significantly enhanced by EC. Our results indicate that the enhancement of EGCg incorporation into the cells by EC should involve a simple physicochemical process.

Table 3. Amount of tea catechins incorporated into the lipid bilayers with various electrical charges

Tea catechin	Incorporation into lipid bilayers (%)			
	Control	10% PS	10% DCP	10% SA
EGC	0.0 ± 0.0	0.0 ± 0.0	0.0 ± 0.0	0.0 ± 0.0
EC	9.2 ± 0.4	3.7 ± 0.0	6.0 ± 0.0	8.4 ± 0.2
EGCg	36.9 ± 0.7	4.6 ± 0.2	7.1 ± 0.5	37.8 ± 0.3
ECg	53.2 ± 0.4	11.1 ± 0.1	21.1 ± 0.2	56.5 ± 0.6

Note: Each catechin solution (100 nmol) in PBS was added to liposomes of PC in the presence or absence of 10% PS, DCP or SA. The mixture was incubated (20°C for 20 min) and centrifuged. The proportion (%) was calculated by dividing the amount incorporated by the amount added. The liposomes-containing PC alone were used as the control. Each result is shown as the mean ± SD of four independent experiments. Source: From Ref. [34] with permission from the Publisher.

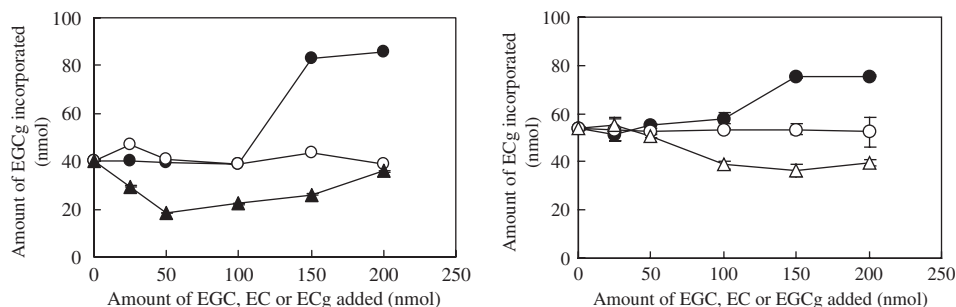


Fig. 8. Amount of a catechin incorporated into lipid bilayers in the presence of other catechins. (A) Incorporation of EGCg and (B) ECg in the presence of ●, EC; ○, EGC; ▲, ECg; and △, EGCg. (From Ref. [34] with permission from the Publisher.)

Fujimura *et al.* [41] reported that EGCg bound to the cell surface and highly associated with plasma membrane microdomains, lipid rafts, on the human basophilic cells. They suggest that the lipid rafts may also play a possible role in the interaction of EGCg with mammalian cells.

4.2. Location of catechin in the lipid bilayers

The location of catechins incorporated into liposomes was investigated by fluorescence quenching of 2-AS and 12-AS with catechins. Kitano *et al.* [29] investigated the location of EGCg incorporated into MLV by fluorescence quenching of 2-AS and 10-AS. They concluded that EGCg was located on the surface region of the lipid bilayer, because EGCg quenched the fluorescence of 2-AS more strongly than that of 10-AS. This effect by fluorescence quenching of 2-AS and 12-AS with *cis*- and *trans*-type catechins was confirmed by the method described in Section 2.2. If a catechin is present in the lipid bilayers, the fluorescence of 2-AS or 12-AS is quenched according to the location of each catechin. The anthroyl group of 2-AS should be located on the surface of the bilayer membrane, while that of 12-AS in a hydrophobic core of the membrane (Fig. 9). Consequently, if a tea catechin locates on the surface of the lipid bilayers, it quenches the fluorescence of 2-AS. On the other hand, if it locates in the hydrophobic core of the lipid bilayers, it quenches that of 12-AS. Figure 10 [33] shows that the quenching effect of ECg on the fluorescence of 2-AS was the highest among *cis*-type catechins, followed by those of EGCg and EC, and the quenching effect of Cg on the fluorescence of 2-AS was the highest among *trans*-catechins, followed by those of GCg and C. EGC and GC had no quenching effect on the fluorescence of 2-AS. These results indicated that ECg, EGCg, EC, Cg, GCg and C located on the surface region of the lipid bilayer. Furthermore, the quenching effect of *trans*-type catechins was lower than that of the corresponding of *cis*-type catechins. Thus, the degree of fluorescence quenching was closely

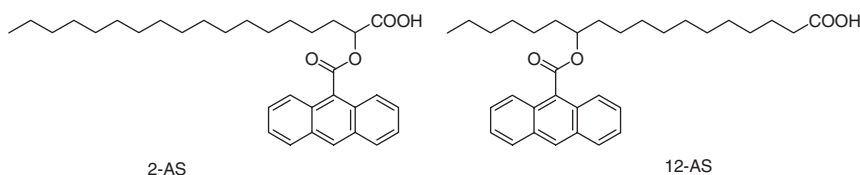


Fig. 9. Chemical structures of 2-AS and 12-AS.

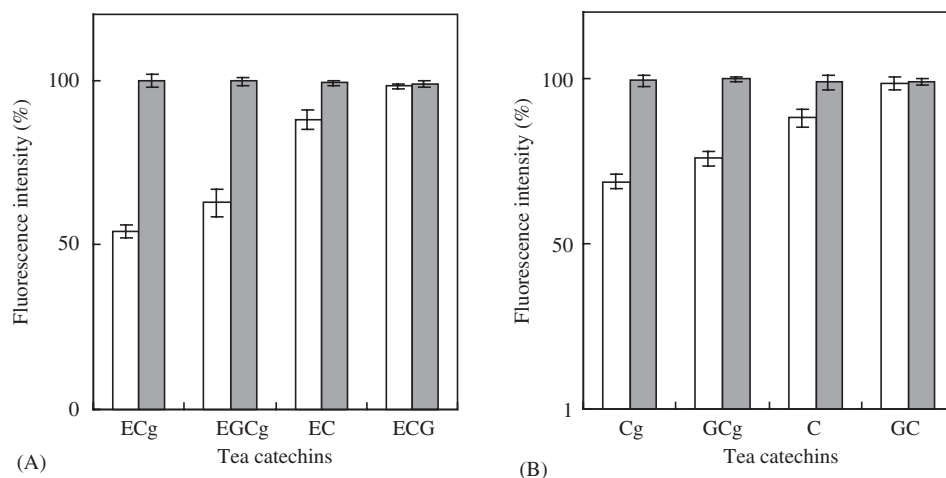


Fig. 10. Effects of (A) *cis*-type catechins and (B) *trans*-type catechins on the fluorescence intensity of 2-AS or 12-AS. The ratio (%) was calculated by dividing the fluorescence intensity by the fluorescence intensity of control solution in the absence of any catechins. The results are shown as the mean value of four independent experiments with the SD. Open bars, 2-AS; grey bars, 12-AS. (From Ref. [33] with permission from the Publisher.)

correlated with the amount of compound incorporated into the lipid bilayers, which is partly attributed to the stereochemical structure.

4.3. Membrane damage caused by catechins

The membrane structure may be altered by the catechins present in the lipid bilayers. Membrane damage of liposomes, caused by a catechin, was analyzed by the method described in Section 2.3. The catechins with galloyl moiety dose-dependently increased calcein leakage (Fig. 11). The effect of ECg was greater than those of EGCg. No effect of EC and ECG was observed. These results suggest that the ratio of calcein leakage, as an index of the membrane damage, also reflects their incorporated amounts. Effects of ECg and EGCg on the physical properties of phospholipid model membranes and the correlation with their antibacterial capacities was examined in detail [42].

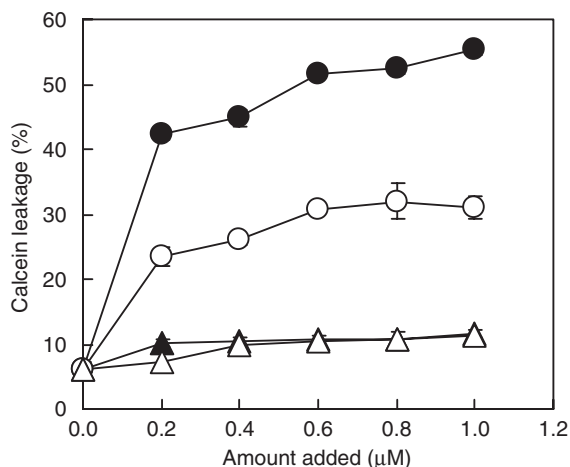


Fig. 11. Dose effects of tea catechins on the calcein leakage from calcein-trapped liposomes. The results are shown as the mean value of four independent experiments with the SD. ●, ECg; ○, EGCG; ▲, EC; △, EGC.

4.4. Antibacterial activity of (+)-catechin derivatives and their interaction with liposomes

The antibacterial activity of various teas and tea catechins has been investigated [43–50]. In these studies, it was found that tea catechins with a galloyl moiety have higher activity than those without a galloyl moiety. It has been suggested that the mechanism of antibacterial activity is associated with the membrane injury activity including effects on the membrane fluidity. Thus, the intensity of the antibacterial activity of tea catechins can partly be explained by the findings described in Section 4.3. It has been reported that the antibacterial activity of EC derivatives with alkyl chain has higher than that of EC [47]. The studies using these derivatives indicated that the antibacterial activity was related to the partition coefficients of these derivatives [51]. We prepared the derivatives with alkyl chain at the 6- and 8-positions of the A-ring of (+)-catechin by the reaction of (+)-catechin with various aldehydes in the presence of methyl mercaptan [52]. These (+)-catechin derivatives were termed C1–C10, according to the carbon number of the reacted aldehyde (Fig. 12).

The antibacterial activity of (+)-catechin derivatives was assayed by the liquid dilution method [53] against six kinds of Gram-positive bacteria (*B. cereus*, *B. circulans*, *B. subtilis*, *S. aureus*, *S. xylosus* and *E. faecalis*) [52]. Since the minimum inhibitory concentration (MIC) changes, by respective derivatives, were quite similar against all six bacteria, Figure 13 shows a typical result, that is the MIC against *B. subtilis*. The MIC of (+)-catechin, C1 and C2 for all tested bacteria was above 400 μg/ml. The MIC decreased with elongating the alkyl chain lengths of the derivatives C1–C4. The antibacterial activities of compounds

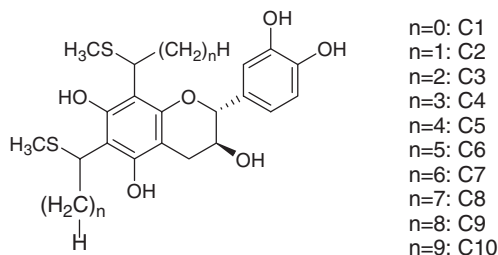


Fig. 12. Chemical structures of the derivatives from (+)-catechin.

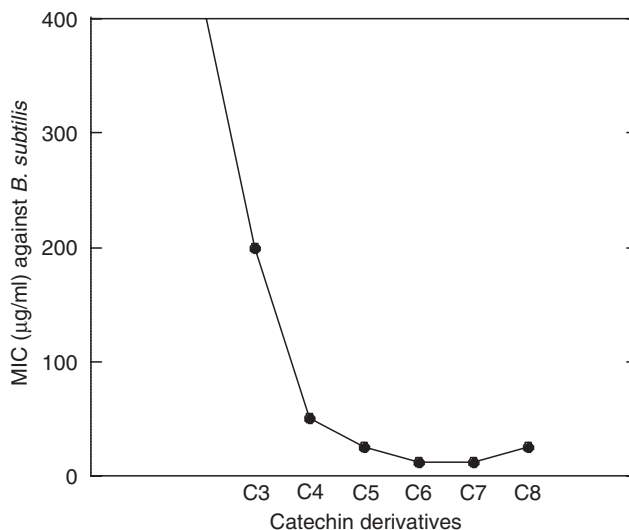


Fig. 13. Minimum inhibitory concentration (MIC) of (+)-catechin derivatives against *B. subtilis* (µg/ml). MICs were determined by the liquid medium dilution method in Mueller–Hinton broth supplemented [53]. (From Ref. [52] with permission from the Publisher).

C4–C7 were very strong. In the case of compounds C9 and C10, the exact antibacterial activity at concentration higher than 100 µg/ml could not be evaluated, because of their low solubility in the medium. Therefore, the effects of C1–C7 on the interaction with the liposomes were investigated further.

The percentage incorporation of the (+)-catechin derivatives into liposomes increased with elongating the alkyl chain lengths of the derivatives (Table 4). The antibacterial activity of (+)-catechin derivatives also increased with elongating the alkyl chain lengths of the derivatives (Fig. 13). The results shown in this table can be summarized as follows. Antibacterial activity: (+)-catechin < C1 < C2 < C3 < C4 < C5, C6, C7; amount incorporated into the lipid bilayers: (+)-catechin < C1 < C2 < C3, C4, C5, C6, C7; ratio of calcein leakage: (+)-catechin, C1, C2, C3 < C4 < C5 < C6 < C7. These results indicate that the antibacterial activity of the

Table 4. Percent incorporation of (+)-catechin derivatives into liposome and their effects on calcein leakage

Test compound	% Incorporation	% Calcein leakage (60 μ M)	% Calcein leakage (10 μ M)
(+)-catechin	13.4 \pm 0.4	7.1 \pm 0.1	
C1	57.1 \pm 2.0	5.6 \pm 2.8	
C2	81.3 \pm 1.7	10.2 \pm 2.2	
C3	101.4 \pm 0.1	8.4 \pm 3.6	
C4	101.0 \pm 0.5	26.3 \pm 2.0	
C5	100.0 \pm 0.0	56.8 \pm 1.9	32.5 \pm 5.4
C6	99.1 \pm 0.4		39.7 \pm 1.6
C7	100.0 \pm 0.2		54.6 \pm 6.5

Note: Each result is shown as the mean value of four independent experiments with the SD. The concentrations of the test compounds to examine the calcein leakage are 60 μ M for (+)-catechin and C1–C5, and 10 μ M for C5–C7. A small amount of calcein leakage (6.2 \pm 1.1%) was observed even in the absence of catechins.

Source: From Ref. [52] with permission from the Publisher.

(+)-catechin derivatives and their interaction with the bacterial membrane are closely correlated. The percentage incorporation of C3–C7 into the liposomes was almost 100%, but the antibacterial activity of C3 was weaker than those of C4–C7. Table 4 shows that C4 or more caused significant calcein leakage, but C3 did not. Thus it is presumed that the antibacterial activity of the (+)-catechin derivatives is associated with both the affinity for the lipid bilayer and the disruption of the membrane structure.

5. DIRECT EVIDENCE OF INCORPORATION OF EGCG INTO LIPID BILAYERS BY SOLID-STATE NUCLEAR MAGNETIC RESONANCE

The findings obtained by the experiments described so far indirectly show that the polyphenols were incorporated into and/or interacted with the lipid bilayers. In order to directly verify the incorporation of catechins into lipid bilayers, the interaction of EGCG with dimyristoylphosphatidylcholine (DMPC) bilayers was investigated by solid-state ^{31}P and ^2H NMR spectroscopy [54]. ^{31}P NMR of the phosphocholine head-group of DMPC provided information about the behavior of the surrounding bilayers when EGCG is incorporated. Further, the orientational and motional properties of [4- ^2H]EGCG, deuterium-labeled at 4-position of EGCG (Fig. 14), incorporated into DMPC liposomes were analyzed by the solid-state ^2H NMR.

Figure 15(A) shows the ^{31}P NMR spectra of EGCG incorporated into DMPC bilayers at temperatures between 40 and 10°C, together with (B) the spectra of DMPC bilayers without EGCG in the right panel. An axially symmetrical powder pattern, which is characteristic of the liquid crystalline phase, was observed

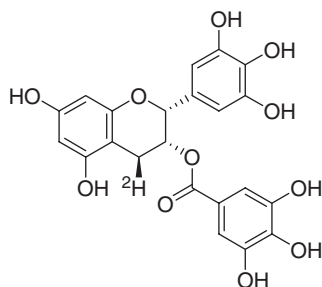


Fig. 14. Chemical structure of [4-²H]EGCg. [4-²H]EGCg deuterated at the 4-position in the C-ring.

irrespective of the phase transition temperature at 23°C. It is worth of note that ³¹P chemical shift anisotropy of DMPC in the presence of EGCg was decreased as compared with that in the absence of EGCg (Table 5) at the same temperature. These findings suggest that EGCg is actually incorporated into the lipid bilayers and affects the head-group motion of the phospholipids. EGCg is assumed to be located on the surface of the lipid bilayers by fluorescence quenching of 2-AS in Section 4.2. The ³¹P NMR study also indicates that EGCg is located in the head-group region of the phospholipids in the lipid bilayers.

On the one hand, Fig. 16(a) shows the ²H NMR spectrum of [4-²H]EGCg in DMPC bilayer. On the other, Fig. 16(b) shows the ²H NMR spectrum of [4-²H]EGCg in the solid phase. The observed ²H spectrum in DMPC bilayers consists of two components. The central line arises from the residual HDO (half-deuterated water consisting one hydrogen, one deuterium, and one oxygen) signal or free EGCg molecule in aqueous solution. The other component shows the quadrupole splitting, indicating that EGCg is incorporated into DMPC bilayers. The observed ²H quadrupole splitting (*Dq*) of [4-²H]EGCg incorporated into DMPC bilayer, 30 kHz, is much smaller than that in the solid state 125 kHz. Obviously, such reduction of the quadrupole splitting is associated with the presence of accompanied large amplitude motions of EGCg within the lipid bilayer.

In general, the ²H quadrupole splitting *Dq* for a certain direction of C–²H bond is related to the angle of the principal axis of the electric field gradient tensor (C–²H vector) with respect to the applied magnetic field (θ)

$$Dq = \frac{3}{4} \left(\frac{e^2qQ}{h} \right) (3\cos^2\theta - 1) \quad (1)$$

Where e^2qQ/h is the quadrupole coupling constant, 167 kHz for sp³ hybridized C–²H pair [55]. For rigid polycrystalline solids, all values of θ are possible and we obtained a powder pattern ²H NMR spectrum with a splitting of 125 kHz for the perpendicular component. Actually, the ²H NMR spectrum of [4-²H]EGCg in the solid state gave rise to the characteristic deuterium quadrupole splitting of ca. 125 kHz. On the other hand, the reduced quadrupole splittings in ²H NMR

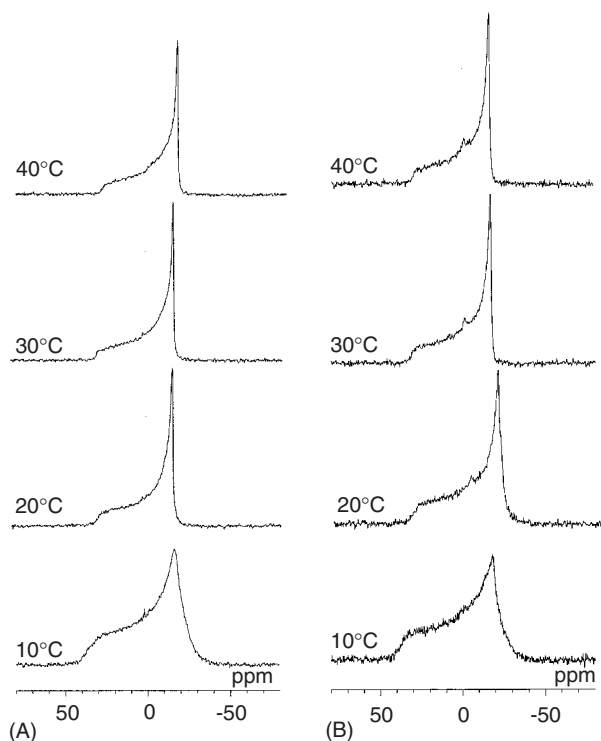


Fig. 15. ^{31}P NMR spectra of DMPC liposomes at various temperatures: (A) in the presence of EGCg; (B) in the absence of EGCg. For ^{31}P NMR measurements, 5 mg of EGCg and 148 mg of DMPC were dissolved in chloroform/methanol (1:1, v/v) with an EGCg-to-DMPC molar ratio of 1:20, and the solvent was subsequently evaporated *in vacuo*, followed by hydration with 1 ml of Tris buffer (20 mM Tris, 100 mM NaCl and pH 7.5). ^{31}P NMR spectra were recorded at the resonance frequency of 161.99 MHz under static conditions. A single-pulse excitation method with dipolar decoupling was used to obtain ^{31}P NMR spectra using a recycle delay of 2 s and proton decoupling field of 50 kHz. The number of scans was typically 1200. An exponential multiplication with a 20 Hz Lorentzian line broadening was applied to all ^{31}P free induction decays prior to Fourier transformation. The chemical shifts of 85% H_3PO_4 served as the reference for ^{31}P NMR spectra.

(From Ref. [54] with permission from the Publisher).

spectrum of $[4\text{-}^2\text{H}]\text{EGCg}$ in DMPC bilayer arises from motional averaged splittings due to the presence of anisotropic molecular motion as expressed by $3\cos^2\theta - 1$ in contrast to the case of the static state in equation (1). The presence of single ^2H quadrupolar splitting is consistent with the previous observation for 12-O- $[20\text{-}^2\text{H}]$ tetradecanoylphorbol-13-acetate in DMPC bilayer [56]. This means that there exists at least one kind of EGCg molecule with rotational motion in lipid bilayers. Alternatively, such splitting could be explained by the asymmetric electric field gradient, which was created by partial molecular motion [57]. In any

Table 5. Chemical shift anisotropy for phosphorus at the head-group of DMPC

Temperature(°C)	EGCg/DMPC (ppm)	DMPC (ppm)
40	43.8 ^a	45.2 ^a
30	44.9 ^a	46.7 ^a
20	44.6 ^b	46.6 ^b
10	49.8 ^b	52.3 ^b

^a Chemical shift difference with an uncertainty of ± 0.3 ppm.

^b Chemical shift difference with an uncertainty of ± 0.5 ppm.

Source: From Ref. [54] with permission from the Publisher.

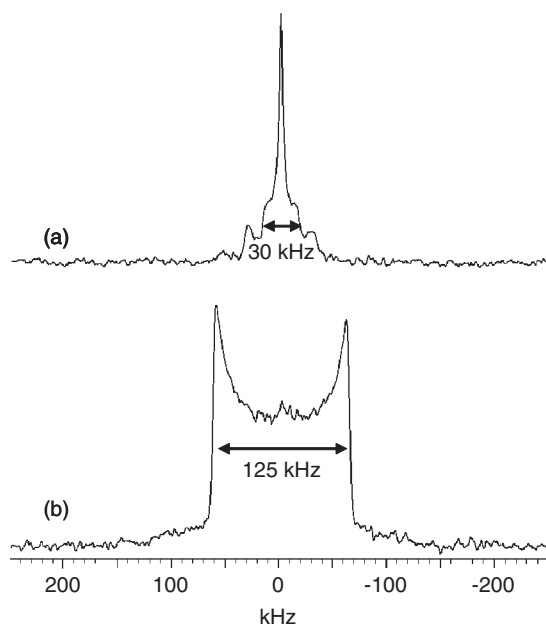


Fig. 16. ²H NMR spectrum of [4-²H]EGCg (a) in DMPC liposomes and (b) in the solid phase. For ²H NMR measurements, [4-²H]EGCg and deuterium-depleted water were used instead of EGCg and Tris buffer, respectively. A freeze–thaw cycle was repeated for several times until a homogeneous suspension of liposomes was obtained. These samples were placed in glass sample tubes and sealed with glue to prevent dehydration. ²H NMR spectra were recorded at the resonance frequency of 61.4 MHz using the quadrupole echo pulse sequence (90°–τ–90°–τ–echo) at 30 °C. Typical acquisition parameters were a 90° pulse length of 2.5 ms, a pulse interval of 60 ms and a recycle delay of 500 ms. The number of scans was typically 180,000. The time domain data were left-shifted to the echo maximum, and Lorentzian line broadening of 2 kHz was applied before Fourier transformation.

(From Ref. [54] with permission from the Publisher).

case, the results of ^2H NMR are consistent with the view that EGCg is incorporated into the lipid bilayers.

6. CONCLUSION

- (1) We developed several methods to investigate interaction of polyphenols with lipid bilayers using liposomes with a dense internal aqueous phase. After incubation of a polyphenol in the medium-containing liposomes, the supernatant was easily separated from the precipitate by centrifugation. This enabled us to measure the amount of a polyphenol incorporated into the liposomes, investigate its location in the lipid bilayers and estimate its activity to cause the membrane damage, more selectively and precisely than before.
- (2) Following factors governing the affinity of polyphenols for lipid bilayers were elucidated by the measurement of the amount of a polyphenol incorporated into the liposomes: chain length of alkyl moiety, number of hydroxyl groups, position of hydroxyl groups, presence of galloyl moiety in catechins, steric effect, ionic concentration in the medium, electric charges of a polyphenol, electric charges of lipid bilayers, presence of glycosides in the structure and presence of other polyphenols in the medium. The orders of the affinity of a series of polyphenols for the lipid bilayers correlate well with the orders of their biological activity evaluated by *in vitro* experiments.
- (3) Tea catechins locate on the surface of the lipid bilayers.
- (4) Some catechins cause membrane damages, which correlated to their antibacterial activity.
- (5) Interaction of EGCg with lipid bilayers was directly proved by solid-state NMR.

ACKNOWLEDGMENTS

This work was supported by a Grant-in Aid (no. 15580110) and Special Coordination Funds of the Ministry of Education, Culture, Sports, Science, and Technology of the Japanese government.

REFERENCES

- [1] H. Tachibana, K. Koga, Y. Fujimura, K. Yamada, A receptor for green tea polyphenol EGCg, *Nat. Struct. Mol. Biol.* 11 (2004) 380–381.
- [2] Y. Kobayashi, M. Suzuki, H. Satsu, S. Arai, Y. Hara, K. Suzuki, Y. Miyamoto, M. Shimizu, Green tea polyphenols inhibit the sodium-dependent glucose transporter of intestinal epithelial cells by a competitive mechanism, *J. Agric. Food Chem.* 48 (2000) 5618–5623.
- [3] T. Nakayama, T. Niimi, T. Osawa, S. Kawakishi, The protective role of polyphenols in cytotoxicity of hydrogen peroxide, *Mutat. Res.* 281 (1992) 77–80.
- [4] T. Nakayama, M. Yamada, T. Osawa, S. Kawakishi, Suppression of active oxygen-induced cytotoxicity by flavonoids, *Biochem. Pharmacol.* 45 (1993) 265–267.

- [5] T. Nakayama, M. Hiramitsu, T. Osawa, S. Kawakishi, The protective role of gallic acid esters in bacterial cytotoxicity and SOS responses induced by hydrogen peroxide, *Mutat. Res.* 303 (1993) 29–34.
- [6] T. Nakayama, M. Yamada, T. Osawa, S. Kawakishi, Inhibitory effects of caffeic acid ethyl ester on H₂O₂-induced cytotoxicity and DNA single-strand breaks in Chinese hamster V79 cells, *Biosci. Biotechnol. Biochem.* 60 (1996) 316–318.
- [7] T. Nakayama, I. Haraguchi, K. Hashimoto, Y. Sugiyama, T. Osawa, Suppression of hydrogen peroxide-induced cytotoxicity toward Chinese hamster lung fibroblasts by chemically modified curcumin, *Food. Sci. Technol. Int. (Tokyo)* 3 (1997) 74–76.
- [8] T. Nakayama, K. Ono, K. Hashimoto, Affinity of antioxidative polyphenols for lipid bilayers evaluated with a liposome system, *Biosci. Biotechnol. Biochem.* 62 (1998) 1005–1007.
- [9] T. Nakayama, Affinities of dietary phenolic antioxidants for lipid bilayers, in: F. Shahidi, C.-T. Ho (Eds.), *Phytochemicals and Phytopharmaceuticals*, AOCS Press, Champaign, 2000, pp. 349–359.
- [10] D. Grunberger, R. Banerjee, K. Eisinger, E.M. Oltz, L. Eφος, M. Caldwell, V. Estevez, K. Nakanishi, Preferential cytotoxicity on tumor cells by caffeic acid phenethyl ester isolated from propolis, *Experientia* 44 (1988) 230–232.
- [11] K. Kajiya, M. Ichiba, S. Kumazawa, T. Nakayama, Role of lipophilicity and hydrogen peroxide formation in the cytotoxicity of flavonols, *Biosci. Biotechnol. Biochem.* 65 (2001) 1227–1229.
- [12] H. Adlercreutz, W. Mazur, Phyto-oestrogens and Western diseases, *Finnish Med. Soc. DUODECIM Ann. Med.* 29 (1997) 95–120.
- [13] A.H. Lichtenstein, Soy protein isoflavones and cardiovascular disease risk, *J. Nutr.* 128 (1998) 1589–1592.
- [14] G.G.J.M. Kuiper, J.G. Lemmen, B. Carlsson, J.C. Corton, S.H. Safe, P.T. Van der Saag, B. Van der Burg, J. Gustafsson, Interaction of estrogenic chemicals and phytoestrogens with estrogen receptor β , *Endocrinology* 139 (1998) 4252–4263.
- [15] R. Kato, K. Kajiya, H. Tokumoto, S. Kumazawa, T. Nakayama, Affinity of isoflavonoids for lipid bilayers evaluated with liposomal systems, *BioFactors* 19 (2003) 179–187.
- [16] J. Hwang, A. Sevanian, H.N. Hodis, F. Ursini, Synergistic inhibition of LDL oxidation by phytoestrogens and ascorbic acid, *Free Radic. Biol. Med.* 29 (2000) 79–89.
- [17] H. Wiseman, J.D. O'Reilly, H. Adlercreutz, A.I. Mallet, E.A. Bowey, I.R. Rowland, T.A.B. Sanders, Isoflavone phytoestrogens consumed in soy decrease F2-isoprostane concentrations and increase resistance of low-density lipoprotein to oxidation in humans, *Am. J. Clin. Nutr.* 72 (2000) 395–400.
- [18] M.B. Ruiz-Larrea, A. Mohan, G. Paganga, N.J. Miller, G.P. Bolwell, C.A. Rice-Evans, Antioxidant activity of phytoestrogenic isoflavones, *Free Radic. Res.* 26 (1997) 63–70.
- [19] K. Iwashita, M. Kobori, K. Yamaki, T. Tsushida, Flavonoids inhibit cell growth and induce apoptosis in B16 melanoma 4A5 cells, *Biosci. Biotechnol. Biochem.* 64 (2000) 1813–1820.
- [20] H.G. Shertzer, A. Puga, C. Chang, P. Smith, D.W. Nebert, K.D.R. Setchell, T.P. Dalton, Inhibition of CYP1A1 enzyme activity in mouse hepatoma cell culture by soybean isoflavones, *Chem.-Biol. Interact.* 123 (1999) 31–49.
- [21] S.E. Kulling, M. Metzler, Induction of micronuclei, DNA strand breaks and HPRT mutations in cultured Chinese hamster V79 cells by the phytoestrogen coumestrol, *Food Chem. Toxicol.* 35 (1997) 605–613.
- [22] L. Movileanu, I. Neagoe, M.L. Flonta, Interaction of the antioxidant flavonoid quercetin with planar lipid bilayers, *Int. J. Pharm.* 205 (2000) 135–146.
- [23] S. Okabe, M. Suganuma, M. Hayashi, E. Sueoka, A. Komori, H. Fujiki, Mechanisms of growth inhibition of human lung cancer cell line, PC-9, by tea polyphenols, *Jpn. J. Cancer Res.* 88 (1997) 639–643.
- [24] M. Tezuka, H. Suzuki, Y. Suzuki, Y. Hara, S. Okada, Inactivation effect of tea leaf catechins on human type-A influenza virus, *Jpn. J. Toxicol. Environ. Health (in Japanese)* 43 (1997) 311–315.

- [25] T. Ishikawa, M. Suzukawa, T. Ito, H. Yoshida, M. Ayaori, M. Nishiwaki, A. Yonemura, Y. Hara, H. Nakamura, Effect of tea flavonoid supplementation on the susceptibility of low-density lipoprotein to oxidative modification, *Am. J. Clin. Nutr.* 66 (1997) 261–266.
- [26] S. Miura, J. Watanabe, T. Tomita, M. Sano, I. Tomita, The inhibitory effects of tea polyphenols (flavan-3-ol derivatives) on Cu^{2+} mediated oxidative modification of low density lipoprotein, *Biol. Pharm. Bull.* 17 (1994) 1567–1572.
- [27] Y. Hara, M. Watanabe, Antibacterial activity of tea polyphenols against *clostridium botulinum*, *Nippon Shokuhin Kogyo Gakkaishi* (in Japanese) 36 (1989) 951–955.
- [28] H. Tsuchiya, Effects of green tea catechins on membrane fluidity, *Pharmacology* 59 (1999) 34–44.
- [29] K. Kitano, K.-Y. Nam, S. Kimura, H. Fujiki, Y. Imanishi, Sealing effects of (–)-epigallocatechin gallate on protein kinase C and protein phosphatase 2A, *Biophys. Chem.* 65 (1997) 157–164.
- [30] K. Saeki, S. Hayakawa, M. Isemura, T. Miyase, Importance of a pyrogallol-type structure in catechin compounds for apoptosis-inducing activity, *Phytochemistry* 53 (2000) 391–394.
- [31] H. Tsuchiya, Stereospecificity in membrane effects of catechins, *Chem.-Biol. Interact.* 134 (2001) 41–54.
- [32] T. Hashimoto, S. Kumazawa, F. Nanjo, Y. Hara, T. Nakayama, Interaction of tea catechins with lipid bilayers investigated with liposome systems, *Biosci. Biotechnol. Biochem.* 63 (1999) 2252–2255.
- [33] K. Kajiya, S. Kumazawa, T. Nakayama, Steric effects on interaction of tea catechins with lipid bilayers, *Biosci. Biotechnol. Biochem.* 65 (2001) 2638–2643.
- [34] K. Kajiya, S. Kumazawa, T. Nakayama, Effects of external factors on the interaction of tea catechins with lipid bilayers, *Biosci. Biotechnol. Biochem.* 66 (2002) 2330–2335.
- [35] M. Hattori, I.T. Kusumoto, T. Namba, T. Ishigami, Y. Hara, Effect of tea polyphenols on glucan synthesis by glucosyltransferase from *Streptococcus mutans*, *Chem. Pharm. Bull.* 38 (1990) 717–720.
- [36] A. Mukoyama, H. Ushijima, S. Nishimura, H. Koike, M. Toda, Y. Hara, T. Shimamura, Inhibition of rotavirus and enterovirus infections by tea extract, *Jpn. J. Med. Sci. Biol.* 44 (1991) 181–186.
- [37] M. Toda, S. Okubo, H. Ikigai, T. Suzuki, Y. Suzuki, Y. Hara, T. Shimamura, The protective activity of tea catechins against experimental infection by *Vibrio cholerae* O1, *Microbiol. Immunol.* 36 (1992) 999–1001.
- [38] H. Ikigai, T. Nakae, Y. Hara, T. Shimamura, Bactericidal catechins damage the lipid bilayer, *Biochem. Biophys. Acta* 1147 (1993) 132–136.
- [39] M. Suganuma, S. Okabe, Y. Kai, N. Sueoka, E. Sueoka, H. Fujiki, Synergistic effects of (–)-epigallocatechin gallate with (–)-epicatechin, sulindac, or tamoxifen on cancer-preventive activity in the human lung cancer cell line PC-9, *Cancer Res.* 59 (1999) 44–47.
- [40] M. Suganuma, S. Okabe, N. Sueoka, E. Sueoka, S. Matsuyama, K. Imai, K. Nakachi, H. Fujiki, Green tea and cancer chemoprevention, *Mutat. Res.* 428 (1999) 339–344.
- [41] Y. Fujimura, H. Tachibana, K. Yamada, Lipid raft-associated catechin suppresses the $\text{Fc}\epsilon\text{RI}$ expression by inhibiting phosphorylation of the extracellular signal-regulated kinase1/2, *FEBS Lett.* 556 (2004) 204–210.
- [42] N. Caturla, E. Vera-Samper, J. Villalain, R. Mateo, V. Micol, The relationship between the antioxidant and the antibacterial properties of galloylated catechins and the structure of phospholipid model membranes, *Free Radic. Biol. Med.* 34 (2003) 648–662.
- [43] R. Amarowicz, R.B. Pegg, D.A. Bautista, Antibacterial activity of green tea polyphenols against *Escherichia coli* K12, *Nahrung* 44 (2000) 60–62.
- [44] Y.-K. Yee, M.W.-L. Koo, Anti-*Helicobacter pylori* activity of Chinese tea: *in vitro* study, *Aliment. Pharmacol. Ther.* 14 (2000) 635–638.

- [45] S. Sakanaka, M. Kim, M. Taniguchi, T. Yamamoto, Antibacterial substances in Japanese green tea extract against *Streptococcus mutans*, a cariogenic bacterium, *Agric. Biol. Chem.* 53 (1989) 2307–2311.
- [46] K. Mabe, M. Yamada, I. Oguni, T. Takahashi, *In vitro* and *in vivo* activities of tea catechins against *Helicobacter pylori*, *Antimicrob. Agents Chemother.* 43 (1999) 1788–1791.
- [47] P.E. Laks, M.S. Pruner, Structure/activity relations of flavonoid phytoalexin analogues, *Phytochemistry* 28 (1989) 87–91.
- [48] N. Horiba, Y. Maekawa, M. Ito, T. Matsumoto, H. Nakamura, A pilot study of Japanese green tea as a medicament: antibacterial and bactericidal effects, *J. Endocrinol.* 17 (1991) 122–124.
- [49] M. Shetty, K. Subbannayya, P.G. Shivananda, Antibacterial activity of tea (*Camellia sinensis*) and coffee (*Coffea arabica*) with special reference to *Salmonella typhimurium*, *J. Comp. Dis.* 26 (1994) 147–150.
- [50] O. Kayser, H. Kolodziej, Antibacterial activity of extracts and constituents of *Pelargonium sidoides* and *Pelargonium reniforme*, *Planta Med.* 63 (1997) 508.
- [51] P.E. Laks, Flavonoid biocides: phytoalexin analogues from condensed tannins, *Phytochemistry* 26 (1987) 1617–1621.
- [52] K. Kajiya, H. Hojo, M. Suzuki, F. Nanjo, S. Kumazawa, T. Nakayama, Relationship between antibacterial activity of (+)-catechin derivatives and their interaction with a model membrane, *J. Agric. Food Chem.* 52 (2004) 1514–1519.
- [53] Japanese Society of Chemotherapy, Method for determination of minimum inhibitory concentration (MIC) of aerobic bacteria by microdilution method, *Chemotherapy* 38 (1990) 102–105.
- [54] S. Kumazawa, K. Kajiya, A. Naito, H. Saito, S. Tuzi, M. Tanio, M. Suzuki, F. Nanjo, E. Suzuki, T. Nakayama, Direct evidence of interaction of a green tea polyphenol, epigallocatechin gallate, with lipid bilayers by solid-state nuclear magnetic resonance, *Biosci. Biotechnol. Biochem.* 68 (2004) 1743–1747.
- [55] H.H. Mantsch, H. Saito, I.C.P. Smith, Deuterium magnetic resonance, application in chemistry, physics and biology, *Prog. Nucl. Magn. Reson. Spectrosc.* 11 (1977) 211–272.
- [56] H. Saito, R. Tabeta, M. Kodama, C. Nagata, Y. Sato, Direct evidence of incorporation of 12-O-[20-²H₁] tetradecanoylphorbol-13-acetate into artificial membranes as determined by deuterium magnetic resonance, *Cancer Lett.* 22 (1984) 65–69.
- [57] R.A. Kinsey, A. Kintanar, E. Oldfield, Dynamics of amino acid side chains in membrane proteins by high field solid state deuterium nuclear magnetic resonance spectroscopy: phenylalanine, tyrosine, and tryptophan, *J. Biol. Chem.* 256 (1981) 9028–9036.

This page intentionally left blank

CHAPTER 5

Cationic Liposomes as Transmembrane Carriers of Nucleic Acids

An Cao,^{1,*} Dominique Briane¹ and Robert Coudert²

¹Laboratoire Biophysique Moléculaire, Cellulaire et Tissulaire (BIOMOCETI), CNRS UMR 7033, UFR de Médecine, Université Paris 13, 74 rue Marcel Cachin, F93017 BOBIGNY Cedex, France

²Laboratoire de Physicochimie des Interfaces et des Milieux Réactionnels (PIMIR), EA 2098, UFR des Sciences et Techniques, Parc de Grandmont, 37200 TOURS, France

Contents

Abbreviations	136
1. Introduction	138
2. Cationic Lipids and Cationic Liposomes	142
2.1. Chemical structure of cationic lipids	142
2.2. Elaboration of cholesterol-based cationic lipids	143
2.3. Cationic liposomes	144
2.3.1. Liposome preparation	144
2.3.2. Conditioning	145
2.4. Formation of complex with nucleic acids: lipoplex	145
2.4.1. Nucleic acids	145
2.4.2. Complexation with DNA	146
3. Properties of Cationic Liposomes and Lipoplexes	146
3.1. Characterization of cationic liposomes	146
3.1.1. Determination of lipid concentration	146
3.1.2. Sizing and ultrastructure of cationic liposomes	147
3.1.3. ζ -potential measurement	150
3.2. Uptake of nucleic acids by cationic liposomes	151
3.2.1. Efficiency of the oligonucleotide/liposome complex formation	151
3.2.2. Gel retardation control of the plasmid/liposome complex formation	153
3.3. Techniques for investigation of cationic liposomes	154
3.3.1. NMR and FTIR spectroscopy	154
3.3.2. Atomic force microscopy	155
3.3.3. Small-angle X-ray scattering	155
3.3.4. Differential scanning calorimetry	155
3.3.5. Fluorescence resonance energy transfer	155
3.3.6. Lipid mixing	156
4. Delivery of DNA in Cells: Lipofection	156
4.1. Cytotoxicity of cationic liposomes	156
4.2. Delivery of nucleic acids: transfection efficiency	157
4.2.1. Measurements of transfection level	158
4.2.2. Evaluation of transfection yield	158
4.2.3. GFP expression and flow cytometry	159
4.3. Cellular trafficking	160

*Corresponding author. Tel. +33-1-48-38-76-88; Fax: +33-1-48-38-77-77;
E-mail: cao@smbh.univ-paris13.fr

4.3.1. Fluorescence and confocal microscopy	160
4.3.2. Transmission electron microscopy	162
4.3.3. Observation of exogenous DNA internalized in the nucleus	164
4.3.4. Mechanism of lipoplex delivery	166
4.3.5. Endocytosis or fusion for lipoplex internalization?	167
5. Factors Affecting Lipofection	168
5.1. Effect of chemical structure	168
5.2. Effect of colipid DOPE on the lipofection	169
5.3. Effect of conditioning (lyophilization) on hydroxyethylated cationic liposomes	170
5.3.1. Effect of conditioning on efficiency in vitro	170
5.3.2. Effect of lyophilization on ³¹ P NMR spectra	171
5.4. Effect of serum on transfection level	172
5.5. Role of proteoglycans	173
6. Targeting	174
6.1. Targeting to receptors on cell surface	174
6.2. Intracellular targeting	174
6.2.1. Transfection of mitochondria	174
6.2.2. Delivery and persistence of vectorized PONC in cultured cells	175
7. Lipofection <i>In Vivo</i>	176
7.1. Intratumoural injection of B16-F10 tumours in nude mice[31]	176
7.2. Effect of erythrocyte haemagglutination by cationic lipids/DNA complexes	177
8. Delivery of DNA of Interest	179
8.1. Transfer of suppressor gene p16 into mesothelioma cells	179
8.1.1. Delivery and persistence of gene p16 observed by immunofluorescence	179
8.1.2. Dose and time effect on proliferation of transfected FR mesothelioma cells	181
8.2. Inhibition of Her2/neu	181
Acknowledgements	181
References	182

Abstract

Cationic liposomes constitute a new class of bilayer, which are able to form complexes with nucleic acids (DNA or RNA), help to cross the cellular membranes, and then deliver them into cells. This interesting property opens several applications for cationic liposomes, in particular in gene therapy, vaccination and biotechnology. The aim of this chapter is to review the structural properties of these liposomes and to describe the methods of characterization as well as methods to observe their pathway in cells after the passage through the cellular barrier. After the description of chemical structures of cholesterol-based cationic lipids investigated in our laboratory, their formation into liposomes, their interaction with nucleic acids and the internalization of complexes in cells will be dealt with. The cytotoxicity and the transfection level are outlined, and applications of cationic liposomes for transfer of interest DNA are illustrated.

ABBREVIATIONS

AMPGD [3-4(-methoxyspiro(1,2-dioxetane-3,2'-tricyclo(3.3.1.1) decane-4-yl)]phenyl-β-D-galactopyranoside

BSA	bovine serum albumin
CMV	cytomegalo virus
DAC-Chol	3 β -(<i>N,N,N</i> -dimethylaminoethane)-carbamoyl cholesterol chloride
DAPI	4', 6-diamidino-2-phenylindole
DOPE	dioleoyl phosphatidyl ethanolamine
DC-Chol	dimethyl aminoethane carbamoyl cholesterol [3 β -(<i>N,N,N</i> -dimethylaminoethane)-carbamoyl]cholesterol]
DDAB	dimethyldioctadecylammonium bromide
DMEM	Dulbecco's-modified Eagle medium
DMF	<i>N,N</i> dimethyl formamide
DMRIE	1,2-dimyristyloxypropyl-3- <i>N,N</i> -dimethyl hydroxyammonium bromide
DMSO	dimethylsulfoxide
DOGS	Dioctadecylamidoglycyl spermine
DOTAP	<i>N</i> -(1-(2,3-dioleyloxy)propyl)- <i>N,N,N</i> -trimethylammonium methylsulfate
DOSPA	2,3-dioleyloxy- <i>N</i> -(2(spermine carboxamido)ethyl)- <i>N,N</i> -dimethyl-1-propanaminium trifluoroacetate
DOTMA	<i>N</i> -(1-(2,3-dioleyloxy)propyl)- <i>N,N,N</i> -trimethylammonium chloride
DTT	dithiothreitol
Fab	fragment antigen binding
EGFP	enhanced green fluorescent protein
FCS	fetal calf serum
FITC	fluorescein isothiocyanate
FTIR	Fourier transform infrared spectroscopy
GAG	glycosaminoglycans
Lip(+)	cationic lipid
MTT	3-(4,5-dimethylthiazol-2-yl)-2,5-diphenyl tetrazolium bromide
NBD-PE	7-nitrobenzo-2-oxa-1,3-diazole labelled phosphatidylethanolamine
O.D.	optical density
ODN	oligodeoxynucleotide
OptiMEM	Opti minimum essential medium (Eagle)
PBS	phosphate-buffered saline
pCMV- β	plasmid containing β -galactosidase gene, promoter cytomegalovirus
PEI	polyethyleneimine
PG	proteoglycans
PONC	peptide-oligonucleotide conjugate
QLS	quasi-elastic light scattering
RLU	relative light unit
SDS	sodium dodecyl sulfate

TEAPC-Chol	(3 β (N-(N',N',N'-triethylaminopropane)-carbamoyl)cholesterol iodide)
TEAEC-Chol	(3 β (N-(N',N',N'-triethylaminoethane)-carbamoyl)cholesterol iodide)
TMAPC-Chol	(3 β (N-(N',N',N'-trimethylaminopropane)-carbamoyl)cholesterol iodide)
TMAEC-Chol	(3 β (N-(N',N',N'-trimethylaminoethane)-carbamoyl)cholesterol iodide)
TEM	transmission electron microscopy. X-gal, 5-bromo-4-chloro-3-indolyl β -D-galactopyranoside. p16 ^{INK4a} is also known as MTS1, cdk4i or cdkN2.

1. INTRODUCTION

Since 15 years, there is an increase in the development of a new kind of synthetic amphiphiles, the so-called cationic lipids, which present an interesting ability to complex with nucleic acids and to deliver them into cells [1–5]. Positively charged, cationic liposomes easily form lipoplexes with nucleic acids by electrostatic interaction. The efficacy of liposomes to complex with DNA, evaluated by gel electrophoresis retardation showed that the total amount of nucleic acid, either short oligonucleotides or long plasmids, should be considered when the charge lipid/DNA molar ratio was appropriately chosen. The lipophilic character then allows the passage across the cellular membrane and the delivery of nucleic acids.

In comparison with viral carriers, which are efficient but potentially hazardous for health, the non-viral method for gene transfer using cationic liposomes is very attractive and promising. Their main advantages are their low cytotoxicity and an apparent tolerance by the immune system, their versatility and their ease of use. Another advantage of cationic lipids over viral methods of cellular gene delivery is their ability to carry large pieces of DNA and the facility in the fabrication. They are usually pre-formed, very stable and can be added at any desired ratio to DNA [4,5].

The techniques of delivery are often necessary because of the low penetration of nucleic acids across cellular membranes. If the efficiency of cationic lipids of the first generation is still relatively small, several studies on new lipids and formulations showed much higher transfection abilities both *in vitro* and *in vivo*.

A cationic lipid molecule is typically composed of a hydrophobic part bound to a hydrophilic cationic part by a linker or other designed molecules. The hydrophobic moiety is generally constituted either by aliphatic chains or by a cholesteryl tail. In liposomes, the cationic lipid is usually associated with a colipid such as dioleoyl

phosphatidyl ethanolamine (DOPE) to form stable liposomal bilayers. Such liposomes instantaneously interact with DNA and form complexes commonly known as lipoplexes. Incubated with cultured cells, most prepared in excess of positive charge, liposome/DNA complexes interact with the negatively charged plasma membrane. The lipoplexes are internalized by endocytosis, even if fusion with plasma membrane cannot be excluded. Cell surface proteoglycans (PG) also participate in the internalization process. Probably due to the effect of the cationic lipid and of the fusogene colipid in endosomal acidic conditions, a destabilization of the endosome occurred, allowing the release of DNA into the cytosol. After this step, with appropriate lipids, the nuclear localization of DNA was observed and with suitable targeting, the internalization of DNA in mitochondria occurred.

Since the first transfection by lipofectin in 1987, cationic lipids have been extensively studied [3–6]. It was shown that DNA can be efficiently transferred by cationic lipids and cationic liposomes in a variety of cell lines in culture. Attempts for transfection *in vivo* were successful and cationic lipid-mediated transfection has shown promise for vaccination and gene therapy clinical trials [7,8]. While the ultimate goal was to have more efficient lipids and to find optimal conditions for their use, investigations have helped in the understanding of physical and chemical processes from which cellular transfection can result.

The central question was the process through which DNA is delivered in cells. Such a delivery should proceed in four essential steps: (i) elaboration of a carrier, (ii) loading of nucleic acids by the carrier, (iii) the passage through the cell membrane barrier and (iv) the release of DNA inside the cell. Through these steps the transported nucleic acid must be protected against destruction by various agents, such as nucleases outside or inside the cells, and the competition by negatively charged proteins or other components in the culture medium or in the blood.

For the elaboration of such carriers, after the cationic liposomes prepared from *N*-(1-(2,3-dioleoyloxy)propyl)-*N,N,N*-trimethylammonium chloride (DOTMA) [1] several other cationic lipids were intensively designed [2,9–17] and a number of these have been commercialized. Most cationic lipids contain acyl double chains as the hydrophobic part. Acyl chains are natural components of cellular membrane lipids facilitating their internalization into cells [1,18–20]. Using the same idea, a second family of cationic lipids were developed deriving from cholesterol, which is an other natural component of biological membranes [21,22]. Among lipids with the cholesteryl ring constituting the hydrophobic part, the most studied is dimethyl aminoethane carbamoyl cholesterol (DC-Chol), which was successfully used for *in vivo* assays [4,23,24]. DC-Chol contains a tertiary amine with two methyl groups in the polar head, linked to the cholesteryl moieties by a carbamoyl and two carbons in the spacer. Recently, other cholesterol-based cationic lipids have been developed [25–31]. The direction of the development of these derivatives was essential to modify either the structure of the polar head or the linker to affect binding with negatively charged DNA. There were suggestions that the structure of the positively charged amino group plays not only a role to

form complexes with DNA, but also with other agents being able to bind to the cationic group, affecting the stability of the complexes with respect to pH.

The liposome formulation, the uptake of DNA and their implication in the transfection process were intensively investigated. Hence, the complexation yield, the characterization of the lipoplexes and their stability have been studied [8,32–44].

About the internalization in cells, there are an increasing number of works to investigate the cellular pathway of DNA/lipid complexes [37,45–52]. The fate in cells of DNA vectorized by cationic lipids called for investigations to elucidate the ways by which DNA/lipid complexes after their entry into cells in order to understand the expression observed. Most reports supports endocytosis to be the route for the passage of these complexes across the cell membrane. [37,44,47,48,51,52]. However, there are different views among the reports about the route of DNA after the release in the cytosol. Investigating the pathway of oligonucleotides carried by monocationic liposomes prepared from dimethyldioctadecylammonium bromide (DDAB) and polycationic liposomes from 2,3-dioleoyloxy-*N*-(2(spermincarboxamido)ethyl)-*N,N*-dimethyl-1-propanaminium trifluoroacetate (DOSPA), Lappalainen *et al.* [48] have observed microscopic patterns showing different routes for oligonucleotides depending on liposomes used. For plasmids carried by liposomes prepared from *N*-(1-(2,3-dioleoyloxy)propyl)-*N,N,N*-trimethylammonium chloride (DOTMA/DOPE), Friend *et al.* [47] described vesicular and reticular intranuclear membranes probably resulting from the fusion of liposomes with the nuclear envelope. It appears that the cellular pathway of DNA/lipid complexes depends on the nature of the lipid used, and the cells to be transfected. In the paper of Friend *et al.* [47], the presence of DNA in the nucleus has not been mentioned whereas with various techniques, plasmids were observed only in the perinuclear area [37,50,51]. This important question remained obscure knowing that the expression was generally observed in most studies using reporter genes transferred into cells by cationic liposomes. It is clear that in the nucleus-containing chromatin, exogenous DNA must be labelled to be distinguished from the endogenous DNA. For long circular plasmids, the labelling was known but still is rarely used. As a result of recent developments, DNA can be marked with digoxigenin (DIG) or other labels allowing its immunogold labelling and therefore its detection at ultrastructural level by electron microscopy [51,53]. With transmission electron microscopy (TEM), following the staining by uranyl acetate, we observed the penetration of complexes into cells by endocytosis, their internalization in endosomes, followed by their release into the cytosol and their presence in the perinuclear area. However, the observation of un-labelled plasmids in nuclei not being possible, the delivery of functional plasmids into cell nuclei has been observed by means of an immuno-gold labelling and attested by expression of transgenes [54].

To date, the efficiency of liposomes used *in vivo* is still relatively low and investigation of the limiting factors in order to improve gene delivery level is

necessary. Besides the upstream factors such as the chemical nature of the lipids and the formulation of liposomes including the conditioning of liposomes and lipoplexes, several other factors such as the molar lipid/DNA charge ratio, the effect of serum in the blood, etc. affect the delivery efficiency. In most of the cited experiments, transfections were made in media exempt from serum and the transfection efficiency *in vivo* is still low [55,56]. Therefore, more progress is necessary to overcome this drawback.

Efforts have been deployed to establish relationships between the physico-chemical basis of cationic lipids and their biological effects, but they were often limited to *in vitro* investigations [14,27,57,58]. *In vivo* investigations have begun to highlight those factors that determine liposome-mediated gene transfer efficiency [31,55,56,59–64]. These efforts were deployed either to change the formulation of the liposome composition or to design new cationic lipids. At present, attention is generally focused on the role of the hydrophobic part or of the polar head and rarely on the role of the spacer though that appears not negligible. In the first cationic lipid DOTMA (1), double acyl chains are linked to a quaternary ammonium polar head by ether bonds. Although this lipid is effective in transfecting a variety of mammalian cells *in vitro* and *in vivo*, it exhibits toxicity for some cells due to the ether bonds in the molecule [22]. Recent works showed that not only the amino group and the hydrophobic tail but also the linker between them affects the stability and the cytotoxicity of cationic lipids. After DC-Chol, Huang and collaborators [21,22] synthesized other derivatives of cholesterol with amide and carbamide linkers. It was suggested that these linkers facilitate biodegradability and reduce cytotoxicity.

The stability of the carriers or the complexes is another factor contributing to the delivery efficiency. It has been proved that the storage conditions affect their stability for which the lyophilization (freeze-drying) is often pharmaceutically recommended. Attempts to address the physical instability of these complexes involved variations in solution conditions and methods of preparation. Steric stabilization and lyophilization to improve physical stability have recently received more attention. There were proofs that mixing with polyethylene glycol (PEG) or lyophilization may reduce the aggregation resulting in maintenance of biological activity [33]. Till date, cationic liposomes are generally stored in liquid form at 4 °C as recommended by manufacturers, while freezing was required for shipping. Lyophilization was suggested only for phospholipid liposomes [67] or DNA/cationic lipid complexes [33,68]. Lyophilization of the complexes implies the pre-determination of their formulation (DNA, charge ratio, etc.) and this parameter cannot be adjusted as per requirement. Moreover, even for one cell line, the optimal lipid/DNA ratio is different and depends on *in vitro* or *in vivo* transfection. Thus, in order to have flexibility of choice, it may be more useful that stable lipid and DNA are available separately just before use.

In this context, this chapter is devoted to reviewing various methods for investigating each transfection step, from the synthesis of cationic lipids and the

formation of liposomes, till their use in cells *in vitro* and *in vivo*. The chemical composition and physical characteristics of liposomes are determined by spectroscopy methods and microscopy. Transfection efficiency is assessed by light or electron microscopy and by inhibition of protein expression using antisense oligodeoxynucleotide (ODN), or genes incorporated into plasmids. Transfection level is evaluated by luminometric measurement or cytological detection of the protein expressed by reporter genes as β -galactosidase, luciferase or green fluorescence protein. For applications, a signal peptide-coupled oligonucleotide has been helped by cationic liposomes to cross the cellular membrane and be delivered into mitochondria of human fibroblast cells [69]. Finally, DNA of interest as tumour suppressor genes p16 have been delivered by cationic liposomes and evaluated by their final biological effect [70].

2. CATIONIC LIPIDS AND CATIONIC LIPOSOMES

2.1. Chemical structure of cationic lipids

Typically, a cationic lipid molecule is an amphiphilic molecule containing a hydrophobic part linked to the positively charged polar head by a linker via a spacer. Corresponding to each one of these parts, there are properties characteristic of the lipid molecule. It is generally believed that ionic interaction between the positive charges of lipids and the negative charges of the phosphate groups in DNA is involved. Otherwise, the chemical structure of the polar head, of the hydrophobic part and of the spacer between them is always an important point to be conceived and thus inspires new designs.

For cationic lipids in the first generation, the linkage is of the head-to-tail type, hydrophobic and hydrophilic parts occupying two separate domains [1,11,18]. While the positive charge should favour the complexation with negatively charged DNA and facilitate to go close to the negatively charged plasma membrane, the hydrophobic part of the lipid permits an easy permeation across the plasma membrane and thus allows the internalization of the DNA–lipid complex in the cell.

The hydrophobic part of cationic lipids can be an acyl double chain or a cholesteryl group to which the name of the lipid is usually attached. DOTMA, *N*-(1-(2,3-dioleoyloxy)propyl)-*N,N,N*-trimethylammonium methylsulfate (DOTAP), 1,2-dimyristyloxypropyl-3-*N,N*-dimethyl hydroxyammonium bromide (DMR1E) and DOSPA are typical examples of cationic lipids of the first kind [1,14], and DC-Chol of the second kind [21,26,71]. Recently, other cationic lipids have been synthesized for which the hydrophobic part may be derived from 1,4-dihydropyridine [72], *N*-*t*-butyl-*N'*-tetradecyl-3-tetradecylaminopropionamidine [20] or carbobenzyloxyglycine [73]. Moreover, the double acyl chain can be symmetric or asymmetric [72]. Although there were not systematic comparative studies of the effect of these hydrophobic parts on the cytotoxicity and on the transfection level,

some evidences have suggested that the length effect seems to be in the order $C_{14} > C_{oleyl} > C_{16} > C_{18}$ [14,72].

The polar head of most cationic lipids contains a mono-, a polyamine group or a tertiary or quaternary ammonium ion. These lipids can be derived from known molecules such as spermine, spermidine, poly-L-lysine [72] or ornithine [74], which easily interact with nucleic acids. It seems rational to predict that polycationic lipids have more potential to bind to DNA. However, the strength of this binding must match two constraints: it must be sufficiently tight to carry DNA through the process, but sufficiently weak to release DNA inside the host cell. Therefore, depending upon the nucleic acid to be carried and upon the cell to be transfected, monocationic lipids such as DMRIE-C or polycationic lipids such as DOSPA (lipofectamine) showed comparable levels. Recently, it was shown that under some particular conditions, a better interaction with DNA can be obtained with a polar head possessing not an amine but a phosphine or an arsenine [75].

The linker in a cationic lipid also plays an important role. It is related to the cleavage of the molecule and then associated to the biodegradability of the lipid once the transport process is achieved. Linkers are usually of five types: ether (–O–); carbonyl (–CO–); ester (–OCO–); amido (–CONH–) or carbamoyl (–OCONH–). The fragility is directly related to the digestion of the lipid molecule, and therefore its biodegradability or the cytotoxicity depends then on the linker. It has been shown that an ether linker is very stable and, consequently, of relatively high toxicity. A carbamoyl linker is more biodegradable [22].

It is to be noted that other molecules were elaborated [76–81], in particular with facial amphiphilicity [82] in which the hydrophobic part may be derived from cholic acids.

Although not directly concerned in the transport process of nucleic acid, counterions of cationic lipids seem to contribute to the transfection level in cells. Results found by Bennett *et al.* [83] showed that levels observed *in vivo* (Balb/C mice lung) using cytofectins prepared with various counterions are in the order: bisulfate = triflate > iodide > bromide > acetate > sulfate.

2.2. Elaboration of cholesterol-based cationic lipids

In our work, liposomes were prepared from cholesterol-based cationic lipids. The efficiency of these liposomes in both *in vitro* and *in vivo* transfection has been shown in previous studies [52,84–86]. The cationic lipids studied contain either a trimethylated, triethylated or hydroxyethylated polar head with a spacer of either 2C or 3C. A comparative study was undertaken to investigate the effect of the structural change on the yield of the liposome–DNA complex formation, the cytotoxicity of the complexes as well as on the efficiency of cellular and intratumoral gene transfer.

A series of five cationic lipids (I), (II), (III), (IV) and (V) was synthesized. These lipids differ with regard to their polar heads from the well-known cationic lipid DC-

Chol [21]. The syntheses have been described in earlier works [69,84–86]. The purity was monitored by chromatography after repeated recrystallizations.

- (I) TMAEC-Chol: (3 β [*N*-(*N*,*N*,*N*-trimethylaminoethane)-carbamoyl] cholesterol) iodide. Chol–O–CO–NH–(CH₂)₂–N⁺(CH₃)₃, I[–]
- (II) TMAPC-Chol: (3 β [*N*-(*N*,*N*,*N*-trimethylaminopropane)-carbamoyl] cholesterol) iodide. Chol–O–CO–NH–(CH₂)₃–N⁺(CH₃)₃, I[–]
- (III) TEAPC-Chol: (3 β [*N*-(*N*,*N*,*N*-triethylaminopropane)-carbamoyl] cholesterol) iodide. Chol–O–CO–NH–(CH₂)₃–N⁺(C₂H₅)₃, I[–]
- (IV) TEAEC-Chol: (3 β [*N*-(*N*,*N*,*N*-triethylaminoethane)-carbamoyl] cholesterol) iodide. Chol–O–CO–NH–(CH₂)₂–N⁺(C₂H₅)₄, I[–]
- (V) DMHAPC-Chol (3 β [*N*-(*N*,*N*,*N*-dimethylhydroxyethylaminopropane)-carbamoyl] cholesterol) iodide. Chol–O–CO–NH–(CH₂)₂–N⁺(CH₃)₂(CH₂)₂–OH, I[–]

In this series, TEAEC-Chol and TEAPC-Chol differ from TMAPC-Chol and TMAEC-Chol in that they have three ethyl groups instead of three methyl groups in the polar head; DMHAPC-Chol contains 3C and a hydroxyethylated head group.

2.3. Cationic liposomes

Cationic liposomes, multilamellar or unilamellar, are generally pre-fabricated and then mixed with DNA at any desired ratio to obtain lipoplexes. They can also be prepared in the presence of DNA, which will be entrapped inside the liposomes and shielded against DNAses [87].

2.3.1. Liposome preparation

Cationic liposomes can be prepared according to standard methods. Usually, depending upon the type and size of liposomes needed, vortexing, sonication or extrusion are used and liposomes of diameter 100–200 nm are obtained. Vortexing, even vigorously, gives multilamellar liposomes (MLV), moderated sonication by bath gives unilamellar liposomes while with extrusion, homogenous distribution in sizes can be expected [14,74,87].

Typically, for experiments in our laboratory, cationic liposomes were formed employing the cationic lipids formulated with the neutral co-lipid DOPE [85]. Cationic lipid and DOPE at desired ratio were dissolved and mixed in chloroform and the solution was dried in a rotating evaporator. Solvent trace was removed under vacuum overnight. The following day, sterile water was added and the mixture was sonicated for 1 h in cycles of 15 min (13 min followed by 2 min rest) to clarity. Centrifugation was used to eliminate aggregates. The preparations can be extruded throughout bicarbonate membranes with chosen pore diameter. Usually, liposomes with homogeneous sizes are obtained.

The liposomes size was characterized by quasi-elastic light scattering using polystyrene latex spheres of 109 nm in aqueous solution for the calibration. Cationic lipid concentrations were monitored by UV spectroscopy at 226 nm and adjusted to the final concentration of 1.50 mM before use.

For some experiments, the liposome suspension was lyophilized by freezing at -80°C and drying under vacuum in a freeze-drier before re-hydrating at the same concentration. In another method, after the freezing, dry liposomes were pre-warmed at a temperature higher than the transition point of the lipid and rehydrated. This is known as dehydrated–rehydrated vesicles (DRV) [87]. This method was shown to be efficient to entrap drugs or DNA when drugs or DNA are present in the rehydration step, but in any case, as will be shown below, the yield is smaller than that in the complexation of pre-fabricated cationic liposomes and DNA.

2.3.2. *Conditioning*

Cationic liposomes are usually preserved in aqueous medium at 4°C . Their size is very stable over time. If freeze-drying is used, liposome characteristics change, but advantageously for DNA delivery, as can be seen in Section 4.3.

2.4. Formation of complex with nucleic acids: lipoplex

Cholesterol-based cationic liposomes easily form complexes with DNA of various lengths. The complexes formed are commonly known as lipoplexes. Theoretically, there is no limit of DNA length to complex with cationic liposomes and to be delivered into cells. Assays in our laboratory were made with oligodeoxynucleotides (ODN) and interferent RNA (siRNA) of 10–30 bases or plasmid DNA of 5–7 kb. These nucleic acids were chosen for evaluating either the transfection level or a biological effect.

2.4.1. *Nucleic acids*

Oligodeoxynucleotides: One of the ODN used for results presented in this paper was a short oligomer (28 bases with the sequence 5'-FG3AG2AG2AG2CG2A-G2AG2A2GAG2A) to inhibit the expression of HER2/neu [52]. For fluorescence microscopy, ODN were labelled at the 5'-end with FITC (green fluorescence). For mitochondrial delivery, ODN was coupled with a signal peptide (peptide–oligonucleotide conjugate, assigned thereof by PONC) [69].

Plasmids: Plasmid DNA used for assays in our work are usually plasmids containing a reporter gene encoding β -galactosidase (pCMV- β gal), luciferase (pCMV-luc) or green fluorescent proteins (pEGFP-N1) [52,84–86]. Plasmid pCMV- β gal was a plasmid of 7.164 kb containing the β -galactosidase reporter gene sequence under the control of the cytomegalovirus promoter (pCMV). The plasmid coding for enhanced green fluorescent protein (pEGFP-N1) was purchased from Clontech. The concentration of plasmid was measured by UV absorption at 260 nm and

plasmid DNA purity was controlled using agarose gel electrophoresis and A_{260}/A_{280} ratios. pUT650 was a plasmid of 5.149 kb containing the firefly luciferase reporter gene sequence under the control of the promoter CMV. Plasmids were conditioned in Tris-EDTA buffer (pH 8) except pUT650, which was conditioned by lyophilization and rehydrated with sterile water as recommended.

2.4.2. Complexation with DNA

Typically, for the formation of DNA/liposome complex at any desired lipid/DNA molar charge ratio, stock solutions of DNA (ODN or plasmid DNA $1 \mu\text{g}/\mu\text{L}$) and liposomes (1.5 mM cationic lipid) were separately diluted in equal volumes of sterile water and then DNA was dropped into the liposome. The lipoplexes formed instantaneously and were used within 30 min for transfection. The order to mix DNA with liposomes is very important to avoid the aggregation of the complexes.

In some applications for particular cell lines, this protocol has been modified to enhance the transfection level by a pre-condensation of plasmids by polycations. So, for mesothelioma cells, plasmids were mixed with spermine before complexation with cationic liposomes. β -Galactosidase activity in cells was highest when spermine was added to plasmids before complex formation, at ratios 3–4 nmol/ μg DNA, depending on the cationic liposome used.

3. PROPERTIES OF CATIONIC LIPOSOMES AND LIPOPLEXES

3.1. Characterization of cationic liposomes

3.1.1. Determination of lipid concentration

Knowledge of the concentration is necessary for an accurate preparation of complexes with DNA at a desired molar charge ratio. Because of a usual lack of absorption in the UV region, the measurement of cationic lipid concentration became a severe problem. To resolve this difficulty, an indirect measurement of cationic lipid concentration can be used [86]. This simple and original method consists of measuring DOPE concentration by a colorimetric technique [88] and determining the cationic lipid/DOPE molar ratio by FTIR using a calibration curve established prior to measurements. The calibration plot represents the peak–height ratio corresponding respectively to the carbonyl groups of cationic lipid and DOPE as a function of known molar ratios. This two-step method becomes a relatively simple routine handling, easier than the evaporative light scattering detector, one of the rare published methods used to detect cationic lipid [89].

3.1.1.1. Determination of the DOPE/cationic lipid ratio

Typically, DOPE/DMHAPC-Chol ratio in the liposomes was monitored by FTIR spectroscopy. The DOPE content was calculated from the ratio of the intensity of

a band associated with the carbonyl stretching at 1743 cm^{-1} to that of the band at 1712 cm^{-1} , corresponding to the carbonyl of DMHAPC-Chol. A calibration curve was established from spectra of DOPE/DMHAPC-Chol mixtures with various ratios. For these FTIR experiments, DOPE and DMHAPC-Chol were mixed in chloroform at desired ratios and the solution was placed directly on a zinc selenide trough and evaporated. Infrared spectra were acquired on a Perkin Elmer 2000 spectrometer equipped with a Deuterium triglycine sulfate (DTGS) detector at ambient temperature. For each spectrum, three scans were collected with a final resolution of 1 cm^{-1} . A linear function was used to fit the baseline in this region prior to the determination of the absorbance. To characterize samples with unknown DOPE/DMHAPC-Chol ratios, the aqueous lipid suspension was lyophilized and dissolved in chloroform.

An example of this method is given with DOPE/DMHAPC-Chol liposomes. Two calibration plots were established, one corresponding to the DOPE quantification (Fig. 1A) and the other representing the variation of the ratio between the IR absorption peak heights at 1712 and 1743 cm^{-1} of, respectively, the carbonyl groups in DMHAPC-Chol and in DOPE as a function of the DOPE/cationic lipid ratio (Fig. 1B). For samples used, the concentration of DOPE was typically 2.1 mM , as determined by the colorimetric method of Stewart so that the concentration of cationic lipid DMHAPC-Chol was 2.5 mM with an accuracy of about 10%.

3.1.2. Sizing and ultrastructure of cationic liposomes

Liposomes and complexes at various ratios with plasmid DNA were characterized by quasielastic light scattering (QLS) and TEM after negative staining using uranyl acetate.

3.1.2.1. Size characterization by quasielastic light scattering

QLS results indicated a size distribution of liposomes with a mean value between 104 and 129 nm , depending on the cationic lipids and a polydispersity factor (a parameter indicating the width of the size distribution) between 20 and 30% (Table 1). The liposome size was practically defined by the preparation conditions. There was little difference in these characteristics from one preparation to another. These liposomes were very stable and could be preserved at $4\text{ }^{\circ}\text{C}$ for many months without noticeable alteration in size distribution.

For complexes DMHAPC-Chol/DOPE liposomes with pCMV- β , sizes varied from 80 nm for uncomplexed liposomes to 180 nm for complexes, with maximum size and scattered intensity observed for cationic/DNA molar change ratio $X = 1.5$.

3.1.2.2. Ultrastructure observed by TEM

There has been an increasing number of investigations to elucidate the ultrastructure of the DNA/lipid complexes [34,90–92] and the correlation between the

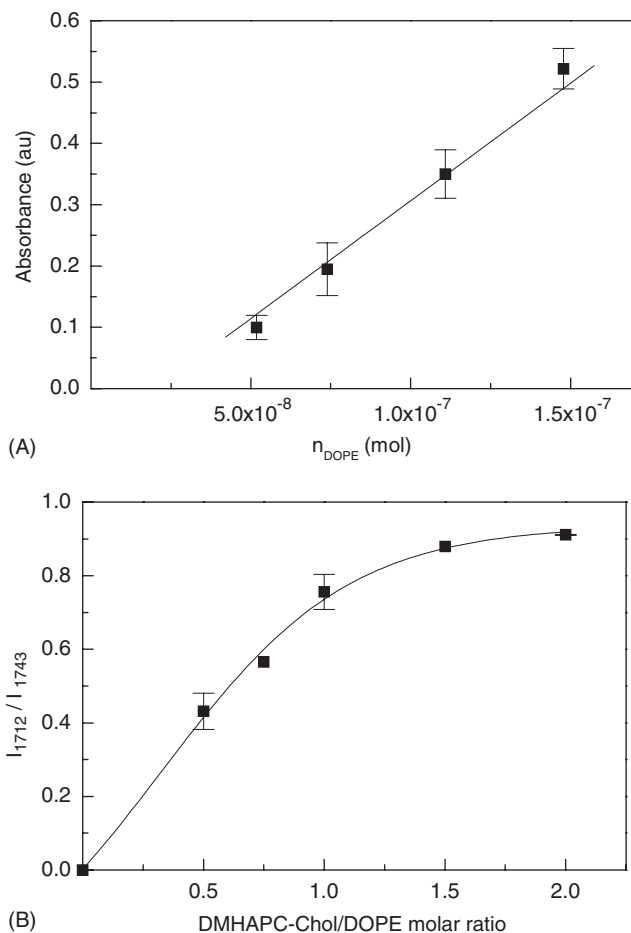


Fig. 1. Determination of the cationic lipid concentration. (A) Calibration curve used to estimate the DOPE content in CHCl_3 solutions following the colorimetric method of Stewart. The absorbance was measured in the organic solution at 468–472 nm for binary DMHAPC-Chol/DOPE (1:1) mixtures with known DOPE concentrations. (B) Calibration curve plotted to determine the DOPE content in the DMHAPC-Chol/DOPE mixtures. I_{1712}/I_{1743} represents the height ratio of the carbonyl band attributed to DMHAPC-Chol over the carbonyl band attributed to DOPE in the FTIR spectra of anhydrous DMHAPC-Chol/DOPE mixtures. Each result represents the mean \pm SE of three spectra. (Reprinted from Percot *et al.* [86]. Copyright 2004, with permission from Elsevier.)

ultrastructure of these complexes with the transfection efficiency. There is evidence that the ultrastructure of the DNA/cationic lipid complexes depends on the charge ratio, and that the transfection level varies as a function of charge ratio. However, the results found in the literature are not entirely in accordance with the structure of the DNA/cationic lipid complexes. While Zabner *et al.* [37] showed various types of complexes prepared with the same lipid/DNA ratio,

Table 1. Size and polydispersity of liposomes characterized by QLS

	Average size (nm)	Polydispersity factor ^a
TMAEC-Chol/DOPE (1:1)	121	0.20
TEAEC-Chol/DOPE (1:1)	128	0.30
TMAPC-Chol/DOPE (1:1)	112.6	0.23
TEAPC-Chol/DOPE (1:1)	104	0.23
DMHAPC-Chol/DOPE(1:1)	80	0.27
DC-Chol/DOPE (1:1)	129	0.28

^a Polydispersity factor is a dimensionless parameter indicating the width of the size distribution of liposomes.

Sternberg [90] found a spaghetti-like shape of DNA coated with lipids. Yoshikawa [93] observed a nucleosome-like structure with DNA wrapping the cationic lipids. It seems that the structure of complexes with DNA also depends on the nature of the cationic lipid used. Concerning cholesterol-based cationic liposomes elaborated in our laboratory, complexes containing beads with size same as of liposomes were observed [52,86].

Typically, TEM results on complexes of TMAEC/DOPE liposomes with 28-mer oligonucleotides at molar charge lip⁺/PO₂⁻ ratio $X = 2$ showed that the lipoplexes are rather globular with sizes of about 180 nm, i.e., slightly larger than liposomes [52]. Assuming a diameter of about 1 nm and a length of 9.52 nm for each oligonucleotide and taking into account the hydration layer, it can be speculated that short DNA such as oligonucleotides are simply adhered onto the surface of the liposomes.

Figure 2 depicts liposomes and complexes of TEAPC/DOPE liposomes with plasmids pCMV- β [31]. At various molar charge ratios X of lip⁺/PO₂⁻ ranging from 0.5 to 4, it was shown that for $X = 0.5$, the lipoplexes are rather globular with sizes varying from 260 to 520 nm [52]. If short oligonucleotides form globular lipoplexes, plasmids form complexes with different structures depending on the charge ratio X —globular shape with $X < 2$ and showing a blackberry feature for higher values. It is important to note that if the liposome structure was conserved, the neutral charge ratio lip⁺/PO₂⁻ should be 2 because there is only half the number of lipid molecules in the outer side of liposomes exposed to DNA. On the contrary, if the liposome structure was destroyed, all the cationic lipid molecules would be associated with DNA, the neutral charge ratio must be 1. In the light of the above, we suppose that with charge ratios in the range of 1–2, there would be formation of a heterogenous distribution of complexes. The variation of shape and size of aggregates of TMAEC-Chol/DOPE liposomes and plasmids is similar to the variation of aggregation of anionic liposomes induced by the presence of polycation, such as polylysine [94]. Such a variety of complex types was also observed by Zabner *et al.* [37] with DMRIE/DOPE and DOSPA/DOPE cationic liposomes. However, a more thorough examination of the micrographs showed

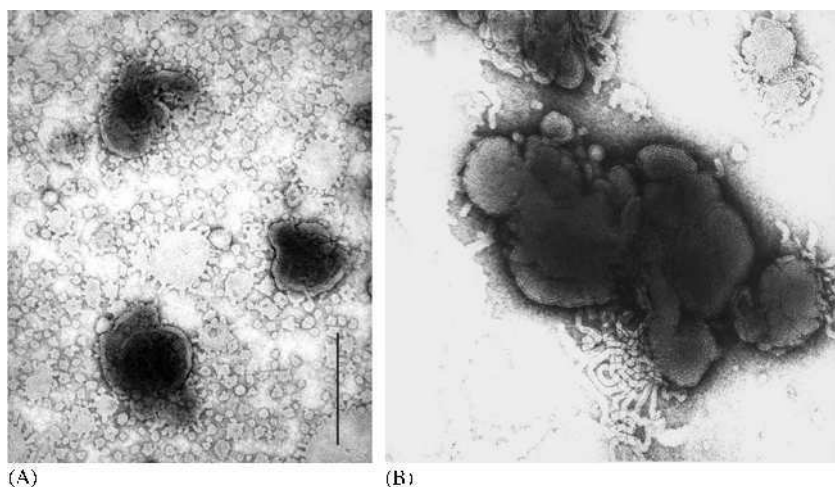


Fig. 2. Ultrastructures observed by TEM. (A) Cationic liposomes TEAPC-Chol/DOPE (1:1), and (B) complexes with plasmid in the molar charge ratio $X = 2$. Samples were spread on Formvar/C grids, treated with a solution of bacitracin (1 mg/mL), stained with uranyl acetate (0.75 mg/mL) and observed using an EM300 Philips microscope operating under a voltage of 60 kV. Scale bar, 200 nm. (Reproduced with permission from Reynier *et al.* [31].)

that in these aggregates there are smaller “beads” with size of about 90–100 nm, practically the same size as of liposomes. These findings indicate that in the complexes of cationic liposomes TMAEC/DOPE and plasmids pCMV- β , the liposomal structure is more or less preserved [52,86].

DNA in complexes was observed by the immuno-gold labelling technique [86]. With this technique, although the entire shape of DNA was not observable keeping in mind the difference of two orders in their sizes, liposomes with 100 nm in diameter and DNA with 2 nm in section, simultaneous observations of the presence of DNA and liposomes were possible in the same field scale. We observed that in both cases (untreated and lyophilized liposomes), plasmid was detected on the surface of the global substructures. These results support the hypothesis of an aggregation between liposomes with DNA as a bridge [86].

3.1.3. ζ -potential measurement

Because of the electrostatic nature of interaction with DNA, the surface potential or ζ -potential is one of the most interesting characteristics of cationic liposomes and lipoplexes. ζ -potential can be measured using laser Doppler spectroscopy or electrophoretic light scattering [44,95]. ζ -potential is related to the apparent proton binding, and then its value depends on pH and ionic strength of the medium [44,96]. Its value is generally calculated using a model where the size and the shape of the surface must be taken into account. As cationic liposomes are usually in serum-free medium and slightly saline buffer must be used [97], the

weak ionic strength should not change the liposome size. For cholesterol-based cationic liposomes such as DC-Chol, ζ -potential is positive, about 60 mV in water and 5 mV in serum-free medium [98–100]. Its value is decreased and becomes negative when liposomes are complexed with DNA (–59.3 mV for the liposome/DNA ratio of 0.67). The variation was in the range from +40 to –40 mV for DOTAP [97]. The ζ -potential is annulled when neutral complexes are obtained approximately with the lipid/DNA molar charge ratio being between 1 and 2, depending on the cationic liposome composition [38]. It seems that the geometry of the system liposomes/DNA can play a role to prevent DNA from coming close to the cationic sites of the liposome. In contrast to *in vitro* transfections where positively charged lipoplexes are believed to be efficient, it was shown that *in vivo* transfection was favoured when lipoplexes with negative ζ -potential was used [31,98].

3.2. Uptake of nucleic acids by cationic liposomes

Depending upon the size of DNA, various techniques can be used to determine the uptake by cationic liposomes and allow the determination of the lipid/DNA ratio for which the totality of DNA was taken. With short oligonucleotides, filtration allows to obtain unbound DNA after mixing with liposomes. With plasmids, gel retardation electrophoresis can be used.

3.2.1. Efficiency of the oligonucleotide/liposome complex formation

As an example, the interaction of TMAEC/DOPE liposomes and phosphodiester oligodeoxynucleotides was monitored by QLS and UV spectroscopy [52]. QLS results showed that the mean size and the polydispersity factor were only slightly changed. Oligonucleotides in complexes were indirectly determined by the titration of oligonucleotides unbound to liposomes. After mixing 20 nmol of oligonucleotides and the desired amount of liposomes, the mixture was filtered through a Millipore filter with the MW lower cut-off of 30 kDa. Only unbound oligonucleotides could pass through the filter and were titrated. UV spectra were recorded and the absorbance relative to the peak at approximately 260 nm was determined. This allowed the determination of the complex formation efficiency. Blank assays were made with oligonucleotides of the same concentration, titrated before and after filtration using Millipore filters.

If C_1 (constant) is the molar concentration of nucleotides before the mixing, C_2 and C those of lipids and unbound nucleotides, respectively, the plot in Fig. 3 represents the variation of the C/C_1 fraction of oligonucleotides passed in the filtrate as a function of the C_2/C_1 lipid/oligomer molar charge ratio between the cationic TMAEC-Chol lipid concentration and that of oligonucleotide, expressed in nucleotide or PO_2^- molar concentration. The percentage was calculated relative

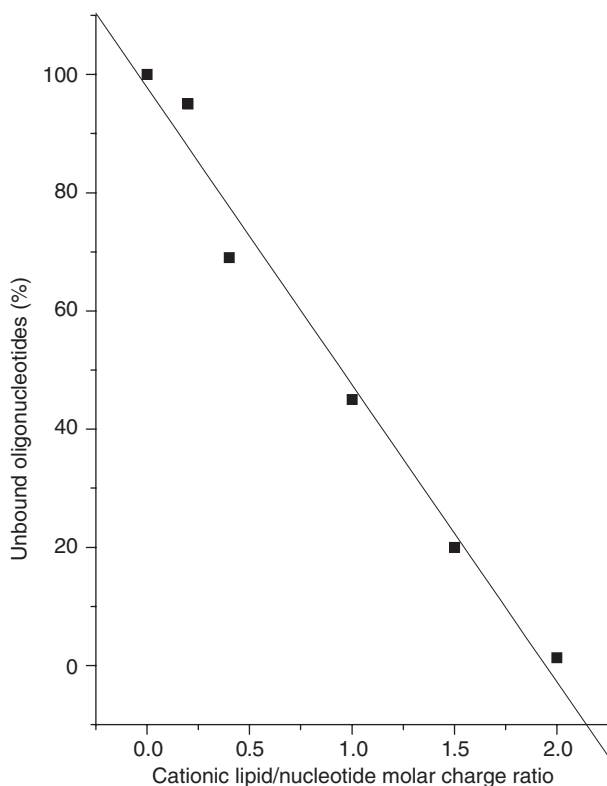


Fig. 3. Efficiency in complex formation of TMAEC-chol/DOPE liposomes with oligonucleotides. The plot represents the percentage of unbound oligonucleotides as a function of the molar charge ratio X between cationic lipid and nucleotides. Oligonucleotides: 20 nmol was mixed with liposomes before filtration. See text for other details of the preparation of complexes. (Reproduced with permission from Cao *et al.* [52].)

to the concentration of oligonucleotides when pure oligonucleotides were filtered. For small contents of liposomes, the plot shows a linear concentration dependence of the unbound oligonucleotide fraction. When there were many more liposomes, the amount of unbound oligonucleotides is decreased. At charge ratios higher than 2, results indicated no unbound oligonucleotides—this means that oligonucleotides were entirely adhered to the liposomes and retained by the filter. The straight line of Fig. 3 can be fitted by the equation $C/C_1 = 1 - kC_2/C_1$ with $k = 1/2$. This can be explained as follows: one nucleotide (assuming with one negative charge) was bound to one cationic lipid molecule (with one positive charge) on the external surface of the liposomes and therefore only one half of the number of cationic lipid molecules is necessary. This result indicates the electrostatic behaviour of the binding of phosphodiester oligonucleotides to TMAEC/DOPE liposomes.

3.2.2. Gel retardation control of the plasmid/liposome complex formation

Formation of complexes between pCMV- β gal plasmid DNA and cationic liposomes results in a retardation of DNA electrophoretic migration and can be monitored by gel retardation control, which allows to estimate the yield of complex formation with different cationic liposomes. Figure 4 indicates changes in the pattern of plasmid DNA electrophoretic migration when pCMV- β gal plasmid DNA is mixed with liposomes at different Lip + /DNA molar charge ratios X ranging from 0.5 to 2. Migration of pCMV- β gal is gradually slowed down when the cationic lipid/DNA (Lip + /DNA) charge ratio X is increased from 0.5 to 1.3. Beyond the charge ratio of 1.3, no migration was observed as indicated by other lanes in Fig. 4A. In lane 5 there are traces of plasmids that are not entirely retained by liposomes but there is no sign of free plasmids in lane 6, indicating a complete complexation of plasmids with liposomes when the molar charge ratio of lip + /DNA is greater than 1.3. Gel electrophoresis showed similar patterns of DNA migration indicating similar ability of the cationic liposomes to complex plasmid DNA.

These results indicate once more the electrostatic behaviour of the binding between DNA to TMAEC/DOPE liposomes assuming one positive electronic charge for each cationic lipid molecule on the outer side of the liposome and one negative charge for every nucleotide of DNA. The uptake of DNA is affected by the presence of serum as shown in Fig. 4B where the lipid/DNA ratio for total uptake of DNA is higher than 2. In any case, the yield of the formation of liposome–DNA can reach 100% for plasmids when the molar charge ratio was appropriately chosen, as for ODN.

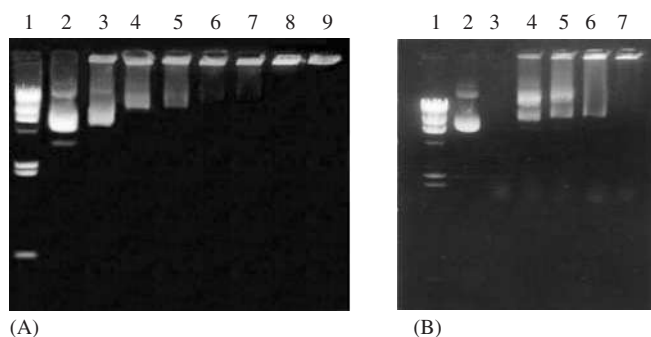


Fig. 4. Gel retardation assay of DNA/liposome complexation. (A) In medium without serum. Lane 1, molecular weight marker (λ *Hind* III); Lane 2, plasmid DNA alone; Lanes 3–9, plasmid DNA complexed with TEAPC-Chol/DOPE at molar charge ratio $X = 0.5$ (Lane 3); $X = 1$ (Lane 4); 1.3 (Lane 5); $X = 1.5$ (Lane 6); $X = 1.7$ (Lane 7); $X = 2$ (Lane 8) and $X = 4$ (Lane 9). (B) In medium containing serum. Lane 1, molecular weight marker (λ *Hind* III); Lane 2, plasmid alone; Lane 3, fetal calf serum (13%); Lanes 4–7, plasmid complexed with TEAPC-Chol/DOPE in the presence of fetal calf serum (13%) at charge ratio $X = 0.5$ (Lane 4); $X = 1$ (Lane 5); $X = 2$ (Lane 6) and $X = 4$ (Lane 7). (Reprinted from Lesage *et al.* [84]. Copyright 2002, with permission from Elsevier.)

This result should be in relation to the effect of charge ratio on the transfection level of B16-F10 cells in culture (Section 3.2). Indeed, *in vitro* results indicated high level of transfection with TEAPC-Chol/DOPE (1:1) in the cationic lipid/DNA molar charge ratio of 2. At a higher X ratio, the transfection level decreased, probably because the cationic lipid in excess significantly altered the net charge of the membranes and affected cellular metabolism or adhesion properties [57,101]. For cells in culture, in the presence of serum, optimal transfection was obtained with an increase in charge ratio compared to that observed in the absence of serum (at about $X = 6$). This is undoubtedly in relation with the results by gel retardation, indicating that a complete association of DNA with liposomes can be obtained with a higher Lip(+)/DNA charge ratio. Yang *et al.* [32] and Lesage *et al.* [84] have also showed that the increase in charge ratio allowed to overcome the inhibitory effect of serum. This revealed competition between negatively charged DNA and anionic components of serum for binding to positively charged lipids, leading to dissociation of the complex [102].

3.3. Techniques for investigation of cationic liposomes

Besides the currently used techniques QLS and TEM described above, cationic lipids and complexes with DNA have been investigated by various physical techniques [60,101–105] such as isothermal titration, differential scanning calorimetry (DSC), fluorescence, NMR and FTIR spectroscopies, cryo-electron microscopy, atomic force microscopy (AFM) and small-angle X-ray scattering (SAXS) [33–44].

3.3.1. NMR and FTIR spectroscopy

These techniques give information about the structure of the lipids or DNA, and insights on their interactions. All lipids were characterized by FTIR and $^1\text{H-NMR}$ spectroscopy [85,86]. Results can be used to analyse a mixture of cationic lipid with DOPE. Typically, for DMHAPC-Chol, the comparison of dry cholesterol and cationic lipid FTIR spectra revealed the disappearance of a band at 1052 cm^{-1} corresponding to the C–O stretching of the alcohol group of the cholesterol and the apparition of two bands at 1250 and 1712 cm^{-1} corresponding to the C–O stretching of the ester group and to the carbonyl stretching of DMHAPC-Chol.

FTIR spectroscopy, commonly used in the 1980s as a tool for investigation of phospholipid bilayers, was recently introduced by Choosakoonkriang *et al.* [41] to study cationic liposomes. Changes of IR absorption bands, concerning lipids, in three spectral regions corresponding to hydrophobic methyl and methylene groups, to the carbonyl bond $\text{C} = \text{O}$ and to the PO_2^- or the $\text{N}^+(\text{CH}_3)_3$ groups were investigated. The wave frequencies of the peaks of the bands at about 2850 and 2920 cm^{-1} indicated the gel or crystalline state of the hydrophobic part of lipid molecules, while those at 1740 cm^{-1} indicated the existence or absence of interaction with the carbonyl bond $\text{C} = \text{O}$, or more precisely, showed this bond in

the hydrated or dehydrated state. FTIR also gave indications in conformation changes of plasmid DNA in interaction.

NMR, considered as more effective than FTIR, is a technique to characterize cationic lipid molecules by their characteristic peaks from which groups in the lipid molecule are identified. ^1H -NMR spectra were obtained for DHMAPC-Chol cationic lipid where peaks are assigned to different groups of the molecule [86]. For the colipid phosphatidylethanolamine (DOPE) or phospholipids, ^{31}P NMR can be used to explore the structure of the PO_2^- group. Hafez *et al.* [42] have investigated the interactions of cationic lipid DOTAP and anionic phospholipids mimicking endosomal membranes. Their results suggested the adoption of the H_{II} phase in anionic phospholipids/cationic lipids equimolar mixtures.

3.3.2. Atomic force microscopy

Liposomes and lipoplexes can be imaged with AFM, using a multimode scanning probe and operating in the tapping mode under constant tapping forces. Samples are usually deposited on freshly cleaved mica surface for a few minutes exposed to air after absorbing excess solution using a paper filter. Images are shown at height mode or amplitude mode [44,101].

3.3.3. Small-angle X-ray scattering

Important insights into the structural organization of cationic lipid–DNA complexes have been obtained by SAXS. In liposomes prepared with pyridinium amphiphiles (SAINT), depending on the absence or the presence of the helper lipid DOPE, either a lamellar or a two-dimensional hexagonal lattice (H_{II}) organization was observed [40,105]. X-ray diffraction experiments performed with both macroscopically oriented and capillary-mounted powder samples of DM-TAP indicated that the lamellar crystalline phase is a highly ordered and substantially dehydrated structure in which the hydrocarbon chains are essentially immobilized [102].

3.3.4. Differential scanning calorimetry

The thermometric phase behaviour of lipid membranes can be monitored by DSC [102]. For acyl-based cationic lipids, this technique provides information about the transition point and the enthalpy characteristic of the lipidic system phase transition.

3.3.5. Fluorescence resonance energy transfer

Fluorescence resonance energy transfer (FRET) between a donor/acceptor of fluorophores such as fluorescein isothiocyanate (FITC) and Texas Red contributed to investigating the preservation of short ODN [106,107]. Indeed, such a transfer is operational when the distance between the donor and the acceptor is

not longer than a critical length of a few nanometers, so that the integrity of a doubly labelled ODN molecule in cells after transfection can be assessed when the donor is excited in the blue and the red fluorescence of the receptor is observed [108].

3.3.6. *Lipid mixing*

Lipid mixing during the formation of the lipoplex can be measured using the double label of Rhodamine-labelled phosphatidylethanolamine (Rh-PE) and 7-nitrobenzo-2-oxa-1,3-diazole labelled phosphatidylethanolamine (NBD-PE) for cationic liposomes [97]. Labelled and non-labelled liposomes are mixed. Because of the fluorescence energy transfer between this couple donor/acceptor of fluorophores, NBD emission was greatly reduced in close proximity to Rh-PE. When DNA was added to cationic liposomes, lipid mixing between labelled and unlabelled liposomes resulted in the dilution of the fluorescence label and thus an increase on the NBD-PE fluorescence. The fraction of lipid mixing can be calculated from the maximum dequenching of the NBD emission, the observed fluorescence and the NBD emission intensity. Moreover, this technique was used to monitor the fusion between cell membranes and lipoplexes and study the mechanism of cellular internalization of the latter [44].

4. DELIVERY OF DNA IN CELLS: LIPOFECTION

Transfection of adherent cells can be obtained by simple addition of lipoplexes solution. Usually serum-free OPTIMEM or culture medium must be used for at least 3–6 h before being replaced with serum-containing culture medium. Depending upon the concentration of added lipoplexes, the internalization of lipoplexes can disturb the cell life.

4.1. Cytotoxicity of cationic liposomes

Cytotoxicity is one of the most important characteristics of a carrier. Therefore, prior to investigating its transfection potential, a study of its toxicity is necessary. For this purpose, usually viability of transfected cells is undertaken by MTT test. This test is based on the formation of coloured formazan by reduction of 3-(4,5-dimethylthiazol-2-yl)-2,5-diphenyl tetrazolium bromide (MTT) reagent in the presence of mitochondrial dehydrogenases of viable cells. The tested cells include human breast carcinoma cells MCF7, human cultured skin fibroblasts, mesothelioma cells, rat gliosarcoma cells 9L and murine melanoma cells B16-F10.

Typically, sub-confluent cells were trypsinized, harvested and re-suspended. The following day, cells were transfected for 48 h. Later, cells were washed with medium and a solution of MTT was added for a further 3 h. The formazan crystals were dissolved in dimethylsulfoxide (DMSO). Absorbance was measured

at 570 nm on a P450 microplate reader (Bio-Rad, Hercules, CA, USA), which allowed the determination of the cationic lipid concentration IC_{50} at which 50% of cells were viable, compared with untransfected cells.

Viability of B16-F10 melanoma cells after incubation in the absence or in the presence of cationic liposomes at various concentrations was detected by MTT test. In B16-F10 cells, statistical analysis of results showed an order of toxicity which was TMAPC-Chol < TEAPC-Chol = TMAEC-Chol < DC-Chol < TEAEC-Chol. The comparison of the IC_{50} between the two opposite chemical structures indicates a factor of 3.5 (Table 2). It seems that a lipid with quaternary ammonium in the polar head is more toxic with three ethyl groups than with three methyl groups. Likewise, three carbon atoms appear to be better than two carbons in the spacer with no meaningful difference between TMAEC-Chol/DOPE and TEAPC-Chol/DOPE [85].

For hydroxyethylated DMHAPC-Chol/DOPE liposomes, with a given cationic lipid concentration, plasmid DNA at different doses has no effect on the cell viability [86].

4.2. Delivery of nucleic acids: transfection efficiency

Transfection efficiency was evaluated from the measurements of transfection level by chemiluminescence and of transfection yield by counting the number of transfected cells. These measurements also indicate the functionality conservation of the transported gene. For this purpose, plasmids containing a reporter gene coding for an enzyme, such as β -galactosidase (β -gal), luciferase (luc) [109] or green fluorescence protein (GFP) [110] were used and the activities of the expressed protein measured either by chemiluminescence or by colouring obtained with an appropriate reagent. Using a luminometer, the transfection level is measured for the whole ensemble of expressed proteins extracted from cells. Microscopy, or flow cytometry method allows the individual counting of the transfected cells and then furnishes the ratio of positively transfected cells.

Table 2. Comparison of cytotoxicity in B16-F10 cells for liposomes prepared from different cationic cholesterol derivatives and DOPE

Transfection reagents	IC_{50} (μ M) ^a
TMAEC-Chol/DOPE	61.5 ± 0.7
TEAEC-Chol/DOPE	28.0 ± 0.7
TMAPC-Chol/DOPE	86.0 ± 1.1
TEAPC-Chol/DOPE	54.9 ± 0.6
DC-Chol	47.3 ± 0.7

^a IC_{50} was defined as the cationic lipid concentration corresponding to 50% of cell viability.

4.2.1. Measurements of transfection level

In order to determine the transfection levels, usually cells were seeded in a six-well Falcon plate (3×10^5 cells/well) on the day preceding transfection. Just before transfection, culture medium was replaced with 1 mL OPTIMEM without serum, then plasmids (3 nmol), liposomes alone or liposome–plasmid complexes at desired charge ratio were added. After 6 h, OPTIMEM was removed, replaced with culture medium containing serum and cells and incubated at 37 °C. After the desired incubation time, cells were washed twice with PBS and the transfection level was measured using the chemiluminescence of luciferase or β -galactosidase. Detection kits are available.

For luciferase, transfection level was measured using chemiluminescence in the presence of ATP and luciferin substrates with a Tropic kit (Applied Biosystems, Bredford, MA, USA). Following the procedure of the supplier, after lysing the transfected cells with a lysis solution containing 1 mM of dithiothreitol (DTT) freshly added, 20 μ L of the cell extract was incubated with 100 μ L of the reagent A before 100 μ L of the reagent B was added. Immediately after mixing, luminometric measurement was made using a BCL luminometer (Govteyron Technologies, Vals de Puy, France) operating at integration mode for 10 s. Protein was titrated by using the Bio-Rad DC Protein assay kit, in order to normalize results expressed in relative light unit per mg of protein (RLU/mg).

For β -galactosidase, a similar protocol was used with the Tropic kit β -galactolight along with using the chemiluminescence of β -galactosidase in the presence of [3-4(-methoxyspiro(1,2-dioxetane-3,2'-tricyclo(3.3.1.1)decane-4-yl)]phenyl- β -D-galactopyranoside (AMPGD). The noise or endogenous β -galactosidase level of untransfected cells was measured and subtracted.

The total chemiluminescence of luciferase, represented in RLU, was measured in B16-F10 melanoma cell lysates after gene transfer [31]. *In vitro*, our previous works showed that no transfection level was detected with naked plasmid DNA and that luciferase activity was optimal with a charge ratio X of 2. Results showed that the transfection level obtained with the cationic lipids presenting three carbons in the spacer is better than the group of cationic lipids with two carbons. The transfection efficiencies of TMAPC-Chol and TEAPC-Chol were, respectively, 2.5 and 7.8-fold significantly higher than that of DC-Chol, the best-known cholesterol-based cationic lipids. Thus, the chemical structure of the polar head seems to influence gene transfer. The transfection level obtained with TEAPC-Chol with three ethyl groups in the polar head was 3.2-fold higher than that obtained with TMAPC-Chol with three methyl groups. So, among the group of cationic lipids with the spacer 3C, which could take an important place in gene transfer, a quaternary ammonium with three ethyl groups for the polar head offers the best results [31,85].

4.2.2. Evaluation of transfection yield

Two techniques are usually used to determine the transfection yield of cells. The first one uses the cytoenzymatic detection of β -galactosidase, the X-gal test

consisting of colouring the expressed protein with the reagent X-gal (5-bromo-4-chloro-3-indolyl β -D-galactopyranoside) followed by counting under a microscope. The second one uses the expression of GFP gene and counting by flow cytometry.

4.2.2.1. β -Galactosidase expression and X-gal test

The presence of expressed β -galactosidase was observed by the blue staining with X-gal reagent. For this test, a four-well permanox Lab-Tek plate (Nunc) was seeded with 4×10^4 MCF7 cells/well. Plasmids pCMV- β (0.5 or 1 μ g) and cationic liposomes at $X = 2$ were complexed and incubated with cells for 48 h at 37 °C in 5% CO₂. After the incubation time, cells were washed with PBS, fixed with paraformaldehyde (1%) and glutaraldehyde (0.02%) for 3 min before the X-gal reagent was added. After 6 h, they were observed under a microscope.

The transfection efficiency of TMAEC-Chol/DOPE in MCF7-cells was estimated by X-gal test [54]. Untransfected cells were used as control, and showed no blue stain due to endogenous β -galactosidase. Cells transfected with unvectorized plasmids present practically no fraction of blue-stained cells. The aspect is very different with cells transfected with plasmids showing large blue blobs. For cells transfected with 0.5 and 1 μ g pCMV- β , vectorized by liposomes, the fraction of blue-stained cells was estimated to be around 50% [54].

4.2.3. GFP expression and flow cytometry

GFP expression can be investigated by microscopy and/or by flow cytometry. For fluorescence microscopy assay, after the desired incubation time, cells were rinsed twice with PBS followed by a fixation step with 4% paraformaldehyde in PBS and mounted in Mowiol before microscopy observation.

For flow cytometry, cells were seeded on six-well plates (3×10^5 cells/well), and plasmid pEGFP-N1 containing GFP gene was used. After the transfection time, cells were detached with a non-enzymatic cell dissociation solution and washed with PBS. After re-suspension, propidium iodide (PI) was added and only IP-negative viable cells were gated to quantify GFP-positive cells. The cells were incubated in the dark at room temperature for 15 min before flow cytometric analysis. For each sample, at least 75,000 events were analysed using an Epics XL flow cytometer (Beckman Coulter, Miami, FL, USA) equipped with an argon ion laser tuned at 488 nm wavelength used for excitation. The emission filters used were 530 ± 30 nm band pass for green fluorescence of GFP, and 620 nm long pass for red fluorescence of PI.

Transfection yields in B16-F10 cells were investigated [85]. The results were obtained with 1 μ g of pEGFP-N1 plasmid complexed with different cationic lipids/DOPE (1:1) at the molar charge ratio of 2 after 24 h of transfection. The auto-fluorescence of untransfected B16-F10 cells has been used as control to estimate transfected cells, indicated by the shift of more than two magnitudes in intensity shown in each panel. From at least 75,000 events marked in the ledger

and analysed, with 1–5% of IP⁺-cells, the percentage of positively transfected viable cells was determined and was found to be in the range between 25 and 30%. Compared with the control, the shift of GFP-positive cell distribution obtained with TMAEC-Chol was of two magnitudes, while it was of three magnitudes with TEAPC-Chol. In spite of the difference in these distributions, the mean values of fluorescence intensity of GFP were approximately equal for all lipids of the series. The ability of TEAPC-Chol to deliver plasmid DNA with a high efficacy was ideally correlated with transfection level results. These results by cytometry were consistent with data of chemiluminescence [84,85].

4.3. Cellular trafficking

Cellular trafficking of lipoplexes is one of the most studied subjects [52,54,106,111]. The information obtained is necessary for understanding the transfection mechanism and then highlighting the parameters to be adjusted for an optimal use of the carriers. Cellular pathway of lipoplexes can be observed by appropriate labelling of DNA and liposomes, followed by fluorescence or electron microscopy observation.

4.3.1. Fluorescence and confocal microscopy

For fluorescence or confocal microscopy, several markers can be purchased from Molecular Probes but fluorescein isothiocyanate (FITC) and lissamine rhodamine are often used for labelling of DNA and lipid, respectively. Lissamine rhodamine-marked phosphatidylethanolamine is generally used as colipid. For comparative observation and to locate the exogenous DNA or lipid with respect to the nucleus, nuclear staining 4',6-diamidino-2-phenylindole (DAPI) can be used. In the case of mitochondrial localization, rhodamine 123 is a good marker for mitochondrial-specific fluorescent dye [112].

4.3.1.1. Delivery and pathway of lipid/oligonucleotides complexes

Observations of cellular internalization in MCF7 cells by 28-mer ODN or in fibroblasts by oligopeptides PONC by confocal microscopy are illustrated by Fig. 5 [52,69]. Cells were plated in a four-well Lab-Tek plate (4×10^4 cells/well). After 24 h, the medium was replaced with serum-free OPTIMEM for 20–30 min at room temperature. The FITC-labelled ODN or FITC-labelled PONC and the lissamine rhodamine-labelled liposome were gently mixed in sterile water and then added to the cells. After 6 h at 37 °C, the transfection medium was replaced with serum containing culture medium and incubated for 24 h at 37 °C. The cells were then washed, fixed in 4% paraformaldehyde for 15 min and then mounted in Mowiol.

Samples were observed using a MRC-600 Bio-Rad confocal laser scanning microscope (CLSM). An Ar⁺ laser was used for double fluorescence of fluorescein and rhodamine with excitation at 515 nm. A 540 DF 30 band pass filter

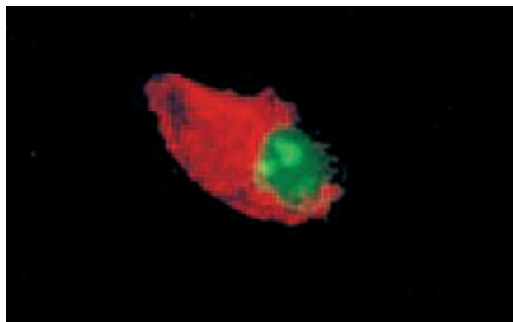


Fig. 5. Internalization of 28-mer oligonucleotides labelled with fluorescein and delivered by TMAEC liposomes into MCF7 cells, observed by CLSM. 28-mer HER2/neu oligodeoxynucleotides (5'-FG3AG2AG2AG2CG2AG2AG2A2GAG2A) were labelled with fluorescein (green fluorescence) and vectorized by TMAEC-Chol/DOPE liposomes into MCF7 cells. The liposomes were labelled with rhodamine (red fluorescence). One can observe the penetration of oligonucleotides (in green) in the nucleus and they were dissociated from the liposomes (in red) in the cytoplasm. See text for the transfection protocol and sample preparation. Micrograph was obtained at 24 h after transfection: picture of a Z-cut section of a transfected MCF7 cell.

combined with an EF 600 LP long pass filter was used for separation of the green emission of fluorescein and the red emission of rhodamine lissamine. To show the relative positions of the labelled liposomes or oligonucleotides with respect to the cells, pictures of the same field were compared. For this purpose, an optical set-up with a channel for green fluorescence and a channel for a red fluorescence allowed to obtain separately the pictures of the same field, which could then be superimposed. There are several advantages of using confocal microscopy: the sample preparation is easy, the observation is quick and almost one can confirm or not the penetration of lipoplexes inside the observed cells. Incorporation of lissamine rhodamine-conjugated DOPE in TMAEC/DOPE liposomes and the use of oligonucleotides 28-mers labelled with fluorescein allowed the observation of (i) the internalization of TMAEC liposomes and of the oligo-liposome complexes into cells; (ii) the dissociation of oligonucleotides from the vectors; (iii) the penetration of oligonucleotides into the cell nuclei; (iv) the persistence of the oligonucleotide with a resident time as long as 72 h in cells and (v) the degradation of liposomes [52].

Naked oligonucleotides did not show transfection in MCF7 cells (results not shown). In Fig. 5, the red fluorescence indicates the presence of lissamine rhodamine-containing lipids, the green fluorescence is due to fluorescein-labelled 28-mer oligonucleotides and the yellow indicates the presence of colocalized lipids and oligomers or complexes. The micrographs showed that complexes penetrated in cells where oligonucleotides were delivered. With confocal microscopy facilities, cells were examined in Z-planes at different levels. This allowed confirmation of the penetration of the oligomers *inside* the nuclei. The results (not

shown) indicated that after 30 min, or even earlier, the transfection was already observable. However the peak fluorescence was observed very much later. At 24 h, while the red (or orange-yellow) fluorescence was observed in the cytoplasm, the pure green fluorescence was seen in the nuclei. It is observed that the labelled lipids diffused throughout the cytoplasm, probably in the intracellular membranes as attested by the reticulated pattern of the red fluorescence. On the other hand, the pure green fluorescence in nuclei indicated oligonucleotides dissociated from liposomes. Even after 72 h, the presence of oligonucleotides in the nuclei was still observed [52]. The lipids were probably degraded or exocytosed. This degradation or exocytosis may contribute to the reduction of cytotoxicity of the transfected cells.

4.3.2. *Transmission electron microscopy*

The fate of the DNA vectorized in cells by cationic lipids is an aspect not yet entirely elucidated, and inspired investigations to understand the route taken by DNA/lipid complexes after having been internalized in cells. TEM is a powerful tool to observe details and offers better resolution than confocal microscopy. TEM was used to observe the ultrastructure of liposome/plasmid complexes and their cellular route after transfection of MCF7 cells. About the passage across the cell membrane, most reports are in favour of endocytosis [47,48] even if excluding the possibility of fusion of liposome/DNA complexes with the plasma membrane is not straightforward [44,45]. If the penetration of the DNA/cationic lipid in cells is the first condition for an efficient transfection, it is also necessary for DNA and lipid to be dissociated and DNA moves towards the target. Accordingly, the residence time of the transported DNA and the degradation or exocytosis of the carriers are other parameters governing a successful transfection. For a transfer of reporter genes or DNA of interest, the penetration into the nucleus is necessary [113].

For observation of the penetration of plasmids into cells, ultrathin-section EM was done on transfected MCF7 cells. Cells were detached by a cell dissociation solution (Sigma, C1594), pelleted at 1500 *g* for 10 min, fixed with 3% glutaraldehyde in 0.1 M cacodylate buffer (pH 7.4) at 4 °C and postfixed with 1% osmium tetroxide for 1 h. Samples were stained with 1% uranyl acetate, dehydrated with a series of ethanol dilutions and propylene oxide, and embedded in Epon 812 resin. Thin sections of 100 nm thickness were cut using a Reichert ultramicrotome and stained with lead citrate and uranyl acetate. Sections were viewed and photographed using a Philips transmission electron microscope operating at 60 kV. The complexes were formed from mixtures of TMAEC-Chol liposomes and plasmids at a charge ratio $X = 2$, corresponding to the optimal transfection level observed in the absence of serum. To follow the route and the fate of liposome/plasmid complexes after transfection, cells were fixed after incubating for 15 min, 30 min, 1 h and 2 h. The micrographs in Fig. 6 showed the features of MCF7 cells exposed to complexes. These micrographs indicate that the technique used allowed to clearly

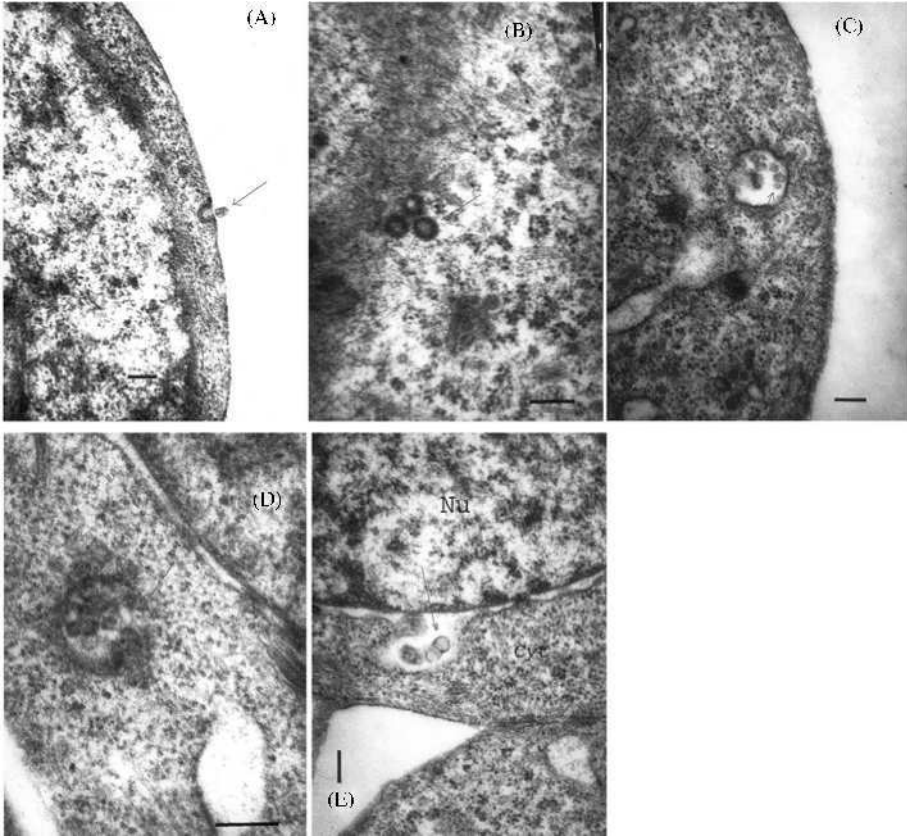


Fig. 6. Cellular route in MCF7 cells of complexes between cationic lipids prepared with TMAEC-Chol/DOPE (1:1) and pCMV- β observed by TEM. Arrowhead highlights complexes. (A) Beginning of endocytosis. (B) and (C) Internalization into endosomes. (D) Opening of endosomes. (E) Entry inside the perinuclear membrane. Nu denotes the nucleus side and Cy the cytoplasm side. Bars represent 200 nm. (Reproduced with permission from Cao *et al.* [52].)

observe the cytoplasm and the nuclei. For transfected cells, the features of cytoplasm are shown in Figs. 6A–E. Figure 6A shows complexes near coated invagination of the plasma membrane indicating the beginning of an endocytosis process. In Fig. 6B, vesicles with a thick wall formed by complexes and the membrane coated with clathrin during the endocytosis process are seen. Figure 6C shows many patterns of endosomal compartments in which dense particles are seen. These particles are probable complexes with size varying from 80 to 130 nm. Figure 6D shows an opened endosome with complexes probably being released. Figure 6E depicts a cell at 2 h after being exposed to complexes; there were not many endosomal compartments with complexes inside at 2 h when compared with that at 15 min. This may indicate that after the uptake of complexes in endosomes, the complexes were very likely to be released rapidly. Feature of complexes similar

to dense particles in endosomal compartments was observed in other cells, such as COS-1 cells transfected with DMRIE/DOPE lipids [37] or CV-1 cells with DDAB/DOPE lipids [47] and in endothelial cells [49]. Complexes already trapped in the vicinity of the nuclear membranes were observed in Fig. 6E.

4.3.3. *Observation of exogenous DNA internalized in the nucleus*

To observe exogenous DNA in cells, it is advantageous to use a marker that distinguishes it from endogenous DNA [54]. For TEM observation, several techniques can be used. One of the most practical methods is to label DNA with digoxigenin (DIG) and to use an anti-DIG antibody conjugated with gold nanoparticles. Commercial kits are available for this purpose.

Plasmids pCMV- β were labelled with DIG and detected by anti-DIG Fab coupled with ultra-small gold particles. The size of gold particles was increased by silver enhancement reagent. In a sterile vial, reactive DIG (DIG-Chem-Link from Roche Diagnostics, Meylan, France) was added to pCMV- β plasmid. After incubation for 30 min at 50 °C in a waterbath, the reaction was stopped by adding the stop solution. The preparation was controlled by gel electrophoresis and results showed no perceptible difference compared to unlabelled plasmids.

Cells dissociated from the wells of plates were fixed at 4 °C for 20 min with 1% paraformaldehyde and 0.1% glutaraldehyde in 0.1 M phosphate buffer (PB) pH 7.4. After washing, the cells were treated with 0.05% NaBH₄ and 0.1% glycine in PB for 10 min, to block the free aldehyde groups and to permeabilize the cells. The cells were then rinsed in PB and pre-incubated in 0.2% acetylated BSA (BSA-C) in PB for 30 min. They were then incubated for 2 h at room temperature with diluted ultra-small gold-labelled anti-DIG antibody fragments (Fab) in 0.2% BSA-C in PB. The cells were rinsed in 0.2% BSA-C in PB, then in PB and refixed with 2.5% glutaraldehyde for 10 min. After washing in PB, the samples were post-fixed with 0.5% OsO₄ in PB for 20 min, washed in deionized water and treated with the silver enhancement reagent. After washing in distilled water, samples were stained with 0.5% uranyl acetate in 50% ethanol, dehydrated in a graded series of alcohols, embedded in Epon resin, sectioned and examined with a Philips EM300 transmission electron microscope operating at 60 kV.

Controls by untransfected cells treated with silver alone or with antibodies followed by silver did not show any dark staining. The kinetics of plasmids carried by TMAEC-Chol/DOPE liposomes was studied; TEM showed that after the cytoplasmic step DNA penetrate inside the nucleus as revealed by immuno-gold labelling. The time course was respected: when cells were incubated with complexes at 15 min, black gold particles were seen only at the cell surface or in cytoplasm but no particles were observed in the nucleus. At 30 min of incubation gold particles were observed only in the cytoplasm and not in the nucleus. Cell components slightly stained by uranyl acetate do not contribute to these very dark patterns. After 24 h, there are many more plasmid copies, especially in the nucleus.

The micrograph in Fig. 7A, devoted to a MCF7 cell transfected for 1 h, shows numerous gold particles but only in the cytoplasm, and in electron-dense vesicles. No gold particle is seen in the nucleus. This indicates that there are already plasmids, or at least plasmid/lipid complexes internalized in the cell. The dense vesicles may be endosomes containing plasmid/lipid complexes. In the micrographs describing cells after 5 h (Fig. 7B), particles are still present in the cytoplasm and a few begin to appear in the nucleus of some cells. Almost with all cells observed at 24 h of transfection, there are many more plasmids in the nucleus although there are still some gold particles outside the nucleus (Fig. 7C and D). Occasionally, gold particles are still present in protrusions of the cell surface. Magnifications of some portions of nuclei show several gold particles in the nucleolus and nucleus (Fig. 7C and D). Most cells observed after 24 h of incubation have an immunopositivity of their nucleus.

Nuclear localization of plasmids was also detected with liposomes prepared from another lipid in the series. This indicates a similar behaviour of the series of cationic lipids containing a quaternary ammonium group. The internalization of

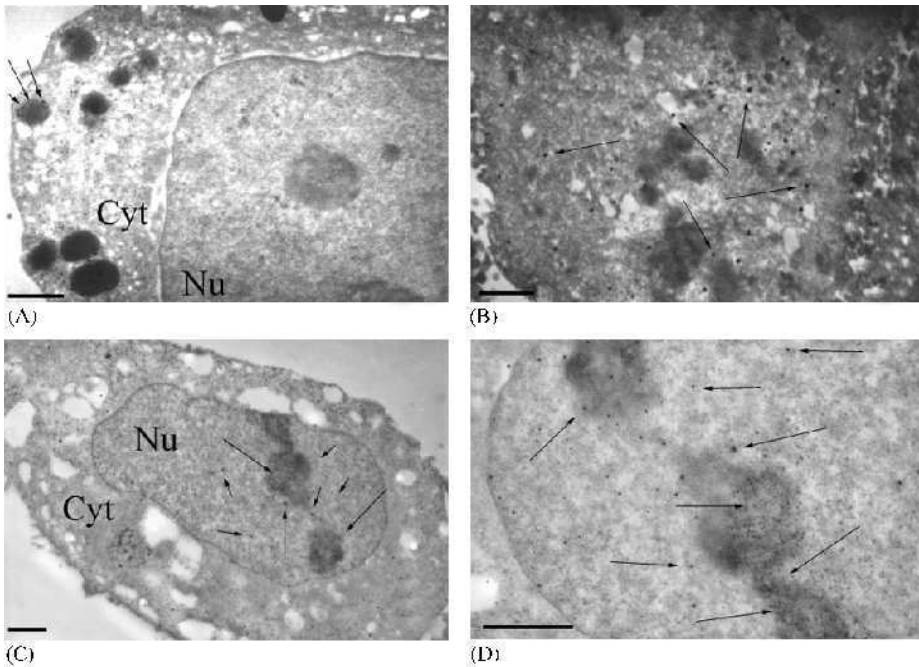


Fig. 7. Cellular route in MCF7 cells of plasmids pCMV- β vectorized by cationic liposomes TMAEC-Chol/DOPE (1:1) observed by TEM. Plasmids were labelled with DIG, detected by antibodies conjugated with gold particles enhanced by colloidal silver, indicated by arrows. (A) Cell transfected with plasmid vectorized by liposomes, 1 h. (B) Cell transfected with vectorized plasmid, 5 h. (C, D) Cell transfected with vectorized plasmid at 24 h. Bars represent 1 μ m. (Reproduced with permission from Briane *et al.* [54].)

plasmids vectorized by TMAEC-Chol/DOPE liposomes was not limited to MCF7 cells alone; transfection has been observed also in gliosarcoma cells 9L [54,84].

Although liposomes were not labelled, the concentration of gold particles in the dense vesicles observed in Fig. 7A undoubtedly corresponds to endosomes observed previously with uranyl acetate-stained complexes. It appears that the membrane of endosomal compartment was destabilized allowing the release of DNA from the complexes and then the entry of DNA in the cytosol as shown by separated gold particles revealing the presence of labelled plasmids. As in most formulations of cationic liposomes [114–116], DOPE was used with TMAEC-Chol and TEAPC-Chol. This destabilization of endosomal membranes may be achieved by cationic lipids or by the colipid DOPE. In the present case, it was not possible to visualize the dissociation of plasmids and liposomes as has been observed with oligonucleotide/liposome complexes in previous work. However, since it is already known that liposomes did not penetrate into the nucleus, it is obvious that with plasmids detected in the nucleus here, the dissociation did occur. At this point, it is necessary to emphasize that the dissociation from lipids and the entry into nuclei was observed with modified oligonucleotides [106] as well as with unmodified oligonucleotides transferred by TMAEC/DOPE liposomes in MCF7 cells [52].

4.3.4. Mechanism of lipoplex delivery

The mechanism of lipoplex delivery is one of the most developed areas of research which contributes to understanding of how DNA can be delivered into cells and how the transfection can be monitored. Indeed, after the passage across the cellular membrane, TEM indicated that lipoplexes entered in and then escaped from the endosomes. This is a crucial step before complexed DNA was released into the cytosol. In order to explain the escape of lipoplexes from endosomes, Zelphati [106] and Hafez [42] have mimicked plasma and endosome membrane by phospholipid liposomes and studied their interaction with lipoplexes.

ODN displacement from lipoplex was studied by FRET. Zelphati *et al.* [106] showed that the release of DNA oligonucleotides was a rapid process, since after 100 s fluorescein fluorescence increased to a plateau regardless of the composition of the negatively charged liposomes. This was 2–3 times slower with ODN/dioctadecylamidoglycyl spermine (DOGS) complexes but still is in the time scale of an endocytic event. Three formulations of liposomes have been showed efficient in releasing ODN: PG/DOPE/DOPC, PS/DOPE/DOPC and PI/DOPE/DOPC. These anionic liposomes mimicked the cytoplasmic-facing monolayer of the cell membrane. Their results also showed that the fluid phase of the liposomes is required regardless of the physical state of the cationic liposomes. The authors proposed that after internalization by endocytosis, lipoplex induces flip-flop of anionic lipids from the cytoplasmic-facing monolayer. Anionic lipids laterally diffuse into the lipoplex and form a charged neutralized ion pair with cationic

lipids. This leads to displacement of the ODN from the cationic lipid and its release into the cytoplasm.

Hafez *et al.* [42] studied the interaction of cationic lipids DODAC, DC-Chol, DOTMA, DOTAP and lipid systems containing anionic phospholipid DOPS using ^{31}P NMR. Their findings were that cationic lipids such as DOTAP/DOPE or DOTAP/cholesterol systems exhibit the ability to induce non-bilayer H_{II} phase structure in anionic lipid systems. In particular, the helper lipids DOPE or cholesterol also promote H_{II} phase organization. Their results suggested that the ability of cationic lipids to deliver DNA arises at least in part from an ability to destabilize endosomal or plasma membranes by inducing non-bilayer lipid structures. Another lipid such as DOPC is not able to induce a H_{II} phase structure and was inefficient for transfection [114].

The internalization of lipoplex and the release of DNA can be modelled by the following steps: (i) lipoplex moves close to the plasma membrane; (ii) endocytosis; (iii) lipoplex is transferred to endosomal compartment; (iv) the membrane of the lipoplex fuses with the endosomal membrane (this is due to the tendency of positively and negatively charged membranes to adhere and fuse, leading to lipid mixing between lipoplex and endosomal lipids); and (v) anionic lipids from the endosomal membrane displace cationic lipids from DNA, leading to DNA release [106] and further formation of non-bilayer structures [43].

After being released into the cytosol, DNA was observed in the nucleus. This is proof of a necessary step for the expression of reporter genes. This passage across the nuclear envelope may be due to various mechanisms. First, there may be a machinery permitting the association of plasmids with nucleus-targeted proteins, which carry DNA into the nuclei. For example, Dowty *et al.* [117] have suggested a “facilitated process” by implying karyophilic proteins. The transport across nuclear envelopes may also occur by signal-mediated factors as discussed in detail by Nigg [118]. Second, although it is generally considered that the nuclear pores are too small (hole size of nuclear pores is about 9 nm) to allow the free passage of macromolecules being the size of plasmids, a close examination shows that this entry is possible. DNA may enter the nucleus during the mitosis of the cell when the nuclear envelopes disappeared as demonstrated by Mortimer *et al.* [119] and Tseng *et al.* [120]. This possibility is limited by the short time of the mitosis, about 1 h compared with the total duration of about 48 h for the cell cycle. Moreover, plasmids dissociated from lipids may be under a stretched supercoiled conformation, which may allow them to have the minimum transverse size about only twice the DNA section, and passing through the nuclear pores.

4.3.5. Endocytosis or fusion for lipoplex internalization?

For most studies including ours, using monensin to prevent endocytosis, with experimental proofs from TEM, this question has been nearly resolved in favour of endocytosis. However, recently, in using fusion inhibitor (100 μM Z-Phe-

Phe-Gly) and that of endocytosis inhibitor (1 $\mu\text{g}/\text{mL}$ of antimycin A, 10 mM NaF and 0.1% (w/w) sodium azide), Almofti *et al.* [44] showed that although the transfection of A431 cells by lipoplexes formed by DC-6-14/cholesterol/DOPE cationic liposomes was completely abolished in the presence of endocytosis inhibitor suggesting that endocytosis is the main route of lipoplexes, the lipofection was also strongly inhibited by the fusion inhibitor suggesting that fusion process is also necessary for lipoplex internalization. With lipid mixing assay, they showed that fusion occurs mainly at the plasma membrane level and thus triggers endocytosis process.

5. FACTORS AFFECTING LIPOFECTION

Lipofection is the result of several factors. In the above sections, we have seen the effect of molar lip+ /DNA molar charge ratio and that of DOPE in the formulation. In this section, we discuss other important factors. Beside the chemical nature and formulation of liposomes, charged components on the cell surface, in the extra- or intracellular media, may be agents that affect the structure of lipoplexes and consequently are implied in the transfection level. In the sections that follow, we will particularly deal with the chemical structure of the lipids, the conditioning of liposomes and the role of cell surface PG.

5.1. Effect of chemical structure

Several comparative studies suggested that the chemical structure affects transfection efficiencies [14,22,75]. First of all, the cationic lipid hydrophilic moieties globally play a major role. It seems that chemical structure of the polar domain affected the DNA delivery by influencing the cellular uptake of lipoplexes or the escape of DNA from the endosome. Indeed, we have observed that the number of transfected cells measured by cytometry in B16-F10 cell line using pEGFP-N1 was not significantly changed with quaternary ammonium cationic lipids in the series studied but was dramatically affected by a ternary ammonium polar head (DC-Chol). Thus, the variation of transfection level observed by chemiluminescence from a cationic lipid to the other in the series was probably due to the differences in the intracellular fate of liposome–DNA complexes and especially to the ability of DNA to escape from the endosome. In these events, the chemical nature of the polar head seems to be determinant. Previous works have reported the cellular pathway of plasmids vectorized by TMAPC-Chol and TEAPC-Chol and the presence of complexes in endosome-like vesicles [52,54]. This was confirmed by the recent work of Hasegawa *et al.* [30], who have highlighted the implication of the polar head group on the release of DNA in cytosol and then on the transfection efficiency.

Changes in toxicity and transfection level were observed in assays with structural differences in the spacer length of the cationic cholesterol derivatives [85].

From these data, it is interesting to note that the lipids showing the least cytotoxicity, TMAPC-Chol and TEAPC-Chol, gave the best transfection efficiencies, for *in vivo* and *in vitro* respectively. These cationic lipids TMAPC-Chol and TEAPC-Chol present the longest spacer (three carbons). Similar results were observed by Floch *et al.* [75] with phosphonolipids, who have shown that the increase of spacer length was correlated with a decrease in the cytotoxicity index *in vitro* and *in vivo*. On the other hand, with the same spacer length, but different cross-sectional area of polar domain, Reynier *et al.* showed that the substitution of methyl groups by ethyl groups increased the toxicity and enhanced the transfection activity of the reagent *in vitro* [85].

With hydroxyethylated DMHAPC-Chol, the level observed at a charge ratio $X = 0.5$ was enhanced by a factor of 26-fold compared to unvectorized plasmid. For comparison, we also measured the levels obtained with DC-Chol and four cationic liposomes in the same series with trimethylated (trimethylaminoethane-carbamoyl cholesterol iodide (TMAEC-Chol) or trimethylaminopropane-carbamoyl cholesterol iodide (TMAPC-Chol)) or triethylated (triethylaminoethane-carbamoyl cholesterol iodide (TEAEC-Chol) and triethylaminopropane-carbamoyl cholesterol iodide (TEAPC-Chol)) polar heads, with spacers of 2C or 3C [86]. All the formulations contain DOPE in equimolar proportion. While DC-Chol and the short lipids TMAEC-Chol and TEAEC-Chol 2C spacers give low transfection levels, TEAPC-Chol and TMAPC-Chol with 3C spacers increased 10- and 30-fold, respectively, the transfection level with respect to the control. The results presented clearly showed the superiority of the cationic lipids constituted by three carbons in the spacer, i.e., TEAPC-Chol, DMHAPC-Chol and TMAPC-Chol and the probable influence of the hydration of the polar head.

5.2. Effect of colipid DOPE on the lipofection

The helper lipid DOPE affected transfection levels *in vitro* and *in vivo* as observed in tumour cells B16-F10. For three different liposome formulations with TEAPC-Chol/DOPE in the ratios 1:0.5, 1:1 and 1:2 used to complex with 15 μg of plasmid pUT650 at molar charge ratio $X = 0.5$ before intratumoral injection in B16 tumour, results showed that the formulation 1:1 allowed the best transfection level of DNA inside tumour cells [31].

It is believed that DOPE plays a double role. On the one hand, DOPE stabilizes most types of cationic lipids in a lipid bilayer and on the other, it allows DNA entry into the cytosol by destabilizing the endosome membrane [114–116]. Intra-tissue gene delivery using DOPE-containing lipoplexes has been shown to be very efficient [121]. The TEAPC-Chol/DOPE (1:1) formulation offers the better compromise to transfer DNA directly inside tumour cells more than 10-fold than unvectorized DNA. In systemic delivery, it seems that DOPE decreases the *in vivo* activity of lipidic vectors [9,62,122].

5.3. Effect of conditioning (lyophilization) on hydroxyethylated cationic liposomes

Assays in B16-F10 cells showed that lyophilization of liposomes prepared with hydroxyethylated cationic lipid and DMHAPC-Chol cationic lipid improved DNA delivery level. Till date, the effect of lyophilization on liposomes was only investigated from a structural point of view [8,65–67]. This surprising result in transfection may open a new way for pharmaceutical uses of cationic liposomes. The lyophilization presents several advantages. First, lyophilization allows to avoid the storage of liposomes under the liquid state, which is generally the cause of instability. Second, it facilitates liposome shipping. Third, the storage of cationic liposomes separately with respect to the storage of DNA will allow the complexation with any DNA of choice and at any desired ratio, for use in a precise purpose. Freeze–thawing of lipoplexes also gave an increase in transfection level. Both lyophilization and freeze–thawing are associated with liposomes aggregation. In the latter case, transfection is largely increased by this pre-treatment of the complexes. During freezing of the complexes, a rearrangement of DNA and cationic lipids in complexes may be responsible for the transfection improvement.

Results of electron microscopy showed that the unlyophilized liposomes are relatively homogenous in size, while lyophilized liposomes present at least four kinds of shapes, ranging from globular structures with the presence of spherical units inside, to chain structures with liposomes fusing on the periphery [86].

5.3.1. Effect of conditioning on efficiency *in vitro*

The lyophilization of the liposomes and the freeze-drying of the complexes substantially influence the transfection efficiency of the lipidic carrier [86]. The conditioning effect on DNA delivery of DMHAPC-Chol/DOPE was estimated for lyophilized and rehydrated liposomes and for lipid/DNA complexes subjected to three cycles of freeze–thawing prior to transfection. The results of β -galactosidase expression 24 h after transfer in B16-F10 cells are indicated in Fig. 8 as a function of the molar cationic lipid/DNA charge ratio. Depending on the conditioning, DMHAPC-Chol/DOPE liposomes showed a maximum transfection level varying from $X = 1.5$ for liposomes, $X = 2$ for lyophilized and rehydrated liposomes and $X = 1.5$ for frozen and thawed complexes. The transfection level obtained with lyophilized and rehydrated liposomes is 4- to 5-fold higher in comparison with unlyophilized liposomes.

Transfection levels in B16-F10 cells of DMHAPC-Chol/DOPE liposomes were compared with those of liposomes in the same chemical series and to commonly known commercial reagents using protocols as recommended by the manufacturers. At the molar charge ratio $X = 1.5$, lipoplexes subjected to three cycles of freeze–thawing gave a transfection level up to fivefold greater than unfreeze–thawed ones and this is similar for DMRIE-C. Results indicated that in comparison to Transfast (Promega) and DMRIE-C (Invitrogen), unlyophilized

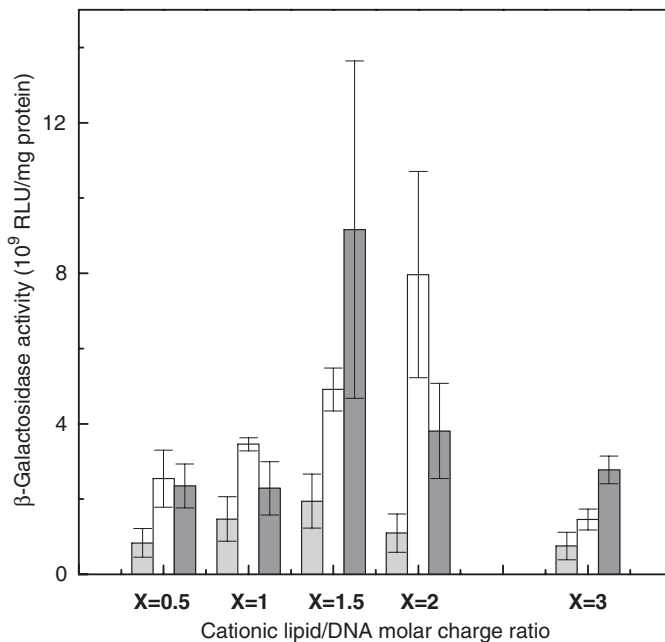


Fig. 8. Transfection level in B16-F10 cells of β -galactosidase plasmid delivered by cationic liposomes DMHAPC-Chol/DOPE. 0.5 μ g of pCMV- β gal plasmid DNA containing the β -galactosidase gene was complexed with liposomes (light grey), lyophilized and rehydrated liposomes (white) and frozen and thawed complexes (dark grey). The charge ratios were ranging from $X = 0.5$ to 3. Each result represents the mean \pm SE of three experiments. (Reprinted from Percot *et al.* [86]. Copyright 2004, with permission from Elsevier.)

DMHAPC-Chol/liposomes present a significantly lower level, but the lyophilized and rehydrated liposomes gave a comparable level [86]. A similar enhancement of transfection level was obtained by freeze–thawing of complexes DNA/lipofectamine without cryoprotectant [33].

5.3.2. Effect of lyophilization on ^{31}P NMR spectra

Changes induced by lyophilization from a molecular point of view were investigated by ^{31}P NMR [86]. The phosphorous spectrum of pure dry DOPE powder in CDCl_3 showed one signal at 0.9 ppm, corresponding to the phosphate group belonging to DOPE polar head. No change was observed when the sample was lyophilized and re-dissolved in the same solvent. The ^{31}P spectrum of the equimolar mixture DMHAPC-Chol/DOPE powder directly dissolved in CDCl_3 presented only one peak at 0.62 ppm.

When the liposomes DMHAPC-Chol/DOPE (1:1) prepared in H_2O were lyophilized and then dissolved in CDCl_3 , two signals, one at 0.64 ppm, which corresponds to the signal already found in CDCl_3 and a new resonance at

-1.07 ppm appeared. When DOPE lipid was first dispersed in H₂O, lyophilized and then dissolved in CDCl₃, two large signals were also present in the ³¹P spectrum at 0.88 and -0.32 ppm. The latter may be due to a modification of the PO₂⁻ group environment of DOPE in the bilayer during lyophilization and indicated two different environments for DOPE phosphate groups in these samples, first dispersed in H₂O and then lyophilized.

Most cationic lipids do not form liposomes alone but need the presence of DOPE. The ability of this lipid to form bilayers in L_α state or to exist in inverted hexagonal phase was known [22,37,114]. It was suggested that DOPE helps cationic lipids to form bilayers and also once the liposome/DNA complex is internalized in cellular endosomes, it destabilizes the latter to release DNA in the cytosol [42,106]. This should be directly related to the transfection level. During the freezing phase of lyophilization, probably ice was locally formed but heterogeneously so that the environment of phosphate groups of DOPE was affected with different hydration states [123], which conferred to the liposomes a structure favouring a better transfection. After lyophilization, the rehydration may be incomplete for a fraction of PO₂⁻ sites, favouring the existence of DOPE in the hexagonal inverted phase. This should be favourable for the destabilization of endosomal membrane and the release of DNA in cytosol, which in turn enhance the transfection level.

5.4. Effect of serum on transfection level

As a complementary information about the behaviour of lipoplexes in physiological environment, the level of transfection was measured in the presence of serum [85]. At the optimal charge ratio used *in vivo* ($X = 0.5$), TMAEC-Chol, TMAPC-Chol and TEAPC-Chol were used to vectorize pUT650 plasmid DNA in B16-F10 cells, in the presence of 0, 10 and 25% of serum (Fig. 9). Regardless of the chemical structure of the cationic lipids, transfection levels were higher with 10 and 25% serum than that obtained without serum. The increase was maximal at 10%. This stimulant effect on *in vitro* transfection could be explained by the proliferative effect of the serum during the period of transfection. Other possible mechanisms, such as endocytosis stimulation or endosomal destabilization, could contribute to the enhancement of the transfection level [124].

It is to be noted that *in vitro* transfection results in the presence of 10 or 25% of serum showed that the chemical nature of the polar domain strongly modulates the ability of reagents to deliver DNA inside cells. Indeed, *in vitro* results showed that the lipids with longer spacers presented an advantage for transfection. With the same spacer length, the more hydrophilic head group favours the DNA transfer. This is also true for *in vivo* transfection. Thus, the interactions with serum play a major role on the ability of these lipids to transfect tumour cells *in vivo*. In the presence of serum, TMAPC-Chol with a spacer 3C appeared as the most efficient lipid in the series studied.

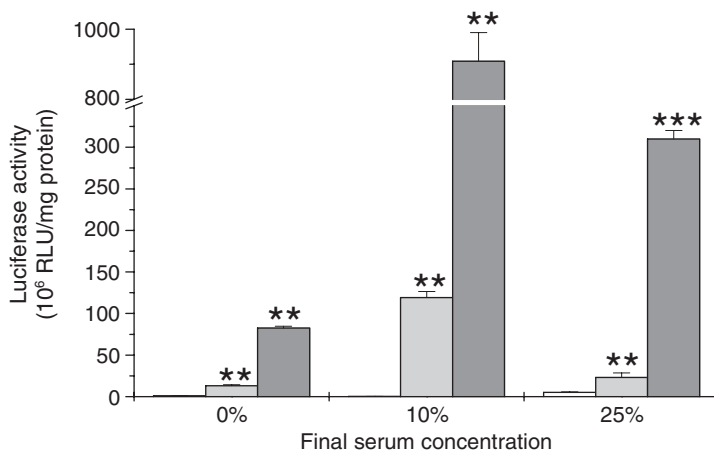


Fig. 9. Effect of variable amounts of serum on transfection level in cultured B16-F10 cells. One microgram of pUT650 plasmid DNA containing the luciferase gene was complexed with different cationic lipids/DOPE (1:1) formulations with the charge ratio $X = 0.5$ used *in vivo*. TMAEC-Chol (white), TEAPC-Chol (light grey) and TMAPC-Chol (dark grey). Each result represents the mean \pm SD of triplicate determinations. Statistic analysis: (**) $p < 0.01$; (***) $p < 0.001$. (Reproduced with permission from Reynier *et al.* [85].)

5.5. Role of proteoglycans

PG are molecules consisting of a protein covalently associated with negatively charged glycosaminoglycans (GAG) chains, including heparan, dermatan and chondroitin sulfates; PG exist as linked membrane proteins at the cell surface and also as major components of extracellular matrix of many tissues [125].

The roles for PG as cell receptors in liposomal gene delivery have been suggested from studies about effect on transfection of cell surface alterations by inhibition of GAG sulfation with chlorate, by their enzymatic removal or by mutations in their biosynthetic pathways [126,127]. However, the presence of free PG and GAG in the extracellular medium of cell culture is known to limit the transfection efficiency of cationic polymers and liposomes [128,129]. In some cases, the competition effects of GAG cannot be explained only by the decreased cellular uptake of complexes but also by an alteration of their intracellular behaviour, especially in endosomes [128,130]. Moreover, these works showed that delivery systems with endosomal buffering capacities (PEI, DOGS) were more affected by the inhibitory effects of GAG on gene transfer than fusogenic liposomes with DOPE as colipid, which were the most resistant carriers. In the same way, the types and the amounts of the cell surface GAG can affect not only the uptake of DNA complexed with cationic polymers or liposomes but also its pathway influencing the transgene expression as shown recently [131].

6. TARGETING

6.1. Targeting to receptors on cell surface

The main goal of the delivery is to selectively target the cell of interest, while sparing the normal tissues. For cancer cells, the targeting seems to be favoured by the expression of specific membrane proteins. It should be possible to use these unique molecular cell surface markers as targets.

From this idea, several methods can be conceived. For a chosen cell type, the first method was the use of Fab corresponding to the target surface protein. The second method was to use small peptides. Comparing these possibilities, there were arguments to favour the use of peptides as ligands. Despite target specificity, the high molecular weight of Fab is a major drawback. Moreover, peptides are nearly invisible to the immune system and are expected to cause minimal side effect [132,133].

6.2. Intracellular targeting

Besides the natural mechanism discussed above (Section 3.3) which depends upon the cell, DNA has been associated with appropriate peptides to be delivered in nuclei [134] or in mitochondria [69]. In the frame of this chapter, we describe an example of mitochondrial transfection.

6.2.1. *Transfection of mitochondria*

The mitochondrial respiratory chain catalyses oxidative phosphorylation, i.e., the oxidation of fuel molecules by oxygen and the concomitant energy transduction into adenosine triphosphate (ATP) [69]. Most of the proteins involved in this process are encoded by nuclear genes; however, 13 of them are encoded by mitochondrial DNA (mtDNA). Point mutations and large rearrangements of mtDNA have been reported in patients with various clinical presentations [135]. In most cases, both normal and mutant mtDNA molecules coexist – a phenomenon called heteroplasmy – the phenotypic expression requiring a minimum threshold number of re-arranged molecules.

To date, there were few studies to investigate mitochondrial transfection [136–140]. A strategy for a therapy of mitochondrial genomes requires a specific orientation of oligonucleotides or plasmids towards the anomalous mitochondria. A cationic lipid was used to deliver an oligonucleotide targeting the mitochondria into the cell.

For this purpose, a 5' fluorescein-labelled oligonucleotide (5'-CTC-CCT-CAC-CAT-TGG-CAG-CCT-A-3') was synthesized and then coupled to the C-terminal of ornithine transcarbamylase mitochondrial targeting sequence (H₂N-MLFNLRILLNNAAFRNGHNFMRNFRCGQPLQN-COOH, Eurogentec). The peptide-oligonucleotide conjugate, assigned thereof by PONC, was conditioned

in PBS. Complexes of PONC and TMAEC-Chol/DOPE liposomes are prepared following the above standard protocol. Measurements showed that at the molar charge ratio cationic lipid/PONC equal to 2, there is no unbound peptide oligonucleotide conjugate.

6.2.2. Delivery and persistence of vectorized PONC in cultured cells

Cultured skin fibroblasts transfected with the PONC–liposome complex were observed by confocal microscopy. It was observed that the rhodamine lissamine-labelled liposome (red fluorescence) and the fluorescein-labelled PONC (green fluorescence) were restricted to the cytoplasm of the cells, demonstrating efficient transfection in these cells [69]. The diffuse and homogenous aspect of rhodamine lissamine-labelled liposome suggests a large diffusion of the liposome throughout the cytoplasm, probably in the intracellular compartments. Conversely, the fluorescein-labelled PONC showed a punctate fluorescence. Moreover, liposome and PONC are differently distributed in the cell, indicating dissociation of PONC from liposome and delivery of PONC in the cytoplasm. No fluorescence can be detected in the nucleus. To facilitate the observation of the PONC, non-labelled liposomes were used. The fluorescein-labelled PONC showed a reticulated aspect (Fig. 10) resembling that obtained with rhodamine 123, a vital dye currently used to selectively stain and visualize mitochondria (not shown). The pattern observed with FITC-oligonucleotides strongly suggests a mitochondrial localization of the PONC. Non-transfected skin fibroblasts as well as fibroblasts incubated with PONC unvectorized by cationic liposome did not

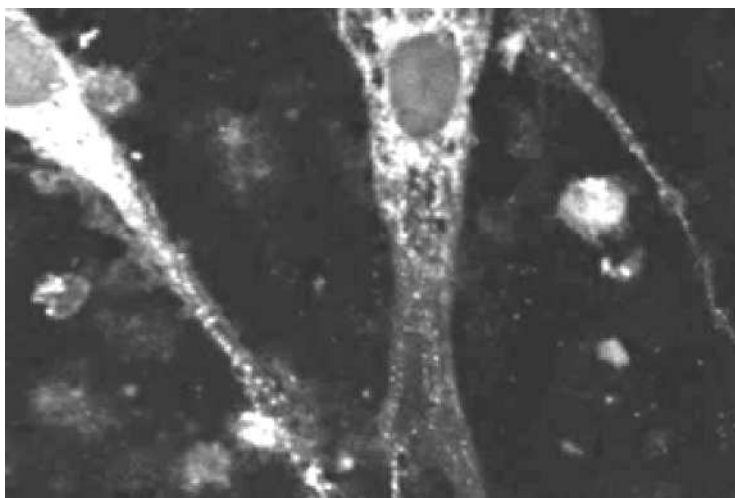


Fig. 10. Mitochondria transfection in fibroblast cell. Peptide oligonucleotide PONC was labelled with fluorescein and complexed to unlabelled TMAEC-Chol/DOPE liposome. The transfection conditions are described in the text. Bar represents 25 μm . (Reproduced with permission from Geromel *et al.* [69].)

show any fluorescence, indicating that only PONC complexed to the liposome can enter the cell.

It is important to note that the oligonucleotides were dissociated from the vectors after entry into the cells but they penetrated into cell mitochondria. This is due to the ornithine transcarbamylase signal peptide, recognized by the mitochondrial protein import machinery. The import of such an oligonucleotide in human cultured skin fibroblasts is the result of the combination of cationic liposomes, which allowed the oligonucleotide to cross the cell membrane and the signal peptide, which targeted it to the mitochondrial matrix.

7. LIPOFECTION *IN VIVO*

In vivo assays are a necessary step for the selection of a carrier. Such assays for analysis of bio-distribution or biological effect can be investigated by intravenous injection. In some particular cases, local inhalation or direct injection in the tumour was usually undertaken.

7.1. Intratumoural injection of B16-F10 tumours in nude mice [31]

Tumours were inoculated into immunodeficient nude mice. When convenient tumour volume was obtained, tumours were injected with lipoplexes (15 µg of plasmid pUT650) prepared at various cationic lipid/DNA ratios X [31]. The lipoplexes were administered by central bolus and the same amount of naked DNA was diluted in sterile water and injected as control. After 24 h post-injection, mice were sacrificed and tumours were removed for analysis. They were crushed and centrifuged. Then supernatants were collected for luciferase activity measurements. As seen in *in vitro* assays, results confirmed that the charge ratio was a critical parameter for transfection of solid tumours induced by B16-F10 melanoma cells in nude mice. Results on the efficiency of TEAPC-Chol/DOPE to carry DNA at different X molar charge ratios (0.5, 1, 2, 4 and 6) into tumours showed that noticeable transfection level was detected for naked plasmid DNA pUT650. The maximum level was obtained with $X = 0.5$ and there was reduction in transgene expression when the molar charge ratio was increased. Compared to non-vectorized plasmid, the transfection level observed with $X = 0.5$ was enhanced by a factor of five.

It is interesting to note that the best transfection level in tumours was obtained with a low charge ratio. In comparing this with gel retardation assay and *in vitro* transfection in the presence of serum (optimal transfection level obtained with $X = 6$, data not shown), this was an unexpected result. This abnormal behaviour may be due to multiple reasons. One of them is that assays *in vivo* were made with high cationic lipid concentration (for 45 nmol nucleotide in 100 µL), colloidal properties were modified with aggregation and precipitation of cationic Lip(+)

DNA complexes. The shift of the optimal charge ratio towards lower values seems not to depend on cationic lipids or solid tumour model but could be a general phenomenon, as observed by other authors as well [55,141,142]. Concerning environmental conditions, Schatzlein suggested that lower ratios of polymer to DNA with less excess positive charge are used with an advantage for targeting *in vivo* because positive charge in excess can form the basis for extensive non-specific interaction with cells, proteins, erythrocytes or other molecules *in vivo* [5,32,143].

Results in our laboratory showed (i) the superiority of the cationic lipids constituted by three carbons in the spacer, i.e., TEAPC-Chol and especially TMAPC-Chol and (ii) the probable influence of the hydration of the polar head. Transfection results with a hydroxyethylated lipid (DMHAPC-Chol) has shown transfection level comparable with that obtained with methylated TMAPC-Chol [86].

7.2. Effect of erythrocyte haemagglutination by cationic lipids/DNA complexes

To understand the *in vivo* compartment of cationic liposomes/DNA complexes presenting a differential sensibility to physiological environment and particularly to blood components, the interactions between cationic lipids/DNA complexes and erythrocytes were analysed [85].

For haemagglutination assay, erythrocytes were prepared as reported by Sakurai *et al.* [143]. Briefly, fresh blood from nude mice was collected with a heparinized syringe. Erythrocytes were washed three times with physiological buffer on ice by centrifugation (1000 *g* for 10 min) to remove mouse plasma and re-suspended in 150 mM NaCl, 10 mM Hepes buffer. One volume of lipoplexes, at variable charge ratios, was combined with 7.5 volumes of red blood cells and incubated for 10 min at 37 °C before fresh state observation using light microscopy.

The interactions of lipoplexes with erythrocytes were studied [85]. These are the main blood cells and so they could interact with lipoplexes. Interaction between erythrocytes and the TMAPC-Chol/DOPE (1:1) liposomes was explored as a function of the charge ratio. After 10 min of incubation, no haemagglutination and no significant change was observed when erythrocytes were incubated with the lipoplexes at the charge ratio of $X = 0.5$ and $X = 1$. When the charge of the lipoplexes was increased, haemagglutination was observed at $X = 2$ and leading to strong haemagglutination at $X = 4$.

In the same study, the effect of DOPE formulated with TEAPC-Chol on haemagglutination was highlighted. At two charge ratios ($X = 1$ and 2), the pictures depicted that haemagglutination increases with the amount of DOPE in the formulation. We can note that this effect was more pronounced with $X = 2$. Similar results were obtained with other lipids in the series for the effects of charge ratio

and DOPE. These results afford some insights into the transfection *in vivo*. Indeed, the major barriers to cationic lipid-mediated gene transfer *in vivo* are upstream of the interactions lipoplexes/cells, i.e., all the non-specific interactions with the tumour environment, such as anionic GAG of the extracellular matrix, endothelial cells of neovasculature, tumour-infiltrating lymphocytes and the whole blood. In solid tumours, cancer cells often occupy less than 50% of a tumour mass. One to 10% of the volume is made up by the vasculature [144] and the rest of the tumour volume consists predominantly of collagen-rich matrix. Although for *in vitro* transfection, the positive charge of lipoplexes is the main reason for the superiority of cationic liposomes in comparison with anionic or pH-sensitive liposomes [145], the best transfection levels *in vivo* have been obtained with negatively charged lipoplexes [12,31].

It was shown that no interaction was observed between negatively charged lipoplexes (low charge ratio, here $X = 0.5$) and the red blood cells known to expose sialic acid groups on the membrane surface. On the other hand, when the complex charge became positive, haemagglutination processes occurred, clearly due to the interaction between lipoplexes and negatively charged red blood cells. This contributes to underlining the major role of the lipoplex charge on intratumoural transfection. The haemagglutination decreases the number of lipoplexes available to the transfection that, in turn, diminishes the transfection level. It seems that in this process the chemical structure of cationic cholesterol derivatives is apparently not implied. Although the presence of DOPE favours interactions between lipoplexes and erythrocytes as indicated by the above results and as reported by Sakurai *et al.* [143], the use of a small charge ratio made it possible to avoid haemagglutination and to enhance the lipofection *in vivo*.

The non-specific interactions as mentioned above can be reduced using cationic lipids presenting a polar head with more hydrophilicity in the chemical structure. Both TMAPC-Chol and TEAPC-Chol lipids having the same spacer length but differing in nitrogen substituents exhibited different activity in transfection *in vivo*. The best cationic lipid-mediated gene transfer *in vivo* was obtained with TMAPC-Chol. The chemical structure of the hydrophilic part of TMAPC-Chol corresponds to the phosphatidylcholine (PC), a natural phospholipid of plasma membrane. In TEAPC-Chol, the methyl groups were substituted by bulky and more hydrophobic ethyl groups, which should be therefore less hydrated. So this may affect the opsonization, a phenomenon that can trap the lipoplexes or destabilize them and facilitate their elimination. Similar strategies have been investigated with the PEG used to make “stealth” liposomes in systemic administration and minimize opsonization [146]. Recent works have shown that cationic poly(ethylene glycol) lipids incorporated into pre-formed vesicles can enhance binding and uptake to cells [147]. However, the best level was obtained *in vitro* with the lipid having the less hydrophilic head, TEAPC-Chol. Castresana *et al.* [148] have proposed that the lamellar–hexagonal transition was accompanied by a weakening in the shell of hydrogen-bonded water, and thus hexagonal

phase formation requires partial dehydration of the phospholipid phosphate group. This should have a consequence on the destabilization of the endosomal membrane and the delivery of DNA in the cytosol.

It seems that the beneficial effect of the lipid head group with less hydrophilicity inside the cell is compensated *in vivo* by the non-specific interactions with extracellular compounds, which were reduced by a higher hydrophilicity. The apparent contradiction between *in vitro* and *in vivo* results can be explained in part in this way.

8. DELIVERY OF DNA OF INTEREST

With successful DNA transfer assays, a promising area of research is gene therapy [2–6,149]. In the scope of this chapter, we illustrate this by a transfer of a suppressor gene in a cell line of mesothelioma in which long exposition to asbestos is usually implied [150].

8.1. Transfer of suppressor gene p16 into mesothelioma cells

Actually, several studies on tumour suppressor gene (*p16*, *BRCA1* and *BRCA2*) replacement have been developed for the treatment of malignancies due to cells deficient of these genes. Among the expressed proteins, p16^{INK4a} is found to be mutated or deleted in many transformed cell lines and some primary tumours derived from multiple human tissues, including pancreas, skin, brain, bladder, lung and pleura [150]. p16^{INK4a} participates in controlling the G1–S cell cycle checkpoint through its indirect interaction with pRb protein [151–153]. So far, the suppressor gene p16^{INK4a} had been transferred using viral vectors [154,155]. Although limited [156], tumour suppressor gene p16 has been imported successfully in a human-cultured pleural mesothelioma cell line by using cationic liposomes. This delivery was demonstrated by tests of its functionality and its effect on the cell proliferation [70].

8.1.1. Delivery and persistence of gene p16 observed by immunofluorescence

Mesothelioma cells transfected with pCMV-p16 plasmids complexed with TMAEC-Chol/DOPE and TEAPC-Chol/DOPE liposomes are illustrated in micrographs of Fig. 11. Untransfected cells did not show any presence of p16, indicating that mesothelioma FR cells do not express p16 (Fig. 11A). Cells transfected with unvectorized pCMV-p16 showed only low level of p16 in the nucleus (Fig. 11C) whereas cells transfected with pCMV-p16 vectorized by TMAEC-Chol/DOPE and TEAPC-Chol/DOPE cationic liposomes showed higher labelling (Figs. 11E and 11G, respectively). Comparison with cells stained with

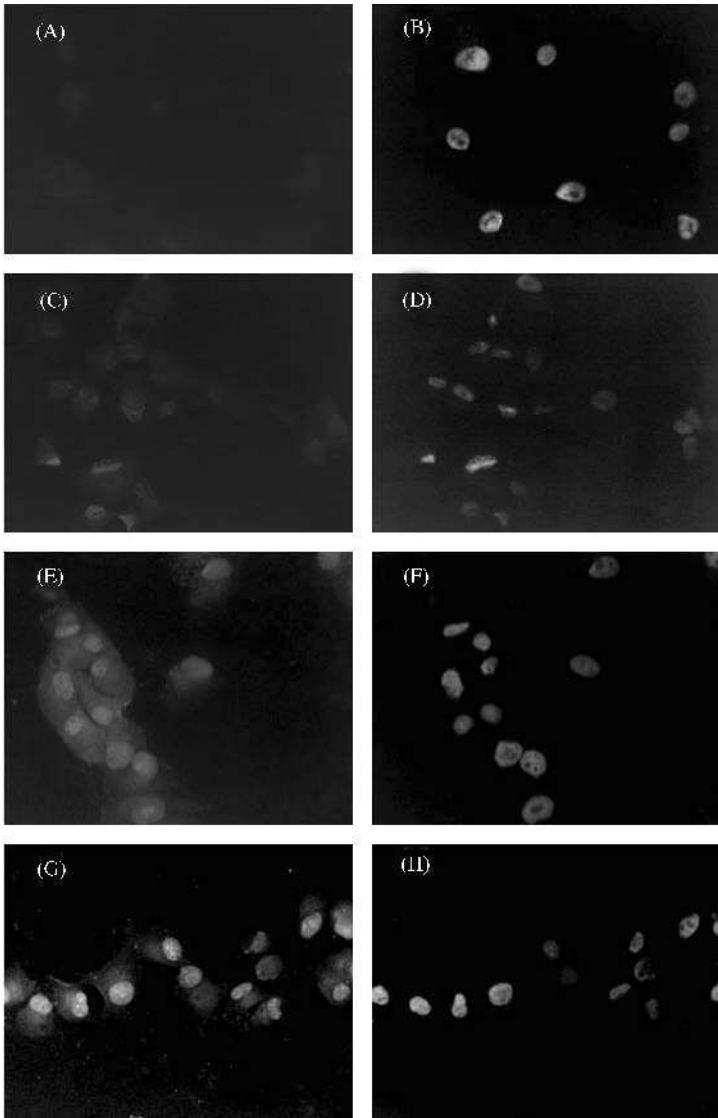


Fig. 11. Transfer of p16 into mesothelioma cells FR, observed by immunofluorescence using antibodies against anti-p16, labelled with fluorescein. Cells were transfected in OPTIMEM with pCMV-p16 complexed with cationic liposomes for 24 h. (A) Control untransfected cells FR. (C) Control FR cells transfected with pCMV-p16 unvectorized by liposomes. (E) FR cells transfected with pCMV-p16 complexed with TMAEC-Chol/DOPE liposomes. (G) FR cells transfected with pCMVp16 complexed with TEAPC-Chol/DOPE liposomes. Amount of plasmids: 3 μ g. Molar charge ratio cationic lipid/DNA: $X = 2$. (B, D, F, H): same fields observed with DAPI staining. (Reprinted from Piperno-Neumann *et al.* [70]. Copyright 2003, with permission from Elsevier.)

DAPI, a nuclear staining (Figs. 11B, D, F and H), shows that the expression was rather nuclear. The fluorescence is only slight, diffuse in the cytoplasm and much more intense in the nucleus as expected. It seems that there is slightly more expression of p16 with TEAPC-Chol/DOPE liposomes than with TMAEC-Chol/liposomes. These observations were confirmed by Western blotting analysis. Delivered by TMAEC-Chol/DOPE or TEAPC-Chol/DOPE liposomes, the transgene p16 strongly expressed in the nucleus and slightly in the cytoplasm, as attested by a pattern that was much more fluorescent inside than outside the nucleus. Moreover, the nuclear fluorescence was diffuse and not punctate, suggesting that the protein is not located in limited areas of the nucleus.

8.1.2. Dose and time effect on proliferation of transfected FR mesothelioma cells

The efficacy of the delivered gene was assessed by the effect on cell proliferation. Three days after transfection, a dose-dependence effect was already observed. An inhibition of about 30% was obtained in cells incubated with 8 μ g of pCMVp16. This inhibition was only transient because cell growth attained the level of the control after 6 days. However with repeated doses, the inhibition was maintained and reached about 50 and 63% after 6 and 9 days, respectively [70]. This inhibition effect agreed with the deficiency of p16 in the FR cells studied by which, the delivery of p16 prevented cell growth. This inhibition rate is in the same order as that observed by Frizelles on cells incubated with p16 gene delivered by the viral route [155].

8.2. Inhibition of Her2/neu

The efficacy of TMAEC-Chol to carry short DNA has been studied in using the oligodeoxynucleotide 28C designed against the gene Her2/neu overexpressed in tumoural cells MCF7. For this purpose, a kit neu/c-erb-2 ELISA of Oncogene Research was used. Details of the protocol were described in Porumb *et al.* [157]. Results indicate that the maximum inhibition of Her2/neu in MCF7 cells was observed after an incubation time 6 h as reported in the previous paper, and the inhibition obtained with oligonucleotides transported by TMAEC-Chol/DOPE liposomes is 15% more efficient than with oligodeoxynucleotides transported by lipofectin [52].

ACKNOWLEDGEMENTS

We thank F. Maille for reading the paper and N. Bouchemal, G. Fadda, D. Lesage, N.Lièvre, R. Naejus, E. Olsman, A. Percot, S. Piperno-Neumann, P. Reynier and J. Vassy for the data used in this chapter.

REFERENCES

- [1] P.L. Felgner, Th.R. Gadek, M. Holm, R. Roman, H.W. Chan, M. Wenz, J.P. Northrop, G.M. Ringold, M. Danielson, Lipofection: a highly efficient, lipid-mediated DNA-transfection procedure, *Proc. Natl. Acad. Sci. USA* 84 (1987) 7413–7417.
- [2] X. Gao, L. Huang, Cationic liposome-mediated gene transfer, *Gene Ther.* 2 (1995) 710–722.
- [3] J. Zabner, Cationic lipids used in gene transfer, *Adv. Drug Deliv. Rev.* 27 (1997) 17–28.
- [4] A.P. Rolland, From genes to gene medicines: recent advances in nonviral gene delivery, *Crit. Rev. Ther. Drug* 15 (1998) 143–198.
- [5] A.G. Schatzlein, Non-viral vectors in cancer gene therapy: principles and progress, *Anticancer Drug* 12 (2001) 275–304.
- [6] R.J. Lee, L. Huang, Lipid vector systems for gene transfer, *Crit. Rev. Ther. Drug* 14 (1997) 173–206.
- [7] G.J. Nabel, A.E. Chang, E.G. Nabel, G.E. Plautz, W. Ensminger, B. Fox, P. Felgner, S. Shu, K. Cho, Immunotherapy for cancer by direct gene transfer into tumors, *Hum. Gene Ther.* 5 (1994) 57–77.
- [8] G. Gregoriadis, R. Saffie, J.B. de Souza, Liposome-mediated DNA vaccination, *FEBS Lett.* 402 (1997) 107–110.
- [9] F. Liu, H. Qi, L. Huang, D. Liu, Factors controlling the efficiency of cationic lipid-mediated transfection *in vivo* via intravenous administration, *Gene Ther.* 4 (1997) 517–523.
- [10] R. Stribling, E. Brunette, D. Liggitt, K. Gaesler, R. Debs, Aerosol gene delivery *in vivo*, *Proc. Natl. Acad. Sci. USA* 89 (1992) 11277–11281.
- [11] J.P. Behr, B. Demeneix, J.P. Loeffler, J. Perez-Mutul, Efficient gene transfer into mammalian primary endocrine cells with lipopolyamine-coated DNA, *Proc. Natl. Acad. Sci. USA* 86 (1989) 6982–6986.
- [12] B. Schwartz, C. Benoist, B. Abdallah, D. Scherman, J.P. Behr, B.A. Demeneix, Lipospermine-based gene transfer into the newborn mouse brain is optimized by a low lipospermine/DNA charge ratio, *Hum. Gene Ther.* 6 (1995) 1515–1524.
- [13] J.S. Remy, C. Sirlin, P. Vierling, J.P. Behr, Gene transfer with a series of lipophilic DNA-binding molecules, *Bioconjugate Chem.* 5 (1994) 647–654.
- [14] J.H. Felgner, R. Kumar, C.N. Sridhar, C.J. Wheeler, Y.J. Tsai, R. Border, P. Ramsey, M. Martin, P.L. Felgner, Enhanced gene delivery and mechanism studies with a novel series of cationic lipid formulations, *J. Biol. Chem.* 269 (1994) 2550–2561.
- [15] G. McLachlan, D.J. Davidson, B.J. Stevenson, P. Dickinson, H. Davidson-Smith, J.R. Dorin, D.J. Porteous, DOTAP as a vehicle for efficient gene delivery *in vitro* and *in vivo*, *Biochemica* 11 (1994) 19–21.
- [16] M.J. Bennett, R.P. Aberle, J.G. Balasubramaniam, R.W. Malone, M.H. Nantz, Cationic lipid-mediated gene delivery to murine lung: correlation of lipid hydration with *in vivo* transfection activity, *J. Med. Chem.* 40 (1997) 4069–4078.
- [17] A.V. Kabanov, V.A. Kabanov, DNA complexes with polycations for the delivery of genetic material into cells, *Bioconjugate Chem.* 6 (1995) 7–20.
- [18] R. Leventis, J.R. Silvius, Interactions of mammalian cells with lipid dispersions containing novel metabolizable cationic amphiphiles, *Biochim. Biophys. Acta* 1023 (1990) 124–132.
- [19] J.K. Rose, L. Buonocore, M.A. Whitt, A new cationic liposome reagent mediating nearly quantitative transfection of animal cells, *Biotechniques* 10 (1991) 520–525.
- [20] J.M. Ruyschaert, A. Ouahabi, V. Villeaume, G. Huez, R. Fuks, M. Vandenbranden, P. Di Stefano, A novel cationic amphiphile for transfection of mammalian cells, *Biochem. Biophys. Res. Commun.* 203 (1994) 1622–1628.
- [21] X. Gao, L. Huang, A novel cationic liposome reagent for efficient transfection of mammalian cells, *Biochem. Biophys. Res. Commun.* 179 (1991) 280–285.

- [22] H. Farhood, R. Bottega, R.M. Epand, L. Huang, Effect of cationic cholesterol derivatives on gene transfer and protein kinase C activity, *Biochim. Biophys. Acta* 1111 (1992) 239–246.
- [23] E.G. Nabel, D. Gordon, Z.Y. Yang, L. Xu, H. San, G.E. Plautz, B.Y. Wu, X. Gao, L. Huang, G.J. Nabel, Gene transfer *in vivo* with DNA–liposome complexes: lack of autoimmunity and gonadal localization, *Hum. Gene Ther.* 3 (1992) 649–656.
- [24] M.J. Stewart, G.E. Plautz, L. Del Buono, Z.Y. Yang, L. Xu, X. Gao, L. Huang, E.G. Nabel, G.J. Nabel, Gene transfer *in vivo* with DNA–liposome complexes: safety and acute toxicity in mice, *Hum. Gene Ther.* 3 (1992) 267–275.
- [25] E.R. Lee, J. Marshall, C.S. Siegel, C. Jiang, N.S. Yew, M.R. Nichols, J.B. Nietupski, R.J. Ziegler, M.B. Lane, K.X. Wang, N.C. Wan, R.K. Scheule, D.J. Harris, A.E. Smith, S.H. Cheng, Detailed analysis of structures and formulations of cationic lipids for efficient gene transfer to the lung, *Hum. Gene Ther.* 7 (1996) 1701–1717.
- [26] J.P. Vigneron, N. Oudrhiri, M. Fauquet, L. Vergely, J.C. Bradley, M. Basseville, P. Lehn, J.M. Lehn, Guanidinium-cholesterol cationic lipids: efficient vectors for the transfection of eukaryotic cells, *Proc. Natl. Acad. Sci. USA* 93 (1996) 9682–9686.
- [27] R. Okayama, M. Noji, M. Nakanishi, Cationic cholesterol with a hydroxyethylamino head group promotes significantly liposome-mediated gene transfection, *FEBS Lett.* 408 (1997) 232–234.
- [28] K. Fife, M. Bower, R.G. Cooper, L. Stewart, C.J. Etherridge, R.C. Coombes, L. Buluwela, A.D. Miller, Endothelial cell transfection with cationic liposomes and herpes simplex-thymidine kinase mediated killing, *Gene Ther.* 5 (1998) 614–620.
- [29] A. Sochanik, I. Kaida, I. Mitrus, A. Rajca, S. Szala, A new cholesterol derivative suitable for transfecting certain type of cells in the presence of 10% serum, *Cancer Gene Ther.* 7 (2000) 513–520.
- [30] S. Hasegawa, N. Hirashima, M. Nakanishi, Comparative study of transfection efficiency of cationic cholesterol mediated by liposomes-based gene delivery, *Bioorg. Med. Chem. Lett.* 12 (2002) 1299–1302.
- [31] P. Reynier, D. Briane, A. Cao, R. Naejus, P. Bissieres, J.L. Salzmman, E. Taillandier, *In vitro* and *in vivo* transfection of melanoma cells B16–F10 mediated by cholesterol-based cationic liposomes, *J. Drug Target.* 10 (2002) 557–566.
- [32] J.P. Yang, L. Huang, Overcoming the inhibitory effect of serum on lipofection by increasing the charge ratio of cationic liposome to DNA, *Gene Ther.* 4 (1997) 950–960.
- [33] T.J. Anchordoquy, J.F. Carpenter, D.J. Kroll, Maintenance of transfection rates and physical characterization of lipid/DNA complexes after freeze-drying and rehydration, *Arch. Biochem. Biophys.* 348 (1997) 199–206.
- [34] B. Sternberg, K. Hong, W. Zheng, D. Papahadjopoulos, Ultrastructural characterization of cationic liposome–DNA complexes showing enhanced stability in serum and high transfection activity *in vivo*, *Biochim. Biophys. Acta* 1375 (1–2) (1998) 23–35.
- [35] B.A. Lobo, S. Rogers, C.M. Wiethof, S. Choosakoonkriang, S. Bogdanovich-Knip, C.R. Middaugh, Calorimetric analysis of the interaction between cationic lipids and plasmid DNA using isothermal titration calorimetry, *Arch. Biochem. Biophys.* 386 (2001) 95–105.
- [36] Y.S. Tarahovski, V.A. Rakhmanova, R.M. Epand, R.C. MacDonald, High temperature stabilization of DNA in complexes with cationic lipids, *Biophys. J.* 82 (1 Pt 1) (2002) 264–273.
- [37] J. Zabner, A.J. Fasbender, T. Moninger, K.A. Poellinger, M.J. Welsh, Cellular and molecular barriers to gene transfer by a cationic lipid, *J. Biol. Chem.* 270 (1995) 18997–19007.
- [38] N.J. Zuidam, Y. Barenholz, Electrostatic and structural properties of complexes involving plasmid DNA and cationic lipids commonly used for gene delivery, *Biochim. Biophys. Acta* 1368 (1998) 115–128.
- [39] S. Huebner, B.J. Battersby, R. Grimm, G. Cevc, Lipid–DNA complex formation: reorganization and rupture of lipid vesicles in the presence of DNA as observed by cryoelectron microscopy, *Biophys. J.* 76 (1999) 3158–3166.

- [40] C.R. Safinya, Structures of lipid–DNA complexes: supramolecular assembly and gene delivery, *Curr. Opin. Struct. Biol.* 11 (2001) 440–448.
- [41] S. Choosakoonkriang, C.M. Wiethoff, T.J. Anchordoquy, S. Koe, J.G. Smith, C.R. Middaugh, Infrared spectroscopic characterization of the interaction of cationic lipids with plasmid DNA, *J. Biol. Chem.* 276 (2001) 8037–8043.
- [42] I.M. Hafez, N. Maurer, P.R. Cullis, On the mechanism whereby cationic lipids promote intracellular delivery of polynucleic acids, *Gene Ther.* 8 (2001) 1188–1196.
- [43] I.V. Zhigaltsev, N. Maurer, K.F. Wong, P.R. Cullis, Triggered release of doxorubicin following mixing of cationic and anionic liposomes, *Biochim. Biophys. Acta* 1565 (2002) 129–135.
- [44] M.R. Almofti, H. Harashima, Y. Shinohara, A. Almofti, Y. Baba, H. Kiwada, Cationic liposome-mediated gene delivery: biophysical study and mechanism of internalization, *Arch. Biochem. Biophys.* 410 (2003) 246–253.
- [45] X. Zhou, L. Huang, DNA transfection mediated by cationic liposomes containing lipopolylysine: characterization and mechanism of action, *Biochim. Biophys. Acta* 1189 (1994) 195–203.
- [46] I. Wrobel, D. Collins, Fusion of cationic liposomes with mammalian cells occurs after endocytosis, *Biochim. Biophys. Acta* 1235 (1995) 296–304.
- [47] D.S. Friend, D. Papahadjopoulos, R.J. Debs, Endocytosis and intracellular processing accompanying transfection mediated by cationic liposomes, *Biochim. Biophys. Acta* 1278 (1996) 41–50.
- [48] K. Lappalainen, R. Miettinen, J. Kellokoski, I. Jaaskelainen, S. Syrjanen, Intracellular distribution of oligonucleotides delivered by cationic liposomes: light and electron microscopic study, *J. Histochem. Cytochem.* 45 (1997) 265–274.
- [49] J.W. McLean, E.A. Fox, P. Baluk, P.B. Bolton, A. Haskell, R. Pearlman, G. Thurston, E.Y. Umemoto, D.M. McDonald, Organ-specific endothelial cell uptake of cationic liposome–DNA complexes in mice, *Am. J. Physiol.* 27 (1997) H387–H404.
- [50] V. Escriou, C. Ciolina, F. Lacroix, G. Byk, D. Scherman, P. Wils, Cationic lipid-mediated gene transfer: effect of serum on cellular uptake and intracellular fate of lipopolyamine/DNA complexes, *Biochim. Biophys. Acta* 1368 (1998) 276–288.
- [51] A. El Ouahabi, M. Thiry, S. Schiffmann, R. Fuks, H. Nguyen-Tran, J.M. Ruyschaert, M. Vandenbranden, Intracellular visualization of BrdU-labeled plasmid DNA/cationic liposome complexes, *J. Histochem. Cytochem.* 47 (1999) 1159–1166.
- [52] A. Cao, D. Briane, R. Coudert, J. Vassy, N. Lievre, E. Olsman, E. Tamboise, J.L. Salzmman, J.P. Rigaut, E. Taillandier, Delivery and pathway in MCF7 cells of DNA vectorized by cationic liposomes derived from cholesterol, *Antisense Nucl. Acid Drug Dev.* 10 (2000) 369–380.
- [53] G. Tarrason, D. Bellido, R. Eritja, S. Vilaro, J. Piulats, Digoxigenin-labeled phosphorothioate oligonucleotides: a new tool for the study of cellular uptake, *Antisense Res. Dev.* 5 (1995) 193–201.
- [54] D. Briane, D. Lesage, A. Cao, R. Coudert, N. Lievre, J.-L. Salzmman, E. Taillandier, Cellular Pathway of plasmids vectorized by cholesterol-based cationic liposomes, *J. Histochem. Cytochem.* 50 (2002) 983–991.
- [55] N.K. Egilmez, Y. Iwanuma, R.B. Bankert, Evaluation and optimization of different cationic liposome formulations for *in vivo* gene transfer, *Biochem. Biophys. Res. Commun.* 221 (1996) 169–173.
- [56] P.R. Clark, A.T. Stopeck, M. Ferrari, S.E. Parker, E.M. Hersh, Studies of direct intratumoral gene transfer using cationic lipid-complexed plasmid DNA, *Cancer Gene Ther.* 7 (2000) 853–860.
- [57] S.J. Eastman, C. Siegel, J. Tousignant, A.E. Smith, S.H. Cheng, R.K. Scheule, Biophysical characterization of cationic lipid: DNA complexes, *Biochim. Biophys. Acta* 1325 (1997) 41–62.
- [58] A.J. Lin, N.L. Slack, A. Ahmad, I. Koltover, C.X. George, C.E. Samuel, C.R. Safinya, Structure and structure-function studies of lipid/plasmid DNA complexes, *J. Drug Target.* 8 (2000) 13–27.

- [59] Y.K. Song, F. Liu, S. Chu, D. Liu, Characterization of cationic liposome-mediated gene transfer *in vivo* by intravenous administration, *Hum. Gene Ther.* 8 (1997) 1585–1594.
- [60] C.R. Dass, Biochemical and biophysical characteristics of lipoplexes pertinent to solid tumour gene therapy, *Int. J. Pharm.* 241 (2002) 1–25.
- [61] S.C. Semple, A. Chonn, P.R. Cullis, Influence of cholesterol on the association of plasma proteins with liposomes, *Biochemistry* 35 (1996) 2521–2525.
- [62] N.S. Templeton, D.D. Lasic, P.M. Frederik, H.H. Strey, D.D. Roberts, G.N. Pavlakis, Improved DNA: liposome complexes for increased systemic delivery and gene expression, *Nat. Biotechnol.* 15 (1997) 647–652.
- [63] O. Zelphati, L.S. Uyechi, L.G. Barron, F.C. Szoka Jr., Effect of serum components on the physico-chemical properties of cationic lipid/oligonucleotide complexes and on their interactions with cells, *Biochim. Biophys. Acta* 1390 (1998) 119–133.
- [64] S. Li, W.C. Tseng, D.B. Stolz, S.P. Wu, S.C. Watkins, L. Huang, Dynamic changes in the characteristics of cationic lipidic vectors after exposure to mouse serum: implications for intravenous lipofection, *Gene Ther.* 6 (1999) 585–594.
- [65] J.Y. Chern, P.V.D. Wetering, H. Talsma, D.J.A. Crommelin, W.E. Hennink, Stabilization of polymer-based gene delivery systems, *Int. J. Pharm.* 183 (1999) 25–28.
- [66] S. Allison, M.dC. Molina, T.J. Anchordoquy, Stabilizing of lipid/DNA complexes during the freezing step of the lyophilization process: the particle isolation hypothesis, *Biochim. Biophys. Acta* 1468 (2000) 127–138.
- [67] E.C.A. Van Winden, W. Zhang, D.J.A. Crommelin, Effect of freezing rate on the stability of liposomes during freeze-drying and rehydration, *Pharm. Res.* 14 (1997) 1151–1160.
- [68] M.dC. Molina, S. Allison, T.J. Anchordoquy, Maintenance of nonviral vector particle size during the freezing step of the lyophilization process is insufficient for preservation of activity: insight from other structural indicators, *J. Pharm. Sci.* 90 (2001) 1445–1455.
- [69] V. Geromel, A. Cao, D. Briane, J. Vassy, A. Rotig, P. Rustin, R. Coudert, J.P. Rigaut, A. Munnich, E. Taillandier, Mitochondria transfection by oligonucleotides containing a signal peptide and vectorized by cationic liposomes, *Antisense Nucl. Acid Drug Dev.* 11 (2001) 175–180.
- [70] S. Piperno-Neumann, O. Oudar, P. Reynier, D. Briane, A. Cao, M.C. Jaurand, R. Naejus, M. Kraemer, J.L. Breau, E. Taillandier, Transfer into mesothelioma cells of plasmid encoding tumor suppressor gene p16 by cationic lipids, *Biochim. Biophys. Acta* 1611 (2003) 131–139.
- [71] M.J. Lee, S.S. Cho, J.R. You, Y. Lee, B.D. Kang, J.S. Choi, J.W. Park, Y.L. Suh, J.A. Kim, D.K. Kim, J.S. Park, Intraperitoneal gene delivery mediated by a novel cationic liposome in a peritoneal disseminated ovarian cancer model, *Gene Ther.* 9 (2002) 859–866.
- [72] Z. Hyvönen, A. Plotniece, I. Reine, B. Chekavichus, G. Duburs, A. Urtti, Novel cationic amphiphilic 1,4-dihydropyridine derivatives for DANN delivery, *Biochim. Biophys. Acta* 1509 (2000) 451–466.
- [73] J.G. Lewis, K.Y. Lin, A. Kothavale, W.M. Flanagan, M.D. Matteucci, R.B. DePrince, R.A. Mook Jr., R.W. Hendren, R.W. Wagner, A serum resistant cytofectin for cellular delivery of antisense oligodeoxynucleotides and plasmid DNA, *Proc. Natl. Acad. Sci. USA* 93 (1996) 3176–3181.
- [74] J. Heynes, D. Niculesu-Duvaz, R. Cooper, C. Springer, Synthesis of novel cationic lipids: effect of structural modification on the efficiency of gene transfer, *J. Med. Chem.* 45 (2002) 99–114.
- [75] V. Floch, S. Loisel, E. Guenin, A.C. Hervé, J.C. Clément, J.J. Yaouanc, H. des Abbyes, C. Férec, Cation substitution in cationic phosphonolipids: a new concept to improve transfection activity and decrease cellular toxicity, *J. Med. Chem.* 43 (2000) 4617–4628.
- [76] M.J. Bennett, A.M. Aberle, R.P. Balasubramaniam, J.G. Malone, M.H. Nantz, R. Malone, Considerations for the design of improved cationic amphiphile-based transfection reagents, *J. Liposome Res.* 6 (1996) 545–565.

- [77] F.H. Cameron, M.J. Moghaddam, V.J. Bender, R.G. Whittaker, M. Mott, T.J. Lockett, A transfection compound series based on a versatile Tris linkage, *Biochim. Biophys. Acta* 11417 (1999) 37–50.
- [78] L.A.M. Ruppert, D. Hoekstra, J.B.F.N. Engberts, Fusogenic behavior of didodecyltrimethylammonium bromide bilayer vesicles, *J. Am. Chem. Soc.* 107 (1985) 2628–2631. L.A.M. Ruppert, J.B.F.N. Engberts, D. Hoekstra, *J. Am. Chem. Soc.* 108 (1986) 3920–3925.
- [79] T. Serikawa, N. Suzuki, H. Kikuchi, K. Tanaka, T. Kitagawa, A new cationic liposome for efficient gene delivery with serum into cultured human cells: a quantitative analysis using two independent fluorescent probes, *Biochim. Biophys. Acta* 1467 (2000) 419–430.
- [80] Y.K. Ghosh, S.S. Visweswariah, S. Bhattacharya, Advantage of ether linkage between the positive charge and the cholesterol skeleton in cholesterol-based amphiphiles as vectors for gene delivery, *Bioconjugate Chem.* 13 (2002) 378–384.
- [81] N. Kiso, M. Ariatti, T. Moodley, A novel cationic cholesterol derivative, its formulation into liposomes, and the efficient transfection of the transformed human cell lines HepG2 and HeLa, *Drug Deliv.* 9 (3) (2002) 161–167.
- [82] S. Walker, M.J. Sofia, R. Kakarla, N.A. Kogan, L. Wierichs, C.B. Longley, K. Brucker, H.R. Axelrod, S. Midha, S. Babu, D. Kahne, Cationic facial amphiphiles: a promising class of transfection agents, *Proc. Natl. Acad. Sci. USA* 93 (1996) 1585–1590.
- [83] M.J. Bennett, A.M. Aberle, R.P. Balasubramaniam, J.G. Malone, M.H. Nantz, R.W. Malone, Considerations for the design of improved cationic amphiphile-based transfection reagents, *J. Liposome Res.* 6 (1996) 545–565.
- [84] D. Lesage, A. Cao, D. Briane, N. Lievre, R. Coudert, M. Raphael, J.-L. Salzmann, E. Taillandier, Evaluation of *in vitro* transfection of gliosarcoma 9L cells using cationic liposomes derived from cholesterol, *Biochim. Biophys. Acta* 1564 (2002) 393–402.
- [85] P. Reynier, D. Briane, R. Coudert, G. Fadda, N. Bouchemal, P. Bissieres, E. Taillandier, A. Cao, Modifications in the head group and in the spacer of cholesterol-based cationic lipids promote transfection in melanoma B16–F10 cells and tumours, *J. Drug Target.* 58 (2004) 25–38.
- [86] A. Percot, D. Briane, R. Coudert, P. Reynier, N. Bouchemal, N. Lièvre, E. Hantz, J.L. Salzmann, A. Cao, A hydroxyethylated cholesterol-based cationic lipid for DNA delivery: effect of conditioning, *Int. J. Pharma.* 278 (2004) 143–163.
- [87] G. Gregoriadis, B. McCormack, Y. Morrison, R. Saffie, B. Zadi, Liposomes in drug targeting (2nd edition), in: J.E. Celis, (Ed.), *Cell Biology: A Laboratory Handbook*, Vol. 4, Academic Press, New York, 1998, pp. 131–140.
- [88] J.C.M. Stewart, Colorimetric determination of phospholipids with ammonium ferrioxalate, *Analyt. Biochem.* 104 (1980) 10–14.
- [89] J.H. Felgner, Separation and quantitation of cationic liposome components by high performance liquid chromatography with evaporative light-scattering detection, *Pharm. Res.* 14 (1997) 1269–1271.
- [90] B. Sternberg, F.L. Sorgi, L. Huang, New structures in complex formation between DNA and cationic liposomes visualized by freeze-fracture electron microscopy, *FEBS Lett.* 356 (1994) 361–366.
- [91] J. Gustafsson, G. Arvidson, G. Karlsson, M. Almgren, Complexes between cationic liposomes and DNA visualized by cryo-TEM, *Biochim. Biophys. Acta* 1235 (1995) 305–312.
- [92] F.M.P. Wong, D. Rimer, M.B. Bally, Cationic lipid binding to DNA: characterization of complex formation, *Biochemistry* 35 (1996) 5756–5763.
- [93] Y. Yoshikawa, N. Emi, T. Kanbe, K. Yoshikawa, H. Saito, Folding and aggregation of DNA chains induced by complexation with lipospermine: formation of a nucleosome-like structure and network assembly, *FEBS Lett.* 396 (1996) 71–76.
- [94] P.L. Felgner, G.M. Ringold, Cationic liposome-mediated transfection, *Nature* 337 (1989) 387–388.

- [95] C. Tanford, *Physical Chemistry of Macromolecules*, Wiley, New York, 1961.
- [96] R. Kraayenhof, G.J. Sterk, H.W.W.F. Sang, K. Krab, R.M. Epand, Monovalent cations differentially affect membrane surface properties and membrane curvature, as revealed by fluorescent probes and dynamic light scattering, *Biochim. Biophys. Acta* 1282 (1996) 293–302.
- [97] Y. Xu, S.W. Hui, P. Frederick, F.C. Szoka Jr., Physicochemical characterization and purification of cationic lipoplexes, *Biophys. J.* 77 (1999) 341–353.
- [98] K.K. Son, D.H. Patel, D. Tkach, A. Park, Cationic liposome and plasmid DNA complexes formed in serum-free medium under optimum transfection condition are negatively charged, *Biochim. Biophys. Acta* 1466 (2000) 11–15.
- [99] K.I. Takeuchi, M. Ishihara, C. Kawaura, M. Noji, T. Furuno, M. Nakanishi, Effect of zeta potential of cationic liposomes containing cationic cholesterol derivatives on gene transfection, *FEBS Lett.* 397 (1996) 207–209.
- [100] D.C. Litzinger, L. Huang, Biodistribution and immunotargetability of ganglioside-stabilized dioleoylphosphatidylethanolamine liposomes, *Biochim. Biophys. Acta* 1104 (1992) 179–187.
- [101] C. Kawaura, A. Noguchi, T. Furuno, M. Nakanishi, Atomic microscopy for studying gene transfection mediated by cationic liposomes with a cationic cholesterol derivative, *FEBS Lett.* 421 (1998) 69–72.
- [102] R.N.A.H. Lewis, S. Tristram-Nagle, J.F. Nagle, R.N. McElhaney, The thermotropic phase behaviour of cationic lipids: calorimetric, infrared spectroscopic and X-ray diffraction studies of lipid bilayer membranes composed of 1,2-di-*O*-myristoyl-3-*N,N,N*-trimethylaminopropane, *Biochim. Biophys. Acta* 1510 (2001) 70–82.
- [103] M.C. Pedroso de Lima, S. Simoes, P. Pires, H. Faneca, N. Duzgunes, Cationic lipid–DNA complexes in gene delivery: from biophysics to biological applications, *Adv. Drug Deliv. Rev.* 47 (2001) 277–294.
- [104] Y. Perrie, G. Gregoriadis, Liposome-entrapped plasmid DNA: characterisation studies, *Biochim. Biophys. Acta* 1475 (2000) 125–132.
- [105] J. Smisterova, A. Wagenaar, M.C.A. Stuart, E. Polushkin, G. ten Brinke, R. Hulst, J.B.F.N. Engberts, D. Hoekstra, Molecular shape of the cationic lipid controls the structure of cationic lipid/DOPE–DNA complexes and the efficiencies of gene delivery, *J. Biol. Chem.* 276 (2001) 47615–47622.
- [106] O. Zelphati, F.C. Szoka Jr., Mechanism of oligonucleotide release from cationic liposomes, *Proc. Natl. Acad. Sci. USA* 93 (1996) 11493–11498.
- [107] Y. Xu, F.C. Szoka Jr., Mechanism of DNA release from cationic liposome/DNA complexes used in cell transfection, *Biochemistry* 35 (1996) 5616–5623.
- [108] M. Refregiers, B. Jolles, L. Chinski, A. Laigle, Intracellular fate of oligodeoxynucleotides: a microspectro FRET study, *Biol. Cell* 91 (1999) 227–280.
- [109] I. Bronstein, J. Fortin, P.E. Stanley, G.S.A.B. Stewart, L.J. Kricka, Chemiluminescent reporter gene assays, *Anal. Biochem.* 219 (1994) 169–181.
- [110] B.G. Reid, G.C. Flynn, Chromophore formation in green fluorescent protein, *Biochemistry* 36 (1997) 6786–6791.
- [111] M. Brisson, W.C. Tseng, C. Almonte, S. Watkins, L. Huang, Subcellular trafficking of the cytoplasmic expression system, *Hum. Gene Ther.* 10 (1999) 2601–2613.
- [112] L.V. Johnson, M.L. Walsh, B.J. Bockus, L.B. Chen, Localization of mitochondria in living cells with rhodamine 123, *Proc. Natl. Acad. Sci. USA* 77 (1980) 990–994.
- [113] V.A. Morozov, P. Noguez-Helin, S. Laune, E. Tamboise, J.L. Salzmann, D. Klatzmann, Plasmovirus: replication cycle of a novel nonviral/viral vector for gene transfer, *Cancer Gene Ther.* 4 (1997) 286–293.
- [114] M.J. Hope, B. Mui, S. Ansell, Q.F. Ahkong, Cationic lipids, phosphatidylethanolamine and the intracellular delivery of polymeric, nucleic acid-based drugs, *Mol. Membr. Biol.* 15 (1998) 1–14.
- [115] H. Farhood, N. Serbina, L. Huang, The role of dioleoyl phosphatidylethanolamine in cationic liposome mediated gene transfer, *Biochim. Biophys. Acta* 1235 (1995) 289–295.

- [116] A.J. Fasbender, J. Marshall, T.O. Moninger, T. Grunst, S. Cheng, M.J. Welsh, Effect of co-lipids in enhancing cationic lipid-mediated gene transfer *in vitro* and *in vivo*, *Gene Ther.* 4 (1997) 716–725.
- [117] M.E. Dowty, P. Williams, G. Zhang, J.E. Hagstrom, J.A. Wolff, Plasmid DNA entry into postmitotic nuclei of primary rat myotubes, *Proc. Natl. Acad. Sci. USA* 92 (1995) 4572–4576.
- [118] E.A. Nigg, Nucleocytoplasmic transport: signals, mechanisms and regulation, *Nature* 386 (1997) 779–787.
- [119] I. Mortimer, P. Tam, I. MacLachlan, R.W. Graham, E.G. Saravolac, P.B. Joshi, Cationic lipid-mediated transfection of cells in culture requires mitotic activity, *Gene Ther.* 6 (1999) 403–411.
- [120] W.C. Tseng, F.R. Haselton, T.D. Giorgio, Mitosis enhances transgene expression of plasmid delivered by cationic liposomes, *Biochim. Biophys. Acta* 1445 (1999) 53–64.
- [121] C.J. Wheeler, P.L. Felgner, Y.J. Tsai, J. Marshall, L. Sukhu, S.G. Doh, J. Hartikka, J. Nietupski, M. Manthorpe, M. Nichols, M. Plewe, X. Liang, J. Norman, A. Smith, S.H. Cheng, A novel cationic lipid greatly enhances plasmid DNA delivery and expression in mouse lung, *Proc. Natl. Acad. Sci. USA* 93 (1996) 11454–11459.
- [122] K. Hong, W. Zheng, A. Baker, D. Papahadjopoulos, Stabilization of cationic liposome–plasmid DNA complexes by polyamines and poly(ethylene glycol)-phospholipid conjugates for efficient *in vivo* gene delivery, *FEBS Lett.* 400 (1997) 233–237.
- [123] P.W. Sanderson, W.P. Williams, B.A. Cunningham, D.H. Wolfe, L.J. Lis, The effect of ice on membrane lipid phase behavior, *Biochim. Biophys. Acta* 1148 (1993) 278–284.
- [124] S. Simoes, V. Slepishkin, P. Pires, R. Gaspar, M.C. Pedroso de Lima, N. Duzgunes, Human serum albumin enhances DNA transfection by lipoplexes and confers resistance to inhibition by serum, *Biochim. Biophys. Acta* 1463 (2000) 459–469.
- [125] R.V. Iozzo, Matrix proteoglycans: from molecular design to cellular function, *Annu. Rev. Biochem.* 67 (1998) 609–652.
- [126] K.A. Mislick, D. Baldeschwieler, Evidence for the role of proteoglycans in cation-mediated gene transfer, *Proc. Natl. Acad. Sci. USA* 93 (1996) 12349–12354. C.M. Wiethoff, J.G. Smith, G.S. Koe, C.R. Middaugh, The potential role of proteoglycans in cationic lipid-mediated gene delivery, *J. Biol. Chem.* 276 (2001) 32806–32813.
- [127] L. Mounkes, W. Zhong, G. Cipres-Palacin, T.D. Heath, R. Debs, Proteoglycans mediate cationic liposome–DNA complex-based gene delivery *in vitro* and *in vivo*, *J. Biol. Chem.* 273 (1998) 26164–26170.
- [128] M. Ruponen, S. Yla-Herttuala, A. Urtti, Interactions of polymeric and liposomal gene delivery systems with extracellular glycosaminoglycans: physicochemical and transfection studies, *Biochim. Biophys. Acta* 1415 (1999) 331–341.
- [129] M. Belting, P. Petersson, Intracellular accumulation of secreted proteoglycans inhibits cationic lipid-mediated gene transfer, *J. Biol. Chem.* 274 (1999) 19375–19382.
- [130] M. Ruponen, S. Ronkko, P. Honkakoski, J. Pelkonen, M. Tammi, A. Urtti, Extracellular glycosaminoglycans modify cellular trafficking of lipoplexes and polyplexes, *J. Biol. Chem.* 276 (2001) 33875–33880.
- [131] M. Ruponen, P. Honkakoski, M. Tammi, A. Urtti, Cell-surface glycosaminoglycans inhibit cation-mediated gene transfer, *J. Gene Med.* 6 (2004) 405–414.
- [132] M. Shadidi, M. Sioud, Selective targeting of cancer cells using synthetic peptides, *Drug Resist. Update* 6 (2003) 363–371.
- [133] P. Harvie, B. Dutzar, T. Galbraith, S. Cudmore, D. O'Mahony, P. Anklesaria, R. Paul, Targeting of lipid–protamine–DNA (LPD) lipoplexes using RGD motifs, *J. Lipos. Res.* 13 (2003) 231–247.
- [134] M.A. Zanta, P. Belguise-Valladier, J.P. Behr, Gene delivery: a single nuclear localization signal peptide is sufficient to carry DNA to the nucleus, *Proc. Natl. Acad. Sci. USA* 96 (1999) 91–96.
- [135] MITOMAP, Human mitochondrial genom database, Center for Molecular Medicine, Emory University, Atlanta, GA USA (<http://www.gen.emory.edu/mitomap.html>).

- [136] M. Seibel, C. Bachmann, J. Schmiedel, N. Wilken, F. Wildeilde, H. Reichmann, G. Isaya, P. Seibel, Processing of artificial peptide–DNA-conjugates by the mitochondrial intermediate peptidase (MIP), *Biol. Chem.* 380 (1999) 961–967.
- [137] R. Taylor, P.F. Chinnery, D.M. Turnbull, R.N. Lightowers, Selective inhibition of mutant mitochondrial DNA replication *in vitro* by peptide nucleic acids, *Nat. Genet.* 15 (1997) 212–215.
- [138] P.F. Chinnery, R.W. Taylor, K. Diekert, R. Lill, D.M. Turnbull, R.N. Lightowers, Peptide nucleic acid delivery to human mitochondria, *Gene Ther.* 6 (1999) 1919–1928.
- [139] P. Seibel, J.S. Trappe, G. Villani, Th. Klopstock, S. Papappa, H. Reichmann, Transfection of mitochondria: strategy towards a gene therapy of mitochondrial DNA diseases, *Nucl. Acids. Res.* 23 (1995) 10–17.
- [140] G.G.M. D'Souza, R. Rammolan, S.M. Cheng, V.P. Torchilin, V. Weissig, DQAsome-mediated delivery of plasmid DNA toward mitochondria in living cells, *J. Control Release* 92 (2003) 189–197.
- [141] T. Nomura, K. Yasuda, T. Yamada, S. Okamoto, R.I. Mahato, Y. Watanabe, Y. Takakura, M. Hashida, Gene expression and antitumor effects following direct interferon (IFN)-gamma gene transfer with naked plasmid DNA and DC-chol liposome complexes in mice, *Gene Ther.* 6 (1999) 121–129.
- [142] K.K. Son, D. Tkach, K.J. Hall, Efficient *in vivo* gene delivery by the negatively charged complexes of cationic liposomes and plasmid DNA, *Biochim. Biophys. Acta* 1468 (2000) 6–10.
- [143] F. Sakurai, T. Nishioka, H. Saito, T. Baba, A. Okuda, O. Matsumoto, T. Taga, F. Yamashita, Y. Takakura, M. Hashida, Interaction between DNA–cationic liposome complexes and erythrocytes is an important factor in systemic gene transfer via the intravenous route in mice: the role of the neutral helper lipid, *Gene Ther.* 8 (2001) 677–686.
- [144] R.K. Jain, Delivery of molecular and cellular medicine to solid tumors, *Adv. Drug Deliv. Rev.* 46 (2001) 149–168.
- [145] J.Y. Legendre, F.C. Szoka Jr., Delivery of plasmid DNA into mammalian cell lines using pH-sensitive liposomes: comparison with cationic liposomes, *Pharm. Res.* 9 (1992) 1235–1242.
- [146] M.C. Woodle, D.D. Lasic, Sterically stabilized liposomes, *Biochim. Biophys. Acta* 1113 (1992) 171–199.
- [147] D.B. Fenske, L.R. Palmer, T. Chen, K.F. Wong, P.R. Cullis, Cationic poly(ethylene glycol) lipids incorporated into pre-formed vesicles enhance binding and uptake to BHK cells, *Biochim. Biophys. Acta* 1512 (2001) 259–272.
- [148] J. Castresana, J.L. Nieva, E. Rivas, A. Alonso, Partial dehydration of phosphatidylethanolamine phosphate groups during hexagonal phase formation, as seen by i.r. spectroscopy, *Biochem. J.* 282 (Pt 2) (1992) 467–470.
- [149] A.M. Boylan, Mesothelioma: new concepts in diagnosis and management, *Curr. Opin. Pulm. Med.* 6 (2000) 157–163.
- [150] M.C. Jaurand, L. Kheang, L. Magne, J. Bignon, Chromosomal changes induced by chrysotile fibres or benzo(3-4)pyrene in rat pleural mesothelial cells, *Mutat. Res.* 169 (1986) 141–148. L. Zeng, J. Fleury-Feith, I. Monnet, C. Boutinn, J. Bignon, M.C. Jaurand, Immunocytochemical characterization of cell lines from human malignant mesothelioma, *Hum. Pathol.* 25 (1994) 227–234.
- [151] W.H. Liggett Jr., D.J. Sidransky, Role of the p16 tumor suppressor gene in cancer, *J. Clin. Oncol.* 16 (1998) 1197–1206.
- [152] M. Ruas, The p16INK4a/CDKN2A tumor suppressor and its relatives, G. Peters, *Biochim. Biophys. Acta* 1378 (1998) F115–F177.
- [153] C.J. Sherr, Cancer cell cycles, *Science* 274 (1996) 1672–1677.
- [154] K. Sumitomo, E. Shimizu, A. Shinohara, J. Yokota, S. Sone, Activation of RB tumor suppressor protein and growth suppression of small cell lung carcinoma cells by reintroduction of p16INK4a gene, *Int. J. Oncol.* 14 (1999) 1075–1080.

- [155] S. Frizelle, J. Grim, J. Zhou, P. Gupta, D.t. Curiel, J. Geradts, R.a. Kratzke, Re-expression of p16INK4a in mesothelioma cells results in cell cycle arrest, cell death, tumor suppression and tumor regression, *Oncogene*. 16 (1998) 3087–3095.
- [156] C.D. Porter, K.V. Lukacs, G. Box, Y. Tadeuchi, M.K. Collins, Cationic liposomes enhance the rate of transduction by a recombinant retroviral vector *in vitro* and *in vivo*, *J. Virol.* 72 (1998) 4832–4840.
- [157] H. Porumb, H. Gousset, R. Letellier, V. Salle, D. Briane, J. Vassy, M. Amor-Gueret, L. Israel, E. Taillandier, Temporary *ex vivo* inhibition of the expression of the human oncogene HER2 (NEU) by a triple helix-forming oligonucleotide, *Cancer Res.* 56 (1996) 515–522.

Molecular Interactions between Lipid and its Related Substances in Bilayer Membranes

Tomohiro Imura,¹ Shoko Yokoyama² and Masahiko Abe^{3,4,*}

¹*Research Institute for Innovation in Sustainable Chemistry, National Institute of Advanced Industrial Science and Technology (AIST), Tsukuba Central 5-2, Higashi 1-1, Tsukuba, Ibaraki 305-8565, Japan*

²*School of Pharmaceutical Sciences, Kyushu University of Health and Welfare, 1714-1 Yoshino, Nobeoka, Miyazaki 882-8508, Japan*

³*Faculty of Science and Technology, Tokyo University of Science, 2641 Yamazaki, Noda, Chiba 278-8510, Japan*

⁴*Institute of Colloid and Interfacial Science, Tokyo University of Science, 1-3 Kagurazaka, Shinjyuku, Tokyo 162-8601, Japan*

Contents

1. Interaction Between Nonionic Surfactant and Phospholipid	192
2. Interaction Between Lipophilic Substance and Phospholipid	194
3. Interaction between Steroid and Phospholipid	197
4. Interaction between Glycolipid and Phospholipid	201
5. Interaction between Mangostin and Phospholipid	204
6. Interaction between Ceramide and Phospholipid	205
7. Interaction between Metal Ion and Phospholipid	210
8. Interaction between Water-soluble Polymer and Phospholipid	213
9. Interaction between Protein and Phospholipid	216
10. Novel Liposome Preparation Method Using Supercritical Carbon Dioxide	219
References	224

Abstract

Liposomes are colloidal structures formed by the self-assembly of phospholipid molecules in aqueous solution. It is widely accepted that liposomes, lipid bilayer membranes, are of great importance as models for biological membranes. Recently, widespread applications have been considered in the areas of drug delivery systems, food chemistry, cosmetics, and so on, because they can encapsulate both water- and lipid-soluble molecules or even macromolecules.

Many studies have been performed on the pharmacological aspects of liposomes in vivo and/or in vitro. However, only a few studies have been done on the physicochemical properties of liposomes, in particular the molecular interactions between phospholipid and its related substances in a lipid bilayer membrane. Investigation of these interactions is of great importance not only practically, but also theoretically.

In this chapter, we review the molecular interactions between phospholipid and related substances such as nonionic surfactants, lipophilic substances, steroids, glycolipids, mangostin, ceramides, metal ions, water-soluble polymers, and proteins in a lipid bilayer. Moreover, we describe a novel liposome preparation method that allows us to prepare the

*Corresponding author. Tel./Fax: +81-4-7124-8650;
E-mail: abemasa@rs.noda.tus.ac.jp

liposomes in a single step using supercritical carbon dioxide instead of a toxic organic solvent.

1. INTERACTION BETWEEN NONIONIC SURFACTANT AND PHOSPHOLIPID

To enhance the functionality of liposomes (for example, targetability for a specific organ and/or cell), a molecular recognition element such as an amphoteric compound having good biodegradability should be incorporated into the lipid bilayers of liposomes [1]. In this section, we have solubilized some nonionic surfactants having different polyoxyethylene chain lengths into the bilayers as a model of molecular recognition elements: the nonionic surfactants used were hexadecyl polyoxyethylene ethers ($C_{16}POE_n$; $n = 10, 20, \text{ and } 40$).

The liposomes including nonionic surfactants were prepared according to the following procedure. After $L\text{-}\alpha$ -dipalmitoylphosphatidylcholine (DPPC, Nihon Oil & Fats Co. Ltd.) dissolved in a chloroform solution, multilamellar vesicle (MLV) including 2 mM of DPPC was prepared by the method of Bangham *et al.* [2]. The obtained MLV was irradiated with ultrasonic waves for 5 h at 50°C to form small unilamellar vesicles (SUV), followed by the addition of a given concentration of nonionic surfactants. These mixtures were stirred for an appropriate time (12 h) with a thermostat at 30°C to reach their equilibrium.

Figure 1 shows the effects of the concentration of various nonionic surfactants on the particle sizes of liposomes. The particle size of the liposomes including

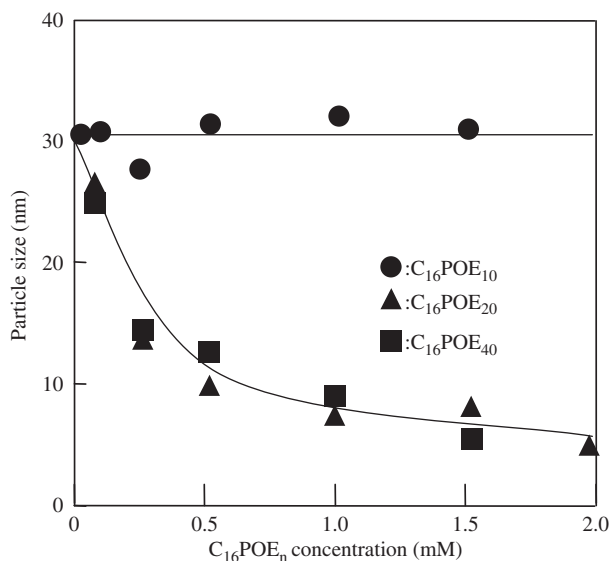


Fig. 1. Effects of the concentrations of various nonionic surfactants on the particle sizes of liposomes at 30°C .

nonionic surfactants with short-polyoxyethylene chains ($C_{16}POE_{10}$) was nearly independent (about 30 nm) of surfactant concentration, whereas the particle size of the liposomes including nonionic surfactants with long-polyoxyethylene chains ($C_{16}POE_{20}$ and $C_{16}POE_{40}$) decreased less than 10 nm, as the surfactant concentration increased. As the minimum value of liposome size is generally known to be 20 nm, above 0.5 mM of nonionic surfactant having long-polyoxyethylene chains, the DPPC liposome is unable to be formed; a molecular aggregate such as micelles would be obtained instead. To ascertain this, the trapping efficiency for Calcein (3,6-dihydroxy-2,3-bis[*N,N*-di(carboxymethyl)-aminomethyl]fluoran), which is the aqueous model material and that is encapsulated into an inner water phase of liposomes, was determined. Although the trapping efficiency for the $C_{16}POE_{10}$ system was little changed (only 10% reduced) by the addition of the surfactant, those for the $C_{16}POE_{20}$ or $C_{16}POE_{40}$ decreased rapidly, as the surfactant concentration increased and then became nearly zero above 1 mM of the surfactant. This means that the molecular aggregate forms without an inner water phase, indicating the destruction of the bilayer structure formed by DPPC above this surfactant concentration.

To ascertain whether $C_{16}POE_{10}$ molecules become incorporated into liposomes or not, after ultracentrifuging (10^5G , 5 h, $40^\circ C$), chemical analysis of the precipitates was performed according to the method of Takayama *et al.* [3]. The amount of DPPC was independent of surfactant concentration, and all the DPPC molecules added existed in the precipitates. At the same time, all the $C_{16}POE_{10}$ molecules also existed in the precipitate. We also investigated molecular interactions between $C_{16}POE_{10}$ and DPPC molecules in bilayers of liposomes by differential scanning calorimetry (DSC) measurement; the cooperative effect of the phase transition of DPPC molecules decreased because of the penetration of the nonionic surfactant into the DPPC molecules.

Liposomes prepared only from phospholipid are unstable because of the lack of charged materials on their surface. Liposomes usually contain dicetyl phosphate (DCP), which is a charged material, to prevent the coagulation of liposome [4]. When liposomes are administered in the human body, those with negatively charged materials have little toxicity [5]. Therefore, we prepared the liposomes with DCP and then investigated the effects of the concentration of nonionic surfactant on the zeta potential of liposomes. We found that every absolute value of zeta potential decreased considerably with increasing nonionic surfactant concentrations. Moreover, the degree of depression increased with increasing polyoxyethylene chain lengths. It can be postulated that the alkyl chains of the nonionic surfactant penetrate into the DPPC bilayers. The polyoxyethylene chain hydrophilic moieties cover up the liposome surface.

In summary, the particle size and trapping efficiency of the liposomes decrease rapidly with increasing concentration of nonionic surfactant possessing a long-oxyethylene chain ($C_{16}POE_{20}$ and $C_{16}POE_{40}$), but show virtually no change in the case of a short-oxyethylene chain ($C_{16}POE_{10}$). The cooperative effect on the

physical properties of a bilayer caused by interaction among DPPC molecules decreases with increasing concentration of the nonionic surfactant. The absolute value of the zeta potential for the liposomes also decreases following the addition of a nonionic surfactant. The addition of a long-polyethoxylated nonionic surfactant to DPPC liposome solution induces structural changes of molecular assembly and in particular, in the presence of excess amounts of C₁₆POE₂₀ and C₁₆POE₄₀, the DPPC liposome with nonionic surfactant does not form. Recent interesting findings related to liposomes with nonionic surfactants were achieved by Matsumoto *et al.* [6,7]. They reported that L- α -dimyristoyl phosphatidylcholine (DMPC) liposomes with dodecyl polyoxyethylene ethers exhibit a highly inhibitory action against the growth of tumor cells as well as intercellular responses against leukemia cells (HL-60) related to apoptosis. The differences in the physicochemical properties of the liposome including nonionic surfactants, which we revealed might cause these attractive biological activities.

2. INTERACTION BETWEEN LIPOPHILIC SUBSTANCE AND PHOSPHOLIPID

Liposomes are spherical molecular assemblies composed of a lipid bilayer membrane and an inner water phase [8]. Thus, water-soluble (hydrophilic) molecules can be incorporated into the inner water phase of liposomes, and at the same time a hydrophobic molecule can also be incorporated into the lipid bilayer membranes forming a hydrophobic moiety. In particular, numerous recent drugs give rise to an enhanced utilization of lipid-soluble molecules.

In this section, we describe incorporation of lipophilic substances having different hydrophilic groups such as octane, 1-octanol, and octanoic acid into the lipid bilayer membrane. Preparation of liposomes including lipophilic substances was almost the same as the method mentioned above (Section 1). The only differences were the composition of liposomes (DPPC/cholesterol/DCP = 7:4:0.7) and the total concentration of lipid (10 mM).

First, we investigated the variation of absorbance of the liposome solutions including lipophilic substances with incubation time. Figure 2 shows the relationship between absorbance and incubation time of liposomes incorporating various lipophilic substances (30 mM) at 30°C. Here, arrows indicate the time required to attain a constant absorbance. As can be seen in Figure 2, the time required to achieve constant absorbance decreased with increasing hydrophilicity of lipophilic substances (octanoic acid < 1-octanol < octane). We previously reported [9] on the solubilization of lipophilic substances by surfactant micelles: octane, being a nonpolar compound, is solubilized into the hydrocarbon core of the surfactant micelles, whereas 1-octanol and octanoic acid, being polar substances, thrust the polar group out of the surface of the surfactant micelles and their alkyl chains penetrate the palisade layers of the surfactant micelles.

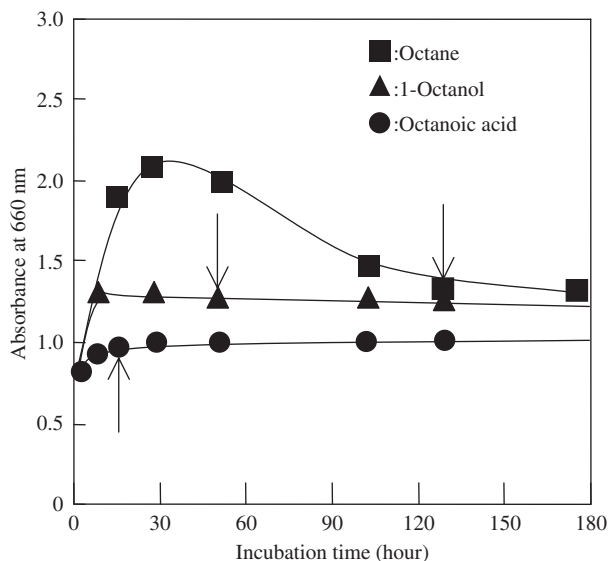


Fig. 2. Relationship between absorbance and incubation time of liposomes incorporating various lipophilic substances at 30°C.

Moreover, 1-octanol, having a weaker hydrophilicity than octanoic acid, is deeply solubilized into the palisade layers of the micelles. Furthermore, compounds having strong hydrophilic groups offer little solubilization in micelles [10] because of their strong interaction with water molecules. The addition of suitable amounts of alcohols and/or fatty acids into the solutions containing surfactant molecules promotes the formation of a molecular aggregate such as a microemulsion. Thus, for lipophilic compounds having a cooperative effect for forming an aggregate with DPPC molecules (in other words, strongly hydrophilic compounds), the time to attain distribution equilibrium of lipophilic compounds between the inside and outside of the liposomes is short, whereas for compounds without a cooperative effect with DPPC (e.g. octane) the time for the establishment of equilibrium becomes longer.

Furthermore, the trapping efficiency measurement of glucose revealed that the aggregates will change from a bilayer structure to a monomolecular structure without an inner water phase at higher concentrations of 1-octanol and octanoic acid. The trapping efficiency for the system with added octane without hydrophilic groups became a constant (0.6%) above 100 mM of octane, whereas that for 1-octanol and octanoic acid with hydrophilic groups became nearly zero above 100 mM of lipophilic substances. The trapping efficiency being zero means an absence of an inner water phase in the molecular aggregate, as mentioned previously.

The microenvironment, such as micropolarity determined by the fluorescence probe method, is important in investigations of the solubilization sites of lipophilic

substances in the bilayer membranes of liposomes. Pyrene is a well-known typical fluorescence probe, like aromatic hydrocarbons, which exists in the hydrocarbon region of a bilayer membrane. Pyrene monomer fluorescence shows five predominant peaks. In the present case of pyrene, peak 3, which is strong and allowed, shows minimal intensity variation with polarity. Peak 1 shows significant intensity enhancements in polar solvents. Thus, the intensity ratio of peak 1/peak 3 serves as a measure of polarity [11]. Figure 3 exhibits the relationship between the I_1/I_3 ratio of pyrene in liposomes and the concentration of lipophilic substances. Pyrene concentration was $12.5 \mu\text{M}$. Here, the I_1/I_3 ratio of pyrene in the bilayer membrane of liposomes was considerably larger than that in pure decane (0.581). As shown in Fig. 3, the micropolarity (I_1/I_3) for the added octanoic acid system was almost independent of the concentration of octanoic acid. On the other hand, the micropolarity for the added 1-octanol system was slightly decreased, and that for the added octane system was considerably decreased with an increasing concentration of the lipophilic substance. It can be postulated that the I_1/I_3 ratio of pyrene solubilized in the bilayer membrane (micropolarity) is dependent on the change of environment of pyrene solubilized and the influence of water molecules existing both in continuous and inner phases. In other words, when the lipophilic substances are incorporated into the hydrocarbon core of the bilayers or are prevented from interacting with water molecules, the I_1/I_3 of pyrene (in other words, micropolarity) will decrease. Namely, for the added octane system, as the I_1/I_3 ratio decreased considerably with an increasing concentration of

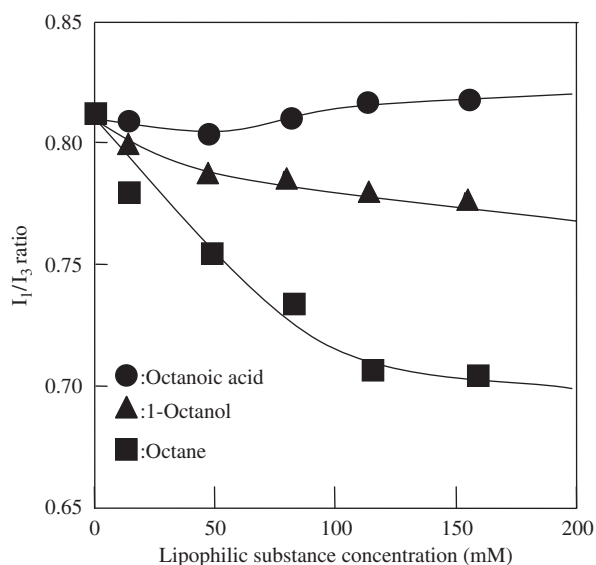


Fig. 3. Relationship between I_1/I_3 ratio of pyrene in liposomes and concentration of lipophilic substances at 30°C .

octane, which means that the octane exists in surroundings with the pyrene molecules solubilized in the hydrocarbon core of liposomes, where the pyrene is protected from interaction with water molecules. For the 1-octanol system, the I_0/I_3 decreased slightly with an increase in concentration of 1-octanol, which means the pyrene solubilized in the hydrocarbon core is slightly affected by water molecules because of the extension of lipid bilayers caused by a deep penetration of 1-octanol molecules. For the added octanoic acid system, I_0/I_3 was nearly independent of the concentration of octanoic acid, which means that the octanoic acid molecules penetrate the bulky palisade layer of the liposomes and avoid the pyrene solubilized in the hydrocarbon core of the liposomes.

From the results mentioned above, the solubilization site of lipophilic substances in the liposomes strongly depends on their hydrophilicity. The lipophilic substance having higher hydrophobicity exists inside the bilayers, and that having higher hydrophilicity exists near the liposome surfaces. Moreover, the excess addition of substances having hydrophilicity is likely to cause a change of aggregate structures. These facts should be considered when liposomes are used in practice as carriers for lipophilic drugs.

3. INTERACTION BETWEEN STEROID AND PHOSPHOLIPID

Liposomes are generally composed of a phospholipid, DCP (a charged lipid), and cholesterol (a steroid that serves to prevent coagulation) to minimize leakage of the entrapped materials [12–14]. However, only a few studies have been done on the physicochemical properties of liposomes, in particular, the molecular interactions between phospholipids and some steroids in a bilayer membrane. In this section, we describe the chemical and structural effects of steroids on the molecular interaction between phospholipid and some steroids.

The liposomes used in this section were prepared by the reverse-phase evaporation method [15]. Briefly, the DPPC, steroids, and DCP (7:3:1) were dissolved in a mixture of diethyl ether and ethanol and then 0.28 mol L^{-1} glucose solution was added with a proper volume. The water in oil (W/O) emulsion was formed by sonication (bath type; Branson B-220, Tokyo, Japan) for 10–20 min. After the solvent of the emulsion was removed using a rotary evaporator, a gel was formed. Finally, reverse-phase evaporation vesicles (REV) were obtained after being shaken on a Vortex mixer for several minutes.

First, we examine the surface pressure–area isotherms of the mixed DPPC/steroid monolayers at the air–water interface because we have previously reported that the two-dimensional (2D) intermolecular interaction in a lipid monolayer is corrected with the lateral interaction in a lipid bilayer [16]. As can be seen in Fig. 4, each DPPC/steroid-mixed monolayer is found to form a condensed monolayer for the different types of steroids. The compressibilities of the mixed monolayer of DPPC with steroids (cholesterol, β -cholestanol, β -sitosterol, and

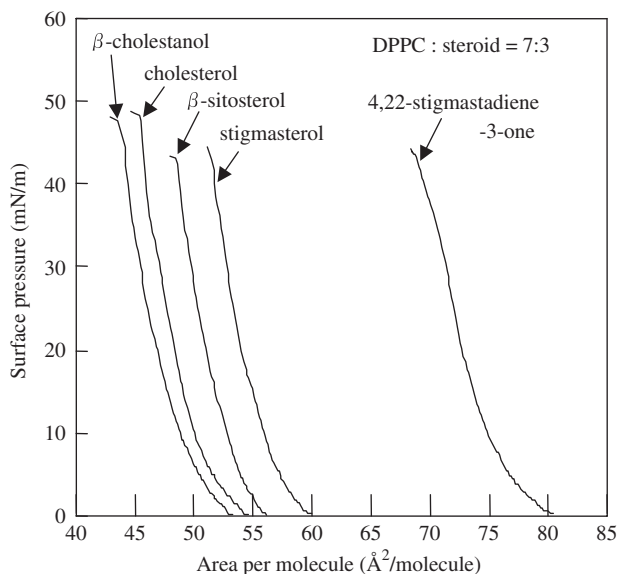


Fig. 4. Surface pressure (π)-area (A) curves (DPPC/steroid = 7:3).

stigmasterol), which have the same hydrophilic group (OH group), were almost the same, but that of the mixed monolayer of DPPC with 4,22stigmastadien-3-one, which has a quinone group, was different from the others (Table 1). The compressibility was determined by the cross point of the tangent line of the surface pressure-area curves near the collapse pressure and the X-axis.

From the results of a limiting area, it can be postulated that the steroids having a hydroxyl group (OH group) as a hydrophilic group orient vertically at the interface, while the 4,22stigmastadien-3-one having a quinone group (O: group) as its hydrophilic group slopes slightly at the interface, because the formation of conjugated double bonds of quinone groups with steroid rings and steroid ring-containing quinone groups form a planar molecule.

In the case of the mixed monolayer of DPPC/steroids having the same OH group, the collapse pressure for the mixture of steroids having smaller side chains as cholesterol or β -cholestanol was larger than for the mixture of steroids having a branched side chain as β -sitosterol and stigmasterol. When the limiting areas of the mixed monolayers are compared with steroids for which the collapse pressure is almost the same, those for stigmasterol with a double bond in the side chain are found to be larger than those for β -sitosterol without such a bond. This may be attributed to the fact that, when a double bond exists in a side chain, the rotation of molecules does not occur, leading to a loose orientation and an increase in the limiting area. Meanwhile, the limiting area of cholesterol with a double bond in the steroid ring and β -cholestanol without it had almost the same values. The interaction of hydrophobic groups between DPPC and steroid

Table 1. Limiting area, collapse pressure, and compressibility for steroid (DPPC/steroid = 7:3)

	Cholesterol	β -Cholestanol	β -Sitosterol	Stigmasterol	4,22-Stigmastadien-3-one
Limiting area ($\text{\AA}^2/\text{molecule}$)	48.1	46.4	52.0	55.5	77.9
Collapse pressure (mN/M)	47	48	43	42	41
Compressibility (mN/m) $\times 10^{-3}$	1.3	1.1	1.6	1.9	3.3

increases with a decrease in the number of side chains and double bonds in the order, cholesterol = β -cholestanol > β -sitosterol > stigmasterol.

The permeability of the bilayer membrane was then estimated by a glucose dialysis method. Figure 5 represents the time course of the glucose leakage from the liposomes. The glucose leakage from the liposomes was decreased by the addition of steroids, indicating that incorporation of steroids into a bilayer membrane results in an increase in the stability of the liposomes. Moreover, the extent of leakage depends on the kinds of steroids. It is clear that the order of the stability of the bilayer membrane can be considered to be cholesterol > β -cholestanol > β -sitosterol > stigmasterol. As this tendency is almost consistent with the propensity, mentioned above, of the molecular interaction between DPPC and steroids (cholesterol = β -cholestanol > β -sitosterol > stigmasterol), the permeability of a bilayer membrane is likely to increase with a decrease in the interaction between DPPC and the steroids.

It was found that the molecular interaction between DPPC and steroids in the hydrophobic membrane depends on the structure of the side chains of the steroids, if the hydrophilic group of the steroids is the same, and the interaction decreases with increasing branching and number of double bonds of the side chains of the steroids. The permeability of water-soluble glucose through the membrane depends on the interactions between lipid and steroid; consequently, the permeability increases, while the interactions decrease.

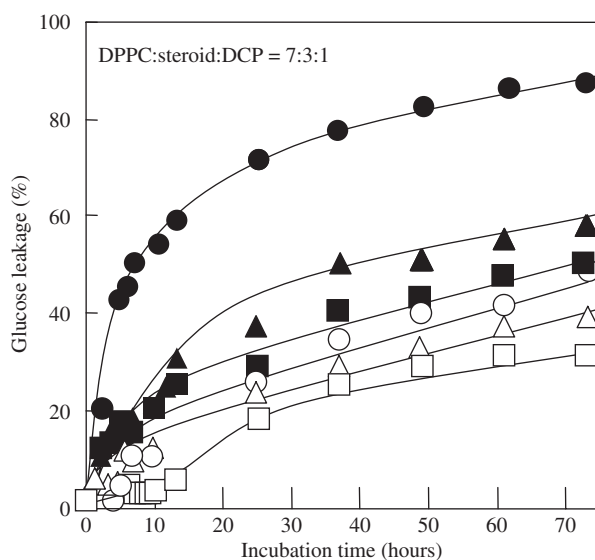


Fig. 5. Time dependence of glucose leakage (DPPC/steroid/DCP = 7:3:1). ●, without steroid; ▲, 4,22-stigmastadien-3-one; ■, stigmasterol; ○, β -sitosterol; △, β -cholestanol; □, cholesterol.

4. INTERACTION BETWEEN GLYCOLIPID AND PHOSPHOLIPID

For DDS, it has been reported that the orientation of carbohydrate groups on the surface of a liposomal membrane provides target specificity for the internal organs [17,18]. For example, terminal galactose residues of glycolipids are effective for the liver [19]. In this section, liposomes composed of phospholipids (DPPC), cholesterol (Chol), charged materials (DCP), and glycolipids having a terminal galactose residue in the molecule were prepared to investigate the molecular interactions between glycolipids and phospholipid in liposomes.

Liposomes including glycolipid were prepared by the Bangham method as described in Section 1. The glycolipids used were 1,2-diacyl [β -D-galactopyranosyl (1'-3)]-*sn*-glycerol (monogalactosyl diglyceride, MG) and 1,2-diacyl [α -D-galactopyranosyl (1'S-6') β -D-galactopyranosyl (1'-3)]-*sn*-glycerol (digalactosyl diglyceride, DG).

We examined the effect of the glycolipids on the permeability of liposomes. Figure 6 depicts the glucose leakage from the liposomes. In both liposome systems, i.e. with cholesterol (Fig. 6(a)) and without cholesterol (Fig. 6(b)), the release of glucose from the liposomes increased with time. Moreover, a two-stage release of glucose molecules from the liposomes could be observed. Both with and without cholesterol, the early stage was more rapid than the later stage. The leakage of glucose from the liposomes without cholesterol, however, was more rapid than that from those with cholesterol in both stages. Thus, in the absence of cholesterol in these liposome systems, the bilayer membranes are less stable, as mentioned in the above section. The glucose leakage in those liposomes including DG was less than in those including MG. This means that the sugar chains in the glycolipids inhibit permeability.

Some lectins can interact with specific saccharide molecules on the cell surface. A galactose-specific lectin, *Ricinus Communis* agglutinin (RCA₁₂₀), [20] was used. A 1 mL portion of 200 $\mu\text{g mL}^{-1}$ RCA₁₂₀ was added rapidly to a 1 mL portion of 0.5 $\mu\text{mol mL}^{-1}$ liposomes including glycolipids. The mixture was vortexed and immediately transferred to a submicron particle size analyzer. The agglutination was determined by monitoring the increasing particle size with time.

Figure 7 shows the time required to increase the particle size of the liposomes in the presence of RCA₁₂₀. Both with and without cholesterol, the time course of the liposome particle size without glycolipids was independent of RCA₁₂₀ concentration, while that of the liposome particle size with glycolipids was fairly dependent on the RCA₁₂₀ concentration level.

The particle size was increased with an increase in the amount of glycolipids added. In DG-including systems, an enlarging effect was observed upon the addition of RCA₁₂₀ to the liposomes; little effect was seen in MG-including systems. This increase in the liposome particle size may be caused by the agglutination of galactose groups in the glycolipids when RCA₁₂₀ molecules are

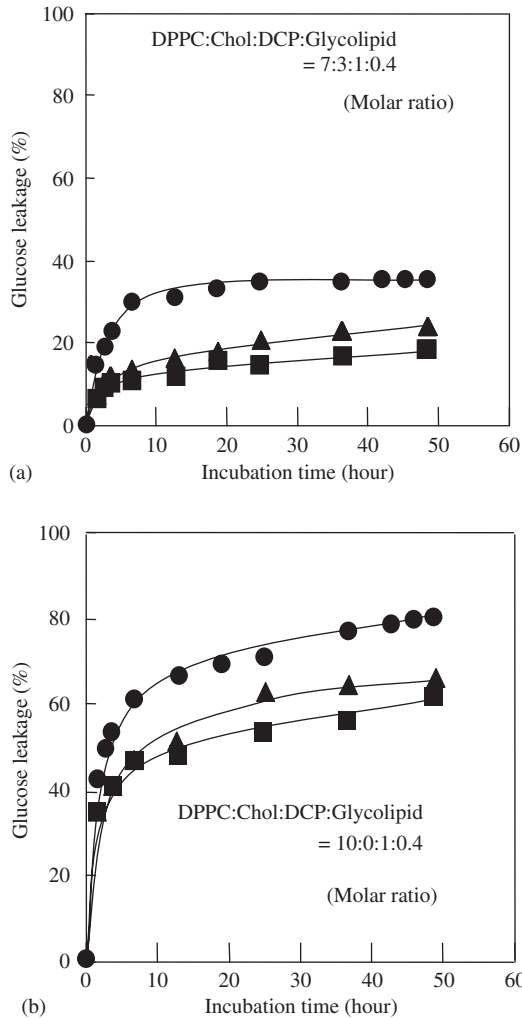


Fig. 6. Permeability of liposomes including glycolipids studied by the measurement of glucose leakage from the liposomes at 37°C. (a) DPPC/Chol/DCP/glycolipid = 7:3:1:0.4; (b) DPPC/Chol/DCP/glycolipid = 10:0:1:0.4. ●, without glycolipid; ▲, MG; ■, DG.

involved. It can be postulated that increasing the numbers of galactose groups in the glycolipids added to the liposomes results in an improvement in the recognition of RCA₁₂₀.

Next, the effect of sugar groups in the glycolipids on the zeta potential of the liposomes was examined. The zeta potential of the liposomes without glycolipids was about -29 mV (with cholesterol) and -30 mV (without cholesterol). These negative zeta potentials are due to the ionization of DCP, which is a negatively charged lipid. The absolute value of the zeta potential decreased with an increase

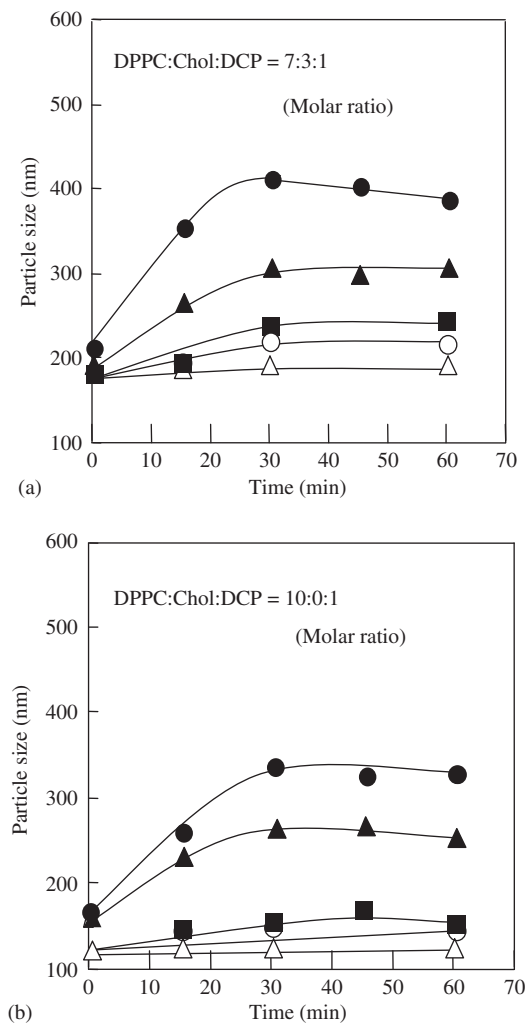


Fig. 7. Increasing particle size upon the addition of RCA₁₂₀ to liposomes at 37°C. (a) DPPC/Chol/DCP/glycolipid = 7:3:1:*n*; (b) DPPC/Chol/DCP/glycolipid = 10:0:1:*n*, where (Δ) *n* = 0; (○) *n* = 0.4 (MG); (■) *n* = 0.8 (MG); (▲) *n* = 0.4 (DG); (●) *n* = 0.8 (DG).

in the mole fraction of the glycolipids. In DG-including systems, the absolute value of the zeta potential was smaller than that in MG-including systems.

In summary, liposomal bilayer membranes are stabilized by the addition of glycolipids. The sugar groups in the glycolipids can then improve the interaction between the liposomes and lectin. The absolute value of the zeta potential of the liposomes decreases with the addition of glycolipids, resulting in a decrease in the dispersibility of the liposomes. The liposomes with glycolipid prepared in this section would be effective for targeting the liver.

5. INTERACTION BETWEEN MANGOSTIN AND PHOSPHOLIPID

Liposomes have a lot of advantages when they are applied as drug carriers [21]. For example, many highly toxic agents encapsulated in liposome show a reduction in normal tissue side effects. An improvement in the pharmacological effects of various agents, which are poorly soluble or insoluble, can also be achieved. Numerous agents, both synthetic and natural extracts, have been encapsulated in liposomes. However, mangostin, a xanthone compound, extracted from the fruit hull of the mangosteen (*Garcinia mangostana*, Linn. (Guttiferae)) with hexane followed by extensive rapid column chromatography [22], has never been studied in liposomes.

Several studies have revealed a number of pharmacological activities, i.e. cardiogenic, antimicrobial, and anti-hepatotoxic effects, as well as an anti-inflammatory activity of mangostin and its derivatives. It was found that mangostin at a dose of 50 mg kg^{-1} exhibits pronounced anti-inflammatory activity in the carrageenin-induced paw edema, cotton pellet implantation, and granuloma pouch models [23]. The entrapment of mangostin, a hydrophobic compound, in liposomes can be of pharmacological advantage, since enhancement of the absorption through the biological membrane by entrapment or solubilization of mangostin in the bilayers of liposomes is anticipated.

In this section, liposomes composed of phospholipids, cholesterol, charged materials, and mangostin (1,3,6-trihydroxy-7-methoxy-2,8-bis-(3-methyl-2-butenyl)-9-xanthenone) were prepared to investigate the molecular interactions between mangostin and phospholipid. Three types of liposome were prepared by the Bangham method: uncharged liposomes (Unc.L) composed of DPPC and Chol (molar ratio 1:1), negatively charged liposomes (Neg.L) composed of DPPC, Chol, and DCP (7:3:1), and positively charged liposomes (Pos.L) composed of DPPC, Chol, and stearyl amine (SA) (7:3:1).

First, the effects of the liposome formation on the addition of mangostin were examined by measuring the amount of DPPC used for liposome formation. In the case of Unc.L, up to the addition of 5 wt.% mangostin, all the DPPC was able to contribute to the formation of liposomes. Beyond this additive amount, not all the DPPC was utilized. Similar to the case of Unc.L, the DPPC amount contributing to the formation of liposomes was changed at the additive point of 15 wt.% mangostin for Neg.L and 10 wt.% mangostin for Pos.L.

The effects of mangostin on the microscopic state of the liposomal bilayer membrane were then investigated. Fluorescent fatty acid probes were used in this study to interpret the microviscosity at different depths in the membranes. It is generally known that 2-(9-anthroyloxy)-palmitic acid (2-AP) can probe the region close to the membrane surface, while 12-(9-anthroyloxy)-stearic acid (12-AS) can probe the region near the bilayer center [24]. The microviscosity, which is related to the fluorescence polarization, can be calculated using Perrin–Weber's equation [25]. It is also known that fluorescence polarization increases with increasing

microviscosity. The fluorescence polarization (P) was calculated using the following equation [24]:

$$P = \frac{I_P - GI_V}{I_P + GI_V} \quad (1)$$

Where I_p and I_v are the fluorescence intensities of the emitted light polarized parallel and verticle to the exciting light, respectively, and G is the grating correction factor. Figure 8(a) (2-AP probe) and 8(b) (12-AS probe) denote the relationship between fluorescence polarization and the amount of mangostin added. In all types of liposomes, both the microviscosity at the region close to the membrane surface of the bilayer membranes and at the region near the bilayer center were increased with the addition of more mangostin. An increase in the amount of mangostin added seems to correspond to an increase in the component number of the liposomal bilayer. Mangostin solubilized in bilayers is found to cause the fluidity of the acyl group to decrease and the microviscosity to increase, owing to the tight packing of lipids.

We further examined the effects of mangostin on the permeability of liposomes. Figure 9 displays the glucose leakage from the liposome. In each liposome (Unc.L, Neg.L, and Pos.L or blank liposome and mangostin liposome), the leakage of glucose from liposomes increased with time. However, the glucose leakage for mangostin liposomes (in all types) was depressed compared with that for blank liposomes. This is a result of the tight packing of the bilayer membrane, which is caused by mangostin solubilized between lipids.

In this section, we reveal that there is a maximum additive concentration (MAC) of mangostin for each individual liposome (Unc.L, Neg.L, and Pos.L). Liposomal bilayer membranes are stabilized by the solubilization of mangostin in each liposome type, which results in restriction of glucose leakage from liposomes. These changes in the physicochemical properties of liposomes should be considered for practical application of mangostin liposomes (liposome-solubilized mangostin).

6. INTERACTION BETWEEN CERAMIDE AND PHOSPHOLIPID

Liposomes are also very promising drug carriers in external drug application because they remain on the skin or in the stratum corneum after application, releasing effective amounts of enclosed drugs in a sustained manner [26–28,29]. Moreover, externally applied drug-including liposomes are reported to enhance transdermal absorption of the drug [30].

Human skin consists of the epidermis, dermis, subcutaneous tissue, and stratum corneum. In particular, the stratum corneum lipids construct the water-permeability barrier, in which the control of water permeability is essential for survival in any living system. The stratum corneum lipids are composed of 50% ceramides, 5% cholesterol, 10% cholesterol esters, and 20% free fatty acids. A

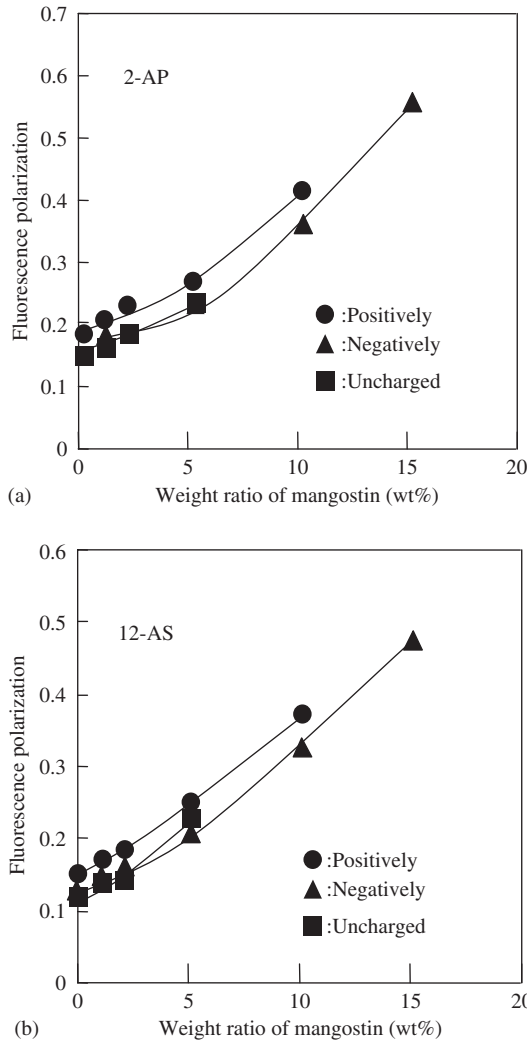


Fig. 8. Relationship between fluorescence polarization and amount of mangostin added at 37°C: (a) fluorescence polarization obtained with 2-AP probe; (b) fluorescence polarization obtained with 12-AS probe.

decreased level of ceramides in the stratum corneum of atopic dermatitis has been found, suggesting that an application of a small amount of ceramides may be effective for dry skin dermatitis [31]. The manufacturing of a ceramide product is, however, a difficult problem because ceramides can barely be dispersed in an aqueous medium. It is expected that the dispersibility of ceramides will be improved by liposome formation with phospholipid.

In this section, the liposomes composed of phospholipids and ceramides were prepared to examine the effects of ceramides on the physicochemical properties of liposomes.

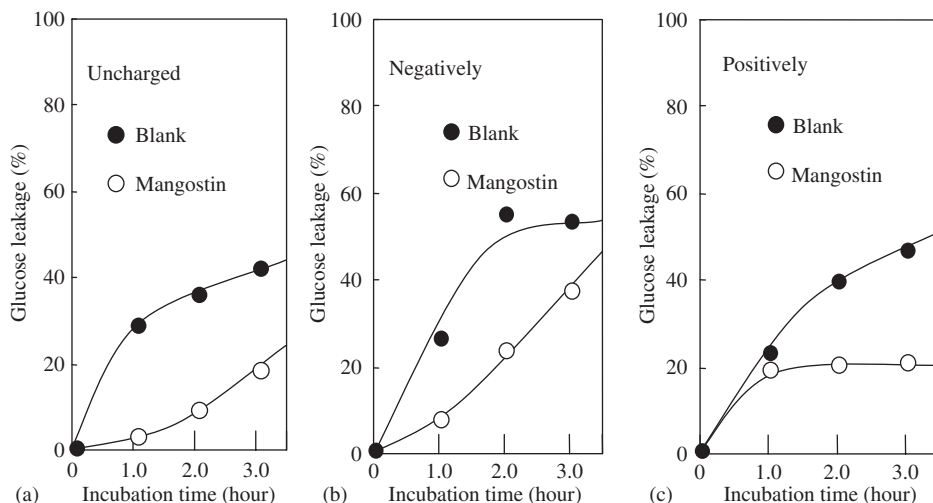


Fig. 9. Permeability of liposome studied by measurement of glucose leakage from liposomes at 37°: (a) uncharged liposomes; (b) negatively charged liposomes; (c) positively charged liposomes.

The liposomes were prepared by the Bangham method and the composition of liposomes in this section was as follows: DPPC/2S,3S, 4R-2-stearoylamide-1,3,4-octadecanetriol (Ceramide 3)/DCP = 10:(0~1.5):1. Ceramide 3 was chosen as a ceramide since Ceramide 3 exists with higher concentration in the epidermis and the stratum corneum.

The effect of Ceramide 3 on the formation of liposomes was examined by measuring the amount of DPPC that forms liposomes. All the DPPC was able to contribute to the formation of liposomes including Ceramide 3 up to 0.130 mol fraction of Ceramide 3, but not all the DPPC was utilized at higher mole fractions of Ceramide 3. Agglutination of Ceramide 3 was also observed with optical microscopy for liposome solutions containing more than 0.166 mol fraction of Ceramide 3.

The effect of Ceramide 3 on the microviscosity of liposomes was investigated using 1,6-diphenyl-1,3,5-hexatriene (DPH) as a fluorescent probe. Figure 10 shows the relationship between the fluorescence polarization of DPH and temperature. The fluorescence polarization of DPH in the DPPC bilayer membranes without Ceramide 3 suddenly decreased above 42°C, which agrees with the phase transition temperature of DPPC. The phase transition temperature was raised by the addition of Ceramide 3. The microviscosity of liposomal bilayer membranes in the liquid crystalline state was increased with increasing mole fraction of Ceramide 3, while that in the gel state was independent of the mole fraction of Ceramide 3. Ceramide 3 is likely to affect the microviscosity in the hydrophobic region of liposomal bilayer membranes in the liquid crystalline state. The results shown in Fig. 10 suggest that the intermolecular interactions in the liposomal bilayer

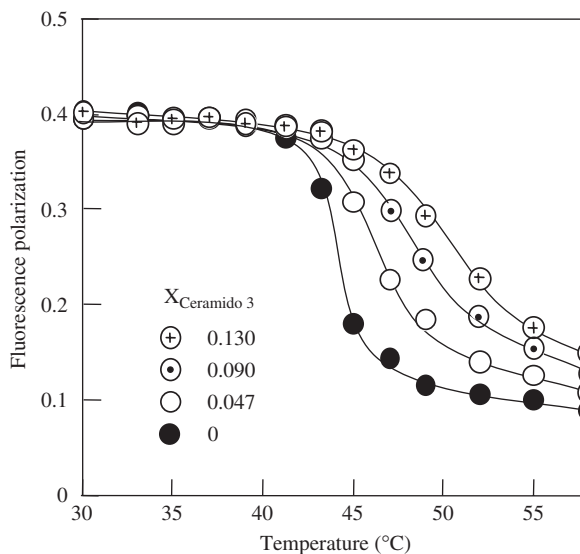


Fig. 10. Relationship between fluorescence polarization of DPH and temperature for liposomes including various amounts of Ceramide 3.

membranes in the liquid crystalline state are strengthened and the packing density in the membranes becomes rigid by the addition of Ceramide 3.

The DSC curves for the mixed DPPC/Ceramide 3 liposomal bilayer membranes were then obtained by varying the mole fraction of Ceramide 3, and the results are shown in Fig. 11. Ceramide 3 had no peaks for at least 0–100°C (the DSC curve is not presented in Fig. 11). This phenomenon is consistent with the fact [27] that Ceramide 3 forms only the liquid-condensed film, as observed for the surface pressure measurement of the Ceramide 3 monolayer. An endothermic peak at about 41°C corresponds to the gel–liquid crystalline phase transition temperature of DPPC. The phase transition temperature of DPPC bilayer membranes was shifted upward with the addition of Ceramide 3, indicating that the liposomal bilayer membranes became thermostable by the addition of Ceramide 3. The shift of the main phase transition temperature to a higher temperature implies a cooperative interaction between DPPC and Ceramide 3 molecules, indicating also that Ceramide 3 is miscible with DPPC. The phase transition between the gel and liquid crystalline phases observed for phospholipid bilayers is related to the phase transition of phospholipid monolayers, from the liquid-expanded film to the liquid-condensed film. An attractive interaction between Ceramide 3 and DPPC in the liquid-expanded films of the mixed DPPC/Ceramide 3 monolayers has been reported in our previous paper [27].

A sharp DSC peak observed for the pure DPPC system became broad in the mixed DPPC/Ceramide 3 liposomal bilayer membranes. Furthermore, a DSC peak was noted to split at higher mole fractions of Ceramide 3. The split peak is

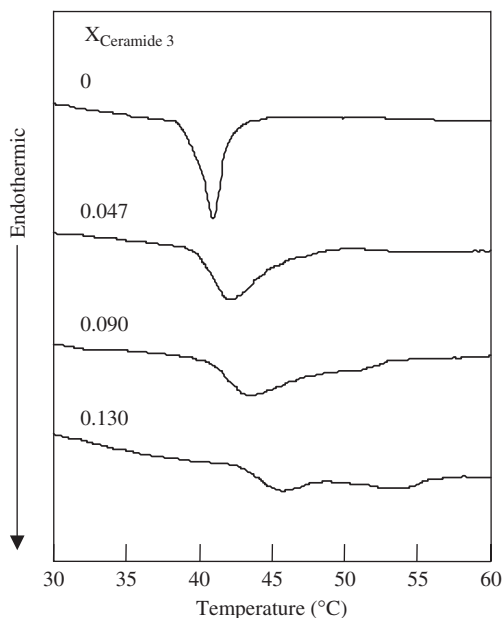


Fig. 11. DSC curves of liposomes including various amounts of Ceramide 3. DSC curves were obtained under the conditions: scanning rate, 1 K min^{-1} ; sensitivity, $0.1 \text{ mcal}^{-1} \text{ s}^{-1}$.

suggested to be caused by the phase separation in the liposomal bilayer membranes. We have also published atomic force microscope (AFM) images of the mixed DPPC/Ceramide 3 monolayers [27], in which elliptical domains and matrix caused by the phase separation between the liquid-condensed and the liquid-expanded films were found; the domains and the matrix observed for the mixed DPPC/Ceramide 3 monolayers correspond to the liquid-condensed and the liquid-expanded films. The DSC curves shown in Fig. 11 should be considered in connection with the AFM images. As an example, in the DSC curve for the mixed DPPC/Ceramide 3 system whose mole fraction of Ceramide 3 is 0.130, the peaks at a lower temperature (about 46°C) and at a higher temperature (about 54°C) may possibly correspond to the matrix and domains in the AFM images, where the matrix and domains are poor and rich in Ceramide 3, respectively. The decrease in the calorie of the DSC peak at a lower temperature is also consistent with the decrease in the matrix area at a higher mole fraction of Ceramide 3 in the AFM images.

In summary, in the preparation of mixed DPPC/Ceramide 3 liposomes, all the DPPC is able to contribute to the formation of liposomes up to 0.130 mol fraction of Ceramide 3. The microviscosity of the liposomal bilayer membranes in the liquid crystalline state is increased with increasing mole fraction of Ceramide 3, while that in the gel state is independent of the mole fraction of Ceramide 3. The phase transition temperature of DPPC bilayer membranes is shifted upwards with

the addition of Ceramide 3, indicating a cooperative interaction between DPPC and Ceramide 3 molecules. However, the sharp DPPC peak becomes broad in the mixed DPPC/Ceramide 3 systems and is split at higher mole fractions of Ceramide 3. The split peak is possibly caused by the phase separation in the liposomal bilayer membranes. The split DSC peak for the mixed DPPC/Ceramide 3 bilayer membranes may possibly be related to the domain formation observed for the mixed DPPC/Ceramide 3 monolayers.

In addition, the dispersibility of liposomes including Ceramide 3 is maintained for at least 15 days: this indicates that the liposomes composed of DPPC and Ceramide 3 could be available as a ceramide product.

7. INTERACTION BETWEEN METAL ION AND PHOSPHOLIPID

Divalent metal ions such as Ca^{2+} and Mg^{2+} are distributed in all mammalian cells and play important roles in biological functions [32–35,36]. The interactions of these metal ions with the lipid membrane have been studied in terms of the basic properties of lipid assemblies and possible physiological implications of interest. The fusogenic activity of cations for phosphatidylserine with cholesterol systems has been reported by Shavnin *et al.* [37]. The phenomena mentioned above are interpreted according to the dehydration ability of the metal ions.

In this section, attenuated total reflection (ATR) Fourier transform infrared (FT-IR) spectroscopy and DSC are applied to liposome systems to elucidate the interactions between metal ions and phospholipid bilayers.

Liposomes were prepared by sonication with a bath-type sonicator (Branson B-220) in which phospholipids were suspended in *N*-Tris (hydroxymethyl) methyl-2-aminoethanesulfonic acid (TES) buffer solution (100 mM NaCl, 2 mM *N*-Tris-(hydroxymethyl)methyl-2-aminoethanesulfonic acid, pH 7.4) for 1 h at 50°C. Two kinds of phospholipids, DPPC and *L*- α -dipalmitoylphosphatidylglycerol (DPPG), were used.

First, we examined the effect of divalent metal ions on the hydrophobic region of DPPC and DPPG liposomes. Figure 12 depicts the change in the antisymmetric CH_2 stretching wavenumber for DPPC and DPPG liposome as a function of the Ca^{2+} ion to phospholipid concentration ratio, at a temperature both above and below the phase transition temperature (70 and 22°C). In the gel phase, the pure DPPC and DPPG liposomes showed the same wavenumber (2918 cm^{-1}), while in the liquid crystalline phase, the band of the DPPG liposome without ions shifted to higher wavenumbers than that of the DPPC liposome (2923 and 2921 cm^{-1} respectively). These results imply that the DPPG liposome exists in a more disordered state than the DPPC liposome in the liquid crystalline phase as a result of the inflation of gauche conformers. Furthermore, the addition of Ca^{2+} to the liposome solution caused the frequency shift to disappear in the DPPG

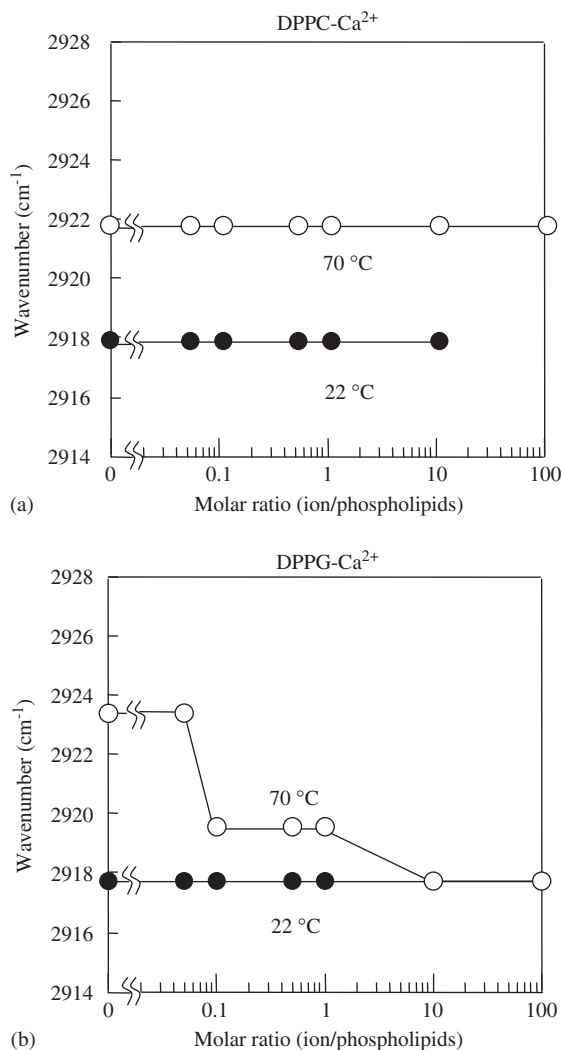


Fig. 12. Infrared spectra of the antisymmetric CH₂ stretching wavenumbers for (a) DPPC and (b) DPPG at various molar ratios of Ca²⁺ ion to phospholipids in TES buffer (pH 7.4).

liposome. It is considered that the hydrocarbon part of the fatty acyl chain of the DPPG liposome changes to a highly ordered *trans* form by Ca²⁺-induced isothermal crystallization [38]. From these results, a higher concentration of Ca²⁺ (molar ratio 10) is needed to the entire gel transition of the fatty acyl chain. Frequency shifts of antisymmetric CH₂ stretching were not observed by addition of Mg²⁺ and Ba²⁺. On the other hand, the antisymmetric CH₂ stretching band for the DPPC liposome was independent of the metal ion concentration.

The effect of divalent metal ions on the hydrophilic region of DPPC and DPPG liposomes was then examined. Infrared spectra of the phosphate-stretching region of DPPC and DPPG liposomes with various metal ions at an ion to phospholipid ratio of 10 in the liquid crystalline phase are shown in Fig. 13. The antisymmetric and symmetric phosphate-stretching absorptions were observed at 1223, 1087 cm^{-1} for DPPC and at 1215, 1091 cm^{-1} for DPPG, respectively. The antisymmetric phosphate-stretching band for DPPC was observed at a significantly higher frequency than for DPPG, suggesting that the phosphate group for DPPC is restricted by other nearby molecules such as water and/or the choline group in the neighborhood of the phospholipid molecule. The symmetric (1067 cm^{-1}) stretching mode of the C–O–C band overlapping the strong PO_4^- band was observed at the same frequency for DPPC and DPPG liposomes. In the presence of Ca^{2+} , the antisymmetric phosphate-stretching band of DPPC was shifted to higher frequency. This frequency shift is due to loss of bound water from the DPPC phosphate group. In the case of the DPPG liposome, the metal ion effect was significant. With Ca^{2+} , the C–O–C band frequency of the DPPG liposome was shifted to lower frequency. This shift is due to intramolecular nonequivalence of the two ester groups. Furthermore, the bandwidth of the

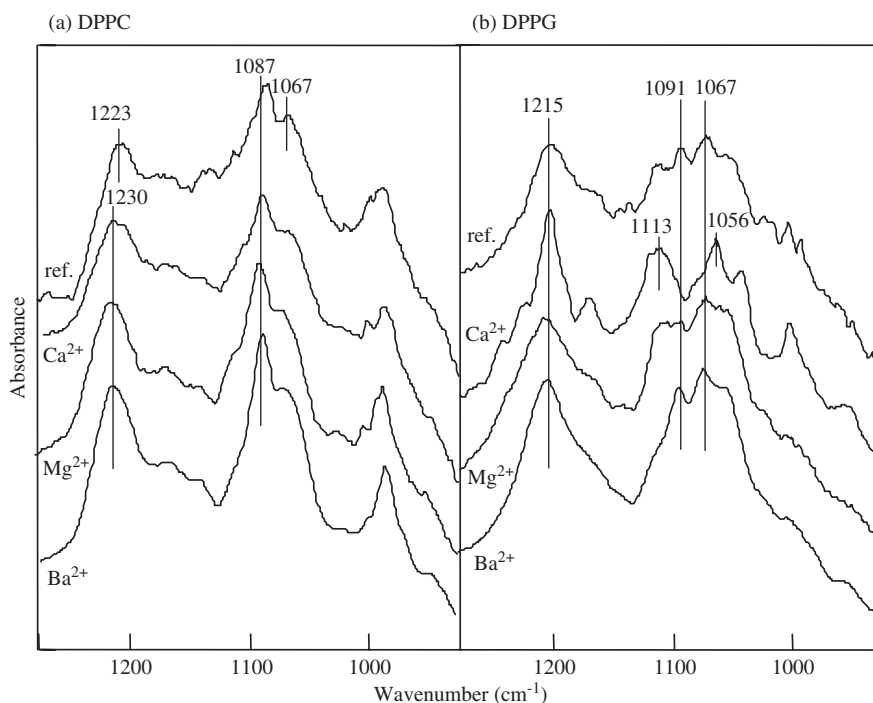


Fig. 13. Infrared spectra of the phosphate-stretching region for (a) DPPC and (b) DPPG liposomes with various ions, Ca^{2+} , Mg^{2+} , and Ba^{2+} (ion to phospholipid molar ratio is 10) at 70°C.

antisymmetric phosphate-stretching peak narrowed and the wavenumber of the symmetric one was observed at a higher side, reflecting the immobilization of the phosphate group as a result of the Ca^{2+} ion binding. The symmetric phosphate-stretching band was split into four bands in the presence of Mg^{2+} , 1120, 1108, 1103, 1095, and 1090 cm^{-1} . The split is attributed to the antiplanar–antiplanar conformation of the torsional angles of the two P–O ester bonds [39]. These splittings may reflect intra- and intermolecular nonequivalence of the ester groups. In the presence of Ba^{2+} , the phosphate band of DPPG was somewhat sharpened. The effects of Ca^{2+} and Mg^{2+} on the DPPG liposome were cumulative, while the effect of Ba^{2+} was not.

The metal ion concentration dependence of the infrared spectra of the symmetric phosphate-stretching region for DPPG liposome was then examined. The DPPG liposome was revealed to be almost independent of Ba^{2+} concentration. This indicates that there is no strong interaction or chelate formation between Ba^{2+} and the phosphate group of DPPG molecules. Being at high Mg^{2+} concentration, the phosphate group remained in a somewhat hydrated state. The symmetric phosphate-stretching band was sharpened due to complete dehydration by Ca^{2+} ion. From these results it can be seen that the ability of metal ions to dehydrate the phosphate group decreases in the order of $\text{Ca}^{2+} \gg \text{Mg}^{2+} > \text{Ba}^{2+}$.

The phase transition temperature estimated by DSC measurement of DPPG liposomes was gradually shifted to 90°C with Ca^{2+} , to 68°C with Mg^{2+} , and to 47°C with Ba^{2+} (metal ion concentration 40 mM). It may be noted that the transition temperature of the hydrated DPPG remains at 50°C in high Mg^{2+} ion concentration solution. This thermogram corresponds to the result of the infrared spectrum of symmetric $-\text{PO}_4^-$ stretching band in which the $-\text{PO}_4^-$ remained in a somewhat hydrated state with Mg^{2+} . These results suggest that the dehydration ability of the metal ion is a contributing factor to shifting the phase transition temperature.

In summary, the infrared spectra revealed that DPPG liposomes are more unstable than DPPC liposomes with changes in temperature and in the presence of metal ions. The dehydration ability of metal ions decreases in the order $\text{Ca}^{2+} \gg \text{Mg}^{2+} > \text{Ba}^{2+}$ in the phosphate ester group of DPPG. The effect of increasing Ca^{2+} and Mg^{2+} concentration is cumulative; however, Ba^{2+} does not demonstrate a concentration dependence. The infrared spectra and DSC thermograms indicate that dehydration is the main cause of the transition temperature shift of liposomes.

8. INTERACTION BETWEEN WATER-SOLUBLE POLYMER AND PHOSPHOLIPID

When liposomes are used as drug carriers and administered into the blood, it is possible to interact with cells and/or blood components [40–43]. The dynamic

behavior of liposomes *in vivo* must be dependent on the interaction between the cell and liposomes. However, only a few studies have been conducted on the physicochemical properties of liposomes, particularly on the interactions between lipid bilayers and cells from a molecular point of view. In fact, investigations on those interactions are unequivocally of great importance, not only practically but theoretically as well.

In this section, chondroitin sulfate (CS), a water-soluble polymer, was used as one of the acidic mucopolysaccharides of the biological membranes [44], and the molecular interactions between CS and phospholipid bilayers with different charges were investigated.

Three types of liposomes were prepared by the Bangham method: uncharged liposomes (Unc.L) composed of DPPC and Chol (molar ratio 7:3), negatively charged liposomes (Neg.L) composed of DPPC, Chol, and DCP (7:3:0.7), and positively charged liposomes (Pos.L) composed of DPPC, Chol, and stearyl amine (SA) (7:3:0.7). The only difference from the liposomes used in Section 5 was the lipid composition. A liposome solution with CS was prepared as follows: given amounts of CS were dissolved in phosphate-buffered saline (PBS), and this was added to the liposomal dispersion. This mixture was incubated at 37°C for 1 h. The final concentration of DPPC was 1 mM.

First, we examine the effect of CS on the zeta potential of three kinds of liposomes. Figure 14 shows the relationship between the zeta potential of liposomes and CS concentration at pH 7.2. In the case of Unc.L and Neg.L, zeta potential was unchanged by the addition of CS. It should be noted, however, that the zeta potential of Pos.L decreased with an increase in the concentration of CS from 18 to -10 mV. This drastic change in the zeta potential of Pos.L (from a positive to a negative value) suggests that CS is adsorbed on the surface of Pos.L due to an electrostatic interaction. These results are supported by the results of gel-filtration chromatography on these liposome–CS systems. Furthermore, the addition of CS to Pos. L solution results in the increasing turbidity of Pos. L, while the turbidity of Unc. L and Neg. L was unchanged, indicating the aggregation of liposomes.

It is well known that uncharged polysaccharides such as dextran and hydroxyethyl starch promote the aggregation of blood cells due to their adsorption [45]. Sunamoto *et al.* [46] reported that polysaccharides, which have straight-chain structure, can aggregate liposomes easily due to the bridging mechanism. Pos.L aggregates by the adsorption of CS due to electrostatic interactions and continuous bridging-structure formation, since CS is a straight-chain molecule.

The effects of CS on the microscopic-state of liposomes was then investigated using 2-AP and 12-AS as fluorescent probes. Figure 15(a) (2-AP probe) and (b) (12-AS probe) show the relation between the fluorescence polarization and the CS concentration. In the Pos.L, which adsorbs CS, both the microviscosity at

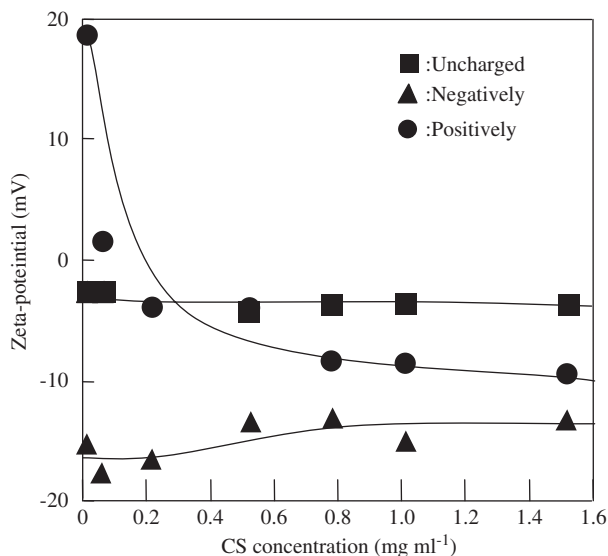


Fig. 14. Relationship between zeta potential of liposomes and CS concentration at 37°C.

the region close to the membrane surface and at the region near the bilayer center were increased with an increase in the CS concentration, whereas the microviscosity of the other liposomes was unchanged. An increase in the microviscosity is caused by the tight packing of lipids, which is dependent on the fluid depression of the acyl chains. When CS is adsorbed on the surface of Pos.L, the fluidity is decreased not only in the head group region but also in the acyl chain region. As a result, the microviscosity, both at the region close to the membrane surface and near the bilayer center, is thought to be increased.

The effect of CS on the phase transition temperature (T_c) of DPPC liposomes was then investigated by DSC measurement. In this experiment, liposomes prepared without Chol were used to measure the T_c clearly. In the case of Unc.L and Neg.L, T_c was not changed with the addition of CS. However, T_c of Pos.L was shifted to a higher temperature by the addition of CS. T_c shift toward the higher temperature results from the increase in the cooperative unit of phase transition.

In summary, the microscopic morphology of liposomes is dramatically changed by the addition of CS to Pos.L, while Unc.L and Neg.L are unchanged. The drastic change in the zeta potential of Pos.L (from a positive to a negative value) suggests that CS is adsorbed on the surface of Pos.L due to the electrostatic interaction. The phase transition temperature of Pos.L is then changed after the addition of CS. However, these values for other liposomes do not change with the addition of CS. These results suggest that CS is adsorbed on the surface of Pos.L and changes the aggregation state significantly.

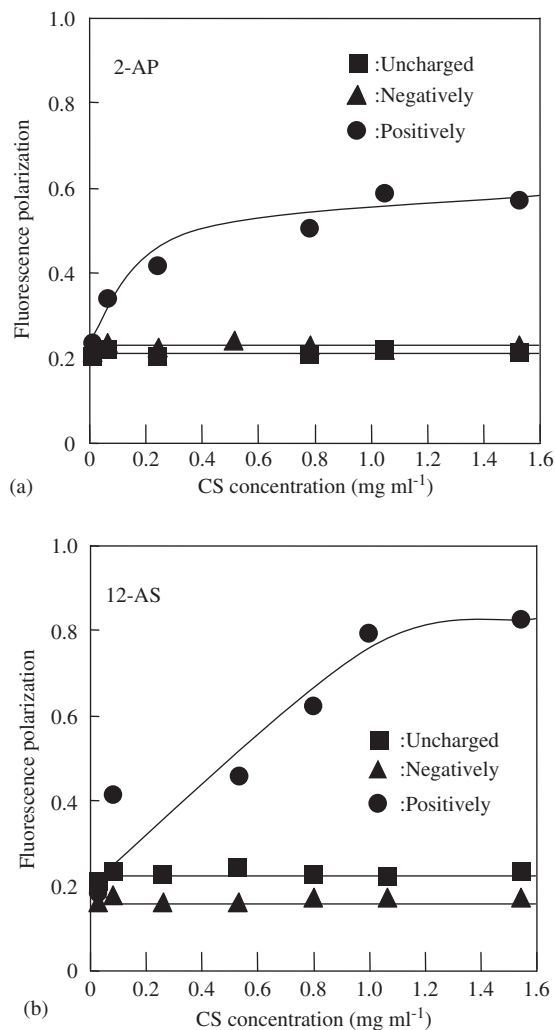


Fig. 15. Relationship between fluorescence polarization of lipid probes ((a) 2-AP and (b) 12-AS) and CS concentration at 37°C.

9. INTERACTION BETWEEN PROTEIN AND PHOSPHOLIPID

When liposomes are administered into the blood, a part of the liposomal bilayer membrane is destroyed by the interaction with components in the blood [47,48]. It is, therefore, important to know the stability and the pharmacokinetics of liposome products in the blood. Serum albumin accounts for 50–55% of all serum protein. In this section, we use bovine serum albumin (BSA) as a model for protein in the blood. The interaction between BSA and liposomal membrane was investigated, and the results were compared with that of lysozyme (LSZ). The isoelectric point of LSZ is 11.1 [49], so LSZ is positively charged in body fluid. The remarkable

difference between LSZ and BSA is the isoelectric point: namely, the isoelectric point of BSA is 4.8 [49], so that BSA is negatively charged in body fluid. It is then interesting to investigate the effect of adsorption of proteins having different amounts of electric charge on liposomal membrane characteristics.

DPPG liposomes, prepared by the Bangham method, were used in this section since the dispersibility of DPPG liposomes is superior to that of the other phospholipid liposomes.

The adsorption isotherms of LSZ and BSA on DPPG liposome are shown in Fig. 16(a) and 16(b), respectively. The adsorption equilibrium of LSZ was attained at a free LSZ concentration of about 20 mg mL^{-1} and the saturated

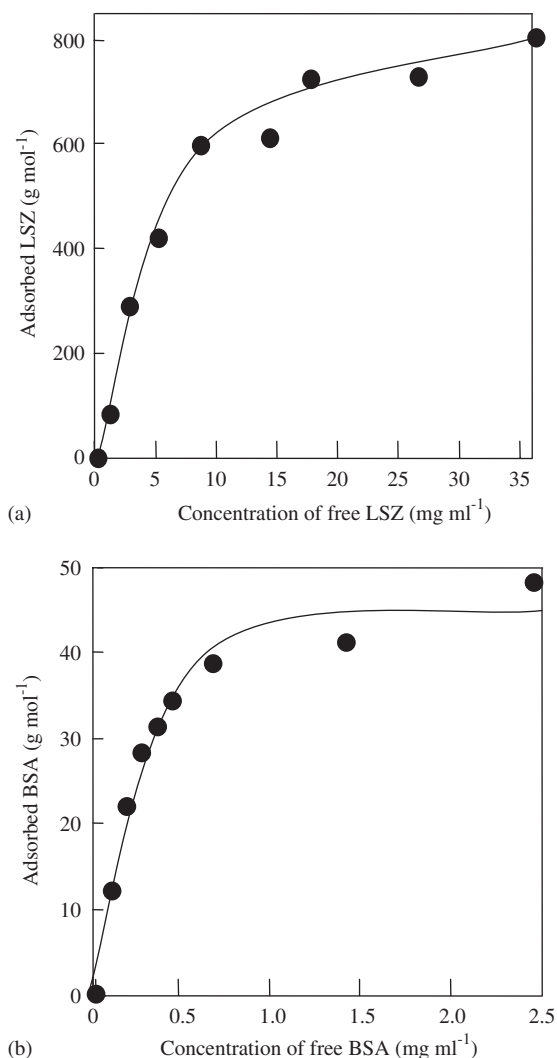


Fig. 16. Adsorption isotherms of (a) LSZ and (b) BSA on DPPG liposomes.

adsorption amount of LSZ was approximately 720 g mol^{-1} of liposomal DPPG, while the adsorption equilibrium of BSA was attained at about 1 mg mL^{-1} free BSA and the saturated adsorption amount of BSA was approximately 44 g mol^{-1} of liposomal DPPG: in other words, the saturated adsorption amount of LSZ on DPPG liposomes was 16 times greater than that of BSA. The molar mass of LSZ is $14,700 \text{ g mol}^{-1}$, while that of BSA is $67,000 \text{ g mol}^{-1}$ [49]. Hence, the greater amount of adsorption of LSZ cannot be explained only by the molecular size.

Since BSA with negative charges adsorbs on negatively charged liposomes, the hydrophobic interactions may cause the adsorption. LSZ is positively charged in the experimental condition (pH 7.4), the greater adsorption amount of LSZ on DPPG liposomes can then be considered to be due probably to an electrostatic interaction between LSZ and DPPG.

The effects of LSZ and BSA on the microviscosity of DPPG liposomal bilayer membranes were investigated by the DPH fluorescent method. Figure 17 shows the relationship between the fluorescence polarization of DPH solubilized in DPPG liposomes and temperature. The fluorescence polarization of DPH in DPPG bilayer membranes dramatically decreased above 41°C , the gel-liquid crystalline phase transition temperature. No significant change was found in phase transition temperature by the addition of LSZ or BSA, whereas the microviscosity of DPPG bilayer membranes above 41°C increased remarkably with increasing concentration of LSZ or BSA. The effect of LSZ on the microviscosity of the DPPG bilayer membranes was greater than that of BSA. The increase in microviscosity in the hydrophobic region of the liposomal bilayer membranes is likely to be due to a restricted swing of DPPG molecules around the LSZ or BSA molecules. The observed increase in microviscosity of DPPG bilayer membranes could then be interpreted as being produced by inhibition of the phase transition from the gel to liquid crystalline state of boundary DPPG molecules. Protein-induced lipid lateral phase separation and protein-induced microdomain formation were observed in the systems of mixed DPPC liposomes including phosphatidylserine or phosphatidic acid [50]. A temporary gap is formed by the phase separation in the lipid bilayer membranes [51], thereby increasing the permeability of the lipid bilayer membranes. We also observed that the percentage of Calcein leaked from DPPG liposomes increased through adsorption of LSZ or BSA on the liposomes. The effect of LSZ on the permeability of the liposomal bilayer membranes was greater than that of BSA. The barrier function of membranes with constituent protein is actually lower than that of lipid membranes without protein [52].

In summary, two kinds of proteins, LSZ and BSA, adsorb on DPPG liposomes. The saturated adsorption amount of LSZ is 16 times larger than that of BSA. The adsorption of LSZ or BSA gives an increase in the microviscosity in the hydrophobic region of liposomal bilayer membranes, and it also causes an increase in the permeability of the membranes. The effect of LSZ on the microviscosity and permeability of liposomal bilayer membranes is larger than that of BSA. These

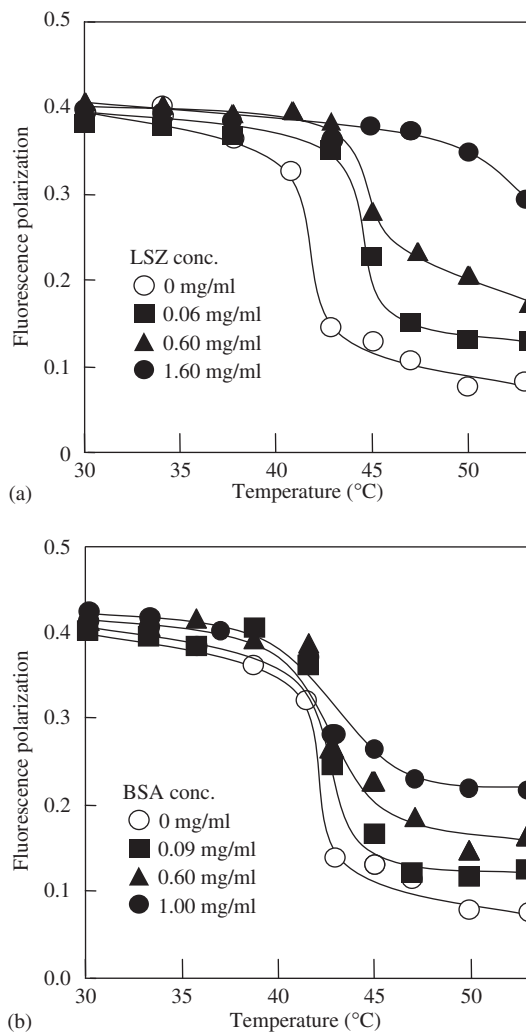


Fig. 17. Relationship between fluorescence polarization (microviscosity of liposomal bilayer membranes) and concentration of added (a) LSZ and (b) BSA.

findings suggest that boundary DPPG makes no contribution to the phase transition and that boundary DPPG and bulk DPPG are in the phase-separated state, thereby increasing the permeability of liposomal bilayer membranes.

10. NOVEL LIPOSOME PREPARATION METHOD USING SUPERCRITICAL CARBON DIOXIDE

The potential use of liposomes as vehicles for drug delivery has generated growing interest, as we explained in the previous sections [53–56]. So far, many

methods have been reported for the preparation of liposomes such as the Bangham method [2], organic solvent injection method [57], and reverse-phase evaporation method [15]. However, these methods need a large amount of organic solvents that are harmful to the environment and the human body. The use of organic solvents must be avoided as much as possible in their preparation, because complete removal of the remaining organic solvent is required. Also, all of these methods are not suitable for mass production of liposomes because they have many steps. Therefore, few examples of effective use of liposomes are known, even though their advantages have been widely recognized.

Supercritical fluids are those fluids that are noncondensable and highly dense at temperatures and pressures beyond the critical values. They are highly functional solvents whose solvent properties can be altered remarkably through control of temperature and pressure. Supercritical carbon dioxide (scCO_2), in particular, has attracted attention as an environment-friendly alternative solvent that can replace organic solvents because it has a low critical temperature ($T_c = 31^\circ\text{C}$) and pressure ($P_c = 73.8\text{ bar}$) and is nontoxic, inflammable, and cheap. This fluid is now widely used in the extraction of physiologically active substances, perfumes, and so forth [58].

In this section, we aim to develop a liposome preparation method that gives liposomes with a high trapping efficiency for water-soluble substances and easily enables production scale-up, using nontoxic and environment-friendly scCO_2 instead of organic solvent.

Figure 18 shows a schematic diagram of the experimental apparatus for liposome preparation. It consists mainly of three parts, a variable volume view cell (model HP-1, Tama Seiki Co.), a HPLC pump (Shodex DS-4) for feeding aqueous solution into the view cell, and a high-pressure pump (model HP-1, Tama

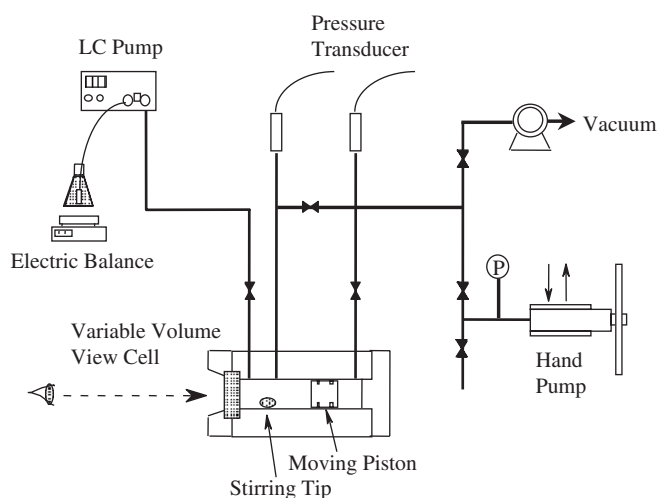


Fig 18. Apparatus for preparation of liposomes.

Seiki Co.) for CO₂ feed and pressure control. The temperature of the view cell is measured and maintained with a temperature controller equipped with a Pt resistance thermometer. Pressures on the front and backsides of the cell are measured with two strain gauges (PG-500KU, Kyowa Co.). The amount of aqueous solution fed into the cell is measured with an electric balance (BX 4200H, Shimadzu Co.). The volume of the view cell is ca. 50 cm³.

Liposome preparation using scCO₂ was performed as follows: After DPPC (0.3 wt.% against CO₂) and ethanol (0–15 wt.% against CO₂) were sealed in the view cell, CO₂ (13.74 g) was introduced into the cell. The cell temperature was then raised to 60°C, a temperature higher than the phase transition temperature (41°C) of DPPC, while the pressure was kept at 200 bar. After several tenths of a minute for equilibration, an aqueous D-(+)-glucose solution (0.2 mol L⁻¹) for measurement of the trapping efficiency for a water-soluble substance was slowly (0.05 mL min⁻¹) introduced into the cell through the HPLC pump till the desired amount of solution was attained. The pressure was then reduced to release CO₂, thereby giving a homogeneous liposome dispersion. The inside of the cell was stirred with a magnetic stirring tip during the experiments.

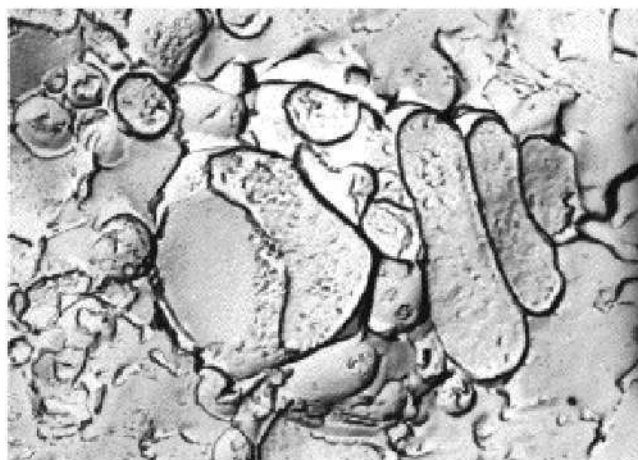
First, the solubility of DPPC without a cosolvent was measured. Visual observations revealed very low solubility of DPPC in scCO₂ (13.749 g). Solid DPPC powder was observed in the bottom of the cell at 60°C and at pressure up to 500 bar. The trapping efficiency was extremely low when water was added to the cell in the presence of solid DPPC. This would suggest a need for complete dissolution of DPPC in scCO₂ for liposome preparation. Thus, the solubility of DPPC in scCO₂ using ethanol as a cosolvent was improved (60°C, 200 bar). When the amount of the ethanol was small, no complete dissolution of DPPC was observed and solid DPPC remained undissolved in the cell bottom. The amount of undissolved DPPC decreased with increasing ethanol concentration, and the lipid completely dissolved in scCO₂ above 7 wt.% addition. On the basis of this finding, the experiments were carried out thereafter at 7 wt.% ethanol addition against scCO₂ because the addition of a higher amount of ethanol is known to prevent liposome formation.

Liposome preparation was conducted by introducing water into a homogeneous mixture of scCO₂, DPPC, and ethanol. While the amounts of introduced water were small, the inside of the cell remained transparent with no appearance of a water phase. When the amount of introduced water was increased, the inside of the cell became opaque. This would indicate that DPPC forms reverse micelles (W/CO₂ microemulsion) at small amounts of introduced water and the microemulsion turns to a macroemulsion as the amount of introduced water increases. With a further increase in the amount, the introduced water gave a water phase in the cell bottom. The water phase was initially transparent and became turbid when more water was introduced with vigorous stirring. As already reported, the change of the phase state from W/CO₂ to CO₂/W emulsion in scCO₂/water/surfactant three-component systems depends on the

amount of introduced water [59]. The turbid aqueous phase observed in our system may contain liposome or CO₂/W emulsion. If this were the case, by analogy with the reverse-phase evaporation, liposomes would have been formed in the water phase through the phase inversion from CO₂/W emulsion to liposomes in the pressure reduction process. Therefore, we gave the name *super-critical reverse phase evaporation* (scRPE) method to our method of liposome preparation.

Figure 19 shows typical freeze-fracture electron micrographs of liposomes (DPPC concentration 10 mM) prepared by the scRPE method. The bar length was 400 nm. The figure shows large ellipsoidal unilamellar liposomes (LUV) with diameter of 0.1–1.2 μm. The reason the liposomes have an ellipsoidal shape is their low stability compared with spherical multilamellar liposomes (MLV). An increasing tendency was also found for the shape of liposomes to become spherical with decreasing liposome size. These findings demonstrate that the scRPE method allows an efficient preparation of LUV.

Figure 20 shows the DPPC concentration dependence of the trapping efficiency of liposomes prepared by the scRPE method for glucose. The abscissa represents the amount of DPPC against the volume of added glucose solution, and the concentration of DPPC becomes higher when the volume of glucose solution introduced into the cell is lower. For comparison, the figure also shows the DPPC concentration dependence of the trapping efficiency of liposomes prepared by the Bangham method (MLV). The trapping efficiency of the former was more than five times higher than that of the latter. Also, it was as high as those of LUV prepared by the conventional reverse-phase evaporation method



400 nm

Fig. 19. Freeze-fracture electron micrographs of liposomes prepared by scPRE method.

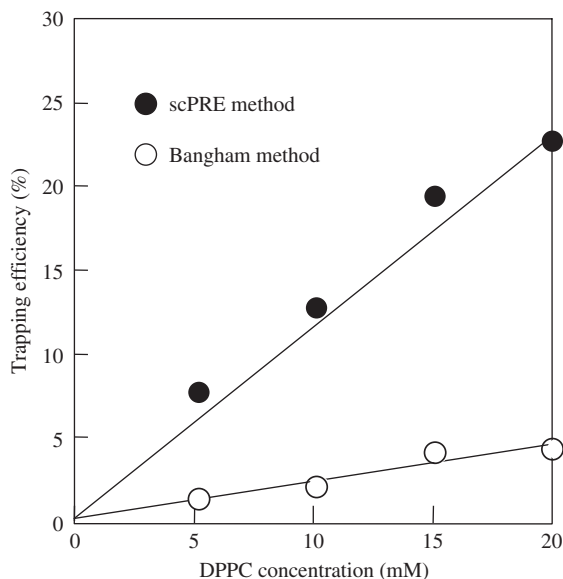


Fig. 20. Relationship between trapping efficiency of liposomes and DPPC concentration.

and the freezing–melting method when a comparison was made at the same DPPC concentration (20 mM).

In general, the trapping efficiency of liposomes (more exactly, their inner aqueous phase) depends on physicochemical properties such as the size and the number of bilayers of liposomes and it is higher for those consisting of a smaller number of bilayers. This difference in the structure then results in the higher trapping efficiency of liposomes prepared by the scRPE method than that of multilamellar liposomes prepared by the Bangham method.

Frederiksen *et al.* [60] have reported a method for preparation of liposomes using scCO₂. They prepared LUV with a diameter of about 200 nm by a rapid expansion of a homogeneous scCO₂/phospholipid/ethanol mixture and simultaneous mixing with an aqueous solution succeeded by passing the resultant gas/water mixture through a specially designed mixing column. Their method can then be regarded as a rapid expansion of supercritical solution (RESS) method. The trapping efficiency of the LUV for fluorescein isothiocyanate-dextran (FITC-dextran) was $20 \pm 5\%$, which is as high as our result on glucose. In contrast to their method, the scRPE method we have developed truly uses supercritical fluids. At the same time, the diameter of liposomes obtained ranges from 0.1 to 1.2 μm and is considerably larger than the diameter of liposomes prepared by their method. Moreover, the amount of carbon dioxide needed in our preparation method seems smaller than that needed in Frederiksen *et al.*'s study.

In summary, we have succeeded in preparing LUV with diameters from 0.1 to 1.2 μm and a high-trapping efficiency for a water-soluble substance using

environment-friendly scCO_2 in the absence of organic solvent toxic to the human body. We also make it possible to control the size and lamellarity of liposomes by changing the preparation pressure and the amount of ethanol [55]. Our method would enable encapsulation with ease into liposomes proteins and genes that are denatured through contact with organic solvent. Because the method is of only one step and uses no inflammable, volatile, or toxic organic solvent, scale-up of liposome production would be easy. Therefore, we believe that the method will greatly contribute to putting liposomes into practical use.

REFERENCES

- [1] M. Abe, T. Hiramatsu, H. Uchiyama, H. Yamauchi, K. Ogino, Molecular interactions between phospholipid and nonionic surfactants in a lipid bilayer, *J. Jpn. Oil Chem. Soc.* 41 (1992) 136–141.
- [2] A.D. Bangham, M.M. Standish, J.C. Watkins, Diffusion of univalent ions across the lamellae of swollen phospholipids, *J. Mol. Biol.* 13 (1965) 238–252.
- [3] M. Takayama, S. Itoh, T. Nagasaki, I. Tanimizu, A new enzymatic method for determination of serum choline-containing phospholipids, *Clin. Chem. Acta* 79 (1977) 93–98.
- [4] P.R. Strom-Jensen, R.L. Magin, F. Dunn, Ultrasonic evidence for structural relaxation in large unilamellar liposomes, *Biochim. Biophys. Acta* 769 (1984) 179–186.
- [5] D.A. Tyrrel, T.D. Heath, C.M. Colley, B.E. Ryman, New aspects of liposomes, *Biochim. Biophys. Acta* 457 (1976) 259–302.
- [6] Y. Matsumoto, C. Imamura, T. Ito, C. Taniguchi, R. Ueoka, Specific hybrid liposomes composed of phosphatidylcholine and polyoxyethylenealkyl ether with markedly enhanced inhibitory effects on the growth of tumor-cells *in-vitro*, *Biol. Pharm. Bull.* 18 (1995) 1456–1458.
- [7] Y. Matsumoto, T. Kato, Y. Kemura, M. Tsuchiya, M. Yamamoto, R. Ueoka, Intracellular response of hybrid liposomes against leukemia cells related to apoptosis with antitumor activity, *Chem. Lett.* (1999) 53–54.
- [8] M. Abe, Y. Takao, T. Yamamoto, K. OK. Kwon, H. Yamauchi, K. Ogino, Molecular interactions between phospholipid and lipophilic substances in a lipid bilayer, *J. Jpn. Oil Chem. Soc.* 41 (1992) 404–409.
- [9] M. Abe, A. Shimizu, K. Ogino, Dielectric properties of solutions of oily materials solubilized by sodium dodecyl sulfate in aqueous solutions, *J. Colloid Interface Sci.* 88 (1982) 319–325.
- [10] M. Abe, Y. Tokuoaka, H. Uchiyama, K. Ogino, Solubilization of synthetic perfumes by sodium dodecyl sulfate, *J. Jpn. Oil Chem. Soc.* 39 (1990) 565–571.
- [11] K. Kalyanasundaram, J.K. Thomas, Environmental effects on vibronic band intensities in pyrene monomer fluorescence and their application in studies of micellar systems, *J. Am. Chem. Soc.* 30 (1977) 2039–2044.
- [12] H. Yamauchi, Y. Takao, M. Abe, K. Ogino, Molecular interactions between lipid and some steroids in a monolayer and a bilayer, *Langmuir* 9 (1993) 300–304.
- [13] Y. Takao, H. Yamauchi, J. Manosroi, A. Manosroi, M. Abe, Molecular interactions between lipids and some steroids in a monolayer and a bilayer 2, *Langmuir* 11 (1995) 912–916.
- [14] M. Abe, K. Hashizaki, Y. Yokouchi, Y. Takao, J. Manosroi, A. Manosroi, H. Sakai, S. Yokoyama, H. Yamauchi, Effects of steroids and vitamin D_3 on the permeability of liposomal bilayer membranes, *J. Jpn. Oil Chem. Soc.* 48 (1999) 215–220.
- [15] F. Szoka Jr., D. Papahadjopoulos, Procedure for preparation of liposomes with large internal aqueous space and high capture by reverse-phase evaporation, *Proc. Natl. Acad. Sci. USA* 75 (1978) 4194–4198.

- [16] K. Ogino, M. Goto, M. Abe, Interaction between L- α -phosphatidylcholines and water molecules, *Jpn. Oil Chem. Soc.* 37 (1988) 640–647.
- [17] A. Sekiguchi, H. Yamauchi, A. Manosroi, J. Manosroi, M. Abe, Molecular interactions between phospholipids and glycolipids in a lipid bilayer, *Colloids Surf. B* 4 (1995) 287–296.
- [18] A. Sekiguchi, K. Ogino, H. Yamauchi, M. Abe, Molecular interactions between phospholipids and sphingoglycolipids in a lipid bilayer, *J. Jpn. Oil Chem. Soc.* 44 (1995) 184–191.
- [19] R.S. Spangler, R.L. Treadway, J.M. Higgins, Selective insulinization of the liver by means of targeted liposomes in conscious diabetic dogs, *Diabetologia* 27 (1984) 333–334.
- [20] D.H. Boldt, S.F. Speckart, R.L. Richards, C.R. Alving, Interactions of plant lectins with glycolipids in liposomes, *Biochem. Biophys. Res. Commun.* 74 (1977) 208–214.
- [21] A. Yoshida, A. Manosroi, J. Manosroi, H. Yamauchi, M. Abe, Molecular interactions between phospholipids and mangostin in a lipid bilayer, *Colloids Surf. B* 4 (1995) 423–432.
- [22] W. Mahabusarakam, P. Wiriyachitra, W.C. Taylor, Chemical-constituents of *Garcinia mangostana*, *J. Nat. Prod.* 50 (1987) 474–478.
- [23] C. Gopalakrishnan, D. Shankaranarayanan, L. Kameswaran, S.K. Nazimudeen, Effect of mangostin, a xanthone from *Garcinia mangostana* Linn. in immunopathological and inflammatory reactions, *Indian J. Exp. Biol.* 18 (1980) 843–846.
- [24] T. Inoue, Y. Muraoka, K. Fukushima, R. Shimozaawa, Interaction of surfactants with vesicle membrane of dipalmitoylphosphatidylcholine: fluorescence depolarization study, *Chem. Phys. Lipids* 46 (1988) 107–115.
- [25] K. Kinoshita, K. Mihashi, Application of Fluorescence Spectrometry to Biochemistry Research, Gakkai Shuppansha, Tokyo, 1988, p. 19.
- [26] T. Imura, H. Sakai, H. Yamauchi, C. Kaise, K. Kozawa, S. Yokoyama, M. Abe, Preparation of liposomes containing ceramide 3 and their membrane characteristics, *Colloids Surf. B* 20 (2001) 1–8.
- [27] T. Imura, H. Sakai, H. Yamauchi, K. Kozawa, S. Yokoyama, M. Matsumoto, M. Abe, Atomic force microscopic study on the surface properties of phospholipids monolayers containing ceramide 3, *Colloids Surf. B* 19 (2000) 81–87.
- [28] T. Imura, H. Sakai, H. Yamauchi, C. Kaise, M. Matsumoto, K. Kozawa, S. Yokoyama, M. Abe, Domain formation and phase separation in mixed phosphatidylcholine/ceramide 3 monolayers and bilayers, *J. Jpn. Oil Chem. Soc.* 49 (2000) 373–377.
- [29] P. Perugini, I. Genta, F. Pavanetto, B. Conti, S. Scalia, A. Baruffini, Study on glycolic acid delivery by liposomes and microspheres, *Int. J. Pharm.* 196 (2000) 51–61.
- [30] G.M.M. El Maghraby, A.C. Williams, B.W. Barry, Skin delivery of oestradiol from deformable and traditional liposomes: mechanistic studies, *J. Pharm. Pharmacol.* 51 (1999) 1123–1134.
- [31] G. Imokawa, A. Abe, K. Jin, Y. Higaki, M. Kawashima, A. Hidano, Decreased level of ceramides in stratum corneum of atopic dermatitis: an etiologic factor in atopic dry skin? *J. Invest. Dermatol.* 96 (1991) 523–526.
- [32] K. OK, Kwon, M.J. Kim, M. Abe, T. Ishinomori, K. Ogino, Thermotropic behavior of a phospholipid bilayer interaction with metal ions, *Langmuir* 10 (1995) 1415–1420.
- [33] K. OK, Kwon, M. Abe, K. Ogino, M.J. Kim, H. Oshima, Effects of calcium ions on phospholipids aggregates at subzero temperatures, *Colloids Surfaces B* 3 (1994) 25–30.
- [34] K. OK, Kwon, M. Abe, K. Ogino, M.J. Kim, H. Oshima, Calcium ion adsorption on phospholipid bilayers, *J. Jpn. Oil Chem. Soc.* 43 (1994) 23–30.
- [35] K. OK, Kwon, M. Abe, T. Ishinomori, K. Ogino, Effects of divalent metal ions on hydration of phospholipid molecules, *J. Jpn. Oil Chem. Soc.* 43 (1994) 403–408.
- [36] T. Ozawa, M. Fukuda, M. Nara, A. Nakamura, Y. Komine, K. Kohama, Y. Umezawa, How can Ca²⁺ selectively activate recovering in the presence of Mg²⁺? Surface plasmon resonance and FT-IR spectroscopic studies, *Biochemistry* 39 (2000) 14495–14503.

- [37] S.A. Shavnin, M.C.P. Delima, J. Fedor, P. Wood, J. Bentz, N. Duzgunes, Cholesterol affects divalent cation-induced fusion and isothermal phase transitions of phospholipid membranes, *Biochim. Biophys. Acta* 946 (1988) 405–416.
- [38] S. Choi, W. Ware Jr., S.R. Lauterbach, W.M. Phillips, Infrared spectroscopic studies on the phosphatidylserine bilayer interacting with calcium ion: effect of cholesterol, *Biochemistry* 30 (1991) 8563–8568.
- [39] H.L. Casal, H.H. Mantsch, H. Hauser, Infrared studies of fully hydrated saturated phosphatidylserine bilayers: effect of lithium and calcium, *Biochemistry* 26 (1987) 4408–4416.
- [40] A. Yoshida, H. Yamauchi, H. Sakai, N. Kawashima, M. Abe, Molecular interactions between lipid bilayers and a water-soluble polymer, *Colloids Surfaces B* 8 (1997) 333–342.
- [41] A. Yoshida, K. Hashizaki, M.E. Mahdy, H. Yamauchi, H. Sakai, S. Yokoyama, M. Abe, Molecular interactions between surface-modified lipid bilayers and a water-soluble polymer, *J. Jpn. Oil Chem. Soc.* 47 (1998) 1323–1329.
- [42] A. Yoshida, K. Hashizaki, H. Yamauchi, H. Sakai, S. Yokoyama, M. Abe, Effect of lipid with covalently attached poly(ethylene glycol) on the surface properties of liposomal bilayer membrane, *Langmuir* 15 (1999) 2333–2337.
- [43] K. Hashizaki, C. Itoh, H. Sakai, S. Yokoyama, H. Taguchi, Y. Saito, N. Ogawa, M. Abe, Freeze-fracture electron microscopic and calorimetric studies on microscopic states of surface-modified liposomes with poly(ethylene glycol) chains, *Colloids Surf. B* 17 (2000) 275–282.
- [44] Q. Wang, J.S. Dordick, R.J. Linhardt, Synthesis and application of carbohydrate-containing polymers, *Chem. Mater.* 14 (2000) 3232–3244.
- [45] M. Minetti, P. Aducci, V. Viti, Interaction of neutral polysaccharides with phosphatidylcholine multilamellar liposomes: phase transitions studied by the binding of fluorescein-conjugated dextrans, *Biochemistry* 18 (1979) 2541–2548.
- [46] J. Sunamoto, K. Iwamoto, H. Kondo, S. Shinkai, Liposomal membranes. 6. Polysaccharide-induced aggregation of multilamellar liposomes of egg lecithin, *J. Biochem.* 88 (1980) 1219–1226.
- [47] T. Tsunoda, T. Imura, M. Kadota, T. Yamazaki, H. Yamauchi, K. OK, Kwon, S. Yokoyama, H. Sakai, M. Abe, Effects of lysozyme and bovine serum albumin on membrane characteristics of dipalmitoylphosphatidylglycerol liposomes, *Colloids Surfaces B* 20 (2001) 155–163.
- [48] Y. Yokouchi, T. Tsunoda, T. Imura, H. Yamauchi, S. Yokoyama, H. Sakai, M. Abe, Effect of adsorption of bovine serum albumin on liposomal membrane characteristics, *Colloids Surf. B* 20 (2001) 95–103.
- [49] H. Zhu, M. Nyström, Cleaning results characterized by flux, streaming potential and FTIR measurements, *Colloids Surf. A* 138 (1998) 309–321.
- [50] A. Raudino, F. Castelli, A thermodynamic study of protein-induced lipid lateral phase-separation -effect of lysozyme on mixed lipid vesicle, *Colloid Polym. Sci.* 270 (1992) 1116–1123.
- [51] D. Kashchiev, D. Exerowa, Bilayer lipid membrane permeation and rupture due to hole formation, *Biochim. Biophys. Acta* 732 (1983) 133–145.
- [52] A.T.M. Van der Steen, B. De Kruijff, J. De Gier, Glycophorin incorporation increases the bilayer permeability of large unilamellar vesicle in a lipid-dependent manner, *Biochim. Biophys. Acta* 691 (1982) 13–23.
- [53] K. Otake, T. Imura, H. Sakai, M. Abe, Development of a new preparation method of liposomes using supercritical carbon dioxide, *Langmuir* 17 (2001) 3898–3901.
- [54] T. Imura, K. Otake, S. Hashimoto, T. Gotoh, M. Yuasa, S. Yokoyama, H. Sakai, J.F. Rathman, M. Abe, Preparation and physicochemical properties of various soybean lecithin liposomes using supercritical reverse phase evaporation method, *Colloids Surf. B* 27 (2002) 133–140.
- [55] T. Imura, T. Gotoh, K. Otake, S. Yoda, Y. Takebayashi, S. Yokoyama, H. Takebayashi, H. Sakai, M. Yuasa, M. Abe, Control of physicochemical properties of liposomes

- using a supercritical reverse phase evaporation method, *Langmuir* 19 (2003) 2021–2025.
- [56] T. Imura, T. Gotoh, S. Yoda, K. Otake, H. Takebayashi, M. Yokosuka, H. Sakai, M. Abe, Development of continuous batch system for mass production of liposomes, *Mater. Technol.* 21 (2003) 30–35.
- [57] S. Batzri, E.D. Korn, Single bilayer liposomes prepared without sonication, *Biochim. Biophys. Acta* 298 (1973) 1015–1019.
- [58] M. Poiana, R. Fresa, B. Mincione, Supercritical carbon dioxide extraction of bergamot peels: extraction kinetics of oil and its components, *Flavour Fragrance J.* 14 (1999) 358–366.
- [59] C.T. Lee Jr., P.A. Psathas, K.P. Johnston, Water-in-carbon dioxide emulsions: formation and stability, *Langmuir* 15 (1999) 6781–6791.
- [60] L. Frederiksen, K. Anton, P. van Hoogevest, H.R. Keller, H. Leuenberger, Preparation of liposomes encapsulating water-soluble compounds using supercritical carbon dioxide, *J. Pharm. Sci.* 86 (1997) 921–928.

This page intentionally left blank

Cell-Mimicking Supramolecular Assemblies Based on Polydiacetylene Lipids: Recent Development as “Smart” Materials for Colorimetric and Electrochemical Biosensing Devices

Chunyan Sun¹ and Jinghong Li^{1,2,*}

¹*State Key Laboratory of Electroanalytical Chemistry, Changchun Institute of Applied Chemistry, Chinese Academy of Sciences, Changchun 130022, China*

²*Department of Chemistry, Tsinghua University, Beijing 100084, China*

Contents

1. Introduction	230
2. Supramolecular Biosensing Assemblies Based on Polydiacetylenes and their Chromism	231
3. Application in Biosensing Devices	233
3.1. Colorimetric detection of molecular recognition interactions between receptor and ligand	233
3.1.1. Colorimetric detection of virus and toxin	233
3.1.2. Colorimetric detection of physiological ions	237
3.1.3. Rapid colorimetric screening of the activities of antibacterial peptides	239
3.1.4. Rapid screening of membrane penetration enhancers	240
3.1.5. Colorimetric detection of small molecules	241
3.2. Colorimetric detection of enzymatic catalysis	241
3.3. Colorimetric immunoassay	242
3.4. Electrochemical biosensors	245
4. Conclusions and Outlook	248
Acknowledgement	249
References	249

Abstract

Design and synthesis of simplified models of cell membranes that mimic their self-organization and functions represent great technical challenge, yet have opened doors to innovative diagnostic and therapeutic methods. Functionalized supramolecular polydiacetylene (PDA) assemblies exhibit unique blue–red colorimetric transitions upon specific interactions with a variety of biological analytes in aqueous solutions. The chemical assemblies include conjugated PDA, responsible for the chromatic transitions, and the molecular recognition elements, which are either chemically or physically associated with the PDAs. The supramolecular assemblies therefore integrate both molecular recognition and signal transduction functions. Langmuir–Blodgett thin films and vesicle bilayers

*Corresponding author. Tel./Fax: +86-10-62795290;
E-mail: jhli@mail.tsinghua.edu.cn

provide ideal configurations for precise delivery of the biological binding entity to the sensing interface, and for control of molecular orientation for effective biomolecular interaction. By incorporation of specific recognition elements, the systems based on PDAs have proved to be versatile and sensitive sensors for a wide range of biological analytes, including viruses, toxins, ions, antibacterial peptides, membrane penetration enhancers, interfacial enzymatic catalysis, and antibodies. The rapid and specific color transitions observed in the “smart” PDA systems will open wide-range of possibilities for biosensor, drug discovery, and diagnostic applications.

1. INTRODUCTION

From the materials science point of view, the biological cell membrane may be considered a highly evolved self-assembled biosensing system that integrates molecular recognition and signal transduction functions. The surface of the membrane is heavily functionalized with recognition molecules, primarily in the forms of glycosylated lipids and proteins. These recognition sites specifically recognize other molecules or other cell surfaces, resulting in a cascade of events such as the opening of ion channels, activation of cellular enzymes, or altering the rate of transport, secretion, or oxidative metabolism. Design, synthesis, and characterization of functional supramolecular assemblies that mimic the self-organization and functions of the cell membrane have advanced substantially in the past two decades [1,2]. Significant progress has been made in exploitation and manipulation of molecular self-organization properties, incorporation of molecular recognition capacities into supramolecular systems, and development of novel membrane-mimicking materials [3]. Mimicking cell membrane, particularly in its biomolecular recognition properties, can facilitate development of new diagnostic and therapeutic devices.

Polymerizable amphiphiles have been used as the building blocks of Langmuir–Blodgett (LB) thin films and liposomes since the late 1970s [4]. Polymerized molecular assemblies are attractive candidates for biological applications because of their enhanced stability compared to their non-polymerized counterparts. Polydiacetylenes (PDAs) form a unique class of polymeric materials that couple highly aligned and conjugated backbones with tailorable pendant side groups and terminal functionalities. They can be structured in the form of bulk materials [5], multilayer and monolayer films [6,7], polymerized vesicles [8,9], and even incorporated into inorganic host matrices to form nanocomposites [10,11]. The unique optical and electrical properties of these conjugated PDA polymers can be exploited for many applications, for example, as “smart” materials for biosensing [3,12–14]. The artificial mimic membranes based on PDAs (thin films and liposomes) are constructed to resemble natural cell membranes at the interfacial region by being chemically modified with bio-recognition molecules, and the π -conjugation of the polymer’s backbone signals analyte binding by undergoing a color transition. Therefore, the ligand-modified PDA supramolecular assemblies are analogous to the cell membrane in which molecular

recognition is directly linked to signal transduction within a single supramolecular assembly.

Herein, we simply summarize the essential properties of PDAs, and then briefly review the diverse applications of cell-mimicking supramolecular assemblies based on PDAs for optical and electrochemical biosensing and simultaneously summarize our recent investigations in this area.

2. SUPRAMOLECULAR BIOSENSING ASSEMBLIES BASED ON POLYDIACETYLENES AND THEIR CHROMISM

The PDA polymer is formed by 1,4 addition of the diacetylene monomers, initiated by 254 nm UV irradiation. The photopolymerization occurs *via* topochemical polymerization from a well-ordered solid state, leading to extremely linear, aligned polymerized domains. The resulting polymer, which has a conjugated backbone of alternating triple and double bonds, is intensely colored, typically a deep blue. The conjugated polymer backbone has a unique visible absorption caused by a $\pi \rightarrow \pi^*$ electronic transition, the frequency of which is dependent on the effective conjugation length within the polymer structure. Previous studies have shown the existence of two predominant phases (blue and red phases) and the occasional occurrence of an additional phase (purple phase) in PDA molecular assemblies, and these phases have been identified based on their color. The blue phase shows an absorption transition centered at ~ 640 nm, with the purple and red phases centered at ~ 600 and ~ 540 nm, respectively. These transitions result from the excitonic absorption of the polymer backbone, where the conjugation length of the red form is diminished relative to the blue form.

The most attractive aspect of PDAs is the chromogenic transition they exhibit. The PDA materials have been shown to undergo visible color transitions from blue to red in response to a variety of environmental perturbations, including optical exposure (photochromism) [15], heat (thermochromism) [16–19], applied stress (mechanochromism) [20,21], changes in chemical environment such as pH [17,18,22] or solvent [23]. While the mechanism of the blue–red color transitions is not fully elucidated, it is generally believed that the transition arises from changes in the conjugation length and bond angle of the PDA backbone. Additionally, small conformational changes in the polymer side chains can also affect the electronic properties of the polymer backbone.

Charych *et al.* [7,8,24] have found that self-assembled structures of PDAs undergo similar chromatic transitions in response to specific molecular recognition events occurring at the interface of the materials. The color transition is triggered when “receptor-lipid” molecules incorporated into the PDA matrix bind specifically to virus or protein molecules. This process is called biochromic induction (affinochromism/biochromism). In this case, the conjugated polymer backbone serves as an optical probe to detect the specific receptor–ligand

interaction. This is a simplified pathway that mimics the more complex signal transduction pathways of biological membranes.

Biochromism was evaluated by colorimetric response (CR) through visible absorption spectra, which is a quantitative scale for the extent of blue–red transition. The visible absorption spectrum of the film (or a liposome solution) before exposure to virus was analyzed as B_0 equation (1), which is defined as the absorption intensity of blue phase divided by the sum of the absorption intensities of the blue and red phases. The film that was exposed to virus was analyzed in the same way as B_1 (equation (2)), which represents the new ratio of absorbance intensities after incubation with the virus. The CR of a film is defined as the percentage change in B upon exposure to virus (equation (3)). In principle, higher CR values indicate more reddish appearance of the film or liposome solution, compared to the blue control sample. A relative color change of 10% or more is observed clearly with the naked eye.

$$B_0 = I_{\text{blue}} / (I_{\text{red}} + I_{\text{blue}}) \text{ initially} \quad (1)$$

$$B_1 = I_{\text{blue}} / (I_{\text{red}} + I_{\text{blue}}) \text{ after exposure to the virus} \quad (2)$$

$$\text{CR} = [(B_0 - B_1) / B_0] \times 100\% \quad (3)$$

The potential flexibility in the chemical and architectural features of diacetylene self-assembling materials allows investigation of a variety of design strategies for the colorimetric sensors. So far, biosensors based on PDA matrices have been constructed mainly in two molecular architectures: liposomes in solution, which are spherically closed lipid lamellar structures enclosing an aqueous compartment, much as do cell membranes; and LB monolayers on solid supports, which consist of organized thin films with molecular-scale control of packing, orientation, and thickness. All architectures have two common components: a biological element that recognizes target analyte molecules, and a physical transducer (the conjugated polymer backbone), which translates molecular recognition into a measurable colorimetric shift. By suitable modification of receptor structure, PDA-based supramolecular assemblies can be used to the analysis of various biomolecular recognitions at cellular membranes, ligand–receptor-binding events, and other processes having biotechnological significance.

In addition to these two supramolecular architectures, two different approaches have been used to functionalize the surface of the assemblies with recognition element. First, the diacetylene monomer lipid can be directly derivatized with the appropriate receptor by synthetic coupling, allowing direct cross-linking of the “receptor-lipid” with the surrounding PDA matrix. Specific, desirable properties can be built into the receptor-lipid molecule to enhance binding and stability. Alternatively, a receptor molecule can be non-covalently incorporated into the PDA matrix in a manner analogous to the heterogeneous mixing of molecules in cell membranes. The second approach avoids potentially complex procedures involved in the synthesis of receptors attached to the diacetylene lipids.

3. APPLICATION IN BIOSENSING DEVICES

Apart from the enhanced stability provided by the polymerized backbone, the unique optical and electronic properties of PDAs can be exploited for many biological applications. Several groups, starting with Charych *et al.* [3,12–14] have produced a substantial body of work demonstrating the use of PDAs as specific colorimetric detectors of biological interactions.

3.1. Colorimetric detection of molecular recognition interactions between receptor and ligand

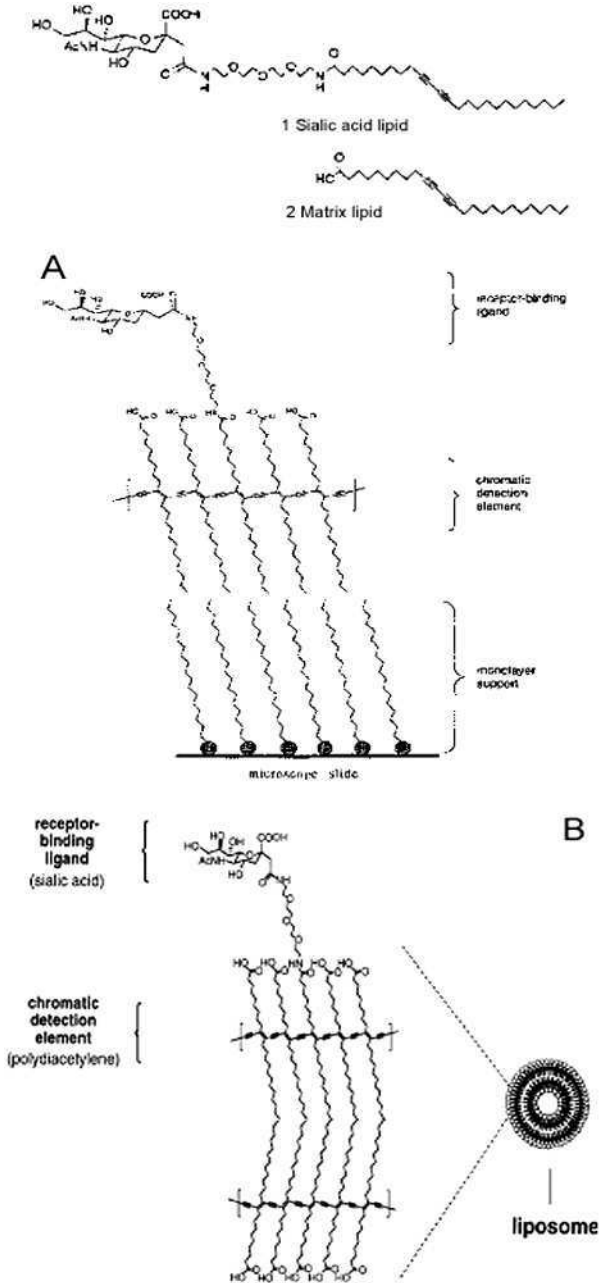
3.1.1. Colorimetric detection of virus and toxin

Charych *et al.* [7,8,24] have derivatized 10,12-pentacosadiynoic acid (PCDA, compound 2 in Scheme 1) with a variety of biologically active molecules such as amino acids, carbohydrates, and biotin. These derivatized diacetylene monomers, such as sialic acid lipid (compound 1 in Scheme 1), can be covalently incorporated into mixed, polymerized thin films or liposomes. Receptor–ligand interactions occurring at the surface of these assemblies, such as the binding of influenza virus to sialic acid, could induce an irreversible biochromic transition. Thus, binding and detection occur within the same supramolecular assembly.

The bilayer assembly (Scheme 1A) is composed of a self-assembled monolayer (SAM) of octadecyltriethoxysilane and a LB monolayer of sialic acid lipid mixed with matrix lipid PCDA [24]. Exposure to influenza virus drastically altered the optical properties of sialic acid-functionalized PDA assemblies. Initially, the film has an absorption maximum at 620 nm and appears blue. After incubation of the film with influenza virus (PBS buffer, pH 7.4), it appears red and the absorption maximum shifts to 550 nm.

The PDA monomers can also be assembled into liposomes (Scheme 1B) by probe or water bath sonication [8]. Relative to blue liposomes, purple liposomes underwent more sensitive biochromism in response to influenza virus. The susceptibility of the liposomes to red-phase conversion in biochromism was clearly enhanced as the material was irradiated longer, suggesting a cooperative effect for the blue–red transition and metastability of the blue form.

For both architectures of thin film and liposomes, control experiments demonstrate the PDA color transition arising from receptor–ligand affinity binding (affinochromism) rather than thermal annealing (thermochromism). No color change was observed when the blue film (or liposomes) was incubated with a blank solution of PBS buffer; similarly, the color of the system remained blue after exposure to virus if the sialic acid lipid 1 was removed from the molecular assembly. Additionally, the specific nature of the interaction between the influenza virus and the sialic acid-functionalized PDA assemblies was also confirmed by competitive inhibition assays. The addition of an excess of monomeric



Scheme 1. Schematic diagrams of (A) the polymerized bilayer assembly and (B) liposome prepared from mixtures of lipids 1 and 2. These assemblies were functionalized with a carbohydrate capture molecule, sialic acid, which binds to the influenza virus lectin, hemagglutinin. The conjugated polymer backbones of alternating double and triple bonds constitute the chromatic detection element. A variety of capture molecules may be co-assembled with or grafted onto the PDA-assemblies. (Scheme 1A was adapted with permission from ref. [7], Fig. 1; Scheme 1B was adapted with permission from Ref. [12], Fig. 2.)

α -O-methyl sialic acid resulted in no color change due to competitive inhibition. As expected, no inhibition was observed with β -O-methyl sialic acid or glucose that does not compete for binding to viral hemagglutinin. The response of the colorimetric biosensors is directly proportional to the quantity of target analyte, influenza virus. Vesicular sensors for influenza virus are more sensitive than thin film sensors. An amount of virus giving a 30% CR in thin film sensors can typically induce \sim 80% CR values in similarly constructed vesicle sensors [3].

PDA thin films and liposomes functionalized with sialic acid molecular recognition groups can bind and colorimetrically detect influenza virus. For biochromism, it is possible that the specific binding of biomolecules by receptors incorporated in PDA matrices can affect the lipid side chain conformations in a manner analogous to thermal chromism, altering the effective conjugation length of the PDA backbone and resulting in detectable shifts in the optical absorption spectrum of the material [7]. The reduced conjugation results in absorption of shorter wavelengths, so red light is reflected. Direct colorimetric detection of receptor–ligand binding offers wide-ranging applications in the areas of diagnostics and drug screening.

Our group and collaborators have prepared PDA films decorated with α -D-mannose using LB technique, which were composed of PCDA and its derivative *P*-10, 12-pentacosadiyne-1-*n* (3,6,9-trioxa-undecylamide) α -D-mannopyranoside (MPDA) [25]. The functionalized film could interact with *Escherichia coli* (*E. coli*) and the interaction led to the blue–red color transition of the film. Control assays demonstrated that this color change resulted from the specific bio-recognition between mannose inserted in the monolayer assembly and *E. coli*.

The affinochromism of the mixed PCDA/MPDA monolayer in response to *E. coli* was enhanced by modifying the terminal carboxyl group of PCDA with CdS nano-crystallites with the aid of LB technology [26]. CdS not only triggered the strong tropism of the bacteria but also reduced the rigidity of the PCDA/MPDA backbone, resulting in the enhanced affinochromism.

Natural lipid receptors, such as gangliosides GM1, can be incorporated into artificial supramolecular assemblies to construct colorimetric biosensors with highly specific recognition properties. Gangliosides are lipid molecules that are located in the plasma membrane of cells and have a carbohydrate recognition group attached to the extracellular surface. Two representative members are the GM1 and GT1b gangliosides, which are respectively the primary targets of cholera toxin and botulinum neurotoxin. The PDA thin-film biosensor for neurotoxin is doped with “promoter” PDA molecules (sialic acid lipid 1 or lactose-derivatized PDA lipid) to facilitate the chromatic transition in the toxin-binding experiments [27]. The mechanism by which the promoter increases film sensitivity to toxin binding is unknown, but may involve reduction of the activation barrier of the chromatic transition through changes in lipid packing and effective conjugated length of the backbone. Promoter molecule may also function as a structural mediator between the non-conjugated receptor and the conjugated backbone.

However, promoters do not act as toxin molecular recognition sites: films containing the promoter but no genuine receptor do not change color in the presence of analyte. In the thin film biosensors, the molecular recognition can be directly linked to signal transduction.

Naturally derived lipophilic molecules not only can be incorporated into PDA LB films, but also can be formed into liposomes when mixed with a polymerizable monomer lipid. For example, the ganglioside GM1 could be incorporated into PDA liposomes with matrix lipid 5,7-docosadiynoic acid (DCDA) [28]. Protein-ligand molecular recognition occurring at the interfacial region of polymerized liposomes resulted in a change of the membrane color, and the CR is directly proportional to the quantity of target analyte, cholera toxin. In this case, the color change is best observed when the diacetylene unit is moved closer to the interface, as with DCDA. Influenza virus has approximately 500 hemagglutinin receptors on its surface capable of binding to the sialic acid ligand on the liposomes. This multipoint binding sufficiently stresses the backbone of the PDA material, distorting the initially planar structure of the polymer backbone. The cholera toxin system is only pentavalent and therefore requires a system more sensitive to binding-induced perturbations. By moving the diacetylenic optical reporter group closer to the interfacial region, the system becomes more sensitive to lower valency binding.

By using lipids with different ligand headgroups, it is possible to create a variety of simple, one-step biosensor devices. Functionalized PDA vesicles have been developed to detect *E. coli*, where the synthetic glycolipid receptors, dioctadecyl glyceryl ether- β -glucosides (DGG) [29] or α -D-mannoside-hexadecyl (MC₁₆) [30,31] were inserted into PDA matrix by physical force rather than directly by covalent cross-linking between the chromophore and the receptor. The signal scales with the amount of virus added to the liposomes suspension.

Resonance Raman spectra (RRs) analysis for PCDA/MC₁₆ vesicles recognized by *E. coli* provided molecular information of this bio-interaction [30]. Results demonstrated that the relative amount of the double bonds to the triple bonds increased during biochromism, and this could be attributed to a configuration transformation from acetylene to butatriene [32]. Therefore, it can be speculated that the specific *E. coli*-mannose interaction may alter side chain conformation, causing the electrical structure of the polymer backbone to change from acetylene to butatriene, and inducing blue-red transition in liposomes.

The effects of some familiar transition metal and alkali earth metal cations on the molecular recognition between mannose and *E. coli* have been studied *in vitro* through the specific biochromism of PCDA/MC₁₆ vesicles [30]. When incubated with *E. coli*, liposomes containing various metal cations exhibited different signal responses (Fig. 1). Apparently, the presence of Cd²⁺, Ca²⁺, Mg²⁺, Ba²⁺, and Ag⁺ enhanced the biochromatic degree of the system. A possible enhancement mechanism was proposed that these metal cations, existing in the form of dissociated ions in the liposome suspension [33], favored bacterial adhesion to

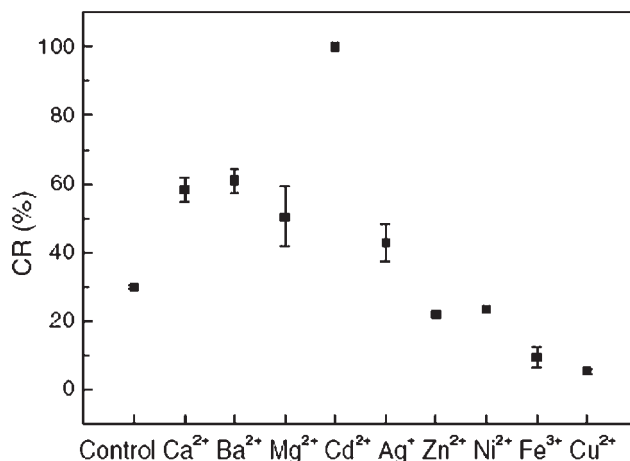


Fig. 1. Effects of the metal cations (1.0×10^{-4} M) on CRs of PCDA/MC₁₆-*E. coli*. Every CR value was the average of results obtained in three independent experiments. (Adapted with permission from Ref. [30], Fig. 3.).

the receptor on the liposome surface [34]. On the contrary, Cu²⁺, Fe³⁺, Ni²⁺, and Zn²⁺ inhibited the biochromism, which cooperated with diacetylene lipid with a carboxylic group [35] and increased the rigidity of the liposomal outer leaflet, blocking changes in the side chain conformation and electrical structure of PDA polymer during biochromism. Both the enhancing and inhibitory effects became more distinct at higher metal concentrations. There was a cooperative effect between metal ions and *E. coli* to modulate the blue–red transition of liposomes. These discoveries would aid to broaden the practical applications of chromatic biosensors, improving detection speed and sensitivity for biological molecules, and developing a novel direct chromatic detection method for metal cations.

We investigated the bactericidal effect of TiO₂ colloid through colorimetric detection of the interaction between mannose-functionalized vesicles with *E. coli* [31]. With various pre-incubation and irradiation time, the quantity of the bacteria could be controlled in real time under the bactericidal effect of TiO₂ colloid. Thus, controllable conjugated bio-interaction between two bio-interfaces was obtained through the introduction of the third factor and monitored in real time.

3.1.2. Colorimetric detection of physiological ions

Development of selective ion-sensors is highly desirable because of the physiological importance of ions such as potassium, sodium, calcium, and others. Currently available ion assays, however, are somewhat limited due to low-ionic selectivity, for example, between K⁺ and Na⁺. R. Jelinek *et al.* [36] have developed supramolecular assemblies composed of ionophores and phospholipids embedded in a PDA matrix, which exhibit visible and rapid color changes in the

presence of specific cations in solution. Ionophores, such as valinomycin or monensin, are generally hydrophobic cyclic molecules, which selectively bind cations and transport them across membranes.

The blue–red color transitions of the dimyristoylphosphatidylcholine (DMPC)/PDA vesicles incorporating ionophores are directly related to binding of the cations to the ionophores, and their association with the lipids. The ionic selectivity of ionophore/DMPC/PDA vesicles is consistent with the established binding affinities of the ionophore molecules. Valinomycin, for example, forms complexes with cations in the following decreasing affinity: $\text{Rb}^+ > \text{K}^+ > \text{Cs}^+ \gg \text{Na}^+ > \text{Li}^+$ [37]. Indeed, the color changes correlate the relative strengths of the ion-bound complexes of valinomycin. Monensin, on the other hand, displays the highest affinity toward Na^+ ions [38], and the colorimetric results are consistent with this property. The CRs of DMPC/PDA vesicles incorporating divalent-pyrrole ionophore, A23187, decrease in the order $\text{Co}^{2+} > \text{Ba}^{2+} > \text{Sr}^{2+} > \text{K}^+$, which are also consistent with the published ionic affinities of A23187 [39]. These results demonstrate that the ionic selectivity is clearly determined by the affinities of the ionophore molecules incorporated into the vesicles, thus allowing for general applicability of the system as a selective ion sensor. The system demonstrates a significant ionic selectivity, in particular between the physiologically important ions Na^+ and K^+ (Fig. 2), further showing that the blue–red color transitions are highly dependent upon the cation–ionophore pair employed.

This assay could be applied for rapid determination of physiological ionic species, and might be extended for microscopic colorimetric determination of

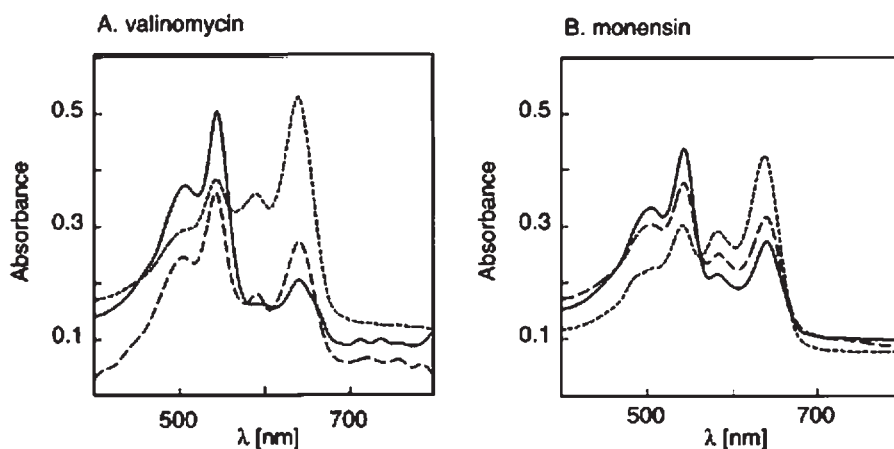


Fig. 2. UV-vis absorption spectra of ionophore/DMPC/PDA vesicle solutions containing K^+ and Na^+ ions. *Valinomycin*: solid line, 10 mM KCl; short dash, 10 mM NaCl; long dash, 9.97 mM NaCl + 0.03 mM KCl (around 350:1 molar ratio). *Monensin*: solid line, 5 mM NaCl; short dash, 5 mM KCl; long dash, 4.87 mM KCl + 0.13 mM NaCl (around 40:1 molar ratio). (Adapted with permission from Ref. [36], Fig. 6.).

intra- and extracellular ion concentrations, as well as for evaluation of the performance and selectivity of putative ion-binding compounds and metal-binding peptides.

3.1.3. Rapid colorimetric screening of the activities of antibacterial peptides

An important step toward a more general applicability of PDA-based materials for biological and diagnostic uses has been the introduction of natural lipids into the PDA matrix. The lipid molecules in the colorimetric vesicles essentially form “microdomains” within the PDA matrix and do not affect the polymerization and blue color of the vesicle solution. Natural membrane lipids embedded within the PDA framework well-mimic lipid-bilayer environments, and biochemical events leading to physical or chemical disruption of the lipid assembly, such as ion transport, peptide–membrane interactions, interfacial enzyme catalysis, and antigen–antibody recognition, can give rise to blue–red colorimetric transitions, induced through structural perturbations of the adjacent PDA network.

Short membrane-associated peptides (10–30 residues) are prevalent in nature as part of the intrinsic defense mechanisms of most organisms, and have been proposed as a blueprint for the design of novel antimicrobial agents. Assays providing rapid and easy evaluation of interactions between membrane peptides and lipid bilayers could significantly benefit both the elucidation of structural and functional properties of membrane peptides as well as the improvement of screening for substances having effective antibacterial properties. The phospholipid/PDA vesicle assay has been successfully applied for screening of membrane-active antibacterial peptides [40,41]. The binding of peptides gives rise to extensive molecular reorganization within the phospholipid domains, thereby inducing structural perturbations in the adjacent PDA matrix, resulting in the blue–red colorimetric transitions. Figure 3 depicts titration curves of the membrane peptides alamethicin, melittin, and magainin added to mixed DMPC/PDA vesicles. The different degree of colorimetric transitions is attributed to the distinct mechanisms of peptide–membrane interactions. Addition of melittin induced different color changes in PDA assemblies incorporating DMPC, dimyristoylphosphatidylethanolamine (PE), and the mixtures of PE and dimyristoylphosphatidylglycerol (PG), and cardiolipin. The different color changes most likely depend on the size and charge of the lipid headgroups, which affect the binding and the degree of penetration of the peptide into the lipid assembly [42].

The color transitions of the phospholipid/PDA vesicles, which are directly related to adoption of helical conformations by the peptides and their association with the lipids, are correlated with important molecular parameters, such as the mechanisms of peptide–lipid binding, and the degree of penetration of the peptides into lipid bilayers. More extreme blue–red transitions are induced by

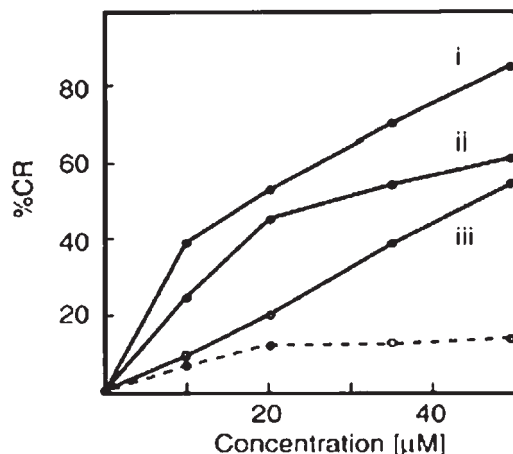


Fig. 3. The changes in CRs upon titration of DMPC/PDA vesicles (2:3 mol ratio) with membrane peptides: (i) magainin, (ii) melittin, and (iii) alamethicin. The dashed line shows the results with melittin added to pure PDA vesicles (background). (Adapted with permission from Ref. [41], Fig. 3B.).

peptides which strongly bind at the lipid–water interface, compared with peptides penetrating into the hydrophobic cores of lipid membranes [43]. For example, relative to native melittin, its non-active analogue differing by only a single amino acid in the sequence, induced more pronounced reddish color. This could be ascribed to the analogue’s reduced helical content, and its inability to fully penetrate into the lipid membrane [44]. The biomimetic phospholipids/PDA vesicles have also been used to study the membrane binding and penetration by polymyxin B derivatives [45] and indolicidin analogs [46], indicating that lipopolisaccharide promoted preferred binding and incorporation of the peptides at the lipid/water interface.

3.1.4. Rapid screening of membrane penetration enhancers

The lipid/PDA vesicle assemblies can also be applied for rapid screening of the activities of membrane penetration enhancers [47]. Identification of chemical substances that induce, or assist, insertion of pharmaceutical compounds into target cells is particularly important to pharmaceutical research and development. PDA matrices containing various lipid molecules exhibit high sensitivity to the type and effectiveness of penetration enhancer added to the solutions, such as oleic acid, Tween-20, and menthol. The sensitivity of the system to the activities of the penetration enhancers is evident even in PDA vesicles incorporating ceramide rather than phosphatidyl choline (PC). This is significant, since important physiological membranes, such as the stratum corneum (the outer layer of the

epidermis in the skin) contain mostly ceramides, rather than phospholipids. The colorimetric system also indicates that interactions of penetration enhancers with membranes depend upon the lipid phase, as well as the self-assembly properties of the enhancer molecules.

The color changes induced in the lipid/PDA solutions occur within seconds after addition of the antibacterial peptides or membrane penetration enhancers. This colorimetric assay can be applied for rapid screening of the activities of antibacterial peptides and membrane penetration enhancers, and could provide structural and functional information on peptide–membrane interactions and mechanisms of membrane permeability.

3.1.5. Colorimetric detection of small molecules

The colorimetric changes of PDA thin films could be induced by conformational changes of the enzyme (hexokinase) immobilized on the sensor surface, which were caused by the binding of glucose to the enzyme active site [48]. Upon binding glucose, hexokinase undergoes a large conformational change. The two domains that form the active site move together in a jaw-like fashion to capture the glucose molecule, and the movement of one domain relative to the other is approximately 8 Å. Coupling the conformational change of the enzyme to the chromatic unit of the PDA film is achieved through protein amine coupling. A series of control experiments demonstrated that the conformational change resulting from the binding of glucose to hexokinase provided the mechanical driving force that causes the sensor to change color. Although a number of more effective sensors for glucose are available, this type of sensor design demonstrated that a protein conformational change could be used as a trigger mechanism for a low-cost, colorimetric solid-state sensor. The marriage of colorimetric biomaterials with biological recognition elements has the potential to yield enormous applications for a wide array of substrates.

3.2. Colorimetric detection of enzymatic catalysis

Interfacial catalysis on biomembranes plays a key role in extra- and intracellular processes and covers a range of enzyme classes such as lipolytic enzymes, acyltransferases, protein kinases, and glycosidases. Phospholipases, which play central roles in various signaling and inflammation processes [49], in particular, are an important class of interfacial enzymes. Owing to the limitation of conventional assays, the method for measuring enzyme activity using non-labeled, naturally occurring substrate is highly desirable. The biochromic vesicles offer a one-step approach to measuring enzyme activity through detection of a color change of PDA “signaling” lipids that surround the natural enzyme substrate [50,51]. DMPC/PDA vesicle solutions undergo rapid blue–red color changes

following interactions with phospholipases, such as phospholipase A₂ (PLA₂), phospholipase C (PLC), or phospholipase D (PLD), even though the enzymatic cleavage sites within the DMPC molecule are different. PLA₂ acts closer to the lipid tail, whereas PLC and PLD act specifically at the hydrophilic headgroup region. The color change is modulated by altering the mole percentage of the natural lipid DMPC in the PDA vesicle and the vesicles that do not contain DMPC remain in their blue phase. The color change of the DMPC/PDA vesicles can be suppressed with known inhibitors to PLA₂, such as MJ33 [52]. Inactivation of PLA₂ is also observed upon removal of Ca²⁺, the catalytic cofactors for PLA₂, from the buffer solution; PLA₂ prepared in buffer containing Zn²⁺ instead of Ca²⁺ ions does not induce a color change of the vesicles. The color transformations were directly associated with enzymatic cleavage of the phospholipid molecules incorporated within the PDA framework. The mechanism of color change is ascribed to lipid reorganization and destabilization of the vesicles by hydrolysis of the DMPC embedded in the PDA signaling matrix.

³¹P and ¹H nuclear magnetic resonance experiments verified the occurrence of interfacial catalysis by phospholipases and revealed the fate of the cleavage products [50,51]. The color change (i.e. destabilization) of the PDA vesicles induced by PLA₂, PLC, and PLD occurs by different pathways, depending on the specific enzyme. Although the PLA₂ hydrolysis products are removed from the vesicles, PLC destabilizes the vesicles through formation of diacylglycerol, and the products of PLD become condensed upon interaction with calcium ions.

Vesicles of DMPC/PDA can also be used for the detection of toxins that exhibit enzyme-like activity. For example, DMPC/PDA vesicles are responsive to the presence of β -bungarotoxin, which acts specifically at the presynaptic motor nerve termini to alter neurotransmitter release and the distribution of aminophospholipids in the inner- and outer-membrane leaflets [53]. The practical bio-analytical applications of the colorimetric assay for interfacial enzymatic cleavage are exemplified in Fig. 4, which reveals the high specificity of the colorimetric transitions in response to membrane-associated enzyme–substrate recognition events [54].

Overall, the phospholipid/PDA system pointed to promising applications both for identification of substances having lipase enzymatic properties as well as for rapid screening of potential enzymatic inhibitors. In both cases, the phospholipid/PDA assembly offers a simple, robust, and inexpensive alternative to existing assays, such as radioactive labeling.

3.3. Colorimetric immunoassay

Immunoassays are based on the use of an antibody that reacts specifically with an antigen to be tested. Immunoassay techniques, such as enzyme-linked immunosorbent assays, radioimmunoassays, immunoagglutination assays, and

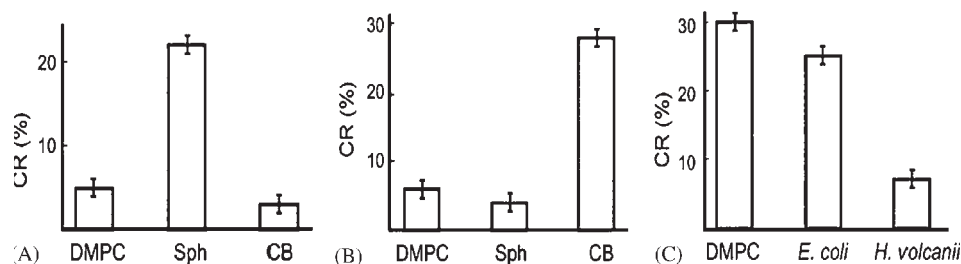


Fig. 4. Selective colorimetric response induced by enzymatic lipid cleavage. CR calculated from the visible absorption spectra of solutions of PDA vesicles containing different lipids (DMPC, Sph (sphingomyelin), CB (cerebroside), *E. coli*, *H. volcanii*) mixed with enzymes: (A) sphingomyelinase, (B) galactosidase, (C) PLA₂. (Adapted with permission from Ref. [54], Fig. 1.).

fluorescent immunoassays, play an important role in medical diagnostics, food, and environmental analyses. However, a common feature of these assay techniques is that they require a label to detect the interaction of a biocompound with an analyte. Jelinek *et al.* [55] have developed a novel molecular system in which interactions between antibodies and peptide epitopes displayed at a biomimetic membrane interface can be detected through induction of visible, spectroscopically quantified, rapid color transitions. The colorimetric assembly consists of a phospholipid/PDA matrix anchoring a hydrophobic peptide displaying the epitope at its *N*-terminus. The combined epitopepeptide/phospholipid/PDA molecular aggregates undergo rapid colorimetric transitions only when they come in contact with antibodies that specifically recognize the epitopes. Diagrams in Fig. 5 show the CRs of DMPC/PDA assemblies incorporating different epitopes, following interactions with various antibodies, demonstrating the general applicability of the system for detection of epitope–antibody recognition.

The binding between the antibodies, which are relatively big macromolecules, and the displayed epitopes at the lipid–water interface is expected to result in significant perturbations of the particle surface, giving rise to the observed color changes within the PDA matrix. Significantly, the color changes occur after a single-mixing step, without further chemical reactions or enzymatic processing. The new colorimetric molecular system could be utilized for studying antigen–antibody interactions and peptide–protein recognition, epitope mapping, and rapid screening of biological and chemical libraries.

A new approach of chromatic immunoassay based on PDA vesicles has been described recently [56]. Using *N*-hydroxysuccinimide (NHS) and 1-ethyl-3-(3-dimethyl aminopropyl) carbodiimide (EDC), antibodies were covalently coupled with mixed vesicles of 10,12-tricosadiynoic acid (TCDA) and DMPC *via* a peptide bond. After antigen injection, specific immunoreactions took place at the polymerized vesicle surface leading to a blue–red color change. The CR values increase with an increase of antigen amount, and incorporation of DMPC in the

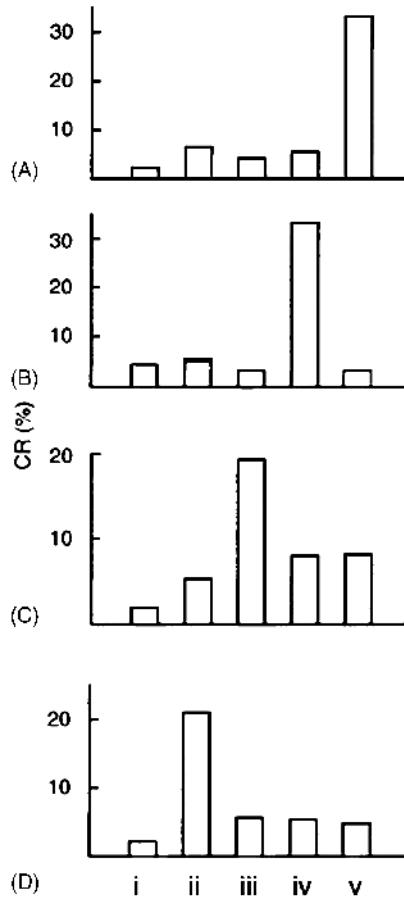


Fig. 5. Diagrams depicting the CRs recorded following addition of antibodies to solutions containing DMPC/PDA particles incorporating different displayed epitopes: (A) c-myc-L7A7K4G (c-myc epitope, EQKLISEEDL, displayed at the N-terminus of the L7A7K4G peptide); (B) HA-L7A7K4G (YPYDVPDYA); (C) FLAG-L7A7K4G (DYKDDDDK); (D) p8 coat protein of fd filamentous bacteriophage. Antibodies, separately added to the particle solutions: (i) control, PBS buffer solution (no antibody added); (ii) anti-fd, 700 $\mu\text{g}/\text{mL}$; (iii) anti-FLAG mAb, 400 $\mu\text{g}/\text{mL}$; (iv) anti-HA mAb, 200 $\mu\text{g}/\text{mL}$; (v) anti-c-myc mAb, 100 $\mu\text{g}/\text{mL}$. Antibodies were dialyzed in 0.01 M PBS, 70 mM sodium chloride, pH 7.4, prior to mixing with the particles. (Adapted with permission from Ref. [55], Fig. 3.).

mixed vesicles increases the sensitivity of the chromatic immunoassay. This chromatic immunoassay is simple, rapid, and sensitive.

Gill *et al.* [57] have produced highly responsive solid-state chromatic biosensors by encapsulating PDA–phospholipid vesicles modified with immunoglobulin (IgG) in hybrid sol–gel materials composed of silica and functionalized siloxanes. Encapsulation of the IgG-PDA-phospholipid vesicles provided transparent blue,

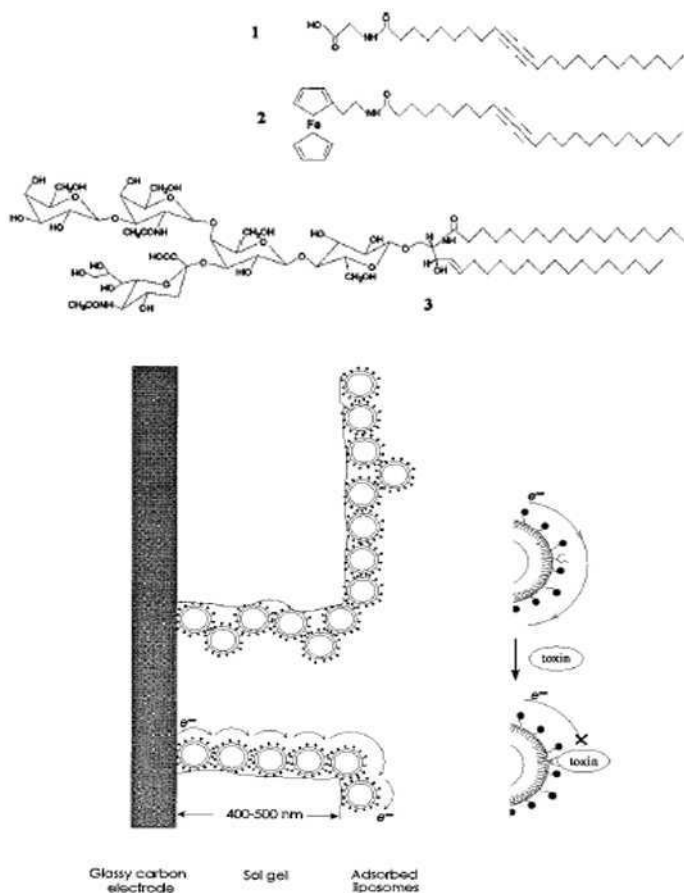
mesoporous composites which were deposited as thick films onto cellulose, nylon, polycarbonate, alumina, silica, and glass. Only slight color changes (<7%) were observed upon sol–gel entrapment of the blue-form vesicles, which indicates that encapsulation did not have a sufficient effect on the vesicle structure so as to trigger switching of the PDA conformation and that the liposomes were largely encapsulated in their native state. More importantly, exposure of the IgG-PDA sol–gels to antigens resulted in the blue–red color changes characteristic of IgG-PDA-phospholipid solutions, which demonstrates that both the biomolecular recognition of IgG and structural transition functions of PDA were preserved upon entrapment. The materials of IgG-PDA sol–gels nanocomposites are rugged and processable and can be fabricated as monoliths, thick films, and microarrays, and furnish colorimetric biosensors that are sensitive and show short response time. The successful fabrication of reagentless solid-state IgG-PDA sol–gel biosensors offers a potentially simple and generic route to solid-state colorimetric sensor and microarray platforms.

3.4. Electrochemical biosensors

Supramolecular assemblies (redox liposomes) prepared from ferrocenic diacetylene lipid and the cell surface receptor ganglioside GM1 (Scheme 2) are utilized to construct an amperometric biosensor for *E. coli* heat-labile enterotoxin on a sol–gel thin-film electrode [58,59]. The design allows for direct inspection of the dependency of electron transport on the state and extent of biomolecular recognition that has taken place on the vesicles and, thus, provides a method for direct measurement of *E. coli* heat-labile enterotoxin binding by electrochemistry.

In the absence of the redox-active Fc-PDA, no voltammetric response was observed for the adsorbed vesicles on the electrode. However, well-defined current responses were obtained for Fc-PDA-containing vesicles. The current peaks show diffusion characteristics and indicate that the redox reactions for the vesicles are chemically reversible. With addition of *E. coli* enterotoxin, a sharp drop in the anodic current of ferrocene was observed (Fig. 6, inset). The response is time-dependent and the current decays in an exponential manner (Fig. 6). Control experiments indicated that the sensor was specific to *E. coli* heat-labile enterotoxin. These results clearly demonstrate that the toxin molecules in the solution diffuse onto the electrode surface and interact with the receptor on vesicles. The toxin–receptor complex appears to block the charge-transfer route on the electrode surface and gradually diminishes the current response.

As for receptor-modified electrodes, the amperometric signal decreased quickly with increasing concentration of the toxin. The dynamic range for the assay extends between 0.5×10^{-5} and 8×10^{-5} g/mL. A detection limit of 3×10^{-6} g/mL (3.6×10^{-8} M) was determined using a 3σ standard deviation cutoff. However, no current change was found on the electrode without the



Scheme 2. Schematic illustration of gel-crack-assisted electron transport on the sol-gel thin-film electrode. The redox/receptor liposomes are composed of *N*-(10,12-pentacosadiynoyl)glycine (GLY-PDA, **1**), *N*-(10,12-pentacosadiynoyl)acetylferrocene (Fc-PDA, **2**), and ganglioside GM1 (**3**). (Adapted with permission from Ref. [58], Chart 1 and Fig. 2.).

receptor GM1, demonstrating the important role of GM1 in defining the sensor's specificity.

A gel-crack-assisted electron transport mechanism (Scheme 2) is thus suggested to explain the large ferrocene current and its response to enterotoxin binding. The oxidation of ferrocene first occurs between the glassy carbon electrode and the liposomes trapped in the gel cracks. As the concentration of ferrocene is depleted at the interface, the process requires, for charge neutrality, ionic migration from the bulk into the area. The response is a typical diffusion-controlled process, and this suggests that ferrocene species near and far from the gelcrack sites participate in the electron transfer. When the enterotoxin is

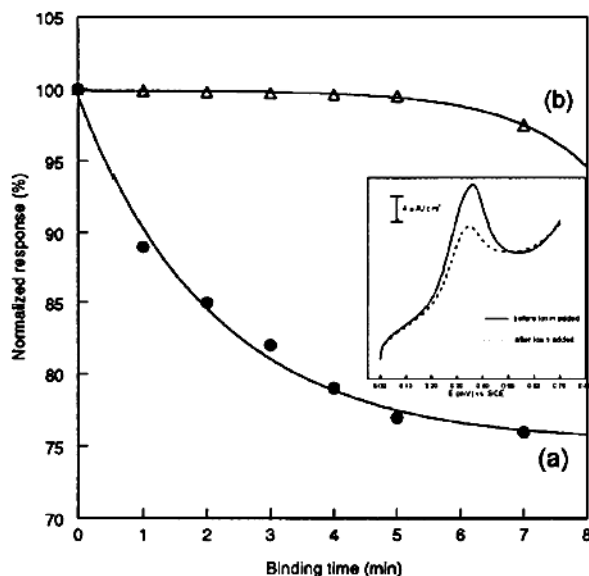


Fig. 6. Effect of toxin binding on amperometric response as a function of time. (a) *E. coli* heat labile enterotoxin (80 ppm), (b) bovine serum albumin (1000 ppm, control). Inset is the anodic current response for redox liposomes (—) without and (···) with 80 ppm enterotoxin. (Adapted with permission from Ref. [58], Fig. 1.).

added, its binding to the receptor sites on the liposomes blocks the electron transport path, resulting in a decrease in current magnitude.

By using supramolecular assemblies composed of PCDA/MPDA supported on the SAM of octadecanethiol on a gold electrode, we reported that the bio-interaction between *E. coli* and mannose could be detected by electrochemical method [60]. Before the electrode was incubated with *E. coli*, a very broad current peak appeared in the cyclic voltammogram (Fig. 7a). There was no redox substance in the bilayer, so the broad current peak resulted from the defects within the bilayer consisting of PCDA/MPDA and the SAM of octadecanethiol on the gold electrode that permitted the probe molecules ($K_3Fe(CN)_6/K_4Fe(CN)_6$) in solution to exchange electrons with the underlying gold electrode surface [61]. After the electrode was incubated with *E. coli* for 3 min, the peak current gradually decreased and appeared plateau-shaped at potential past the redox potential of probe molecules (Fig. 7b). This can be explained by a low density of micro- or nanometer scale defects within the bilayer, and each defect could behave as a single ultramicroelectrode [62]. After the electrode was incubated with *E. coli* for 5 min, the current decreased exponentially (Fig. 7c). Chidesy *et al.* [61] reported that the change was attributed to the decrease of defect density within the bilayer. In other words, there were no defect sites through which probe molecules can completely or partially penetrate.

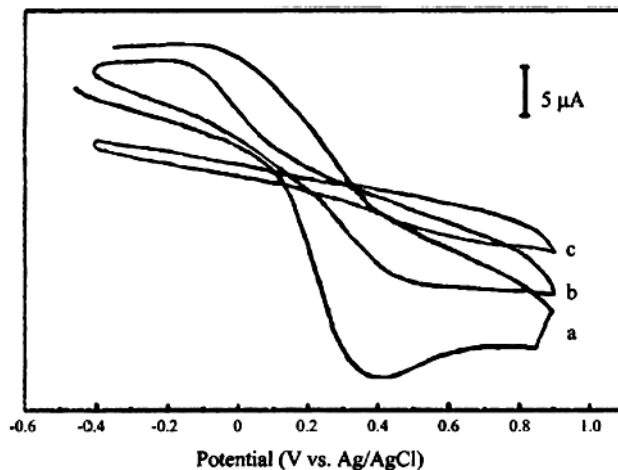


Fig. 7. Cyclic voltammograms for 5 mM $K_3Fe(CN)_6/K_4Fe(CN)_6$ in 0.1 M KCl solution on the bilayer consisting of PCDA/MPDA and the SAM of the octadecanethiol modified gold electrode. Scan rate, 200 mV/s. Concentration of *E. coli* in solution, 9×10^8 cells/mL. (a) Before incubation with *E. coli* and (b, c) after incubation with *E. coli* for 3 and 5 min, respectively. (Adapted with permission from Ref. [60], Fig. 5.).

The amperometric response decreased noticeably with time in bacterial solution, but no significant current drop was observed in background solution. The bacterium cells in saline solution diffused onto the electrode surface and bound with the receptor (mannose) on the bilayer. The binding appeared to change the bilayer structure and gradually diminish the current response. No current change was found on the electrode without the receptor. However, as for receptor-modified electrodes, the amperometric signal decreased quickly with increasing concentration of the bacterium, and there was a linear relationship within the range of 1×10^8 – 7×10^8 cells/mL. These results demonstrate the specificity of the interactions between *E. coli* and mannose.

The direct electrochemical detection of molecular recognition by PDA supramolecular assemblies might not only open a new path for the use of these membranes in the area of biosensor development but also offer new possibilities for diagnostic applications and screening for binding ligands.

4. CONCLUSIONS AND OUTLOOK

Induction of colorimetric transition in PDA-based assemblies by molecular recognition is a recent, but exciting development in biosensors. The results obtained so far have pointed to the potential of the “smart” systems as effective colorimetric biosensors. PDA vesicles and thin films modified with “receptor lipid” can

be used to detect the presence of viruses or toxins through a blue–red color transition. In particular, the incorporation of natural lipids into the PDA matrix enables the vesicles to successfully mimic environments of cellular membranes, thus opening the way to a variety of biochemical applications. Experiments that have been reported demonstrated the application of the phospholipid/PDA vesicle system for detection of various biochemical processes and biological analytes, including soluble ions, peptide–membrane interactions, enzymatic lipid cleavage, antigen–antibody interactions, and for screening of pharmacologically active compounds.

Applications of these PDA-assemblies in molecular electronics and sensors are at a very early stage, but the simplicity of design and synthesis of these assemblies makes them very promising prototype platforms for detection of bioactive materials. In particular, the seamless integration of signal transduction with biomolecular recognition allows device miniaturization and offers potential for simultaneous, multi-channel orthogonal detection techniques. The colorimetric sensors have the potential to be commercially successful, provided certain key problems regarding detection sensitivity, consistency of the initial optical state, sensor stability, and durability can be solved.

In the future, more attention will be focused on addressing sensitivity and durability issues by chemical modification of the synthetic membranes.

ACKNOWLEDGEMENT

This work was financially supported by the National Natural Science Foundation of China (No. 20125513, No. 20435010), Li Foundation, USA, and a Foundation for the Author of National Excellent Doctoral Dissertation of PR China.

REFERENCES

- [1] H. Ringsdorf, B. Schlarb, J. Venzmer, Molecular architecture and function of polymeric oriented systems: models for the study of organization, surface recognition, and dynamics of biomembranes, *Angew. Chem. Int. Ed. Engl.* 27 (1988) 113–158.
- [2] J.H. Fendler, *Membrane Mimetic Chemistry*, Wiley Interscience, New York, 1982.
- [3] J. Song, Q. Cheng, S.M. Zhu, R.C. Stevens, “Smart” materials for biosensing devices: cell-mimicking supramolecular assemblies and colorimetric detection of pathogenic agents, *Biomed. Microdevices* 4 (2002) 213–221.
- [4] D. Day, H. Ringsdorf, Polymerization of diacetylene carbonic acid monolayers at the gas-water interface, *J. Polym. Sci., Polym. Lett. Ed.* 16 (1978) 205–210.
- [5] D. Bloor, R.R. Chance, *Polydiacetylenes: Synthesis, Structure, and Electronic Properties*, Dordrecht, Martinus Nijhoff, 1985.
- [6] D.Y. Sasaki, R.W. Carpick, A.R. Burns, High molecular orientation in mono- and trilayer polydiacetylene films imaged by atomic force microscopy, *J. Colloid Interface Sci.* 229 (2000) 490–496.
- [7] W. Spevak, J.O. Nagy, D.H. Charych, Molecular assemblies of functionalized polydiacetylene, *Adv. Mater.* 7 (1995) 85–89.

- [8] A. Reichert, J.O. Nagy, W. Spevak, D. Charych, Polydiacetylene liposomes functionalized with sialic acid bind and colorimetrically detect influenza virus, *J. Am. Chem. Soc.* 117 (1995) 829–830.
- [9] U. Jonas, K. Shah, S. Norvez, D.H. Charych, Reversible color switching and unusual solution polymerization of hydrazide-modified diacetylene lipids, *J. Am. Chem. Soc.* 121 (1999) 4580–4588.
- [10] Y.F. Lu, Y. Yang, A. Sellinger, M.C. Lu, J.M. Huang, H.Y. Fan, R. Haddad, G. Lopez, A.R. Burns, D.Y. Sasaki, J. Shelnut, C.J. Brinker, Self-assembly of mesoscopically ordered chromatic polydiacetylene/silica nanocomposites, *Nature* 410 (2001) 913–917.
- [11] Y. Yang, Y. Lu, M. Lu, J. Huang, R. Haddad, G. Xomeritakis, N. Liu, A.P. Malanoski, D. Sturmayer, H. Fan, D.Y. Sasaki, R.A. Assink, J.A. Shelnut, F. van Swol, G.P. Lopez, A.R. Burns, C.J. Brinker, Functional nanocomposites prepared by self-Assembly and polymerization of diacetylene Surfactants and silicic Acid, *J. Am. Chem. Soc.* 125 (2003) 1269–1277.
- [12] S. Okada, S. Peng, W. Spevak, D. Charych, Color and chromism of polydiacetylene vesicles, *Acc. Chem. Res.* 31 (1998) 229–239.
- [13] R. Jelinek, Colorimetric sensors for drug discovery and biomedical diagnostics, *Drug Develop. Res.* 50 (2000) 497–501.
- [14] R. Jelinek, S. Kolusheva, Polymerized lipid vesicles as colorimetric biosensors for biotechnological applications, *Biotechnol. Adv.* 19 (2001) 109–118.
- [15] B. Tieke, G. Lieser, G. Wegner, Polymerization of diacetylenes in multilayers, *J. Polym. Sci. Polym. Chem. Ed.* 17 (1979) 1631–1644.
- [16] A. Lio, A. Reichert, D.J. Ahn, J.O. Nagy, M. Salmeron, D.H. Charych, Molecular imaging of thermochromic carbohydrate-modified polydiacetylene thin films, *Langmuir* 13 (1997) 6524–6532.
- [17] D.J. Ahn, E.-H. Chae, G.S. Lee, H.-Y. Shim, T.-E. Chang, K.-D. Ahn, J.-M. Kim, Colorimetric reversibility of polydiacetylene supramolecules having enhanced hydrogen-bonding under thermal and pH stimuli, *J. Am. Chem. Soc.* 125 (2003) 8976–8977.
- [18] Q. Cheng, M. Yamamoto, R.C. Stevens, Amino acid terminated polydiacetylene lipid microstructures: morphology and chromatic transition, *Langmuir* 16 (2000) 5333–5342.
- [19] R.W. Carpick, T.M. Mayer, D.Y. Sasaki, A.R. Burns, Spectroscopic ellipsometry and fluorescence study of thermochromism in an ultrathin poly(diacetylene) film: reversibility and transition kinetics, *Langmuir* 16 (2000) 4639–4647.
- [20] R.A. Nallicheri, M.F. Rubner, Investigations of the mechanochromic behavior of poly(urethane-diacetylene) segmented copolymers, *Macromolecules* 24 (1991) 517–525.
- [21] R.W. Carpick, D.Y. Sasaki, A.R. Burns, First observation of mechanochromism at the nanometer scale, *Langmuir* 16 (2000) 1270–1278.
- [22] Q. Cheng, R.C. Stevens, Charge-induced chromatic transition of amino acid-derivatized polydiacetylene liposomes, *Langmuir* 14 (1998) 1974–1976.
- [23] R.R. Chance, Chromism in polydiacetylene solutions and crystals, *Macromolecules* 13 (1980) 396–398.
- [24] D.H. Charych, J.O. Nagy, W. Spevak, M.D. Bednarski, Direct colorimetric detection of a receptor–ligand interaction by a polymerized bilayer assembly, *Science* 261 (1993) 585–588.
- [25] B.L. Ma, Y. Fan, L.G. Zhang, X.G. Kong, Y.J. Li, J.H. Li, Direct colorimetric study on the interaction of *Escherichia coli* with mannose in polydiacetylene Langmuir–Blodgett films, *Colloids Surfaces B: Biointerfaces* 27 (2003) 209–213.
- [26] Y.J. Zhang, B.L. Ma, Y.J. Li, J.H. Li, Enhanced affinochromism of polydiacetylene monolayer in response to bacteria by incorporating CdS nano-crystallites, *Colloids Surfaces B: Biointerfaces* 35 (2004) 41–44.
- [27] D. Charych, Q. Cheng, A. Reichert, G. Kuziemko, M. Stroh, J.O. Nagy, W. Spevak, R.C. Stevens, A ‘litmus test’ for molecular recognition using artificial membranes, *Chem. Biol.* 3 (1996) 113–120.

- [28] J.J. Pan, D. Charych, Molecular recognition and colorimetric detection of cholera toxin by poly(diacetylene) liposomes incorporating Gm1 ganglioside, *Langmuir* 13 (1997) 1365–1367.
- [29] Z.F. Ma, J.R. Li, M.H. Liu, J. Cao, Z.Y. Zou, J. Tu, L. Jiang, Colorimetric detection of *Escherichia coli* by polydiacetylene vesicles functionalized with glycolipid, *J. Am. Chem. Soc.* 120 (1998) 12678–12679.
- [30] C.Y. Sun, Y.J. Zhang, Y. Fan, Y.J. Li, J.H. Li, Mannose – *Escherichia coli* interaction in the presence of metal cations studied *in vitro* by colorimetric polydiacetylene/glycolipid liposomes, *J. Inorg. Biochem.* 98 (2004) 925–930.
- [31] Y.J. Zhang, Y. Fan, C.Y. Sun, D.Z. Shen, Y.J. Li, J.H. Li, Functionalized polydiacetylene-glycolipid vesicles interacted with *Escherichia coli* under the TiO₂ colloid, *Colloids Surfaces B: Biointerfaces* 40 (2005) 137–142.
- [32] H.W. Beckham, M.F. Rubner, Structural characterization of the cross-polymerization of a diacetylene-functionalized polyamide, *Macromolecules* 26 (1993) 5192–5197.
- [33] B. Tieke, G. Wegner, D. Nägele, H. Ringsdorf, Polymerization of tricoso-10,12-dienoic acid in multilayers, *Angew. Chem. Int. Ed. Engl.* 15 (1976) 764–765.
- [34] G. Xu, *Molecular Medicine Bacteriology*, Science Publishing Company, Beijing, 2000.
- [35] X. Huang, M.H. Liu, Chirality of photopolymerized organized supramolecular polydiacetylene films, *Chem. Commun.* (2003) 66–67.
- [36] S. Kolesheva, T. Shahal, R. Jelinek, Cation-selective color sensors composed of ionophore–phospholipid–polydiacetylene mixed vesicles, *J. Am. Chem. Soc.* 122 (2000) 776–780.
- [37] B.C. Pressman, Biological applications of ionophores, *Annu. Rev. Biochem.* 45 (1976) 501–530.
- [38] P.W. Reed, Ionophores, *Methods Enzymol.* 55 (1979) 435–454.
- [39] J.S. Puskin, T.E. Gunter, Electron paramagnetic resonance of copper ion and manganese ion complexes with the ionophore A23187, *Biochemistry* 14 (1975) 187–191.
- [40] S. Kolesheva, L. Boyer, R. Jelinek, A colorimetric assay for rapid screening of antimicrobial peptides, *Nature Biotechnol.* 18 (2000) 225–227.
- [41] S. Kolesheva, T. Shahal, R. Jelinek, Peptide–membrane interactions studied by a new phospholipid/polydiacetylene colorimetric vesicle assay, *Biochemistry* 39 (2000) 15851–15859.
- [42] W.T. Heller, K. He, S.J. Ludtke, T.A. Harroun, H.W. Huang, Effect of changing the size of lipid headgroup on peptide insertion into membranes, *Biophys. J.* 73 (1997) 239–244.
- [43] T. Sheynis, J. Sykora, A. Benda, S. Kolesheva, M. Hof, R. Jelinek, Bilayer localization of membrane-active peptides studied in biomimetic vesicles by visible and fluorescence spectroscopies, *Eur. J. Biochem.* 270 (2003) 4478–4487.
- [44] E. Perez-Paya, R.A. Houghten, S.E. Blondelle, The role of amphipathicity in the folding, self-association, and biological activity of multiple subunit small proteins, *J. Biol. Chem.* 270 (1995) 1048–1053.
- [45] M. Katz, H. Tsubery, S. Kolesheva, A. Shames, M. Fridkin, R. Jelinek, Lipid binding and membrane penetration of polymyxin B derivatives studied in a biomimetic vesicle system, *Biochem. J.* 375 (2003) 405–413.
- [46] R. Halevy, A. Rozek, S. Kolesheva, R.E.W. Hancock, R. Jelinek, Membrane binding and permeation by indolicidin analogs studied by a biomimetic lipid/polydiacetylene vesicle assay, *Peptides* 24 (2003) 1753–1761.
- [47] D. Evrard, E. Touitou, S. Kolesheva, Y. Fishov, R. Jelinek, A new colorimetric assay for studying and rapid screening of membrane penetration enhancers, *Pharm. Res.* 18 (2001) 943–949.
- [48] Q. Cheng, R.C. Stevens, Coupling of an induced fit enzyme to polydiacetylene thin films: colorimetric detection of glucose, *Adv. Mater.* 9 (1997) 481–483.
- [49] M. Waite, *The Phospholipases*, Plenum Press, New York, 1987.
- [50] S.Y. Okada, R. Jelinek, D. Charych, Induced color change of conjugated polymeric vesicles by interfacial catalysis of phospholipase A₂, *Angew. Chem. Int. Ed.* 38 (1999) 655–659.

- [51] R. Jelinek, S. Okada, S. Norvez, D. Charych, Interfacial catalysis by phospholipases at conjugated lipid vesicles: colorimetric detection and NMR spectroscopy, *Chem. Biol.* 5 (1998) 619–629.
- [52] M.K. Jain, W. Tao, J. Rogers, C. Arenson, H. Eibl, B.-Z. Yu, Active-site-directed specific competitive inhibitors of phospholipase A₂: novel transition-state analogs, *Biochemistry* 30 (1991) 10256–10268.
- [53] A. Ghassemi, P. Rosenberg, Effects of snake venom phospholipase A₂ toxins (β -bungarotoxin, notexin) and enzymes (*Naja naja atra*, *Naja nigricollis*) on amino-phospholipid asymmetry in rat cerebrocortical synaptosomes, *Biochem. Pharmacol.* 44 (1992) 1073–1083.
- [54] S. Rozner, S. Kolusheva, Z. Cohen, W. Dowhan, J. Eichler, R. Jelinek, Detection and analysis of membrane interactions by a biomimetic colorimetric lipid/polydiacetylene assay, *Anal. Biochem.* 319 (2003) 96–104.
- [55] S. Kolusheva, R. Kafri, M. Katz, R. Jelinek, Rapid colorimetric detection of antibody-epitope recognition at a biomimetic membrane interface, *J. Am. Chem. Soc.* 123 (2001) 417–422.
- [56] Y.L. Su, J.R. Li, L. Jiang, Chromatic immunoassay based on polydiacetylene vesicles, *Colloids Surfaces B: Biointerfaces* 38 (2004) 29–33.
- [57] I. Gill, A. Ballesteros, Immunoglobulin–polydiacetylene sol–gel nanocomposites as solid-state chromatic biosensors, *Angew. Chem. Int. Ed.* 42 (2003) 3264–3267.
- [58] Q. Cheng, T.Z. Peng, R.C. Stevens, Signaling of *Escherichia coli* enterotoxin on supramolecular redox bilayer vesicles, *J. Am. Chem. Soc.* 121 (1999) 6767–6768.
- [59] T.Z. Peng, Q. Cheng, R.C. Stevens, Amperometric detection of *Escherichia coli* heat-labile enterotoxin by redox diacetylenic vesicles on a sol–gel thin-film electrode, *Anal. Chem.* 72 (2000) 1611–1617.
- [60] Y.J. Li, B.L. Ma, Y. Fan, X.G. Kong, J.H. Li, Electrochemical and Raman studies of the biointeraction between *Escherichia coli* and mannose in polydiacetylene derivative supported on the self-assembled monolayers of octadecanethiol on a gold electrode, *Anal. Chem.* 74 (2002) 6349–6354.
- [61] M.D. Porter, T.B. Bright, D.L. Allara, C.E.D. Chidesy, Spontaneously organized molecular assemblies. 4. Structural characterization of *n*-alkyl thiol monolayers on gold by optical ellipsometry, infrared spectroscopy, and electrochemistry, *J. Am. Chem. Soc.* 109 (1987) 3559–3568.
- [62] E. Sabantai, I. Rubinstein, Organized self-assembling monolayers on electrodes. 2. Monolayer-based ultramicroelectrodes for the study of very rapid electrode kinetics, *J. Phys. Chem.* 91 (1987) 6663–6669.

Budding of Liposomes – Role of Intrinsic Shape of Membrane Constituents

Ales Iglic^{1,*} and Veronika Kralj-Iglic²

¹Laboratory of Applied Physics, Faculty of Electrical Engineering, University of Ljubljana, Trzaska 25, SI-1000 Ljubljana, Slovenia

²Institute of Biophysics, Faculty of Medicine, University of Ljubljana, Lipiceva 2, SI-1000 Ljubljana, Slovenia

Contents

1. Introduction	253
2. The Single-Constituent Energy	255
3. Liposomes Composed of a Single Kind of Phospholipid Molecules	256
3.1. The two-state model	256
3.2. Global thermodynamic equilibrium	260
3.3. Solution of the variational problem – the equilibrium shape and orientational distribution	263
3.4. Stability of the narrow neck(s)	268
3.5. Stability of the pear shape and the ADE model	269
4. Spherical Budding in Liposomes Composed of Two Kinds of Molecules	271
5. Conclusion	276
References	278

Abstract

The budding of phospholipid bilayer membrane is studied theoretically. The description starts from a single-constituent energy that reflects intrinsic shape of the constituent, and uses methods of statistical physics to obtain membrane free energy. The membrane free energy is minimized to yield the equilibrium shape and distribution functions of constituents. It is shown that two mechanisms based on internal degrees of freedom: in-plane orientational ordering of phospholipids in the narrow neck connecting the bud with the mother membrane and clustering of membrane inclusions in the budding region, are complementary mechanisms that promote budding of liposomes.

1. INTRODUCTION

The budding of the bilayer membrane is a process that is vitally important for cells. Accordingly, it is of interest to understand the mechanisms that are involved in the budding. For this, the budding in bilayer membrane vesicles composed of a single phospholipid species have been investigated [1–3]. Changes in the suspension of vesicles, such as changes in temperature and changes in shape of vesicles may in certain conditions induce formation of buds of the

*Corresponding author. Tel.: +386-1-4250-278; Fax: +386-1-4768-850;
E-mail: ales.iglic@fe.uni-lj.si

membrane bilayer [4]. The cell membrane is a multi-component structure, therefore it is of special interest to study the budding of multi-component bilayer membranes. In such membranes, laterally mobile membrane constituents that favor certain membrane curvature, distribute between buds and the mother membrane [5]. Buds may develop into vesicles that alienate from the mother body leading to a loss of the mother membrane material [6]. This is especially significant in vesicles composed of more than one species, since due to the redistribution of the membrane constituents certain substances are accumulated in buds/daughter vesicles [7]. Lateral distribution of membrane constituents can be considered as an internal degree of freedom. The constituents distribute in such a way so as to minimize the membrane free energy [1,8–12]. Besides the lateral distribution of membrane constituents, another internal degree of freedom – lateral distribution of the in-plane orientational ordering of anisotropic constituents – has recently been considered [13–15]. A method has been developed [9,17] starting from the microscopic description of the membrane constituents and applying methods of statistical physics to obtain the membrane free energy. To obtain the equilibrium configuration of the vesicle, the membrane free energy is minimized taking into account the relevant geometrical constraints. The intrinsic properties of membrane constituents and interactions between them are thereby revealed in macroscopic features such as the equilibrium shape of the vesicle. Here, we apply this method while focusing on the effect of the intrinsic shape of the membrane constituents on the internal degrees of freedom, i.e. the equilibrium configuration of the membrane (the orientational ordering and/or the equilibrium membrane shape and the corresponding lateral distribution of constituents). The results presented may contribute to the understanding of abrupt changes in curvature derivatives, the stability of narrow necks that connect buds with the mother membrane, the stability of pear shapes and mechanisms of raft accumulation on the buds.

The description is based on the energy of a single constituent, which depends on the intrinsic shape of the constituents. The introduction of the single-inclusion energy is followed by the statistical mechanical model of the membrane composed of a single species of phospholipid molecules that may undergo in-plane orientational ordering, and a rigorous solution of the variational problem (the minimization of the free energy) yielding equilibrium shapes and the corresponding orientational order distributions of the one-component phospholipid vesicles. Then, the same formalism for the single-inclusion energy and the statistical mechanical model are used to describe spherical budding in the two-component membrane. The solution of the variational problem by a simple parametrical model yields the equilibrium shape and the corresponding lateral distribution of the membrane constituents. The role of the intrinsic shape of the membrane constituents can be recognized throughout the presentation.

2. THE SINGLE-CONSTITUENT ENERGY

Any membrane constituent may be treated as a very small inclusion in a two-dimensional continuum curvature field imposed by other membrane constituents. We assume that the inclusion, due to its structure and local interactions, energetically would prefer a local geometry that is described by the two-intrinsic principal curvatures C_{1m} and C_{2m} . The intrinsic principal curvatures are in general not identical (Fig. 1). If they are identical ($C_{1m} = C_{2m}$), then the in-plane orientation of the inclusion is irrelevant. Such inclusion is called isotropic. If $C_{1m} \neq C_{2m}$ the inclusion is called anisotropic. The orientation of such inclusion is important for its energy. It is assumed that the inclusion will spend on an average more time in the orientation, which is energetically most favorable, than in any other orientation.

If the area and the volume of the vesicle are fixed, the shape cannot attain the curvatures that would equal the intrinsic curvatures in all its points and the energy of the molecules is increased. The energy of a single inclusion derives from the mismatch between the actual membrane shape given by the two principal curvatures C_1 and C_2 and the intrinsic shape given by the intrinsic principal

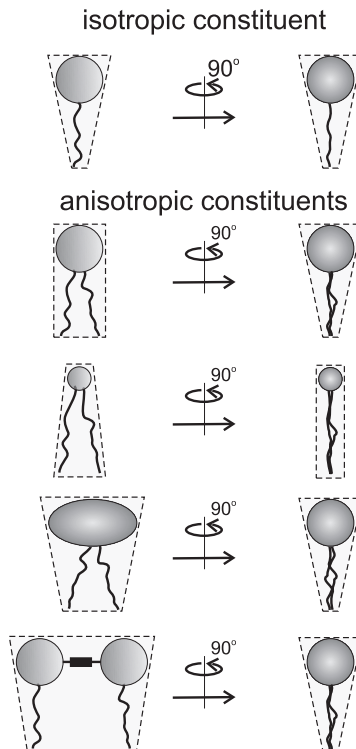


Fig. 1. Schematic representation of different intrinsic shapes of some membrane constituents. Front and side views are shown. Upper: isotropic constituent ($C_{1m} = C_{2m}$), lower: examples of anisotropic constituents ($C_{1m} \neq C_{2m}$).

curvatures C_{1m} and C_{2m} [16,17],

$$E(\omega) = \frac{\xi}{2}(H - H_m)^2 + \frac{\xi + \xi^*}{4}(\hat{C}^2 - 2\hat{C}\hat{C}_m\cos(2\omega) + \hat{C}_m^2) \quad (1)$$

where ξ and ξ^* are constants describing the strength of the interaction between the inclusion and the surrounding membrane continuum and in the case of larger multicomponent flexible membrane inclusion also the bending rigidity of the inclusion. $H = (C_1 + C_2)/2$ is the mean curvature of the membrane, $H_m = (C_{1m} + C_{2m})/2$ is the mean curvature of the continuum intrinsic to the inclusion, $\hat{C} = (C_1 - C_2)/2$, $\hat{C}_m = (C_{1m} - C_{2m})/2$ and ω is the orientation of the principal axes of the intrinsic shape relative to the principal axes of the local curvature of the continuum.

It can be seen from equation (1) that the single-inclusion energy attains a minimum when $\cos(2\omega) = 1$, i.e., when the two systems are aligned or mutually rotated by an angle π , while the single-inclusion energy attains a maximum when $\cos(2\omega) = -1$, i.e., when the two systems are mutually rotated by an angle $\pi/2$ or $3\pi/2$. In the first case the single-inclusion energy is

$$E_{\min} = \frac{\xi}{2}(H - H_m)^2 + \frac{\xi + \xi^*}{4}(D^2 + D_m^2) - \frac{\xi + \xi^*}{2}DD_m \quad (2)$$

whereas in the second case the single-inclusion energy is

$$E_{\max} = \frac{\xi}{2}(H - H_m)^2 + \frac{\xi + \xi^*}{4}(D^2 + D_m^2) + \frac{\xi + \xi^*}{2}DD_m \quad (3)$$

where $D = |\hat{C}|$ and $D_m = |\hat{C}_m|$ are the curvature deviator and the intrinsic curvature deviator, respectively. The states $\omega = 0, \pi$ and the states $\pi/2, 3\pi/2$, respectively, are degenerate so that the ordering is quadrupolar.

3. LIPOSOMES COMPOSED OF A SINGLE KIND OF PHOSPHOLIPID MOLECULES

3.1. The two-state model

A single phospholipid molecule is treated as a very small inclusion in a two-dimensional continuum curvature field imposed by other phospholipid molecules. We assume that the phospholipid molecule, due to its structure and local interactions, energetically would prefer a local geometry that is described by the two principal curvatures C_{1m} and C_{2m} . As the phospholipid molecule is composed of two tails and a headgroup, the intrinsic principal curvatures are not identical (Fig. 1), i.e., the intrinsic shape of the phospholipid molecule is anisotropic [18].

Each monolayer is described separately. The contributions to the free energy of the two monolayers are then summed to obtain the energy of the bilayer membrane.

The monolayer area is divided into small patches that, however, contain a large number of molecules so that the methods of statistical physics can be used. The membrane curvature is taken to be constant over the patch. This curvature field is produced by the molecules themselves, i.e., the molecules pack together in such way as to form the local shape of the membrane. We consider that every phospholipid molecule in the patch is subject to this field. The lattice statistics approach is used, drawing an analogy from the problem of non-interacting magnetic dipoles in an external magnetic field [19], the curvature deviator D taking the role of the external magnetic field.

In the idealized case, we assume a simple model where we have M equivalent molecules in the patch, each existing in one of the two possible states corresponding to the energies E_{\min} and E_{\max} , respectively (equations (2) and (3)); N molecules are taken to be in the state with higher energy E_{\max} and $(M-N)$ molecules are taken to be in the state with lower energy E_{\min} . The energy of the lipid molecules within the patch in the mean curvature field, divided by kT where k is the Boltzmann constant and T is the temperature, is

$$\frac{E_D}{kT} = N \frac{E_{\max}}{kT} + (M - N) \frac{E_{\min}}{kT} \quad (4)$$

Inserting equations (2) and (3) into equation (4) gives

$$\frac{E_D}{kT} = M \frac{E_q}{kT} - (M/2 - N) d_{\text{eff}} \quad (5)$$

where

$$\frac{E_q}{kT} = \frac{\xi}{2kT} (H - H_m)^2 + \frac{\xi + \xi^*}{4kT} (D^2 + D_m^2) \quad (6)$$

and

$$d_{\text{eff}} = \frac{(\xi + \xi^*) D_m D}{kT} \quad (7)$$

We call d_{eff} the effective curvature deviator.

Direct interactions between the membrane constituents are taken into account. Here we assume that the relative orientation of two anisotropic molecules gives rise to a contribution to the direct interaction that is the most important and neglect all other contributions. In describing the direct interaction between the nearest-neighbor molecules, we propose it should be taken into account that the molecules that are oriented in such way that their orientational energy in the mean curvature field is lower, also exhibit more favorable packing. By attaining the shape that is in tune with the local-curvature field, the tails of the favorably oriented molecules come, on the whole, closer together, which gives rise to additional lowering of the energy of the patch due to direct interactions, relative to the situation where the molecules are randomly oriented within the patch. On the

other hand, if we consider that the molecules that are oriented in such way that their orientational energy in the mean curvature field is higher, exhibit less favorable packing, in which the tails are on the whole further apart. This causes a rise of the energy of the interaction between such oriented molecules within the patch with respect to the situation where the molecules are randomly oriented. The effect depends on the local-curvature field, on the intrinsic shape of the molecule and the strength of the interaction. We consider the effect to be proportional to the local effective curvature deviator. The direct interaction of N molecules in the patch that have higher energy E_{\max} with their neighbors is therefore described by a positive contribution [14],

$$\frac{E_N}{kT} = \frac{\tilde{k}}{kT} N d_{\text{eff}} \quad (8)$$

where \tilde{k} is the interaction constant. Accordingly, the direct interaction of $(M-N)$ molecules that have lower energy E_{\min} , with their neighbors is described as

$$\frac{E_{M-N}}{kT} = -\frac{\tilde{k}}{kT} (M-N) d_{\text{eff}} \quad (9)$$

The total energy of the patch due to direct interaction E_i/kT is $(E_N/kT + E_{M-N}/kT)/2$, where we divide by 2 as to avoid counting each molecule twice. Therefore,

$$\frac{E_i}{kT} = -\frac{\tilde{k}}{kT} (M/2 - N) d_{\text{eff}} \quad (10)$$

The total energy of the patch E^P is obtained by summing the contribution of the orientation of the molecules according to the local curvature deviator E_D and the contribution of the direct interaction between the molecules within the patch E_i ,

$$\frac{E^P}{kT} = \frac{E_D}{kT} + \frac{E_i}{kT} \quad (11)$$

$$\frac{E^P}{kT} = M \frac{E_q}{kT} - \left(1 + \frac{\tilde{k}}{kT}\right) (M/2 - N) d_{\text{eff}} \quad (12)$$

It follows from the above equation that the direct interactions renormalize (enhance) the interaction of the phospholipid molecule with the deviatoric field.

The chosen patch is considered as a system with a constant area A^P and a constant number of molecules M . The system is immersed in a heat bath so that its temperature T is constant. There are two possible energy states for the molecules in the patch. Within the given energy state the molecules are treated as indistinguishable. We assume that the system is in thermodynamic equilibrium and follow the description of a two-orientation model of noninteracting magnetic dipoles [19]. Analogous, if there are N molecules in the state with higher (maximal) energy and $(M-N)$ molecules in the state with lower (minimal) energy, the number of possible arrangements consistent with this N is $M!/N!(M-N)!$, while the

corresponding energy of the system is E^P . However, when calculating the partition function, we must consider all possibilities, e.g., N can be any number from 0 to M ; $N = 0$ means that all the molecules are in the state with lower energy, $N = 1$ means that one molecule is in the state with higher energy while $M-1$ molecules are in the state with lower energy, etc. The canonical partition function $Q^P(M, T, D)$ of M molecules in the small patch of the membrane is therefore

$$Q^P = \sum_{N=0}^M \frac{M!}{N!(M-N)!} \exp\left(-\frac{E^P}{kT}\right) \quad (13)$$

where k is the Boltzmann constant.

Considering equations (2–13) and using the binomial (Newton) formula in summation of the finite series yields

$$Q^P = (2q \cosh(d_{\text{eff}}(1 + \tilde{k}/kT)/2))^M \quad (14)$$

where

$$q = \exp\left(-\frac{E_q}{kT}\right) \quad (15)$$

The Helmholtz free energy of the patch is $F^P = -kT \ln Q^P$,

$$\begin{aligned} F^P = & \frac{M(3\zeta + \zeta^*)}{4} H^2 - M\zeta H H_m - \frac{M(\zeta + \zeta^*)}{4} C_1 C_2 \\ & - MkT \ln \left(2 \cosh \left(\frac{d_{\text{eff}}(1 + \frac{\tilde{k}}{kT})}{2} \right) \right) \\ & + \frac{M\zeta}{2} H_m^2 + \frac{M(\zeta + \zeta^*)}{4} D_m^2 \end{aligned} \quad (16)$$

where

$$D^2 = H^2 - C_1 C_2 \quad (17)$$

The energy of the membrane bilayer is then obtained by summing the contributions of the all patches in both monolayers,

$$F = \int_{A_{\text{out}}} m_{\text{out}} F^P(C_1, C_2) dA + \int_{A_{\text{in}}} m_{\text{in}} F^P(-C_1, -C_2) dA \quad (18)$$

where m_{out} and m_{in} are the area densities of the lipid molecules in the outer and in the inner monolayer, respectively, while F^P is given by equation (16). It is considered that the signs of the principal curvatures in the inner layer are opposite to the signs of the principal curvatures in the outer layer.

We assume that $m_{\text{out}} = m_{\text{in}} = m_0$. Also, in integration, we neglect the difference between the areas of the two monolayers ($A_{\text{out}} = A_{\text{in}} = A_0$), where A is the membrane area. The latter approximation is not valid for strongly curved membranes, but in the system that will be considered in this work, the area

corresponding to strong curvature (i.e. the area of the neck(s)) is small compared to the area of the entire vesicle. It follows from equations (16) and (18) that

$$F = \frac{(3\zeta + \zeta^*)}{8} m_0 \int (2H)^2 dA - \frac{(\zeta + \zeta^*)m_0}{2} \int C_1 C_2 dA - 2m_0 kT \int \ln \left(2 \cosh(d_{\text{eff}}(1 + \frac{\tilde{k}}{kT})/2) \right) dA \quad (19)$$

The first two terms of the above expression yield the bending energy of a nearly flat thin membrane [20]. In the following, the constant contribution $-2m_0 kT A \ln 2$ that is included in the third term of equation (19) is omitted. Also the second term in equation (19) is not considered further since according to the Gauss–Bonnet theorem it is constant for the closed surfaces that are considered in this work. Therefore, we will further consider the expression for the free energy F [14],

$$F = \frac{(3\zeta + \zeta^*)}{8} m_0 \int (2H)^2 dA - 2m_0 kT \int \ln \cosh(d_{\text{eff}}(1 + \tilde{k}/kT)/2) dA \quad (20)$$

The average number of molecules in each of the energy states represents the local quadrupolar ordering of the molecules. Knowing the canonical partition function of a patch Q^P we can calculate the average fraction of the molecules with higher energy within the patch (E_{max}) [14],

$$\frac{\langle N \rangle}{M} = \frac{1}{1 + e^{d_{\text{eff}}(1 + \tilde{k}/kT)}} \quad (21)$$

while the average fraction of the molecules in the lower energy state E_{min} is [14],

$$\frac{\langle M - N \rangle}{M} = \frac{1}{1 + e^{-d_{\text{eff}}(1 + \tilde{k}/kT)}} \quad (22)$$

It can be seen from equations (21) and (22) that at $d_{\text{eff}} = 0$, i.e. when the principal curvatures are equal, both energy states are equally occupied ($\langle N \rangle/M = \langle M - N \rangle/M = 1/2$). The fraction of the number of molecules in the lower energy state increases with increasing d_{eff} to 1, while the fraction of molecules in the higher energy state decreases to 0.

3.2. Global thermodynamic equilibrium

The equilibrium configuration of the system (the equilibrium shape and the corresponding distribution of the quadrupolar ordering) is sought by minimizing the membrane free energy

$$\delta F = 0 \quad (23)$$

under relevant geometrical constraints. We require that the membrane area A

be fixed, that the enclosed volume V be fixed and that the average mean curvature $\langle H \rangle$ be fixed,

$$\int dA = A, \int dV = V, \frac{1}{A} \int HdA = \langle H \rangle \tag{24}$$

For clarity, the above problem is expressed in dimensionless form. We introduce the dimensionless curvatures $c_1 = R_s C_1, c_2 = R_s C_2, h = R_s H, h_m = R_s H_m, \langle h \rangle = R_s \langle H \rangle, d = R_s D, d_m = R_s D_m$, the relative area $a = A/4\pi R_s^2 = 1$, the relative volume $v = 3V/4\pi R_s^3$, the relative area element $da = dA/4\pi R_s^2$ and the relative volume element $dv = 3dV/4\pi R_s^3$. The normalization unit R_s is the radius of the sphere of the required area A , $R_s = \sqrt{A/4\pi}$. The free energy of the phospholipid bilayer F (equation (20)) is normalized relative to $(3\xi + \xi^*)2\pi m_0$,

$$f = w_b + f_d \tag{25}$$

where

$$w_b = \frac{1}{4} \int (c_1 + c_2)^2 da \tag{26}$$

$$f_d = -\kappa \int \ln \cosh(d_{\text{eff}}(1 + \tilde{k}/kT)/2) da \tag{27}$$

and

$$\kappa = 4kTR_s^2/(3\xi + \xi^*) \tag{28}$$

We consider only axisymmetric shapes. The geometry of the shape is described in terms of the arc length l . We use the coordinates $\rho(l)$ and $z(l)$ where ρ is the perpendicular distance between the symmetry axis and a certain point on the contour and z the position of this point along the symmetry axis. The principal curvatures are

$$c_1 = \frac{\sin\psi}{\rho}, \quad c_2 = \frac{d\psi}{dl} \equiv \psi_l \tag{29}$$

where ψ is the angle between the normal to the surface and the symmetry axis. The dimensionless area element is $da = \rho dl/2$ and the dimensionless volume element is $dv = 3\rho^2 \sin\psi dl/4$. Using the above coordinates, the dimensionless free energy is

$$f = \int \frac{1}{8} \left(\frac{\sin\psi}{\rho} + \psi_l \right)^2 \rho dl - \int \frac{\kappa\rho}{2} \ln \cosh \left(\vartheta \left(\frac{\sin\psi}{\rho} - \psi_l \right) \right) dl \tag{30}$$

where

$$\vartheta = \frac{(\xi + \xi^*)D_m}{4kTR_s} \left(1 + \frac{\tilde{k}}{kT} \right) \tag{31}$$

while the dimensionless global constraints are

$$\int \frac{1}{2} \rho \, dl = 1, \quad \int \frac{3}{4} \rho^2 \sin \psi \, dl = \nu, \quad \int \frac{1}{4} (\sin \psi + \psi_l \varrho) \, dl = \langle h \rangle \quad (32)$$

Also, we must consider a local constraint between the chosen coordinates,

$$\frac{d\rho}{dl} = \cos \psi \quad (33)$$

A functional is constructed, $G = \int L \, dl$, where

$$\begin{aligned} L = & \frac{1}{8} \left(\frac{\sin \psi}{\varrho} + \psi_l \right)^2 \rho - \frac{\kappa \rho}{2} \ln \cosh \left(\vartheta \left(\frac{\sin \psi}{\varrho} - \psi_l \right) \right) \\ & + \lambda_a \frac{\rho}{2} + \lambda_\nu \frac{3}{4} \rho^2 \sin \psi + \lambda_{\langle h \rangle} \frac{1}{4} \left(\frac{\sin \psi}{\varrho} + \psi_l \right) \rho + \lambda (\rho_l - \cos \psi) \end{aligned} \quad (34)$$

λ_a, λ_ν and $\lambda_{\langle h \rangle}$ are the global Lagrange multipliers and λ is the local Lagrange multiplier. The above variational problem is expressed by a system of Lagrange–Euler differential equations,

$$\frac{\partial L}{\partial \rho} - \frac{d}{dl} \left(\frac{\partial L}{\partial \rho_l} \right) = 0 \quad (35)$$

$$\frac{\partial L}{\partial \psi} - \frac{d}{dl} \left(\frac{\partial L}{\partial \psi_l} \right) = 0 \quad (36)$$

It follows from equations (35) and (34) that [14]

$$\begin{aligned} \frac{d\lambda}{dl} = & \frac{1}{8} \left(\frac{\chi^2 - \sin^2 \psi}{\rho^2} \right) + \frac{\lambda_a}{2} + \frac{3}{2} \lambda_\nu \varrho \sin \psi + \frac{1}{4} \lambda_{\langle h \rangle} \frac{\chi}{\rho} \\ & - \frac{\kappa}{2} \ln \cosh \left(\vartheta \left(\frac{\sin \psi - \chi}{\varrho} \right) \right) + \frac{\kappa \vartheta}{2 \rho} \sin \psi \tanh \left(\vartheta \left(\frac{\sin \psi - \chi}{\varrho} \right) \right) \end{aligned} \quad (37)$$

while, it follows from equations (36) and (34) that [14]

$$\frac{d\chi}{dl} = \frac{A}{B} \quad (38)$$

where

$$B = \left(1 - \frac{2\kappa \vartheta^2}{\cosh^2(\vartheta(\sin \psi - \chi)/\varrho)} \right) \quad (39)$$

$$A = \frac{\sin \psi \cos \psi}{\rho} \left(1 + \frac{2\kappa \vartheta^2}{\cosh^2\left(\vartheta\left(\frac{\sin \psi - \chi}{\varrho}\right)\right)} \right) - \frac{4\kappa \vartheta^2 \chi \cos \psi}{\rho \cosh^2\left(\vartheta\left(\frac{\sin \psi - \chi}{\varrho}\right)\right)}$$

$$+3\lambda_v \varrho^2 \cos\psi + 4\lambda \sin\psi - 4\kappa \vartheta \cos\psi \tanh\left(\vartheta \left(\frac{\sin\psi - \chi}{\varrho}\right)\right) \quad (40)$$

and

$$\psi_l = \frac{\chi}{\rho} \quad (41)$$

At the poles $\psi_l = \sin\psi / \rho$.

It follows from equations (38) and (39) that a singularity in $d\chi/dl$ occurs when the denominator (39) becomes equal to 0,

$$1 - \frac{2\kappa\vartheta^2}{\cosh^2(\vartheta(\sin\psi/\rho - \psi_l))} = 0 \quad (42)$$

equation (42) is fulfilled when

$$\frac{\sin\psi}{\rho} - \psi_l = \pm \frac{1}{\vartheta} \ln(\sqrt{2\kappa\vartheta} + \sqrt{2\kappa\vartheta^2 - 1}) \quad (43)$$

i.e. when the curvature deviator attains a certain constant value determined by the constants κ and ϑ . This singularity occurs at sites where the opposing effects of isotropic and deviatoric bending become equal in magnitude, i.e., where the deviatoric effects renormalize the isotropic bending to zero. A geometry is reached where the curvature is so high that the approximate model is no longer valid.

3.3. Solution of the variational problem – the equilibrium shape and orientational distribution

The system of Lagrange–Euler differential equations (37) and (38) is solved numerically. The contour of the axisymmetric equilibrium shape is then given by the two coordinates (ρ, z) , where $dz/dl = \sin\psi$. In order to solve the problem numerically, the model constants should be estimated: the interaction constant ζ^* was for reasons of simplicity taken to be equal to ζ , $\zeta = \zeta^* = k_c a_0$, where k_c is the bilayer bending constant and a_0 is the area per phospholipid molecule, $k_c \simeq 20kT$, $a_0 = 60 \times 10^{-20} \text{m}^2$, R_s is 10^{-5}m , $T = 300\text{K}$, $D_m = 2 \times 10^8 \text{m}^{-1}$, $\vartheta \simeq 1.5 \times 10^{-4}$, $\kappa \simeq 7 \times 10^6$ and $\tilde{k}/kT \simeq 1$ [14]. As $a_0 m_0 = 1$, it follows from above and from the normalization given after equation (24) that the normalization factor of the energies is $(3\zeta + \zeta^*)2\pi m_0 = 8\pi k_c$.

Figure 2 shows how the global Lagrange multipliers of an almost globular shape with chosen relative volume and average mean curvature and a chosen constant κ change upon increase of the constant ϑ . It could be expected that the singularity would eventually be reached for high-enough values of ϑ . We call the shape where the singularity first occurs, the critical shape. We were able to overcome the interval of ϑ corresponding to shapes with at least one singularity by extrapolating the solution (the Lagrange multipliers and the boundary conditions) over

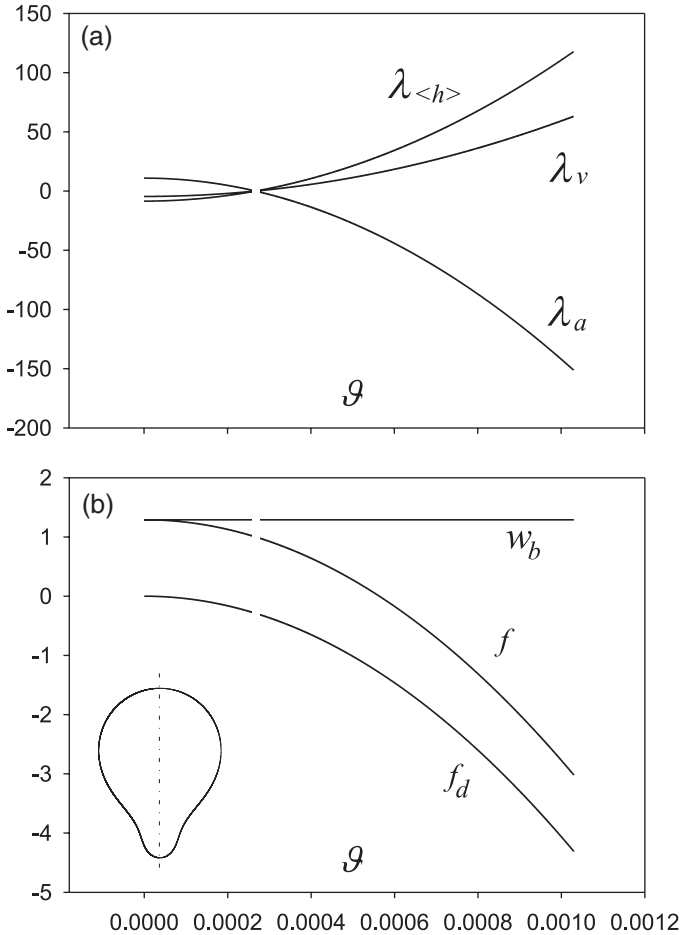


Fig. 2. (a) Lagrange coefficients as a function of the interaction constant ϑ . (b) Bilayer membrane free energy f and the energy contributions: energy of isotropic bending w_b , and contribution of orientational ordering f_d as a function of the interaction constant ϑ . The values of model parameters are $\nu = 0.95$, $\langle h \rangle = 1.0422$, $\kappa = 7 \times 10^6$ (from Kralj-Iglic *et al* [14]).

this narrow interval. Within this interval we could not solve the variational problem numerically. This is indicated by the gap in the curves (Figs. 2a,b). It can also be seen in Fig. 2a that all the Lagrange multipliers approach zero within this interval.

Figure 2b shows the corresponding dependence of the energy contributions on the value of the constant ϑ . The isotropic bending energy w_b , the deviatoric energy f_d and the sum of these two terms $f = w_b + f_d$ are depicted. It can be seen that close to the interval where the singularity occurs and the Lagrange multipliers approach zero, the dependence of the energy on ϑ indicates no discontinuity. When the interaction constant ϑ is increased over the entire range where the

shapes could be calculated (Fig. 2) the shape change is so minute that the shape appears the same (see inset).

Increasing the constant ϑ in a shape that attains many different values of c_1 and c_2 along the contour (such as the pear-shape with a narrow neck) would first yield a singularity (reach the critical shape) at a single point on the contour (on a ring of axisymmetric shape) in the neck region. It is of interest to study the behavior of the solutions of the variational problem close to the critical shape. Starting with the constants κ and ϑ that are high enough to yield a solution above the interval where the singularity occurs in at least one point on the contour, we approached the critical shape with a somewhat narrower neck by decreasing the constant κ .

Figure 3 shows the contour of the shape and the corresponding fraction of the molecules in the lower energy state, i.e., the ordering of the phospholipid molecules; gray lines correspond to the shape that is more remote to the critical ϑ while black lines correspond to the shape that is closer to the critical ϑ . It can be seen in both cases that the fraction of the molecules in the lower energy state increases in the neck region. In the neck, the curvature deviator is higher and the orientational ordering becomes more pronounced. As the critical ϑ is approached, the maximum of the orientational distribution function becomes narrower and the peak becomes sharper. The neck of the pear-shape becomes shorter and exhibits a more abrupt width change for the shape that is closer to the critical ϑ .

Figure 4 shows the numerator (equation (40)), the denominator (equation (39)) and the derivative $d\chi/dl$ along the contour as a function of the symmetry axis of the shapes depicted in Fig. 3. In the shape that is closer to the critical shape (case b) the denominator attains lower absolute values along the whole contour, while it approaches 0 at a certain point in the neck region. Correspondingly, the derivative $d\chi/dl$ reaches higher values and changes abruptly in the vicinity of this point forming sharp peaks. In the shape that is more remote to the critical shape (case a), the absolute values of the denominator and of the numerator are higher, while the values of the derivative $d\chi/dl$ are lower. The peaks formed by the derivative $d\chi/dl$ are milder. The arc length, where the derivative $d\chi/dl$ strongly changes diminishes as the critical shape is approached.

Figure 4 shows that the derivative $d\chi/dl$ increases when we approach the critical shape, while the numerator and the denominator both decrease over the entire shape. In the point on the contour close to the narrowest width of the neck, the denominator approaches zero. From the numerical results we could not come to a definite conclusion that the regularity condition can be imposed. We could not exclude the possibility that the derivative $d\chi/dl$ may in some cases increase beyond any limit. This would mean that the discontinuity in the meridian curvature that is consistent with divergence in $d\chi/dl$ corresponds to a finite energy. Changes of the meridian curvature over a minute arc length were recently observed in two-component phospholipid vesicles with added cholesterol, where the two phospholipids were in two different liquid phases (ordered/disordered) [21].

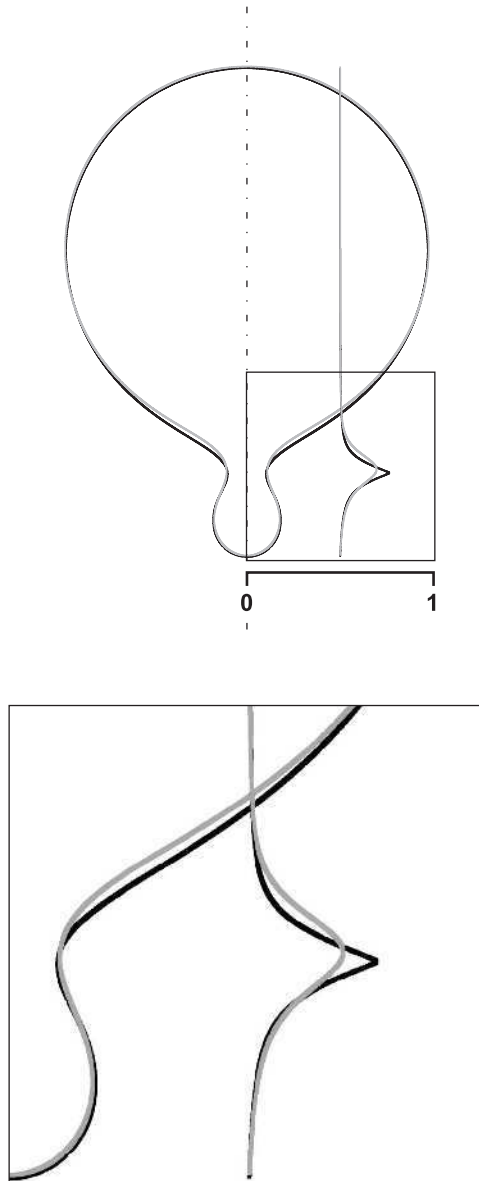


Fig. 3. Two shapes illustrating the approach to the critical shape with singularity in the Euler–Lagrange differential equation and the corresponding orientational distribution functions. The shape that is closer to the critical shape ($\kappa = 1735.5$, black) has a shorter neck and a sharper distribution peak than the shape that is more remote from the critical shape ($\kappa = 2800$, gray). For both shapes $\nu = 0.95$, $\vartheta = 0.02456$, $\langle h \rangle = 1.11543$ (from Kralj-Iglic *et al* [14]).

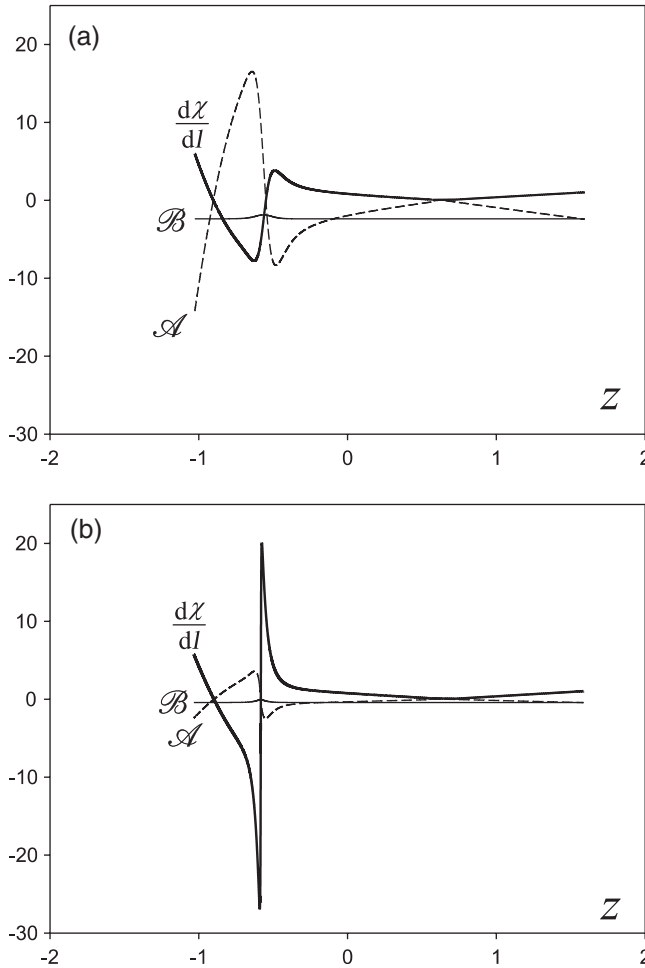


Fig. 4. Approach to the critical shape with singularity in the Lagrange–Euler differential equation. The numerator A , the denominator B and the derivative $d\chi/dl$ are shown for both shapes (a and b, respectively) presented in Fig. 3 (from [14]).

Segregation of the phospholipid was observed whereby an abrupt change in the meridian curvature could be noted in some of the two-photon micrographs. The abrupt changes in curvature appear close to the line where the two phases are in contact, but rather within the disordered phase region. In some shapes, the abrupt change in meridian curvature appears within the disordered phase. It is argued [21] that the shape is determined by the preference of the phospholipid for a certain curvature and by the effects on the edges where the two phases meet; however, the abrupt changes in the curvature within a given phase are not explained.

3.4. Stability of the narrow neck(s)

We studied the sequence of shapes of increasing average mean curvature within the class of pear shapes [2]. It was observed in experiments that the shapes with narrow neck(s) show increased stability [4,17]. For example, in spontaneous transformation of pure palmitoyl oleyl phosphatidylcholine (POPC) vesicles, where the initially long thin protrusion shortens with time, a shape composed of a globular mother vesicle and almost spherical protrusion connected by a narrow neck is attained. Further, the opening of the neck starts; however, the process reverses so that the neck becomes very thin again (Fig. 5). There may be several such oscillations before the neck opens and the vesicle attains its flaccid shape. This indicates an energy minimum of the shape composed of two globular parts connected by a narrow neck. It will be shown below that the orientational ordering of phospholipid molecules in the narrow neck may explain stability of shapes with narrow neck(s).

Figure 6 shows how the free energy of the vesicle changes upon increase of the average mean curvature for a vesicle of a given relative volume $v = 0.95$ and size $R_s = 10^{-5}$ m. Case a corresponds to isotropic bending only, case b corresponds to the quadrupolar ordering of independent molecules ($\tilde{k}/kT = 0$), while case c also considers direct interactions between phospholipid molecules ($\tilde{k}/kT = 1$). The energy of isotropic bending w_b increases along the sequence [22], while the energy of deviatoric bending f_d decreases along the sequence. The behavior of the sum of the two contributions exhibits the difference in the relative rate of change of the two contributions. In case b (if the molecules are considered as independent) the decrease of the energy of the deviatoric bending is not strong enough to overcome the increase of the energy of isotropic bending w_b and f increases with increasing $\langle h \rangle$. In case c (if direct interaction between phospholipid molecules is considered), the increase of the energy of isotropic bending w_b is overcome and the vesicle free energy decreases with increasing $\langle h \rangle$. The rigorous solution of the variational problem (Fig. 6) shows that the effect of quadrupolar ordering on the free energy of the vesicle is also important in shapes, where there are no regions of very high-curvature deviator. Except for in the vicinity of the singularity, the local ordering is low over most of the membrane

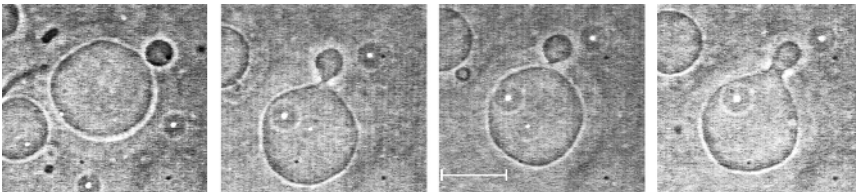


Fig. 5. Oscillations of the neck width before the neck opens and the vesicle attains its flaccid shape indicating that the shape with the narrow neck is energetically favorable, bar = 20 μm (adapted from Iglic and Kralj-Iglic [17]).

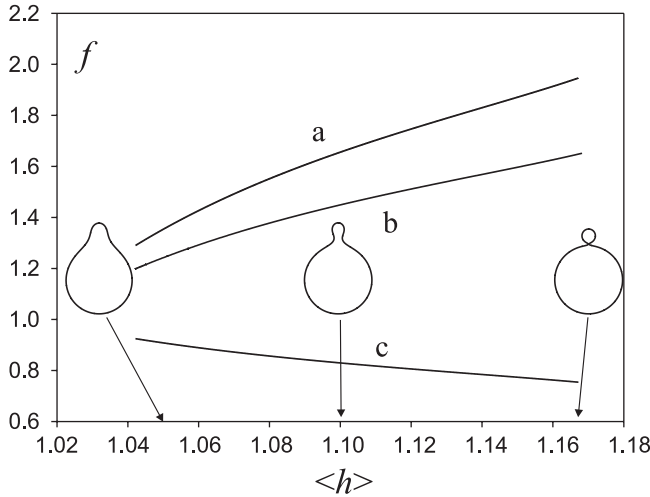


Fig. 6. Bilayer membrane free energy as a function of the average mean curvature of the vesicle with $\nu = 0.95$; (a) isotropic bending, (b) orientational ordering of independent molecules $\vartheta = 1.5 \times 10^{-4}, \kappa = 7 \times 10^6$, c: orientational ordering of interacting molecules $\vartheta = 3 \times 10^{-4}, \kappa = 7 \times 10^6$ (adapted from [14]).

area, while the equilibrium shape could hardly be distinguished from the corresponding shape calculated by minimization of the Helfrich local bending energy. However, as the values of the free energy are considerably affected, the quadrupolar ordering of phospholipid molecules provides a particular interpretation of the trajectories representing the observed processes within the phase diagram of possible shapes. The formation of the neck is energetically favorable for any initiation mechanism. The membrane free energy decreases as the region of increasing curvature deviator increases, while the free energy values remain within the same range (Fig. 6). Similar to exovesiculation (Fig. 4), an energy decrease could also be expected for endovesiculation, by using the same values of the model constants (ϑ and κ). The deviatoric effects could not determine the general direction of the shape change of the globular vesicle, but once the neck(s) start(s) to form, the deviatoric effects provide a mechanism for its stabilization.

3.5. Stability of the pear shape and the ADE model

The mechanism of quadrupolar ordering is complementary to the mechanisms of local and non-local isotropic elasticity of the area-difference-elasticity (ADE) model [3]. The contribution of the non-local isotropic elasticity to the membrane free energy is expressed within the ADE model as [23,3]

$$W_{ADE} = 2k_r A(\langle H \rangle - H_0)^2 \tag{44}$$

where k_r is the non-local bending constant and H_0 determines the average mean curvature of the membrane under lowest possible stress. The contribution of the non-local isotropic bending normalized by $(3\xi + \xi^*)2\pi m_0 = 8\pi k_c$ is

$$w_{ADE} = q(\langle h \rangle - h_0)^2 \quad (45)$$

where $q = k_r/k_c$ and $h_0 = H_0 R_s$.

Within the ADE model, where the free energy consists of the local (26) and non-local (45) isotropic bending, the absolute minimum of the free energy may be by an appropriate choice of the parameters q and h_0 shifted to the limit shape composed of the two spheres connected by an infinitesimal neck. However, a higher value of q than the experimentally estimated one [24] is needed to obtain this effect [3], while the values of h_0 should be taken much larger than any of $\langle h \rangle$ within the sequence of pear shapes, which gives a significant increase in the free energy and concomitant tension within the membrane. It seems unlikely that the vesicle would favor high tension within the membrane as it may develop processes to relax, such as transient pore formation [25,26]. It will be shown below that a decrease of the free energy due to the orientational ordering of phospholipid molecules may complement the non-local isotropic bending in stabilizing pear shapes, including shapes with neck(s).

Figure 7 shows the dependence of the free energy of the vesicle on the average mean curvature $\langle h \rangle$ including the non-local bending of the ADE model for two choices of the parameter h_0 (A: $h_0 = 1.9$, B: $h_0 = 2.1$). Cases a, show the isotropic local and non-local bending (ADE model) while, cases b show the isotropic local and non-local bending and the deviatoric bending due to the quadrupolar ordering of independent molecules ($\tilde{k}/kT = 0$). Since in both cases, A and B, the constant h_0 is larger than any $\langle h \rangle$ of the sequence ($\langle h \rangle < 1.74$), adding a quadratic term of non-local bending to the isotropic local bending increases the membrane free energy (Fig. 7, curves a). If the energy contribution of the deviatoric bending is considered (Fig. 7, curves b), a shallow minimum is obtained for $h_0 = 1.9$ close to the limit shape (at $\langle h \rangle = 1.16$) (A), while for $h_0 = 2.1$ (B) the free energy is decreasing toward the shape with the narrow neck. It can be seen that without considering the deviatoric effect (ADE model alone) the formation of the neck is not favored if the experimental value of the parameter $q = 2$ [24] and the values of h_0 that are comparable to the values of $\langle h \rangle$ within the sequence of the pear shapes are considered. Including the deviatoric effect to the membrane local and non-local isotropic bending renders a minimum close to the shape with the narrow neck. The quadrupolar ordering diminishes the increase of the free energy due to local isotropic bending. Therefore, the sequence becomes more sensitive to the effect of the non-local isotropic bending.

By varying constants ϑ, κ and h_0 within the range that still gives contributions to the free energy that are comparable to the isotropic bending energy, it is also possible to obtain stable pear shapes with a wider neck and deeper minima of the free energy that would exceed the energies of thermal fluctuations. Figure 8

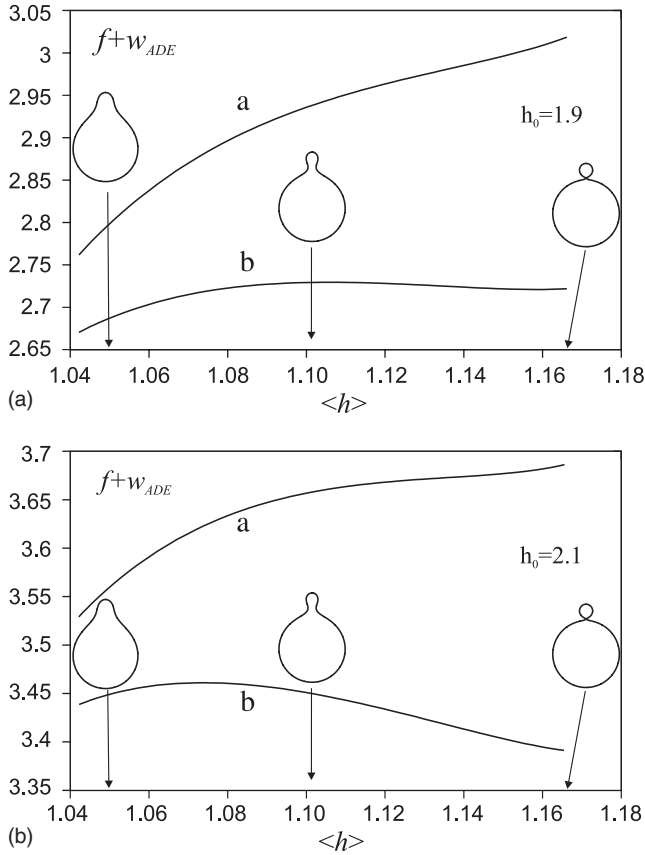


Fig. 7. Bilayer membrane free energy including non-local isotropic bending as a function of the average mean curvature of the vesicle with $\nu = 0.95$ and $q = 2$. Curves a: local and non-local isotropic bending ($\vartheta = 0, \kappa = 0$). Curves b: local and non-local isotropic bending and deviatoric bending due to the orientational ordering ($\vartheta = 1.5 \times 10^{-4}, \kappa = 7 \times 10^6$).

shows the dependence of the free energy of the vesicle on the average mean curvature including the non-local bending of the ADE model for three choices of the parameter h_0 as given in the figure. It can be seen that it is possible to obtain an absolute minimum also for the shape with a wider neck.

4. SPHERICAL BUDDING IN LIPOSOMES COMPOSED OF TWO KINDS OF MOLECULES

We consider a system composed of phospholipid molecules and membrane-inserted molecules that form together with distorted nearby phospholipid molecules the membrane inclusions [15,22,27]. It is assumed that the inclusions

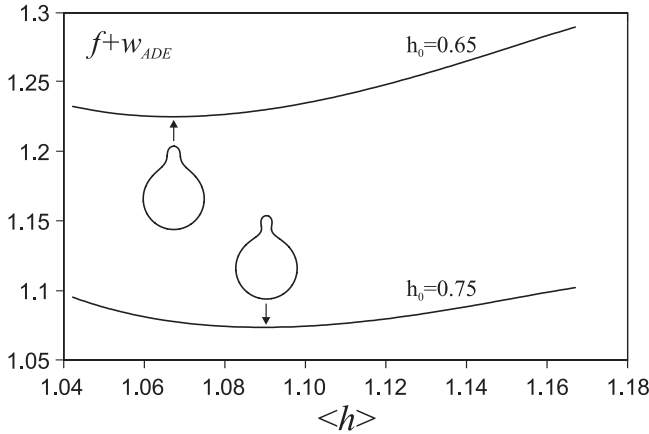


Fig. 8. Bilayer membrane free energy including non-local isotropic bending as a function of the average mean curvature of the vesicle with $\nu = 0.95$ and $q = 2$ for two choices of the parameter h_0 , as given in the figure. The respective shapes, which correspond to the absolute minimum of the free energy within the class of the pear shapes are shown. The values of the model parameters are $\vartheta = 3 \times 10^{-4}, \kappa = 7 \times 10^6$.

are formed by complexes seeded for example by a protein or a detergent molecule. As such inclusions can be rather large, we take that the energy of a single phospholipid molecule is much smaller than the energy of a single inclusion and will therefore be neglected. For simplicity, inclusions are considered to distribute only in one layer of the bilayer. Due to the lateral mobility of inclusions they accumulate in regions of favorable curvature, while they are depleted from regions of unfavorable curvature [5,22,28]. The influence of the intrinsic shape of the phospholipid molecules on the equilibrium configuration of the system has been described in detail in the previous section, therefore, here we study the effect of the intrinsic shape of larger membrane inclusions seeded, for example, by the intercalated protein or detergent molecule in the membrane.

In order to avoid too high local lateral densities of the inclusions we consider the excluded volume principle, i.e., the finite volume of the membrane components by applying the lattice statistics [19].

As previously, the outer monolayer area is divided into small patches that, however, contain a large number of molecules so the methods of statistical physics can be used. The membrane curvature is taken to be constant over the patch. A lattice is imagined with all its M sites occupied either with a phospholipid molecule or an inclusion. In the chosen patch, there are N inclusions with energy E_N and $(M-N)$ phospholipid molecules with energy 0. The inclusions are taken to be isotropic so that $D_m = 0$. It follows from equation (1)

$$E_N = \frac{\xi}{2}(H - H_m)^2 \tag{46}$$

In this case direct interactions between isotropic inclusions are taken into account by using the Bragg–Williams approximation [19]. We assume that the direct interactions [29] are possible only between the inclusions, while there is no direct interaction between the inclusion-phospholipid pairs,

$$W_{ii} = \bar{N}_{ii}w \quad (47)$$

where w is the interaction energy of an inclusion–inclusion pair (for $w < 0$ the interaction between the inclusions is attractive) and \bar{N}_{ii} is the average number of nearest–neighbor inclusions,

$$\bar{N}_{ii} = \frac{1}{2}Nc\frac{N}{M} \quad (48)$$

where, c is the number of nearest neighbors ($c = 4$ for two-dimensional square net). The factor $1/2$ was inserted in order to avoid counting each inclusion–inclusion pair twice. Such direct-interaction energy was used in [8].

The canonical partition function of the inclusions in the patch is

$$Q^P = \exp(-E_N/kT) \exp(-cN^2w/2MkT) \frac{M!}{N!(M-N)!} \quad (49)$$

The Helmholtz free energy of the patch is $F^P = -kT \ln Q^P$,

$$F^P = N\frac{\xi}{2}(H - H_m)^2 + \frac{cwN^2}{2M} + kT \ln(N/M) + kT(M - N) \ln((M - N)/M) \quad (50)$$

The membrane free energy is obtained by summing the contributions of all patches in the outer layer. The contribution of the inner layer composed of phospholipid molecules yields a constant contribution since the energy of the phospholipid molecules is taken to be 0, and since all the lattice sites are occupied by equal and indistinguishable molecules. This constant contribution is omitted. Free energy of the vesicle is therefore

$$F = \int_A \frac{\xi m_0}{2} (H - H_m)^2 n \, dA + \int_A \frac{cwm_0}{2} n^2 \, dA + kTm_0 \int_A (n \ln n + (1 - n) \ln(1 - n)) \, dA \quad (51)$$

where $n = N/M$ and $m_0 = M/dA$.

The equilibrium configuration of the system (the equilibrium shape and the corresponding distribution of the membrane inclusions) is sought by minimizing the free energy

$$\delta F = 0 \quad (52)$$

under relevant geometrical constraints.

We require that there is a fixed number of inclusions in the membrane

$$\frac{1}{A} \int n \, dA = \bar{n} \tag{53}$$

where, \bar{n} is the average value of n .

For clarity, dimensionless quantities are used. The dimensionless curvatures and the area and volume elements are defined as above (equation (24)). Here, the free energy is normalized relative to kTm_0A ,

$$f = \int \frac{\xi}{2kT} (H - H_m)^2 n \, da + \int \frac{cw}{2kT} n^2 \, da + \int (n \ln n + (1 - n) \ln(1 - n)) \, da \tag{54}$$

The dimensionless form of constraint (53) is

$$\int n \, da = \bar{n} \tag{55}$$

Here, we will rigorously solve the variational problem only with respect to the distribution of the inclusions n . A functional is constructed, $G = \int L \, dl$, where

$$L = \frac{\xi}{2kT} (H - H_m)^2 n + \frac{cw}{2kT} n^2 + (n \ln n + (1 - n) \ln(1 - n)) + \lambda_n n \tag{56}$$

and λ_n is the global Lagrange multiplier. The relevant Lagrange–Euler differential equation

$$\frac{\partial L}{\partial n} = 0 \tag{57}$$

yields

$$\ln \left[\frac{n}{1 - n} \exp \frac{cwn}{kT} \right] = -\lambda - \frac{\xi}{2kT} (H - H_m)^2 \tag{58}$$

For simplicity, we take $\exp(cwn/kT) \approx 1 + cwn/kT$, therefore,

$$\ln \left[\frac{n}{1 - n} \left(1 + \frac{cwn}{kT} \right) \right] = -\lambda - \frac{\xi}{2kT} (H - H_m)^2 \tag{59}$$

After rearrangement, equation (59) is solved to obtain

$$n = - \frac{(1 + e^{-(\lambda+\beta)})kT}{8w} + \frac{(1 + e^{-(\lambda+\beta)})kT}{8w} \sqrt{1 + \frac{(16w/kT)e^{-(\lambda+\beta)}}{(1 + e^{-(\lambda+\beta)})^2}} \tag{60}$$

where, $\beta = \xi n(H - H_m)^2 / 2kT$ and $c = 4$. In the limit of weak interaction (small w) equation (60) transforms into

$$n \cong \frac{\vartheta \exp(-\beta)}{(1 + \vartheta \exp(-\beta))} \left[1 - \frac{4w}{kT} \frac{\vartheta \exp(-\beta)}{(1 + \vartheta \exp(-\beta))^2} \right] \tag{61}$$

where $\vartheta = \exp(-\lambda)$ and $w < 0$ for attractive interactions. The parameter ϑ is determined from constraint (53).

To perform minimization of the membrane free energy with respect to the membrane shape, we use a simple parametric model that we consider relevant to discuss a possible physical mechanism explaining the observed curvature-induced sorting of membrane components. We limit our study to buds that have spherical shape. In the model, the membrane is divided into two parts, the planar part (part 1) with the relative area a_1 and the respective fraction of the area covered by the inclusions n_1 , and spherically curved part of the membrane (part 2) with the constant mean curvature $H = 1/r$, the relative area a_2 and the respective fraction of the area covered by inclusions equal to n_2 . The parameter ϑ is determined numerically from the condition

$$n_1 a_1 + n_2 a_2 = \bar{n} \tag{62}$$

where we take into account

$$a_1 + a_2 = 1 \tag{63}$$

As previously stated, the curved membrane region (region 2) corresponds to the budding (invaginated or evaginated) membrane regions or vesicles.

Figure 9 shows the fraction of the area of the membrane budding (invaginated or evaginated) region covered by inclusions (n_2) as a function of its curvature radius (r) for three values of the intrinsic mean curvature of the inclusions (H_m). It can be seen that for the values of r close to $1/H_m$ the fraction of the membrane curved area occupied by inclusions (n_2) is much larger than \bar{n} even if $w = 0$. This indicates

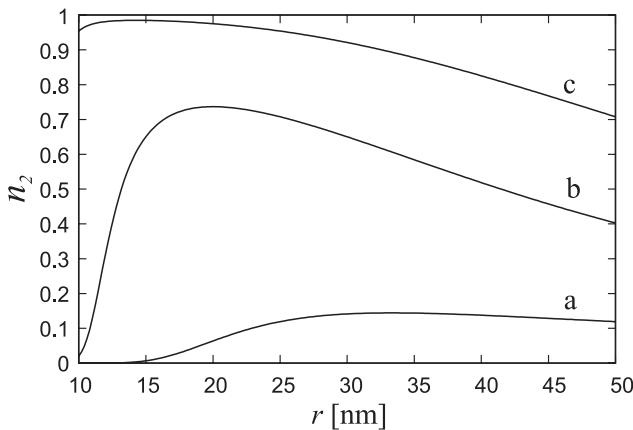


Fig. 9. Fraction of the area of the membrane invaginated or evaginated (budding) region covered by inclusions (n_2) as the function of its curvature radius (r) for three values of the intrinsic mean curvature of the inclusions (H_m): 0.03 nm^{-1} (a), 0.05 nm^{-1} (b) and 0.07 nm^{-1} (c). The values of the other model parameters are: $\bar{n} = 0.02$, $a_2 = 0.02$, $w = 0$ and $\xi = 5000 \text{ kT nm}^{-2}$ [28].

the possibility of the curvature-induced clustering of the membrane inclusions in the highly curved membrane regions, i.e., the formation of rafts on membrane invaginations or evaginations and vesicles, due to the preference of inclusions for certain (non-zero) membrane curvature. It can be also seen in Fig. 9 that for high-enough values of the intrinsic mean curvature of the inclusions (H_m) the value of (n_2) approaches unity indicating the possibility of the lateral phase separation of the inclusions for high-enough values of (H_m). For given H_m , the value of r corresponding to maximum of $n_2(r)$ (Fig. 9) also corresponds to minimum of the free energy F , i.e., this value of r is energetically most favorable for given H_m .

Recently, upgradation of the standard model for the cellular membranes [30] with consideration of lateral inhomogeneities of the membrane constituents – rafts [31,32], indicates that budding is important in formation of rafts. Clustering of membrane constituents into larger domains (rafts) in highly curved spherical regions (invaginations) of cell membranes have been observed in biological membranes [33]. It was suggested that small protein–cholesterol membrane complexes (inclusions) may coalesce into larger domains (rafts) [34] upon curvature-induced enrichment of inclusions in highly curved spherical parts of the budding region [35]. The size of membrane inclusions can be very small, comprising just a few molecules (proteins and lipids) [36], but also larger.

For example, it was indicated recently that after generation of ceramide from sphingomyelin in giant sphingomyelin liposomes, lateral distribution of ceramide becomes non-homogeneous. Lateral phase separation, i.e., the formation of ceramide domains, takes place leading to the formation of ceramide-enriched membrane evaginations/invaginations [5]. It is suggested that the observed lateral segregation of the ceramide molecules may be a consequence of the interdependence between the local-membrane shape, the local area density of ceramide molecules and the intrinsic shape of the ceramide molecules. The role of the direct intermolecular (nearest-neighbor) interactions between ceramide molecules is also indicated [5].

In the presented theoretical consideration the applied value for the interaction constants ξ is considerably larger than the corresponding value for a single phospholipid molecule [18]. This means that the inclusions considered in Fig. 9 can be membrane proteins, protein–lipid complexes or small clusters of lipid molecules (nanorafts). Therefore they can not be considered as completely rigid bodies as they can adjust their shape to local membrane curvature also by bending. As it is shown in Fig. 9 such inclusions may coalesce into larger rafts upon curvature-induced clustering as indicated in previous studies [34,35].

5. CONCLUSION

In-plane orientational ordering of lipids in the narrow neck connecting the bud with the mother membrane and clustering of membrane inclusions in the budding

region are considered to be complementary driving mechanisms in budding of liposomes (Fig. 10). Both these internal degrees of freedom diminish the membrane free energy. Thereby they counteract the mechanism of isotropic bending and contribute to the relaxation of the membrane. In one-component membrane anisotropic shape of phospholipid molecules (Fig. 1) induces an internal degree of freedom exhibited by in-plane orientational ordering of molecules according to the local membrane curvature. Higher degree of ordering is localized in regions with large difference between the two principal curvatures, e.g., narrow neck(s) (Fig. 10). In multi-component membranes, intrinsic shape of the inclusions induces an internal degree of freedom exhibited by segregation of components (Fig. 9).

Inclusions segregate in the buds (Fig. 10), which fit the intrinsic shape of the inclusions (Fig. 9). Attractive direct interactions between the inclusions promote this effect.

Regions of higher order may present an environment that is favorable for raft formation. Budding with internal degrees of freedom may therefore represent a sorting mechanism that regulates composition of the membrane and lateral distribution of its constituents according to their intrinsic shape and mutual interactions.

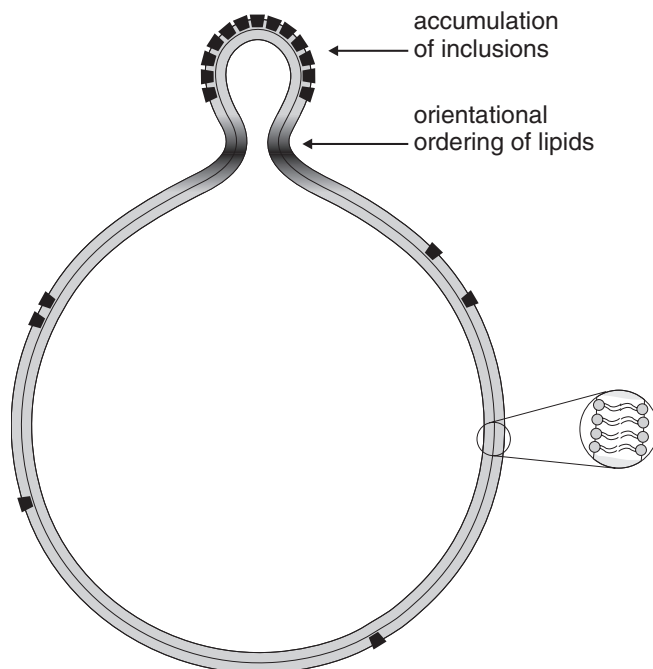


Fig. 10. Schematic presentation of two different complementary driving mechanisms of membrane budding, i.e., clustering of membrane inclusions in the budding region and in-plane orientational ordering of lipids in the narrow neck connecting the bud with the mother membrane.

REFERENCES

- [1] E. Sackmann, Membrane bending energy concept of vesicle and cell shapes and shape transitions, *FEBS Lett.* 346 (1994) 3–16.
- [2] R. Lipowsky, The conformation of membranes, *Nature* 349 (1991) 475–481.
- [3] L. Miao, U. Seifert, M. Wortis, H.G. Döbereiner, Budding transitions of fluid-bilayer vesicles: effect of area difference elasticity, *Phys. Rev. E* 49 (1994) 5389–5407.
- [4] J. Käs, E. Sackmann, Shape transitions and shape stability of giant phospholipid vesicles in pure water induced by area – to – volume change, *Biophys. J.* 60 (1991) 825–844.
- [5] J.M. Holopainen, M.I. Angelova, P.K.J. Kinnunen, Vectorial budding of vesicles by asymmetrical enzymatic formation of ceramide in giant liposomes. *Biophys. J.* 78 (2000) 830–838.
- [6] V. Kralj-Iglic, A. Iglic, H. Hägerstrand, P. Peterlin, Stable tubular microexovesicles of the erythrocyte membrane induced by dimeric amphiphiles, *Phys. Rev. E* 61 (2000) 4230–4234.
- [7] H. Hägerstrand, B. Isomaa, Lipid and protein composition of exovesicles released from human erythrocytes following treatment with amphiphiles, *Biochim. Biophys. Acta* 1190 (1994) 409–415.
- [8] V.S. Markin, Lateral organization of membranes and cell shapes. *Biophys. J.* 36 (1981) 1–19.
- [9] V. Kralj-Iglic, S. Svetina, B. Zeks, Shapes of bilayer vesicles with membrane embedded molecules, *Eur. Biophys. J.* 24 (1996) 311–321.
- [10] P.B.S. Kumar, G. Gompper, R. Lipowsky, Budding dynamics of multicomponent membranes, *Phys. Rev. Lett.* 86 (2001) 3911–3914.
- [11] R. Lipowsky, R. Dimova, Domains in membranes and vesicles, *J. Phys. Condens. Matter* 15 (2003) 531–545.
- [12] M. Laradji, P.B.S. Kumar, Dynamics of domain growth in self-assembled fluid vesicles, *Phys. Rev. Lett.* 93 (2004) 1–4/198105.
- [13] J.B. Fournier, Nontopological saddle splay and curvature instabilities from anisotropic membrane constituents, *Phys. Rev. Lett.* 76 (1996) 4436–4439.
- [14] V. Kralj-Iglic, B. Babnik, D.R. Gauger, S. May, A. Iglic, Quadrupolar ordering of phospholipid molecules in narrow necks of phospholipid vesicles, *J. Stat. Phys.* (2006) (in print).
- [15] M. Fosnaric, K. Bohinc, D.R. Gauger, A. Iglic, V. Kralj-Iglic, S. May, The influence of anisotropic membrane inclusions on curvature elastic properties of lipid membranes, *J. Chem. Inf. Model.* 45 (2005) 1652–1661.
- [16] V. Kralj-Iglic, M. Remskar, G. Vidmar, M. Fosnaric, A. Iglic, Deviatoric elasticity as a possible physical mechanism explaining collapse of inorganic micro and nanotubes, *Phys. Lett.* 296 (2002) 151–155.
- [17] A. Iglic, V. Kralj-Iglic, Effect of anisotropic properties of membrane constituents on stable shape of membrane bilayer structure, in: H. Ti Tien, A. Ottova-Leitmannova (Eds.), *Planar Lipid Bilayers (BLMs) and Their Applications*, Elsevier, Amsterdam, London, 2003, pp. 143–172.
- [18] V. Kralj-Iglic, A. Iglic, G. Gomiscek, F. Sevsek, V. Arrigler, H. Hägerstrand, Microtubes and nanotubes of a phospholipid bilayer membrane, *J. Phys. A: Math. Gen.* 35 (2002) 1533–1549.
- [19] T.L. Hill, *An Introduction to Statistical Thermodynamics*, General Publishing Company, Toronto, 1986, pp. 209–211..
- [20] W. Helfrich, Elastic properties of lipid bilayers – theory and possible experiments, *Z. Naturforsch.* 28c (1973) 693–703.
- [21] T. Baumgart, S.T. Hess, W.W. Webb, Imaging coexisting fluid domains in biomembrane models coupling curvature and line tension, *Nature* 425 (2003) 821–824.
- [22] V. Kralj-Iglic, V. Heinrich, S. Svetina, B. Zeks, Free energy of closed membrane with anisotropic inclusions, *Eur. Phys. J. B* 10 (1999) 5–8.

- [23] E.A. Evans, R. Skalak, *Mechanics and Thermodynamics of Biomembranes*, CRC Press, Boca Raton, FL, 1980.
- [24] W.C. Hwang, R.A. Waugh, Energy of dissociation of lipid bilayer from the membrane skeleton of red blood cells, *Biophys. J.* 72 (1997) 2669–2678.
- [25] J.M. Holopainen, M.I. Angelova, Söderlund, P.J. Kinnunen, Macroscopic consequences of the action of phospholipase C on giant unilamellar liposomes, *Biophys. J.* 83 (2002) 932–943.
- [26] R.M. Raphael, R.E. Waugh, Accelerated interleaflet transport of phosphatidylcholine molecules in membranes under deformation, *Biophys. J.* 71 (1996) 1374–1388.
- [27] S. Marcelja, Chain ordering in liquid crystals II. Structure of bilayer membranes, *Biophys. Biochim. Acta* 367 (1974) 165–176.
- [28] A. Iglic, M. Fosnaric, H. Hägerstrand, V. Kralj-Iglic, Coupling between vesicle shape and the non-homogeneous lateral distribution of membrane constituents in Golgi bodies, *FEBS Lett.* 574/1–3 (2004) 9–12.
- [29] K. Bohinc, V. Kralj-Iglic, S. May, Interaction between two cylindrical inclusions in a symmetric lipid bilayer, *J. Chem. Phys.* 119 (2003) 7435–7444.
- [30] S.J. Singer, G.L. Nicholson, The fluid mosaic model of the structure of cell membranes, *Science* 175 (1972) 720–731.
- [31] D.A. Brown, E. London, Structure and origin of ordered lipid domains in biological membranes, *J. Membr. Biol.* 164 (1998) 103–114.
- [32] K. Simons, E. Ikonen, Functional rafts in cell membranes, *Nature* 387 (1997) 569–572.
- [33] T. Harder, K. Simons, Caveolae, DIGs, and the dynamics of sphingolipid-cholesterol microdomains, *Curr. Opin. Cell. Biol.* 9 (1997) 534–542.
- [34] J.C. Holthuis, G. van Meer, K. Huitema, Lipid microdomains, lipid translocation and the organization of intracellular membrane transport (review), *Mol. Membr. Biol.* 20 (2003) 231–241.
- [35] C. Thiele, M.J. Hannah F. Fahrenholz, W.B. Huttner, Cholesterol binds to synaptophysin and is required for biogenesis of synaptic vesicles, *Nat. Cell. Biol.* 2 (1999) 42–49.
- [36] K. Jacobson, C. Dietrich, Looking at lipid raft? *Trends Cell Biol.* 9 (1999) 87–91.

This page intentionally left blank

Electrical Properties of Aqueous Liposome Suspensions

F. Bordi,^{1,2} C. Cametti^{1,2,*} and S. Sennato^{1,2}

¹*Dipartimento di Fisica, Universita' di Roma "La Sapienza" Piazzale A. Moro 5, I-00185 – Rome, Italy*

²*INFM CRS-SOFT, c/o Università di Roma "La Sapienza" Piazzale A. Moro 5, I-00185 – Rome, Italy*

Contents

1. Introduction	282
1.1. Classification and preparation of liposomes	283
1.2. Applications	284
2. Dielectric Properties of Liposome Suspensions	285
2.1. Dielectric properties of a heterogeneous system	286
2.1.1. The basic formulas	286
2.1.2. Influence of the ion (counterion) distribution	291
2.1.3. Specific effects associated with the liposome structure	295
3. Radio Wave Dielectric Spectra of a DPPC Liposome Suspension: A Typical Example	300
3.1. Liposome preparation	302
3.2. Typical dielectric spectra	302
3.3. Influence of the liposome size	305
3.4. Influence of the temperature	306
4. Electrical Properties of the Liposomal Structure	307
4.1. Effect of surface charge density on the spontaneous formation of vesicles	307
4.2. Effect of an external electric field on vesicle double-layer structure	311
5. Electrorotation of Liposomes	314
References	315

Abstract

The dielectric and conductometric behavior of aqueous liposome suspensions are reviewed in light of the interfacial properties of highly heterogeneous colloidal systems, and the interplay between lipid bilayer properties and an applied electric field is briefly discussed. Since electrostatic interactions play a relevant role in the self-assembly of amphiphilic molecules, the presence of an external electric field strongly influences the organization of the lipids within the bilayer, and, correspondingly, the coupling of an external electric field to these systems furnishes a valuable physical probe to investigate the structure and dynamical properties of the liposome–water interface. After a brief summary of the dielectric theory of heterogeneous systems applied to aqueous liposome suspensions, some recent applications of the radio-wave dielectric spectroscopy, addressed to the investigation of DPPC aqueous liposome suspensions, are presented and discussed here. In particular, we have evidenced how dielectric spectroscopy, in an appropriate frequency range, is capable of furnishing information

*Corresponding author. Tel.: +39-06-49913476; Fax: +39-06-4463158;
E-mail: cesare.cametti@roma1.infn.it

on the structural organization of the lipid bilayer (correlated lipid domains at the lipid–aqueous interface), on the changes in the lipid chain conformation at the pre- and main-transition temperature, and on counterion accumulation effects, in the neighboring bilayer surface. Finally, the effects of the surface charge density on the spontaneous vesicle formation and the influence of an external electric field on the double-layer structure are summarized.

1. INTRODUCTION

Liposomes are vesicular structures formed by a closed lipid bilayer encompassing an aqueous core. In an appropriate environment, these structures, owing to the amphiphilic character of their component molecules, self-assemble. Amphiphilic molecules, being composed of different hydrophobic and hydrophilic parts, give rise in aqueous solution to a variety of morphologically different structures. Among these, unilamellar or multilamellar vesicles (liposomes) are of peculiar interest under several aspects. Liposomes are excellent models of biomembranes, in particular, to study interactions between different lipids and membrane proteins, offering the unique advantage that the lipidic composition of the bilayer can be varied in a well-defined and controlled way. Furthermore, since the lipid bilayer allows the entrapment of hydrophilic material within the aqueous core, and hydrophobic material within the hydrocarbon chain phase, liposomes can be effectively used as drug delivery systems.

The lipid composition, together with the characteristics of the aqueous phase, defines the physicochemical properties of these structures, such as their stability, the surface charge density (at the lipid–aqueous phase interface), the surface hydrophilicity/hydrophobicity ratio, the bilayer rigidity and, moreover, their properties as colloidal particles, such as size, electrophoretic mobility, inter-particle interactions, and interactions with ions and other molecules in the solution. The possibility of a fine-tuning of all these properties suggested a number of applications in various fields. In the last few years, the development of liposome applications has been considerable, especially in clinical and biotechnological fields [1–4].

Although the basic ‘driving force’ for the self-assembling of amphiphilic lipids is represented by the entropic gain obtained when water, avoiding the contact with the hydrophobic part, is not ‘forced’ to assume a structure compatible with a non-polar surface [5], electrostatic interactions play a fundamental role in the aggregation process and in determining the properties of the resulting particles and, more generally, of the suspension as a whole. For this reason, the presence of an external electric field can have a strong influence on the organization of the lipids within the bilayer and, correspondingly, the coupling of an external electric field to the system furnishes a valuable physical probe to investigate the structure and the dynamical properties of the liposome–water interface.

This review, aimed to highlight both these aspects – the dielectric behavior of these systems as a model of a highly heterogeneous colloid and the interplay between lipid bilayer properties and electric fields – is organized as follows. We will first give a brief overview of the various types of vesicles that form under

different conditions. Then we will focus on the main results of the dielectric theory of heterogeneous systems as applied to liposome suspension and we will discuss some recent applications of dielectric spectroscopy addressed to the investigation of these systems, mentioning, for completeness, the more recent developments of the twin technique dielectrophoresis. In the last part, we will review some recent results on the effects of electrostatic interactions on the lipidic structure and on the dynamics of formation of the lipid vesicles. The prominent message from these studies is that small changes in the 'electrostatic environment' can have dramatic effects on the molecular organization at the bilayer level. Investigation of these effects could represent the key to completely understand the mechanisms that allow biological cell to control membrane organization.

1.1. Classification and preparation of liposomes

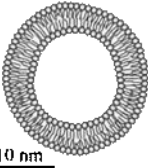
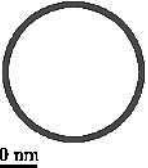
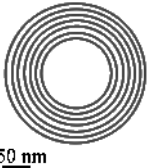
Liposome classification can be made either according to their structural properties, i.e., size and number of lamellae, or on the basis of the preparation method. Four main classes of liposomes can be identified as follows:

1. Small unilamellar vesicles (SUV), with diameter less than 100 nm. This category includes the lowest limit available for lipid vesicles (about 25 nm for dipalmitoyl-lecithin liposomes).
2. Large unilamellar vesicles (LUV), with diameter between 100 nm and 10 μm .
3. Giant unilamellar vesicles (GUV), with diameter larger than 1 μm .
4. Multilamellar large vesicles (MLV), with more concentric lamellae, with diameters larger than 0.5 μm . In the presence of a few number of lamellae, these structures are referred to as oligolamellar liposomes (OLV).

A scheme of the standard liposome nomenclature is shown in Table 1.

Liposomes can be prepared by means of different methods in order to control dimensions and number of the lamellae in the vesicle. Up to now various experimental set-up have been developed to generate homogeneous and reproducible liposome suspensions of appropriate size range, most of them involving two steps, i.e., the lipid hydration and the liposome sizing [6–10]. In the first step, lipids are dissolved in an appropriate organic solvent, which is then dried down in a round-sided glass vessel to form a thin film. Multilamellar aggregates are spontaneously produced by hydrating the thin lipid film when the system is shaken at a temperature higher than the melting transition temperature T_m of the lipid. In the next step, SUVs may be produced by pressure extrusion or ultrasonication, yielding predictable and reproducible particle size distributions [6,7,11]. The extrusion process developed by Hope *et al.* [12] consists in forcing liposome dispersion through polycarbonate membrane filters with controlled pore diameters. Sonication by means of a probe or a bath, continuous or pulse mode power, sonicator has been employed since 1960s [13,14] to reduce the size of multilamellar vesicles and to reshape them to unilamellar ones.

Table 1. Liposome classification and standard nomenclature

		Liposome classification		
		Denomination	Diameter	Morphology
SUV		Small unilamellar vesicles	20–100 nm	
LUV		Large unilamellar vesicles	> 100 nm	
GUV		Giant unilamellar vesicles	> 1 μm	
OLV		Oligolamellar vesicles	0.1–0.5 μm	
MLV		Multilamellar large vesicles	> 0.5 μm	

Other preparation methods are based on the replacement of organic solvents by aqueous media. In the presence of water immiscible solvent, Deamer and Bangham [15] developed the ‘solvent injection’ method, which involves the slow injection of ether or ether–methanol solutions into an aqueous phase, through a narrow bore needle. The solvent is continuously removed by slow evaporation, at elevated temperature and under reduced pressure. Another method, known as the ‘reverse-phase evaporation’ method [16], allows the formation of unilamellar or multilamellar liposomes by emulsifying a lipid-containing water-immiscible solvent (chloroform, ether) with a water phase. In the presence of solvents soluble in water, Batzri and Korn [17] developed the ‘ethanol injection’ method. A solution of lipids in ethanol is injected into an excess of saline or another aqueous medium, and the complete mixing is achieved thanks to the force of the injection. When the ethanol is diluted, phospholipid molecules are dispersed throughout the medium and form liposomes. A fast injection results in the formation of small liposomes, while a slower one yields larger vesicles.

In the attempt to circumvent the lipid dissolution into an organic solvent, high-shear homogenizers are employed for the production, in a single step, of highly concentrated liposomes with diameters smaller than 100 nm [7,18,19].

1.2. Applications

Because of the ‘biocompatibility’ of liposome with the lipid bilayer of biological cell membranes, liposomes are employed in numerous clinical situations [2–4,20–22].

Since 1970 until now, liposomes have been investigated as systems for the delivery or targeting of drugs to specific sites in the body. Many review articles evidence the large expansion of this research over the last 30 years [1–4].

The use of liposomes as drug delivery systems is mainly due to their structural versatility in terms of size, composition, surface charge, bilayer fluidity, and ability to incorporate almost any drug, or to carry cell-specific ligands. Moreover, some specific properties, such as the controlled retention of entrapped drugs in the presence of biological fluids and the vesicle permanence in the blood circulation or in other body compartments, explain the enormous growing up of applications, which appear to become almost limitless.

Liposomes are considered the leading drug delivery systems for the systemic administration of drugs. Efforts in development of new formulations have reduced toxicity and improved efficacy for the delivery of a wide range of drugs, as antitumor agents, antivirals, antifungals, antimicrobials, vaccines, and gene therapeutics [4].

2. DIELECTRIC PROPERTIES OF LIPOSOME SUSPENSIONS

Under the influence of an external electric field, aqueous liposome suspensions undergo a very complex phenomenology driven both by the electrical properties of the lipids organized in the double layer, such as their ionic or zwitterionic character, and by the presence of a large interface with an external medium, making them a suitable model for highly heterogeneous colloidal systems.

Moreover, the typical phenomena shown by these systems occur at very different characteristic times, ranging from times of the order of 1 s or more for fluctuation and/or reorganization of large structures (clusters of liposomes) to times of the order of ps, typical of the motion of a water molecule due to orientational polarization.

Dielectric spectroscopy, extending from some MHz to tenth of GHz, over more than 10^{10} decades of frequency, offers an unique and unreplaceable technique to investigate the electrical properties of aqueous liposome suspensions.

This technique has long been known as a powerful tool in the study of heterogeneous systems such as colloidal particle dispersions [23] and, more generally, it has been successfully employed to investigate the structure and transport properties of cell membranes and lipid bilayers [24,25]. In particular, dielectric spectroscopy measurements on liposome suspensions have been recently advantageously used to investigate the molecular order and the reorientational motions of lipid headgroups at the bilayer surface. Previous investigations on stacked, hydrated planar bilayers revealed the suitability of the method [26], showing that local headgroup dynamics contributes a dielectric relaxation in the frequency range between 10 and 100 MHz, that can be separated from the effects generally present in highly dispersed colloidal systems, such as the ionic contribution at lower frequencies and the dipolar orientational effect or the relaxation of the hydration water, at higher frequencies (close to 100–150 MHz).

Before analyzing in detail the electrical effects that are peculiar to liposome suspensions, in the following section we will summarize the main features of the dielectric theory applied to highly dispersed colloidal systems.

2.1. Dielectric properties of a heterogeneous system

2.1.1. The basic formulas

Within the heterogeneous colloidal system theory [27], an aqueous liposome suspension can be modeled as a collection of spherical (or spheroidal) particles covered by a concentric layer encapsulating an aqueous core phase and uniformly distributed in a continuous aqueous phase.

The dielectric properties of such systems have been described, in their basic expressions, by Pauly and Schwan [28], who considered, within the mean field theory approximation, the average behavior of the whole system as due to the superposition of the dipolar effect that each particle experiences under an applied electric field.

The dielectric and conductometric properties of each one of the different media involved are generally characterized by two parameters, the complex electrical conductivity $\sigma^*(\omega)$ and the complex dielectric constant $\varepsilon^*(\omega)$, both of them depending on the angular frequency ω .

If the bulk properties of each media, i.e., the electrical conductivity σ and the permittivity ε , are independent of the frequency, then the above dielectric parameters can be written as¹

$$\sigma^*(\omega) = \sigma + i\omega\varepsilon_0\varepsilon \quad (5)$$

¹ From a general point of view, the relationship between the complex dielectric constant $\varepsilon^*(\omega)$ and the complex electrical conductivity $\sigma^*(\omega)$ is given by

$$\sigma^*(\omega) = i\omega\varepsilon_0\varepsilon^*(\omega) \quad (1)$$

where ε_0 is the dielectric constant of free space and ω the angular frequency of the applied electric field. The complex dielectric constant $\varepsilon^*(\omega)$, in the presence of an intrinsic dielectric relaxation in the frequency range investigated, can be written as

$$\varepsilon^*(\omega) = \varepsilon'(\omega) - i[\varepsilon''_{\text{diel}}(\omega) + \varepsilon''_{\text{cond}}(\omega)] \quad (2)$$

where the total dielectric loss (the imaginary part) is due to a contribution deriving from the dielectric loss, $\varepsilon''_{\text{diel}}(\omega)$, and a contribution due to a conductivity loss $\varepsilon''_{\text{cond}}(\omega) = \sigma/(\varepsilon_0\omega)$. For samples with $\varepsilon'(\omega) \equiv \varepsilon$ (independent of frequency) and $\varepsilon''_{\text{diel}}(\omega) = 0$, the above relationship reads

$$\sigma^*(\omega) = \sigma + i\omega\varepsilon_0\varepsilon \quad (3)$$

or equivalently as

$$\varepsilon^*(\omega) = \varepsilon + \frac{\sigma}{i\omega\varepsilon_0} \quad (4)$$

or equivalently, as

$$\varepsilon^*(\omega) \equiv \frac{\sigma^*(\omega)}{i\omega\varepsilon_0} = \varepsilon + \frac{\sigma}{i\omega\varepsilon_0} \quad (6)$$

The basic expression for a collection of N spherical particles of radius R with complex dielectric constant $\varepsilon_p^*(\omega) = \varepsilon + \sigma_p/i\omega\varepsilon_0$ covered with a shell of thickness d with complex dielectric constant $\varepsilon_s^*(\omega) = \varepsilon_s + \sigma_s/i\omega\varepsilon_0$, uniformly distributed in a continuous medium of complex dielectric constant $\varepsilon_m^*(\omega) = \varepsilon_m + \sigma_m/i\omega\varepsilon_0$ can be derived from the effective medium approximation (EMA) theory, using the Maxwell argument of equating the external moment $M = NM_a$ of N such spheres in volume V to the moment of a single sphere M_a of this same volume and permittivity ε^* in a medium of permittivity ε_m^* . This can be done considering the spatial dependence of dipolar term in the electrical potential outside a spherical region containing the particle ensemble. This term is derived from the solution of the Laplace equation $\nabla^2\Psi(\vec{r}) = 0$ with the appropriate boundary conditions.

Within these approximations, the complex electrical conductivity $\sigma^*(\omega)$ or, equivalently, the complex dielectric constant $\varepsilon^*(\omega)$ of the shelled particle suspension is given by

$$\frac{\sigma^*(\omega)}{\sigma_m^*(\omega)} = \frac{\sigma_s^*(1 + 2\phi) + 2\sigma_m^*(1 - \phi)(\sigma_p^*(1 - \nu) + \sigma_s^*(2 + \nu))}{\sigma_s^*(1 - \phi) + \sigma_m^*(2 + \phi)(\sigma_p^*(1 - \nu) + \sigma_s^*(2 + \nu))} \bigg/ \frac{(\sigma_p^*(1 + 2\nu) + 2\sigma_s^*(1 - \nu))}{(\sigma_p^*(1 + 2\nu) + 2\sigma_s^*(1 - \nu))} \quad (7)$$

or, equivalently as

$$\frac{\varepsilon^*(\omega)}{\varepsilon_m^*(\omega)} = \frac{\varepsilon_s^*(1 + 2\phi) + 2\varepsilon_m^*(1 - \phi)(\varepsilon_p^*(1 - \nu) + \varepsilon_s^*(2 + \nu))}{\varepsilon_s^*(1 - \phi) + \varepsilon_m^*(2 + \phi)(\varepsilon_p^*(1 - \nu) + \varepsilon_s^*(2 + \nu))} \bigg/ \frac{(\varepsilon_p^*(1 + 2\nu) + 2\varepsilon_s^*(1 - \nu))}{(\varepsilon_p^*(1 + 2\nu) + 2\varepsilon_s^*(1 - \nu))} \quad (8)$$

where $\phi = (4\pi N(R + d)^3)/3V$ is the fractional volume of the dispersed particles and $\nu = [R/(R + d)]^3$ takes into account the volume occupied by the shell.

Equations (7) and (8) can be rearranged to give

$$\frac{\sigma^*(\omega)}{\sigma_m^*(\omega)} \equiv \frac{\varepsilon^*(\omega)}{\varepsilon_m^*(\omega)} = \frac{A - \omega^2 B + i\omega E}{C - \omega^2 D + i\omega F} \quad (9)$$

where the quantities $A-F$, after somewhat cumbersome calculations, are given by

$$\begin{aligned}
 A &= (1 + 2\phi)\sigma_s a + 2(1 - \phi)\sigma_m b \\
 B &= \varepsilon_0^2[(1 + 2\phi)\varepsilon_s c + 2(1 - \phi)\varepsilon_m d] \\
 C &= (1 - \phi)\sigma_s a + (2 + \phi)\sigma_m b \\
 D &= \varepsilon_0^2[(1 - \phi)\varepsilon_s c + (2 + \phi)\varepsilon_m d] \\
 E &= \varepsilon_0[(1 + 2\phi)(\varepsilon_s a + \sigma_s c) + 2(1 - \phi)(\varepsilon_m b + \sigma_m d)] \\
 F &= \varepsilon_0[(1 - \phi)(\varepsilon_s a + \sigma_s c) + (2 + \phi)(\varepsilon_m b + \sigma_m d)]
 \end{aligned} \tag{10}$$

where

$$\begin{aligned}
 a &= (1 + 2\nu)\sigma_p + 2(1 - \nu)\sigma_s \\
 b &= (1 - \nu)\sigma_p + (2 + \nu)\sigma_s \\
 c &= (1 + 2\nu)\varepsilon_p + 2(1 - \nu)\varepsilon_s \\
 d &= (1 - \nu)\varepsilon_p + (2 + \nu)\varepsilon_s
 \end{aligned} \tag{11}$$

Equations (7) and (8) can be rewritten by the method of the partial fractions as the superposition of two contiguous Debye-type relaxation functions

$$\varepsilon^*(\omega) = \varepsilon_\infty + \frac{\varepsilon_{ss} - \varepsilon_{0\infty}}{1 + i\omega\tau_1} + \frac{\varepsilon_{0\infty} - \varepsilon_\infty}{1 + i\omega\tau_2} + \frac{\sigma_{ss}}{i\omega\varepsilon_0} \tag{12}$$

or equivalently as

$$\sigma^*(\omega) = \sigma_{ss} + \frac{i\omega\tau_1(\sigma_0 - \sigma_{ss})}{1 + i\omega\tau_1} + \frac{i\omega\tau_2(\sigma_\infty - \sigma_0)}{1 + i\omega\tau_2} + i\omega\varepsilon_0\varepsilon_\infty \tag{13}$$

where the dielectric parameters of the two contiguous relaxations are given by

$$\begin{aligned}
 \Delta\varepsilon_1 &= \varepsilon_{ss} - \varepsilon_\infty = \frac{\varepsilon_0\varepsilon_m - \sigma_m\tau_1}{\varepsilon_0 C(\tau_1 - \tau_2)\tau_1} (A\tau_1^2 - E\tau_1 + B) \\
 \Delta\varepsilon_2 &= \varepsilon_{0\infty} - \varepsilon_\infty = \frac{\varepsilon_0\varepsilon_m - \sigma_m\tau_2}{\varepsilon_0 C(\tau_1 - \tau_2)\tau_2} (-A\tau_2^2 + E\tau_2 - B) \\
 \varepsilon_\infty &= \varepsilon_m B/D \\
 \tau_1 &= \frac{1}{2C} \left[F + \sqrt{F^2 - 4CD} \right] \\
 \tau_2 &= 2D \frac{1}{F + \sqrt{F^2 - 4CD}} \\
 \Delta\sigma_1 &= \sigma_0 - \sigma_{ss} = \frac{\varepsilon_0}{\tau_1} (\varepsilon_{ss} - \varepsilon_{0\infty}) \\
 \Delta\sigma_2 &= \sigma_\infty - \sigma_0 = \frac{\varepsilon_0}{\tau_2} (\varepsilon_{0\infty} - \varepsilon_\infty) \\
 \sigma_{ss} &= \sigma_m A/C
 \end{aligned} \tag{14}$$

where ε_{ss} and ε_∞ are the low-frequency and high-frequency limit of the permittivity; $\varepsilon'(\omega)$, $\varepsilon_{0\infty}$ the high-frequency limit of the first relaxation and the low-frequency limit of the second relaxation, respectively, whose relaxation times

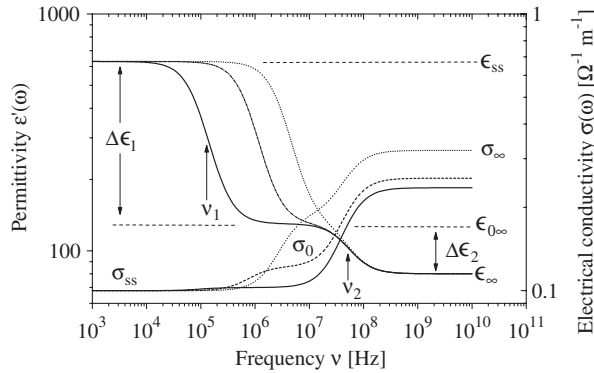


Fig. 1. Typical dielectric and conductometric spectra resulting from the superposition of two contiguous Debye-type relaxation functions. The permittivity $\epsilon'(\omega)$ and the conductivity $\sigma(\omega)$ have been calculated from the real part of equations (12) and (13), respectively. The parameters assume the following values: high-frequency relaxation: $\Delta\epsilon_2 = \epsilon_{0\infty} - \epsilon_{\infty} = 50$, $\tau_2 = 3 \times 10^8$ s, $\epsilon_{\infty} = 80$, $\sigma = 0.1 \Omega^{-1} \text{m}^{-1}$. For the low-frequency relaxation, three relaxation times are compared: $\tau_1 = 6 \times 10^5$ s (full line), $\tau_1 = 5 \times 10^6$ s (dashed line), $\tau_1 = 2 \times 10^7$ s (dotted line). In all cases, the dielectric increment assumes the values $\Delta\epsilon_1 = \epsilon_{ss} - \epsilon_{0\infty} = 500$. In the figure, the asymptotic values of the dielectric parameters, both at low- and at high-frequency limit, are appropriately labeled.

are τ_1 and τ_2 . Analogously, $\Delta\sigma_1$ and $\Delta\sigma_2$ are the corresponding conductivity increments and σ_{ss} the dc electrical conductivity.

Figure 1 sketches typical dielectric spectra of a colloidal particle suspension showing two well-separated relaxation contributions, originating from the two different interfaces of the shell boundaries with the external and the internal medium.

The same procedure can be iterated for a particle covered by two concentric layers, characterized by three different interfaces, resulting in an expression

$$\frac{\epsilon_m^*(\omega)}{\epsilon_m^*(\omega)} = \frac{A - \omega^2 B + i\omega E - i\omega^3 G}{C - \omega^2 D + i\omega F - i\omega^3 H} \tag{15}$$

that, generalized for a number n of adjacent layers, reads

$$\frac{\epsilon_m^*(\omega)}{\epsilon_m^*(\omega)} = \frac{A_0 + \sum_{j=0}^n (j)^{j+1} \omega^{j+1} A_{j+1}}{B_0 + \sum_{j=0}^n (j)^{j+1} \omega^{j+1} B_{j+1}} \tag{16}$$

where A_0, B_0 and $A_{j+1}, B_{j+1} (j = 0, 1, \dots, n)$ are known real functions depending, in a rather cumbersome way, on the electrical parameters, i.e., the permittivity ϵ and the electrical conductivities σ , of the different media, and n is the number of the resulting interfaces by which the heterogeneous system is built up.

Hanay *et al.* [29] have discussed in detail the experimental conditions by which the influence of the different interfaces and consequently the presence of distinct dispersions are measured in a real system. As a general rule, to each interface in the system, corresponds a different dielectric dispersion whose origin, at a macroscopic level, is due to a surface charge distribution. Obviously, in real systems, these different dispersions can fall very close to each other, making difficult the deconvolution of the whole dielectric spectrum, or, in dependence of the particle system investigated, the dielectric strength of some of them may be negligibly small in comparison with the others.

A further difficulty arises if one or more dielectric media undergo an intrinsic dielectric relaxation (associated to the bulk properties of the medium). A typical example for such a system is a simple colloid in an aqueous phase, investigated at a frequency high enough to evidence the orientational polarization of the water molecules. In this case, the complex dielectric constant $\varepsilon_m^*(\omega)$ of the water phase is well accounted for by a single-decay Debye relaxation function

$$\varepsilon_m^*(\omega) = \varepsilon_{W\infty} + \frac{\varepsilon_{WS} - \varepsilon_{W\infty}}{1 + i\omega\tau_w} + \frac{\sigma_w}{i\omega\varepsilon_0} \quad (17)$$

where ε_{WS} , $\varepsilon_{W\infty}$, τ_w and σ_w are the low- and high-frequency limit of the permittivity, the relaxation time and the dc electrical conductivity, respectively. The presence of this further dielectric relaxation makes the overall dielectric spectra more complex, and their interpretation in terms of the single effect requires caution. A general theory of the dielectric behavior of spheroidal particle suspensions with an intrinsic dispersion has been recently discussed by Gao *et al.* [30].

For a suspension of liposome particles, the following approximations generally hold, due to their particular features, i.e., $\sigma_s \ll \sigma_p \cong \sigma_m$, $\varepsilon_s \ll \varepsilon_p \cong \varepsilon_m$, $v \simeq 1 - 3d/R$, considering that the same aqueous phase is present in the inner and outer medium and that the thickness d of the shell is considerably smaller than the radius R of the vesicle.

Under these circumstances, equations (14) reduce to a unique dispersion with dielectric parameters given by

$$\begin{aligned} \Delta\varepsilon &= \varepsilon_{ss} - \varepsilon_{\infty} = \frac{9\phi\varepsilon_s}{(2+\phi)^2 d/R} - \frac{3\phi\varepsilon_m}{(2+\phi)} \\ \tau &= \frac{3\varepsilon_0\varepsilon_s}{(2+\phi)\sigma_m d/R} \\ \varepsilon_{\infty} &= \varepsilon_m \\ \sigma_{ss} &= \sigma_m \frac{3\sigma_s + 2(1-\phi)\sigma_m d/R}{3\sigma_s + (2+\phi)\sigma_m d/R} \cong \frac{2(1-\phi)}{(2+\phi)}\sigma_m \\ \sigma_{\infty} &= 3\sigma_m \left[(1+\phi) \frac{d}{R} \frac{\varepsilon_m}{\varepsilon_s} \right] \end{aligned} \quad (18)$$

For a typical liposomal particle, 100 nm in diameter, dispersed in an aqueous phase characterized by $\varepsilon_m = 80$ and $\sigma_m = 10^{-3}\Omega^{-1}\text{m}^{-1}$, at a concentration

$\phi = 0.10$ with a lipidic bilayer 50 \AA thickness and a permittivity $\epsilon_s = 5$, equations (18) predict a dielectric relaxation with a dielectric increment $\Delta\epsilon = 9$, a conductivity increment $\Delta\sigma = \sigma_\infty - \sigma_{ss} = 1.8 \times 10^{-3} \Omega^{-1} \text{ m}^{-1}$ and a relaxation time $\tau = 1.3 \times 10^{-6} \text{ s}$. In the present case, owing to the particular features of the liposome structure, this basic model justifies only a very small effect, characterized by a very small dielectric increment, compared to the one generally found experimentally.

As we will show in the next section, the observed dielectric behavior of a liposome suspension or, in general, of a colloidal (charged) particle suspension, deeply deviates from the one predicted by the simple picture shown in Fig. 1. Here, the dielectric relaxations are exclusively due to the heterogeneous characters of this system at a submicron scale length, because of the adjacent media whose different polarizability causes the appearance of a surface charge distribution (Maxwell–Wagner relaxation effect). Basically, this model neglects the electrokinetics effects occurring in an aqueous phase bathing a charged or zwitterionic surface, like those generally occurring at the lipid bilayer interfaces.

Although equations (18) are the basic expressions of the dielectric heterogeneous systems theory, the introduction of a further mechanism giving rise to more specific surface effects is required to take into account the generally large extent of the observed dielectric relaxation.

2.1.2. Influence of the ion (counterion) distribution

The situation has changed drastically and the huge discrepancy with the observed behavior strongly reduced by the appearance of the theoretical explanation given by Schwarz [31] and later by Schurr [32] based on the assumption that the particle core may be surrounded by an infinitely thin conducting layer, arising from the confined tangential motion of (partially bound) counterions.

This particular diffusion mechanism results in a further relaxation contribution whose strength is generally very large and can take into account the very big effects observed in the low-frequency range of the dielectric spectrum (this big effect has been called ‘giant’ dielectric dispersion). For example, in an alternating electric field of few kilohertz, a dilute suspension of polystyrene submicron particles in an electrolyte solution has a permittivity of well over three orders of magnitude than the pure solution one [23].

O’Konski [33] first introduced a surface conductivity mechanism in the analysis of the dielectric relaxations of charged colloidal particles, resulting in a term $2\lambda/R$ to be added to the bulk conductivity of the particles. The surface conductivity λ arises from the tangential diffusion of counterions. According to this concept, the basic idea is replacing the complex dielectric constant of a spherical particle covered by a thin conducting shell, originated by the tangential diffusion of the

counterions, with an equivalent complex permittivity $\epsilon_{\text{peq}}^*(\omega)$ given by

$$\epsilon_{\text{peq}}^*(\omega) = \epsilon_{\text{p}}^*(\omega) + \frac{1}{i\epsilon_0\omega} \frac{2}{R} \lambda_{\text{tot}}^*(\omega) \quad (19)$$

where the total surface conductivity

$$\lambda_{\text{tot}}^*(\omega) = \lambda + \frac{i\omega\tau\lambda_0}{1 + i\omega\tau} \quad (20)$$

is due to two terms, the contribution λ , independent of frequency, as in the original model of [33], and the contribution $i\omega\tau\lambda_0/(1 + i\omega\tau)$, dependent on frequency, as in the model developed by Schwarz [31].

The two different values of the surface conductivity lead to a distinction between a bound charge current and a true, or dc, current, which persists in accordance with Ohm's law in the steady state, or equivalently to regard the double layer as consisting in a layer of bound counterions and a diffuse layer, which can exchange with the bulk. The relaxation time τ is given by $\tau = R^2/(2uK_{\text{B}}T)$, where u is the counterion surface mobility (per unit charge) and $K_{\text{B}}T$ the thermal energy.

Nevertheless the surface conductance model was able to take into account remarkably well the low-frequency giant dielectric strength and the relaxation time observed in charged particle colloidal suspensions, this approach has been criticized, for example, by Fixman [34], who observed that the structure of the double layer at the interface is more composite than the one suggested by this model and other interfacial charges need to be taken into consideration, such as diffusion of free ions and, moreover, polarization processes associated to the deformation of the ionic diffuse double layer.

These difficulties can be overcome by replacing, almost partially, the tightly bound counterion layer with a diffuse double layer (for example in the Gouy–Chapman model), where the counterion distributions are governed by the Poisson–Boltzmann equation. In this context, Chew and Sen [35] have derived the dielectric and conductometric behavior of a dilute suspension of spherical particles with a fixed surface charge dispersed in an electrolyte solution, expanding the relevant equations in power series of $(k_{\text{D}}R)^{-1}$ where k_{D} is the inverse of the Debye screening length and R the radius of the dispersed particle.

The second-order solution furnishes, in the limit of small ϕ , the permittivity $\epsilon'(\omega)$ and the conductivity $\sigma(\omega)$, given by

$$\epsilon'(\omega) = 3\phi\epsilon_{\text{m}}\text{Re}\{M\} + \frac{\sigma_{\text{m}}}{\epsilon_0\omega\epsilon_{\text{m}}}\text{Im}\{M\} + \epsilon_{\text{m}} \quad (21)$$

$$\sigma(\omega) = \sigma_{\text{m}} + 3\phi\sigma_{\text{m}}\text{Re}\{M\} - \frac{\omega\epsilon_0\epsilon_{\text{m}}}{\sigma_{\text{m}}}\text{Im}\{M\} \quad (22)$$

where $\text{Re}\{M\}$ and $\text{Im}\{M\}$ are the real and the imaginary part of the induced particle dipole moment eMR^3 given by

$$eMR^3 = -\frac{1}{2} + \lambda \frac{6t^2}{1-t^2} + \lambda^2 - \frac{3i\omega \epsilon_p}{4D \epsilon_m} R^2 + 6\ln(1-t^2) - \frac{24t^2}{(1-t^2)^2} \left(t^2 + \frac{1}{\alpha} \right) \quad (23)$$

where $\lambda = d/R$ and D is the counterion diffusion coefficient, $t = \tanh e\phi_0/4K_B T$ with ϕ_0 the potential at the surface of the particle and α a parameter given by $\alpha = (1 + \sqrt{\omega\tau} - i\sqrt{\omega\tau} - i\omega\tau)/(1 + \sqrt{\omega\tau} - i\sqrt{\omega\tau})$ with $\tau = R^2/2D$. This treatment, which is free from the approximations of previous analytical results, furnishes a dielectric increment of the order of

$$\Delta\epsilon \sim \epsilon_m \frac{t^2}{1-t^2} \quad (24)$$

which can be large, as generally observed experimentally, when $t \rightarrow 1$, i.e., when $e\psi_0/K_B T \gg 1$, resulting in a dielectric increment $\Delta\epsilon$ that increases exponentially with the surface potential ψ_0

$$\Delta\epsilon \sim \phi \epsilon_m e^{e\psi_0/K_B T} \quad (25)$$

which is in agreement with the results obtained by Dukhin and Shilov [36] and by Fixman [34], using more complicated boundary conditions.

Fixman [34], O'Brien [37], and Chew [38] extended the original model of Schwarz and Schurr [31,32] including the diffusion of ions (the exchange of ions) from the counterion surface layer surrounding the charged particle toward the bulk electrolyte. More recently, the effect of a composite structure of the double layer composed of a loosely bound diffuse layer and a tightly bound Stern layer further divided into an inner and outer Helmholtz layers has been discussed by Hu [39].

A somewhat different approach, along the line of the Schwarz–Schurr model [31,32], has been developed by Grosse and Foster [40–42] on the basis of a series of investigations on the electrokinetic phenomena in the diffuse double layer.

This generalization leads to a more complex dielectric behavior resulting in two contiguous dielectric dispersions, characterized by a dielectric increment and a relaxation time (low-frequency relaxation mode) given by, respectively,

$$\Delta\epsilon_1 = \frac{9\phi \epsilon_m (2k_D \lambda_s / \sigma_m)^4}{16((2k_D \lambda_s / \sigma_m^2)(2\lambda_s / R + \sigma_m) + 2)^2} \quad (26)$$

$$\tau_1 = \frac{R^2}{D} \quad (27)$$

and by a dielectric increment and a relaxation time (high-frequency relaxation mode) given by, respectively,

$$\Delta\epsilon_2 = \frac{9\phi\epsilon_m((2\lambda_s/R\sigma_m) - (\epsilon_p/\epsilon_m))^2}{((\epsilon_p/\epsilon_m) + 2)((2\lambda_s/R\sigma_m) + 2)^2} \quad (28)$$

$$\tau_2 = \frac{\epsilon_0\epsilon_m((\epsilon_p/\epsilon_m) + 2)}{\sigma_m((2\lambda_s/R\sigma_m) + 2)} \quad (29)$$

where $k_D = \sqrt{\sigma_m/\epsilon_0\epsilon_m D}$ is the inverse of the Debye screening length, λ_s is the counterion surface conductivity and D the counterion bulk diffusion coefficient. The above relationships hold in the limit $R \gg k_D^{-1}$. The full expressions are given in ref. [42].

In the limit $R \gg k_D^{-1}$, the high-frequency relaxation mode reduces to the Maxwell–Wagner relaxation effect for insulating particle covering by a conducting layer characterized by a surface conductivity λ_s

$$\Delta\epsilon_2 = \frac{9}{2}\phi\epsilon_m \frac{(\lambda_s/R)^2}{(\lambda_s/R) + \sigma_m^2} \quad (30)$$

$$\tau_2 = \frac{\epsilon_0\epsilon_m}{(\lambda_s/R) + \sigma_m} \quad (31)$$

The particular feature of the liposome structure, consisting of a thin closed bulky non-conductive bilayer separating two aqueous phases of the same bulk electrical properties, enforces the dielectric effect associated with the ionic diffusion at the two interfaces, which generally predominates over that induced by the simple heterogeneity of the system.

This fact makes dielectric technique of an unique valuable interest in understanding the complex phenomenology underlying the electrokinetic effect at the charged or zwitterionic interfaces, resulting in low-frequency dielectric dispersions. On the other hand, this dispersion is generally contiguous and partially overlapped with the relaxation due to the electrode polarization effect, that in most cases, masks almost completely the one to be investigated. Consequently, the frequency range investigated so far preferentially deals with that at relatively higher frequencies, above some tenth of kilohertz, where electrode polarization artifacts are moderate or negligible and only few investigations deal with the low-frequency behavior.

Recently, the whole dielectric spectrum of different unilamellar phospholipid vesicles in aqueous suspensions has been measured [43] over a broad frequency range, extending from 1 kHz to 1 GHz. The dependence of the permittivity $\epsilon'(\omega)$ on the frequency, once the electrode polarization was removed by using a

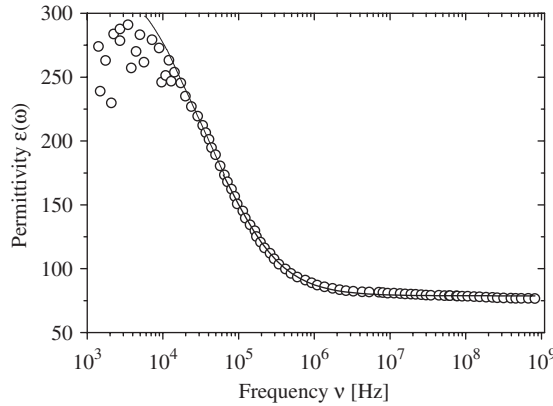


Fig. 2. Dielectric spectrum of DMPC/DMPG 2:8 wt/wt mixture in the frequency range from 1 kHz to 1 GHz together with the calculated curve on the basis of equation (32). Redrawn from Tirado [43].

variable spacing parallel platinum black electrode cell, has been analyzed considering the superposition of the counterion polarization relaxation and the usual interfacial relaxation associated with the lipid bilayer, according to a revisited version of the model developed by Grosse *et al.* [44,45].

These authors derived for the permittivity $\epsilon'(\omega)$ the following expression:

$$\epsilon'(\omega) = \epsilon_{\infty} + \frac{\Delta\epsilon_{\alpha}(1 + \sqrt{\gamma})}{1 + 2\sqrt{\gamma}(1 + \omega\tau_{\alpha}) + 2\gamma + (\omega\tau_{\alpha})^2} + \frac{\Delta\epsilon_{\beta_1}}{1 + (\omega\tau_{\beta_1})^2} + \frac{\Delta\epsilon_{\beta_2}}{1 + (\omega\tau_{\beta_2})^2} \tag{32}$$

where the different quantities $\Delta\epsilon_{\alpha}$, γ , τ_{α} and $\Delta\epsilon_{\beta_1}$, $\Delta\epsilon_{\beta_2}$, τ_{β_1} and τ_{β_2} on the right-hand side of equation (32) depend on the characteristic parameters of the system, such as the diffusion coefficients of the counterions and co-ions and the zeta potential ζ . The full expressions of these parameters are given in Grosse *et al.* [44,45]. This model provides a quantitative interpretation of the data, with the zeta potential as a simple adjustable parameter. A typical dielectric spectrum of dimyristoylglycerophosphocholine (DMPC) and phosphatidylglyceroldimyristoyl (DMPG) 2:8 wt/wt mixture is shown in Fig. 2 together with the calculated value on the basis of equation (32), taking into account the counterion polarization and the membrane charging with the ζ potential as the only adjustable parameter. The theory gives a reasonable good agreement over the whole spectrum, extending from 1 kHz to 1 GHz.

2.1.3. Specific effects associated with the liposome structure

In the case of a liposome particle, however, where the electric structure of the interface, depending on the chemical lipid structure, plays an important role, the

above picture (Fig. 2), typical of charged colloidal suspensions, must be conveniently modified, taking into account the three molecular mechanisms that contribute with peculiar characteristics to the dielectric spectra of phospholipid vesicle aqueous suspensions.

They are the limited translational diffusion of the ionic groups in the lipid molecules and its condensed counterions, whose effects are expected at low frequencies; the rotational diffusion of the zwitterionic phospholipids, where positive and negative charges exist in different parts of the molecule, at intermediate frequencies; and finally the rotational diffusion of the partially bounded water molecules, at higher frequencies.

These molecular mechanisms result in additional dielectric polarization effects that add to those associated with the heterogeneous character of the system and, in part, contribute to make the observed phenomenology even more complex.

In the case of zwitterionic liposomes, where dipolar headgroups located at the bilayer surface originate a microdynamics resulting in the formation of lipid domain structures, a further mechanism must be considered.

Kaatze *et al.* [46,47] and, more recently, Schrader and Kaatze [48] have investigated solutions of unilamellar liposomes built up by dimyristoylphosphatidylcholine (DMPC) and a mixture of dimyristoyl- and dipalmitoylphosphatidylcholine (DPPC) composed of lipids with different length of acyl chains. The dielectric properties of these liposome suspensions, in the frequency range close to the Mega-Hertz region, where the interfacial effects dominate, have been described within the effective medium theory approximation, assuming a correlated motion of the cationic lecithin groups, tangentially to vesicle surface, on circular path around the anionic phosphate groups (Fig. 3).

This approach has been already employed some years ago by the same group in the investigation of different phospholipids–water systems [46,49–53].

Here, we will describe this model in detail since it represents a valuable example of the effectiveness of dielectric relaxation methods in investigating the surface properties of typical heterogeneous liposome systems such as zwitterionic liposome suspensions.

The above-stated mechanism results in an equivalent complex dielectric constant $\varepsilon_{p_{eq}}^*(\omega)$ of the liposome particle given by

$$\varepsilon_{p_{eq}}^*(\omega) = \varepsilon_s^*(\omega) \frac{1 - 2(R/(R+d))^3 (\varepsilon_s^*(\omega) - \varepsilon_p^*(\omega)) / (2\varepsilon_s^*(\omega) + \varepsilon_p^*(\omega))}{1 + (R/(R+d))^3 (\varepsilon_s^*(\omega) - \varepsilon_p^*(\omega)) / (2\varepsilon_s^*(\omega) + \varepsilon_p^*(\omega))} + \frac{8\pi}{(R+d)} \{ \alpha_\zeta(\omega) + \alpha_{core}(\omega) \} \quad (33)$$

where the second term on the right-hand side represents the contribution of the surface polarizability densities deriving from the diffusional reorientation of the zwitterionic headgroups and the restricted motion of the ionic species,

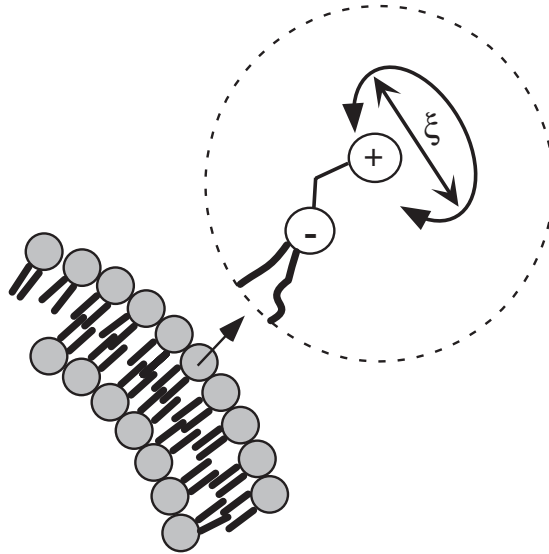


Fig. 3. A sketch of the surface polarizability mechanism in zwitterionic lipids, according to the model suggested by Kaatze *et al.* [46,47], and Schrader and Kaatze [48]. The cationic group in the zwitterionic polar lipid head rotates around the anionic group in circular paths with radius ξ , tangentially to the lipid surface.

respectively, and

$$\epsilon_{\xi}^*(\omega) = \epsilon_m^*(\omega) + \frac{8\pi}{R} \{ \alpha_{\xi}(\omega) + \alpha_{\text{core}}(\omega) \} \tag{34}$$

is the dielectric constant of the liposome core together with the inner polar surface layer.

Kaatze *et al.* [46,47] and Schrader and Kaatze [48] assumed that $\alpha_{\xi}(\omega)$ and $\alpha_{\text{core}}(\omega)$ relax according to a Cole–Cole relaxation function. In particular, the dielectric strength $\Delta\alpha_{\xi}$ can be expressed in terms of the molecular parameters as

$$\Delta\alpha_{\xi} = \frac{\bar{n}g(e\xi)^2}{2K_B T} \tag{35}$$

where \bar{n} is the mean surface number density of the dipoles at the lipid–water interfaces, g a factor that takes into account possible correlations between neighboring dipoles, ξ a characteristic length associated with the dipole that can be interpreted as the radius of a circular path identified by the headgroup rotation. In this picture, the relaxation time τ_{ξ} can be interpreted as due to this rotation and written as $\tau_{\xi} = \xi^2 / uK_B T$, where u is the ‘rotational’ mobility of the headgroup. The contribution due to the inner zwitterions is kept small by the depolarizing electric field effects [54] and has been neglected.

Using a nonlinear least-squares regression analysis procedure, they found the relevant parameters of the model. The parameters which characterize the bilayer

surface polarizability, i.e., $g\xi^3$, that takes into account the extension of the motion of the zwitterionic headgroups, and u/ξ^2 , that represents the mobility of the headgroups normalized to the square of the radius ξ , for the systems investigated by Kaatz *et al.* [47] are shown in Fig. 4.

As can be seen, for both the liposome suspensions, a pronounced effect close to the melting transition temperature T_m is evidenced, resulting in an enhancement of the parallel ordering of the dipolar phospholipid headgroups, larger in the pure DMPC bilayer than in bilayer built up by a lipid DMPC/DPPC mixture. This effect is clearly observable both in the correlation parameter g and in the mobility u , once the displacement ξ is considered independent of the temperature. The formation of correlated dipolar domains produces a further surface dielectric polarization effect that can easily be observed by means of dielectric spectroscopy measurements.

With a similar approach, De Luca *et al.* [55] investigated the organization of clusters formed by gangliosides in lipid bilayer vesicles. Gangliosides are

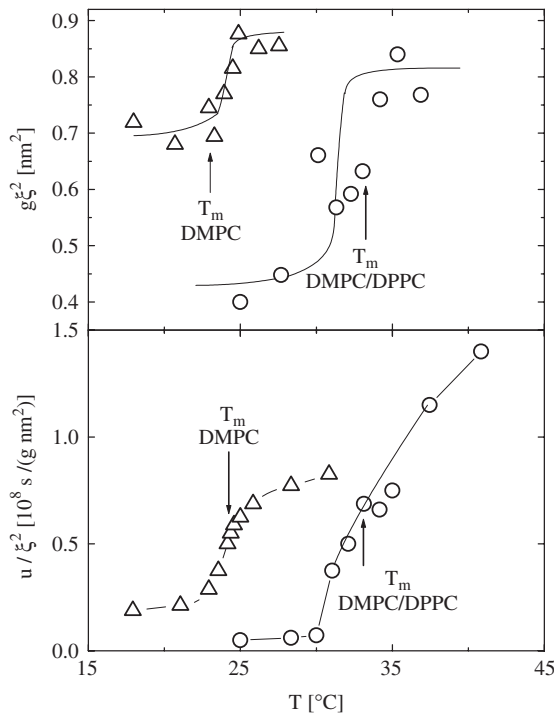


Fig. 4. The parameters of the surface polarizability model as a function of the temperature for two different liposome suspensions (DMPC and mixed 1:1 DMPC/DPPC). The quantity $g\xi^2$, proportional to the surface polarizability $\Delta\alpha_\xi$ (equation (35)) (top) and the quantity u/ξ^2 , proportional to the relaxation frequency τ_ξ (bottom), derived from the analysis of the observed relaxation display a marked increase at the main transition temperature T_m , evidencing the formation of cluster domains (redrawn from Schrader and Kaatz [48]).

glycosphingolipids that contain sialic acid in the headgroup. They are located primarily on the outer leaflet of the lipid bilayer of biological cell membranes and appear to be relevant in different important cell functions, such as cell–cell interactions, antigen recognition, cell activation, and signal transduction. Moreover, gangliosides and cholesterol are credited to be mainly responsible for the formation of ‘rafts’ [56], i.e., segregated domains of more compact and ordered lipids, ‘floating’ in a more fluid lipid matrix, that are supposed to be involved in a number of important membrane cell functions, but whose mere existence is currently a matter of lively debate [57]. Analyzing the dielectric behavior of mixed phospholipid/ganglioside liposomes at different molar ratios, these authors point out that a ganglioside concentration-dependent dielectric dispersion appears, with an amplitude of the order of a few tenths of dielectric units, whose maximum occurs at a well-defined ganglioside/phospholipid molar ratio. This effect is attributed to an excess surface polarizability caused by the surface ganglioside organization. In a previous work, the same authors have shown that the presence of small amounts of gangliosides in mixed ganglioside/phospholipid liposomes causes a marked alteration in the surface conductance of the particles, as reflected in the low-frequency conductivity behavior of a liposome suspension [58].

In mixed lipid bilayers, large domains exist near phase transitions, particularly at the main, or gel/fluid transition, where ordered, gel-like domains appear, separated from the more fluid matrix. However, while near the gel/fluid phase transition temperature, the domain structure is mainly promoted by the isomerization of the lipid acyl chains, in mixed bilayers, steric and/or electrostatic interactions between headgroups play an essential role in determining the formation of segregated domains [59]. Conversely, any change induced in the electrostatic interactions at the bilayer surface (varying the suspension ionic strength, for example) may influence the domain structure.

The interest in the knowledge of the surface structure of mixed liposomes resides in the fact that lateral organization of cell membranes, the possible existence of segregated lipid domains, their structure and their role in membrane functionality are currently debated with much enthusiasm (see, for example, recent reviews appeared on these topics by Edidin [60,61], Barenholz [62], Subczynska and Kusumi [63] and the literature cited therein).

Another example of application of dielectric spectroscopy to the investigation of the dynamics of different molecules within a lipid bilayer is represented by the work of Ermolina *et al.* [64]. These authors, employing time domain dielectric spectroscopy technique, investigated the possible effects of two different ‘skin penetration modulator’ molecules on phosphatidylcholine (PC) bilayer vesicles. These ‘modulators’ are substances that are known to enhance or to retard permeation of solutes through the ‘stratum corneum’ of skin that, with its lipid structured bilayers, represents the main barrier to skin permeation. Although the main components of stratum corneum are ceramides, the authors chose PC liposomes as a simple and suitable model to investigate non-specific effects of

skin modulators on the transport properties of a lipid bilayer. Dielectric spectra were analyzed in terms of the sum of two dielectric relaxation functions, consisting of a Debye dispersion at lower frequencies and a Cole–Davidson relaxation at higher frequencies, according to

$$\varepsilon^*(\omega) = \varepsilon_\infty + \frac{\Delta\varepsilon_1}{1 + j\omega\tau_1} + \frac{\Delta\varepsilon_2}{(1 + j\omega\tau_1)^\beta} \quad (36)$$

These authors assume that the slow, low-frequency Debye-type dispersion is due to the interfacial charging of the vesicle bilayers through the intra- and extra-vesicle solution resistances (Maxwell–Wagner effect), while the fast, high-frequency Cole–Davidson relaxation process is attributed to the reorientation of the PC headgroups in the plane of the bilayer surface. It must be noted that the spreading factor β , introduced in the high-frequency dielectric dispersion, is usually assumed as a measure of the amplitude of a distribution of ‘different environments’ that locally modify the relaxation of a given dipolar species.

Assuming the dipole moment of the PC group independent of temperature and of ‘modulator’ concentration, the authors calculate a dipole correlation factor g from the dielectric increment that they correlate to the presence of defects in the PC headgroup dipoles alignment, possibly induced by the presence of the modulator. Using a statistical, fractal approach they analogously correlate the spreading factor β to an average number of defects. Using this model, they are able to quantify the extent of intermolecular interactions between lipid molecules in the bilayer and moreover how these interactions are influenced by the presence of ‘skin penetration modulators.’

A somewhat particular aspect has been considered by Barker *et al.* [65] who compared the dielectric behavior of liposome suspension over a wide frequency range, from 10^{-2} to 10^5 Hz, under different conditions, with the predictions of different theoretical models. They suggest that the very low-frequency response could be associated with the presence of a layer of liposomes adsorbed onto the electrode surfaces, introducing a further contribution to the overall dielectric spectrum, whose features are partially influenced by the chemical characteristics of the electrode surface.

3. RADIO WAVE DIELECTRIC SPECTRA OF A DPPC LIPOSOME SUSPENSION: A TYPICAL EXAMPLE

In this section, we will present typical dielectric and conductometric spectra of zwitterionic liposomes in aqueous suspension in the radio-wave frequency range and in an extended temperature interval, as an example of application of dielectric methods to liposome electrical characterization. The system chosen for description by no means exhausts the variety of the dielectric phenomena that

can be encountered. It was selected to illustrate the relation between the well-defined dielectric phenomena and the structure and the behavior of the molecules by which the systems are composed.

One set of data has been selected as offering an example of the influence of the liposome radius on the overall dielectric spectra, in particular when the liposome size increases and the lipid bilayer evolves toward a planar unilamellar structure.

In the second aspect, we will deal with the influence of the temperature on the dielectric response whose peculiar feature is caused by the different structural organizations that the system undergoes.

Phospholipid–water systems display a gel–liquid crystalline phase transition attributed to a cooperative melting of the hydrocarbon chains, which produces a change in the bilayer structure. Highly hydrated phospholipids exhibit, moreover, a so-called pretransition, which is thought to have a rippled bilayer structure. This ripple phase (or $P_{\beta'}$ phase), falling between the low temperature $L_{\beta'}$ phase, where the acyl chains are frozen in a rigid extended all-*trans* configuration, and the high-temperature L_{α} phase, where fluid-like melted hydrocarbon chains prevail, is characterized by a one-dimensional high modulation of the bilayer. The temperature strongly influences the liposomal structural organization. A typical effect of temperature on the apparent molecular volume of DPPC molecules is shown in Fig. 5, where the pretransition (at about 36–37 °C) and the main transition (at about 42 °C) are accompanied by well-marked changes reflecting a different spatial organization of the lipid bilayer.

Both the two above-stated changes in the lipid organization, geometrical, induced by varying the liposome radius, and physicochemical, induced by varying

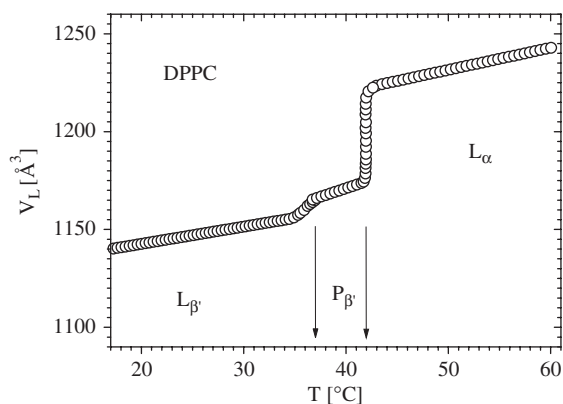


Fig. 5. Effect of temperature on the apparent molecular volume V_L of DPPC molecules in a bilayer. The pretransition (at about 36–37 °C) and the main transition (at about 42 °C) are clearly accompanied by significant changes in the apparent molecular volume, reflecting the spatial organization of the bilayer (from Wiener *et al.* [107]).

the temperature, reflect in dielectric spectra with different characteristics, whose main features represent a valuable probe to investigate the static and dynamical behavior of these structures.

3.1. Liposome preparation

The lipid employed was (DPPC), provided by Sigma Chem. Co. with a purity of 99%. Measurements were done without any further purification. The liposome preparation follows the usual (standard) procedure. The desired amount of lipid (usually, 15 mg) was dissolved in approximately 10 ml of chloroform–methanol (1:1 wt/wt) mixture and subsequently the solvent was removed by rotoevaporation under a reduced pressure until a thin lipid film was formed. The hydration of the lipid film was achieved by addition of 10 ml of deionized water (Q-quality) and allowing the mixture to swell under rotation at a temperature above the main transition temperature of the lipid ($T_m \sim 42^\circ\text{C}$) for 1 h. The resulting liposome suspension was sonicated for a further 1 h in a pulse power mode at a temperature of 25°C until a homogeneous solution was obtained. The desired liposome size was achieved by successive filtration through progressively smaller pore polycarbonate filters (Millipore). Using this procedure, we investigated liposomes of different sizes, varying from about 80 to 1000 nm in diameter. The liposome size and size distribution are determined, as usually, by dynamic light-scattering measurements.

3.2. Typical dielectric spectra

Some typical dielectric and conductometric spectra in the frequency range from 1 kHz to 10 MHz are shown in Figs 6 and 7. Each spectrum is composed of at least two different contributions due to different polarization mechanisms, at different molecular level. The first one, which falls in the lower frequency range and only the high-frequency tail is observed in the frequency range we have investigated, is attributable to the electrode polarization effect, i.e., to the formation of a layer of ions close to the metal electrode surface which acts, in an equivalent circuit scheme, as a capacitance in series with the one caused by the sample under test. This effect, which depends on many physicochemical parameters of the ionic suspension, is outside the scope of this review and it will not be treated anymore in what follows. We want only to point out that many different methods have been described to eliminate or to take into account for this effect. A technique to correct the dielectric data from the electrode polarization effect in the radio wave spectroscopy measurements has been proposed by the present authors and can be found elsewhere [66].

At higher frequencies, the dielectric relaxation attributable to the presence of the dispersed liposomes is observed. This relaxation is generally composed of

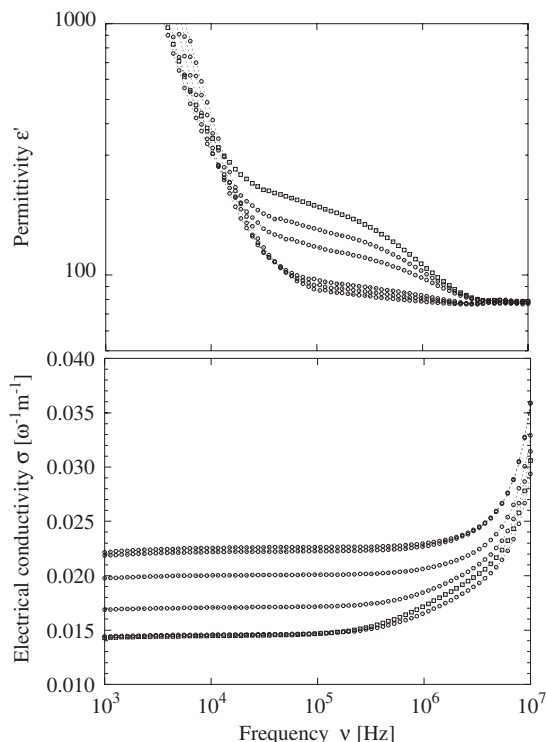


Fig. 6. Dielectric spectra of DPPC liposomes in aqueous suspension in the frequency range from 1 kHz to 10 MHz. Upper panel: the permittivity ϵ' . In the lower frequency range, the large increase of ϵ' is attributable to the combined effects of the electrode polarization and to polarization due to the counterion surface diffusion. At higher frequencies, the interfacial polarization is evidenced. Lower panel: the electrical conductivity σ . The step increase of σ at the higher frequencies is due to the superposition of the low-frequency wing of the aqueous phase relaxation. Each curve refers to a different size of the liposome, changing from 130 to 750 nm in diameter. The lipid concentration is maintained constant to the value of 4% wt/wt and the measurements were taken at the temperature of 20 °C.

two contributions, both of them due to the interfacial polarization effects, even if caused by different molecular mechanisms. The first one is originated by the diffusion layer polarization at the interface between the charged or polar particle surface and the bulk of the dispersing medium. It depends on the motion of counterions in the neighborhood of the particle; and a relevant role is played by tangential diffusion mechanism, according to the models previously stated. This dispersion overlaps with the high-frequency tail of the electrode polarization effect and is partially, and in some cases completely, masked by this predominant effect. Only when favorable conditions apply or a particular experimental set-up is employed, a full investigation of this dispersion is possible. On the other hand, the

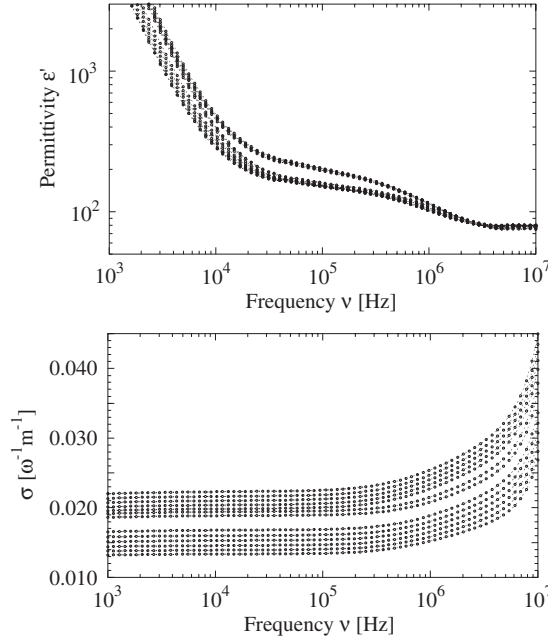


Fig. 7. The dielectric spectra of DPPC liposomes in aqueous suspension in the frequency range from 1 kHz to 10 MHz. Upper panel: the permittivity ϵ' . Lower panel: the electrical conductivity σ . Measurements have been taken at different temperatures from 20.0 to 56.0 °C, step 3.0 °C, covering the whole temperature range where the pretransition and the main transition fall. The liposome diameter is 620 nm and the fractional volume of the dispersed phase is $\phi = 0.04$. At the main transition temperature, a marked increase in both the dielectric increment $\Delta\epsilon$ and the electrical conductivity is evidenced.

characteristic frequency of this effect scales with the inverse of square radius of the particle, so that its frequency localization can be easily assigned.

The second dispersion, falling at somewhat higher frequencies, is attributable to the Maxwell–Wagner effect, modified to take into account that the adjacent media, which cause the interfacial polarization, can have a dissipative character. Moreover, if free charges are present, the counterion distribution is governed by a flux equation to which contribute both the external electric field and the field rising from the surface charge. In this case, the effective medium approximation theory holds, provided the Laplace equation is substituted by the Poisson equation. Obviously, the formal description of the dielectric response is more complex, but the basic assumptions and the approximations employed are essentially the same.

Finally, at higher frequencies, in the microwave range, the orientational polarization of the aqueous phase occurs (the water molecules possesses an electric dipole moment of about 1.8 D) which causes a decrease of the permittivity of water from the static value of about 80 (at room temperature) to the high-frequency limit of about 4.5. The relaxation frequency of pure liquid water is about $\nu_0 = 17$ GHz at

room temperature so that at a decade of frequency before, this effect begins to appear and becomes more and more significant as the frequency increases.

The spectra shown in Figs 6 and 7 deal with the high-frequency tail of the electrode polarization effect (which is considered in this context as an artifact) and with the Maxwell–Wagner polarization effect associated with the interfacial properties of the liposome suspension. The orientational polarization effect of the aqueous phase occurs at higher frequencies, above the high-frequency limit of the frequency window employed.

3.3. Influence of the liposome size

Fig. 6 shows the dielectric and conductometric spectra in the frequency range from 1 kHz to 10 MHz of a DPPC–liposome aqueous suspension at a temperature of 20 °C, for different liposome size, from about 130 to 750 nm in diameter.

Once the dielectric spectra have been corrected for the electrode polarization effect, the data can be analyzed on the basis of a Cole–Cole relaxation function and the relevant dielectric parameters evaluated.

The dielectric increment $\Delta\epsilon$ and the relaxation time τ as a function of the liposome size are shown in Fig. 8. We observe that, with the increase of the liposome size, the dielectric increment $\Delta\epsilon$ increases, linearly at first, showing more marked deviation from linearity as the size of the vesicles increases. Moreover, the relaxation time is proportional to the square of the particle radius (Fig. 8b). This behavior agrees with predictions of equations (26) and (27), indicating that the observed dispersion is attributable to the ion diffusion along the liposome surface. In this case, equation (27) correctly predicts a relaxation time τ that scales as R^2 . In equation (26) the particle radius does not appear explicitly, the dielectric increment being proportional to the fractional volume ϕ of the dispersed phase. However, as the dielectric spectra have been measured at the same lipid concentration, maintaining constant the total number of lipid molecules involved, the volume fraction ϕ scales as $\phi = N_p v / V \sim R$ considering the liposome concentration given by

$$\frac{N_p}{V} = \frac{n_{\text{mol}} a}{8\pi R^2} \quad (37)$$

with n_{mol} the total number of lipid molecules in the suspension, a the area occupied by each molecule at the bilayer surface and $v = 4\pi R^3/3$ the volume of each liposome.

Moreover, when the particle radius increases at constant lipid numerical concentration, the average distance between adjacent vesicles, normalized to radius R , scales as

$$\frac{V^{1/3}}{N_p} \frac{1}{R} \sim R^{-1/3} \quad (38)$$

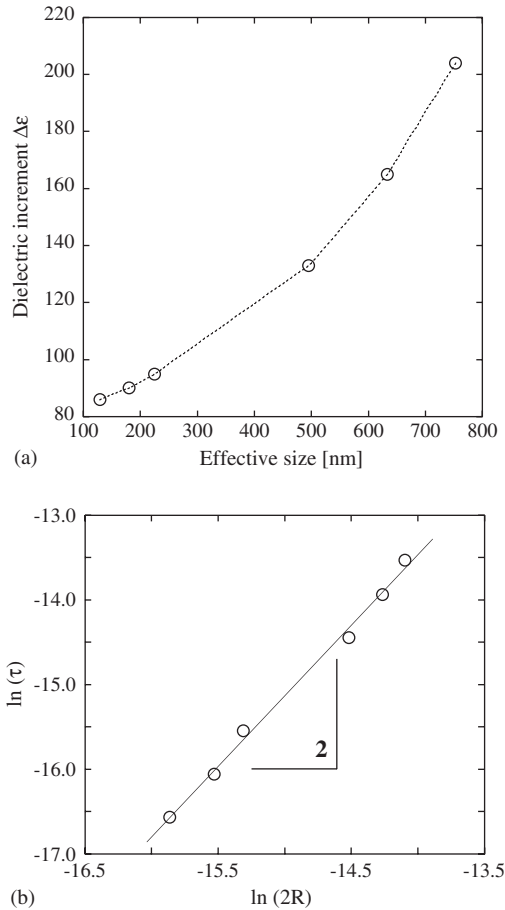


Fig. 8. (a) Dielectric increment $\Delta\epsilon$ as a function of liposome size. As the curvature radius of the bilayer increases, the dielectric strength increases. (b) The relaxation time τ is shown as a function of the logarithm of the liposome size. Over the whole interval of radii investigated, the relaxation time scales as the squared radius, according to equation (27).

suggesting that deviation from linearity might be attributed to an increased particle–particle electrostatic interactions as the vesicle radius R increases.

3.4. Influence of the temperature

Figure 7 shows the dielectric and conductometric spectra in the frequency range from 1 kHz to 10 MHz of a DPPC-liposome 620 nm in diameter aqueous suspension at different temperatures from 20 to 56 °C, covering the range from the pretransition to the main transition temperatures.

The behavior of the dielectric parameters $\Delta\epsilon$ (Fig. 9) and τ (Fig. 10), derived from the analysis of the dielectric spectra employing a Cole–Cole relaxation

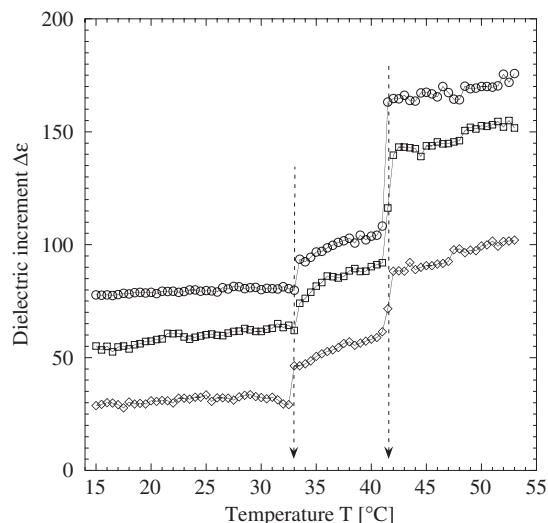


Fig. 9. The dielectric increment $\Delta\epsilon$ of DPPC liposome suspensions as a function of temperature for three different liposome size: (○): 750 nm (□): 620 nm; (◇): 500 nm in diameter. The fractional volume of the dispersed phase is $\Phi = 0.04$. At temperatures close to the pretransition and the main transition temperature, a well-defined increase is observed, marked by the arrows.

function, clearly evidences the effect of the temperature, indicating that either at the pretransition or at the main transition temperature, a marked reorganization of the double layer occurs. As can be seen in Fig. 9, the ripple phase, between the $L_{\beta'}$ and L_{α} phase, is accompanied by an increase of the dielectric strength, until the more fluid conformation of the hydrocarbon chains favors a more marked dipole organization to which a higher dielectric increment is attributed.

4. ELECTRICAL PROPERTIES OF THE LIPOSOMAL STRUCTURE

The influence of the electrical environment on the formation of lipid vesicles is very strong. Here, we will briefly review the main phenomenology induced by the surface charge distribution at the liposome–aqueous interface and by an external electric field, confining ourselves to the treatment of the double-layer structure and to the liposome stability.

4.1. Effect of surface charge density on the spontaneous formation of vesicles

For relatively large vesicles of controlled size, such as those required in biomedical applications, obtained under non-equilibrium conditions, the deformation

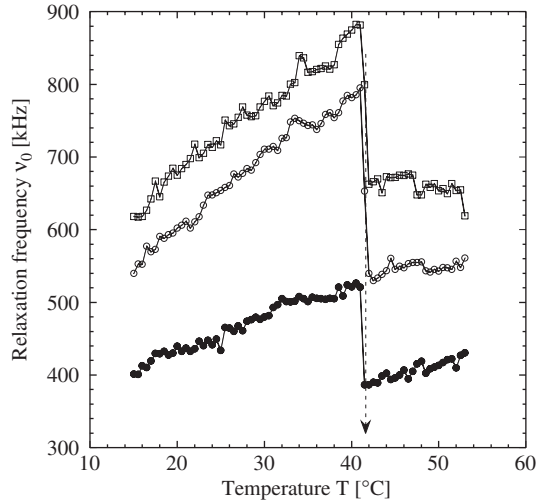


Fig. 10. The relaxation frequency ν_0 of a DPPC liposome suspension as a function of temperature for three different liposome size: (\square): 500 nm; (\circ): 620 nm (\bullet): 750 nm. The fractional volume of the dispersed phase is $\Phi = 0.04$. At temperatures close to the main transition temperature (marked by the arrow), a well-pronounced change in the relaxation frequency value is observed. In this case, the influence of the pretransition is less pronounced.

of the flat double layer into a spherical one is obtained to the cost of some bending energy (for the state-of-the-art on the formation dynamics of vesicles, see the excellent review of Gradzielski [67]). On the contrary, in the case of small vesicles, the free energy increases due to bending which can be compensated if the outer layer contains significantly more molecules than the inner layer. Symmetrical bilayers built up by identical monolayers have zero spontaneous curvature and, according to Helfrich [68], their bending elasticity can be written as

$$dE = \left[\frac{1}{2} \kappa (c_1 + c_2)^2 + \bar{\kappa} c_1 c_2 \right] dA \quad (39)$$

where dE is the free energy cost for bending the elemental area dA of a bilayer with principal local curvatures c_1 and c_2 . Here, κ and $\bar{\kappa}$ represent the mean and Gaussian curvature moduli, respectively.

Vesicles of hundred nanometers in size or more should then rarely form spontaneously, since pure phospholipid bilayers have bending moduli in the order of $5/25 K_B T$, at room temperature, or more [69–71]. However, when the bilayer consists of a mixture of different amphiphiles, characterized by different values of the packing parameter [72], equilibrium vesicles can form [73]. Packing parameter of a surfactant molecule is defined as the ratio between the volume V_0 of hydrophobic tail and the volume of an equivalent cylinder whose basis is the area of the polar head, a_0 , and whose height is the length of the hydrophobic part. If the bilayer is composed of only a single surfactant species, a flat bilayer

represents the status of minimal energy, since the two monolayers have the same ‘natural’ curvature, but an opposite sign. However, if more than one component is present, the different species can distribute in the two monolayers in such a way that the outer surface will have higher spontaneous curvature and equilibrium vesicles can form spontaneously. Moreover, because the vesicles are, in this case, energetically stabilized, a well-defined size is selected, depending on their composition. Consequently, the size distribution is fairly monodisperse.

The bending moduli of charged bilayers can be written as the sum of two contributions: an intrinsic bending elasticity, κ_p and $\bar{\kappa}_p$, arising from packing constraints and a specific electrostatic contribution to the bending free energy, κ_{elec} and $\bar{\kappa}_{elec}$. Hence, the ‘total’ mean and Gaussian bending moduli are written as

$$\begin{aligned}\kappa &= \kappa_p + \kappa_{elec} \\ \bar{\kappa} &= \bar{\kappa}_p + \bar{\kappa}_{elec}\end{aligned}\quad (40)$$

This implies that, beside steric interactions, vesicle stabilization is also influenced by charge density asymmetries on the two layers [70]. When the charge density on the outer surface of the vesicle is larger than that on the inner surface, the energy expenditure for bending the bilayer can be compensated by a reduction in electrostatic repulsion in the outer monolayer, due to its deformation. This is also true when the charges are allowed to flip from one side to the other. Also in this case, the entropic disadvantage due to the unequal charge distribution can be not sufficient to compensate for the reduction in electrostatic energy [71].

The possibility that even in the absence of a charge asymmetry, there could be spontaneous formation of vesicle when the surface charge density exceeds a limiting value, was pointed out by Winterhalter and Helfrich [74] in their analysis of the effect of charge density on membrane curvature moduli, based on the Debye–Hückel approximation. Their theory predicts that κ_{elec} is always positive, but $\bar{\kappa}_{elec}$ may be, in some cases, negative. At a sufficiently high surface charge density and low ionic strength, the negative contribution of $\bar{\kappa}_{elec}$ becomes comparable to the positive κ_{elec} , and entropically stabilized, polydispersed vesicles form. At higher charge densities, $\bar{\kappa}_{elec}$ dominates and the flat bilayer becomes unstable against spontaneous bending, leading to the formation of small, thermodynamically stable vesicles. More recently, Kumaran [70], by using nonlinear Poisson–Boltzman equation, calculated this limiting value of the charge density as $\sigma^* = Cn_\infty/k_D$, where C is a characteristic constant of the model, n_∞ is the number density of counterions (with charge ze) at a large distance from the surface, and k_D is the inverse of the Debye screening length. For $n_\infty = 6 \times 10^{24} \text{ e/m}^3$, corresponding to a molar concentration of 10^{-2} mol/l , the Debye screening length is 4.3 nm (in water, for monovalent counterions and at room temperature) and the corresponding limiting charge density is $\sigma^* = 7.3 \times 10^{17} \text{ e/m}^2$. As an example, for liposomes built up by DOTAP (dioleoyltrimethylammonium-propane), a cationic synthetic lipid commonly used in

biomedical applications, assuming the surfactant to be completely ionized and the area per polar head occupied at the liposome interface by one surfactant molecule $\approx 65 \text{ \AA}^2$ [75], the surface charge is $1.5 \times 10^{18} \text{ e/m}^2$, higher than the above-stated limiting value. In this case, the formation of liposomes stabilized by surface charge effect is expected.

Analyzing the effect of charge density-curvature coupling on the dynamics of fluctuations, it has been argued that when the charges are allowed to move on the membrane surface, the flat state of the membrane is unstable, due to a correlated variation in surface charge density and curvature [76]. Moreover, if fluctuations of counterion concentration in the diffuse layer, due to surface shape perturbations, are considered, instabilities arise also when the charge or the potential at the surface assumes a fixed value [77].

Lau and Pincus [78] proposed a different model, assuming a neutral system of mobile positive and negative charges confined on the surface of the vesicle. Such a scheme may appear appropriate to describe both a highly charged membrane, whose counterions are confined in a sheath near its surface (condensed counterions) and a membrane composed of an equimolar mixture of anionic and cationic surfactants. Within this framework, these authors showed that charge fluctuations contribute a non-analytic term to the bending rigidity, arguing that this term may lead to spontaneous vesicle formation. On the basis of the same model, Kim and Sung [79] were able to explain qualitatively the suppression of spontaneous vesicle formation, observed for different mixtures of ionic surfactants, when simple salts are added.

The effect of surface charge in inducing a double-layer bending and in stabilizing liposomes has been observed in different systems. Brasher *et al.* [80] investigated the behavior of mixed anionic and cationic surfactants in pure water. They observed an equilibrium vesicle phase when the composition in oppositely charged species deviates significantly from stoichiometry. The addition of a monovalent salt alters significantly the phase behavior. In particular, at certain compositions, by increasing the ionic strength, a vesicle-to-micelle transition can be induced. Also the addition of small amounts of an ionic surfactant to the lamellar phase of a nonionic surfactant system has been proved to be effective in inducing spontaneous bending and in the formation of multilamellar 'onion-like' structures [81–84], even though, in some cases, the formation of vesicles or of classical stacked bilayers depends on the procedure of sample preparation [84]. Besides onion-like structures, occurring at moderate surfactant concentration, Oberdisse *et al.* [82] found in their systems also a phase of thermodynamically stable, unilamellar microvesicles (with a radius below 100 \AA), appearing in the very dilute concentration range. The same authors showed that a transition from small to big charged unilamellar vesicles [83] and a region of phase diagram, where small and big vesicles coexist [85], can be predicted on the basis of a (nonlinearized) Poisson–Boltzmann cell model.

Different vesicle-forming surfactants can be protonated at various degrees by changing the pH of the aqueous solution. In particular, in the case of single tail oleyldimethylamine oxide (OleyDMAO) surfactant, there is experimental evidence that protonation decreases the average curvature and induces a change from thread-like micelles in the nonionic state to vesicles at the half-protonated state [86]. However, the observed effect of the protonation cannot be simply explained only in terms of electrostatic repulsion between charges. At decreasing pH (increasing protonation), the bilayer average curvature apparently goes through a maximum at about a half-protonated state, contrary to the expectation of a monotonic decrease with the ionization (protonation, in the case of amine oxides). This behavior has been attributed to an additional short-range attractive interaction [86], probably a hydrogen bond, between the protonated and the non-protonated headgroups of amine oxides.

4.2. Effect of an external electric field on vesicle double-layer structure

Owing to the liquid nature of the lipid matrix, under externally applied electric fields, a redistribution of charges on charged vesicle surface occurs. Experimentally, it has been observed that the application of a tangential electric field to a confined section of a double layer made up of different phospholipids induces a lateral reorganization of charged and uncharged membrane components. Electric field-induced concentration profiles have been investigated in these systems by using epifluorescence microscopy [87]. The results were interpreted on the basis of a thermodynamic model that accounts for the observed critical demixing behavior, i.e., a collective molecular interaction resulting in a spontaneous phase separation, at critical temperature and composition. This interaction has the effect of amplifying the lateral reorganization of the membrane, in response to the stress induced by the applied electric field.

In liposomes built up by a mixture of two different lipids, bearing different charges, a neutral one and a charged one, for example, the charged species, under the influence of an external electrical field, can move within the bilayer so that the external field can cause a surface reorganization. Such a spatial redistribution of the charges on a nonhomogeneously charged object may substantially affect its electrophoretic mobility, to an extent that, if two oppositely charged species are embedded into the membrane, the direction of motion can be reversed, upon the increase of the field intensity [88].

It has been recently shown that the electric stress created by ionic currents across a non-perfectly flat membrane gives rise to a destabilizing surface energy, enhancing undulations [89]. When a fixed electric field is applied across the membrane, the electric stress at the membrane interfaces is due to the force exerted by the conduction charges brought by the field at the interfaces or, in

other words, by the surface charge density induced by the field, whose sign is opposite at the two interfaces. If the membrane is perfectly flat, the electric stress is symmetrically balanced on both sides of the membrane and the field only produces a compression of the membrane itself. However, any membrane curvature that leads to an asymmetry in the charge density between the two interfaces produces an unbalanced net stress, whose order of magnitude can be expressed as $\Sigma_{el} \simeq \epsilon_m E_m^2 d/R$, where d is the membrane thickness and R the local curvature radius, E_m is the electric field inside the membrane and ϵ_m the membrane permittivity. This stress, in turn, tends to enhance the small local undulations of the membrane, since the unbalanced normal stress points toward opposite directions in regions with opposing curvatures. In the presence of a lipid reservoir, the electric field induces a decrease of the interfacial tension, known as the electrocapillary effect (see, for example Kang *et al.* [90] and literature cited therein). On the contrary, for a fixed number of surfactant molecules, the enhancing of the membrane undulation under electric field produces a concomitant mechanical tension, because of deviation from the nominal area per molecule.

For values of the electric field typically in the order of $E \sim 10^3$ V/m, the electrostatic contribution to the surface tension reaches values in excess of about $T_{el} \sim 10^{-3}$ J/m², comparable to the mechanical tension needed for the rupture of a lipid membrane [91].

It has long been known that transmembrane voltage pulses of sufficient amplitude create transient pores in a lipid bilayer. This phenomenon, known as ‘electroporation,’ has been extensively investigated (for a review see Weaver and Chizmadzhev [91] and Tien and Ottowa [92]), and have attracted increasing attention as a powerful technique for introducing DNA and other charged molecules into cells and liposomes, in biomedical and biotechnological applications. Barnett and Weaver [93] and Weaver and Chizmadzhev [91] derived a quantitative theory of electroporation in planar bilayer lipid membranes. These authors assumed that transient aqueous pores of minimal size, created and destroyed by thermal fluctuations, are involved in electroporation. By writing a density function of membrane pore population, depending on a rate r_p of pore formation given by

$$r_p \sim \exp \left[\frac{(a\Delta V)}{(K_B T)} \right] \quad (41)$$

where a is a constant and ΔV the transmembrane voltage, these authors are able to derive an expression for the overall conductance of the electroporated membrane which is in good agreement with experiments. Moreover, also the predictions of theory on the duration and amplitude effect of the charging pulse compare fairly with experiments.

More recently, Chizmadzhev *et al.* [94] reported that the nonconductive pores, termed ‘pre-pores,’ would be induced by an applied voltage and from which the transient hydrophilic (conductive) pore could develop. In this context, the undu-

lation instabilities induced by the external electric field, described by Sens and Isambert [89], could play an important role.

However, Isambert [95] argued that, in general, models that assume a flat membrane under constant mechanical tension are not appropriate for describing the opening of pores in the double layer of a closed vesicle or of a biological cell. In the very short timescale involved in electroporation, the membrane cannot exchange phospholipids with the cell reservoirs and, in this aspect, cell membrane behaves like an artificial vesicle with a fixed number of phospholipids. Analogous to the case of undulation instabilities discussed above, at the curved membrane interfaces, the electric field generates noncancelling electric stresses that tend to deform the vesicle shape. However, both the number of phospholipids in the membrane and the volume of the vesicle are essentially fixed and the cell membrane stretches until a mechanical balance between the surface tension and the sum of the normal (electric) stresses is attained. Starting *ab initio* from the Laplace equation for a shelled sphere in a conducting medium, with the appropriate boundary conditions, Isambert [95] showed that, for the case of unperforated cells (i.e. before electroporation), the radial stress is proportional to the radius of curvature of the membrane and independent of the conductivities of both the inner medium (cytosol) and the bathing (external) solution. When a surface tension value is reached, high enough to cause the membrane rupture, the opening of a pore causes the relaxation of the tension. Considering the bilayer as a viscous film under relaxing surface tension, Isambert [95] showed that the elastic relaxation of the stretched membrane immediately after pores nucleation may follow two dynamic regimes, with an initial 'very slow exponential' or linear increase of the average pore radius, followed by a catastrophic bursting of the film, in good agreement with experiments on artificial bilayers [96].

On the basis of a different theoretical analysis, Lewis [97] comes to the conclusion that, in addition to a compressive stress normal to the membrane plane, an applied electric field also generates traction stresses on the plane of the membrane that are likely to be sufficient to cause electroporation and rupture of the membrane itself.

The now classical experiment of Zhelev and Needham [98] for studying electroporation of lipid membranes was performed using spherical, giant liposomes (from 25 to 55 μm in diameter). Holding a single liposome by a micropipette and controlling the internal pressure by gentle pipette suction, they created a small mechanical tension in the bilayer. The liposomes were filled with a solution having a different refractive index from the one of the bathing medium, so that the formation of a pore could be visualized by the small jet emitted inside the solution. Pore lifetimes could be controlled by adjusting the membrane tension and varied from tenths of a second to several seconds. The pore size was determined from the volumetric flow in the pore region and the measured pressure difference across the bilayer. Pores, with a diameter of $\approx 1 \mu\text{m}$, were in these conditions in a quasi-stationary state and when they collapsed spontaneously, they did so in a few milliseconds. From the measured pore size and the membrane tension, the au-

thors determined a pore line tension in the order of $0.9/3.0 \times 10^{-11}$ N, depending on vesicle composition.

Kakorin and Neumann [99] analyzed the ionic conductivity of lipid membrane pores in terms of electrostatic interactions of the transported ions with low-dielectric pore walls. It is well known that protein channels frequently show non-Ohmic behavior. However, also conductive pores in electroporated lipid bilayer can show a voltage-dependent electrical conductivity. This effect can be explained considering the discontinuity of polarizability between the aqueous medium and the low-permittivity double-layer interior at the pore wall, and described in terms of an image charge that tend to repel the ion from the lipid phase. Assuming a specific shape of the image potential at the pore entrance, Kakorin and Neumann [99], on the basis of the observed conductivity of lipid vesicles, calculated a mean pore radius of ≈ 0.6 nm. In a more recent paper, Griese [100] and his coworkers, by means of the combined use of electro-optic and conductivity relaxation measurements on suspensions of electroporated unilamellar vesicles, pointed out the existence of a contribution to the overall electrical conductivity of the suspension, that could be attributed to the releasing of intravesicular electrolyte through the pores, during the electric pulse.

5. ELECTROROTATION OF LIPOSOMES

A biologic cell or a vesicle suspended in an aqueous medium in a nonuniform electric field is subject to different forces that depend on the particle shape and on the differences in dielectric parameters characterizing the bathing solution and the particle itself. Different patterns of electric field, spatially nonuniform, or time varying, such as rotating or traveling wave, can easily be created by using appropriate microelectrode arrays. These fields induce dipole moments in the particles, and each type of particle responds to the forces produced by the interaction of the induced dipole with the applied field in a unique way. Based on this 'electrokinetic' effect, different techniques have been developed that allows a controlled and selective manipulation of biological cells, vesicles and, more in general, colloidal particles.

In particular, a uniform rotating electric field can be generated by four electrodes arranged in a square symmetry excited with sinusoidal voltages, with 90° phase difference between adjacent electrodes. The rotating electric field will induce in the particle a rotating dipole moment out of phase with the field. The amplitude of the dipole and the phase difference of its rotation with respect to the phase of electric field depends on particle shape and on passive electric properties of both the particle and the bathing medium, at the frequency of the applied field. In stationary conditions, the torque due to the interaction of the rotating field and the induced dipole will cause the particle spinning, at a characteristic frequency. From this frequency, that can easily be measured by eye, using, for

example, a bright field optical microscope, and by using an appropriate geometrical schematization of the particle, the dielectric and conductometric parameters of the particles are obtained. This technique developed in the early 1980s by different groups [101,102] has been termed 'electrorotation'. Electrorotation of liposomes has been used by Pethig *et al.* [103] for the verification of dielectric multi-shell models used to describe biological cells. Different unilamellar, oligolamellar, and multilamellar liposomes of diameters ranging from 5 to 24 μm , well characterized by fluorescence microscopy, flow cytometry and electron spin resonance, were employed as model systems. From their analysis, the authors argued that, although the spectra for multilamellar liposomes appear clearly distinguishable from the spectra of more simple unilamellar or oligolamellar liposomes, the accuracy with which the dielectric parameters of each new concentric membrane compartment could be fitted fell off very rapidly by increasing the numbers of shells. From this, they concluded that, while electrorotation data enable accurate determinations of the dielectric properties of the outermost membrane of multicompartiment membrane structures, quantitative estimates of the parameters of internal compartments are less reliable, even though the technique provides good indications of the level of complexity of the system.

Although very simple and effective, the experimental approach consists in manipulating the particles 'manually', by means of micromanipulators, in order to select and put them in the rotating field and in visual observation under a microscope presents several limitations. Different technical improvements of the experimental setup have recently been developed, aimed to confer some degree of automation to the procedure. As an example, by the combined use of optical tweezers and of a video camera, Mietchen *et al.* [104] implemented an automated apparatus for single shell electrorotation spectroscopy. In electrorotational light scattering (ERLS) [105] or in dielectrophoretic light scattering (DPLS) [106], a different experimental approach is employed. A dynamic light-scattering experiment is carried out on the particle suspension in the presence of a rotating (ERLS) or an oscillating, nonuniform electric field (DPLS). The field induces suspended particles to undergo dielectrophoretic motion, which is detected by the modulation in the dynamic light-scattering autocorrelation function. From this modulated autocorrelation function, by using a suitable dielectric model for the suspended particles, the dielectric characteristics of the cell can be obtained.

REFERENCES

- [1] G. Gregoriadis, A. Florence, Liposomes in drug delivery, Clinical, diagnostic and ophthalmic potential, *Drugs* 45 (1993) 15–28.
- [2] D. Lasic, Novel applications of liposomes, *Trends Biotechnol.* 16 (1998) 307–321.
- [3] R. Banerjee, Liposomes: applications in medicine, *J. Biomater. Appl.* 16 (2001) 3–21.
- [4] T. Lian, R.J. Ho, Trends and developments in liposome drug delivery systems, *J. Pharm. Sci.* 90 (2001) 667–680.

- [5] A. Finkelstein, O.B. Ptitsyn, *Protein Physics*, Academic Press, London, 2002, Chapter. 5.
- [6] D. Lichtenberg, Y. Barenholz, *Liposomes: Preparation, Characterization and Preservation (Methods of Biological Analysis 33)*, Wiley, New York, 1988, pp. 337–461.
- [7] R.R.C. New, *Liposomes: A Practical Approach*, IRL Press at Oxford University Press, Oxford, 1990.
- [8] U.K. Nassander, G. Storm, P.A. Peeters, D.J.A. Crommelin, *Liposomes. Biodegradable Polymers as Drug Delivery Systems*, Marcel Dekker, New York, 1988, pp. 261–338.
- [9] G. Gregoriadis, *Liposome Technology*, 2nd edition, CRC Press, Boca Raton, FL, 1993.
- [10] Y. Barenholz, D.J.A. Crommelin, *Liposomes as Pharmaceutical Dosage Forms. Encyclopedia of Pharmaceutical Technology*, Marcel Dekker, New York, 1994, pp. 1–39.
- [11] F. Szoka, D. Papahadjopoulos, *Liposomes: Preparation and Characterization, (Liposomes: From Physical Structure to Therapeutic Application)*, Elsevier, North-Holland, Amsterdam, 1981, pp. 51–82.
- [12] M.J. Hope, M.B. Bally, G. Webb, P.R. Cullis, Production of large unilamellar vesicles by a rapid extrusion procedure. Characterization of size distribution, trapped volume and ability to maintain a membrane potential., *Biochim. Biophys. Acta* 812 (1983) 55–65.
- [13] L. Saunders, J. Perrin, D. Gammack, Ultrasonic radiation of some phospholipids sols, *J. Pharm. Pharmacol.* 14 (1962) 567–572.
- [14] C.H. Huang, Studies on phosphatidylcholine vesicles: formation and physical characteristics, *Biochemistry* 8 (1969) 334–352.
- [15] D.W. Deamer, A.D. Bangham, Large volume liposomes by an ether injection method, *Biochim. Biophys. Acta* 443 (1976) 629–643.
- [16] F. Szoka, D. Papahadjopoulos, Procedure for preparation of liposomes with larger internal aqueous space and high capture by reverse-phase evaporation, *Proc. Natl. Acad. Sci. USA* 75 (1978) 4194–4198.
- [17] S. Batzri, E.D. Korn, Single bilayer liposomes prepared without sonication, *Biochim. Biophys. Acta* 298 (1973) 1015–1019.
- [18] H. Talsma, A.Y. Ozer, L. Van Bloois, D.J.A. Crommelin, The size reduction of liposomes with a high pressure homogenizer (microfluidizertm). Characterization of prepared dispersions and comparison with conventional methods, *Drug. Dev. Ind. Pharm.* 15 (1989) 197–207.
- [19] M. Brandl, D. Bachmann, M. Drechsler, K.H. Bauer, Liposome preparation by a new high pressure homogenizer Gaulin micron lab 40, *Drug. Dev. Ind. Pharm.* 16 (1990) 2167–2191.
- [20] G. Sessa, G.J. Weissman, Formation of artificial lysosome *in vitro*, *J. Clin. Invest.* 48 (1969) 76a–77a.
- [21] G. Gregoriadis, P.D. Leatwood, B.E. Ryman, Enzyme entrapment in liposomes, *FEBS Lett.* 14 (1971) 95–99.
- [22] M.A. Moses, H. Brem, R. Langer, Advancing the field of drug delivery: taking aim at cancer, *Cancer Cell* 4 (2003) 337–341.
- [23] W.B. Russel, D.A. Saville, W.R. Schowalter, *Colloidal Dispersions*, Cambridge University Press, Cambridge, 1989.
- [24] K. Asami, Characterization of heterogeneous systems by dielectric spectroscopy, *Prog. Polym. Sci.* 27 (2002) 1617–1659.
- [25] Y. Feldman, I. Ermolina, Y. Hayashi, Time domain dielectric spectroscopy study of biological systems, *IEEE Trans. Dielect. Elec. Ins.* 10 (2003) 728–753.
- [26] B. Klösgen, C. Reichle, S. Kohismann, K.D. Kramer, Dielectric spectroscopy as a sensor of membrane headgroup mobility and hydration, *Biophys. J.* 71 (1996) 3251–3260.

- [27] M. Clause, Dielectric properties of emulsions and related systems *Encyclopedia of Emulsion Technology*, Vol. 1, Basic Theory, Marcel Dekker Inc, New York, 1983.
- [28] H. Pauly, H.P. Schwan, Impedance of a suspension of ball-shaped particles with a shell; a model for the dielectric behavior of cell suspensions and protein solutions, *Z. Naturforsch.* 14b (1959) 125–131.
- [29] T. Hanay, H.Z. Zhang, K. Sekine, K. Asaka, K. Asami, The number of interfaces and the associated dielectric relaxations in heterogeneous systems, *Ferroelectrics* 86 (1988) 191–204.
- [30] L. Gao, J.P. Huang, K.W. Yu, Theory of a.c. electrokinetic behavior of spheroidal cell suspensions with an intrinsic dispersion, *Phys. Rev. E* 67 (2003) 021910–022910.
- [31] G. Schwarz, A theory of the low frequency dielectric dispersion of colloidal particles in electrolyte solutions, *J. Phys. Chem.* 66 (1962) 2636–2642.
- [32] J.M. Schurr, On the theory of the dielectric dispersion of spherical colloidal particles in electrolyte solutions, *J. Phys. Chem.* 68 (1964) 2407–2413.
- [33] C.T. O’Konski, Electrical properties of macromolecules. Theory of ionic polarization in polyelectrolyte, *J. Phys. Chem.* 64 (1960) 605–619.
- [34] M. Fixman, Charged macromolecules in external fields. I. The sphere, *J. Chem. Phys.* 72 (1980) 5177–5186.
- [35] W.C. Chew, P.S. Sen, Dielectric enhancement due to electrochemical double-layer: thin double layer approximation, *J. Chem. Phys.* 77 (1982) 4683–4693.
- [36] S.S. Dukhin, V.N. Shilov, *Dielectric Phenomena and the Double Layer in Disperse Systems and Polyelectrolytes*, Halsted, New York, 1974.
- [37] R.W. O’Brien, The response of a colloidal suspension to an alternating electric field, *Adv. Colloid Interface Sci.* 16 (1982) 281–320.
- [38] W.C. Chew, Dielectric enhancement and electrophoresis due to an electrochemical double layer: a uniform approximation, *J. Chem. Phys.* 80 (1984) 4541–4552.
- [39] Y. Hu, Effects of an inner Helmholtz layer on the dielectric dispersion of colloidal dispersions, *Langmuir* 14 (1998) 271–276.
- [40] C. Grosse, K.R. Foster, Influence of bulk diffusion on the counterion polarization in a condensed counterion model, *J. Phys. Chem.* 91 (1987) 6415–6417.
- [41] C. Grosse, K.R. Foster, Permittivity of a suspension of charged spherical particles in electrolyte solution, *J. Phys. Chem.* 91 (1987) 3073–3076.
- [42] C. Grosse, Permittivity of a suspension of charged spherical particles in electrolyte solution. 2. Influence of the surface conductivity and asymmetry of the electrolyte at the low- and high-frequency relaxations, *J. Phys. Chem.* 92 (1988) 3905–3910.
- [43] M. Tirado, C. Grosse, W. Schrader, U. Kaatze, Broad frequency range dielectric spectroscopy of aqueous suspensions of phospholipids vesicles, *J. Non-Cryst. Solids* 305 (2002) 373–378.
- [44] C. Grosse, R. Barchini, C. Halloy, R. Pottel, On the decomposition of the Maxwell mixture formula into a sum of Debye type contributions, *J. Phys. D.* 19 (1986) 1957–1964.
- [45] C. Grosse, *Relaxation mechanisms of homogeneous particles and cells suspended in aqueous electrolyte solutions. Interfacial Electrokinetics and Electrophoresis*, Marcel Dekker, New York, 2001.
- [46] U. Kaatze, A. Dittrich, K. Gopel, R. Pottel, Dielectric studies of water in solutions of purified lecithin vesicles, *Chem. Phys. Lipids* 35 (1984) 279–290.
- [47] U. Kaatze, K. Gopel, R. Pottel, Zwitterion motions of differently aggregated phospholipids in aqueous and methanolic solutions. a dielectric relaxation study, *J. Phys. Chem.* 89 (1985) 2565–2571.
- [48] W. Schrader, U. Kaatze, Zwitterionic headgroup orientation correlation and mobility and the domain structure of membranes, *J. Phys. Chem. B* 105 (2001) 6266–6272.
- [49] U. Kaatze, R. Henze, R. Pottel, Dielectric relaxation and molecular motion in C14/lecithin/water systems, *Chem. Phys. Lipids* 25 (1979) 149–177.

- [50] R. Henze, Dielectric relaxation lecithin/cholesterol/water mixtures, *Chem. Phys. Lipids* 27 (1979) 165–175.
- [51] U. Kaatzte, R. Henze, Orientational correlation and dielectric relaxation of the zwitterionic head groups of dimyristoyl-lecithin multi-bilayer vesicles, *Ber. Bunsenges. Phys. Chem.* 84 (1980) 1102–1108.
- [52] U. Kaatzte, S.C. Muller, H. Heibl, Monoalkyl phosphodiester: synthesis and dielectric relaxations of solutions, *Chem. Phys. Lipids* 27 (1980) 263–280.
- [53] K. Kaatzte, U. Lautscham, R. Pottel, On the changes in the microwave dielectric spectrum of aqueous phospholipid bilayer solutions at the ordered-fluid phase transition, *J. Mol. Liquids* 28 (1984) 249–270.
- [54] R. Pottel, K.D. Gopel, R. Henze, U. Kaatzte, V. Uhlenndorf, The dielectric permittivity spectrum of aqueous colloidal phospholipid solution between 1 kHz and 60 GHz, *Biophys. Chem.* 19 (1984) 233.
- [55] F. De Luca, C. Cametti, A. Naglieri, F. Bordi, R. Misasi, M. Sorice, Cluster organization of glycosphingolipid GD1a in lipid bilayer membranes: a dielectric and conductometric study, *Langmuir* 15 (1999) 2493–2499.
- [56] K. Simons, E. Ikonen, Functional rafts in cell membranes, *Nature* 387 (1997) 569–572.
- [57] S. Munro, Lipid rafts: elusive or illusive? *Cell* 115 (2003) 377–388.
- [58] C. Cametti, F. De Luca, M.A. Macri, B. Maraviglia, R. Misasi, M. Sorice, A. Pavan, T. Garofalo, G.M. Pontieri, F. Bordi, G. Zimatore, Influence of different glycosphingolipids on the conductometric properties of a model phospholipid membrane system, *Colloids Surf. B* 7 (1996) 39–46.
- [59] M. Diociaiuti, I. Ruspantini, C. Giordani, F. Bordi, P. Chistolini, Distribution of GD3 in DPPC monolayers: a thermodynamic and atomic force microscopy combined study, *Biophys. J.* 86 (2004) 321–328.
- [60] M. Edidin, Shrinking patches and slippery rafts: scales of domains in the plasma membrane, *Trends in Cell Biology* 11 (2001) 492–496.
- [61] M. Edidin, Timeline: Lipids on the frontier: a century of cell-membrane bilayers, *Nature* 4 (2003) 414–418.
- [62] Y. Barenholz, Cholesterol and other membrane active sterols: from membrane evolution to “rafts”, *Prog. Lipid Res.* 41 (2002) 1–5.
- [63] W.K. Subczynska, A. Kusumi, Dynamics of raft molecules in the cell and artificial membranes: approaches by pulse EPR spin labeling and single molecule optical microscopy, *Biochim. Biophys. Acta* 1610 (2003) 231–243.
- [64] I. Ermolina, G. Smith, Y. Ryabov, A. Puzenko, Y. Polevaya, R. Nigmatullin, Y. Feldman, Effect of penetration enhancers on the dynamic behavior of phosphatidylcholine headgroups in liposomes, *J. Phys. Chem. B* 104 (2000) 1373–1381.
- [65] S.A. Barker, D.Q.M. Craig, R.M. Hill, K.M.G. Taylor, The low-frequency dielectric response of liposomes, *J. Colloid Interf. Sci.* 166 (1994) 66–72.
- [66] F. Bordi, C. Cametti, T. Gili, Reduction of the contribution of the electrode polarization effect in the radiowave dielectric measurements of highly conducting biological cell membrane, *Bioelectrochemistry* 54 (2001) 53–61.
- [67] M. Gradzielski, Vesicles and vesicle gels—structure and dynamics of formation, *J. Phys.: Condens. Matter* 15 (2003) R655–R697.
- [68] W. Helfrich, Elastic properties of lipid bilayers. theory and possible experiments, *Z. Naturforsch. C* 28 (1973) 693–703.
- [69] G. Brannigan, A.C. Tamboli, F.L.H. Brown, The role of molecular shape in bilayer elasticity and phase behavior, *J. Chem. Phys.* 121 (2004) 3259–3271.
- [70] V. Kumaran, Effect of surface charge on the curvature moduli of a membrane, *Phys. Rev. E* 64 (2001) 0519221–0519229.
- [71] V. Kumaran, Spontaneous formation of vesicles by weakly charged membranes, *J. Chem. Phys.* 99 (1993) 5490–5499.
- [72] J. Israelachvili, *Intermolecular and Surface Forces*, Academic Press, London, 1985.

- [73] S.A. Safran, P.A. Pincus, D. Andelman, F.C. MacKintosh, Stability and phase behavior of mixed surfactant vesicles, *Phys. Rev. A* 43 (1991) 1071–1078.
- [74] M. Winterhalter, Helfrich, Stability and phase behavior of mixed surfactant vesicles, *J. Phys. Chem.* 92 (1988) 6865–6867.
- [75] F. Bordi, C. Cametti, M. Diociaiuti, D. Gaudino, T. Gili, S. Sennato, Complexation of anionic polyelectrolytes with cationic liposomes: evidence of reentrant condensation and lipoplex formation, *Langmuir* 20 (2004) 5214–5222.
- [76] V. Kumaran, Instabilities due to charge-density-curvature coupling in charged membranes, *Phys. Rev. Lett.* 85 (2000) 4996–4999.
- [77] V. Kumaran, Electrohydrodynamic instability of a charged membrane, *Phys. Rev. E* 64 (2001) 0119111–0119118.
- [78] A.W.C. Lau, P. Pincus, Charge-fluctuation-induced nonanalytic bending rigidity, *Phys. Rev. Lett.* 81 (1998) 1338–1341.
- [79] Y.W. Kim, W. Sung, Effects of charge and its fluctuation on membrane undulation and stability, *Europhys. Lett.* 58 (2002) 147–153.
- [80] L.L. Brasher, K.L. Herrington, E.W. Kaler, Electrostatic effects on the phase behavior of aqueous cetyltrimethylammonium bromide and sodium octyl sulfate mixtures with added sodium bromide, *Langmuir* 11 (1995) 4267–4277.
- [81] H. Hoffmann, C. Thunig, P. Schmiedel, U. Munkert, Surfactant system with charged multilamellar vesicles and their rheological properties, *Langmuir* 10 (1994) 3972–3981.
- [82] J. Oberdisse, C. Couve, J. Appell, J.F. Berret, C. Ligoure, G. Porte, Vesicles and onions from charged surfactant bilayers: a neutron scattering study, *Langmuir* 12 (1996) 1212–1218.
- [83] J. Oberdisse, G. Porte, Size of microvesicles from charged surfactant bilayers: neutron scattering data compared to an electrostatic model, *Phys. Rev. E* 56 (1997) 1965–1975.
- [84] J. Hao, H. Hoffmann, K. Horbaschek, A novel cationic/anionic surfactant system from a zwitterionic from a zwitterionic alkyldimethylamine oxide and dihydroperfluorooctanoic acid, *Langmuir* 17 (2001) 4151–4160.
- [85] J. Oberdisse, Transition from small to big charged unilamellar vesicles, *Eur. Phys. J. B* 3 (1998) 463–469.
- [86] H. Kawasaki, M. Souda, S. Tanaka, N. Nemoto, G. Karlsson, M. Almgren, H. Maeda, Reversible vesicle formation by changing pH, *J. Phys. Chem. B* 106 (2002) 1524–1527.
- [87] J.T. Groves, S.G. Boxer, M.H.M., Electric field effects in multicomponent fluid lipid membranes, *J. Phys. Chem. B* 104 (2000) 119–124.
- [88] P. André, D. Long, A. Ajdari, Electrophoretic mobility of heterogeneous vesicles, *Europhys. Lett.* 46 (1999) 530–536.
- [89] P. Sens, H. Isambert, Undulation instability of lipid membranes under electric field, *Phys. Rev. Lett.* 88 (2002) 128102.
- [90] K.H. Kang, I. Kang, C.M. Lee, Wetting tension due to Coulombic interaction in charge-related wetting phenomena, *Langmuir* 19 (2003) 5407–5412.
- [91] J.C. Weaver, Y.A. Chizmadzhev, Theory of electroporation: a review, *Bioelectrochem. Bioenerg.* 41 (1996) 135–160.
- [92] H.T. Tien, A. Ottawa, The bilayer lipid membrane BLM under electrical fields, *IEEE Trans. Dielectrics Electric. Insul.* 10 (2003) 717–727.
- [93] A. Barnett, J.C. Weaver, Electroporation: a unified, quantitative Theory of reversible electrical breakdown and mechanical rupture in artificial planar bilayer membranes, *Bioelectrochem. Bioenerg.* 25 (1991) 163–182.
- [94] K.C. Melikov, V.A. Frolov, A. Shcherbakov, A.V. Samsonov, Y.A. Chizmadzhev, L.V. Chemomordik, Voltage-induced nonconductive pre-pores and metastable single pores in unmodified planar lipid bilayer, *Biophys. J.* 80 (2001) 1829–1836.
- [95] H. Isambert, Understanding the electroporation of cells and artificial bilayer membranes, *Phys. Rev. Lett.* 80 (1998) 3404–3407.

- [96] C. Wilhelm, M. Winterhalter, U. Zimmermann, R. Benz, Kinetics of pore size during irreversible electrical breakdown of lipid bilayer membranes, *Biophys. J.* 64 (1993) 121–128.
- [97] T.J. Lewis, A model for bilayer membrane electroporation based on resultant electromechanical stress, *IEEE Trans. Dielectrics Electric. Insul.* 10 (2003) 769–777.
- [98] D.V. Zhelev, D. Needham, Tension-stabilized pores in giant vesicles – determination of pore-size and pore line tension, *Biochim. Biophys. Acta* 1147 (1993) 89–104.
- [99] S. Kakorin, E. Neumann, Ionic conductivity of electroporated lipid bilayer membranes, *Bioelectrochem.* 56 (2002) 163–166.
- [100] T. Griese, S. Kakorin, E. Neumann, Conductometric and electrooptic relaxation spectrometry of lipid vesicle electroporation at high fields, *Phys. Chem. Chem. Phys.* 4 (2002) 1217–1227.
- [101] W.M. Arnold, U. Zimmermann, Rotating-field-induced rotation and measurement of the membrane capacitance of single mesophyll cells of *Avena sativa*, *Z. Naturforsch. C* 37 (1982) 908–915.
- [102] M. Mischel, A. Voss, H.A. Pohl, Cellular spin resonance in rotating electric fields, *J. Biol. Phys.* 10 (1982) 223–226.
- [103] K.L. Chan, R.C. Gascoiyne, F.F. Becker, R. Pethig, Electrorotation of liposomes: verification of dielectric multi-shell model for cells, *Biochim. Biophys. Acta* 1349 (1997) 182–196.
- [104] D. Mietchen, T. Schnelle, T. Müller, R. Hagedorn, G. Fuhr, Automated dielectric single cell spectroscopy – temperature dependence of electrorotation, *J. Phys. D: Appl. Phys.* 35 (2002) 1258–1270.
- [105] B. Pruger, P. Eppmann, E. Donath, J. Gimsa, Measurement of inherent particle properties by dynamic light scattering: introducing electrorotational light scattering, *Biophys. J.* 72 (1997) 1414–1424.
- [106] F.G. Halaka, Dielectrophoretic dynamic light-scattering (ddls) spectroscopy, *Proc. Natl. Acad. Sci.* 100 (2003) 10164–10169.
- [107] M.C. Wiener, S. Tristram-Nagle, P.A. Wilkinson, L.E. Campbell, J.F. Nagle, Specific volumes of lipids in a fully hydrated bilayer dispersion, *Biochim. Biophys. Acta* 938 (1988) 135–142.

SUBJECT INDEX

A

2-(9-anthroyloxy)stearic acid (2-AS)
111
12-(9-anthroyloxy)stearic acid (12-AS)
111
active site-targeting 1, 7, 16
affinochromism/biochromism 231
aggregation 61, 70, 73
aluminum 79, 81
anionic electrolytes 71
anticancer ether lipids (AELs) 15
Arg–Gly–Asp (RGD) 31
arginine–glycine–aspartic acid 73
ATPase 70

B

biochanin A 115, 116
biological membrane 49, 50, 55, 58,
59
blood proteins 72
Br 67
Bragg–Williams approximation 273
budding of liposomes 253, 254, 271,
275–277

C

Ca²⁺ 54, 66, 71
caffeic acid phenethyl ester 113
calcein-trapped liposomes 111, 124
carbopol 69
cardiolipin 50
catechins 107–111, 116–124, 126,
130
cells 49, 50, 52, 68, 70, 72, 73
ceramide 191, 205–210
charge densities 63, 71
chemiluminescence 157, 158, 160,
168
chinese hamster lung fibroblast 112,
114

chitosan 69
cholesterol 50
chondroitin sulfate (CS) 32
CL 55, 60–63
ClO₄⁻ 67
clustering of membrane inclusions
253, 276, 277
colipid 136, 138, 139, 155, 160, 166,
169, 173
colorimetric detection 229, 233, 235,
237, 241
colorimetric response (CR) 232
conditioning 135, 136, 141, 145, 168,
170
cone-shaped lipids 8
confocal microscopy 136, 160–162,
175
conformation 49, 54, 56, 65, 68
counterion polarization 295
Cs⁺ 65, 66
curcumin 108, 109, 114
curvature deviator 256–258, 263, 265,
268, 269

D

daidzein 115, 116
Debye–Hückel parameter 65
dehydration 9, 54, 70, 83, 86, 102,
179, 210
deviatoric bending 263, 268, 270, 271
dicetylphosphate (DCP) 69, 121
dielectric properties 281, 285, 286,
296, 315
differential scanning calorimetry 57
digoxigenin 140, 164
dimyristoylphosphatidylcholine
(DMPC) 126
dioleoyl phosphatidylcholine 58, 71
dipole 51, 55, 56, 63, 67

direct interactions between the
 membrane constituents 257
dispersed systems 285, 286
DMHAPC-Chol 144, 146–149, 154,
 157, 169–171, 177
DNA delivery 145, 168, 170
DNA transfection 50, 71
DOPE 136, 137, 139, 140, 144,
 146–155, 157, 159, 161,
 163–173, 175–181
DSC 57

E
electric surface properties 49, 63
electrochemical biosensors 229,
 245
electron microscopy 136, 138, 140,
 142, 154, 160, 162, 170
electrorotation 281, 314, 315
electrostatic model 55
endocytosis 136, 139, 140, 162, 163,
 166–168, 172
endosome 139, 140, 163, 165, 166,
 168, 169, 172, 173
endothelial barrier 72
enthalpy 57–59
entropy 51, 57, 58
enzyme-sensitive liposomes 1, 13
epicatechin (EC) 108, 116
epicatechin gallate (ECg) 108,
 116
epidermal growth factor receptor
 (EGFR) 21
epigallocatechin (EGC) 108, 116
epigallocatechin gallate (EGCg) 108,
 116

F
F- 49–73
folate receptor (FR) 16, 21
folate-attached liposomes 21, 22
formononetin 115, 116
FTIR 135, 137, 146–148, 154,
 155
fusion 49, 50, 60, 68, 70, 71
fusogenic peptide 21, 24, 25

G
 β -galactosidase 137, 142, 145, 146,
 157–159, 170, 171
galactose 27–30
galactosylceramide 53, 60
galangin 114
gallic acid esters 107–109, 112, 113,
 117
gel retardation 135, 151, 153, 154,
 176
genistein 115, 116
GFP (green fluorescent protein) 137,
 145
giant unilamellar vesicles (GUV) 52, 53
glucose 60–62, 69
glucosylceramide 60
glycolipids 49–51, 67, 68, 73, 191,
 201–203
glycosaminoglycan 137, 173
glycosphingolipids 59
glycosylated liposomes 26

H
 H^+ 66, 70
head group interactions 58
headgroups 51, 63
hepatocytes 72
heterogeneous systems 281, 283,
 285, 291
hyaluronan 16, 31, 32
hydration 49, 50, 54, 56–60, 65, 67, 70
hydration-structure making 66
hydrophobic peptides 69

I
immunoliposome 1, 16–21, 31
in vivo study 68, 69, 72
integrin 16, 31
intracellular delivery 72
intrinsic principal curvatures 255, 256
intrinsic shape 253–256, 258, 272,
 276, 277
inverted cone shaped lipids 8
ionic strength 51, 52, 63, 65, 66, 71

isoflavones 107–109, 114–116
isotropic bending 263, 264, 268–272,
277

K

K⁺ 65, 66, 70
kaempferol 114
kerasine 60

L

lactosylceramide 60
Langmuir-Blodgett (LB) monolayers
230
large unilamellar vesicles (LUV) 52,
53, 60, 68, 71, 73
lateral phase separation 276
lattice statistics 257, 272
Li⁺ 65, 66
lipid headgroups 63, 65, 66
lipid hydration 58
lipophilic substance 191, 194–197
lipoplex 135, 136, 145, 156, 166–168,
178
liposome structure 281, 291, 294, 295
liposomes 230, 232, 233, 235–237,
245–247, 253, 256, 271, 276,
277, 281–285, 296, 299, 300,
302–304, 309–315
liver 69, 72
luciferase 142, 145, 146, 157, 158,
173, 176
luminometer 157, 158
lyophilization 136, 141, 146, 170–172

M

M 52, 61
macrophage 1, 4, 18, 21, 25–27, 29
mangostin 191, 204–206
mannose 26–28
membrane 79–93, 95–100, 102
membrane fluidity 80, 86–90, 93, 96,
99, 100
membrane inclusion 253, 256,
271–273, 276, 277
mesothelioma 136, 146, 156,
179–181

metal ion 191, 210–213
metals 79–81, 83, 90, 92–97, 101
Mg²⁺ 66
micropolarity 195, 196
microviscosity 204, 205, 207, 209,
214, 215, 218, 219
minimum inhibitory concentration
(MIC) 124, 125
mitochondria 136, 139, 142, 174–176
MLVs 52, 57
Mn²⁺ 66
molecular recognition 192, 229–233,
235, 236, 248
mononuclear phagocytic system 68
mucoadhesive 69, 70
multilamellar vesicles (MLVs) 4, 52,
109

N

N-isopropylacrylamide 68
Na⁺ 65, 66
negative net charges 54
NH₄⁺ 65, 66
NO₃⁻ 67
non-local bending 270, 271
nonionic surfactant 191–194
nucleic acid 135, 136, 138, 139, 143,
145, 151, 157
nude mice 136, 176, 177

O

OH- 66
oligodeoxynucleotide (ODN) 142
orientational distribution 253, 263,
265, 266
osmotic effects 49, 60
oxidative stress 98

P

31P NMR 136, 155, 167, 171
p16 136, 138, 142, 179–181
packing parameter 51
partition coefficient 107, 111, 112,
117, 119, 121, 124
passive accumulation 16
passive targeting 50, 69

PEG 49, 63, 68, 69, 71, 72
 pH-sensitive 67, 68
 pH-sensitive liposomes 1, 7–10, 18,
 19, 29
 phase transition 49, 50, 53, 55, 57–60,
 63, 65, 67
 phase transition temperature 57–59,
 65, 68, 70
 phosphatidic acid 50
 phosphatidyl serine (PS) 121
 phosphatidylcholine 50, 58
 phosphatidylcholine from egg yolk
 (egg PC) 109
 phosphatidylethanolamine 50, 58
 phosphatidylglycerol 50
 phosphatidylinositol 50
 phospholipase 3, 11, 14, 15
 photosensitive liposomes 1, 10, 11
 phrenosine 60
 plant polyphenols 107–109
 plasmid 135, 137, 138, 140, 142,
 145–147, 149–151, 153, 155,
 157–160, 162, 164–169,
 171–174, 176, 179, 180
 polar head groups 50, 53, 54, 57,
 67
 poly(γ -dodecyl-glutamate) 69
 poly(benzyl-glutamate) 69
 poly(leucine) 69
 poly(valine) 69
 polydiacetylenes (PDAs) 230
 polyethylene glycol (PEG) 5
 polyphenols 107–109, 112, 117, 126,
 130
 polyvinyl alcohol (PVA) 69
 positive charge 54, 63, 72, 73
 principal curvatures 255, 256,
 259–261, 277
 prolonged circulation time 68
 propyl and methyl gallates 112
 protein 191, 216–218, 224
 proteoglycan 136, 137, 139, 173

Q

QLS 137, 147, 149, 151, 154
 quercetin 114, 116

R

radio wave dielectric spectroscopy
 302
 Rb^+ 65, 66
 RDG 73
 receptor–ligand interaction 232, 233
 receptor-mediated endocytosis 6, 21,
 24
 reporter gene 140, 142, 145, 146, 157,
 162, 167
 reticulo endothelial organs 73
 reticuloendothelial system (RES) 4
 rupture 59, 71

S

SCN- 67
 serum 136, 137, 141, 150, 151, 153,
 154, 156, 158, 160, 162, 172,
 173, 176
 shrinkage 60–62
 small unilamellar vesicles (SUV) 52,
 57, 71
 SO_4^{2-} 67
 solid state ^{31}P and 2H NMR
 spectroscopy 126
 solid state nuclear magnetic
 resonance 126
 sphingomyelin 50, 58
 sphingomyelinase 14
 spleen 69
 stealth liposome 20
 stearyl amine (SA) 121
 sterically stabilized liposomes (SSL) 1,
 5
 steroid 191, 197–200
 structure breakers 66
 sulfatide 60
 supercritical fluid 220, 223
 supercritical reverse phase
 evaporation method (scRPE
 method) 222
 surface activity 49, 53
 surface charge density 281, 282, 307,
 309, 310, 312
 surface Modification 49, 67, 68, 72,
 73

T

targeting 136, 139, 174, 177
tea polyphenols 108
TEAEC-Chol 138, 144, 149, 157, 169
TEAPC-Chol 138, 144, 149, 150, 153,
154, 157, 158, 160, 166, 168,
169, 172, 173, 176–181
tetracaine 61–63
tetraethylammonium + 65
tetrahydrocurcumin (THC) 114
tetramethylammonium + 66
thermosensitive liposomes 1, 12, 13
TMAEC-Chol 138, 144, 149, 151, 152,
157, 159–166, 169, 172, 173,
175, 179–181
TMAPC-Chol 138, 144, 149, 157, 158,
168, 169, 172, 173, 177, 178
trafficking 136, 160
trans-gauche isomerism 58
transfection 135, 136, 138–143, 145,
146, 148, 151, 154, 156–162,
165–178, 181
transfection in vivo 139, 178

transferrin-attached liposomes 24
trapping efficiency 193, 195, 220–223
triggered drug release 1, 5, 6, 13
trinitrophenol 66
tubulovesicles 70
tumor 67

U

unilamellar vesicles (ULVs) 4
urea 66

V

van der Waals interactions 58
vascoactive intestinal peptide (VIP) 16

W

water permeability coefficient 60
water-soluble polymer 191, 213, 214

Z

zeta potential 63, 65, 66, 193, 194,
202, 203, 214, 215

This page intentionally left blank